Advanced Dielectrophoretic Cell Separation Systems

A thesis submitted to the
Department of Electronics and Electrical Engineering,
University of Glasgow

for the degree of
Doctor of Philosophy

by

David Holmes

To Mum and Dad

Abstract

This thesis describes experimental and theoretical investigations into new particle handling and separation methods and techniques. It makes a major contribution to the rapidly expanding field of cell separation technology. A novel dielectrophoretic cell separation system has been developed, which is capable of processing large sample volumes (~50mL) in a flow through system. Previously reported dielectrophoretic cell separator systems typically process sample volumes in the 100μL range. The electrode configuration developed for this work allows the isolation and concentration of single particle types from large sample volumes; a method which could be further developed into a new rare-cell separation technology. In addition, a new technique of particle fractionation was developed termed 'Dielectrophoretic Chromatography'.

A cell separation chip was designed and built using standard micro-fabrication techniques. Experimental work was undertaken to demonstrate the function and limitations of the device. Numerical modelling of the particle motion in the device is presented and compared with experimental work for a number of different particle types, applied voltages and fluid flow rates.

The dielectrophoretic separation system comprises a microfluidic channel, of cross-section 100μm x 10mm and length 50mm, with two sets of interdigitated microelectrode arrays. The first set of arrays, with characteristic electrode size 40μm, called a focussing device, has electrodes patterned onto the top and bottom surfaces of the flow channel. The second electrode array, which is part of the same device, has an electrode array patterned only on the bottom of the channel. Two sizes of secondary electrode array were used 20μm and 40μm. AC voltages (from 1V to 10V peak) are applied to the microelectrode, with a frequency between 10kHz to 180MHz. A dielectrophoretic force is exerted on the particles as they flow along the channel. The first electrode array uses negative dielectrophoresis to focus the stream of particles entering the device into a narrow sheet (one particle diameter thick) midway between the upper and lower channel surfaces. The second electrode array, down stream from the first is separately controllable. This is used to selectively attract a desired sub-population of particles from the flow stream under positive dielectrophoresis. The separation electrode retains these particles while all other particles flow through to the channel outlet, where they can be collected. Removal of the signal applied to the separation electrodes releases the captured particles, which can then also be collected from the outlet.

Experiments carried out using the new system show it to be capable of the separation of binary mixtures of cell types into their component parts. Mixtures of trophoblast cells were isolated from the chorionic membranes of the human placenta by enzymatic digestion. These cells were

mixed with human peripheral blood cells, that had been isolated on a density gradient and passed through the system at a rate of 1mL/hr. Flow-cytometeric analysis of the samples prior to, and following passage through the separation system showed a 30-fold enrichment of the sample for trophoblast cells. Similar experiments were carried out with mixtures of 6μm latex beads and peripheral blood cells, and demonstrate the ability of the system to selectively capture 100% pure populations of blood cells at the separation electrode.

Dielectrophoretic chromatography was performed using the two-stage separation electrode device. Following focussing using the initial electrode arrays, cells with different dielectric and volumetric properties flow into the secondary electrode array and experience different forces and therefore follow different trajectories. The individual cells or particles are therefore attracted onto the separation electrode array at a position which depends on particle parameters, suspending medium flow rate, suspending medium density, and applied voltage and frequency. The mean banding position of a collection of like particles is shown to be in quantitative agreement with numerical simulations of the particle trajectories.

The efficacy of the system was determined by investigating the separation of two cell types, namely cultured human monocytes cell line (THP-1) and human peripheral blood cells. It was shown that the cells could be separated into sub-populations with a distinct distribution along the length of the separation electrode array. Measurements were performed on the THP-1 cells, allowing the calculation of their dielectric properties, giving a mean value for the specific membrane capacitance of 17.7± 2.7mFm^{-2}, with a cell radius of 6.4 ± 1μm. The dielectric properties of human peripheral blood cells were obtained from the literature. Simulation of the position of the cells was found to be in reasonable agreement with experiment. The ability of the system to concentrate very low number densities of biological particles from large volumes (10mL), containing fewer than 100 cells per mL was demonstrated, using blood cells, bacteria, and sub-micron latex beads (460nm diameter).

Maternal peripheral blood samples (20mL) were obtained from pregnant women expecting male babies. Following pre-treatment these samples were passed through the system under experimental conditions chosen to select for the foetal cells (trophoblast). PCR analysis of the post-sort samples was negative for the presence of the Y-chromosome indicating that the system did not enrich sufficiently for the small numbers of foetal cells that might have been present in the samples. Further work is required to assess the full capabilities of the dielectrophoretic particle separation system for rare cell isolation on maternal samples or other biological materials.

Acknowledgements

I would like to thank Professor Hywel Morgan for giving me the opportunity to work in such an interesting field. His great encouragement and enthusiasm throughout the course of this work has made the experience a good one.

Thanks to Nic Green for all the advice on numerical simulation and many interesting conversations. To all the members of the Bioelectronics group (past and present) thanks for making the place fun, and for putting up with the continuous demands for blood samples. If you look carefully within these pages you might recognise some of the cells… Thanks to Paul and Nigel for lunches and coffee as well as the odd beer. Also cheers to Chris, Martin, and all the rest of the weekly bio-footballers for many hours of fun. A special thanks to Aussie Dave, Mary and Eric for being there as long as me.

I would also like to express my gratitude to all the technical staff in the Department of Electronics and Electrical Engineering at Glasgow, and all those at the Queen Mother's Hospital, and the Royal Infirmary who helped with the 'bits and pieces' along the way. A special thanks goes to Drs Margot Thomas and Steve Campbell for sharing their knowledge of placental physiology with me. And to Mrs Anne Young for the technical help regarding all aspects of my work at the Royal Infirmary.

To Jane and Danielle, Lou, Michael, Alan, Richard, Stephen and Ros and anyone else I'm lucky enough to call my friends you'll be glad to hear – I'M FINALLY FINISHED!

Finally, a great big special thanks to Mairi for being lovely and putting up with me for the last few years - and as promised I've removed the quote about "cooking".

Contents

Chapter One: Introduction

1 Introduction to rare particle separation

The separation of rare cells (less than 1%) from heterogeneous cell suspensions is useful for a variety of clinical and biological applications. The majority of applications requiring the isolation of these cells can broadly be divided into two categories: (1) the positive selection of a particular cell type for analysis or clinical use or (2) the depletion of undesired cells from a population of desired cells. Examples of the first category are the isolation of foetal cells from the maternal circulation [1, 2], and the isolation and detection of cancer cells from the circulation for diagnostic purposes [3]. Examples of the second category are the depletion of residual tumour burden cells from bone marrow or stimulated aphaeresis product [4], and the removal of bacteria from blood products.

A variety of techniques aimed at achieving the separation and/or identification of various cell types (rare and not so rare) have been developed over the years. The history of cell separation dates back to the 1960's, with available separation parameters being exploited as soon as they were identified as being specific for a given cell type. Initially, physical characteristics (e.g., density) or biochemical characteristics were used. For example, L-leucine-methyl ester kills the lysosome-rich monocytes and natural killer (NK) cells and can thus be used for their depletion. Bøyum [5] first described the use of Ficoll-density gradients for the isolation of lymphocytes from blood in 1968. With the development of monoclonal antibodies (mAbs) in the 70's the isolation of cells with distinct functional differences became possible. Polyclonal antibodies are also useful for cell separation but tend to be less specific.

Techniques based on the attachment of mAbs to a variety of substrates (e.g. for panning, immunomagnetics, immunofluorescence, etc.) has lead to the development of highly sophisticated sorting tools capable of detecting and isolating large numbers of cells based on a number of different criteria. Depending on the technique employed cell selection can often be based on multiple criteria at once (e.g. the presence of a number of different antigens on the cell surface). These tools however are often expensive and typically require skilled operators to achieve the optimal results.

Each cell type has its own complement of surface proteins (antigens) specific to that cell type. Antibodies can be produced which recognize these surface antigens and bind specifically to them. It should be noted that other molecules can be used to recognise other surface antigens (e.g. lectins bind to carbohydrates in the cell membrane). If the antibodies are attached to a substrate (e.g. fluorescent molecule, magnetic bead, etc.) their binding to a cell's surface can then allow a variety of separation schemes to be used. For example, once labelled with an antibody, the target cell population can be selectively enriched using flow cytometry, or magnetic separation methods as discussed below.

To date, nearly all separation strategies have been antibody based. Unfortunately, these methods are limited by the lack of specificity of currently available antibodies. As a result, cells other than those targeted can bind the antibody and be positively selected, along with the target cells, resulting in contamination of the "sorted" sample.

The case of foetal cell isolation demonstrates the need for high-resolution sorting schemes capable of discriminating between cell types, without the need for labelling. The search for antibodies specific to any of the foetal cell types present in the maternal blood has proved unfruitful, despite concerted effort by a number of groups working in this area, with the same being true for many other cell types. Although in time, specific antibodies may be produced to address these problems, interest in other non-antibody based separation techniques is growing. One example is the novel AC electrokinetic technique; dielectrophoresis [59], which has been shown to be capable of distinguish between different cell types by using the electrical properties of the cell membrane as the discriminatory factor.

The application of microsystems technology to the fields of biological, chemical and medical science has developed exponentially over the last decade (e.g. [6]). The technology promises great developments, with the miniaturisation of current technologies and the development of entirely novel methods. The field of miniaturised separation science has been transformed by the use of capillary electrophoresis (CE) for the separation of chemicals, proteins, macromolecules, etc (e.g. ref [7-9]). The CE technique has allowed the development of high-speed, high-resolution separations on extremely small sample volumes (<1nL compared with slab electrophoresis which requires sample volumes in the μL range).

The technique of dielectrophoresis is currently experiencing a period of intense interest as a method for bio-particle separation. This thesis presents my work on a novel dielectrophoretic cell separation device.

1.1 Cell types in blood

Whole blood contains a variety of cell types, each with a different physiological role. Red blood cells (RBCs), white blood cells (WBCs) and platelets are all suspended in a proteinaceous fluid called plasma. Plasma, which is 90% water, constitutes about 55% of the blood volume. Plasma contains various proteins (e.g. albumin, fibrinogen, globulins and other clotting proteins). Table 1-1 shows the average concentration of the various cell types found in the peripheral blood of a healthy human.

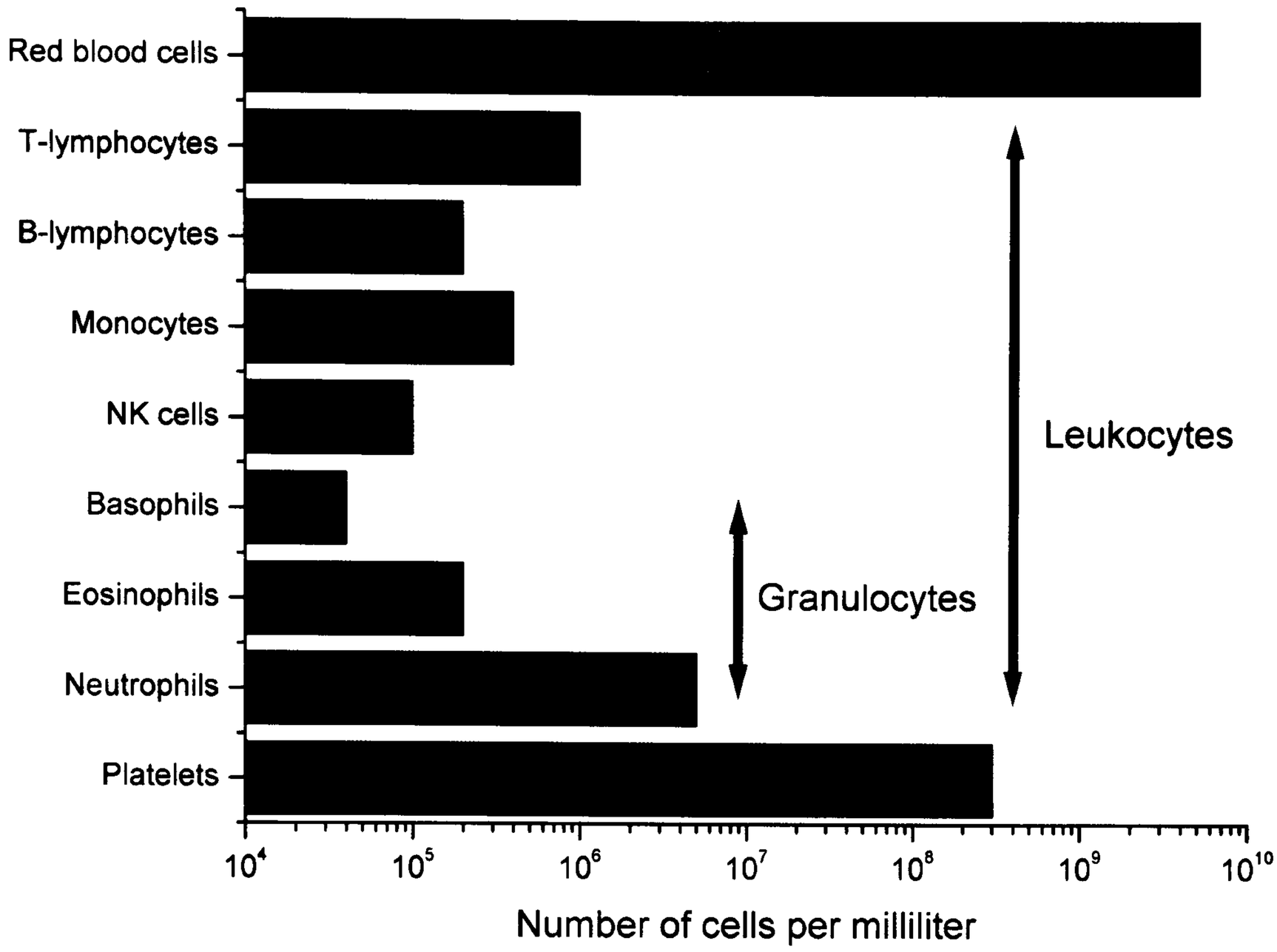

Table 1-1. Concentration of major cell populations in normal adult human blood [10].

1.1.1 Red blood cells (RBCs)

Red blood cells (or erythrocytes) are perhaps the most recognizable component of whole blood. They typically express a bi-concave disc morphology and contain haemoglobin, an iron-containing protein that carries oxygen throughout the body. It is the haemoglobin that gives blood its characteristic red colour. The percentage of blood volume occupied by RBCs (the haematocrit) for an average adult male is 47 percent. Manufactured in the bone marrow, RBCs are continuously being produced and broken down. They live for approximately 120 days in the circulatory system before being removed from the blood by the spleen.

1.1.2 White blood cells

White blood cells (WBCs, also known as leukocytes) are responsible for protecting the body from invasion by foreign substances such as bacteria, fungi and viruses. The majority of WBCs are produced in the bone marrow, where they outnumber RBCs by two to one. However, in the blood stream, there are about 600 RBCs for every WBC. There are several types of WBC, these include; Granulocytes (including Neutrophils, Basophils, Eosinophils) and Monocytes (that

become tissue Macrophages) which protect against infection by destroying invading bacteria and viruses, and Lymphocytes which aid in the immune defence.

1.1.3 Platelets

Platelets (or thrombocytes) are very small cellular components (~1μm) that help with the clotting process by sticking to the lining of blood vessels. Platelets are made in the bone marrow and survive in the circulatory system for an average of 9-10 days before being removed from the blood by the spleen. The platelet is vital to life, because it helps prevent blood loss resulting from trauma, and blood vessel leakage that results from normal daily activity.

1.2 Examples of rare cell isolation

1.2.1 Isolation of foetal cells from maternal blood

The isolation of foetal cells from the maternal circulation has been investigated by a number of groups [1, 2, 11-37]. Over the past 30 years the use of prenatal diagnosis by expectant couples and their doctors has expanded as molecular biology techniques have developed. In the U.K., U.S. and many other countries it is normal to offer cytogenetic diagnosis to pregnant women who will be 35 years or older at the time of delivery. In order to carry out such cytogenetic diagnoses, a sample of foetal nucleated cells must be obtained via an invasive technique such as chorionic villus sampling (CVS) or amniocentesis. The age threshold of 35 years corresponds to the maternal age at which the chance of an infant being born with the most common autosomal aneuploidy, trisomy 21 (Down's syndrome [20]), is equal to the chance of miscarriage due to these procedures (~1 in 250).

Despite the safety and improving accuracy of invasive techniques, the incidence of Down's syndrome births is still about 1 per 1000 for all live births. The reason for this is that although there is an increased likelihood of aneuploidy with increased maternal age, as a group older women are having fewer births when compared with younger women [20]. Of all the Down's syndrome births, 80% of them are to women under 35 years old [20]. This group of women are currently not offered the prenatal diagnostic techniques because the risk from the invasive procedures is greater than the risk of the infant having Down's syndrome. For every positive Down's test, there are four miscarriages of healthy babies resulting from invasive prenatal diagnostic testing. It is therefore clear that a non-invasive method of isolating foetal nucleated cells for cytogenetic diagnosis would be of great value.

Several recent reports have described the isolation of foetal cell types from the maternal blood [11-22]. These cells, originating from the foetus, are released throughout the course of the pregnancy. They find their way across the placenta (from the foetus) and into the maternal blood supply, via a number of physiologically normal routes (see below). The isolation of these foetal cells from samples of maternal blood potentially represents a non-invasive procedure, without risk to the foetus. The maternal blood samples can be safely obtained by vein puncture, usually from the mother's arm. The current methods used for the isolation of these cell types from the maternal blood are still at an early stage of development and are still far from being used as part a routine diagnostics technique. This is primarily due to the complexity and expense of the current technologies.

In 1893 Schmörl [23] first reported observing foetal cells within the maternal vasculature when he described multinucleated syncitiotrophoblast cells in the pulmonary vasculature of a woman who had died of eclampsia. However, the suggestion that these cells might provide a useful source of genetic material for prenatal diagnostic purposes did not arise until 1969 when Walknowska *et al* [24] reported the detection of foetal metaphases in maternal blood. Such a projection has only become possible with recent developments in molecular biology and a better understanding of certain areas of biology.

For many years the existence of foetal cells in maternal blood was considered controversial. However, using recently developed molecular techniques such as polymerase chain reaction (PCR) and fluorescence *in situ* hybridisation (FISH), various groups have demonstrated beyond doubt the existence of foetal cells in maternal blood. Many groups have used PCR to detect Y-chromosome sequences (male DNA) and single gene sequences (e.g. haemoglobin Lepore(Boston)) in maternal blood. FISH has been used to detect the most common chromosomal abnormalities involving chromosomes 21, 18, 13, X and Y, which account for 95 – 98% of all chromosomal abnormalities at birth. Free foetal DNA sequences, as well as freely circulating intact nuclei, have also been shown to exist in maternal blood and plasma [1, 2, 25-27]. These also represent a potential source of foetal DNA for prenatal cytogenetic testing.

1.2.2 Foetal cell types in maternal blood

There are a number of foetal cell types present in the maternal circulation, which could potentially be isolated and used for prenatal cytogenetic diagnosis. What follows is a summary of the various foetal cell types that have been shown to be present in the maternal circulation. These cells are thought to enter the maternal blood stream in either of two ways: (1) when they are dislodged from the placental tissue by the invasion of the maternal vasculature into the placenta or (2) via 'micro bleeds', small haemorrhages of the foetal blood vessels.

1.2.2.1 Foetal lymphocytes

Initial attempts, using flow cytometery, to recover foetal leukocytes were carried out by Herzenberg *et al.* [28, 29]. Foetal lymphocytes clearly exist in the maternal blood but their use is problematic as they can persist in the maternal blood after pregnancy and may become a source of contamination precluding their use for diagnostic purposes in future pregnancies. Bianchi *et al.* [30] studied women who had delivered male children between 6 months and 27 years earlier and found that foetal lymphocytes from these pregnancies were still present in their blood.

1.2.2.2 Foetal granulocytes

To date there has only been one reported investigation showing foetal granulocytes in maternal blood [31]. The authors used flow cytometery to look for cells showing a Y-chromosome signal. As these cells have a short half-life, persistence to another pregnancy is unlikely. At present there is no way of differentiating between foetal and maternal granulocytes making separation impossible.

1.2.2.3 Foetal nucleated red blood cells (fnRBCs)

Erythroblasts, or nucleated red blood cells (nRBCs) are found in the peripheral circulation. Foetal nucleated red blood cells (fnRBCs) have been shown to be present in the maternal circulation by a number of groups (e.g. [11, 15, 17, 21, 32-34]). They are by far the most widely studied cell type, with regard to their isolation from the maternal blood supply. Foetal haemoglobin has been used successfully as a marker for the isolation of these cells by flow cytometry [35, 36].

1.2.2.4 Trophoblast

The trophoblast cells of the placenta form the interface between the conceptus and the mother, with the outer layer of terminally differentiated syncytiotrophoblast cells bathed in maternal blood. The inner layers of mononuclear cytotrophoblast cells proliferate, differentiate and fuse to form the multinucleated syncytiotrophoblast. As the syncytiotrophoblast cells and the underlying mesenchyme and blood vessels continue to proliferate the tissue forms branches called villi. The cavities form initially within the trophoblastic shell during early development. These cavities increase in size and communicate with one another, producing the maternal blood lake within the placenta. This process results in the formation of these cavities or lacunae lined with syncytiotrophoblast cells. The lytic activity of the syncytiotrophoblast cells causes the rupture of both maternal arterial and venous blood vessels with a resultant flow of maternal blood from the arteries into the lacunar spaces and back into the maternal system via the veins.

There are two routes by which trophoblast cells gain access to maternal circulation [115]. Syncytiotrophoblast cells are thought to be shed continuously into the maternal circulation and lodge in the capillary beds of the maternal lungs where most are degraded, however small numbers of these cells may escape into the peripheral circulation [24]. In early pregnancy, the maternal spiral arterioles are invaded by specialised cytotrophoblast cells, and this is essential to the development of a good blood supply for the placenta (see figure 1-1 below). It is therefore probable that there is a heterogeneous population of trophoblast cells present in the maternal bloodstream at different times of gestation, although one would expect that the smaller cytotrophoblast cells be more prevalent than the syncytiotrophoblast cells in the maternal blood.

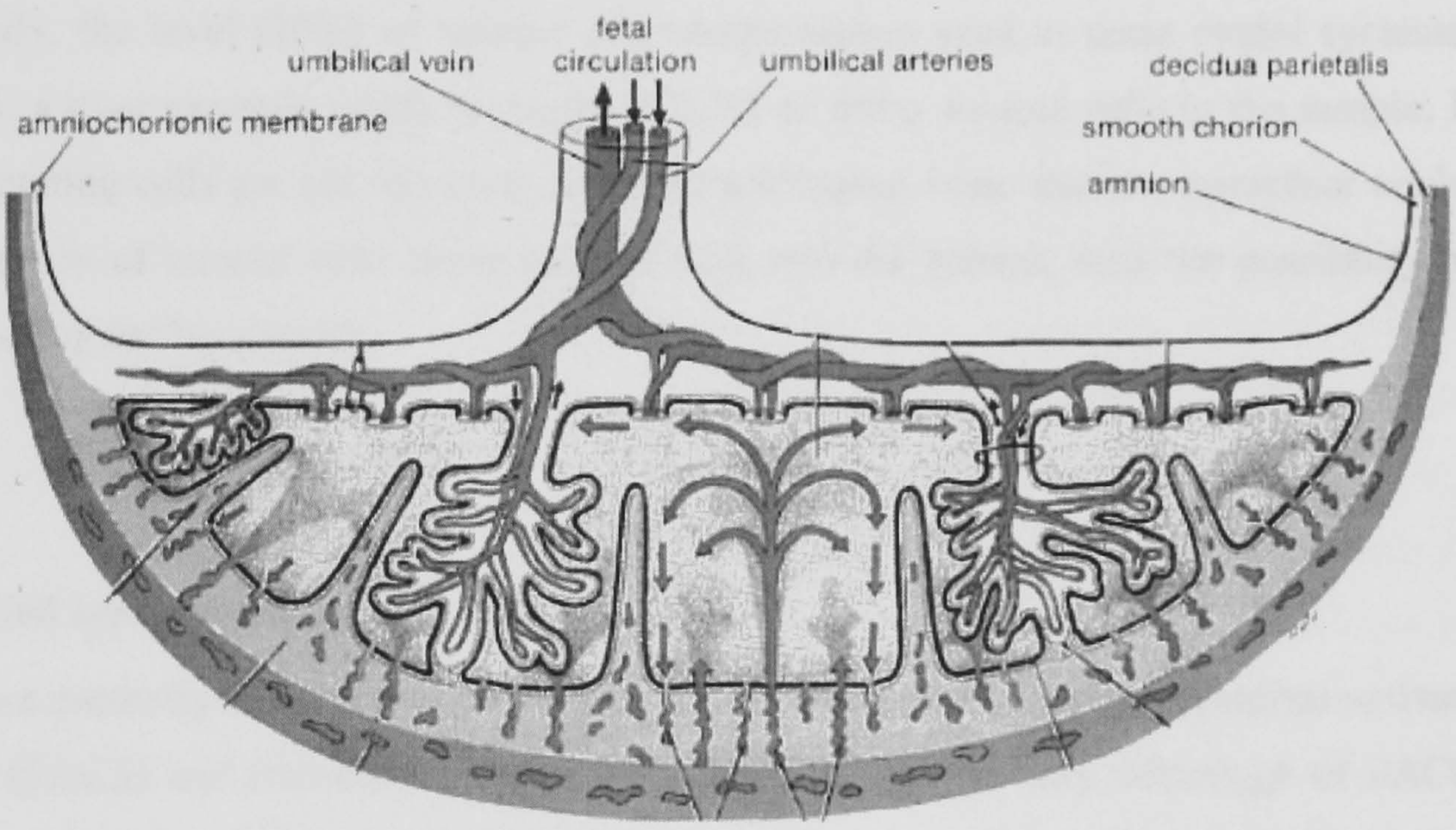

Figure 1-1. Drawing of the placental anatomy [114].

The first report of the isolation of trophoblast from peripheral blood of pregnant women was that by Covone *et al.* [37]. These cells appear early on in gestation (from 6weeks until birth). Trophoblast cells are endothelial cells of placental origin and have quite different physiological functions and properties compared with both foetal and maternal blood cells. One would expect these differences to be reflected in the structure/morphology and protein content of the cellular membrane, and therefore of the foetal cells present in the maternal blood the trophoblast is likely to show the most significant differences in dielectric properties when compared with maternal blood cells. Part of the work presented in this thesis therefore focuses on the isolation of trophoblast from blood.

1.2.3 Cancer cells in the peripheral circulation

The detection and quantitative measurement of rare cancer cells in the blood or bone marrow is potentially very important for diagnostic and therapeutic purposes [3, 38-44]. These cells, if isolated, could be used to determine the likely prognosis and aid in decision-making about the

type and aggressiveness of treatment. Currently used high-dose chemotherapy treatments destroy the haematopoietic system; chemotherapy can then be followed by autologous bone marrow transplantation to restore the patient's blood cell production. The patient's own bone marrow or peripheral blood stem cells are used in autologous transplant and these are collected prior to chemotherapy. In order to avoid the possibility of the re-infusion of the contaminating tumour cells back into the patient, these tissues need to be purged of tumour cells before they can be used therapeutically [45, 46].

Model studies have shown [47, 48] that current state-of-the-art techniques are capable of purging a 10% tumour cell load in a sample of bone marrow by a factor of 10^{-3} to 10^{-4}. Obviously, the level (10%) of tumour cell contamination used in these model systems is not realistic; a truer example might be closer to 0.1% or fewer tumour cells in the sample. If these contaminating cells are not removed, a typical autologous bone marrow transplant could result in thousands of tumour cells being infused back into the patient, with the possibility of these cells causing further disease.

1.3 Cell separation and detection

There are currently two main cell sorting techniques in use; they are fluorescence-activated cell sorting (FACS) and immunomagnetic cell separation. The primary advantage of FACS is its ability to identify individual cells based upon multiple parameters such as cell size, granularity, colour and intensity of fluorescence. FACS has the drawback that its sorting rate is limited to a maximum of about 10^4 cells per second (dedicated research instruments can, when optimally configured achieve sort rates approaching 10^5 cells/s). Immunomagnetic cell separation has the advantage of being fast and simple to operate. However, it can only sort cells on the basis of a single parameter. There are a plethora of other cell separation techniques currently being used to isolate specific cell fractions, but none have the resolution of either the FACS or immunomagnetic cell separation technologies.

The following discussion will concentrate mainly on the detection and separation of cells using flow cytometry, of which FACS is a sub-technique, and immunomagnetics. Other cell separation techniques are discussed briefly and a variety of cell identification and detection technologies are then discussed.

1.3.1 Flow cytometry

A flow cytometer is an instrument that measures the properties of cells in a flowing stream. Strictly speaking, instruments other than those commonly referred to as flow cytometers must

be included if one uses this definition. There are two main types of flow cytometer - analysers and sorters. Sorters have the ability not only to collect data on cells (i.e. analyse) but also to sort the cells based upon their particular wavelength of emission (as defined by fluorescent labelling of the cell sample) and light scattering properties.

Two companies, Becton Dickinson and Beckman Coulter have dominated the commercial flow cytometer market (with both analysers and sorters). There are a number of other companies producing flow cytometers, but they hold only a small percentage of the market. Advances in fluidics, optics, electronics, lasers, computers and software have made flow cytometers considerably more complex, but also easier to use.

1.3.1.1 The Coulter technique

The Coulter technique, originally proposed by Coulter in the 1950's [49], allows the measurement of the number and size of particles suspended in an electrolyte by passing them one-by-one through a small orifice and measuring the change in electrical impedance between a pair of electrodes placed at either side of the orifice. The change in the impedance as a particle passes through the orifice generates a voltage pulse whose amplitude is proportional to the particle's volume. The technique has been applied to count blood cells [49, 50] and bacteria [51, 52] as well as other cell types. The pulses, once amplified, sized and counted give information about the particle size distribution within the suspension.

The Coulter counter operates as shown in figure 1-2, a pressure difference across a small orifice causes a defined volume (typically 0.05ml, 0.5ml, 2ml) of the particle suspension to flow through an orifice. The samples must be sufficiently dilute such that only a single cell will be present in the orifice at any given time. The impedance across the orifice changes and the resultant voltage pulses are processed by the system electronics. To reduce background noise, all pulses above a certain threshold level are counted, thus the count represents the number of and size of particles above a certain minimum size in the defined suspension volume.

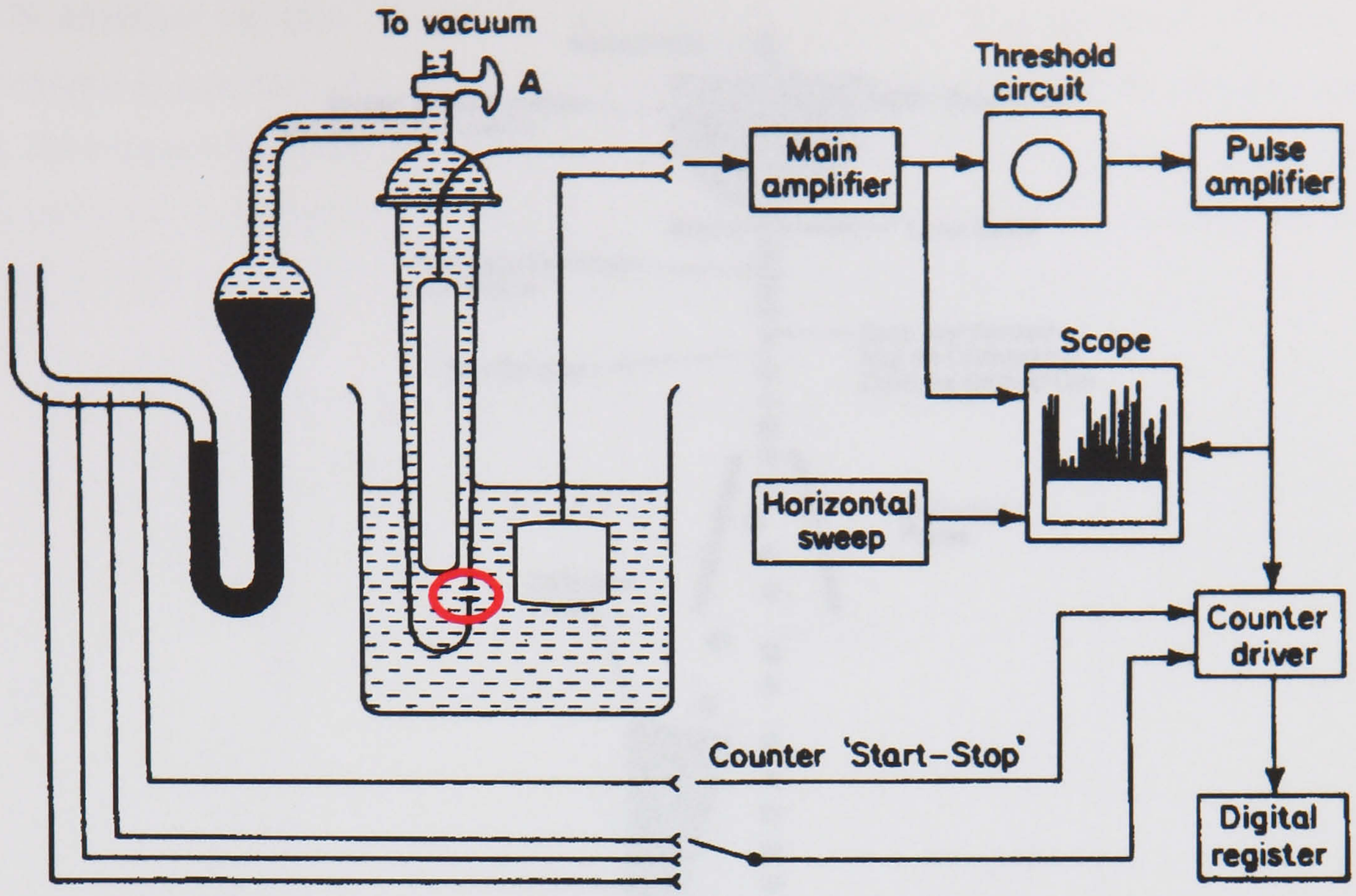

Figure 1-2. Schematic of the Coulter counter [53], the electrodes are positioned on either side of a small orifice (highlighted by the red circle).

The Coulter counter relies upon the basic assumption that the voltage pulse generated by a particle as it passes through the orifice is directly proportional to the particle cross-sectional area. This assumption is true so long as the change in the resistance of the orifice, due to the presence of the particle, does not affect the current flow through the orifice. The external resistance of the circuit is designed to be sufficiently high so as to ensure this constant current.

Coulter counters are generally used to analyse the proportions or numbers of blood cells in a sample. Few cell sorters have been developed using the Coulter technique. Recently, a number of microfabricated devices based on the Coulter principle have been developed, some of which have attempted to integrate sorting capabilities within the system (e.g. [54]).

1.3.1.2 Fluorescence-Activated Cell Sorting (FACS)

The term Fluorescence-Activated Cell Sorting (FACS) describes an instrument that can measure physical, as well as multi-colour fluorescence properties of cells flowing in a stream. The term FACS is applied equally to sorters and analysers.

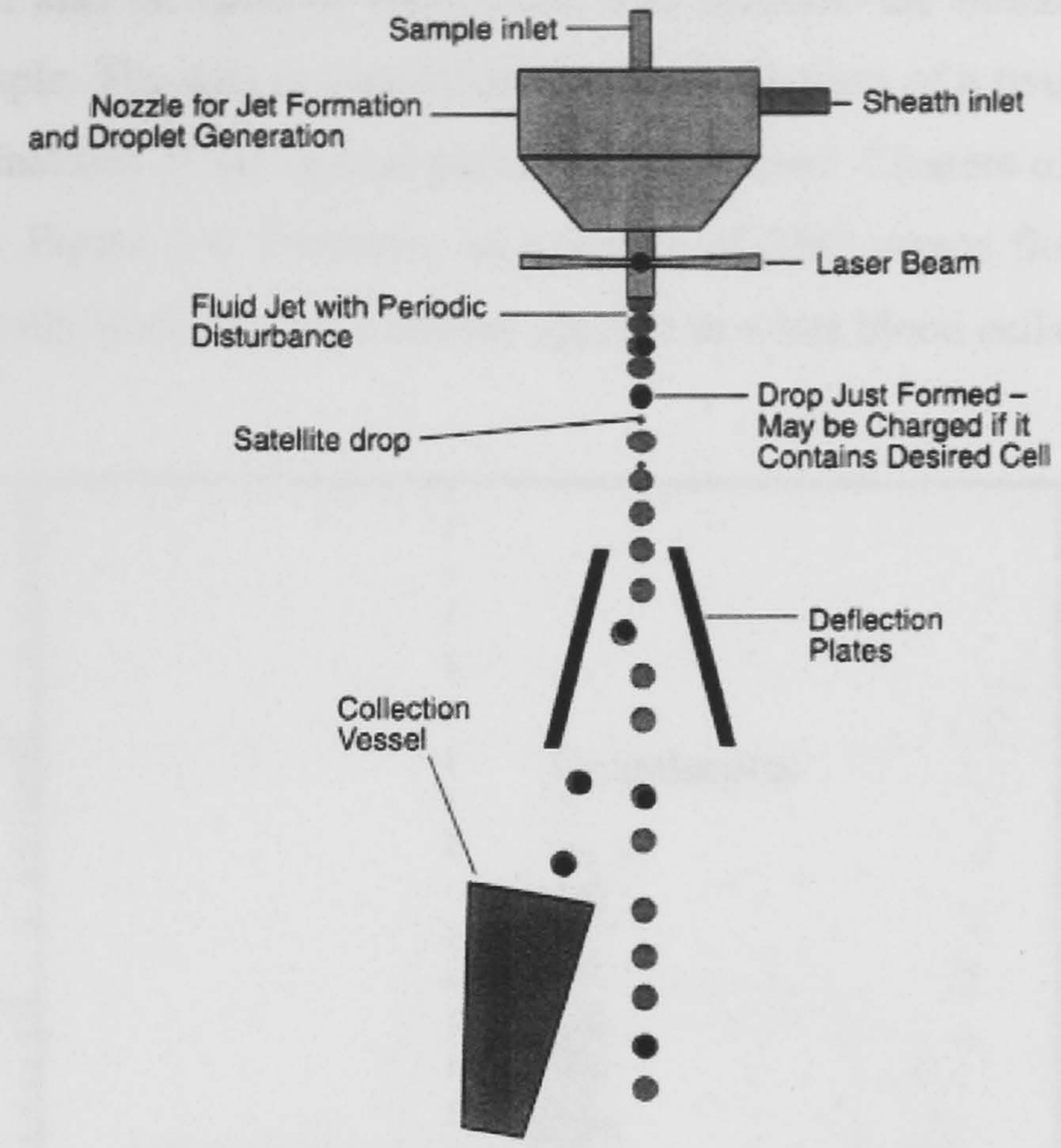

Figure 1-3. Fluorescence- activated cell sorting (FACS) [55].

The principle of FACS is shown in figure 1-3. Antibodies tagged with fluorochromes are attached to the cells. These fluorescent labels allow the identification of particular cell types in liquid suspension, as they flow past an optical sensing zone, where the fluorescent molecules are excited by a laser beam and emit light. An electrical signal is generated by sensors, which detect the emitted and scattered light and control whether or not a specific cell is selected. If a cell fulfils the criteria set by the operator, the droplet containing that cell is electrically charged. The droplets are then passed through an electric field, which deflects charged droplets out of stream and into a collection tube.

The light emitted by the cells as they pass one by one through a laser beam, or other light source is collected by optical elements in both the direction of laser light (forward scatter, FSC) and normal to the direction of the laser (side scatter, SSC). Photomultiplier tubes (PMTs) or photodiodes are used to detect the light and generate an electrical signal, which is processed by the instrument and displayed on a computer screen. FSC correlates mainly with cell size. SSC correlates with the internal contents of the cell as well as its size. For practical purposes SSC can be considered to represent the cell granularity. Fluorescent emission from the particle is filtered and separate detectors are used to detect the various colours (these are typically referred to as FL1, FL2, FL3, etc).

FACS machines can also be used to count cells, and measure the numbers of different cell populations in a sample. The data is usually displayed in the form of a two-dimensional scatter plot, showing combinations of the optical parameters measured. Clusters of dots represent cells of a particular type. Figure 1-4 illustrates an example of SSC versus fluorescence for white blood cells fluorescently labelled with a marker specific to white blood cells.

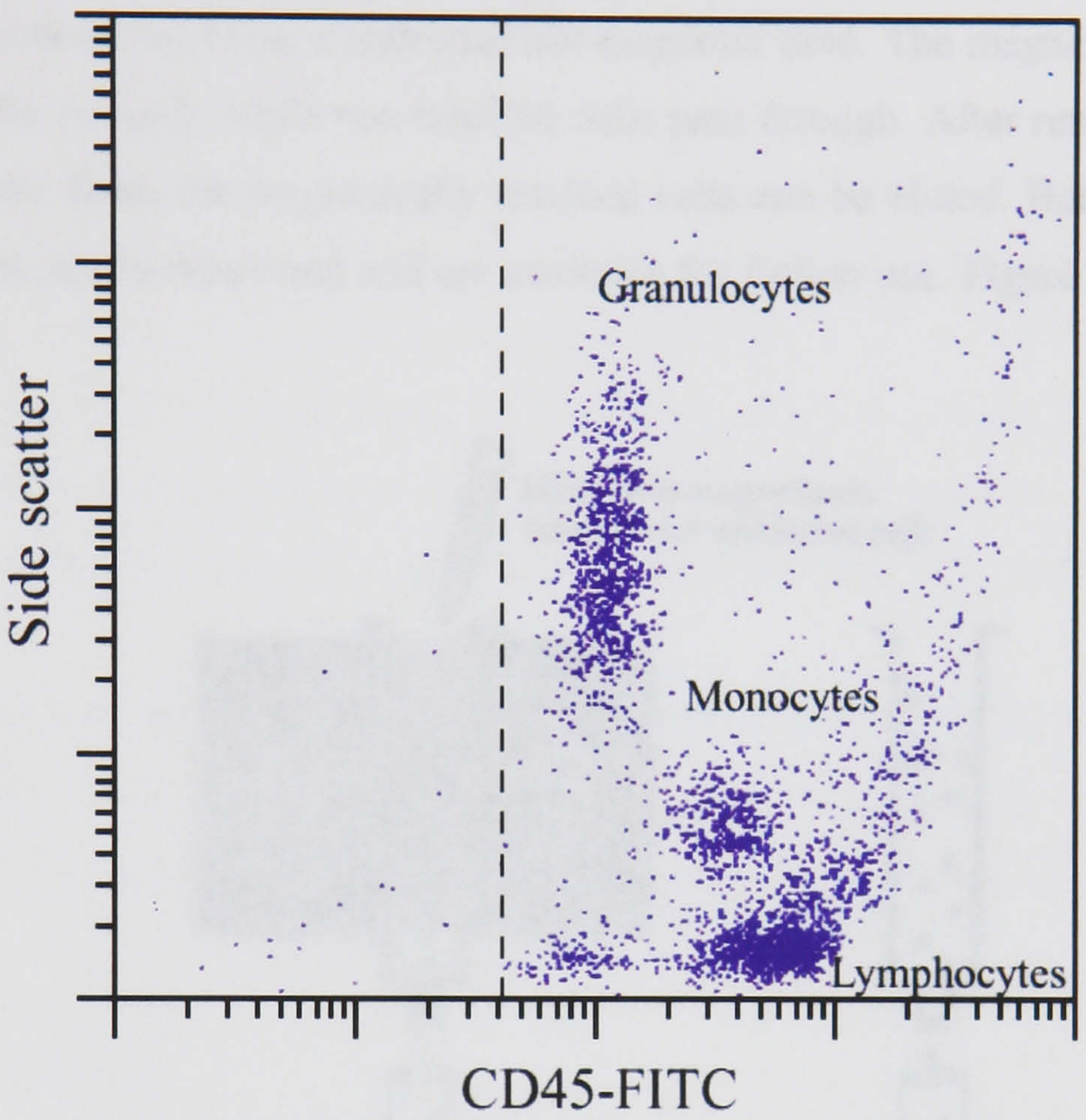

Figure 1-4. Fluorescence versus SSC plot showing relative positions of the WBC subpopulations [56].

Production of new fluorescent probes has seen the development of more flexible instruments so that eight or more parameters of correlated data can be collected at once. Three colour (along with the FSC and SSC information) FACS is most widely used.

1.3.2 Immuno-magnetic techniques

The preparation and labelling of cells for immunomagnetic separation [55-57] is similar to that used in fluorescence flow cytometry. There are a number of magnetic matrices that have been developed for immunomagnetic cell separation, with commercial manufacturers including Polysciences, Bangs Labs, Amersham International. The most widely used matrices are the microspheres from Dynal Inc., and the 'MACS' nanoparticles from Myltenyi Biotech. A discussion of the MACS system as developed by Myltenyi Biotech (this is the system used in the work of this thesis) is given initially; this is then followed by a brief description of the microshperes technology from Dynal.

1.3.2.1 Magnetically activated cell sorting - MACS

Cells of interest are specifically labelled with super-paramagnetic microbeads (co-precipitates of iron oxide and polysaccharides) 20-100nm in diameter. The cells are incubated with the magnetic beads, whose surfaces have been functionalised with antibodies specific to the cell type to be removed from the suspension. After magnetic labelling, the cells are passed through a separation column, which is placed in a strong permanent magnet. The column matrix (usually a fine wire mesh) serves to create a high-gradient magnetic field. The magnetically labelled cells are retained in the column, while non-labelled cells pass through. After removal of the column from the magnetic field, the magnetically retained cells can be eluted. Both labelled and non-labelled fractions can be recovered and are available for further use. Figure 1-5 shows the basic set-up.

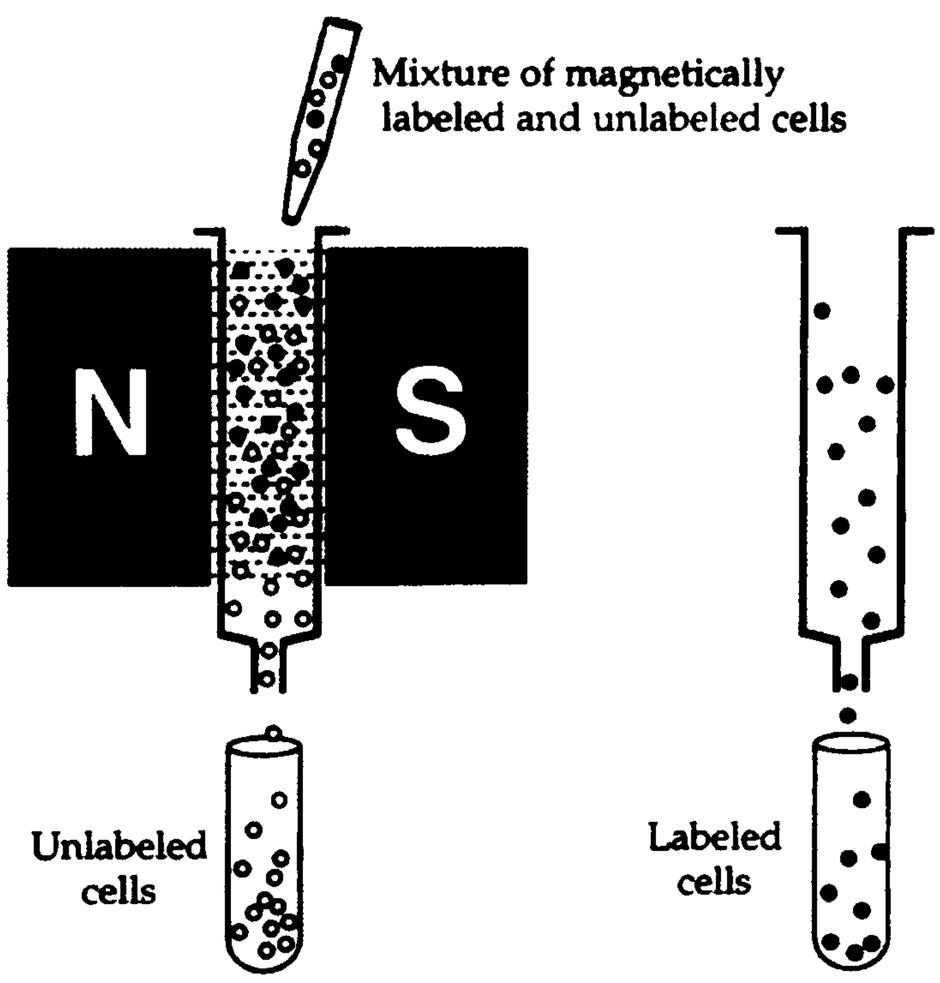

Figure 1-5. Magnetically activated cell separation [55].

The matrix consists of wire wool coated with a thin biocompatible plastic polymer to prevent corrosion. For a permanent magnet of 0.5–1 Tesla (T) and matrix wire of diameter 50 - 100μm, extremely high magnetic field gradients (i.e. high forces) can be generated ($\nabla B^2 > 10^4 T^2 m^{-3}$).

The extremely small size of the MACS microbeads reduces the mechanical stress on the cells and allows short incubation and fast processing times. The beads form a stable colloidal suspension and do not sediment or aggregate in magnetic fields. Their size and composition (iron oxide and polysaccharide) make them biocompatible. They are reported not to activate cells or influence function and viability. Therefore, bead detachment is not required, so positively selected cells (i.e. magnetically labelled ones) can be used immediately after separation for analysis and subsequent experiments.

The MACS system has been used for the isolation of rare cells with concentrations down to 1 rare cell for every 10^8 cells in the sample, with lower frequencies having been isolated using a combination of depletion and positive selection. Haematopoietic stem and progenitor cells, residual tumour cells or antigen-specific B or T cells, have all been isolated. Even the isolation of cells according to the expression of cytoplasmic proteins or selection of live cells based on secreted proteins is feasible. As with FACS the technique is limited by the availability of antibodies specific to the cell type being isolated.

Miltenyi Biotech have developed an automated cell sorting system based on their MACS microbead technology. The autoMACS is an automated bench-top magnetic cell sorter capable of sorting up to 10 million cells per second from samples of up to $4x10^9$ total cells allowing ultra high-speed positive selection as well as depletion. Using the system for positive selection, isolation of up to 2×10^8 pure target cells within a few minutes is possible. Cells as rare as 1 in 10^6 have been enriched to high purity using a double positive selection protocol [56].

MACS microbeads are compatible with flow cytometry. It is therefore possible to fluorescently and magnetically label cells simultaneously. After MACS sorting, cells can be used immediately for flow cytometeric analysis or further fluorescence activated cell sorting.

1.3.2.2 Microspheres

Dynal manufactures a range of magnetic microspheres of different sizes (2.8, 4.5, 5.0μm in diameter) [55]. The M450 polystyrene microspheres are the most widely used for cell separation, they are 4.5μm in diameter and contain ~20% by weight of magnetite (FE_3O_3) dispersed throughout their volume. The particles are super-paramagnetic, meaning they can be collected in a magnetic field, but do not retain any magnetism when the field is removed. The microspheres are available uncoated or precoated with a variety of monoclonal antibodies or other coating suitable for molecular biology applications. The Dynal microspheres have been used to separate or isolate a variety of cell types as well as other sub-cellular components and proteins, DNA and RNA.

The principle of operation is similar to that of the MACS beads described above. However, due to the large size of these microspheres there is no need for a wire wool matrix (used in the MACS system to create large magnetic field gradients). The cells with attached microspheres can simply be held against the side of the separation vessel (typically a tube) with a magnet held on the outer wall of the tube. Non-magnetically labelled cells are then simply decanted from the tube and the labelled cells along with any free microspheres retained within the tube. The cells can be removed from the microspheres by a number of methods.

1.3.3 Other cell separation methods

1.3.3.1 Erythrocyte lysis

Because of the high proportion of RBCs in blood (99%) it is generally useful to remove these cells prior to other isolation procedures. Red blood cells can be selectively removed from a blood sample because of their susceptibility to hypotonic shock, compared with that of leukocytes (white blood cells) and other nucleated cells. Low salt concentration solutions and commercial lysis kits can be used. When the cells are suspended in the lysis solution, of suitable osmotic pressure, the difference in ion concentration between the inside and the outside of the cell membrane results in a flow of water molecules across the cellular membrane into the cell, causing it to swell and burst. Density gradient separation can be used to separate the dead cells (RBCs) from the live (WBCs).

1.3.3.2 Density Gradients

Different cell types differ in their densities. If blood is treated to prevent clotting and permitted to stand in a container, the RBCs (being the densest) will settle to the bottom of the tube; the plasma will stay on top; and the white blood cells and platelets will remain suspended between the plasma and the RBCs. A centrifuge may be used to increase the sedimentation rate and hasten this separation process.

Based on this principle, cells can be separated on single-step or continuous-density gradients. The most commonly used are Ficoll (high molecular weight sugar) and Percoll (colloidal silicate); these allow the preparation of gradients of correct density and osmolality, with low viscosity. Two important uses of Ficoll are the isolation of peripheral blood mononuclear cells (PBMCs) from RBCs, and the separation of live cells (low density) from dead cells (high density). Figure 1-6(a) shows an outline of the density centrifugation procedure using a single step gradient, with the relative positions of the various cell types following centrifugation shown on the right. Figure 1-6(b) shows a photograph of a continuous Percoll density gradient formed by ultra-centrifugation, the different coloured beads have different densities and are placed in the tube to illustrate the density profile. Such gradients can be used to separate different cell types, and when compared with the position of the marker beads the density of a cell type can be estimated.

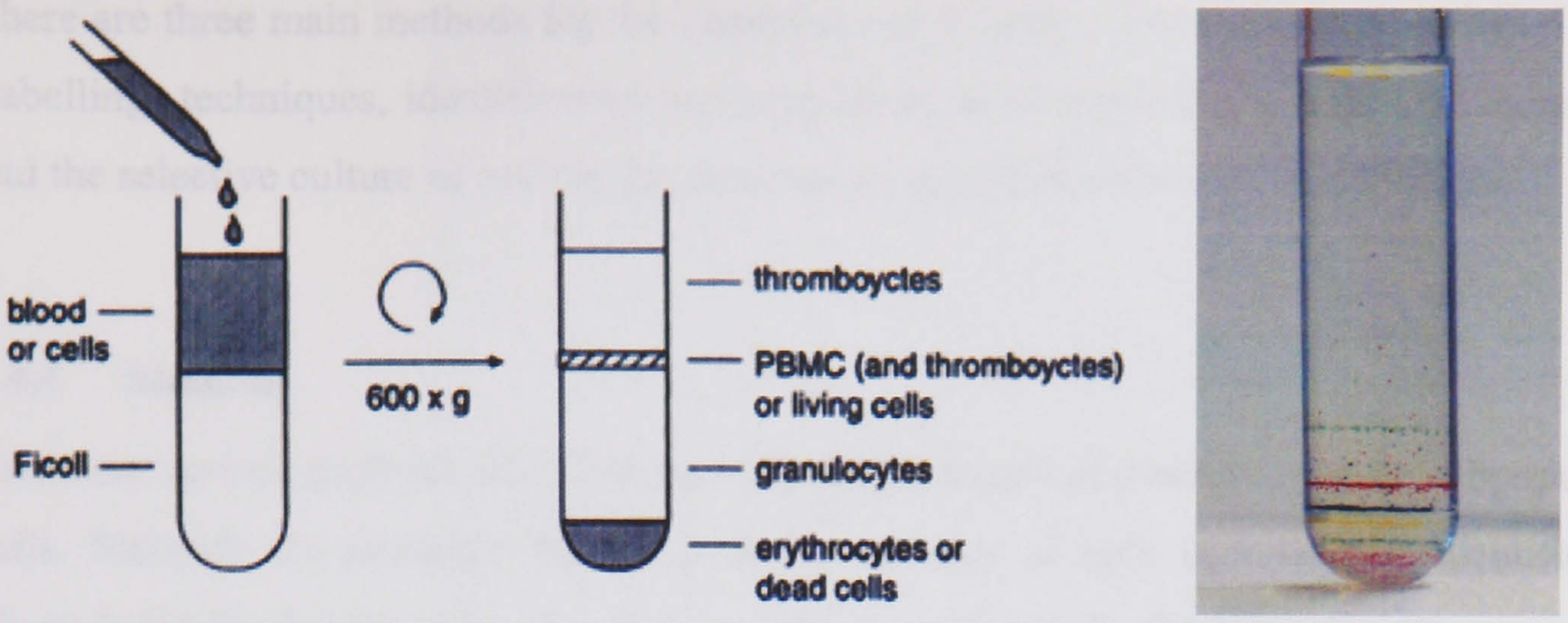

Figure 1-6. (a) Relative position of the various blood cell types after density gradient centrifugation using a single step Ficoll density gradient [55]. (b) Continuous Percoll gradient beads of differing colour have different densities.

1.3.3.3 Panning

Panning utilises antibodies coated onto polystyrene plastic dishes. The cell mixture is poured over the antibody-coated dish and the cells allowed to sediment. Cells expressing surface antigens corresponding to the coating, bind via these surface markers to the antibodies on the dish. Unbound cells are washed off and collected, the bound cells can be scraped off the dish with ice-cold buffer or cultured in the dish [55].

1.3.3.4 Complement lysis

Complement treatment can be used to destroy, or purge, an unwanted cell subpopulation. First the sample is incubated with an antibody specific for the cell type requiring depletion, and then incubated with complement in the form of serum. Upon binding the antibody, complement factors are converted in a cascade, which eventually results in a molecular complex that punches holes in the cell membrane, resulting in the death of the cell.

1.4 Cell identification

A variety of methods are available that allow the accurate identification (and analysis) of the various cell types within a population, or once they have been isolated from a heterogeneous mixture. A brief description of these methods is given here. Those techniques used in the course of this work are described in more detail in chapter three along with details of the methodologies.

There are three main methods for the identification of cells. They include: a variety of staining (labelling) techniques, identification and amplification of specific DNA or mRNA sequences, and the selective culture of cells in the presence of growth accelerators or inhibitors.

1.4.1 Staining

There are various methods that alter the optical appearance of a cell or specific subpopulation of cells. Methods are available for assaying the viability of cells in a sample, identification of physiologically distinct cells, identification of immunologically distinct cells, etc.

1.4.1.1 Dye exclusion

Dye exclusion is one of the simplest, but still widely used methods for identifying the proportion of live to dead cells in a sample. For example, the dye Trypan Blue is mixed with the cell sample, with the dead cells taking up the dye and appearing blue under examination using a light microscope. The dye enters the dead or dying cells by passing through their more permeable cytoplasmic membrane. The proportion of blue to non-blue cells in the sample can thus be counted. A similar method uses membrane permeable fluorescent dyes (e.g. CellTracker^{TM} from Molecular Probes) which when inside a cell are converted to a membrane impermeable form of the dye. In this case the living cells are the ones that retain the dye and fluoresce, the dye will leak out of the dead or dying cells.

1.4.1.2 Fluorescence in situ hybridisation (FISH)

FISH involves the hybridisation of a probe that is complementary to a nucleic acid sequence (DNA or RNA). The probe is labelled with a reporter molecule (usually fluorescent) that allows the visualization of the sequence if present. Using chromosome-specific probes allows the number of copies of chromosomes to be seen within the nucleus of the cell. FISH methods for looking at single gene sequences are also available. Figure 1-7 shows an example of a FISH labelled cell.

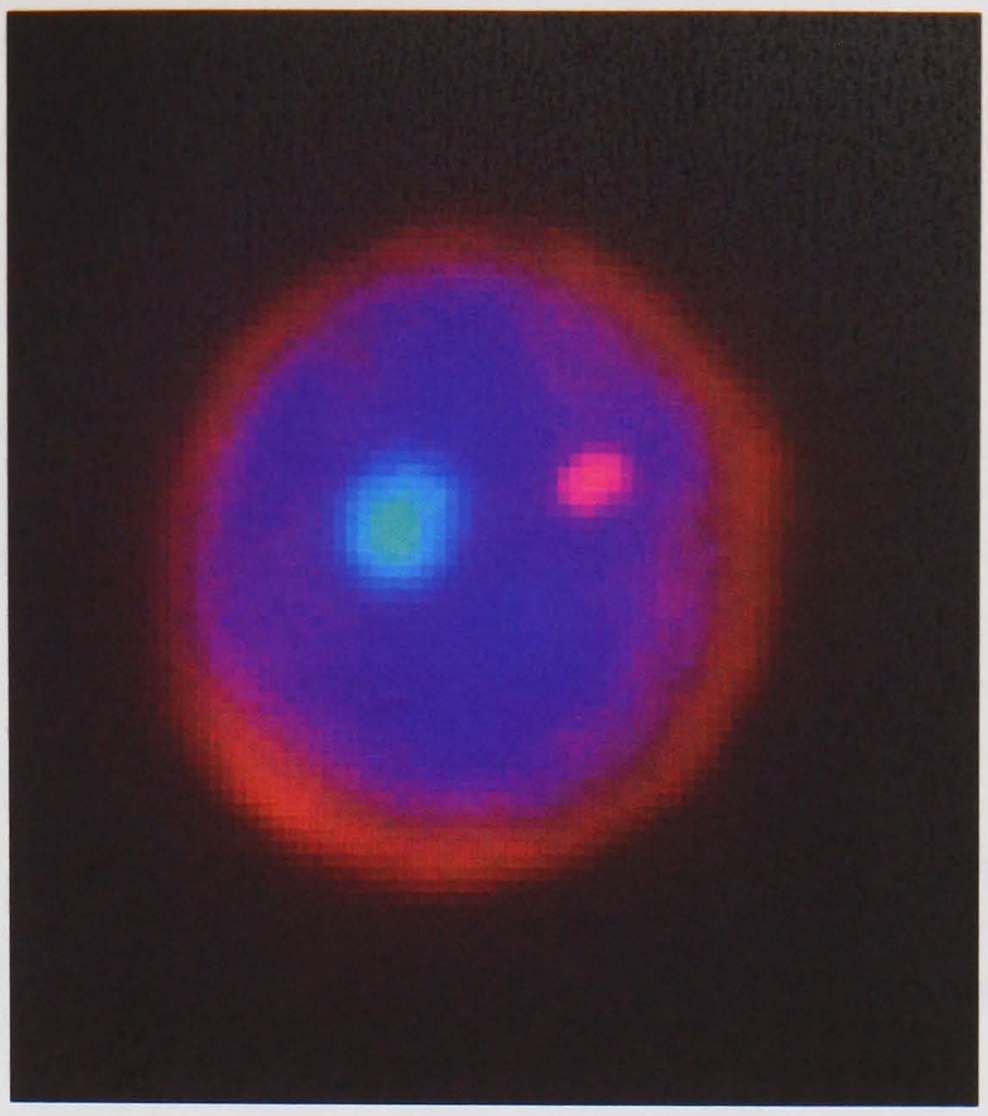

Figure 1-7. Example of a typical FISH image from a male fnRBC isolated from chord blood. The nucleus appears blue, X-chromosome (green), Y-chromosome (red), and foetal haemoglobin stained orange.

1.4.2 Polymerase chain reaction (PCR)

The polymerase chain reaction (PCR) allows the amplification of a specific DNA sequence, thus increasing the number of copies of that sequence to a level at which it can be detected. The basic outline of the procedure for the detection of specific gene sequences using the PCR technique is shown below in Figure 1-8.

The PCR process uses two oligonucleotide primers (short sequences of DNA, which are complimentary to a specific sequence) one at each end of the target DNA segment. The primers are added to the DNA, heating causes them to denature, they are then cooled and allowed to reanneal. The reannealing primers hybridise to opposite strands of the DNA sequence. An enzyme, DNA polymerase, and the four base nucleotides (A-C-G-T) are mixed together and thermally cycled. The DNA denatures with the heat and when cooled the primers reanneal to opposite strands of the DNA at opposite ends of the target sequence. The DNA polymerase adds nucleotides to the 5' end of the primers building up a complementary sequence. The process proceeds for a number of cycles (n=20-30) until sufficient copies of the target DNA are produced. In theory each round of amplification doubles the amount of DNA so that the amount of DNA produce grows exponentially (2^n). In practice PCR is usually about 85% efficient after 20 cycles.

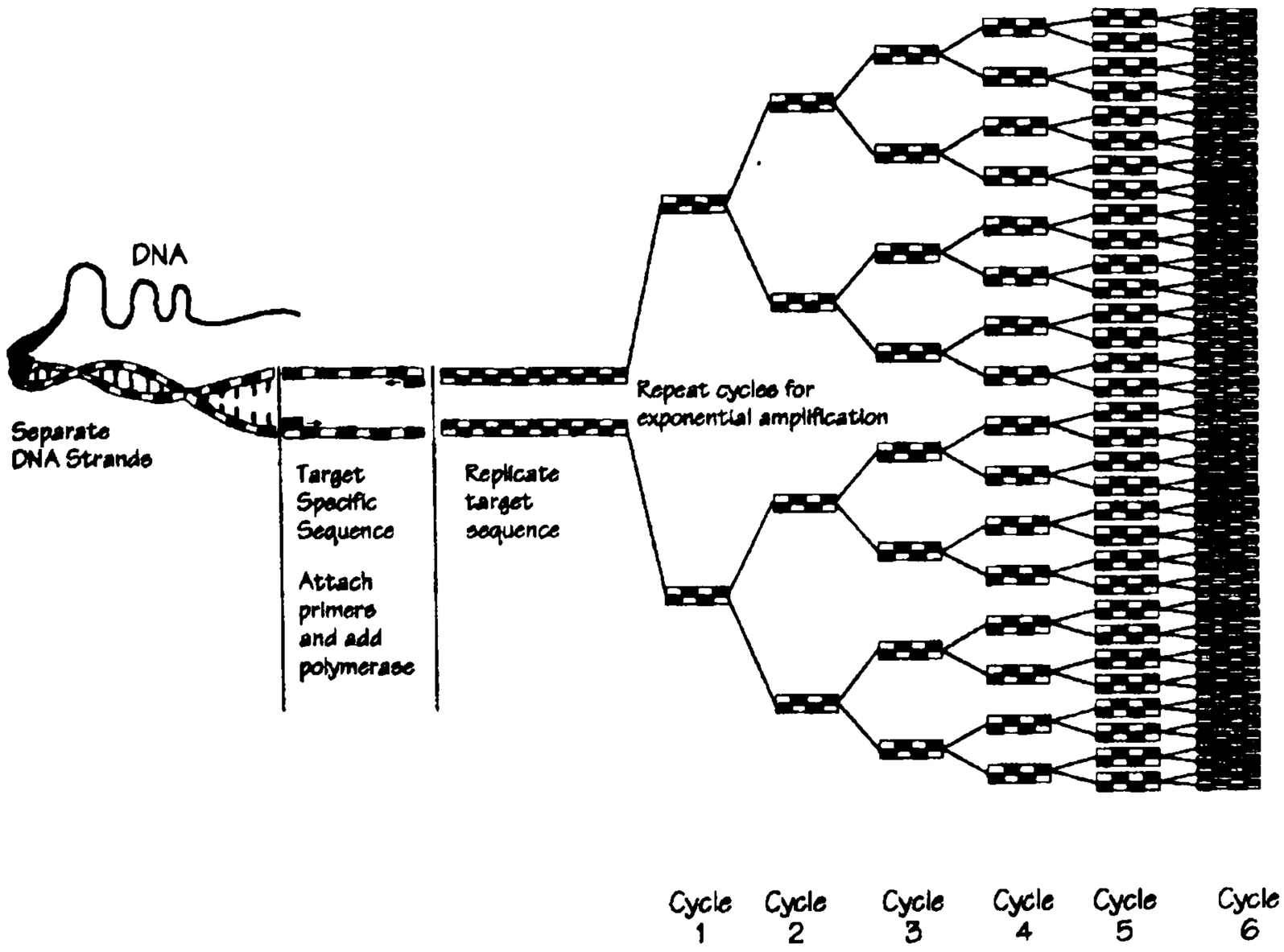

Figure 1-8. Amplification of DNA sequences using the polymerase chain reaction [58].

To detect the DNA sequence, the PCR products are digested with restriction enzymes and the fragments 'run' on an electrophoresis gel. The fragments are labelled with ethidium bromide to allow visualization under ultraviolet light.

1.4.2.1 Use of PCR in prenatal diagnostics

Populations of foetal cells isolated from maternal blood will contain contaminating maternal blood cells, and therefore maternal DNA will always be present. This limits the usefulness of PCR for genetic diagnostics other than looking for DNA sequences specific to the Y-chromosome. Consider for example the case of a Down's syndrome foetus; the difference between the normal maternal cell and the foetal cell is 2:3 copies of chromosome 21. It is therefore impossible to diagnose Down's syndrome using PCR, as the slightly increased amount of chromosome 21 will not be seen.

If a pure sample of cells can be obtained, they may be subjected to quantitative PCR (qPCR) a technique that allows the amount of DNA in the sample to be determined with resolution such that aneuploidy (multiple extra copies of chromosomes) could be detected.

1.4.2.2 Nested PCR

PCR on single cells is possible but with an increased likelihood of false positives, making positive and negative controls very important. Non-specific binding of the primers early on in the PCR process will obviously lead to greater errors in the final product (false positive).

Nested PCR limits the effect of non-specific binding by initially running the PCR reaction with a set of primers slightly outside the sequence (external primers) and then running a second PCR reaction using a set of internal primers within the original primers. The initial primers may amplify other similar sequences present in the genome swamping the specific target sequence; the second PCR reaction will then amplify only sequences present within the initial primer. Nested PCR allows for greater amplification and higher specificity.

1.4.2.3 Ligase chain reaction (LCR)

The ligase chain reaction (LCR) is method for detecting small quantities of a target DNA, and works in a manor similar to PCR. The technique uses four primers instead of two and uses the enzyme DNA ligase to join adjacent synthetic oligonucleotides together after they have bound the target DNA sequence. The small size of the primers means that they are destabilised by single base mismatches, and so form a sensitive test for the presence of mutations in the target sequence. LCR can have greater specificity than PCR and has use in molecular diagnostics.

1.4.2.4 Comparative Genomic Hybridisation (CGH)

Comparative genomic hybridisation (CGH) allows the analysis of the entire genetic complement of a single cell. CGH compares all the genetic information in a control genome (e.g. from one of the mother's cells) with that of the foetal cell under examination. The technique is quantitative and generates large amounts of data allowing the identification of single gene disorders and is therefore far more detailed than the relatively crude method of chromosome counting.

1.5 Cell separation and detection in microsystems

1.5.1 Dielectrophoretic cell separation systems

Dielectrophoresis (DEP) has been applied to the separation and manipulation of a wide array of bioparticles since it was first described by Pohl in 1951 [59-63]. The general theory describing the behaviour of particles in dielectrophoretic systems is described in chapter two. Explained briefly, when a cell is suspended in an electrolyte solution and subjected to an externally applied electric field, the charge distribution on and around the cell membrane is disturbed causing the

cell to polarise [59]. The interaction of this polarisation with the externally applied field results in a force acting on the cell. For the case of a uniform field the net force acting on the cell is zero. If however, the electric field is non-uniform then the particle experiences a force, which moves it towards or away from the regions of high electric field intensity (i.e. towards or away from the electrodes). The direction of the DEP force depends upon the relative polarisabilities of the cells and the suspending media. If the polarisability of the cell is greater than that of the suspending medium the cell will experience a positive DEP force, attracting it to the electrode. If the polarisability of the cell is less than that of the suspending medium the cell will experience a negative DEP force, repelling it from the electrode. DEP has been shown to be a sensitive method for discriminating between sub-populations of cells, allowing the separation of cells based on their intrinsic membrane capacitance and conductance (see below).

The DEP force varies in magnitude and direction with the applied electric field magnitude and frequency, the medium conductivity and permittivity, the cell volume and the intrinsic dielectric properties of the individual cells. These properties are governed by the morphology of the cell, in particular the membrane structure, protein content and charge. Similar cells will therefore experience similar DEP forces. A number of groups have investigated the possibility of using the differences in dielectric properties of various cell types as a means of cell separation, where the difference in the DEP force can be exploited to separate the cells into sub-populations (see below).

1.5.1.1 Characterisation of cells for DEP separation

DEP cell separation methods require that the intrinsic dielectric properties of the various cell types differ sufficiently, such that they experience DEP forces of differing magnitude or direction. It is thus important to measure the cell's properties before separation. A number of methods allow this, e.g. dielectric spectroscopy of suspensions of a single cell type [64, 65], electrorotation measurements of individual cells [66-69], dielectrophoretic crossover measurements [70, 71].

Chan *et al* [71] measured the dielectric properties of trophoblast cells and peripheral blood mononuclear cells using dielectrophoretic crossover and single cell electrorotation methods. Both dielectrophoretic crossover data and electrorotation data gave an average specific membrane capacitance for the peripheral blood mononuclear cells of $11.6 \pm 4.2 mF.m^{-2}$. Trophoblast cells prepared using three different methods had a higher average specific membrane capacitance in the range $13\text{-}18 mFm^{-2}$. The authors suggest that the differences in capacitance between the cell types could be exploited as the basis of an AC electrokinetic system for the separation of trophoblast cells from peripheral blood mononuclear cells.

Yang *et al* [72] used a more sophisticated cell separation protocol, based on magnetically activated cell sorting (MACS) and sheep erythrocyte rosetting methods, to produce almost pure samples of the four main leukocyte subpopulations, namely, B- and T-lymphocytes, monocytes, and granulocytes. They measured the dielectric characteristics by electrorotation over the frequency range 1 kHz to 120 MHz and found the mean specific membrane capacitance values to be 10.5, 12.6, 15.3, and 11.0 $mF.m^{-2}$ for T- and B-lymphocytes, monocytes, and granulocytes, respectively. Scanning electron microscopy (SEM) of the purified cell sub-populations confirmed earlier findings [73] suggesting that these values correlate with the richness of the surface morphologies of the different cell types. Scanning electron micrographs of the four main leukocyte sub-populations are shown in figure 1-9, showing the differences in membrane morphology. From a physical point of view, three possible explanations could account for differences in values of specific membrane capacitance for the different cell types; these are differences in membrane area, thickness, or composition. Yang *et. al.* [73] found that T-lymphocytes (figure 1-9(a)) tend to have fewer surface features than B-lymphocytes (figure 1-9(b)), in agreement with the measured value of membrane capacitance which is slightly lower for the T-lymphocytes. Monocytes (figure 1-9(c)) were found to have the greatest density of folds and ruffles of the four leukocyte populations, and had the largest membrane capacitance of the four cell types. The granulocytes (figure 1-9(d)) have a more complex surface structure than that of lymphocytes, however their specific membrane capacitances is smaller than that of the B-lymphocytes, the authors suggest that this could be due to the composition of the membrane. The group further suggests that dielectrophoretic cell sorters could have the ability to discriminate between, and to separate, leukocyte subpopulations under appropriate conditions.

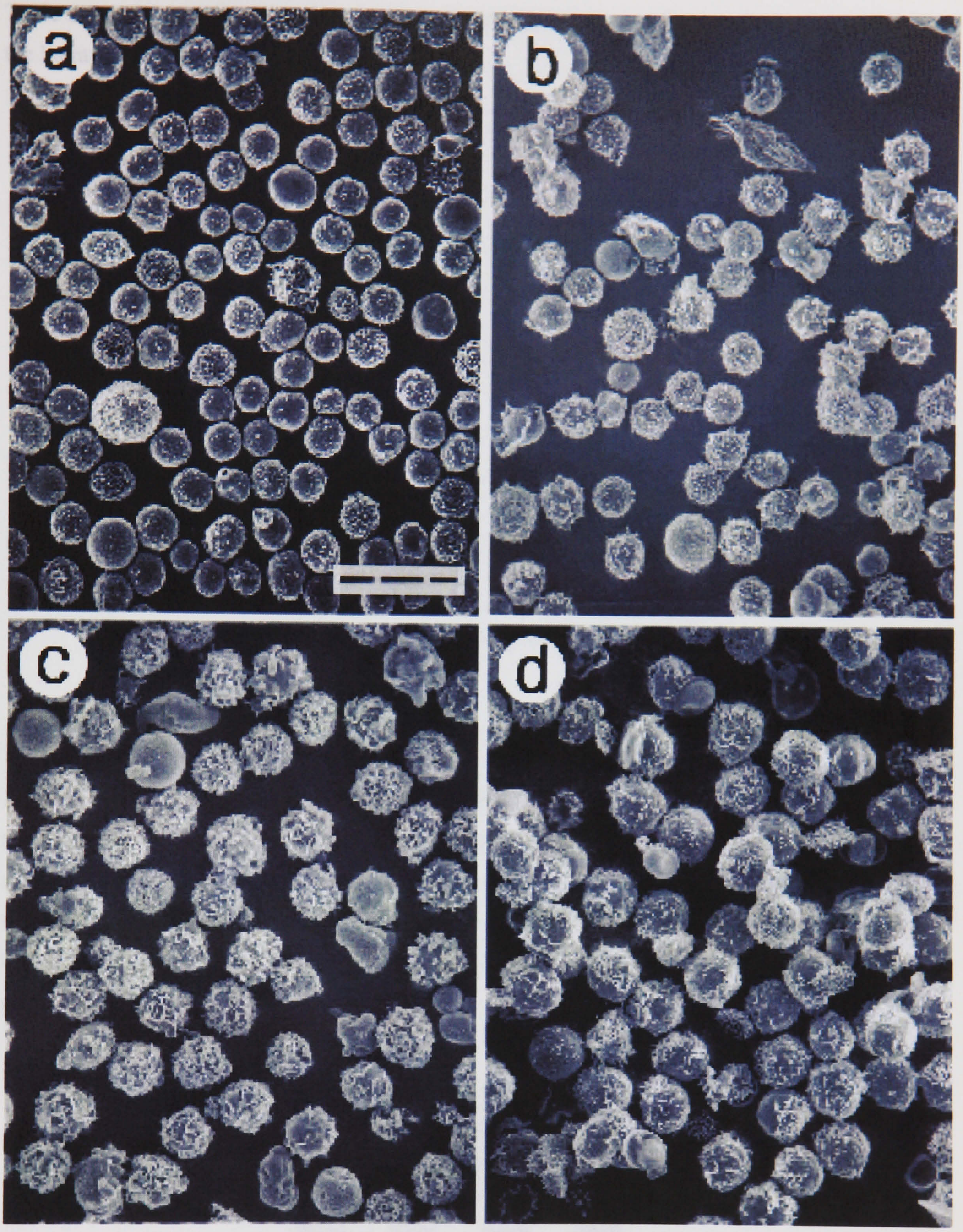

Figure 1-9. SEM image purified samples of the various leukocyte sub-populations (a) T-lymphocytes, (b) B-lymphocytes, (c) Monocytes, (d) Granulocytes showing the differences in their surface morphology, which leads to differences in DEP properties between the cell types. Scale bar 20μm. [72]

Table 1-2 gives the mean specific membrane capacitance for a variety of cell types taken from the literature.

Cell Type	Capacitance (mF/m^2)
Trophoblast [71]	17.8 ± 9.6
Cytotrophoblast [71]	26.6 ± 6.2
T-Lymphocyte [72]	10.5 ± 3.1
B-lymphocyte [72]	12.6 ± 3.5
Monocytes [72]	15.3 ± 4.3
Granulocytes [72]	11.0 ± 3.2
Erythrocyte [63]	9
NRBC [see ch.6]	22.8

Table 1-2. Membrane electrical properties of various cell types.

1.5.1.2 Batch DEP separation

A number of batch DEP separation systems have been developed for the separation of cells and microorganisms. These systems are generally quite simple in construction and operation, usually consist of two glass slides sandwiching a thin gasket material (typically 100-500μm) that defines a flow channel. Arrays of electrodes are patterned on the facing surface of one or both of the glass slides, the commonest electrode design being that of the, castellated electrode shown in figure 1-10.

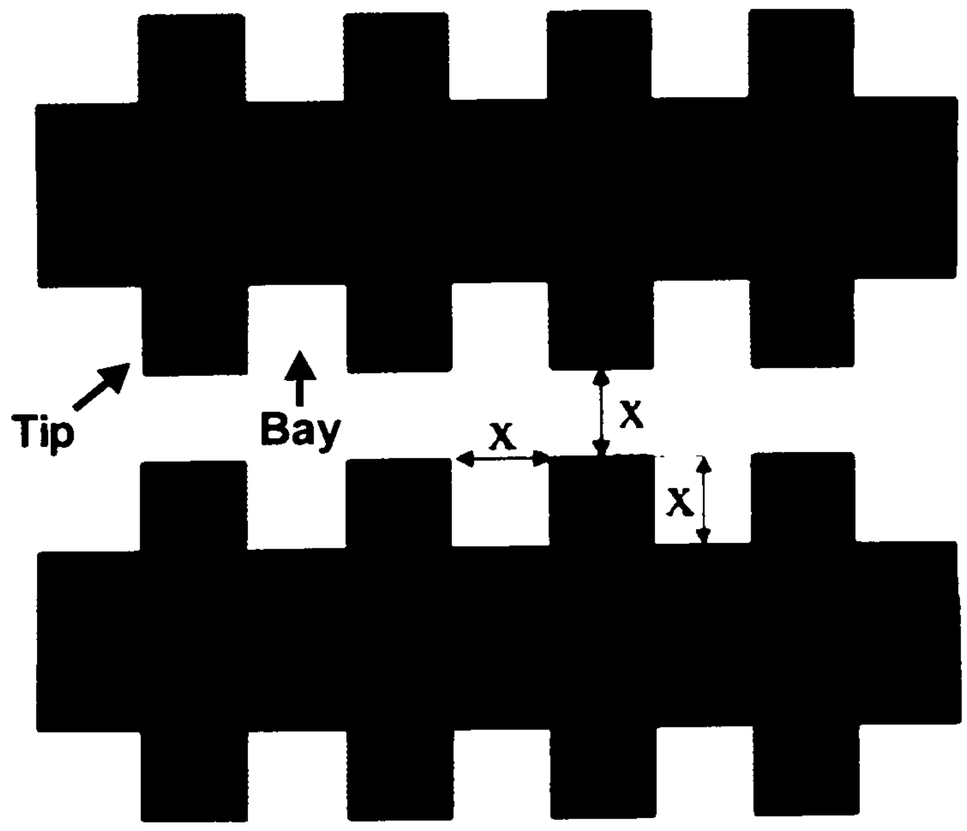

Figure 1-10. Castellated microelectrodes.

Typically, a sample of cell suspension (~100μl) is injected into the separation chamber with the electrodes energised at a frequency and magnitude such that all the cells undergo positive DEP and are held at the electrode edges. Sinusoidal or square wave voltages in the frequency range 100kHz to 10MHz are commonly used with peak-to-peak voltages of between 5V and 20V. Once all the cells are trapped at the electrode edges the flow of cell free medium through the chamber is initiated. A slight reduction in the applied frequency results in the release of one cell type, which can be collected as it elutes from the chamber. Further reductions in the frequency result in the selective release of further cell types, which can also be collected. Finally the release of all the remaining cells from the chamber is achieved by either a further reduction in the frequency of the applied field, or by setting the applied voltage to zero.

The batch separation of a variety of cell types has been demonstrated. These include the separation of viable and non-viable yeast cells [74]; the separation of leukaemia [75], and breast cancer cells [76] from blood; the separation of CD34+ cells from bone marrow and peripheral blood [77, 78]; as well as the separation of various bacteria species from each other and from blood cells [79, 80].

Variations on the batch separation theme have been demonstrated (e.g. the use of time varying conductivity gradients, instead of the variation of the applied frequency [81]). However, all the batch methods to date have been limited by the small sample volumes used, and the problem of steric hindrance. Steric hindrance results in the trapping of cells, that should normally be released (i.e. they are experiencing a –ve DEP force), by cells of a different type that are being held at the electrode edge under a +ve DEP force. Reduction in the sample concentration reduces steric hindrance effects but also reduces the number of cells processed per sample. As a result the purity of the cell fractions obtained after batch separation could be inversely proportional to the initial sample concentration for a given device [74].

1.5.1.3 Continuous dielectrophoretic cell separation

Continuous separation of cells has been demonstrated, where the cell mixture is injected into the centre of the separation chamber and the fluid flow direction and field are switched periodically [82]. The cyclical regime for cell separation is as follows,

- The cell sample is introduced into the centre of the chamber.
- A field frequency is applied such that cells of type A are repelled and move into the electrode bays (see figure 1-10), while cells of type B are attracted to the electrode edges by +veDEP.

- Fluid flow in one direction results in cell type A moving in that direction while cell type B remains held at the electrode edge under the influence of positive DEP (positive DEP exhibits a stronger holding force against the fluid flow than negative DEP).
- The DEP force is removed by switching off the voltage and the whole sample is pumped in the opposite direction.
- Reapplication of the field applied in step two, and fluid flow to the left carries cell type A to the left.

This regime results in sufficient spatial separation of cell types A and B along the electrode array to allow the injection of more cell sample during step one of the next cycle. Separation of the two cell types is thus achieved with collection of cell type A from the channel's left hand port and cell type B from the right hand port.

The continuous separation system described has been used to separate viable and non-viable yeast with 92-97% efficiency. The purity of sorted samples is thought to be a result of reduced steric hindrance as a result of the mixing effects that occur when all the cells are released from the electrodes, moved with the fluid flow and then recaptured when the voltage is reapplied. This process, although capable of processing large samples of cells is slow.

1.5.1.4 DEP-field flow fractionation (DEP-FFF)

Conceptualised in the 1960's, field-flow fractionation (FFF) is a family of separation techniques, all of which involve superimposing a physical field, at right angles to a main channel flow. The principle of FFF is shown schematically in figure 1-11. Directed along the channel length, the main channel flow sweeps sample components from the channel inlet to outlet. The particles in the flow interact with the cross field and are forced into different positions in the parabolic flow profile of the main channel flow. Separation occurs because particles at different heights, in the channel, move with the velocity at which the fluid is moving at that height. Particles closer to the centre of the channel therefore have a higher velocity than those levitated to a position closer to the chamber wall. For FFF to operate successfully it is critical that strict laminar flow be achieved across the thin dimension of a ribbon-like channel.

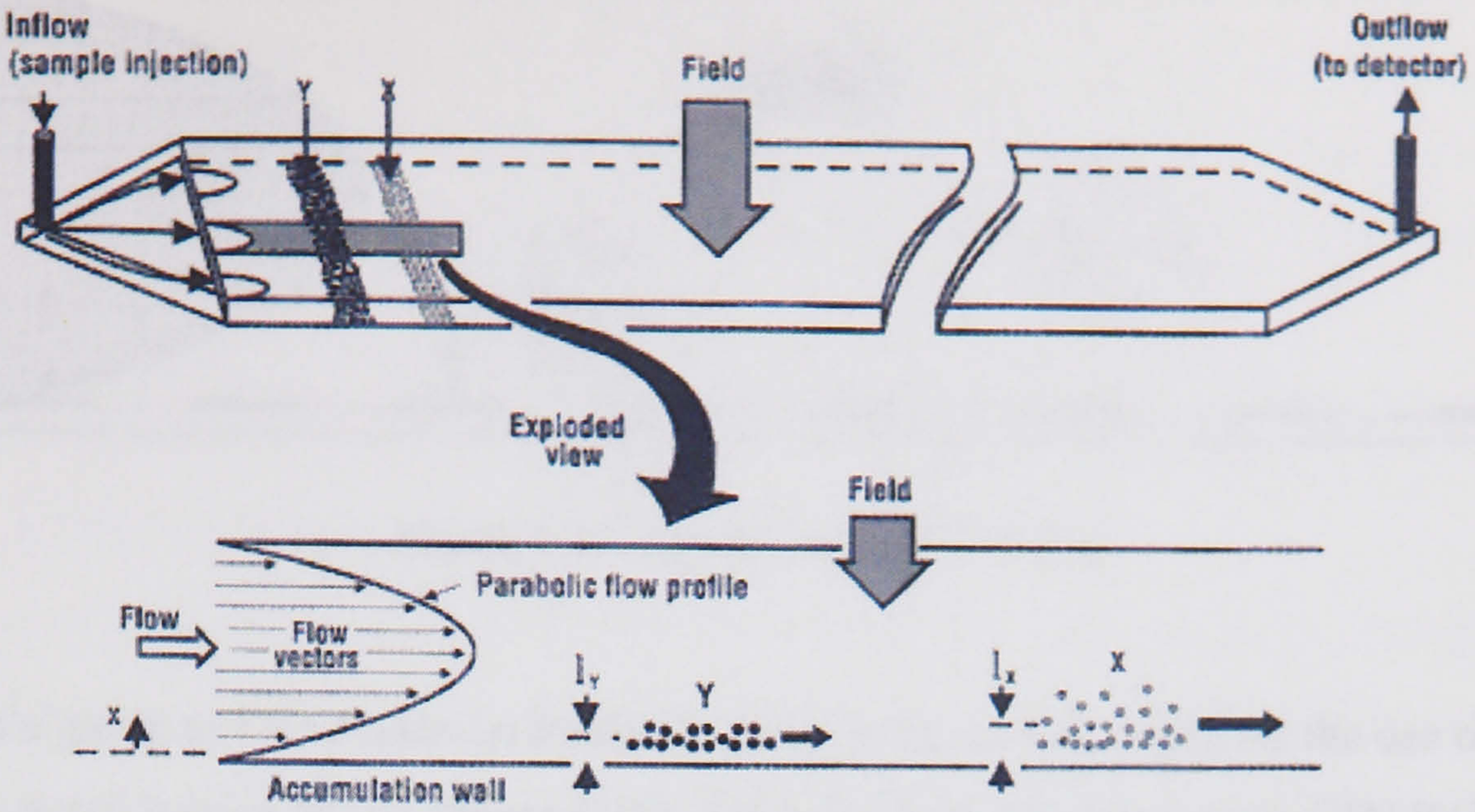

Figure 1-11. Schematic of the principles of field-flow-fractionation [83].

FFF is capable of separating not only cells and cell-sized particles, but also a broad range of particles from approximately 1 nm to 100 μm in diameter. The field itself can be any physical phenomenon and characterizes the specific FFF sub technique; for example electrical, magnetic, thermal gradient, sedimentation or gravitational, flow, and steric field-flow-fractionation methods exist. For more information the reader is referred to one of the many books on the FFF technique (e.g. [83]).

Recently, a further FFF sub-technique has been described in the literature, that of Dielectrophoretic-Field Flow Fractionation (DEP-FFF) or gravitational-DEP-FFF. The basis of the technique (shown in figure 1-12) is to use negative DEP forces to balance the gravitational (sedimentation) forces on particle such that particles of different dielectric properties as well as density are levitated to different heights in the parabolic flow profile. The basic device uses an array of interdigitated microelectrodes, lining the bottom surface of a thin chamber, to generate a dielectrophoretic force that levitates the cells above the electrode array. The DEP force acts counter to the gravitational force causing the different cell types to occupy different equilibrium positions above the electrode array. The height depends on the frequency of the applied field, the applied voltage, and the dielectric properties of the specific cell. Such channels exhibit a parabolic fluid velocity profile, with zero velocity at the top and bottom of the channel surfaces and maximum fluid velocity at the channel centre. The time a cell takes to elute from the channel is therefore related to the height of levitation. Various groups have demonstrated the feasibility of DEP-FFF [84-94].

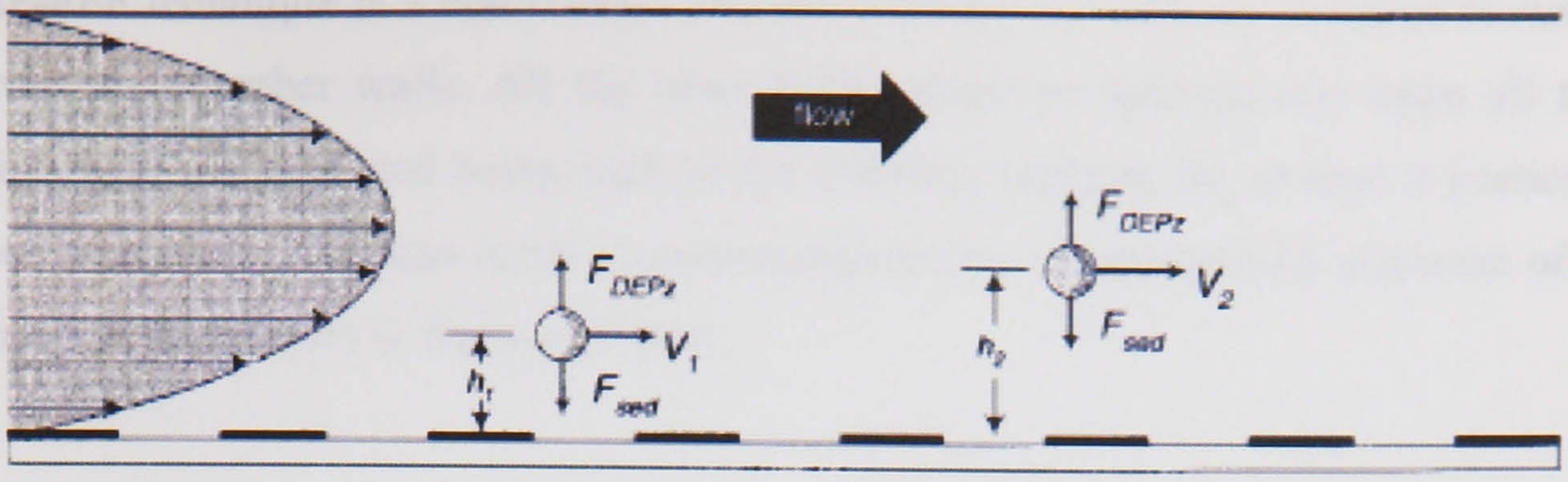

Figure 1-12. Principle of DEP-FFF [72].

Gascoyne's group at MD Anderson Medical Center in Texas have reported the use of the above system to purge human breast cancer MDA-435 cells from haematopoietic CD34(+) stem cells [95]. CD34(+) stem cells were levitated higher and were carried faster by the fluid flow, exiting the separation chamber before the cancer cells. Efficient separation of the cell mixture was observed in less than 12 min, and CD34(+) stem cell fractions with a purity >99.2% were obtained.

Subsequent papers from the same group have demonstrated separation of latex beads of differing size, and surface functionality, also the separation of the various white blood cell subpopulations (i.e. T- and B-lymphocytes, monocytes, and granulocytes) using the combined DEP-field flow fractionation (DEP-FFF) device.

They have also coupled the output port of their DEP-FFF device to the inlet of a flow cytometer, thus enabling online analysis of the fractionation process as shown in figure 1-13. A possible further step would be to use the separation capabilities of the flow sorter to further select cells of interest from the sample.

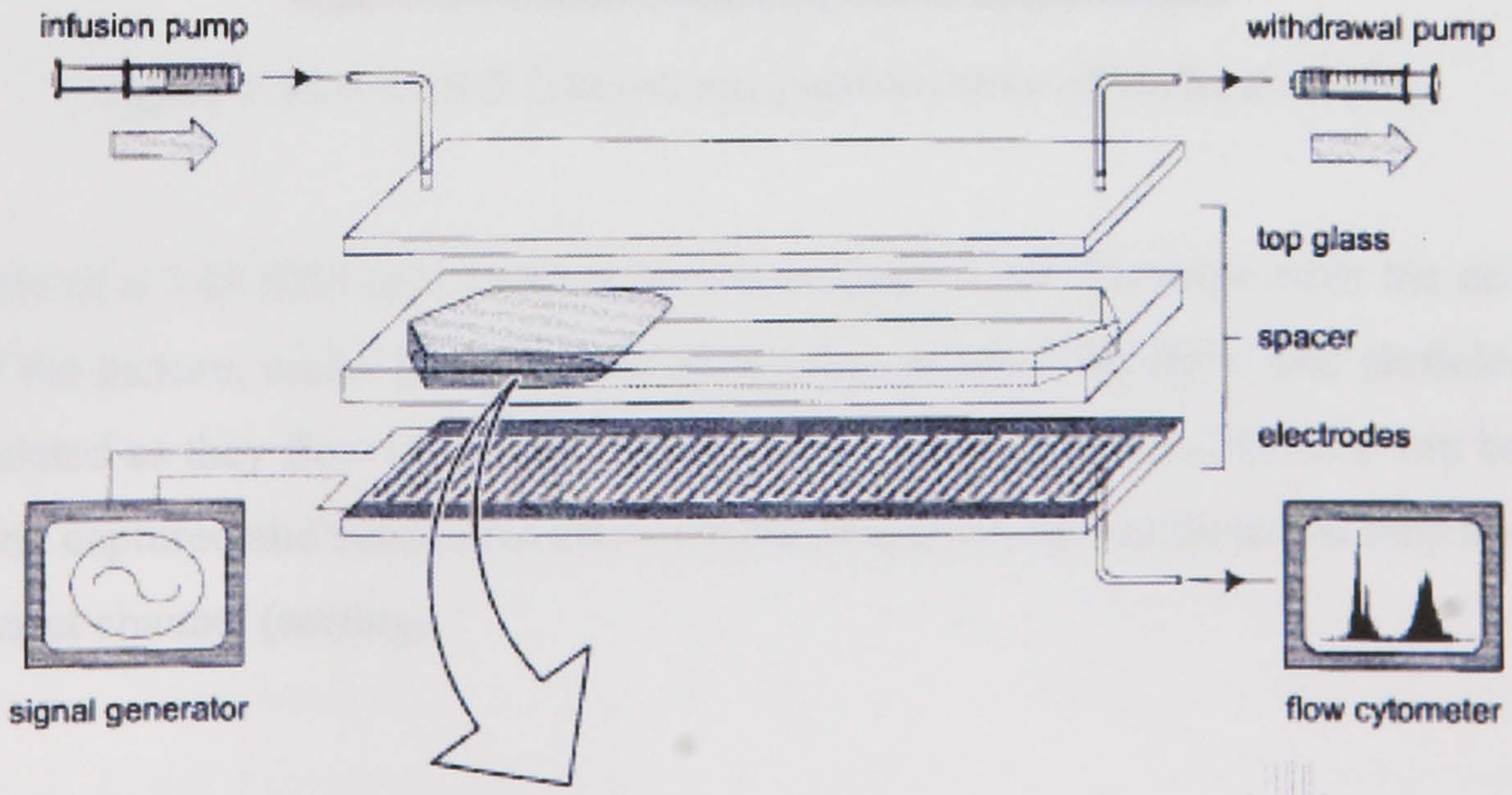

Figure 1-13. Schematic of the DEP-FFF device of Yang *et al* 1999 [72].

The DEP-FFF technique is a non-contact process whereby the cells are retained in suspension away from the chamber walls. All the other DEP separation systems rely upon all the cells interacting with the field and being held at the chamber surfaces for at least a portion of the separation procedure. This can result in contamination due to non-specific adhesion of cells to the chamber surfaces (this is discussed later).

1.5.1.5 3-D cell handling

The group of Fuhr at the Humboldt University in Berlin have designed a number of serial cell/particle manipulation systems [96-100] (these sort particles individually, one after the other). Their particle handling system consists of 3-D microelectrode elements patterned onto two layers (the upper and lower channel walls). They demonstrate the ability of these structures to form 3-D DEP field structures, such as funnels, aligners, cages and switches. The top and bottom electrode structures are separated by a 40μm thick polymer spacer, which forms a flow channel. The electrodes of the funnel, aligner or switch were operated with 5-11 V at 5-15 MHz, and it was found that efficient handling of particles could be achieved with flow rates up to 3500μm/s. Cells could be aligned effectively at flow rates up to 300μm/s in PBS. The group has gone on to commercialise this technology with a company called EVOTEC.

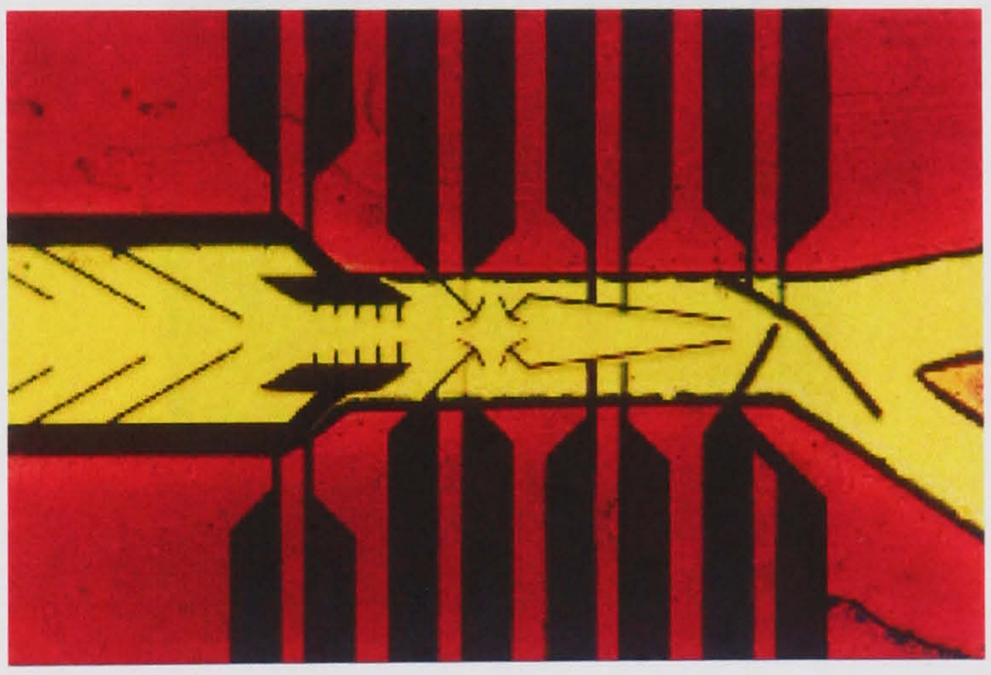

Figure 1-14. 3-D DEP field cell manipulation device of Muller *et al.* [99]

An example of a 3-D DEP cell sorter is shown in figure 1-14. Particles enter the device, from the left of the picture, under the influence of pressure driven fluid flow. The particles can then be manipulated as they flow through a number of electrode elements. Particles can be focussed into a beam, captured and rotated (to allow characterisation), and deflected so they flow into the chosen output channel (sorting).

1.5.2 Micro-flowcytometry

A number of micro-flowcytometric devices have been described in the literature over the last three or four years.

1.5.2.1 μFACS

Ramsey's group at Oakridge have demonstrated a microfabricated flow cytometer based on a cross-shaped channel, etched in glass [101]. Particles are transported electrophoretically by applying potentials to fluid reservoirs at the channel ends. The device uses electrokinetic focusing at the cross intersection to produce a beam of single particles, and detection occurs 50μm downstream from this intersection. Latex particles with diameters of 1 and 2μm were detected and counted using laser light scattering and fluorescence coincidence, with a maximum sample throughput of 34 particles/s. In a separate report, fluorescently labelled *E.coli* were counted at rates from 30 to 85 cells/s [102].

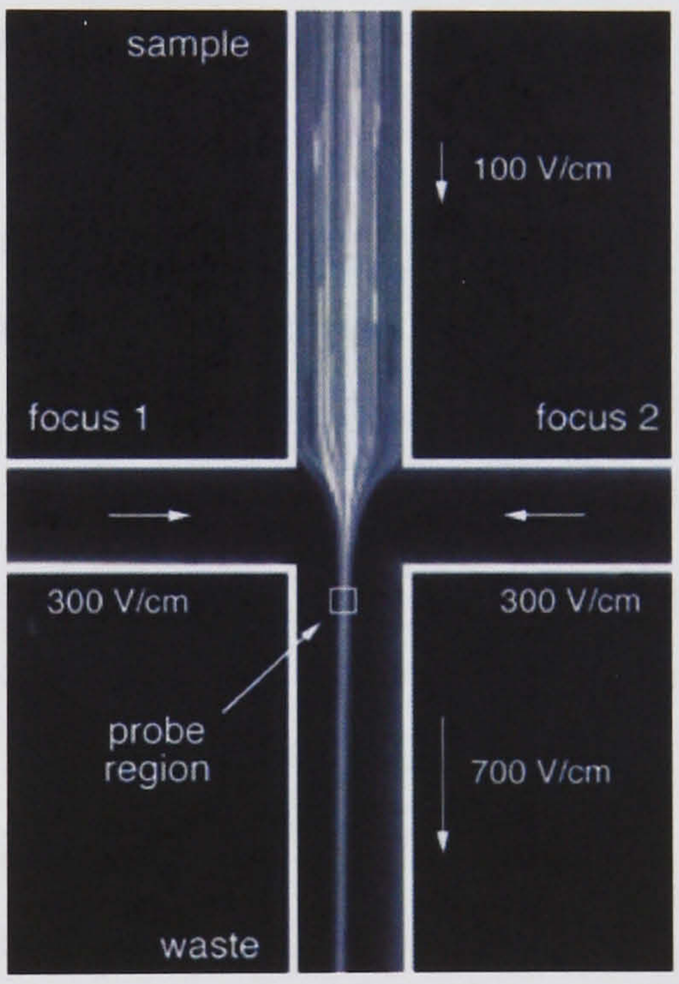

Figure 1-15. Time integrated CCD image of electrokinetically focussed beads [101].

Quake's group at California Institute of Technology describe a 'disposable' microfabricated fluorescence-activated cell sorter [103] fabricated in PDMS (polydimethylsiloxane) using 'soft lithography' [104], the device is shown in figure 1-16. Transport of particles along the T-shaped channel (3μm wide by 4μm deep) is accomplished by electro-osmotic flow, and sorting is achieved at the T-junction by switching the applied voltage, sending particles down one of the two channels. They demonstrate sorting of micron-sized beads of various colours, and the separation of *E.coli* expressing green fluorescent protein (GFP) from a background of non-fluorescent *E.coli*. Sort rates of 20 cells/s have been achieved. The same device has been used to size and sort DNA molecules [105].

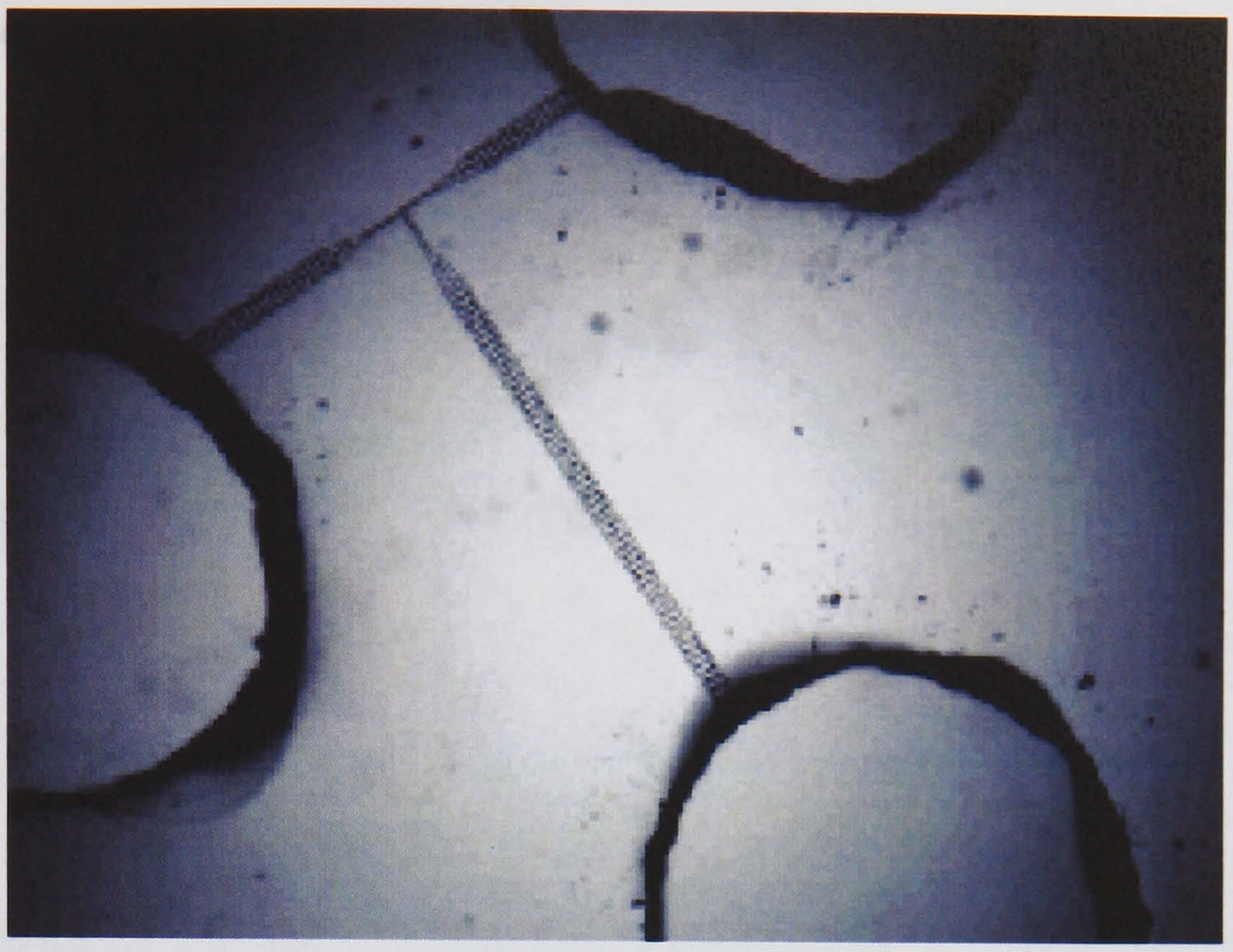

Figure 1-16. μFACS of Quake [103] fabricated in PDMS. The channels narrow from 100μm at the wells to 3μm at the sorting junction, with a channel depth of 4μm [103].

Harrison's group [106] at the University of Alberta have used electroosmotic and/or electrophoretic pumping to drive cell transport within a network of capillary channels fabricated on a glass chip. *Saccharomyces cerevisiae*, canine erythrocytes, and *E.coli* were selected and transported from one location to another within the capillary network, with velocities up to about 0.5 mm/s in capillaries with a 15 x 55μm cross section. Canine erythrocytes were intentionally lysed within the chip, to demonstrate that cell selection and a subsequent reaction could be achieved.

Compared with conventional FACS machines, μFACS devices have the potential to provide higher sensitivity, no cross-contamination, and lower cost. As well as the potential for low power hand held machines that could be used in the field. These devices are also potentially more cell-friendly as the forces required to manipulate particles in a microstructure is orders of magnitude smaller than those used in macroscopic systems.

1.5.2.2 μCoulter counter

Koch *et al* [107] have designed and fabricated a micromachined Coulter counter, shown in figure 1-17. They etched a channel in silicon; sputter coated the channel walls with 100nm of titanium, which was then patterned to form metal electrodes on the channel walls. To seal the channel a Pyrex wafer was anodically bonded on top of the silicon substrate. Passage of 3μm diameter particles through the 5μm wide channel with an electrode spacing of 40μm showed a

relative resistance change of 1.8%. They did not report counting rates or the device's ability to distinguish between particles of different type.

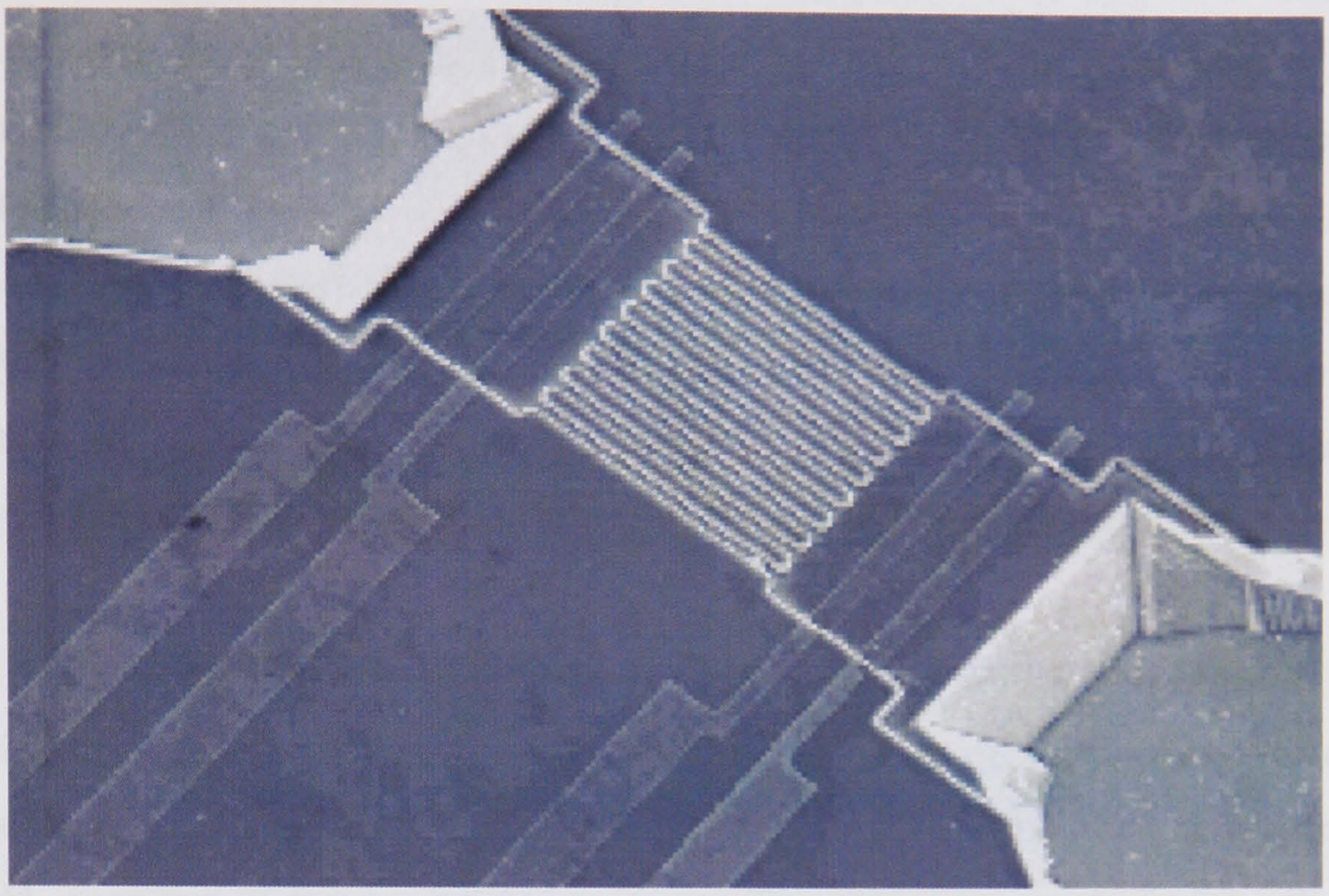

Figure 1-17. Koch's micromachined coulter counter [107].

Saleh *et al* [108] fabricated a microchip Coulter counter on a quartz substrate with a PDMS lid, and used it to detect individual colloidal particles, shown in figure 1-18. The device showed sensitivity proportional to particle size, down to particles as small as 87 nm in diameter, and the ability to distinguish between colloids whose diameters differ by less than 10%. They suggest that further reductions in the pore size would allow the device to measure biological macromolecules, such as DNA and proteins.

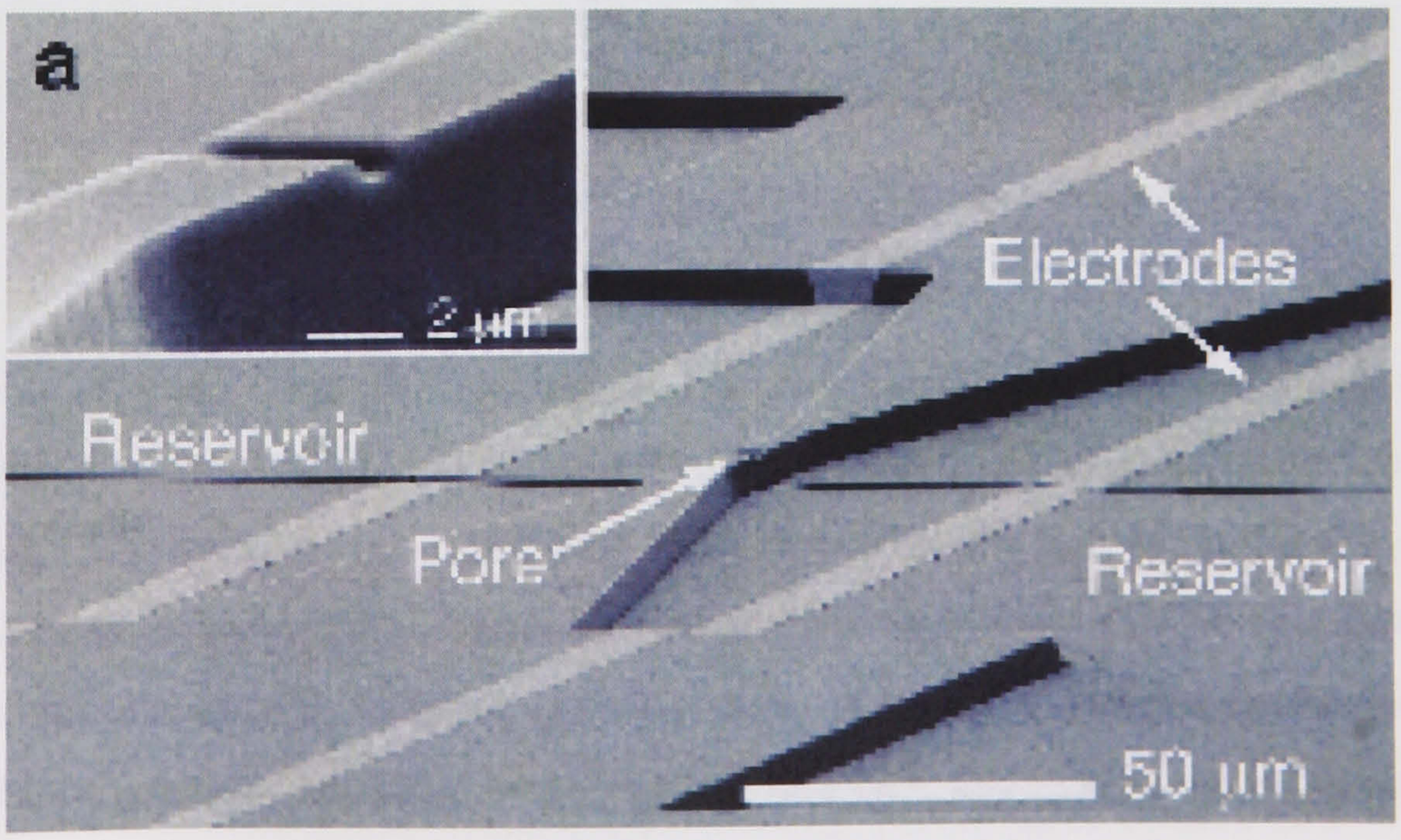

Figure 1-18. μCoulter counter of Saleh *et al*. The electrodes can be seen in the channels either side of the pore, which is shown in the inset [108].

1.5.2.3 μImpedance spectroscopy

Ayliffe *et al* [109] described the first microfabricated device capable of performing microelectronic impedance measurements on femtolitre (10^{-15}) volumes, thus suggesting the possibility of rapid single cell impedance measurement in a flow through system. The device was fabricated on glass and consisted of a 10μm wide by 4μm high epoxy channel (defined using SU-8 photoresist) with integrated gold measurement electrodes. Suspensions of cells were flowed along the channel and passed between the electrode pair, allowing the measurement of the dielectric properties of individual cells as they passed through the sensing zone. Measurements of human leukocytes and teleost fish red blood cells were shown to give statistically different results over a measurement range of 10kHz to 1MHz.

Sohn *et al* at Princeton [110] have developed a PDMS flow through "capacitance cytometry" chip (see figure 1-19) that purports to measure the DNA content of eukaryotic cells. They measure a change in capacitance that is evoked by the passage of individual cells across a 1-kHz electric field. Analysis of the cell-cycle kinetics (cells at different points in the cell cycle have different amounts of DNA) of populations of cells was compared with standard flow cytometry data and the authors reported favourable results.

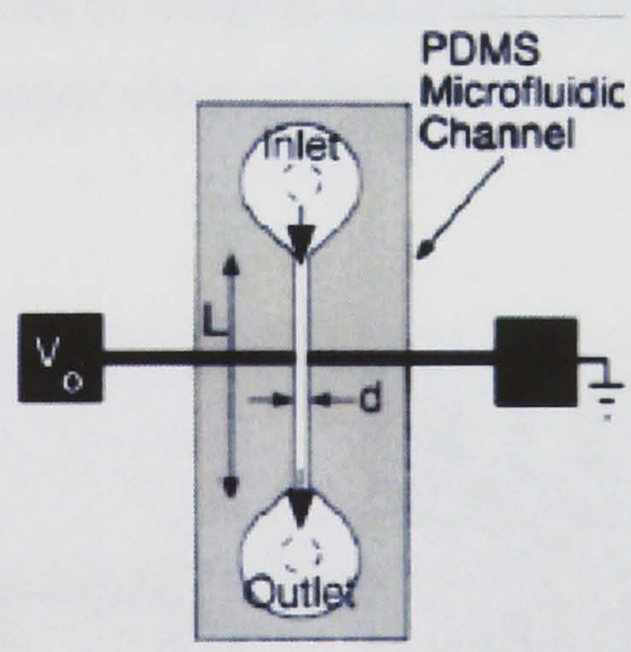

Figure 1-19. Schematic of the Princeton capacitance cytometer [110].

Fuller *et al* [111] have developed (see figure 1-20) a microfabricated flow-through impedance characterization system capable of performing, multi-frequency measurements on cells and other particles. The sensor measures both the resistive and reactive impedance of passing particles, at rates of up to 100 particles/s. With particle impedance measured at three or more frequencies simultaneously, enabling the derivation of multiple particle parameters. Human peripheral blood granulocyte radius, membrane capacitance, and cytoplasmic conductivity were measured and were found to be in agreement with published values.

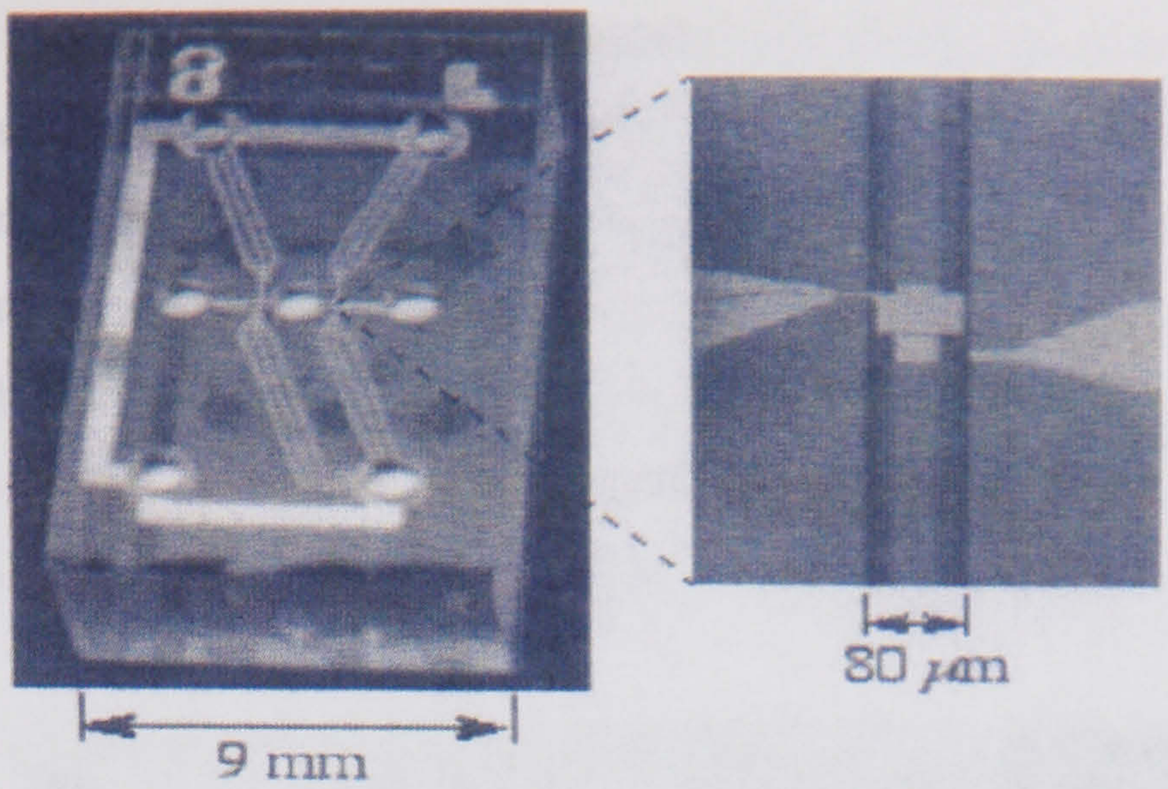

Figure 1-20. Micro flow-through impedance chip of Fuller *et al* [111].

Gawad *et al* [54] at EPFL (l'Ecole polytechnique fédérale de Lausanne), Lausanne describe a device, which measures the spectral impedance of individual cells or particles at a rate of 100 cells/s (figure 1-21). The device consists of a polyimide channel fabricated on glass, with microfabricated electrodes on the channel bottom and a PDMS lid. As the particles flow through the measurement area each particle's impedance is recorded by a pair of micro-electrodes. The cell free media surrounding the cell is used as a reference. They describe the impedance measurements of cells and particles of different sizes and types displaying the data in a similar fashion to that of the graphical output obtained from a FACS analyser. A prototype DEP sorting element was also demonstrated.

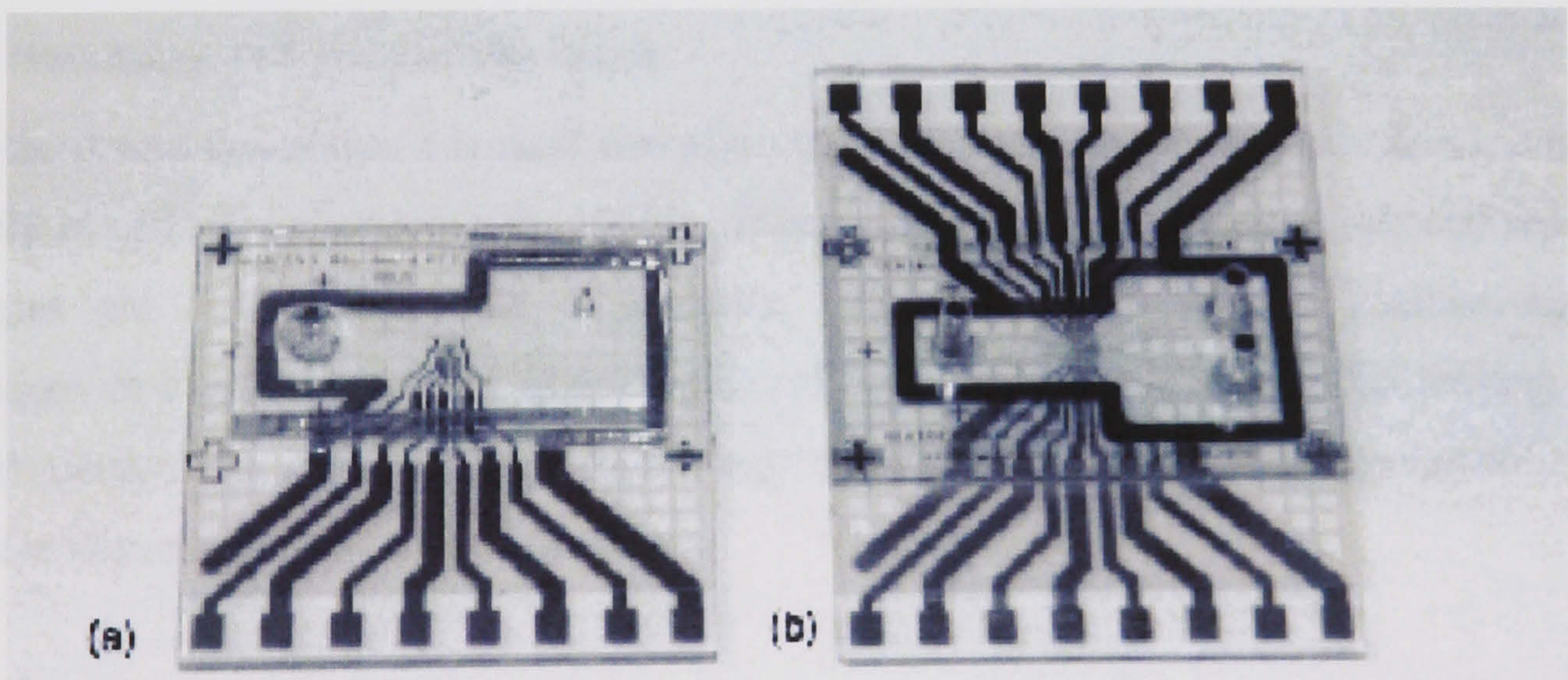

Figure 1-21. Flow-through cell impedance analyser of Gawad *et al* [54].

1.5.3 Micro-structures

Mechanical sorting of cells in microstructure has also been shown to have potential for the separation of cells. Simple filters based on size exclusion have been demonstrated (see [6] for examples). Carlson *et al* [112] constructed a lattice consisting of a set of 5μm wide channels of

varying length, as shown in figure 1-22(a). Forming parallel arrays of these channels, and forcing a drop of human blood containing red and white blood cells through the lattice caused the white cells to self-fractionate into their subpopulations. The pattern of white cells that forms is due to a combination of stretch-activated adhesion of cells with the walls, stochastic sticking probabilities, and hetero-avoidance between granulocytes and lymphocytes. Figure 1-22(b) shows the separation of the leukocyte sub-populations, with monocytes and granulocytes labelled with a green fluorescent probe and T-lymphocytes labelled with a red probe.

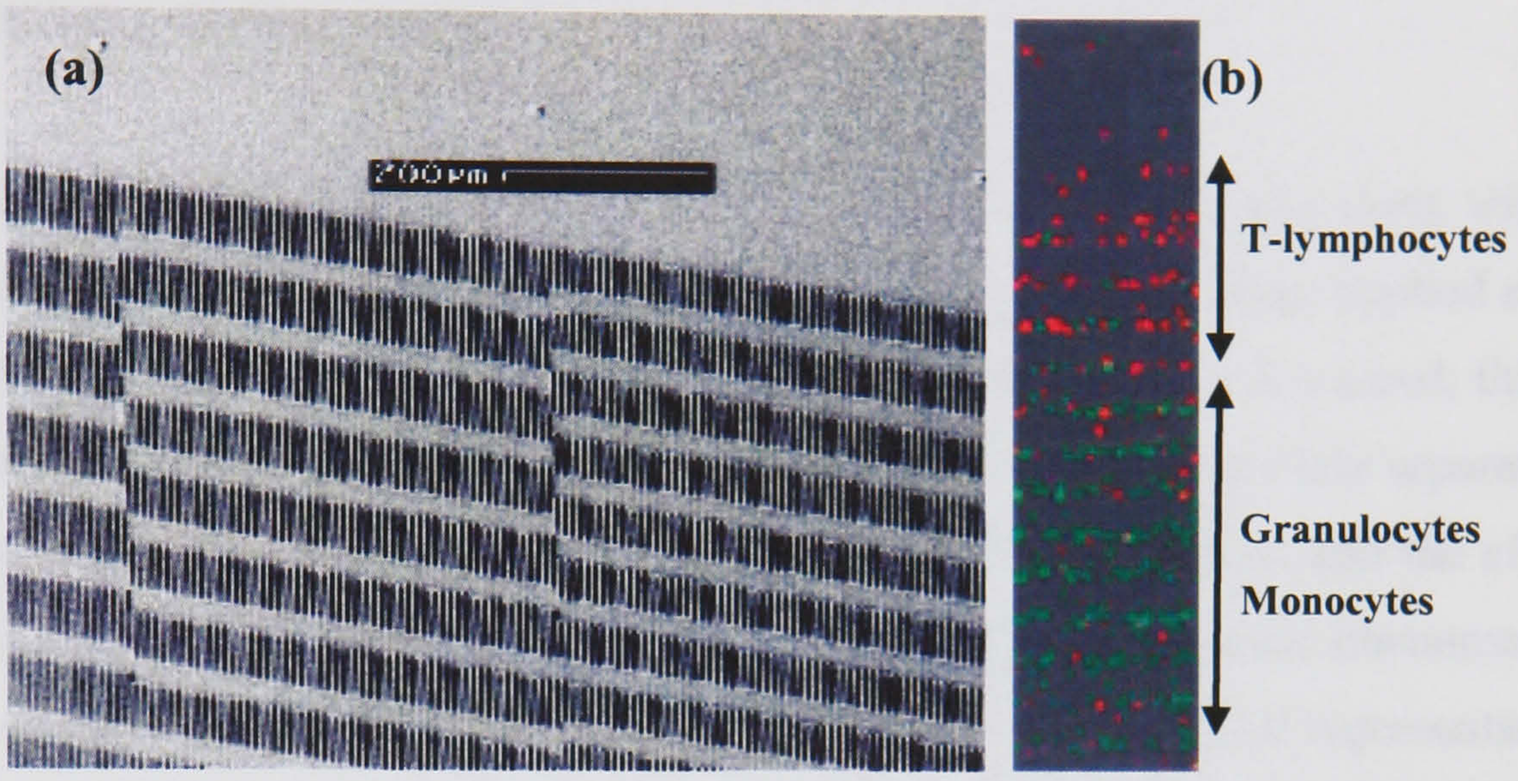

Figure 1-22. (a) Silicon microchannel array of Carlson *et al*. **(b)** Separation of fluorescently labelled white blood cells captured along the length of the lattice. Flow is from top to bottom with granulocytes and monocytes labelled with green fluorescence and T-lymphocytes labelled with red fluorescence [112].

1.6 Summary and aims of this thesis

From the discussion above it is clear that although there have been continuous developments in the field of cell separation since the 1960's, neither macroscopic nor microscopic cell separation strategies are currently capable of isolating rare cells, other than in immuno-magnetic techniques or highly configured flow cytometers in experimental settings, thus making all the current methods for isolating rare particles extremely expensive and usually technically labour intensive requiring highly trained operators.

Although interesting as a cell separation technique, most DEP systems are restricted to the processing of small sample volumes and useful for little more than demonstrating the ability of DEP devices to distinguish between a variety of cell types. Rare cell isolation inherently requires the ability to process large numbers of cells and thus requires a system capable of handling such samples. To overcome this problem a novel electrode design has been developed and tested for this thesis. It is shown that the system can be used to isolate low numbers of particles from dilute suspensions and is capable of continuous handling of large sample volumes in excess of 10ml. A novel method of particle isolation is proposed "Dielectrophoretic

Chromatography". This allows on-chip separation of particles based on the particle dielectric properties, its size and density.

1.6.1 Chapter summary

In chapter one a general introduction to the field of cell and particle separation techniques was presented with focus on the problem of rare cell isolation. Dielectrophoretic particle separation systems were discussed in some detail and the state of the art in area of microfabricated particle separation and detection systems presented.

Chapter two introduces the theory behind the polarisation of dielectric materials, along with a description of the AC electrokinetic phenomena arising from the interaction of an applied non-uniform field and this polarisation. The nature of the dielectrophoretic force is discussed; this is followed by a discussion of the other forces present within micro-fabricated particle separation system as pertinent to this work. These include buoyancy forces, viscous forces, and the effect of thermal forces (i.e. Brownian motion and diffusion). The electrohydrodynamic phenomenon of AC electro-osmotic and electro-thermal fluid flow are discussed. An analytical representation of the DEP force generated by an array of interdigitated bar electrodes is presented. Finally, the theoretical background is given for the dielectric modelling of real particles.

Chapter three gives details of the biological protocols used throughout the thesis. Cell preparation and identification methods are presented here along with the detailed description of the sample preparation for the experimental work. Chapter four gives details of the device fabrication methods used and the devices and equipment developed during the course of this work. Details of any other equipment used are also given.

Chapters five through eight contain the main results from this thesis. Chapter five describes the numerical simulations used to model the motion of the particles as they flow through the dielectrophoretic separation system. The results of the simulations are presented with regard to particle separation in the device and discussed. Chapter six introduces the novel DEP separation method of "Dielectrophoretic Chromatography". Experiments were conducted using a variety of particle types the results are presented and discussed with reference to the simulation work of chapter five.

Chapter seven presents the results of experimental work carried out to separate binary mixtures of cell types. Two model mixture systems are used here; (i) the separation of PBMCs from 6μm latex beads and (ii) the separation of placentally derived trophoblast cells from PBMCs. The

ability of the separation system to isolate and concentrate low numbers of particles (cells, sub-micron latex beads, etc) from large fluid volumes in a continuous flow manner is also presented. Chapter eight presents results of work carried out to isolate foetal cells from clinical samples of maternal peripheral blood obtained from pregnant women. Related to this, the dielectric properties of foetal nucleated red blood cells (fnRBCs) were also measured using crossover measurements and the results are presented. Experimental work to modify the surface chemistry of the separation device is also presented in this chapter. The aim of this is the tailoring of the separation device with antibodies specific to the cell type of interest, while also attempting to block any non-specific binding (i.e. other non-target cell types) within the channel. The study looked at the effect of laminin and other proteins on the adhesion of trophoblast cells and PBMCs to treated glass surfaces.

Chapter nine contains concluding remarks and proposals for future work.

1.7 References

1. Holzgreve, W. and S. Hahn, *Prenatal diagnosis using fetal cells and free fetal DNA in maternal blood.* Clinics in Perinatology, 2001. **28**(2): p. 353-+.
2. Bianchi, D.W. and Y.M.D. Lo, *Fetomaternal cellular and plasma DNA trafficking - The Yin and the Yang*, in *Circulating Nucleic Acids in Plasma or Serum Ii*. 2001, New York Acad Sciences: New York. p. 119-131.
3. Luke, S. and K. Kaul, *Detection of breast cancer cells in blood using immunomagnetic bead selection and reverse transcription polymerase chain reaction.* Molecular Diagnosis, 1998. **3**(3): p. 149-155.
4. Trummer, A., *et al.*, *Competitive cytokeratin 19 RT-PCR for quantification of breast cancer cells in blood cell suspensions.* Journal of Hematotherapy & Stem Cell Research, 2000. **9**(2): p. 275-284.
5. Bøyum, A., *Isolation of mononuclear cells and granulocytes from human blood.* Scand J Clin Lab Invest, 1968. **21**: p. 77.
6. *uTAS2000.* in *Micro Total Analysis Systems 2000, Proceedings*. 2000. Dordrecht: Kluwer Academic Publ.
7. Harrison, D.J., *et al.*, *Capillary Electrophoresis and Sample Injection Systems Integrated On a Planar Glass Chip.* Analytical Chemistry, 1992. **64**(17): p. 1926-1932.
8. Zhang, C.X. and A. Manz, *Narrow sample channel injectors for capillary electrophoresis on microchips.* Analytical Chemistry, 2001. **73**(11): p. 2656-2662.
9. Jacobson, S.C., *et al.*, *High-Speed Separations On a Microchip.* Analytical Chemistry, 1994. **66**(7): p. 1114-1118.

10. Dynal, I., *Dynal, Bioscience Product Catalogue*. 2000.
11. Wachtel, S.S., L.P. Shulman, and D. Sammons, *Fetal cells in maternal blood.* Clinical Genetics, 2001. **59**(2): p. 74-79.
12. Tutschek, B., *et al.*, *Noninvasive Prenatal-Diagnosis of Fetal Cells in Maternal Blood.* Gynakologe, 1995. **28**(5): p. 289-301.
13. Torricelli, F. and C. Pescucci, *Isolation of fetal cells from the maternal circulation: Prospects for the non-invasive prenatal diagnosis.* Clinical Chemistry and Laboratory Medicine, 2001. **39**(6): p. 494-500.
14. Simpson, J.L. and S. Elias, *Isolating fetal cells in the maternal circulation.* Human Reproduction Update, 1995. **1**(4): p. 409-418.
15. Lo, Y.M.D., *Noninvasive Prenatal-Diagnosis Using Fetal Cells in Maternal Blood.* Journal of Clinical Pathology, 1994. **47**(12): p. 1060-1065.
16. Kang, A., S. Hahn, and W. Holzgreve, *Fetal cells in maternal blood: their role in non-invasive prenatal diagnosis and in disease.* Schweizerische Medizinische Wochenschrift, 1999. **129**(46): p. 1740-1743.
17. Holzgreve, W., H.S.P. Garritsen, and D. Ganshirtahlert, *Fetal Cells in the Maternal Circulation.* Journal of Reproductive Medicine, 1992. **37**(5): p. 410-418.
18. Hahn, S., *et al.*, *Fetal cells in maternal blood - An update from Basel.* European Journal of Obstetrics Gynecology and Reproductive Biology, 1999. **85**(1): p. 101-104.
19. Bohmer, R.M., *Fetal cells from maternal blood: Purpose, biological questions, technical challenges.* Intervirology, 1998. **41**(4-5): p. 226-231.
20. Bianchi, D.W., *Fetal cells in the maternal circulation: Feasibility for prenatal diagnosis.* British Journal of Haematology, 1999. **105**(3): p. 574-583.
21. Bianchi, D.W., *Prenatal-Diagnosis By Analysis of Fetal Cells in Maternal Blood.* Journal of Pediatrics, 1995. **127**(6): p. 847-856.
22. Adinolfi, M. and J. Sherlock, *Fetal cells in transcervical samples at an early stage of gestation.* Journal of Human Genetics, 2001. **46**(3): p. 99-104.
23. Schmörl, G., *Pathologisch-anatomische untersuchungen ueber Publereklapmsie.* 1893, Leipzig: Vogel.
24. Walknowska, J., F.A. Conte, and M.M. Grumbach, *Practical and theoretical implications of fetal/maternal lymphocyte transfer.* Lancet, 1969. **i**: p. 1119-1122.
25. Lo, Y.M.D., *Fetal DNA in maternal plasma: application to noninvasive blood group genotyping of the fetus.* Transfusion Clinique Et Biologique, 2001. **8**(3): p. 306-310.
26. Thomas, M.R., *et al.*, *The Time of Appearance and Disappearance of Fetal DNA From the Maternal Circulation.* Prenatal Diagnosis, 1995. **15**(7): p. 641-646.
27. Hahn, S.U., *et al.*, *Both maternal and fetal cell-free DNA in plasma fluctuate*, in *Circulating Nucleic Acids in Plasma or Serum Ii*. 2001, New York Acad Sciences: New York. p. 141-144.

28. Herzenberg, L.A., *et al.*, *Fetal cells in the blood of pregnant women: detection and enrichment by fluorescence-activated cell sorting.* Proceedings of the National Academy of Sciences U.S.A., 1979. **76**(1): p. 1453-1455.

29. Iverson, G.M., *et al.*, *Detection and isolation of fetal cells from maternal blood using the fluorescence-activated cell sorter (FACS).* Prenatal Diagnostics, 1981. **1**(61-73).

30. Bianchi, D.W., *et al.*, *Male fetal progenitor cells persist in maternal blood for as long as 27 years postpartum.* Proceedings of the National Academy of Sciences of the United States of America, 1996. **93**(2): p. 705-708.

31. Wessman, M., K. Ylinen, and S. Knuutila, *Fetal granulocytes in maternal venous blood detected by in situ hybridisation.* Prenatal Diagnosis, 1992. **12**: p. 993-1000.

32. Chen, H., *et al.*, *Evaluating the culture of fetal erythroblasts from maternal blood for non-invasive prenatal diagnosis.* Prenatal Diagnosis, 1998. **18**(9): p. 883-892.

33. Simpson, J.L., *et al.*, *Fetal Cells in Maternal Blood - Prospects For Noninvasive Prenatal-Diagnosis.* Contraception Fertilite Sexualite, 1995. **23**(7-8): p. 445-450.

34. Slungatallberg, A. and S. Knuutila, *Can Nucleated Erythrocytes Found in Maternal Venous-Blood Be Used in the Noninvasive Prenatal-Diagnosis of Fetal Chromosome-Abnormalities.* European Journal of Human Genetics, 1995. **3**(4): p. 264-270.

35. Zheng, Y.L., *et al.*, *Flow Sorting of Fetal Erythroblasts Using Intracytoplasmic Antifetal Hemoglobin - Preliminary-Observations On Maternal Samples.* Prenatal Diagnosis, 1995. **15**(10): p. 897-905.

36. DeMaria, M.A., *et al.*, *Improved fetal nucleated erythrocyte sorting purity using intracellular antifetal hemoglobin and Hoechst 33342.* Cytometry, 1996. **25**(1): p. 37-45.

37. Covone, A.E., *et al.*, *Trophoblast cells in peripheral blood from pregnant women.* Lancet, 1984(Oct 13): p. 841-843.

38. Bilchik, A., *et al.*, *Molecular detection of metastatic pancreatic carcinoma cells using a multimarker reverse transcriptase-polymerase chain reaction assay.* Cancer, 2000. **88**(5): p. 1037-1044.

39. Eaton, M.C., *et al.*, *Immunobead RT-PCR: A sensitive method for detection of circulating tumor cells.* Biotechniques, 1997. **22**(1): p. 100-105.

40. Fodstad, O., *et al.*, *Improved immunomagnetic method for detection and characterization of cancer cells in blood and bone marrow.* Experimental Hematology, 1997. **25**(8): p. 615-615.

41. Grunewald, K., *et al.*, *Mammaglobin gene expression: A superior marker of breast cancer cells in peripheral blood in comparison to epidermal-growth- factor receptor and cytokeratin-19.* Laboratory Investigation, 2000. **80**(7): p. 1071-1077.

42. Inufusa, H., *et al.*, *Correlation of prognosis of breast cancer patients and expression of Le(y) which acts as a cofactor of tumor procoagulant.* International Journal of Oncology, 1998. **13**(3): p. 481-487.

43. Z'Graggen, K., *et al.*, *Biological implications of tumor cells in blood and bone marrow of pancreatic cancer patients.* Surgery, 2001. **129**(5): p. 537-546.

44. Rao, W., *et al.*, *Preparation of immuno-magnetic beads and their separation & detection to ovary cancer cells.* Journal of Wuhan University of Technology-Materials Science Edition, 2001. **16**(2): p. 76-78.

45. Deisseroth, A.b., *et al.*, Blood, 1994. **83**: p. 3068-3076.

46. Glorieux, P., *et al.*, Cancer, 1986. **58**: p. 2136-2139.

47. Kemshed, J.T., Journal of Hematotherapy, 1992. **1**: p. 35-44.

48. Anderson, I.C., *et al.*, Cancer Research, 1989. **49**: p. 4659-4664.

49. Coulter, W.H., Proceedings of the National Electronic Conference, 1956. **12**: p. 1034.

50. Morgan, B.B., Research, 1957. **10**: p. 271.

51. Kubitschek, H.E., Research, 1960. **13**: p. 128.

52. Kubitschek, H.E., Nature, 1958. **182**: p. 234-235.

53. Allen, T., *Particle size characterisation*. 1999.

54. Gawad, S., L. Schild, and P. Renaud, *Micromachined impedance spectroscopy flow cytometer for cell analysis and particle sizing.* Lab on a Chip, 2001. **1**(1): p. 76-82.

55. *Cell separation methods and applications*. 1 ed, ed. D. Recktenwald and A. Radbruch. 1998, New York: Marcel Dekker Inc. 331.

56. Milyenyi Biotech, I., *Instructions for Use, VarioMACS and SuperMACS*: Miltenyi Biotech.

57. Thiel, A., A. Scheffold, and A. Radbruch, *Immunomagnetic cell sorting - pushing the limits.* Immunotechnology, 1998. **4**(2): p. 89-96.

58. Rabinow, P., *PCR: a biotechnology story*. 1997.

59. Pethig, R., *Dielectric and electronic properties of biological materials*. 1979, Chichester: John Wiley & Sons.

60. Pohl, H.A., *The motion and percipitation of suspensoids in divergent electric fields.* Journal of Applied Physics, 1951. **22**: p. 869-871.

61. Pohl, H.A., *Dielectrophoresis*. 1978, Cambridge: Cambridge University Press.

62. Pethig, R., *Dielectrophoresis: Using inhomogeneous AC electrical fields to separate and manipulate cells.* Critical Reviews in Biotechnology, 1996. **16**(4): p. 331-348.

63. Jones, T.B., *Electromechanics of Particles*. 1995, Cambridge: Cambridge University Press.

64. Ermolina, I., Y. Polevaya, and Y. Feldman, *Study of normal and malignant white blood cells by time domain dielectric spectroscopy.* Ieee Transactions On Dielectrics and Electrical Insulation, 2001. **8**(2): p. 253-261.

65. Polevaya, Y., *et al.*, *Time domain dielectric spectroscopy study of human cells - II. Normal and malignant white blood cells.* Biochimica Et Biophysica Acta-Biomembranes, 1999. **1419**(2): p. 257-271.

66. Holzel, R. and I. Lamprecht, *Dielectric-Properties of Yeast-Cells As Determined By Electrorotation.* Biochimica Et Biophysica Acta, 1992. **1104**(1): p. 195-200.

67. Schnelle, T., T. Muller, and G. Fuhr, *Dielectric single particle spectroscopy for measurement of dispersion.* Medical & Biological Engineering & Computing, 1999. **37**(2): p. 264-271.

68. Archer, S., H. Morgan, and F.J. Rixon, *Electrorotation studies of baby hamster kidney fibroblasts infected with herpes simplex virus type 1.* Biophysical Journal, 1999. **76**(5): p. 2833-2842.

69. Markx, G.H. and C.L. Davey, *The dielectric properties of biological cells at radiofrequencies: Applications in biotechnology.* Enzyme and Microbial Technology, 1999. **25**(3-5): p. 161-171.

70. Gascoyne, P., *et al.*, *Dielectrophoretic detection of changes in erythrocyte membranes following malarial infection.* Biochimica Et Biophysica Acta-Biomembranes, 1997. **1323**(2): p. 240-252.

71. Chan, K.L., *et al.*, *Measurements of the dielectric properties of peripheral blood mononuclear cells and trophoblast cells using AC electrokinetic techniques.* Biochimica Et Biophysica Acta-Molecular Basis of Disease, 2000. **1500**(3): p. 313-322.

72. Yang, J., *et al.*, *Dielectric properties of human leukocyte subpopulations determined by electrorotation as a cell separation criterion.* Biophysical Journal, 1999. **76**(6): p. 3307-3314.

73. Huang, Y., *et al.*, *Membrane dielectric responses of human T-lymphocytes following mitogenic stimulation.* Biochimica Et Biophysica Acta-Biomembranes, 1999. **1417**(1): p. 51-62.

74. Markx, G.H., M.S. Talary, and R. Pethig, *Separation of Viable and Nonviable Yeast Using Dielectrophoresis.* Journal of Biotechnology, 1994. **32**(1): p. 29-37.

75. Becker, F.F., *et al.*, *The Removal of Human Leukemia-Cells From Blood Using Interdigitated Microelectrodes.* Journal of Physics D-Applied Physics, 1994. **27**(12): p. 2659-2662.

76. Becker, F.F., *et al.*, *Separation of Human Breast-Cancer Cells From Blood By Differential Dielectric Affinity.* Proceedings of the National Academy of Sciences of the United States of America, 1995. **92**(3): p. 860-864.

77. Stephens, M., *et al.*, *The dielectrophoresis enrichment of CD34(+) cells from peripheral blood stem cell harvests.* Bone Marrow Transplantation, 1996. **18**(4): p. 777-782.

78. Talary, M.S., *et al.*, *Dielectrophoretic Separation and Enrichment of Cd34+ Cell Subpopulation From Bone-Marrow and Peripheral-Blood Stem-Cells.* Medical & Biological Engineering & Computing, 1995. **33**(2): p. 235-237.

79. Wang, X.B., *et al.*, *Selective Dielectrophoretic Confinement of Bioparticles in Potential-Energy Wells.* Journal of Physics D-Applied Physics, 1993. **26**(8): p. 1278-1285.

80. Markx, G.H., *et al.*, *Dielectrophoretic Characterization and Separation of Microorganisms.* Microbiology-Uk, 1994. **140**: p. 585-591.

81. Markx, G.H., P.A. Dyda, and R. Pethig, *Dielectrophoretic separation of bacteria using a conductivity gradient.* Journal of Biotechnology, 1996. **51**(2): p. 175-180.

82. Markx, G.H. and R. Pethig, *Dielectrophoretic Separation of Cells - Continuous Separation.* Biotechnology and Bioengineering, 1995. **45**(4): p. 337-343.

83. Schimpf, M.E., K. Caldwell, and J.C. Giddings, *Field-Flow Fractionation Handbook.* 1 ed. 2000: John Wiley & Sons. 560.

84. Gascoyne, P.R.C., *et al.*, *Cell separation by conventional dielectrophoresis combined with field-flow-fractionation.* Biophysical Journal, 1996. **70**(2): p. TU412-TU412.

85. Huang, Y., *et al.*, *Introducing dielectrophoresis as a new force field for field- flow fractionation.* Biophysical Journal, 1997. **73**(2): p. 1118-1129.

86. Markx, G.H., R. Pethig, and J. Rousselet, *The dielectrophoretic levitation of latex beads, with reference to field-flow fractionation.* Journal of Physics D-Applied Physics, 1997. **30**(17): p. 2470-2477.

87. Markx, G.H., J. Rousselet, and R. Pethig, *DEP-FFF: Field-flow fractionation using non-uniform electric fields.* Journal of Liquid Chromatography & Related Technologies, 1997. **20**(16-17): p. 2857-2872.

88. Muller, T., *et al.*, *Microdevice for cell and particle separation using dielectrophoretic field-flow fractionation.* Journal of Liquid Chromatography & Related Technologies, 2000. **23**(1): p. 47-59.

89. Rousselet, J., G.H. Markx, and R. Pethig, *Separation of erythrocytes and latex beads by dielectrophoretic levitation and hyperlayer field-flow fractionation.* Colloids and Surfaces a-Physicochemical and Engineering Aspects, 1998. **140**(1-3): p. 209-216.

90. Vykoukal, J., *et al.*, *A combined dielectrophoretic and field-flow fractionation microsystem for biomedical separation and analysis*, in *Micro Total Analysis Systems 2000, Proceedings*. 2000, Kluwer Academic Publ: Dordrecht. p. 127-130.

91. Wang, X.B., *et al.*, *Separation of polystyrene microbeads using dielectrophoretic/gravitational field-flow-fractionation.* Biophysical Journal, 1998. **74**(5): p. 2689-2701.

92. Wang, X.B., *et al.*, *Cell separation by dielectrophoretic field-flow-fractionation.* Analytical Chemistry, 2000. **72**(4): p. 832-839.

93. Yang, J., *et al.*, *Differential analysis of human leukocytes by dielectrophoretic field-flow-fractionation.* Biophysical Journal, 2000. **78**(5): p. 2680-2689.

94. Yang, J., *et al.*, *Cell separation on microfabricated electrodes using dielectrophoretic/gravitational field flow fractionation.* Analytical Chemistry, 1999. **71**(5): p. 911-918.

95. Huang, Y., *et al.*, *The removal of human breast cancer cells from hematopoietic CD34(+) stem cells by dielectrophoretic field-flow- fractionation.* Journal of Hematotherapy & Stem Cell Research, 1999. **8**(5): p. 481-490.

96. Fiedler, S., *et al.*, *Dielectrophoretic sorting of particles and cells in a microsystem.* Analytical Chemistry, 1998. **70**(9): p. 1909-1915.

97. Fuhr, G. and S.G. Shirley, *Biological application of microstructures*, in *Microsystem Technology in Chemistry and Life Science*. 1998, Springer-Verlag Berlin: Berlin 33. p. 83-116.

98. Gradl, G., *et al.*, *New micro devices for single cell analysis, cell sorting and cloning-on-a-chip: The Cytocon (TM) instrument*, in *Micro Total Analysis Systems 2000, Proceedings*. 2000, Kluwer Academic Publ: Dordrecht. p. 443-446.

99. Muller, T., *et al.*, *A 3-D microelectrode system for handling and caging single cells and particles.* Biosensors & Bioelectronics, 1999. **14**(3): p. 247-256.

100. Fuhr, G., *et al.*, *Radiofrequency Microtools For Particle and Live Cell Manipulation.* Naturwissenschaften, 1994. **81**(12): p. 528-535.

101. Schrum, D.P., *et al.*, *Microchip flow cytometry using electrokinetic focusing.* Analytical Chemistry, 1999. **71**(19): p. 4173-4177.

102. McClain, M.A., *et al.*, *Flow cytometry of Escherichia coli on microfluidic devices.* Analytical Chemistry, 2001. **73**(21): p. 5334-5338.

103. Fu, A.Y., *et al.*, *A microfabricated fluorescence-activated cell sorter.* Nature Biotechnology, 1999. **17**(11): p. 1109-1111.

104. Xia, Y.N. and G.M. Whitesides, *Soft lithography.* Abstracts of Papers of the American Chemical Society, 1997. **214**: p. 348-PMSE.

105. Chou, H.P., *et al.*, *A microfabricated device for sizing and sorting DNA molecules.* Proceedings of the National Academy of Sciences of the United States of America, 1999. **96**(1): p. 11-13.

106. Li, P.C.H. and D.J. Harrison, *Transport, manipulation, and reaction of biological cells on- chip using electrokinetic effects.* Analytical Chemistry, 1997. **69**(8): p. 1564-1568.

107. Koch, M., *et al.*, *A micromachined particle sorter: Principle and technology*, in *Eurosensors Xii, Vols 1 and 2*. 1998, Iop Publishing Ltd: Bristol. p. 595-598.

108. Saleh, O.A. and L.L. Sohn, *Quantitative sensing of nanoscale colloids using a microchip Coulter counter.* Review of Scientific Instruments, 2001. **72**(12): p. 4449-4451.

109. Ayliffe, H.E., A.B. Frazier, and R.D. Rabbitt, *Electric impedance spectroscopy using microchannels with integrated metal electrodes.* Journal of Microelectromechanical Systems, 1999. **8**(1): p. 50-57.

110. Sohn, L.L., *et al.*, *Capacitance cytometry: Measuring biological cells one by one.* Proceedings of the National Academy of Sciences of the United States of America, 2000. **97**(20): p. 10687-10690.

111. Fuller, C.K., *et al.*, *Microfabricated multi-frequency particle impedance characterization system*, in *Micro Total Analysis Systems 2000, Proceedings*. 2000, Kluwer Academic Publ: Dordrecht. p. 265-268.

112. Carlson, R.H., *et al.*, *Self-sorting of white blood cells in a lattice.* Physical Review Letters, 1997. **79**(11).

113. Yamanishi, D.T., *et al.*, *Biochip based enrichment of fetal cells from maternal blood.* American Journal of Human Genetics, 2001. **69**(4): p. 2881.

114. Moore, K.L., *The developing human*. 5th edition, 1993: WB Saunders, Philadelphia.

115. Kaufmann, P., *et al.*, *Endovascular Trophoblast Invasion: Implications for the Pathogenesis of Intrauterine Growth Retardation and Preeclampsia*. Biology of Reproduction, 2003. **69**: p. 1-7.

Chapter Two: Forces in AC electrokinetic microsystems

2 Introduction

The field of alternating current (ac) electrokinetics is concerned with the investigation of the movement of polarizable particles and liquids in non-uniform ac electric fields. This movement arises from the interaction of an applied electric field with the particle and the fluid. A variety of forces and phenomena result and these can roughly be separated into those that act directly upon the particles and those that act upon the suspending fluid.

This chapter presents the theory behind the polarisation of dielectric materials, along with a description of the ac electrokinetic phenomena arising from the interaction of an applied non-uniform field and this polarisation. Also presented is a discussion of the forces acting within the micro-fabricated particle separation system pertinent to this work.

2.1 Dielectrics and polarisation

Dielectric materials polarize under the influence of an external applied electric field (see [1-7] for theory of the various polarisation processes described below). Polarization is the ability of a material to acquire a dipole through the action of this external electric field. Ideal dielectrics possess no free charge carriers, with all charges being strongly bound to the atoms or molecules of the dielectric material. Upon the application of an electric field these bound charges can only be forced to move slightly, with the positive charges moving one direction and the negative charges moving in the opposite direction. A dielectric in which this charge displacement has taken place is said to be polarized.

For the case of a homogeneous dielectric there are three polarisation processes: electronic α_e, atomic α_a and orientational α_o. In the case of a heterogeneous dielectric system, a further polarisation mechanism is present, interfacial polarisation α_i. The total polarisability of the material α_T is the sum of these processes, $\alpha_T=\alpha_e+\alpha_a+\alpha_o+\alpha_i$. Each of the polarisation processes posses a characteristic time constant, resulting in a dielectric relaxation or dispersion.

2.1.1 Electronic polarisation

Electronic polarisation occurs in both polar and non-polar materials. An applied field causes the nucleus and electrons of an atom to experience oppositely directed forces. The electron orbitals are distorted in such a way that their average position no longer coincides with that of the nucleus. The electric fields generated by the microfabricated electrodes used in dielectrophoretic systems are typically of the order of $10^6 Vm^{-1}$, and considerably smaller than those within the atom $10^{11} Vm^{-1}$. The displacement of the charges is therefore only of the order of 10Å. The

frequency region of this polarisation process is above 10^{14}Hz (UV regions and higher) and therefore of no consequence to this work.

2.1.2 Atomic polarisation

Atomic polarisation occurs as a result of the displacement of differently charged ions within a material, and can contribute greatly to the total polarisation in inorganic compounds. This mechanism only makes a small contribution to the total polarization in organic solvents where there are no ions present. Atomic polarisation occurs in the frequency range above 10^{12}Hz again making it of little consequence to this work.

2.1.3 Orientational polarisation

Orientational polarisation only occurs in polar molecules, i.e. those molecules that contain permanent dipoles in their chemical structure. The permanent molecular dipoles in these materials are free to rotate about their axis of symmetry and to align with an applied electric field. Orientational polarisation is temperature dependent. As the temperature of the material is increased so the thermal agitation of the molecules within the material increases, this results in a reduction in the level of polarisation of the material. This reduction is due to the increased random movement and consequent disordering of the orientation of the molecules in the material.

2.1.4 Debye relaxations

For a homogeneous dielectric the movement or formation of each dipole has a characteristic relaxation time. Due to the physical size of the dipole moment there is a limit to the speed with which it can orient within a time varying electric field. If the applied field has a period much shorter than the relaxation time of the dipole, the dipole is unable to orient with the field and the polarisation no longer occurs.

As just described dipole reorientation is typically the slowest polarisation mechanism in a homogeneous dielectric and is usually the first polarisation term to disappear as the frequency of the field is increased. The atomic and electronic polarisation processes have relaxation frequencies high enough such that their contribution to the total polarisation is unaffected by the angular frequency of the electric fields used in this work. As a consequence, the low frequency limit of polarisation for a homogeneous dielectric is given by the sum of the electronic, atomic and orientational polarisations. While the high frequency limit of polarisation is given by the sum of the electronic and atomic polarisations only.

2.1.5 Interfacial polarisation: Maxwell-Wagner polarisation

When a heterogeneous system is subjected to an applied electric field it generally shows frequency dependent dielectric and conductive properties that are different to those of the constituent parts. Heterogeneous systems therefore exhibit further dispersions due to interfacial phenomenon; these are in addition to the above-mentioned polarisation processes and are known as Maxwell-Wagner interfacial polarizations [1-7]. An accumulation of charges at the structural interface between the dissimilar materials gives rise to the formation of a charge layer at the boundary.

The simplest example of a Maxwell-Wagner interfacial polarization is that of a parallel plate capacitor comprised of two dielectrics of differing thickness (d_1, d_2), permittivities (ε_1,ε_2) and conductivites (σ_1,σ_2) and plate area A, as shown in figure 2-1. Conductivity can be thought of as a measure of the ease with which current flows through a material, while permittivity is a measure of the energy storage in a system [6].

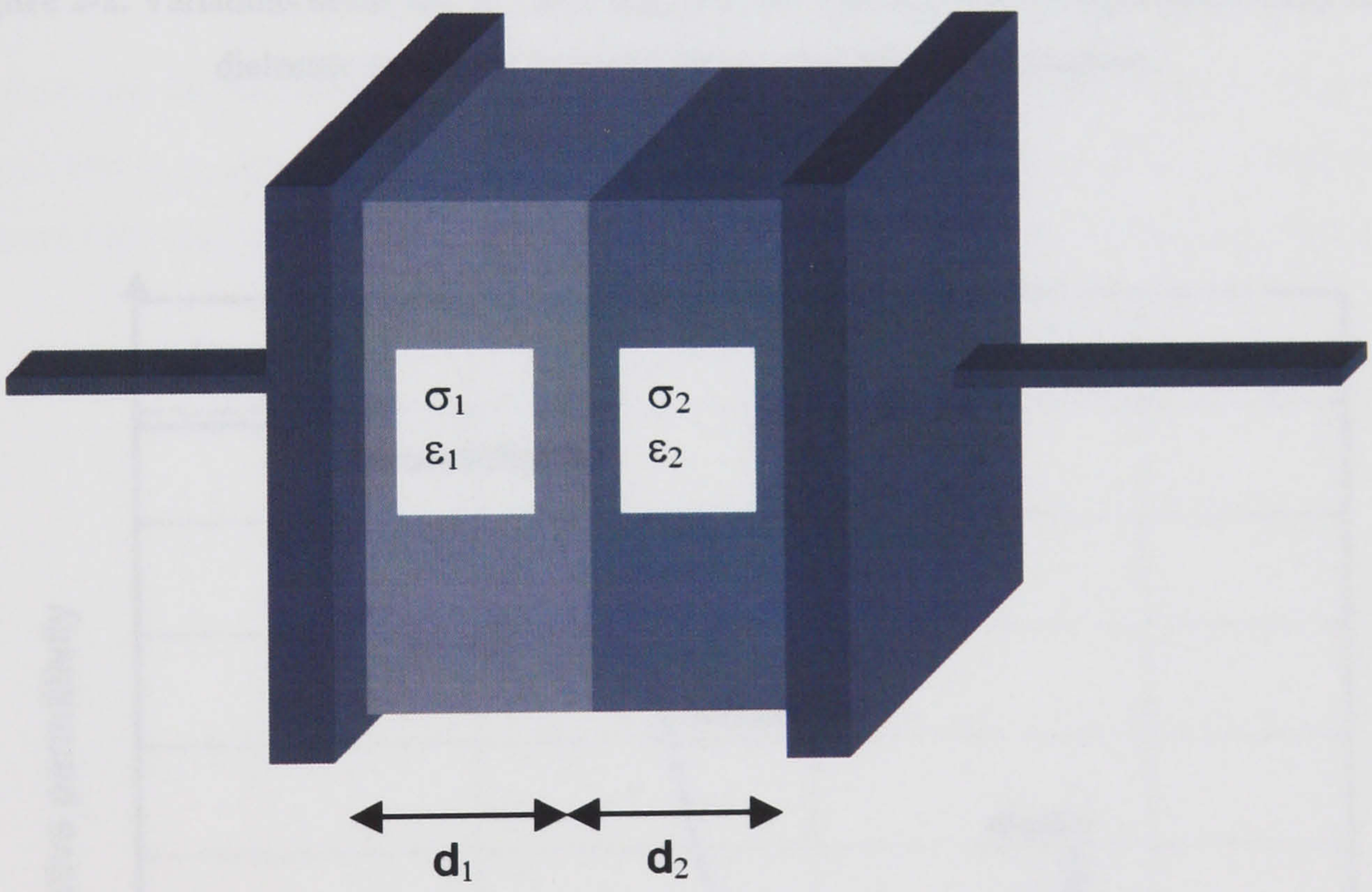

Figure 2-1. Parallel plate capacitor with plate area A and two dielectrics of thickness d_1 and d_2 with permittivities ε_1, ε_2 and conductivities σ_1, σ_2.

The frequency, at which the relaxation due to the Maxwell-Wagner interfacial polarisation occurs, depends on the nature of the interface. Figure 2-2 shows the variation in the real ε' and imaginary ε'' parts of the complex permittivity (ε^* is the complex permittivity given by $\varepsilon^* = \varepsilon_0\varepsilon' - j\varepsilon''$), with frequency for a typical Maxwell-Wagner interfacial polarisation. Δε is the dielectric decrement.

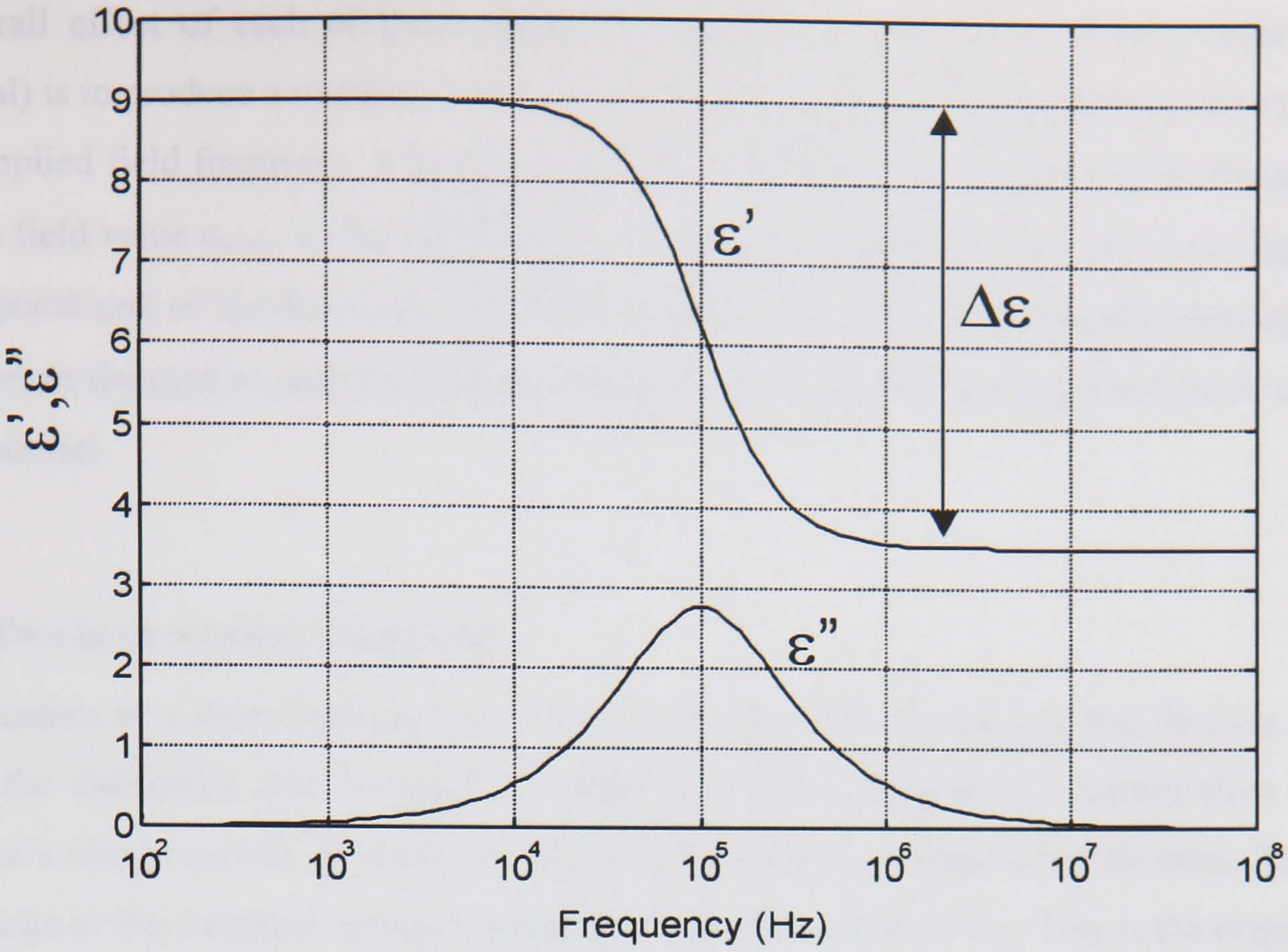

Figure 2-2. Variations of the real (ε') and imaginary (ε'') parts of the complex permittivity for a dielectric exhibiting Maxwell-Wagner interfacial polarisation.

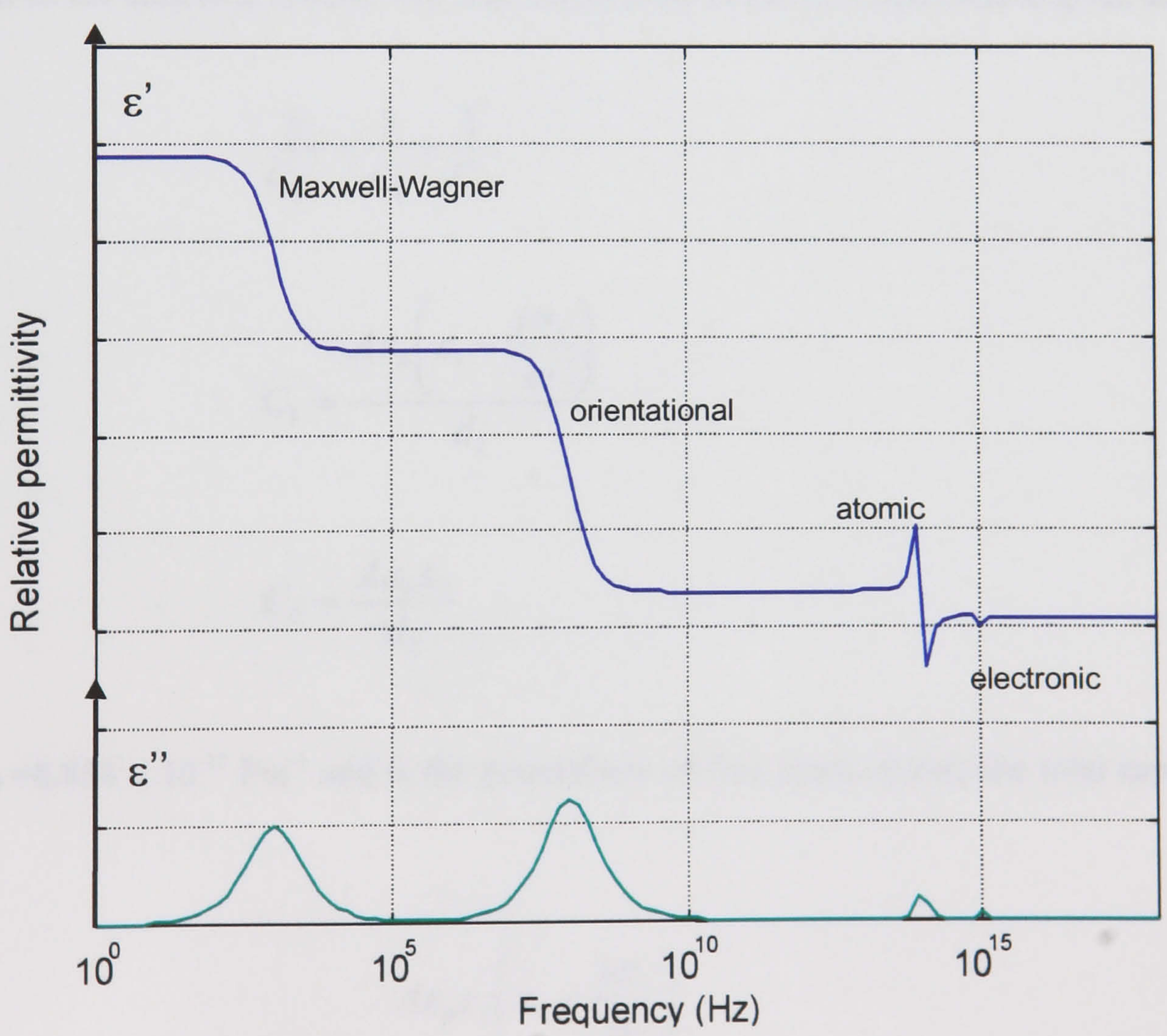

Figure 2-3. The effects of electronic, atomic and orientational and Maxwell-Wagner polarisation on the real (ε') and imaginary (ε'') parts of the complex permittivity of a dielectric.

The overall effect of each of these polarisation processes (electronic, atomic, orientational, interfacial) is to produce a number of dispersions and in the dielectric permittivity of the system. As the applied field frequency is increased from the steady state, the permittivity changes from the static field value $\varepsilon_{\omega\to 0}$, to the high frequency value $\varepsilon_{\omega\to\infty}$ equal to 1, as shown in figure 2-3. At the optical end of the frequency spectrum the electronic and atomic polarisations appear as resonances in the system, and the associated peaks in ε'' characterise the absorption of radiation by the material.

2.1.5.1 Two layer system: simple case

On application of a static field across the two-layer capacitor, the electric flux density flowing through the dielectrics will be equal. In order to ensure continuity of current flow in both dielectrics a charge carrier discontinuity arises at the interface of the two dielectrics. The build up of charge at this interface causes a frequency dependent polarisation. This is the origin of the dielectric dispersions in heterogeneous systems [4, 5].

The system can be modelled as a pair of capacitors in series. Assuming that σ_2 is negligibly small, and that ε_1, ε_2 and σ_1 are frequency independent a simplified expression is obtained for the behaviour of the dielectric system. The total capacitance of the two capacitors is given as,

$$\frac{1}{C_{tot}} = \frac{1}{C_1} + \frac{1}{C_2} \tag{2-1}$$

where,

$$C_1 = \frac{A\varepsilon_o\left(\varepsilon_1 - \frac{j\sigma_1}{\omega}\right)}{d_1} \tag{2-2}$$

and,

$$C_2 = \frac{A\varepsilon_o\varepsilon_2}{d_2} \tag{2-3}$$

where $\varepsilon_0 = 8.854 \times 10^{-12}$ Fm^{-1} and is the permittivity of free space, giving the total capacitance as,

$$C_{tot} = \frac{A\varepsilon_o\varepsilon_2\left(\varepsilon_1 - \frac{j\sigma_1}{\omega}\right)}{d_2\left(\varepsilon_1 - \frac{j\sigma_1}{\omega}\right) + d_1\varepsilon_2} \tag{2-4}$$

from which the low frequency limit ($\omega \rightarrow 0$) of the effective permittivity is given by,

$$\varepsilon_{\omega \to 0} = \frac{\varepsilon_2 d}{d_2} \tag{2-5}$$

and the high frequency limit ($\omega \rightarrow \infty$) of the effective permittivity is given by,

$$\varepsilon_{\omega \to \infty} = \frac{\varepsilon_1 \varepsilon_2 d}{d_2 \varepsilon_1 + d_1 \varepsilon_2} \tag{2-6}$$

If there is a difference between ε_1 and ε_2 the system will exhibit a dielectric dispersion.

2.1.5.2 Two layer system: complete analysis

A fuller analysis of the two-layer system [4] (i.e. not taking σ_2 to be negligibly small, and assuming that ε_1, ε_2 and σ_1 are frequency dependent) demonstrates that the dielectric dispersions can be described in terms of the Debye equations (see section 2.2.4), giving the following expressions for the dielectric parameters of a two-layer system,

$$\varepsilon' = \left(\varepsilon_{\omega \to \infty} + \frac{\varepsilon_{\omega \to o} - \varepsilon_{\omega \to \infty}}{1 + \omega\tau} \right) \varepsilon_0 \tag{2-7}$$

and,

$$\varepsilon'' = \left(\frac{\left(\varepsilon_{\omega \to o} - \varepsilon_{\omega \to \infty}\right)\omega\tau}{1 + \omega^2 \tau^2} + \frac{\sigma}{\omega \varepsilon_0} \right) \varepsilon_0 \tag{2-8}$$

and,

$$\varepsilon_{\omega \to o} = \frac{d\left(\varepsilon_1 d_1 \sigma_2^2 + \varepsilon_2 d_2 \sigma_1^2\right)}{\left(d_2 \sigma_1 + d_1 \sigma_2\right)^2} \tag{2-9}$$

and,

$$\varepsilon_{\omega \to \infty} = \frac{\varepsilon_1 \varepsilon_2 d}{d_2 \varepsilon_1 + d_1 \varepsilon_2} \tag{2-10}$$

where

$$\tau = \frac{\epsilon_o \left(\epsilon_1 d_2 + \epsilon_2 d_1\right)}{d_2 \sigma_1 + d_1 \sigma_2} \tag{2-11}$$

The conductivity of the interfacial system as a whole is given by,

$$\sigma = \frac{d\sigma_1\sigma_2}{d_2\sigma_1 + d_1\sigma_2} \tag{2-12}$$

2.2 Dielectrophoresis (DEP)

As described in section 2.1.5, when an electric field is applied, the interface between a particle and the medium in which it is suspended undergoes Maxwell-Wagner interfacial polarisation. The interaction of the charges (associated with the formation of the effective dipole moment) with the applied electric field results in a force, which acts upon the particle. For a uniform electric field the net force experienced by a neutral particle is zero. However, if the particle is placed in a non-uniform electric field the resulting force imbalance across the particle causes it to move. This movement arises due to the variation in the charge density over the particle. It is important to make the distinction between the phenomenon of dielectrophoresis and electrophoresis.

2.2.1 Electrophoresis

Electrophoresis is the motion of charged matter under the influence of an applied electric field. The direction of motion is always toward the electrode of opposite charge to that of the particle, and it is of no consequence whether the field is uniform or non-uniform. Due to the presence of the double layer, a charged particle when suspended in aqueous solution appears electro-neutral. Despite this, movement of the particle still occurs due to the mobility of the ions in the double later. The velocity of a charged particle due to the electric field is a function of the particle's size and charge as well as the viscosity and conductivity of the suspending liquid (i.e. the thickness of the double layer surrounding the particle). The electrophoretic mobility of a charged particle suspended in solution is given by the function

$$\mu_E = \frac{2\varepsilon\zeta}{3\eta} f(\kappa a) \tag{2-13}$$

where η is the viscosity of the liquid, ϵ the absolute permittivity of the liquid, ζ the particle's zeta potential, and $f(\kappa a)$ is a function of the ratio of the particle radius a to the double layer thickness κ^{-1}. The function $f(\kappa a)$ varies between 1 and 1.5 as the value of κa varies between 0 and ∞(see [6] for further details).

The main application of electrophoresis is in the separation of macromolecules such as DNA and proteins, with the different macromolecules moving with different velocities under the influence of the applied electric field. As the technique will work with any charged particle it is applicable to the separation of cells, which typically have a net negative surface charge at physiological pH [5-6].

2.2.2 The dielectrophoretic force

Dielectrophoresis is distinctly different in nature from electrophoresis. Dielectrophoresis (DEP) is the translational movement of neutral matter as a result of polarisation effects in non-uniform electric fields [4, 5, 7].

Under the influence of a uniform DC electric field, a particle with charge q will experience a net force toward the electrode of opposite polarity to that of itself. A neutral particle will become polarised as a result of the electric field but will experience no net movement in the uniform field, this is shown below in figures 2-4 and 2-5.

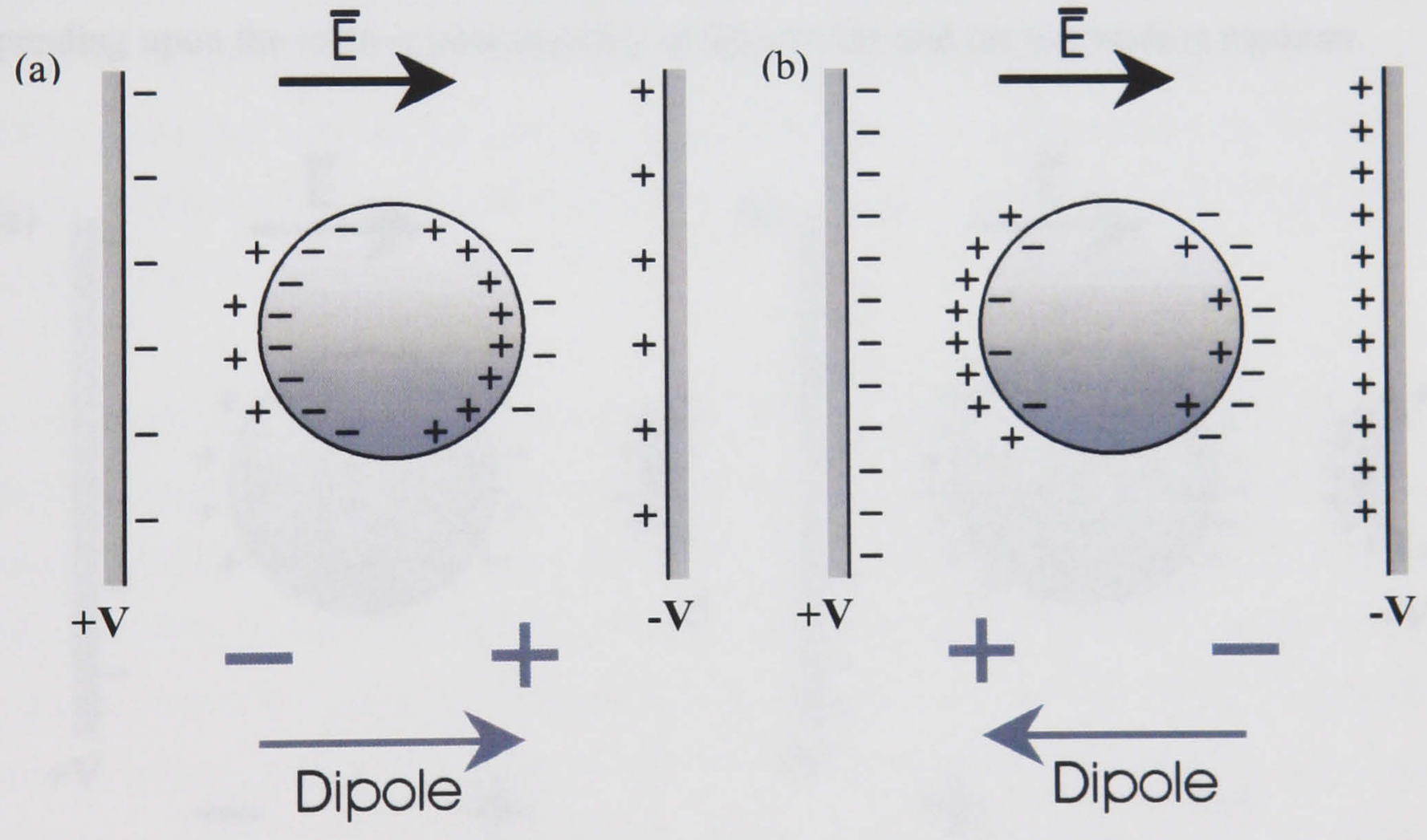

Figure 2-4. Effect of a uniform field on uncharged particles. No net translational force is exerted on the neutral particle. (a) the polarisability of the particle is greater than that of the medium, (b) the polarisability of the particle is less than that of the medium. Adapted from [6].

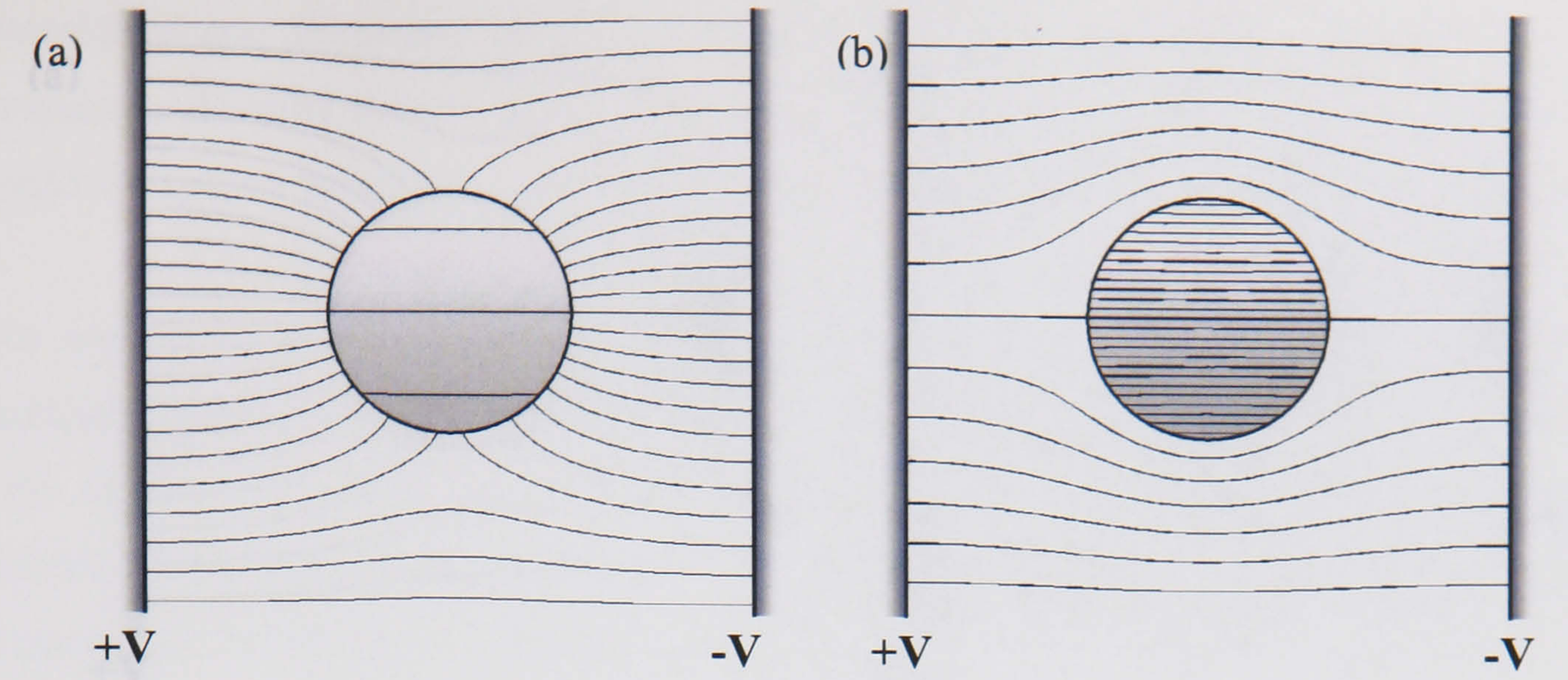

Figure 2-5. Plots of the electric field lines for an uncharged spherical particle placed in a uniform field (a) the polarisability of the particle is greater than that of the medium, (b) the polarisability of the particle is less than that of the medium. Adapted from [6].

If these particles are now placed in a non-uniform DC electric field the situation is somewhat different. The charged particle will still experience a net translational force towards the electrode of opposite polarity. However, the neutral particle will now experience a net translational force, moving it towards or away from the regions of high electric field intensity, depending upon the relative polarisability of the particle and the suspending medium.

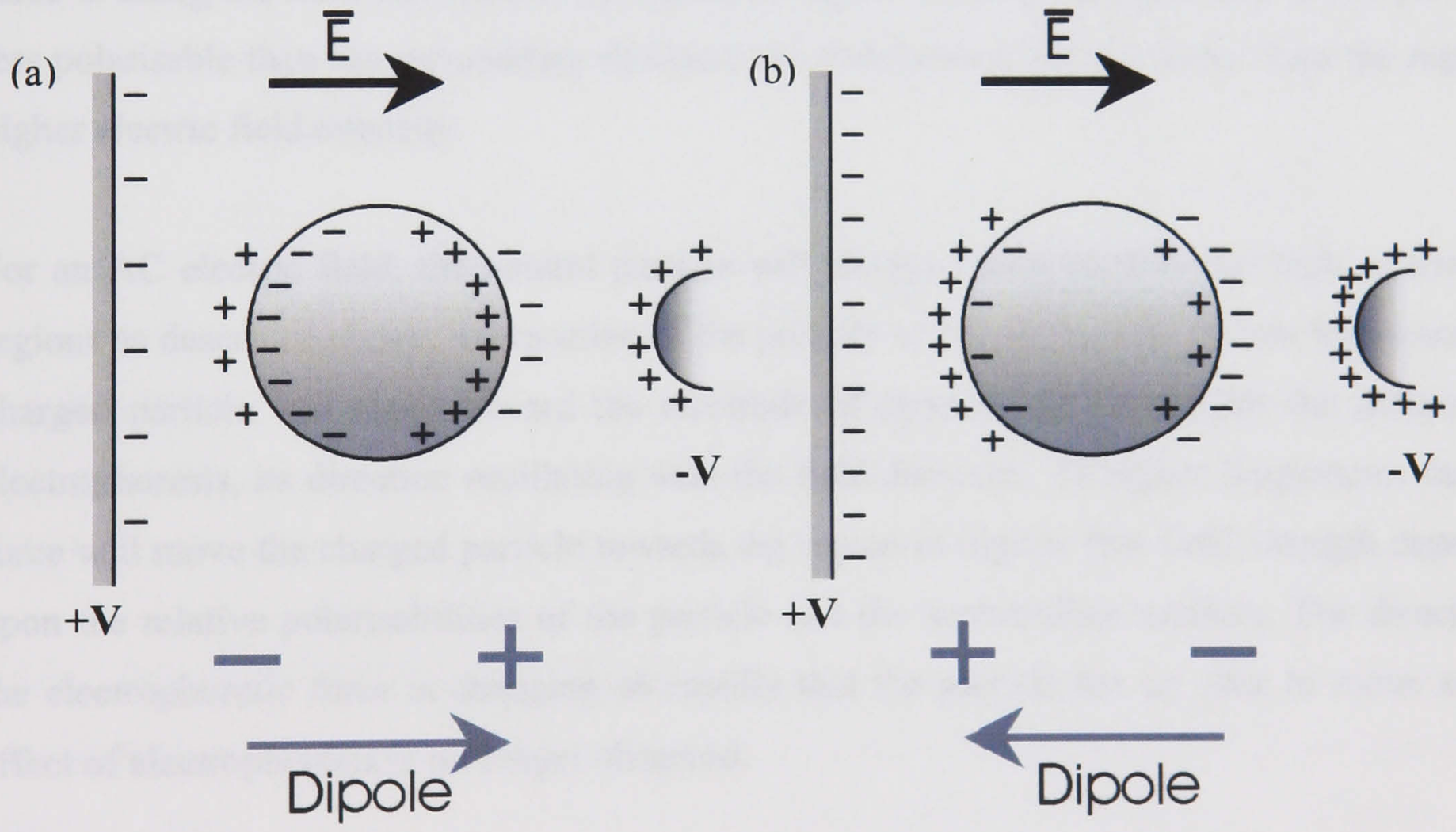

Figure 2-6. Effect of a non-uniform field on uncharged particles. A translational force is exerted on the neutral particle. (a) the polarisability of the particle is greater than that of the medium, (b) the polarisability of the particle is less than that of the medium. Adapted from [6].

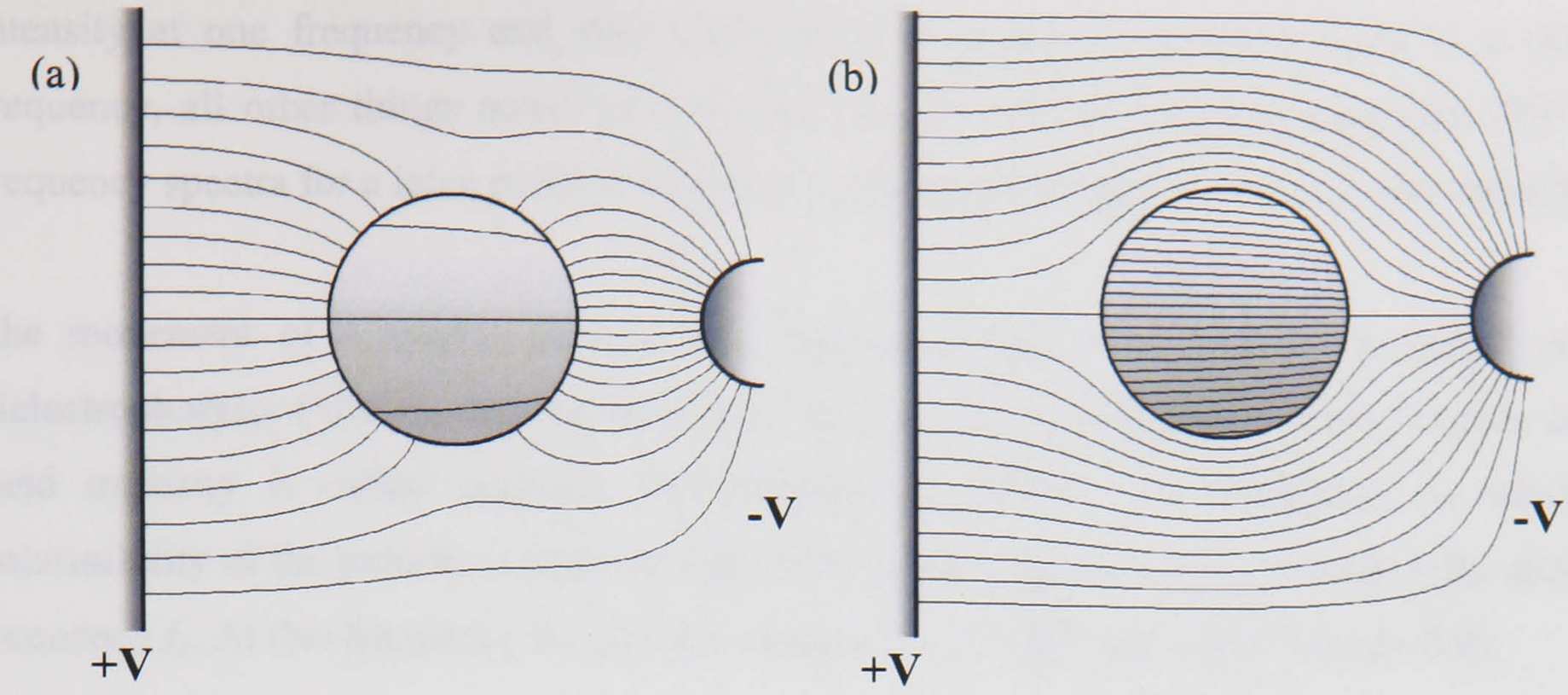

Figure 2-7. Plots of the electric field lines for an uncharged spherical particle placed in a uniform field (a) the polarisability of the particle is greater than that of the medium, (b) the polarisability of the particle is less than that of the medium. Adapted from [6].

The charge redistribution in and around the particle due to the field results in equal amounts of oppositely charged ions facing the electrodes of opposite polarity. However, as the field is non-uniform, the forces experienced by opposite ends of the neutral particle have different magnitudes. The resultant net translational force in this case is therefore non-zero, giving rise to motion. If the neutral particle is more polarisable than the surrounding medium, the translational force is along the field line toward the region of higher electric field intensity. If the particle is less polarisable than the surrounding medium, the translational force is away from the region of higher electric field intensity.

For an AC electric field, the neutral particle will always move towards the high or low field regions as described above, irrespective of the polarity of the electrodes. At low frequencies the charged particle will move toward the electrode of opposite polarity under the influence of electrophoresis, its direction oscillating with the field direction. At higher frequencies the DEP force will move the charged particle towards the region of high or low field strength depending upon the relative polarisabilities of the particle and the surrounding medium. The direction of the electrophoretic force is changing so rapidly that the particle has no time to move and the effect of electrophoresis is no longer observed.

2.2.3 Positive and negative dielectrophoresis

In the previous sections it was shown that the polarisation of a dielectric material is frequency dependent with characteristic dispersions of polarisation occurring at different frequencies. Materials therefore exhibit characteristic dielectrophoretic spectra due to differences in their dielectric properties. Particles may therefore experiences a force towards a region of high field

intensity at one frequency and may experience an oppositely directed force at a different frequency, all other things remaining the same. Figure 2-8 shows the normalised DEP force frequency spectra for a latex particle suspended in water (see section 2-9 for further details).

The movement of a neutral particle to a region of high field intensity is called positive dielectrophoresis (+DEP), and the movement of a neutral particle away from a region of high field intensity is called negative dielectrophoresis (-DEP). The frequency at which the polarisability of the particle is equal to that of the suspending medium is known as the crossover frequency f_x. At this frequency the particle experiences no DEP force (see section 2.9).

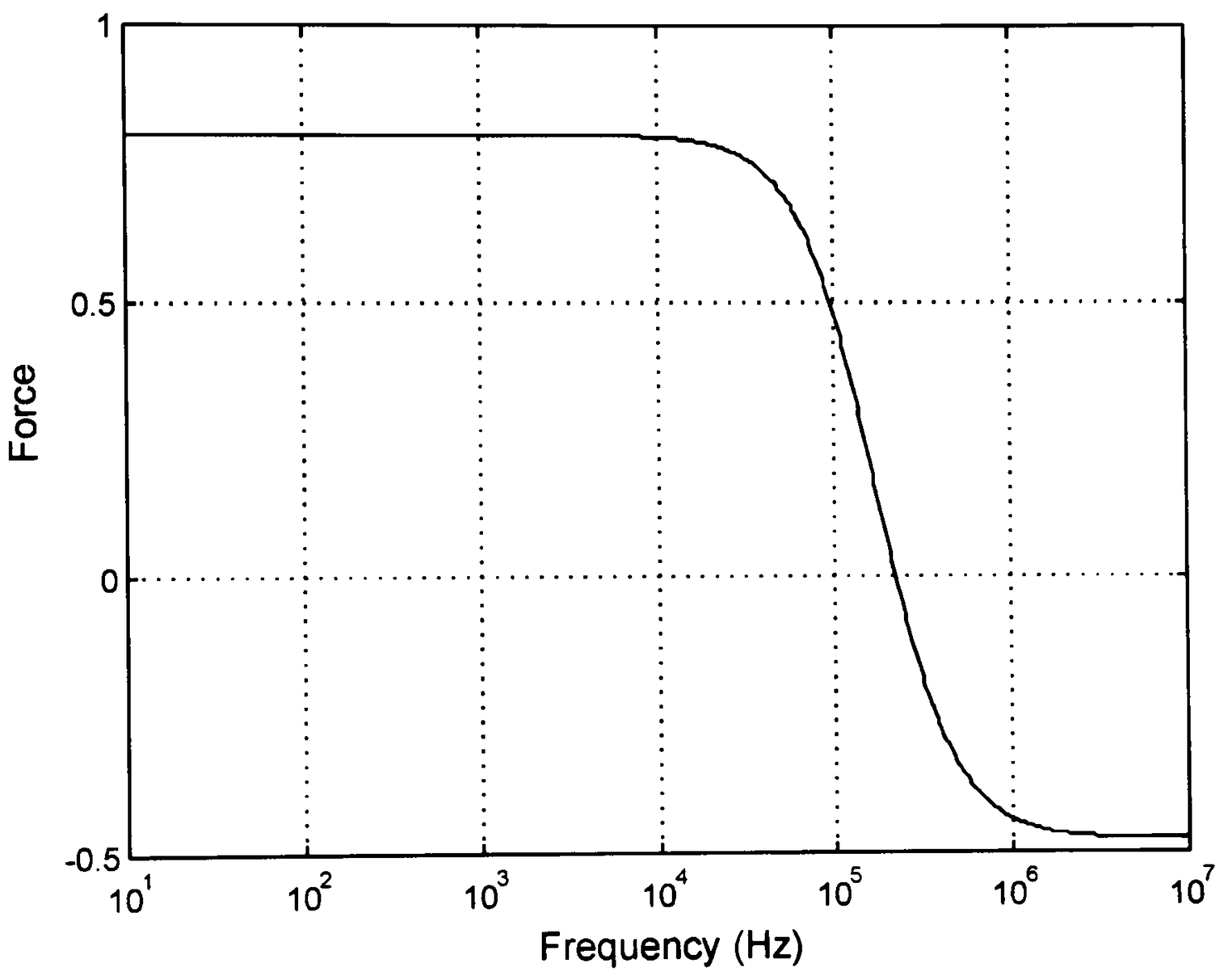

Figure 2-8. Normalised DEP force experienced by a 10μm latex particle suspended in water of conductivity 0.1mSm^{-1}.

2.2.4 Derivation of the force on a dipole

The DEP force acting on a particle can be derived first, by estimating the net force upon a small physical dipole, and then generalising to the force acting on a particle of effective dipole moment $\boldsymbol{p}_{eff}$ (see [4] and [6]).

A neutral particle within an externally applied electric field has an induced dipole moment, with centres of equal positive and negative charge separated by a distance $\boldsymbol{d}$. We assume that no field contributions arise from the dipole itself.

For a dipole in a non-uniform field the positive and negative charges experience different electric field strengths. This gives rise to a total force on the particle of,

$$\boldsymbol{F} = q\boldsymbol{E}(\boldsymbol{r}+\boldsymbol{d}) - q\boldsymbol{E}(\boldsymbol{r}) \tag{2-14}$$

where $\boldsymbol{r}$ is the position vector of $-q$.

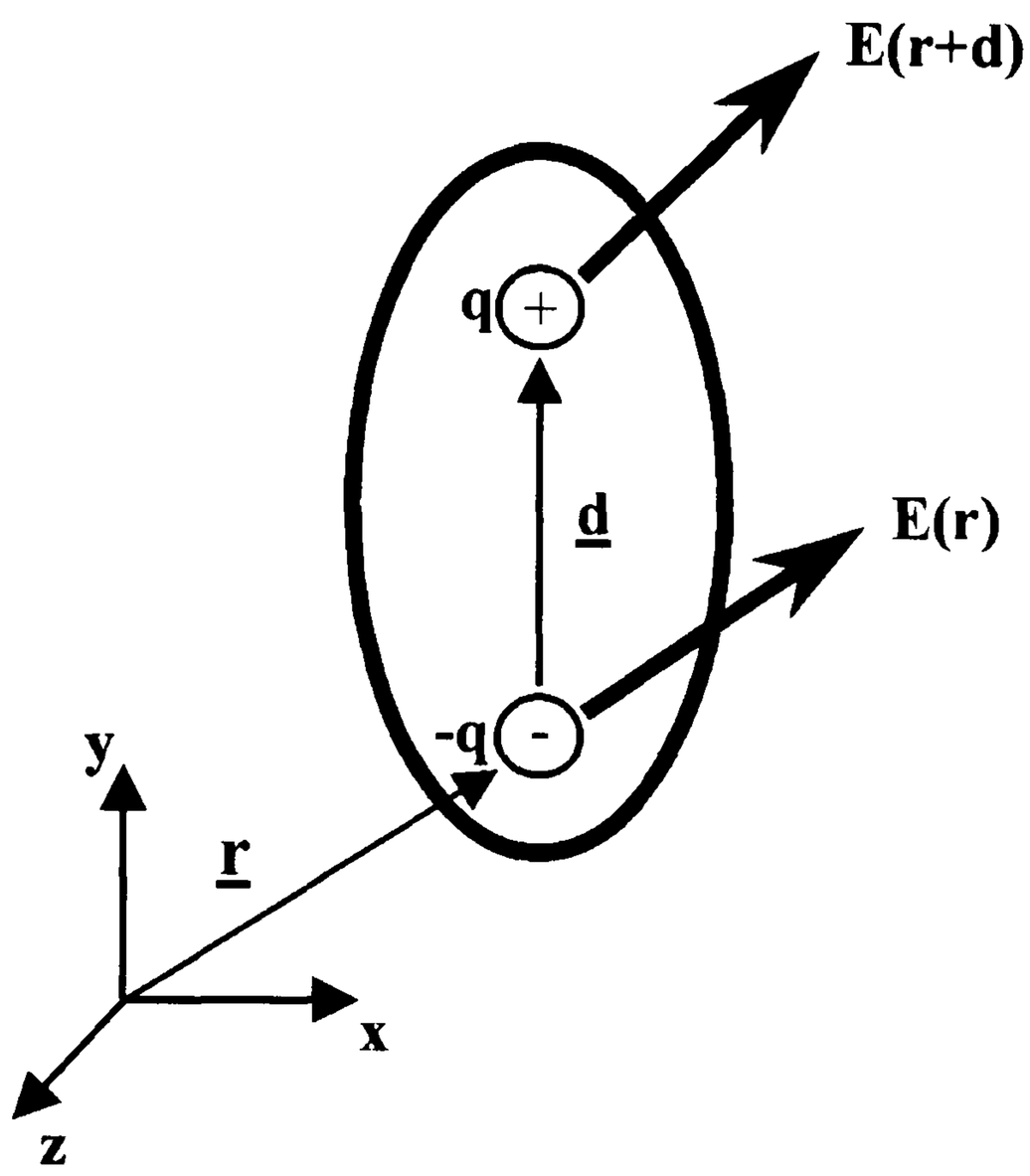

Figure 2-8. The force on a small dipole in a non-uniform electric field.

If the magnitude of $\boldsymbol{d}$ is small compared to the characteristic scale of the electric field non-uniformity, a simplified vector Taylor series (i.e. $\mathbf{A}(\mathbf{x} + \mathbf{dx}) = \mathbf{A}(\mathbf{x}) + \mathbf{dx} \cdot \nabla \mathbf{A}$ + higher order terms) can be used to describe the electric field about position $\boldsymbol{r}$, i.e.

$$\boldsymbol{E}(\boldsymbol{r}+\boldsymbol{d}) = \boldsymbol{E}(\boldsymbol{r}) + \boldsymbol{d} \cdot \nabla \boldsymbol{E}(\boldsymbol{r}) \tag{2-15}$$

where ∇ is the del operator, and all higher terms of $\boldsymbol{d}$ have been neglected. Using the above equations we obtain the force acting on a particle as,

$$\boldsymbol{F} = q\boldsymbol{d} \cdot \nabla \boldsymbol{E} \,. \tag{2-16}$$

From this we obtain the force on a dipole due to an applied electric field,

$$\boldsymbol{F}_{dipole} = (\boldsymbol{p} \cdot \nabla)\boldsymbol{E} \,. \tag{2-17}$$

The above equation is an approximation for the force exerted on any physical dipole. For a polarisable particle of finite size equation 2-17 gives good results if the electric field non-uniformity can be neglected, when measured over a length scale similar to the size of the particle. This approximation generally leads to good results when applied to small micron or sub-micron sized particles interacting with the electric fields produced by the electrodes of the size used in this work [4]. However, when calculating the forces experienced by particles very close to the electrode edge, or the fields generated by mutual particle-to-particle interactions (between closely spaced particles) the approximation can become significantly erroneous. Higher order linear multipolar terms must therefore be included in such situations (see [4, 8-10] for a discussion of linear multipoles).

2.3 The effective dipole moment

From the above discussion (section 2.1.5) it is apparent that a dielectric particle suspended in a liquid will experience Maxwell-Wagner interfacial polarization at the particle/liquid interface, inducing a dipole moment in the particle. The concept of the effective dipole moment, $\boldsymbol{p}_{eff}$ of the particle, can then be defined as the moment of the equivalent point dipole immersed in the same fluid with its position the same as the center of the original particle.

The electrostatic potential ϕ_{dipole} due to a point dipole of moment $\boldsymbol{p}_{eff}$ in a dielectric medium of permittivity ε_m is given by [4],

$$\phi_{dipole} = \frac{\boldsymbol{p}_{eff} cos\theta}{4\pi\varepsilon_m r^2} \tag{2-18}$$

where θ and r are polar coordinates for a spherical system.

The effective complex polarisability α of a homogeneous solid dielectric sphere can be written in terms of the complex dielectric properties of the sphere and the surrounding medium [4],

$$\alpha = 3\varepsilon_m \left(\frac{\varepsilon_p^* - \varepsilon_m^*}{\varepsilon_p^* + 2\varepsilon_m^*} \right) \tag{2-19}$$

where ε^* is the complex permittivity given by $\varepsilon^* = \varepsilon_0 \varepsilon_r - j\frac{\sigma}{\omega}$ and the subscripts m and p refer to the medium and the particle respectively.

The effective dipole moment of a dielectric particle suspended in a liquid is therefore frequency dependent and can be expressed as,

$$\boldsymbol{p}_{eff} = v\alpha \boldsymbol{E} \tag{2-20}$$

where v is the particle volume. This can be written more explicitly as,

$$\boldsymbol{p}_{eff} = 4\pi\varepsilon_m \left(\frac{\varepsilon_p^* - \varepsilon_m^*}{\varepsilon_p^* + 2\varepsilon_m^*} \right) a^3 \boldsymbol{E} . \tag{2-21}$$

The frequency dependence of the effective dipole moment is described by the term in brackets known as the *Clausius-Mossotti* factor,

$$f_{CM} = \frac{\varepsilon_p^* - \varepsilon_m^*}{\varepsilon_p^* + 2\varepsilon_m^*} \tag{2-22}$$

where the *Clausius-Mossotti* factor corrects for the fact that the field acting locally on the dipole is not the same as the external field applied to the system, due to the effect of the fields associated with the neighbouring dipoles.

The above solution is correct under conditions where the radius of the sphere is small compared to the characteristic length of the electric field non-uniformity. This is generally the case for the microfabricated electrodes used in the experimental work carried out for this thesis.

The effective moment method described above simplifies the calculation of the force on a particle and avoids the need for complicated derivations based on the Maxwell stress tensor (see [4] for detail). It may be used to calculate the forces on particles as long as the dielectric loss in the suspending liquid is negligible (i.e. $\varepsilon_m'' << \varepsilon_m'$).

2.3.1 The time averaged dielectric force

The instantaneous force on a dipole in an electric field is given above (2-17). For the case of a time varying electric field ($\boldsymbol{E} = E_o e^{j\omega t}$) the dipole varies with the same angular velocity as the electric field, but with a phase lag θ. The time-averaged force is,

$$\langle \boldsymbol{F} \rangle = \frac{1}{2} Re\left[(\boldsymbol{p} \cdot \nabla) \boldsymbol{E}^* \right] \tag{2-23}$$

where $\boldsymbol{E}^*$ is the complex conjugate of $\boldsymbol{E}$. After manipulation using suitable vector identities and inserting the expression for the effective dipole moment the time averaged DEP force becomes [4],

$$\langle \boldsymbol{F} \rangle = \pi \varepsilon_m a^3 Re\{ f_{CM} \} \nabla |\boldsymbol{E}|^2 \tag{2-24}$$

where $\nabla |\boldsymbol{E}|^2$ is the gradient of the square of the electric field and $Re\{f_{CM}\}$ is the real part of the *Clausius-Mossotti* factor, which is defined by the limit $-0.5 < Re\{f_{CM}\} < 1$.

2.4 Forces other than DEP on particles in solution

There are a number of forces other than DEP experienced by a particle moving in a dielectrophoretic separation system of the type described in this thesis. There are externally imposed forces such as the gravitational and the dielectrophoretic forces, which are the predominant forces acting on particles greater than 1μm. Intrinsic forces, such as Brownian motion and diffusion are also present and must also be accounted for. There is also the effect of the fluid motion, which is transferred into movement of the particles due to viscous drag. There are two types of fluid flow in a DEP separation system; the first is the flow arising from electrohydrodynamic forces on the fluid due to interaction of the electric field and the fluid; and the second is the fluid flow due to the hydrostatic pressure pumping the fluid through the channel.

For the purposes of this thesis particles with diameters ranging from ~100 nm to ~10 μm were investigated. The forces acting on particles in this size range in aqueous suspension can be modelled using Newtonian mechanics. In order to simplify the analysis we will consider the one-dimensional system, the result can easily be generalised to three dimensions.

Figure 2-9 shows the various forces on a particle in a DEP microfluidic system. F_G is the gravitational force, F_S (or F_{drag}) is the Stokes drag force and F_{DEP} is the DEP force on the particle. F_G can act in either direction depending upon the relative density of the medium and the particle. Depending on the relative polarisabilities of the particle and the medium F_{DEP} can act either towards or away from the electrodes.

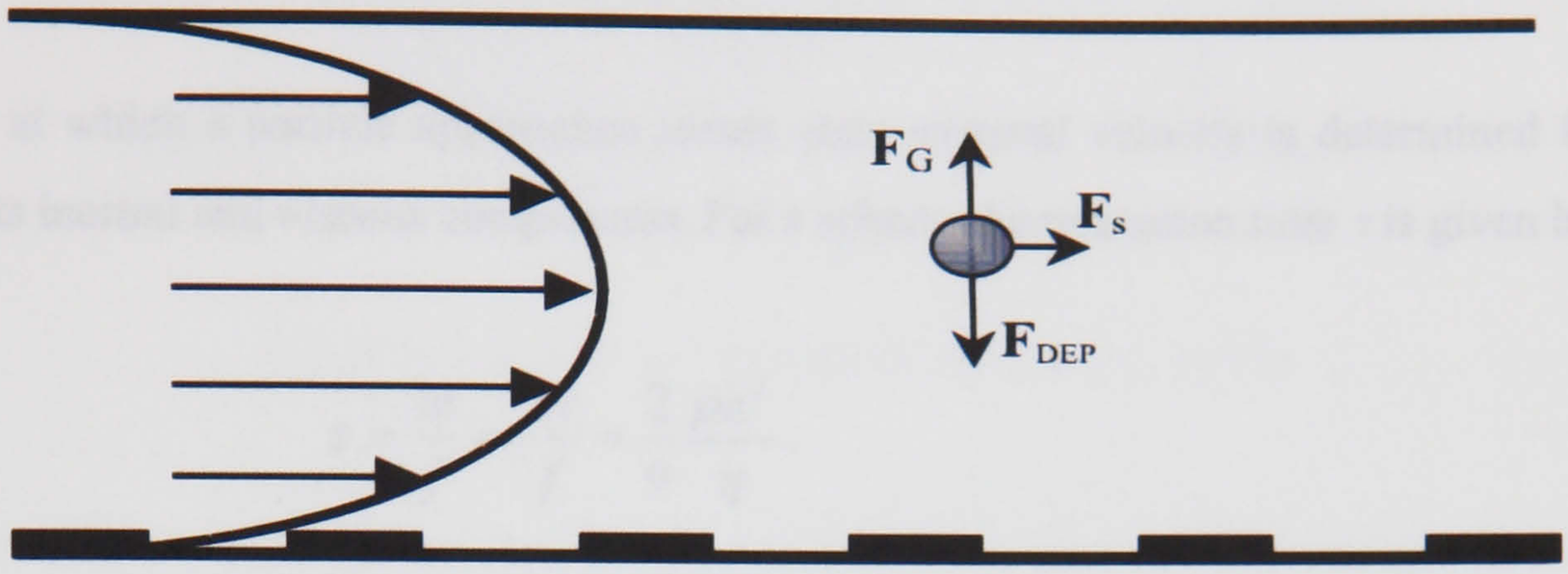

Figure 2-9. Forces on a particle in a DEP flow through system.

2.4.1 Gravitational forces

A particle of volume v and mass density ρ_p, suspended in a fluid of density ρ_m experiences a buoyancy force due to gravity. The net force on the particle can be written as:

$$\boldsymbol{F}_g = m\boldsymbol{g} = v(\rho_m - \rho_p)\boldsymbol{g} \tag{2-25}$$

where g the gravitational acceleration (9.81 ms^{-2}). The force acts with gravity if $\rho_p > \rho_m$ and against gravity if $\rho_p < \rho_m$.

2.4.2 Viscous drag

A particle moving though a liquid medium with velocity **v** experiences a frictional drag force $\boldsymbol{F}_{drag}$, due to the viscous nature of the fluid,

$$\boldsymbol{F}_{drag} = -f\,\mathbf{v} = -f\frac{d\boldsymbol{x}}{dt} \tag{2-26}$$

where f is the friction, or Stokes' drag, factor. For a sphere with radius a moving through a fluid with dynamic viscosity η, the friction coefficient is,

$$f = 6\pi\eta a. \tag{2-27}$$

The mass of a latex bead with radius a can be calculated as,

$$m = \rho v = \rho \frac{4}{3} \pi a^3 \tag{2-28}$$

where $\rho = 1050$ kgm^{-3}, hence a 1μm radius latex bead has a mass $m = 4.398\text{x}10^{-15}$ kg.

The rate at which a particle approaches steady state terminal velocity is determined from the ratio of its inertial and viscous components. For a sphere, the relaxation time τ is given by

$$\tau = \frac{m}{f} = \frac{\rho v}{f} = \frac{2}{9} \frac{\rho a^2}{\eta}. \tag{2-29}$$

A step change in force gives a velocity change,

$$\mathbf{v} = \frac{\boldsymbol{F}}{f} \left(1 - e^{-\left(\frac{f}{m}\right)t} \right). \tag{2-30}$$

Using the value for dynamic viscosity of water, at 20 °C, $\eta = 1\text{x}10^{-3}$ kgm^{-1}s^{-1}, equation 2-30 predicts a 1μm latex bead has relaxation time $\tau = 1.11\text{x}10^{-8}$s. A particle will therefore reach its steady state terminal velocity almost instantaneously, and any measured change in velocity is a result of a change in force on the particle [6].

2.5 Analytical solution of the 2D field gradient

Morgan *et al* [11, 12] have provided an analytical solution for the two-dimensional electric field gradient above an array of interdigitated "bar" microelectrodes (see figure 2-9). Their solution uses Fourier series analysis to obtain an analytical solution for the dielectrophoretic force on a particle generated by this design of electrode array. Solutions for both the dielectrophoretic and traveling wave dielectrophoretic force are given. A full analytical expression is given for the dielectrophoretic force in two-dimensions based on infinite series. A simpler one-dimensional expression is also derived for the force at a distance of the order of the electrode size d above the electrodes to infinity.

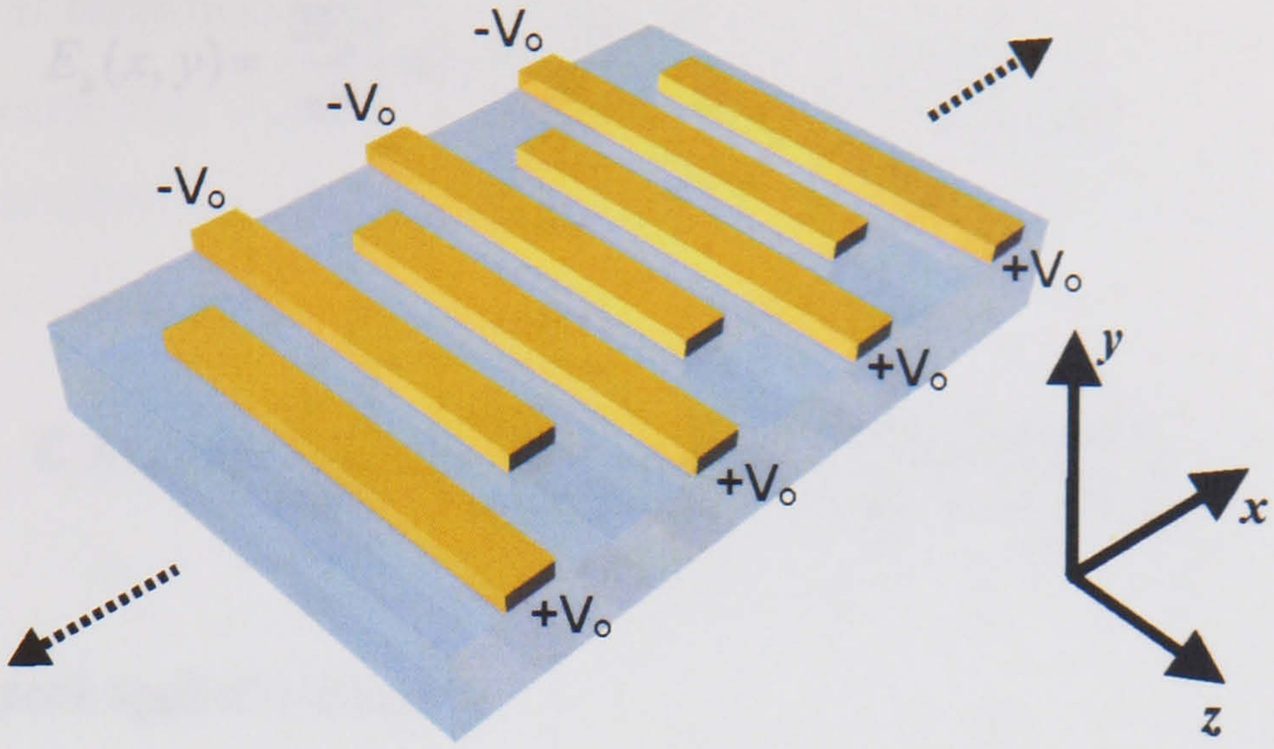

Figure 2-9. Schematic of the interdigitated bar electrodes.

Their analytical solution gives results that are in close agreement with previously published experimental observations [13, 14] and with previously derived analytical solutions obtained using Green's theorem [15-17], as well as other techniques [18]. Figure 2-10 shows a vector plot of the DEP force generated by such arrays of interdigitated bar electrodes.

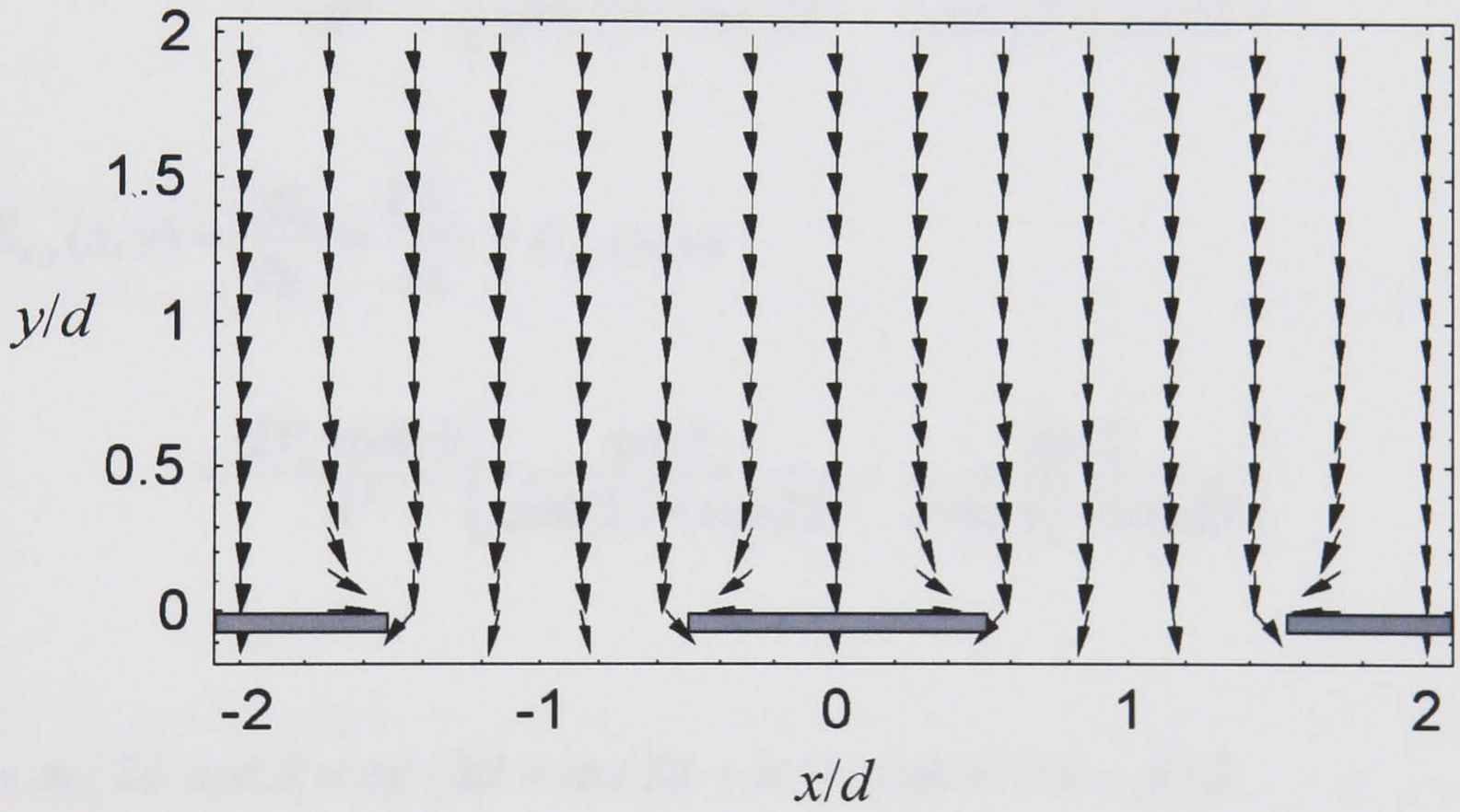

Figure 2-10. Plot of the normalised DEP force vectors above an array of interdigitated bar electrodes. *d* is the width of the electrodes and of the spaces. Adapted from [6].

2.5.1 Full two-dimensional solution of the DEP force

The analytical form for the two-dimensional electric field above an array of interdigitated bar electrodes is given by the sum of an infinite Fourier series. Assuming linear boundary conditions for the potential, and for the special case where $d_1 = d_2 = d$ the closed form expression for the horizontal and vertical components of the field at any point is given by,

$$E_x(x,y)=\frac{2V_o}{\pi d}\left[\tan^{-1}\left(\frac{\sin\hat{x}}{\sinh\hat{y}}\right)-\tan^{-1}\left(\frac{\cos\hat{x}}{\sinh\hat{y}}\right)\right] \tag{2-31}$$

$$E_y(x,y)=\frac{V_o}{d\pi}\left[\ln\left(\frac{\cosh\hat{y}+\cos\hat{x}}{\cosh\hat{y}-\cos\hat{x}}\cdot\frac{\cosh\hat{y}+\sin\hat{x}}{\cosh\hat{y}-\sin\hat{x}}\right)\right] \tag{2-32}$$

where V_0 is the peak applied voltage.

The DEP force is obtained from the derivatives of the electric field components, with explicit expressions for $E_{x,x}$, $E_{x,y}$, $E_{y,x}$ and $E_{y,y}$ given by:

$$\begin{aligned} E_{x,x}(x,y)&=\frac{\partial E_x}{\partial x}=-\frac{\partial E_y}{\partial y}=-E_{y,y}(x,y)\\ &=\frac{2V_o\sinh\hat{y}}{d^2}\left[\frac{\cos\hat{x}}{\cosh 2\hat{y}-\cos 2\hat{x}}+\frac{\sin\hat{x}}{\cosh 2\hat{y}+\cos 2\hat{x}}\right] \end{aligned} \tag{2-33}$$

$$\begin{aligned} E_{x,y}(x,y)&=\frac{\partial E_x}{\partial y}=\frac{\partial E_y}{\partial x}=E_{y,x}(x,y)\\ &=\frac{2V_o\cosh\hat{y}}{d^2}\left[\frac{\cos\hat{x}}{\cosh 2\hat{y}+\cos 2\hat{x}}-\frac{\sin\hat{x}}{\cosh 2\hat{y}-\cos 2\hat{x}}\right] \end{aligned} \tag{2-34}$$

where $\hat{y}=\pi y/2d$ and $\hat{x}=\pi x'/2d=\pi x/2d+\pi/4$, and $x'=x+d/2$.

We can thus write the field gradient as,

$$\nabla(E_x^2+E_y^2)=2\mathbf{u}_x(E_xE_{x,x}+E_yE_{y,x})+2\mathbf{u}_y(E_xE_{y,x}+E_yE_{y,y}) \tag{2-35}$$

where $\mathbf{u}_x$ and $\mathbf{u}_y$ are unit vectors in the x and y directions.

The time averaged DEP force at any point above the electrode array is then expressed as,

$$\langle F_{DEP}\rangle=\frac{1}{4}vRe[\alpha]\nabla(E_x^2+E_y^2) \tag{2-36}$$

2.5.2 Forces at heights greater than the characteristic electrode size

For height y greater than d (where $d = (d_1+d_2)/2$) the higher order terms of the infinite series sum become negligible and all but the first term can be neglected giving the DEP force for the general case, $d_1 \neq d_2 \neq d$ as,

$$\langle F_{DEP} \rangle = -16 \frac{V_o^{\,2} v}{\pi d_2^{\,2} d} Re[\alpha] cos^2\left(\frac{\pi d_1}{4d}\right) e^{-\frac{\pi y}{d}} u_y \tag{2-37}$$

and for the special case where $d_1 = d_2 = d$ the DEP force is,

$$\langle F_{DEP} \rangle = -8 \frac{V_o^{\,2} v}{\pi d^3} Re[\alpha] e^{-\frac{\pi y}{d}} \mathbf{u}_y \tag{2-38}$$

These equations accurately describe the field at heights greater than d above the electrode array but deviate somewhat for values of $y < d$ (this is further discussed in chapter 5).

2.6 Fluid flow in microchannels

The Navier-Stokes equation describes the motion of fluids and can be written as [2],

$$-\nabla \boldsymbol{P} + \eta \nabla^2 \mathbf{v} = \rho\left(\frac{\partial \mathbf{v}}{\partial t} + (\mathbf{v}\cdot\nabla)\mathbf{v}\right) \tag{2-39}$$

where $\boldsymbol{P}$ is the applied pressure, $\mathbf{v}$ is the velocity vector, ρ is the fluid density and η is the viscosity of the fluid. The terms on the left side of equation 2-39 represent the forces on the fluid due to applied pressure and viscosity while the terms on the right side represent the inertial forces.

If we assume that the liquid is incompressible (a good assumption at flow speed much less than the speed of sound) and ρ is therefore constant we have the additional equation,

$$\nabla \cdot \mathbf{v} = 0 \tag{2-40}$$

For any fluid flow a dimensionless number R can be calculated as the ratio of the inertial forces to the viscous forces, i.e.

$$R = \frac{\rho\left(\frac{\partial v}{\partial t} + (\mathrm{v}\cdot\nabla)\mathrm{v}\right)}{\eta\nabla^2\mathrm{v}} = \frac{\rho r^2}{\eta\tau} + \frac{\rho \mathrm{v} r}{\eta} \tag{2-41}$$

where, r is the characteristic size of the channel in which the fluid is flowing, and τ is the time scale over which the velocity is changing (where $u/\tau = \partial u/\partial\tau$).

The Reynolds number is defined as,

$$R_e = \frac{\rho \mathrm{v} r}{\eta} \tag{2-42}$$

and is a measure of the characteristics of the fluid flow behaviour in the steady state, i.e. when $\tau\rightarrow\infty$ and gives an indication of the relative smoothness of the fluid flow (i.e. whether it is laminar or turbulent). For the case of the microfabricated flow channels used in this work, with at least one characteristic dimension in the micrometer range, and with low fluid velocities, it can be shown that the fluid flow is in the low Reynolds number regime ($R_e << 1$). At these low values of Reynolds number the inertial effects, which cause turbulence and secondary fluid flows, are negligible and viscous effects dominate the dynamics of the fluid. This type of flow is termed laminar.

For laminar flow (i.e. low Reynold's number flow) occurring in a system driven by a hydrostatic pressure difference applied along the length of the channel we get so called Pouiselle type flow. This is characterised by a parabolic flow profile across the channel, with the maximum flow velocity at the channel centre and zero flow velocity at the channel walls.

For a rectangular flow channel of width w, length l and height h the mean flow velocity at height y is given as [19],

$$\mathbf{v}_m = 6\langle \mathbf{v}_m \rangle \frac{y}{h}\left(1 - \frac{y}{h}\right) \tag{2-43}$$

where $<\mathbf{v}_m>$ is the mean velocity of the fluid and the bottom channel wall is taken to be $y=0$, and $y=h$ the top of the channel (see figure 2-11). Equation 2-43 assumes that the channel width and length are much greater than the channel height.

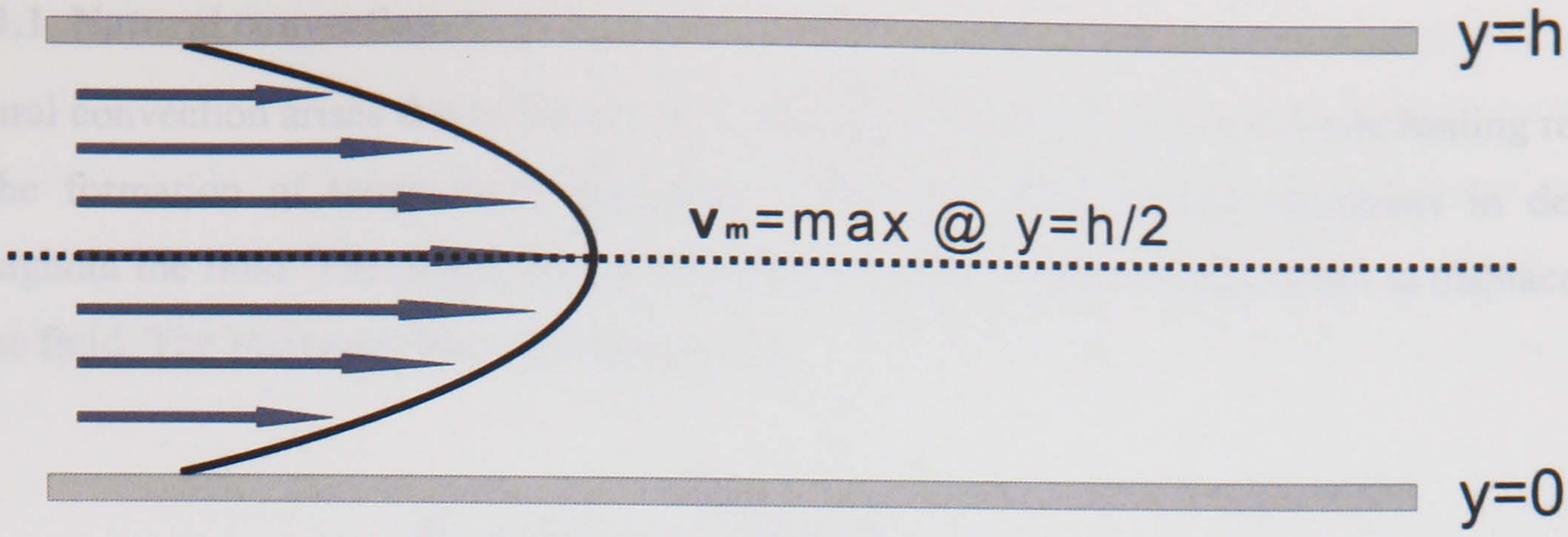

Figure 2-11. Parabolic flow profile characteristic of Pousielle type flow in a micro-channel.

The average volume flow rate Q is given by integrating the fluid velocities over the entire channel cross-section.

2.7 Electrohydrodynamic forces

Electrohydrodynamic (EHD) forces on fluids arise as a result of the interaction of the electric field with the solution causing fluid motion. Particles within the fluid experience drag forces from the fluid resulting in a force on the particle. The types of EHD forces are described below. See chapters six and eight in Morgan and Green's book [6] for a detailed description of EHD phenomena in microsystems.

2.7.1 Electrothermal forces

Due to the small size of the electrodes the application of relatively low voltages can produce very high electrical field strengths (~10^6V/m). These high field strengths can generate a large power dissipation in the fluid surrounding the electrode. The power generated per unit volume is proportional to the conductivity of the medium σ_m and the magnitude of the electric field E squared and is expressed as,

$$W = \sigma_m E^2 . \tag{2-44}$$

The electrical power density can be highly non-uniform due to the non-uniform fields produced by microelectrodes, with the highest power density localised at and close to the electrodes. This results in the formation of temperature gradients in the fluid, leading to gradients in viscosity, density, permittivity and conductivity of the fluid. These gradients can give rise to fluid flow in two ways, natural convection and electrothermal fluid flow.

2.7.1.1 Natural convection

Natural convection arises due to buoyancy forces acting on the fluid. Local Joule heating results in the formation of temperature gradients in the fluid that produce variations in density throughout the fluid. The denser fluid elements move due to gravitational forces to displace less dense fluid. The buoyancy force is expressed as,

$$\boldsymbol{F}_g = \Delta\rho_m \boldsymbol{g} = \frac{\partial\rho_m}{\partial T}\Delta T\boldsymbol{g} \tag{2-45}$$

where ΔT is the temperature rise.

Ramos *et al* [20] estimated the order of magnitude effect of natural convection and found that for all situations involving microelectrode structures, the effects of natural convection can be considered to be negligible when compared with electrical forces.

2.7.1.2 Electrothermal fluid flow

Electrothermal fluid flow arises due to local Joule heating giving rise to gradients in permittivity and conductivity. The electric field interacts with these gradients producing electrical forces. Depending upon the frequency range employed either Coulombic or dielectric forces predominate. The transition from the frequency region where Coulombic forces dominate to that where dielectric forces dominate occurs at a frequency of the order of the inverse of the charge relaxation time of the fluid given by,

$$\tau_c \approx \tau = \frac{\varepsilon}{\sigma} \tag{2-46}$$

2.7.2 AC electro-osmosis

Observation of the low-frequency behaviour of biological particles in DEP systems shows that the motion of the particles cannot be explained by DEP alone. It was assumed [21] that this motion was a result of low frequency negative DEP coupled with electrophoretic effects acting on the particles. Further investigation [20, 22-30] has revealed that these low frequency effects have their origin in fluid movement. The fluid motion described cannot however be explained by electrothermal effects alone.

Planar microelectrodes produce non-uniform electric fields. The electric field has both a normal and a tangential component to the electrode surface. A force similar to DC electro-osmosis

occurs at the electrode surface due to the force generated by the tangential component of the field acting on the double layer. The direction of this force is independent of the applied voltage since the sign of the excess charge in the double layer is always opposite to that of the charge on the electrode, with both the sign of the charge and the tangential component of the field changing every half cycle. The forces on the fluid are shown schematically in figure 2-12 below.

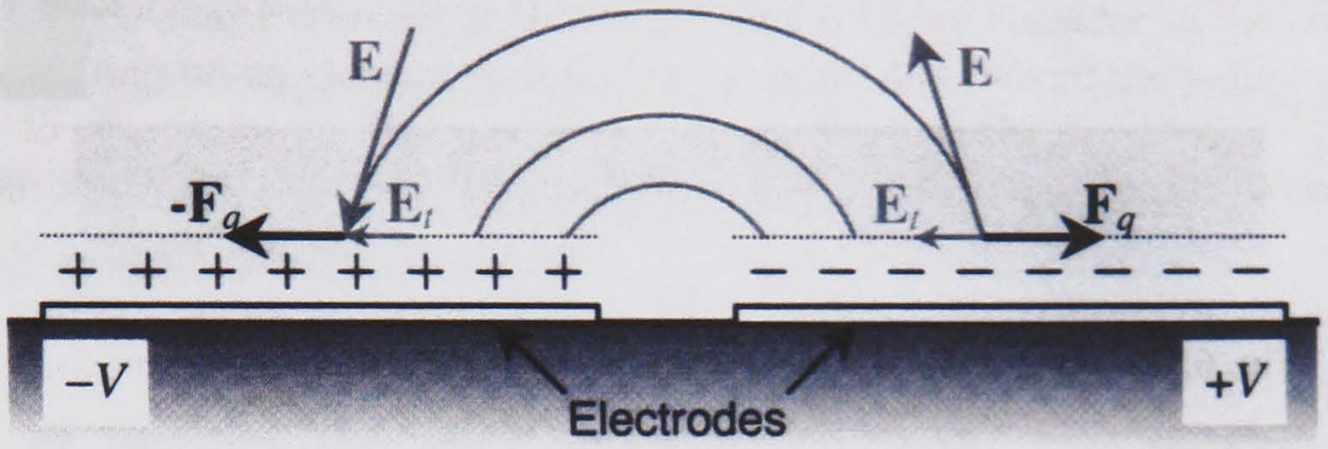

Figure 2-12. Schematic showing the forces acting in AC electroosmosis. Adapted from [6].

2.8 Brownian motion and diffusion

All particles in solution undergo Brownian motion, to a greater or lesser extent depending primarily on the particle size and viscosity of the suspending medium. This irregular motion is due to the transfer of kinetic energy (via random collisions) between the molecules of the fluid and the suspended particles. The collisions are irregular, with the time-averaged displacement being zero. Over time the particle distribution follows a Gaussian profile, with a mean squared displacement, in one dimension given by,

$$\left|\Delta\bar{x}\right|^2 = 2Dt \tag{2-47}$$

where D is the diffusion coefficient. For a sphere of radius a,

$$D = \frac{k_b T}{6\pi\eta a} \tag{2-48}$$

where k_b is the Boltzmann constant.

The equations of motion for an isolated particle suspended in a fluid above an array of DEP microelectrodes can be written in terms of four forces, the acceleration force, the fluid drag

force, the DEP force, and the random thermal force. Summation of these forces gives us the following equation

$$m\frac{d\,\mathbf{v}}{dt} = -f\,\mathbf{v} + \boldsymbol{F}_{DEP} + \boldsymbol{F}_{Brown} \tag{2-49}$$

where m is the mass of the particle, $\mathbf{v}$ the velocity, f the friction factor and $\boldsymbol{F}_{Brown}$ the random Brownian force, and $\boldsymbol{F}_{DEP}$ is the time averaged DEP force. Equation 2-49 is referred to as Langevin's equation [31]. The Langevin equation is only valid for calculations of the movement of single isolated particles. Solving this equation allows the calculation of the trajectories of single particles in microelectrode structures.

For ensembles of particles one must employ a statistical approach to predict particle distributions. The particle-conservation equation can be written as,

$$\frac{\partial c}{\partial t} + v \cdot \nabla c = -\nabla \cdot J_{Tot} \tag{2-50}$$

where c is the concentration of particles per unit volume and J_{Tot} is the total flux of particles comprising the diffusion, sedimentation and DEP fluxes,

$$\boldsymbol{J}_{Tot} = \boldsymbol{J}_{D} + \boldsymbol{J}_{g} + \boldsymbol{J}_{DEP} \tag{2-51}$$

where,

$$\boldsymbol{J}_{D} = -D\nabla c\,, \qquad \boldsymbol{J}_{g} = \frac{c\boldsymbol{F}_{g}}{6\pi\eta a}\,, \qquad \boldsymbol{J}_{DEP} = \frac{c\boldsymbol{F}_{DEP}}{6\pi\eta a}\,. \tag{2-52}$$

Here we are assuming that particle-particle interactions are negligible and can be ignored.

For the case of negative DEP the particle-conservation equation can be used to investigate the confinement of particles within potential energy minima. Particles can be trapped within a region of space whose surface is defined at positions where the thermal and electrical energies are equal. Particles lying outside this region can move freely as their thermal energy is greater than the dielectrophoretic potential energy. Within this region a particle's thermal energy is less than the DEP potential energy the result being that the particle will remain confined within the energy minima. For the case of negative DEP the particle-conservation equation can be expressed as [6],

$$-D\nabla c + \frac{c\boldsymbol{F}_{DEP}}{6\pi\eta a} = 0 \tag{2-53}$$

Equation 2-53 can be integrated to give the steady state concentration of particles across the channel

$$c(y) = C_1 exp\left(\int_0^h \frac{\boldsymbol{F}_{DEP}}{6\pi\eta a D} dy \right) \tag{2-54}$$

where C_1 is an integration constant and h is the channel height in the y direction. Further details of particle concentration profiles are given in chapter five, where the distribution of sub-micron particles between two arrays of interdigitated electrodes is modelled.

2.9 Dielectric models of real particles

2.9.1 Latex beads: surface conductance

For spherical linear solid homogeneous particles such as latex beads, the crossover frequency is related to the surface conductance of the particle. This allows the surface conductance of such particles to be determined from the measurement of their crossover frequency.

The *Clausius-Mossotti* factor f_{CM} and surface conductance K_s are given by the following expressions:

$$f_{CM} = \frac{\varepsilon_p^* - \varepsilon_m^*}{\varepsilon_p^* + 2\varepsilon_m^*} \tag{2-55}$$

and

$$\sigma_p = \frac{2K_s}{a} \tag{2-56}$$

where ε^* is the complex permittivity as described above, σ_p is the particle conductivity, ω is the angular frequency of the applied field and a is the particle radius [32, 33].

At the DEP crossover frequency f_x, the DEP force is zero and Re[f_{CM}] = 0. From equations 2-55 and 2-56, the relationship between bead surface conductance K_s and f_x is then:

$$K_s = \frac{r}{4}\left(-\sigma_m + \left[9\sigma_m^2 - 4\left(\left(\epsilon_p - \epsilon_m\right)\left(\epsilon_p + 2\epsilon_m\right)\left(2\pi f_x\right)^2\right)\right]^{\frac{1}{2}}\right) \quad (2\text{-}57)$$

where for latex ε_p is $2.56\varepsilon_0$, $\varepsilon_m = 78\varepsilon_0$, and ε_0 the permittivity of free space. Thus measurement of the crossover frequencies at a known suspending medium conductivity σ_m, allows K_s to be calculated.

2.9.2 Dielectric Shell models

In general real particles such as cells are not homogeneous in their electrical and physical properties. Take the case of the erythrocyte; in 1913 Höber showed that this cell type could be represented as a conducting sphere surrounded by a resistive membrane. In 1891, Maxwell demonstrated that such a concentric system could be replaced by a homogeneous sphere of the same external radius and effective resistance r_p [3]. This "smeared-out" sphere can be substituted for a heterogeneous sphere without altering the externally applied electric field. Wagner [34] extended the work of Maxwell and derived the effective complex permittivity of a system composed of particles dispersed in a dielectric medium. This theory, and that of a multishell model for cells was further developed [35-39], more recently by Huang *et al* [40]. An ellipsoidal multishell model has also been presented in the literature (e.g. [41]).

2.9.2.1 The spherical multishell model

Biological cells are complex living system and compartmentalisation of their interiors is an integral property of all eukaryotic cells. However, the heterogeneous nature of the cell can be simplified somewhat, with the cell being described as a particle comprised of an outer membrane, composed of lipid molecules, proteins, ion channels, and sugar molecules. This outer membrane encloses the cell interior, comprised of an aqueous cytoplasm rich in ions. Within this cytoplasm lies the cell nucleus comprised of a nuclear membrane, which in turn surrounds the aqueous nucleoplasm as shown in figure 2-13. The membranes actively transport ions across themselves maintaining the differences in the properties of the various cell compartments. This represents a simplified description of the cell but one that has been shown to allow the accurate modelling of biological cells in electric fields in the frequency region encountered in this work.

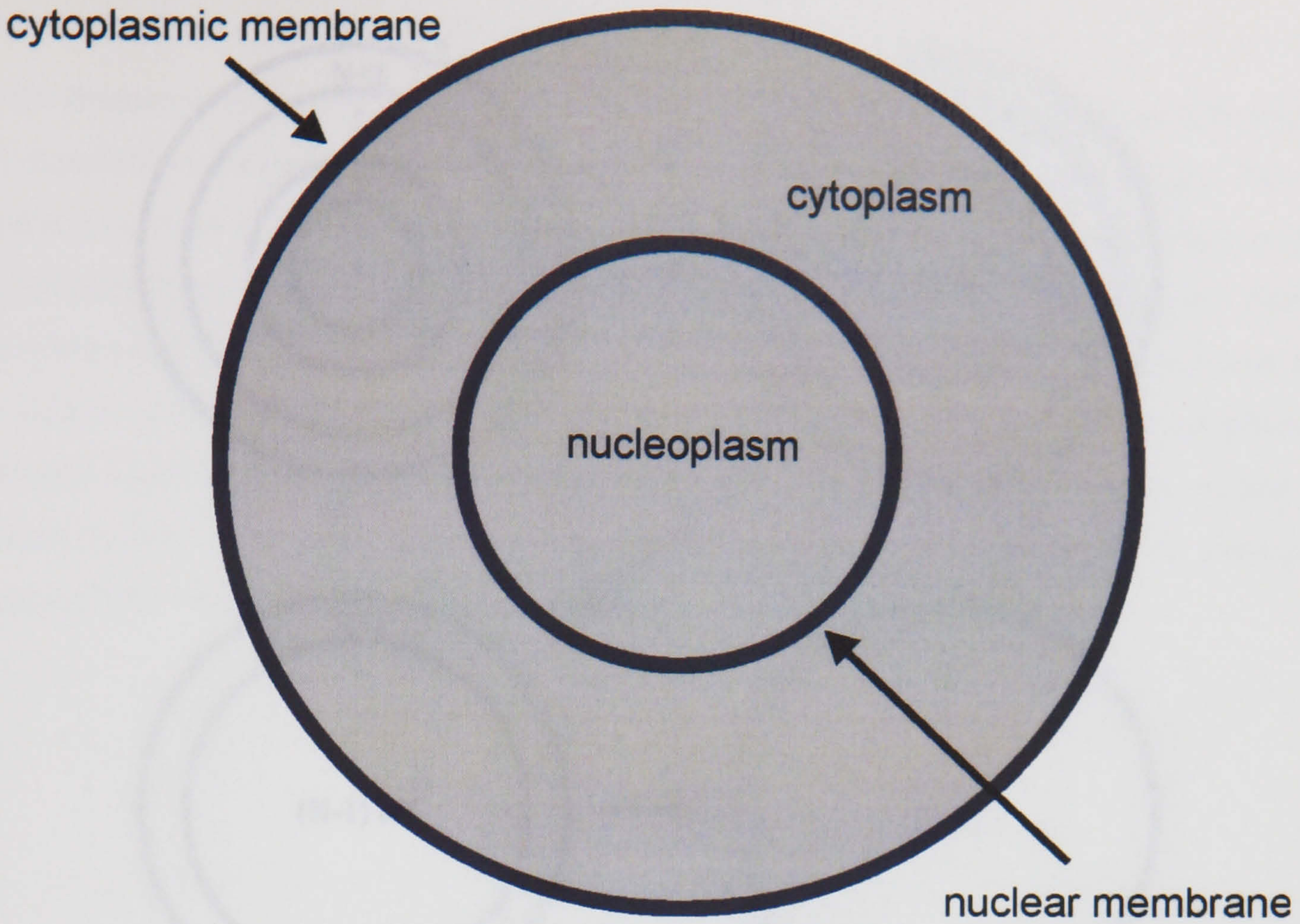

Figure 2-13. Simplified model of a cell.

The spherical multishell model can be used to describe the dielectric properties of cells. If we assume the cell geometry is spherical and the different parts are concentric in their orientation, the spherical multishell model is as follows [37, 40, 42]:

$$\varepsilon^*_{peff} = \varepsilon^*_{Neff} = \varepsilon^*_{N+1}\left[\frac{\left(\frac{R_{N+1}}{R_N}\right)^3 + 2\left(\frac{\varepsilon^*_{N-1eff} - \varepsilon^*_{N+1}}{\varepsilon^*_{N-1eff} + 2\varepsilon^*_{N+1}}\right)}{\left(\frac{R_{N+1}}{R_N}\right)^3 - \left(\frac{\varepsilon^*_{N-1eff} - \varepsilon^*_{N+1}}{\varepsilon^*_{N-1eff} + 2\varepsilon^*_{N+1}}\right)}\right] \tag{2-58}$$

where ε^*_{Neff} is the effective complex permittivity of the N-shelled sphere model. R_N and R_{N+1} is the radius of the Nth-shell and the N+1th shell respectively. ε^*_{N-1eff} is the effective complex permittivity of the N-1th shell working from the innermost shell. ε^*_{N+1eff} is the effective complex permittivity of the N+1th shell. Figure 2-14 shows the N-shelled model.

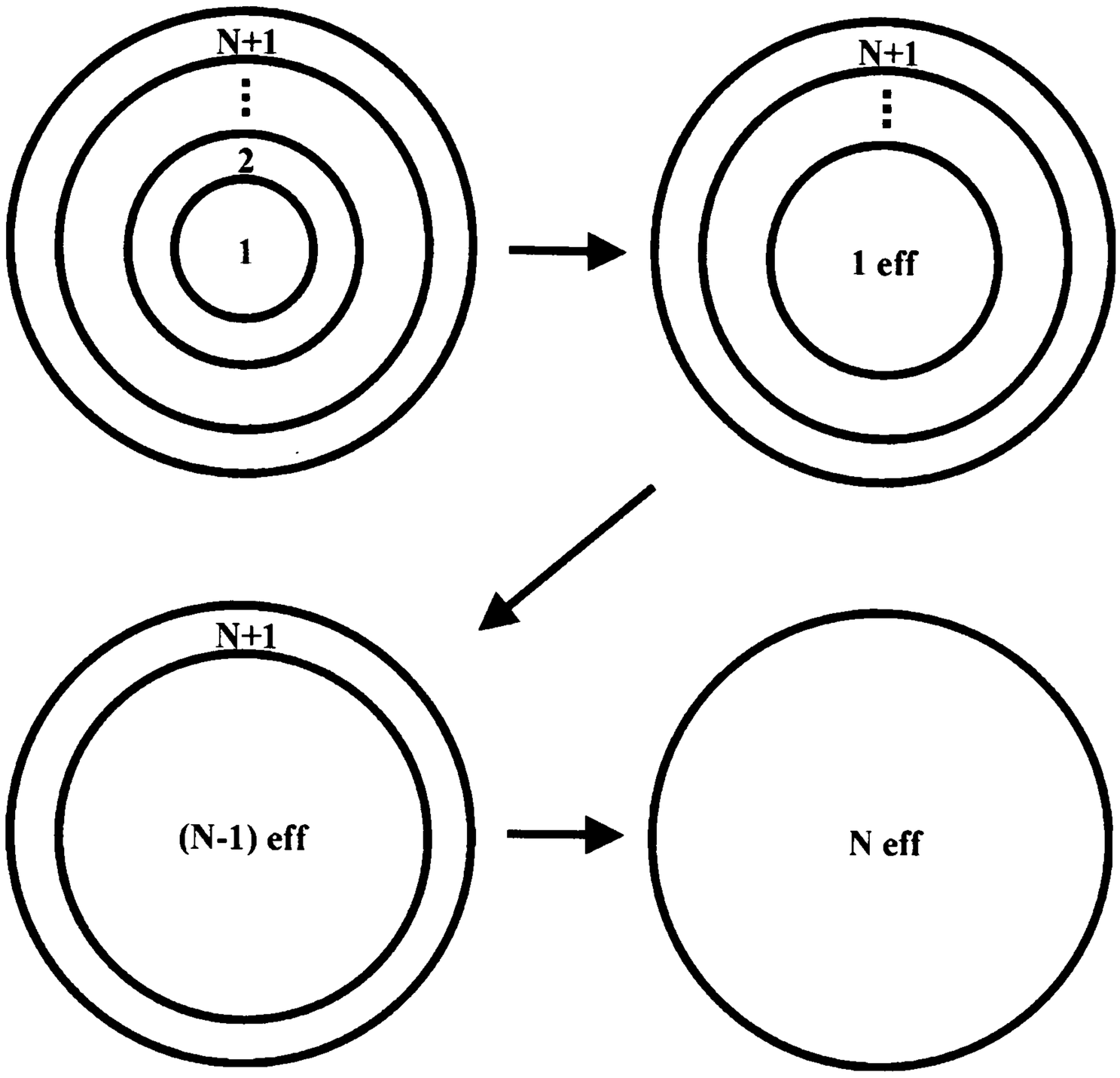

Figure 2-14. Multi-shell model of a spherical dielectric particle.

2.9.2.2 Ellipsoidal multishell model

The above spherical shell model is a special case of the more general ellipsoidal multishell model. Particles may be better modelled using the ellipsoidal model [41] if the particles are distinctly non-spherical, as in the case of certain bacteria. Erythrocytes can be approximated using the ellipsoidal model, however the results are generally not good due to the lack of a more suitable oblate spheroid model. We shall not describe the details of the ellipsoidal model, as it was not used in the present work, suffice it to say that if more detailed descriptions of the properties of non-spherical particles are required this model is available.

2.9.3 Dielectrophoretic cross-over frequency

When there is no translational force acting on a particle, the complex permittivity of the particle and that of the suspending medium are equal. Measurement of the frequency at which this zero net force condition arises allows the calculation of various dielectric properties of the particle under investigation. For the case of a biological cell a value of membrane capacitance can be calculated. For particles such as latex beads a useful parameter, that of surface conductance can be obtained as described above.

2.9.3.1 Membrane capacitance of a cell

As the frequency of the non-uniform AC electric field increases, a particle such as a biological cell experiences a translation force pushing it towards the low field intensity region. The cell experiences negative DEP because the complex permittivity of the cell membrane is less than the complex permittivity of the suspending medium. As the frequency of the applied electric field increases further it becomes sufficiently high to penetrate through the cell membrane into the interior of the cell (into the cytoplasm) where the complex permittivity of the cytoplasm is generally higher than that of the suspending medium (typically $\sigma_{cyto}>\sigma_m$). When this occurs the translation force will move the cell toward the high field intensity region; the cell undergoes positive DEP. There are two interfaces and therefore two dispersions.

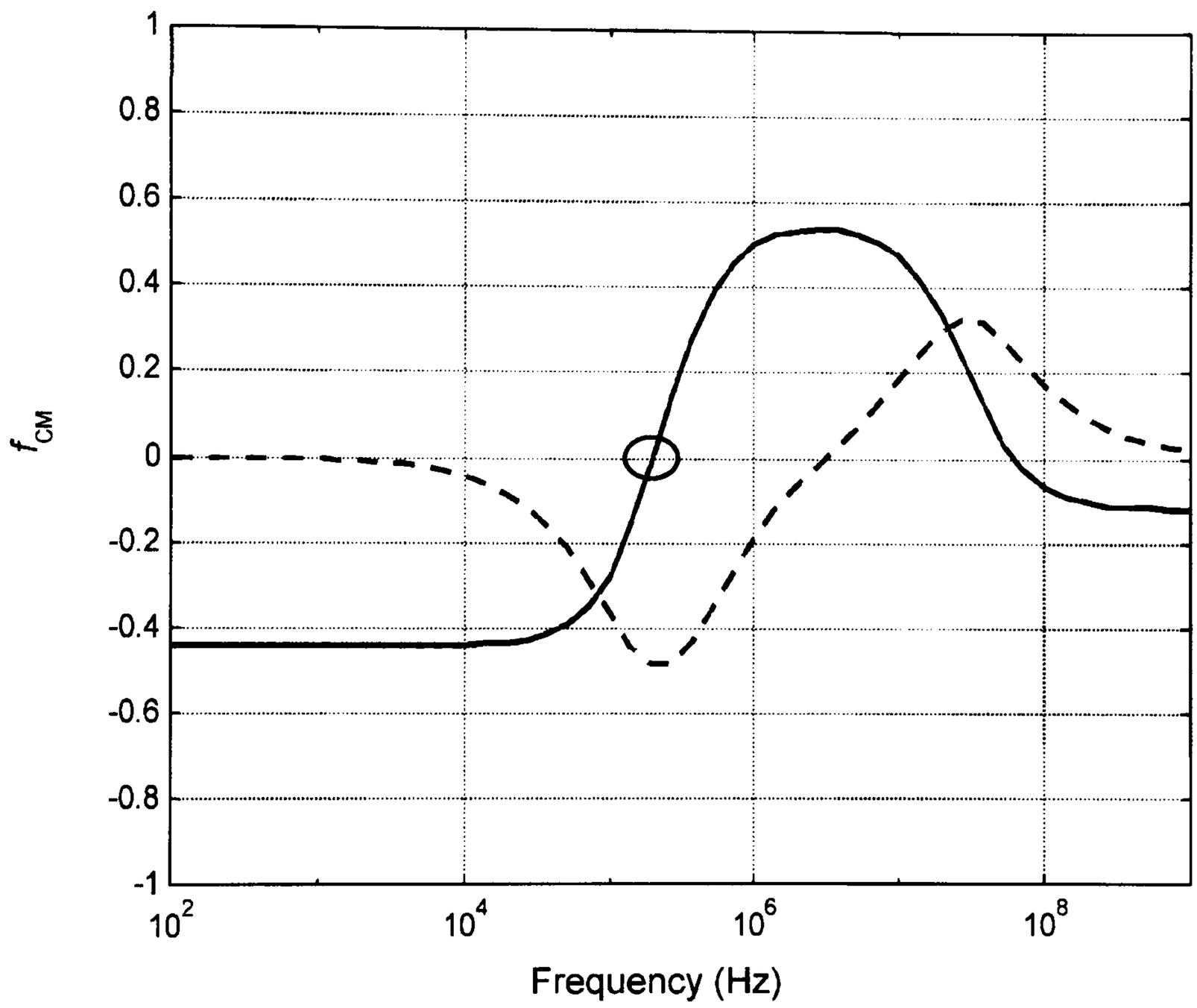

Figure 2-14. The real (solid) and imaginary (dashed) values of the Clausius-Mossotti factor versus frequency for a typical human lymphocyte. Circle shows crossover frequency point for the cytoplasmic membrane.

As the translation force changes from negative DEP to positive DEP, there is a transition period where no net force acts on the cell. This zero force point, known as the dielectrophoretic crossover frequency, occurs because the complex permittivities of the cell and the suspending medium are the same, and the net translation force disappears. Figure 2-14 shows the real and imaginary parts of the *Clausius-Mossotti* factor versus frequency for a biological cell suspended in a low conductivity medium.

Measurement of the dielectrophoretic crossover frequency allows the value of the membrane capacitance of the cell to be calculated. Gimsa [42] gave the first theoretical description of this and others have also given descriptions of the theory (e.g. [43]).

As the complex permittivity of the particle and that of the medium are equal, the real part of the *Clausius-Mossotti* factor is equal to zero, i.e.

$$Re\left(\frac{\epsilon_p^* - \epsilon_m^*}{\epsilon_p^* + 2\epsilon_m^*}\right) = 0\,. \tag{2-59}$$

Substitution for the complex permittivity and rearranging gives the angular frequency of the DEP cross-over frequency as,

$$\omega_x = \left(\frac{(\sigma_m - \sigma_p)(\sigma_p + 2\sigma_m)}{(\varepsilon_0\varepsilon_p - \varepsilon_0\varepsilon_m)(\varepsilon_0\varepsilon_p + 2\varepsilon_0\varepsilon_m)}\right)^{\frac{1}{2}} \tag{2-60}$$

for which the DEP cross-over frequency is $f_x = \frac{\omega_x}{2\pi}$.

Use of the generalised dielectric shell model [40],

$$\varepsilon_p^* = \varepsilon_{mem}^*\left[\frac{\left(\frac{R}{R-d}\right)^3 + 2\left(\frac{\varepsilon_{in}^* - \varepsilon_{mem}^*}{\varepsilon_{in}^* + 2\varepsilon_{mem}^*}\right)}{\left(\frac{R}{R-d}\right)^3 - \left(\frac{\varepsilon_{in}^* - \varepsilon_{mem}^*}{\varepsilon_{in}^* + 2\varepsilon_{mem}^*}\right)}\right] \tag{2-61}$$

where ε_{in}^* and ε_{mem}^* are the complex permittivities of the cell interior and the cell membrane respectively. R and d are the radius of the cell and thickness of the cytoplasmic membrane respectively.

From the above the membrane capacitance of the cell can be calculated. The cytoplasmic membrane of a cell is a thin poorly conducting envelope of low relative permittivity, whereas the cell interior is of relatively high conductivity and permittivity in comparison. At frequencies well below the typical Maxwell-Wagner relaxation frequency for a cell (<1MHz)

$$\left(\frac{\varepsilon_{in}^{*}-\varepsilon_{mem}^{*}}{\varepsilon_{in}^{*}+2\varepsilon_{mem}^{*}}\right)\approx 1. \tag{2-62}$$

The radius R of the cell is substantially larger than the thickness of the cytoplasm d. Taking this into consideration allows us to write equation 2-61 in a simplified form giving the complex permittivity of the cell as,

$$\varepsilon_{p}^{*}=\varepsilon_{mem}^{*}\left(\frac{R}{d}\right) \tag{2-63}$$

where the specific membrane capacitance (capacitance per unit area) can be written as,

$$C_{Smem}=\frac{\varepsilon_{mem}}{d}. \tag{2-64}$$

The permittivity of the cell can thus be described in terms of the specific membrane capacitance.

$$\varepsilon_{p}=C_{Smem}R. \tag{2-65}$$

Given the condition that the conductivity of the medium is very high compared to that of the membrane and $\sigma_{p}\approx 0$, then

$$f_{x}=\frac{\sigma_{m}}{\pi\sqrt{2}\varepsilon_{p}}. \tag{2-66}$$

Substituting 2-65 into 2-66 gives an expression for the specific membrane capacitance of a cell in terms of three measurable quantities; medium conductivity, size and cross-over frequency,

$$C_{Smem}=\frac{\sigma_{m}}{\pi\sqrt{2}f_{x}R}. \tag{2-67}$$

2.10 References

1. Debye, P., *Polar Molecules*. 1947, New York: Dover.
2. Feynman, R.P., R.B. Leighton, and M. Sands, *The Feynman lectures on physics*. 1965: Addison-Wesley Publishing Company.
3. Maxwell, J.C., *A Treatise on Electricity and Magnetism*. Vol. 1. 1881, Oxford: Clarendon Press.
4. Jones, T.B., *Electromechanics of Particles*. 1995, Cambridge: Cambridge University Press.
5. Pethig, R., *Dielectric and electronic properties of biological materials*. 1979, Chichester: John Wiley & Sons.
6. Morgan, H. and N.G. Green, *AC Electrokinetics: Colloids and Nanoparticles*. 1 ed. Microtechnologies and Microsystems Series, ed. R. Pethig. 2003, Baldock, UK: Research Studies Press.
7. Pohl, H.A., *Dielectrophoresis*. 1978, Cambridge: Cambridge University Press.
8. Hartley, L.F., K. Kaler, and R. Paul, *Quadrupole levitation of microscopic dielectric particles*. Journal of Electrostatics, 1999. **46**(4): p. 233-246.
9. Jones, T.B. and M. Washizu, *Multipolar dielectrophoretic and electrorotation theory*. Journal of Electrostatics, 1996. **37**(1-2): p. 121-134.
10. Schnelle, T., T. Muller, and G. Fuhr, *Trapping in AC octode field cages*. Journal of Electrostatics, 2000. **50**(1): p. 17-29.
11. Morgan, H., *et al.*, *The dielectrophoretic and travelling wave forces generated by interdigitated electrode arrays: analytical solution using Fourier series (vol 34, pg 1553, 2001)*. Journal of Physics D-Applied Physics, 2001. **34**(17): p. 2708-2708.
12. Morgan, H., *et al.*, *The dielectrophoretic and travelling wave forces generated by interdigitated electrode arrays: analytical solution using Fourier series*. Journal of Physics D-Applied Physics, 2001. **34**(10): p. 1553-1561.
13. Markx, G.H., R. Pethig, and J. Rousselet, *The dielectrophoretic levitation of latex beads, with reference to field-flow fractionation*. Journal of Physics D-Applied Physics, 1997. **30**(17): p. 2470-2477.
14. Cui, L., D. Holmes, and H. Morgan, *The dielectrophoretic levitation and separation of latex beads in microchips*. Electrophoresis, 2001. **22**(18): p. 3893-3901.
15. Wang, X.B., *et al.*, *Separation of polystyrene microbeads using dielectrophoretic/gravitational field-flow-fractionation*. Biophysical Journal, 1998. **74**(5): p. 2689-2701.
16. Huang, Y., *et al.*, *Introducing dielectrophoresis as a new force field for field- flow fractionation*. Biophysical Journal, 1997. **73**(2): p. 1118-1129.
17. Clague, D.S. and E.K. Wheeler, *Dielectrophoretic manipulation of macromolecules: The electric field - art. no. 026605*. Physical Review E, 2001. **6402**(2): p. 6605-+.

18. Garcia, M. and G. Clague, *The 2D electric field above a planar sequence of independent strip electrodes.* Journal of Physics D-Applied Physics, 2000. **33**(14): p. 1747-1755.

19. Schimpf, M.E., K. Caldwell, and J.C. Giddings, *Field-Flow Fractionation Handbook.* 1 ed. 2000: John Wiley & Sons. 560.

20. Ramos, A., *et al.*, *Ac electrokinetics: a review of forces in microelectrode structures.* Journal of Physics D-Applied Physics, 1998. **31**(18): p. 2338-2353.

21. Pethig, R., *et al.*, *Positive and Negative Dielectrophoretic Collection of Colloidal Particles Using Interdigitated Castellated Microelectrodes.* Journal of Physics D-Applied Physics, 1992. **25**(5): p. 881-888.

22. Green, N.G. and H. Morgan, *Separation of submicrometre particles using a combination of dielectrophoretic and electrohydrodynamic forces.* Journal of Physics D-Applied Physics, 1998. **31**(7): p. L25-L30.

23. Green, N.G. and H. Morgan, *Sub-micrometre AC electrokinetics*, in *Proceedings of the 20th Annual International Conference of the Ieee Engineering in Medicine and Biology Society, Vol 20, Pts 1-6 - Biomedical Engineering Towards the Year 2000 and Beyond.* 1998, I E E E: New York. p. 2974-2977.

24. Green, N.G., *et al.*, *Sub-micrometre ac electrokinetics: particle dynamics under the influence of dielectrophoresis and electrohydrodynamics*, in *Electrostatics 1999.* 1999, Iop Publishing Ltd: Bristol. p. 89-92.

25. Green, N.G., *et al.*, *Fluid flow induced by nonuniform ac electric fields in electrolytes on microelectrodes. I. Experimental measurements.* Physical Review E, 2000. **61**(4): p. 4011-4018.

26. Green, N.G., *et al.*, *Electric field induced fluid flow on microelectrodes: the effect of illumination.* Journal of Physics D-Applied Physics, 2000. **33**(2): p. L13-L17.

27. Green, N.G., A. Ramos, and H. Morgan, *Ac electrokinetics: a survey of sub-micrometre particle dynamics.* Journal of Physics D-Applied Physics, 2000. **33**(6): p. 632-641.

28. Ramos, A., *et al.*, *Fluid flow driven by a.c. electric fields in microelectrodes*, in *Electrostatics 1999.* 1999, Iop Publishing Ltd: Bristol. p. 137-140.

29. Ramos, A., *et al.*, *The role of electrohydrodynamic forces in the dielectrophoretic manipulation and separation of particles.* Journal of Electrostatics, 1999. **47**(1-2): p. 71-81.

30. Ramos, A., *et al.*, *AC electric-field-induced fluid flow in microelectrodes.* Journal of Colloid and Interface Science, 1999. **217**(2): p. 420-422.

31. Langevin, P.C.R., C.R. Academy of Science, 1908. **146**: p. 530.

32. O'Konski, C.T., *Electric properties of macromolecules V: theory of ionic polarization in polyelectrolytes.* Journal of Physical Chemistry, 1960. **64**: p. 605-619.

33. Hughes, M.P., H. Morgan, and M.F. Flynn, *The dielectrophoretic behavior of submicron latex spheres: Influence of surface conductance.* Journal of Colloid and Interface Science, 1999. **220**(2): p. 454-457.

34. Wagner, K.W., *Erklarung der Dielectrischen Nachwirkungsvorgange auf Grund Maxwellsher Forstellungen.* Archiv Elektrotechnik, 1914. **2**: p. 371-389.

35. Fricke, H., *A Mathematical Treatment of the Electric Conductivity and Capacity of Dispersive Systems.* Phys Rev, 1924. **24**: p. 575-587.

36. Hanai, T., *Theory of Dielectric Dispersion Due to Interfacial Polarisation and its Application to Emulsion.* Kolloid Z, 1960. **171**: p. 23-31.

37. Irimajiri, A., T. Hanai, and A. Inouye, *A Dielectric Theory of 'Multi-Stratified Shell' Model with its Application to a Lymphoma Cell.* Journal of Theoretical Biology, 1979.

38. Pauly, H. and Schwan.H.P., Biophysical Journal, 1966. **6**: p. 621-639.

39. Schwan, H.P., *et al.*, Journal of Physical Chemistry, 1962. **66**: p. 2626-2635.

40. Huang, Y., *et al.*, *Differences in the AC electrodynamics of viable and non-viable yeast cells determined through combined dielectrophoresis and electrorotation studies.* Physics in Medicine and Biology, 1992. **37**(7): p. 1499-1517.

41. Kakutani, T., S. Shibatani, and M. Sugai, *Electrorotation of Nonspherical Cells - Theory For Ellipsoidal Cells With an Arbitrary Number of Shells.* Bioelectrochemistry and Bioenergetics, 1993. **31**(2): p. 131-145.

42. Gimsa, J., *et al.*, *Dielectrophoresis and Electrorotation of Neurospora Slime and Murine Myeloma Cells.* Biophysical Journal, 1991. **60**(4): p. 749-760.

43. Gascoyne, P.R.C., *et al.*, *Use of Dielectrophoretic Collection Spectra For Characterizing Differences Between Normal and Cancerous Cells.* Ieee Transactions On Industry Applications, 1994. **30**(4): p. 829-834.

Chapter Three: Materials and methods

3 Introduction

This chapter gives details of the biological protocols used in the rest of this thesis. All blood and placental samples were obtained from patients at the Queen Mother's Hospital, Yorkhill or Glasgow Royal Infirmary (GRI) following informed written consent. The Yorkhill Ethics Committee and Glasgow Royal Infirmary Ethics Committee approved all procedures.

Cord blood samples were obtained and experiments using these samples were carried out while visiting the lab of Dr. Diana Bianchi, at the New England Medical Center (NEMC, Tufts University, Boson, MA, USA) over a period of three weeks in November 1999. Samples were obtained, following the appropriate ethical guidelines as set down by NEMC.

Members of the Bioelectronics group in the Department of Electronics at Glasgow University and research staff from the department of Obstetrics and Gynaecology at the GRI kindly donated all the other blood samples.

All reagents were purchased from Sigma unless stated otherwise.

3.1 Preparation of single cell suspensions from human tissue samples

Tissue samples or other collections of cells often require pre-treatment in order to obtain a mono-disperse sample of the cells. In the case of blood samples, or free-floating culture systems, the cells are already freely suspended in the medium and can easily be re-dispersed in a variety of media. However, the cells of interest are often contained within complex three-dimensional tissue structures, held in place by cell:cell and cell:matrix interactions [1]. A variety of strategies exist to liberate cells from these local attachments. There are three basic methods:

- Mechanical – the tissue is cut, minced, or forced through filters.
- Chemical – divalent cations (e.g. Ca^{2+}, Mg^{2+}) are removed by washing or chelating.
- Digestive – enzymes are used to digest components of the extracellular matrix.

In practice a combination of the above methods are usually required to obtain satisfactory results.

3.1.1 Peripheral blood mononuclear cells (PBMCs) from whole blood

Blood samples were obtained via vein puncture from healthy volunteers. As discussed in chapter one, blood comprises a variety of cell types. These cells can be separated into subpopulations based on differences in cell density [2]. The use of a commercially available media, Histopaque-1077 (a Ficoll based density media) allows the isolation of mononuclear cells (monocytes, T-lymphocytes, B-lymphocytes) from the more dense erythrocytes and polymorphonuclear cells (granulocytes).

Blood samples were processed as follows:

- 5ml of whole blood was collected into a sterile Vacutainer™ tube (Becton Dikinson) containing 4.5mg of EDTA, and inverted several times to ensure mixing.
- Blood was diluted 1:2 with PBS (0.1% w/v EDTA).
- 5ml of diluted blood was pipetted into a centrifuge tube and then gently underlaid with 5ml of Histopaque-1077.
- Centrifuged for 20min at 600g.
- The "buffy coat" (band containing the PBMCs at the blood/Histopaque interface) was pipetted off and resuspended in 10ml Puck's Saline A (PSA) with 25mM Hepes buffer (pH=7.4, Gibco).
- This was centrifuged for 15min at 500g to remove the supernatant (and any residual Histopaque) and the cell pellet resuspended in either fresh PSA or desired media.

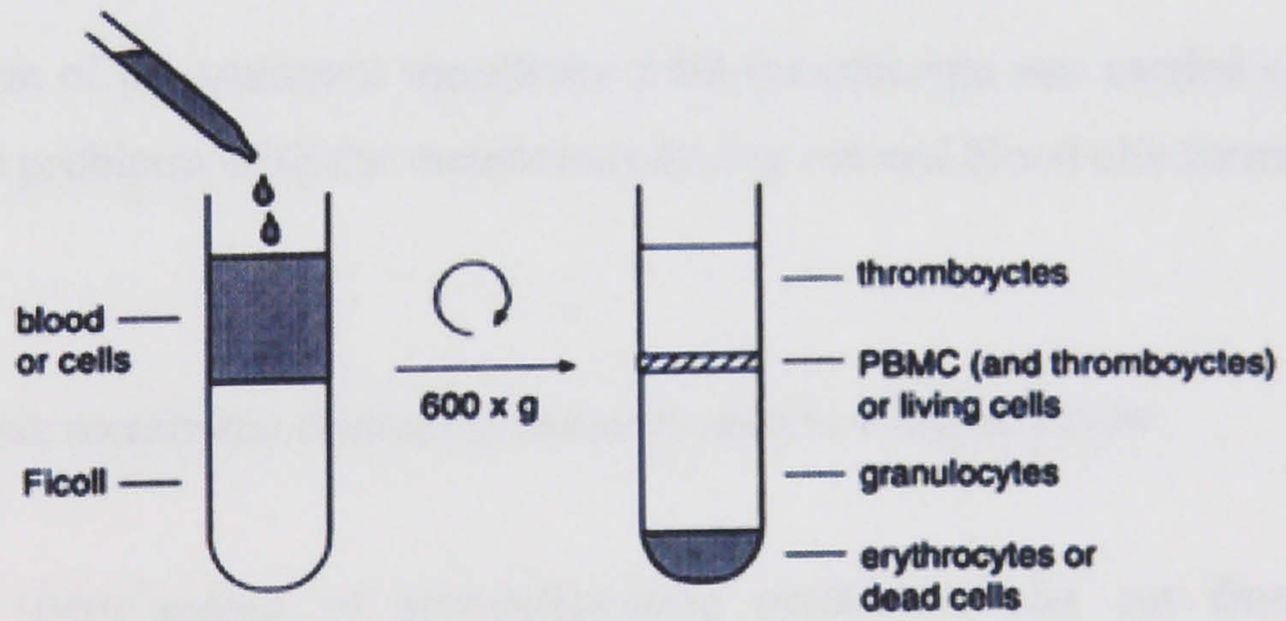

Figure 3-1. Density gradient centrifugation, and the positions of various cell types following centrifugation over Histopaque-1077. The "buffy coat" contains the PBMC layer [3].

EDTA was used as an anti-coagulant. There is little difference between EDTA, Acid citrate dextrose or heparin anticoagulants when working with fresh blood samples. However, EDTA has been shown to be unsuitable for blood storage as it leads to contamination of the PBMC density gradient fraction with RBCs [4].

3.1.2 Retrieval of trophoblast cells from the amnion-chorionic membranes of the human placenta

Normal term placentas were obtained immediately after delivery following Caesarean section or spontaneous vaginal delivery. The cytotrophoblast cells were prepared from the amniochorionic membranes of the placenta (these membranes are attached to the placenta and form the sack surrounding the foetus) using a combination of mechanical and enzymatic digestion techniques [5, 6]. A schematic showing the anatomy of the placenta and the position of these membranes is shown in figure 3-2.

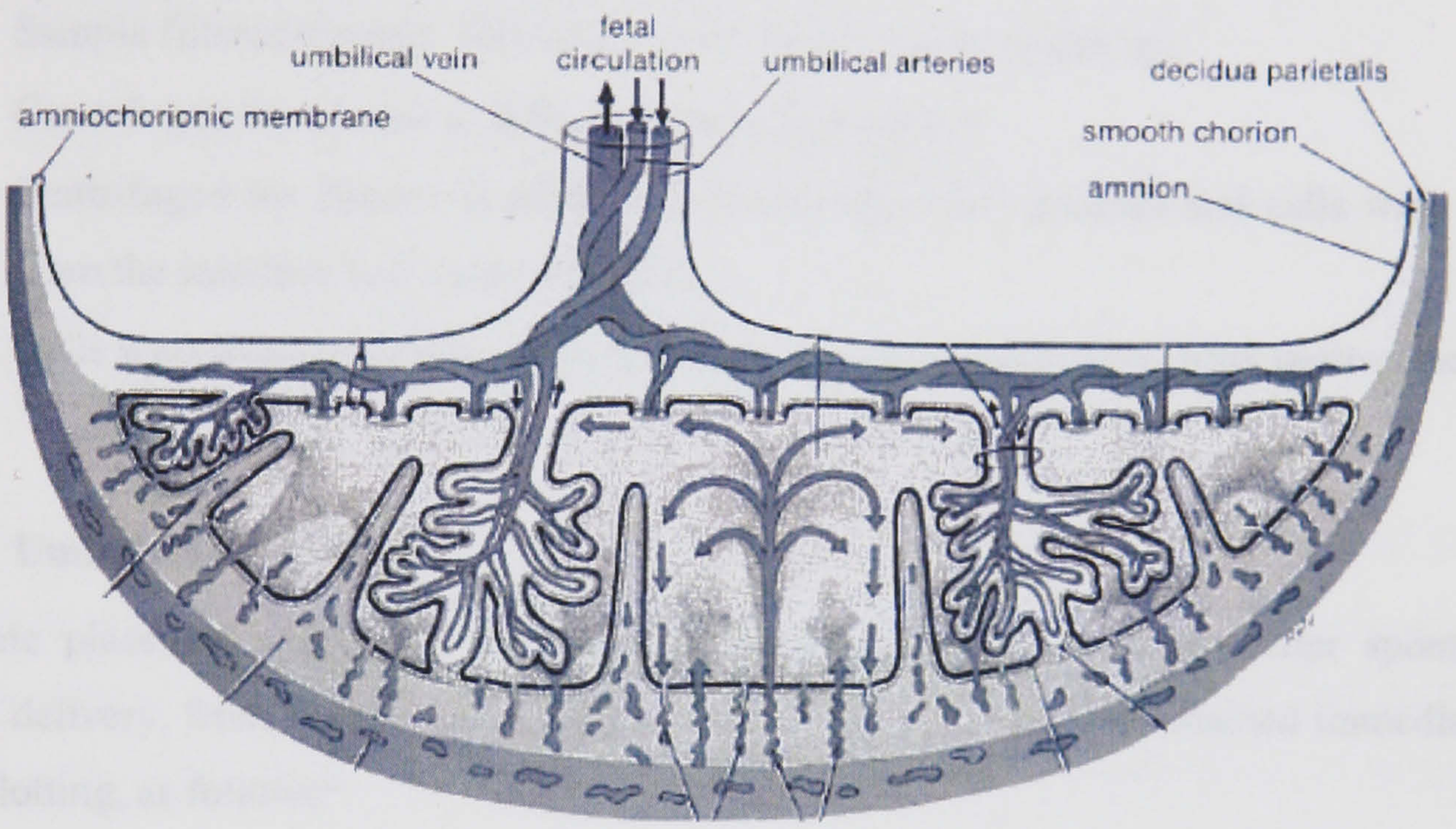

Figure 3-2. Drawing of the placenta showing the amniochorionic membranes [17].

The initial isolation of the amnionic membrane from the placenta was carried out on the labour ward, to avoid the problems with the membranes drying out and blood clot formation.

The amniochorionic membrane dissection protocol used is outlined below:

- 10cm x 10cm pieces of amniochorionic membrane was cut from the placental membranes.
- The amnionic and chorionic membranes were carefully separated (pealed apart) and the chorionic membranes retained.
- The decidua and any blood were gently scraped from surfaces of chorionic membranes using a large flat razor blade.
- Chorionic membranes were washed in PBS and placed in RPMI-1640 culture medium (with 25mM Hepes buffer (pH=7.4), 5% foetal calf serum (FCS)) for transport to lab.

The enzymatic digestion of chorionic membranes was performed in the lab, as follows:

- Chorionic membrane was placed in a universal tube containing 1mg/ml of protease type XXIV (P-8038) in RPMI for 1 hour at 37°C in a 6% CO_2 incubator and agitated gently every 15 min.
- PBS wash to remove enzyme.
- Membrane was placed into a universal tube containing 1mg/ml collagenase type IV (C-5138), 2mg/ml hyaluronidase (H-3506) in RPMI for 90mins at 37°C in 6% CO_2 incubator and agitated gently every 15 min.
- Sample filtered through 100μm gauze to remove tissue fragments.
- Centrifuged for 15mins at 500g to remove supernatant
- Centrifuged for 20mins at 600g on a Histopaque-1077 gradient and cells were collect from the interface and washed in PSA.
- Cells were resuspended to required density in culture medium or other desired media.

3.1.3 Umbilical cord blood

Complete placentas with attached umbilical cord were obtained directly after spontaneous vaginal delivery, from healthy non-smokers. Cord blood samples were obtained immediately to avoid clotting, as follows:

- The end of the cord proximal to the placenta was clamped.
- The placenta was raised with the cord hanging downward.
- Blood within the cord was forced out by squeezing, starting at the proximal end of the cord and moving distally.
- Cord blood was collected, via a plastic collection funnel, into a sterile tube containing 4.5mg of sodium citrate and inverted several times to ensure good mixing.
- Blood samples were stored at 4°C until required (for a maximum of 4 hours).

3.2 Culture of human mononuclear cells

The mononuclear cell line, THP-1 was used. These cells were grown and maintained in culture from an initial gift of cells provided by Ms. S. Robertson and Ms. S. Kitsen at the Deptartment of Haematology, Glasgow Royal Infirmary. The cell lines grow and divide while free-floating in suspension. The fact that these cells grow in suspension and do not require attachment to a solid substrate, means that they can be harvested with the minimum amount of processing.

It should be noted that the convenience of harvesting these cells and using them for experiments, instead of obtaining fresh blood samples, is countered by the need to maintain the cultures. Sterile technique was used throughout to avoiding contamination [7].

3.2.1 THP-1

The THP-1 cell line is a mononuclear cell line derived from a human monocytic leukaemia. These cells will divide and survive indefinitely if kept under suitable conditions.

The following culture medium was prepared and stored in the refrigerator at 4°C:

- 500ml of RPMI-1640 (25mM Hepes and $NaHCO_3$) with,
  - 5ml L-glutamine.
  - 5ml Penicillin/Streptomycin.
  - 2-5ml Fungizone or Amphotocerin B.

Initial samples of cells ("seeds") were obtained from a continuous culture held at the GRI. These cells were resuspended in a sterile culture flask containing 30-50ml of the above culture medium supplemented with 10% foetal calf serum (FCS) (FCS is a nutrient used to feed the cells, and was defrosted and added to the above media just prior to resuspension of the cells).

The cells were then maintained at 37°C in an incubator with 5% CO_2 atmosphere. Every few days the cells were observed using a light microscope and split if necessary. Cells were harvested just prior to experiments and resuspended in the desired media at the required cell concentrations.

3.3 Culture of bacteria - *E.Coli*, K-12

E.coli bacteria were grown in culture. To aid visualisation the bacteria were genetically transformed to express Green Fluorescent Protein (GFP), and selectively cultured to produce a population of cells, all of which expressed GFP. A kit was obtained from Bio-Rad containing all the necessary reagents and a sample of lyophilised *E.coli* K-12 strain.

An outline of the procedure for culture and transformation of the *E.coli* cells is given below, for more detail the reader is referred to the Bio-Rad manual, "Bacterial Transformation The pGLO™ System" [8].

The host organism *E.coli* K-12 strain, the vector coding the recombinant GFP protein, and the subsequent transformants created by their combination are non-pathogenic. As with the mononuclear cell culture, sterile culture techniques were used throughout.

The protocol for culture and transformation of the *E.coli* was as follows:

- Grew *E.coli* K-12 (NCTC 10538) overnight on agar to produce competent cells.
- Picked single colony and dispersed in 250µL of $CaCl_2$ (50mM, pH 7.4) in a micro-centrifuge tube.
- Added 1µl of plasmid vector solution to the tube. Incubated on ice for 10mins.
- Heatshocked tube at 42°C for 50s in a waterbath.
- Removed from water bath and incubated on ice for 2mins
- Removed from ice. Added 250µl of LB broth to the tube. Incubated at room temp. for 10mins.
- Plated 100µl of the transformed solution on an LB agar plate (supplemented with ampicillin and arabinose).
- Incubated overnight at 37°C.
- Following day checked for growth and fluorescence.

Figure 3-3 shows the transformation process in schematic form.

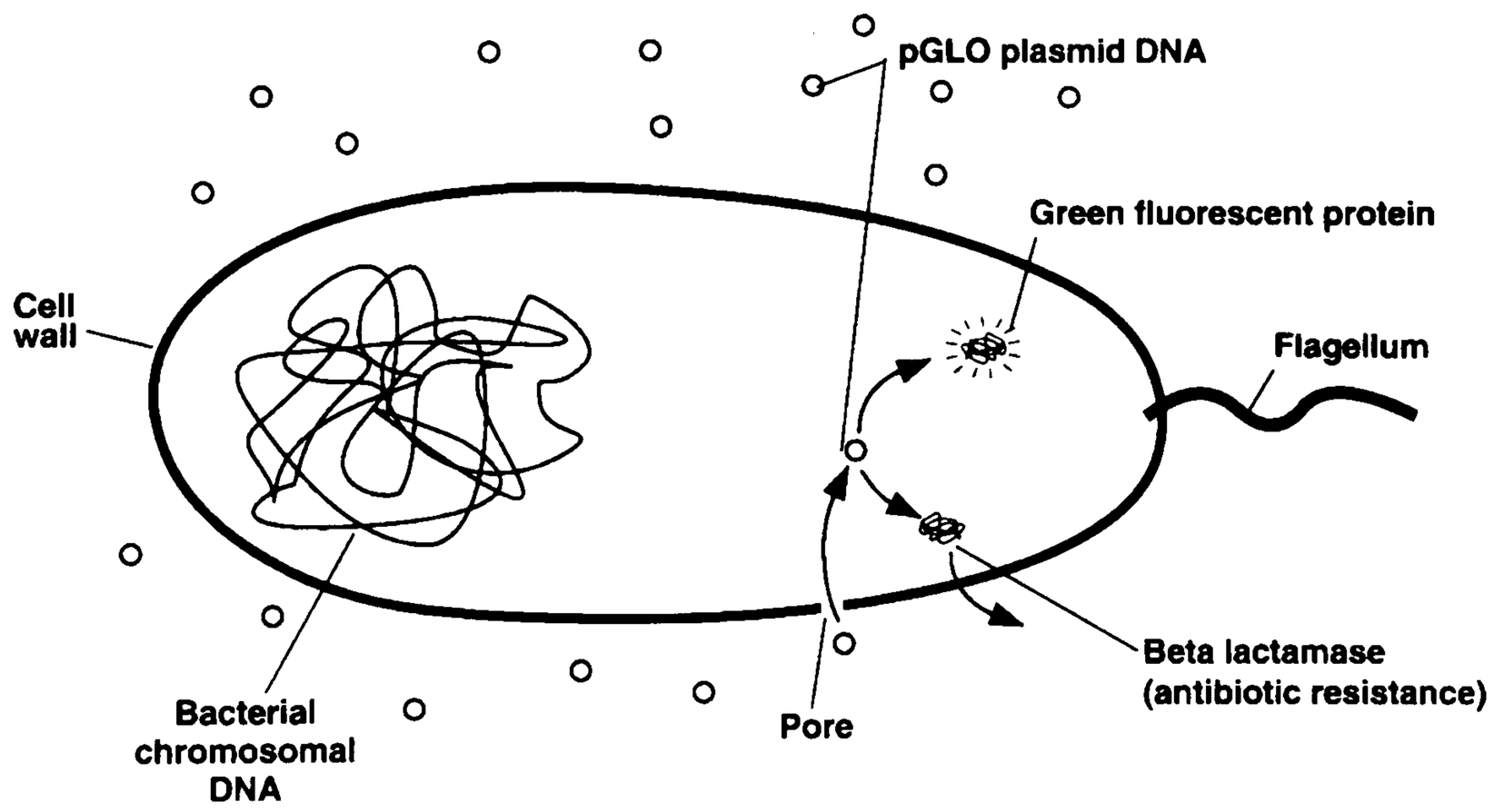

Figure 3-3. Insertion of pGLO gene into bacteria.

After successful transformation and culturing the *E.coli* cells emitted green light (wavelength ~515nm) when excited with blue (488nm) or ultraviolet light. Figure 3-4 shows the streaked *E.coli* cultures under white light conditions and when placed under a handheld UV lamp

emitting light at 365nm. Figure 3-5 shows the *E.coli* in suspension and viewed using a microscope and FITC filter set, with excitation light of 488nm

.

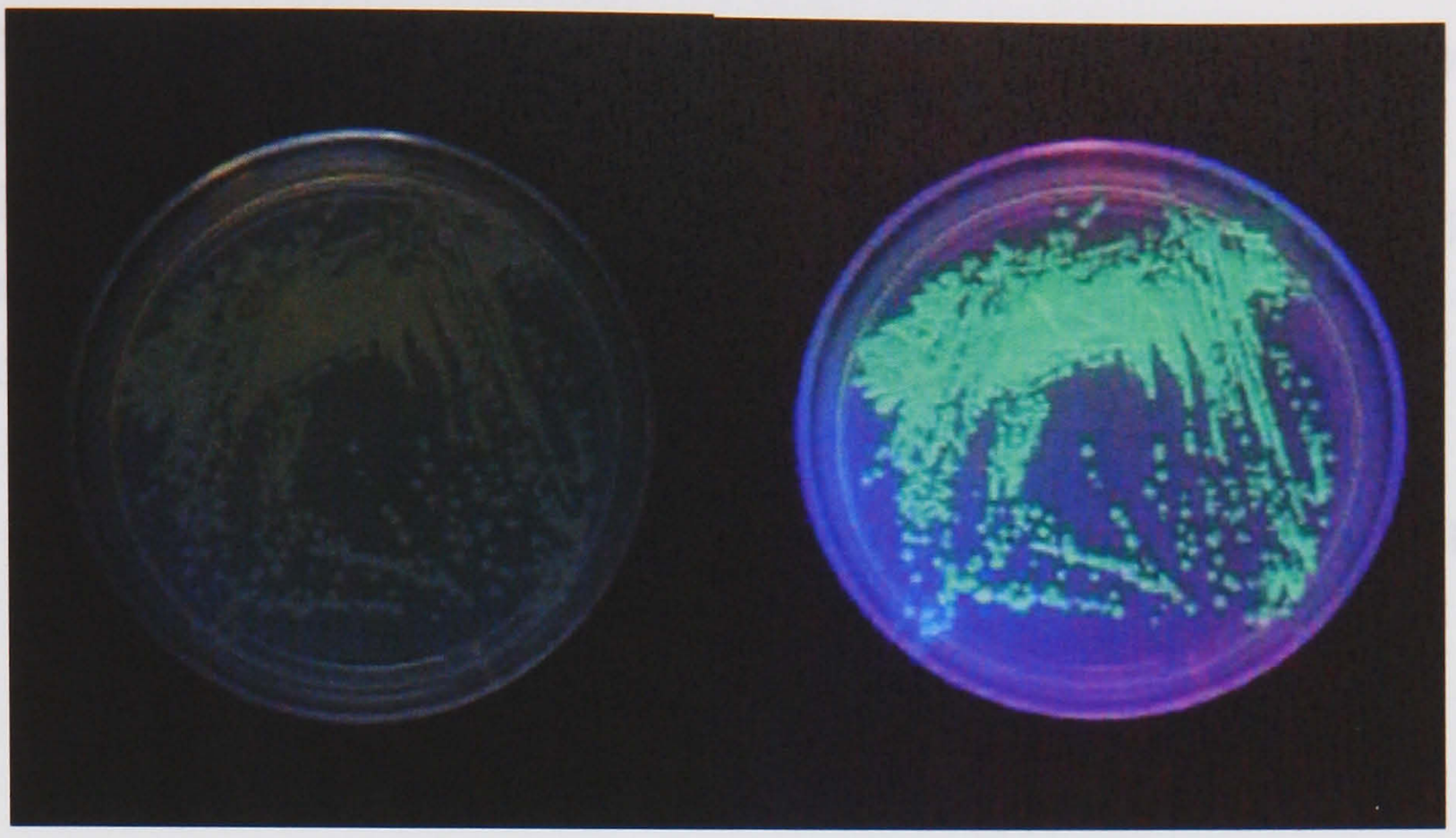

Figure 3-4. Example of the GFP expressing *E.coli* cultured on agar plates. The sample is viewed under white light conditions (left) and illuminated with a UV lamp (right).

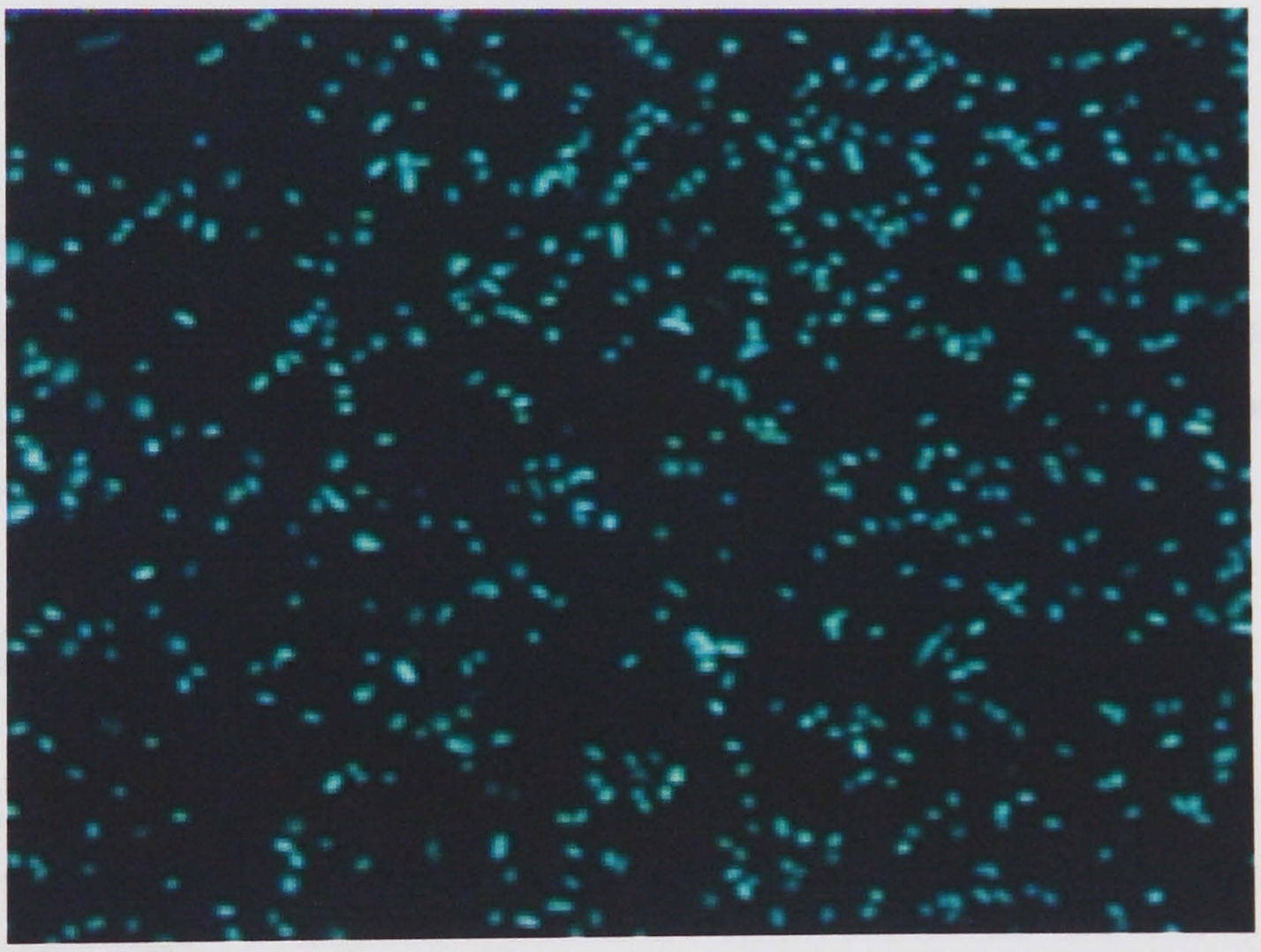

Figure 3-5. GFP expressing *E.coli* in suspension.

3.4 Trypan blue - cell viability

The viability of cells can be assayed simply by observing whether they uptake the dye trypan blue [3]. The test gives an indication of the integrity of the cell membrane as a measure of cell survival.

The protocol is outlined below:

- Obtain the cell sample to be assayed in suspension.
- 0.05ml of cell suspension adjusted to $1x10^6$ cells/ml was added to 0.95ml of trypan blue solution in a small tube and incubated at room temperature for 5mins.
- The tube was tapped to resuspend the cells, and 30µl of cells transferred by pipette to a haemocytometer chamber.
- Count the number of clear unstained cells, and also the total number of cells.

The cell viability is then calculated and expressed as the percentage of unstained cells in the total cell population.

3.5 Flow cytometry analysis

Flow cytometric analysis of cells was performed on a Becton Dickinson FACScan® (Becton Dickinson, UK) flow cytometer in the Dept. of Haematology at GRI. Standard instrument settings were used [9].

3.5.1 Labelling of mononuclear cells for flow cytometry analysis

Direct immunofluorescence staining of cell surface antigens on isolated mononuclear cell preparations (PBMCs) or cultured mononuclear cells (THP-1 or BOB) was performed prior to analysis by FACS.

The following reagents were used:

- FITC, RPE, APC, and/or RPE-Cy5 conjugated monoclonal antibodies to human cellular surface antigens CD14, CD45, and/or CD69 (all purchased from Dako Ltd., High Wycombe, UK).
- PBS (calcium and magnesium free).
- Labelling medium: PBS with 1% w/v BSA.
- Cell fix: 1% w/v paraformaldehyde in PBS.

FITC, RPE, APC, and RPE-Cy5 are fluorescent molecules. These are covalently attached to monoclonal antibodies that recognise specific antigens on the surface of different cell types. This allows identification of the cell type based on the colour of its fluorescence. Anti-CD14,

anti-CD45, and anti-CD69 are monoclonal antibodies specific to Monocytes, Leukocytes and T-lymphocytes respectively (see chapter one for more detail).

The following DAKO [10] labelling protocol was used:

- Cells samples were suspended in labelling medium at concentrations of ~10^7 cells/ml.
- 100 µl of cell suspension (~10^6 cells) was mixed with 10 µl of fluorochrome conjugated antibody. For dual or triple colour labelling, 10µl each of FITC, RPE, APC, and/or RPE-Cy5 conjugated antibody was added to the same sample.
- Cells were incubated in the dark at 4°C for 15-30 minutes.
- Washed with cold PBS (4°C).
- Fixed by resuspending cells in 1ml of PBS with 100µl 1% paraformaldehyde. (optional)

3.5.2 Internal labelling of trophoblast cells using JMB2 and Cyto-7

As discussed in chapter one, trophoblast cells do not express surface antigens for which there are commercially available surface antibodies specific to this cell type. It was therefore necessary to identify these cells using antibodies specific to certain internal proteins within the cytoplasm of the cell. Trophoblast cells were thus labelled prior to FACS analysis using either the JMB2 or Cyto-7 antibodies. These antibodies are specific for cytokeratin, a protein found in epithelial cells and not present in blood cells.

To allow these antibodies access to the inside of the cell, the cellular membrane must be made permeable. A commercially available permeabilization kit was purchased (Fix and Perm, Caltag labs, California).

3.5.1.1 JMB2 and Cyto-7

Anti-JMB2 culture supernatant [11] was kindly donated by Professor McGee, University of Oxford. The JMB2 antibody labels syncytiotrophoblast and both villous and extravillous cytotrophoblast [6]. Titration experiments were carried out using the JMB2 and Cyto-7 (see appendix A.3.1) to obtain the antibody concentrations, which gave the optimal labelling levels.

Cells were labelled using either JMB2 or Cyto-7 (both label cyto-skeletal cytokeratin) according to the same protocol. The optimal concentration of the JMB2 antibody was found to be 1:200 in PBS; and that of Cyto-7 was found to be 1:25 in PBS (see appendix A.3.1 for details).

The following antibodies were used (all purchased from Dako apart from JMB2):

1° antibodies:

- JMB2 1:200 in PBS (250µl).
- Cyto-7 1:25 in PBS (250µl).
- Negative Control; Anti-mouse IgG1-FITC 1:9 in PBS (20µl:180µl).

2° antibodies:

- FITC-conjugated goat anti(mouse IgG) $F(ab)_2$ 1:100 in PBS (100µl)

The JMB2, Cyto-7 and a negative control antibody were each used separately with the following labelling protocol:

- Centrifuge sample 15mins at 500g, resuspend pellet in 100µl of Fix and Perm for 15 mins at room temperature.
- Centrifuge for 15mins at 500g.
- Resuspend pellet and incubate with 1° antibody on ice for 30mins.
- Centrifuge for 15mins at 500g and resuspend in PBS.
- Centrifuge for 15mins at 500g, resuspend pellet with 2° antibody on ice for 30mins in the dark.
- Resuspend cells in PBS for FACS.

3.6 Magnetically activated cell sorting of PBMCs

MACS separations were carried out using the MiniMACS separation system (Myltenyi Biotech, Germany). The labeling procedure was similar to that used for the fluorescent labeling of cell surface antigens for FACS analysis (described above). Cell labeling can be performed at the same time for both FACS and MACS.

For MACS separation, cells were magnetically labeled with MACS MicroBeads and separated on a wire mesh column, which was placed in the intense magnetic field of a MACS separator. The magnetically labelled cells were retained in the column while the unlabelled cells ran through the column and were collected in a test tube. The unlabelled cells were thus separated from the cell type binding the specific MACS Microbeads–antibody combination. After removal of the column from the magnetic field, the cells magnetically retained in the column were eluted and collected in a separate tube.

The MACS labeling protocol was taken from the datasheets [12] provided with the MACS Microbeads and was as follows:

- Cells washed in PBS, centrifuged for 15mins at 500g and re-suspend in 80 µl of MACS buffer (PBS with 0.5 % bovine serum albumin and 2mM EDTA) per 10^7 total cells (for fewer cells, use same volume).
- 20 µl of MACS MicroBeads were added per 10^7 total cells, mixed well and incubate for 15mins at 4°C.
- Add fluorochrome-conjugated antibody, to allow analysis by FACS.
- Cells washed by adding 1-2ml of the MACS labeling buffer, centrifuged at 500g for 15 minutes to remove supernatant.
- Cell pellet was resuspended in MACS buffer (typically 500 µl of buffer per 10^8 total cells).
- Magnetic separation was performed by passing through the MACS column.

3.7 CellTracker fluorescent probes

For increased fluorescence, some experiments were carried out using CellTracker dyes. CellTracker probes can freely pass through a cell's cytoplasmic membrane. However, once inside the cell the dye molecules undergo a glutathione S-transferase mediated reaction producing a cell impermeant reaction product [13]. This product is retained within the cell allowing them to be visualised using either fluorescence microscopy or FACS analysis.

The following CellTracker probes were purchased from Molecular Probes Inc.

- Yellow-green, chloromethyl derivatives of fluorescein diacetate (CMFDA) (C-2925).

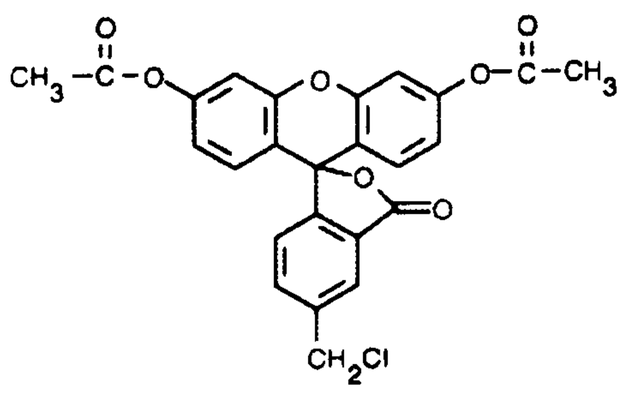

Excitation wavelength - 492nm

Emission wavelength - 516nm

- Blue, chloromethyl derivatives of hydroxycoumarin (CMHC) (C-2111).

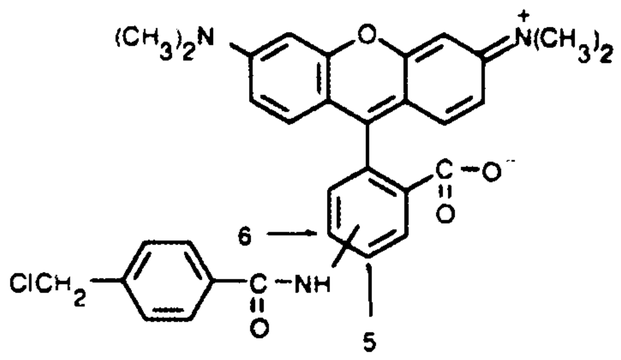

Excitation wavelength - 372nm

Emission wavelength - 470nm

- Orange, chloromethylbenzoylaminotetramethyl-rhodamine (CMTMR) (C-2927).

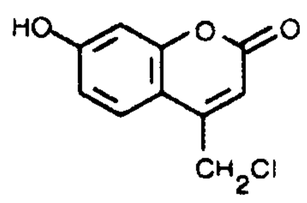

Excitation wavelength - 540nm

Emission wavelength - 566nm

Loading of the CellTracker dyes into cells was achieved by simply adding the diluted probe to the cell suspension, incubating, and then briefly washing with fresh medium before analysis. Stock solutions of the dyes were made up by dissolving each of the dyes in anhydrous dimethylsiloxane (DMSO) to yield a 10mM stock solution. These stock solutions were then divided into 12.5µl aliquots and stored at –70°C.

For labelling cells with CellTracker dyes the protocol was as follows:

- Aliquots of stock were taken from the freezer and thawed.
- 12.5µl of CellTracker stock was added to 4.988ml of warm PBS (37°C) to give a 25µM solution and vortexed to mix.
- Cells were spun down at 500g for 15min and the supernatant was removed
- Cell were resuspended in the dilute stock solution (25µM) and placed in the incubator at 37°C for 15-30mins.
- Centrifuged for 15mins at 500g discarding supernatant, the cell pellet was then resuspended in warm PBS (37°C) and returned to the incubator for a further 30mins.
- Centrifuged for 15mins at 500g and resuspend in PBS or other media.

Figure 3-6 below shows THP-1 cells labelled with the blue (CMHC) CellTracker dye. The image is viewed in epi-fluorescent mode using a DAPI filter, with low-level brightfield illumination from a halogen lamp to allow visualization of the cell shape.

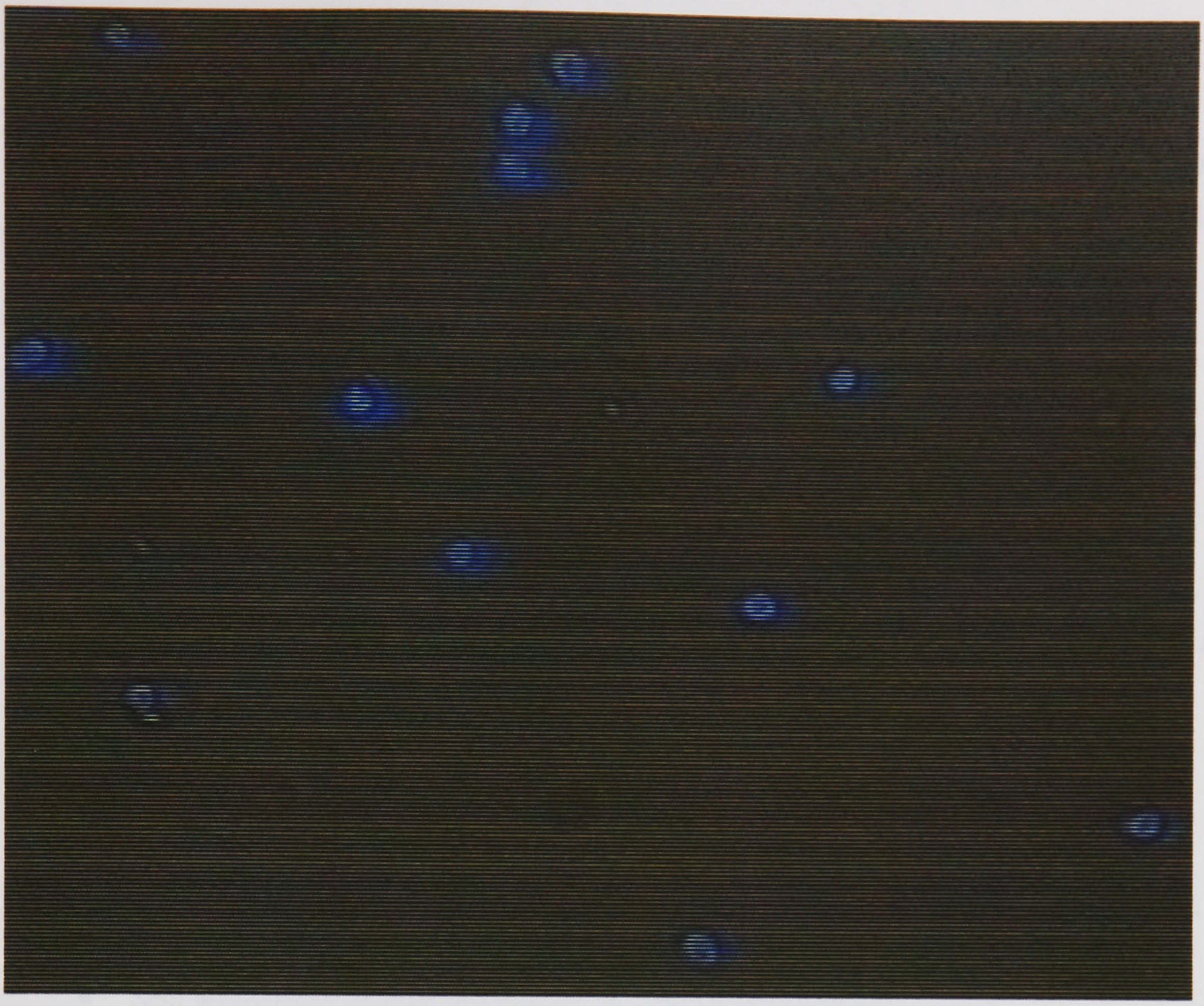

Figure 3-6. Combined transillumination and epi-fluorescence image of THP-1 cells labelled with blue CellTracker dye.

The CellTracker™ dyes are converted within the cell, from a membrane permeable form of the dye, to a membrane impermeable form of the dye. However, the dye is only membrane impermeable if the cells are healthy and have intact cellular membranes. Dead or dying cells tend to have leaky cellular membranes, and therefore the dye leaks out of the cells. The CellTracker™ dyes can thus be used in a similar manner to trypan blue for cell viability studies, with live cells fluorescing and dead or dying cells not fluorescing.

3.8 Polymerase chain reaction (PCR)

All PCR reactions were carried out by staff at the Duncan Guthrie Institute, Yorkhill Hospital, Yorkhill, Glasgow. The primers used allowed the amplification and detection of a portion of the Y (male) chromosome. All reactions were thermally cycled 30 times, unless stated otherwise. Post reaction DNA was incubated with ethidium bromide and run on a gel electrophoresis system. Finally, the bands were visualised under UV illumination and photographed. Adult male and female blood samples were run at the same time as controls.

3.9 FISH

Fluorescence in-situ hybridisation is a technique that involves the hybridisation of a complementary nucleic acid probe to a DNA or RNA sequence in the cell under examination. The probe is labelled with a reporter molecule (usually fluorescent) that allows the visualization of the sequence if it is present in the cell.

FISH reactions were carried out as follows,

- Cells were allowed to sediment onto glass slides.
- These were then fixed by immersion in MeOH:Acetic acid (3:1) for 30mins or longer.
- Wash
    - 2xSSC (3M NaCl, 0.3M sodium citrate; 10ml dH_2O, 40ml SSC) for 5mins at 42°C.
    - 2xSSC / 0.05% Tween20 for 15mins at 42°C.
    - 2xSSC / 0.05% Tween20 for 15mins at 42°C.
    - 2xSSC 5mins at 42°C.
- Dehydrate at room temperature in an ethanol series (70%, 80%, 100%) for 2mins each.
- Place 30µl of hybridisation solution onto sample and cover with a coverslide.
- Seal with rubber cement, cure cement at 42°C for 8mins.
- Denature for 10mins at 90oC, and hybridise at 42°C overnight in a humid slide box.
- Gently remove the coverslide.
- Wash
    - 2xSSC for 5mins at 42°C.
    - 2xSSC / 50% Formamide for 5mins at 42°C.
    - 2xSSC / 50% Formamide for 5mins at 42°C.
    - 2xSSC 5mins at 42°C.
- DAPI stain: 4µl DAPI into 40ml 2xSSC for 5mins at room temperature.
- Place coverslide with antifade solution (Fluroguard™, Bio-Rad 170-3140).
- Observe using fluorescence microscope.

Figure 3-7 shows an example of FISH carried out on a fnRBC at NEMC in Boston. The probes used were specific for the X (Cy-3) and Y (FITC) chromosomes and can be seen in the figure as red and green near the centre of the cell. The blue is the DAPI stained DNA. The orange halo around the cell is the γ-haemoglobin stain used to label the cell for FACS sorting. The X (Cy-3) and Y (FITC) chromosome probes were synthesised in house.

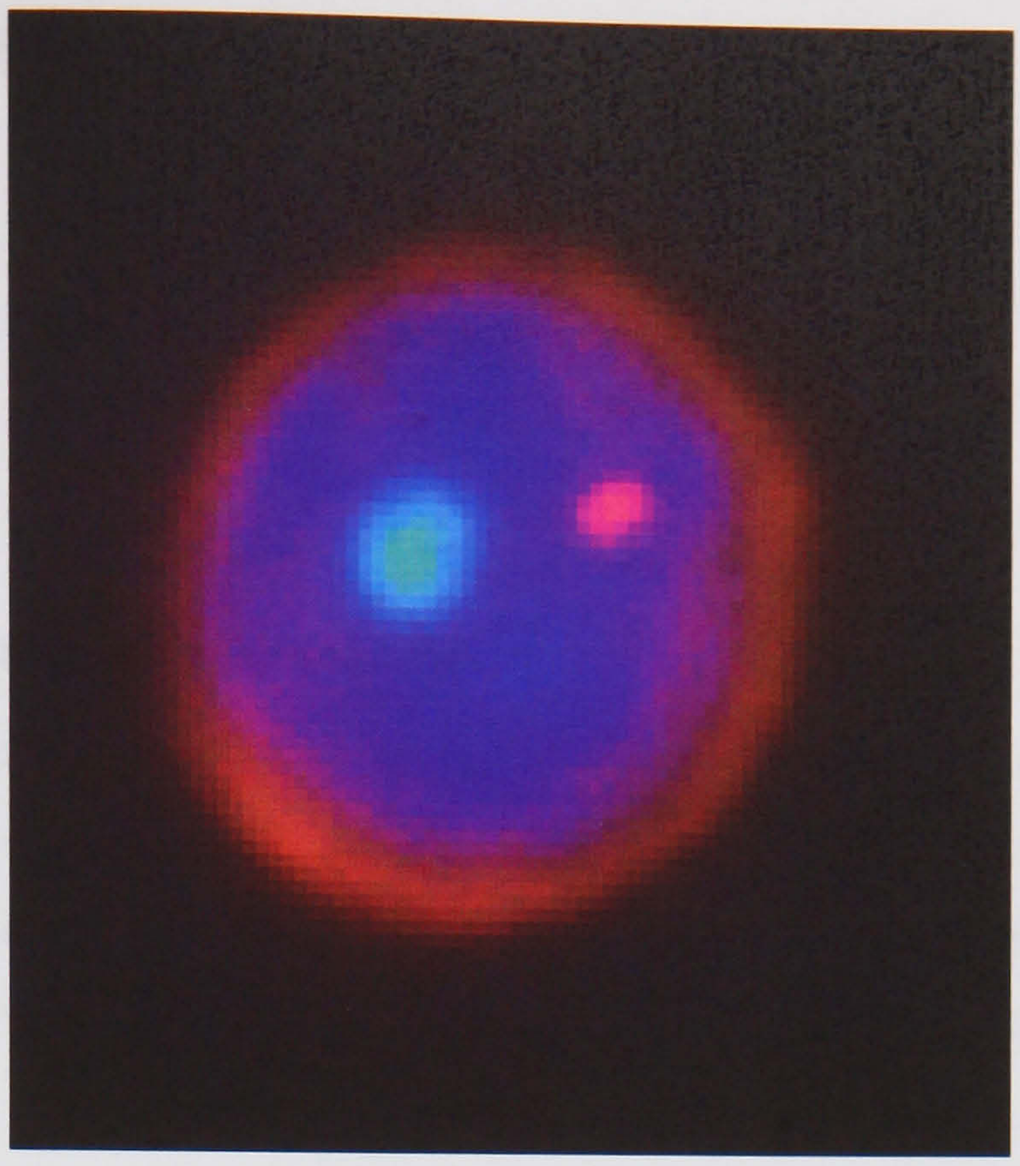

Figure 3-7. FISH image from a male fnRBC isolated from foetal cord blood. The nucleus appears blue (DAPI), X-chromosome (green), Y-chromosome (red), and foetal γ-haemoglobin stained orange.

3.10 SEM of cells

Cell samples were prepared for viewing on the Hitachi S800 scanning electron microscopy. The cells were initially fixed and then dehydrated through a series of solvents.

Fixation was achieved as follows:

- A drop of cell suspension was pipetted onto a glass microscope slide, and the cells allowed to sediment onto the glass.
- Slides were immersed for 15mins in 2% glutaraldehyde in PBS.
- x4 wash in PBS.
- Post-fix soaked in 1% osmium tetroxide in PBS for 15mins.
- x4 wash in PBS.
- x2 wash in dH_2O.

Dehydration involved sequential immersion of the sample (after fixation) in the following:

- 50% Analar ethanol in dH_2O for 10mins.
- 50% Analar ethanol in dH_2O for 10mins.
- 100% Analar ethanol for 10mins.

- 100% hexamethyldisilazane for 10mins.
- Air dried.

Samples were stored in an airtight box until examined using the SEM.

3.11 Dielectrophoretic separation media

A requirement for dielectrophoresis of particles is that the particles are in suspension. The relative polarisabilities of the particle and the suspending medium must also be suitably chosen so as to allow both positive and negative DEP. Generally, this requires that the properties of the suspending media are controlled, rather than trying to alter the dielectric properties of the particle.

3.11.1 Latex beads

Latex particles are generally suspended in low ionic strength media such as distilled water with a small amount of PBS, to adjust the medium conductivity. Figure 3-8 shows the effect on medium conductivity with the addition of PBS to water.

Figure 3-8. Conductivity changes due to the addition of small amounts of PBS to water.

Changing medium conductivity alters a particle's relative polarisability versus frequency characteristics. Figure 3-9 shown the effect of changing the medium conductivity has on a 10μm latex sphere suspended in water, with the particle's surface conductivity $K_s = 2.44x10^{-9}$ S, and the bulk conductivity of the latex $\sigma_p = 1x10^{-9}$ Sm^{-1} [16].

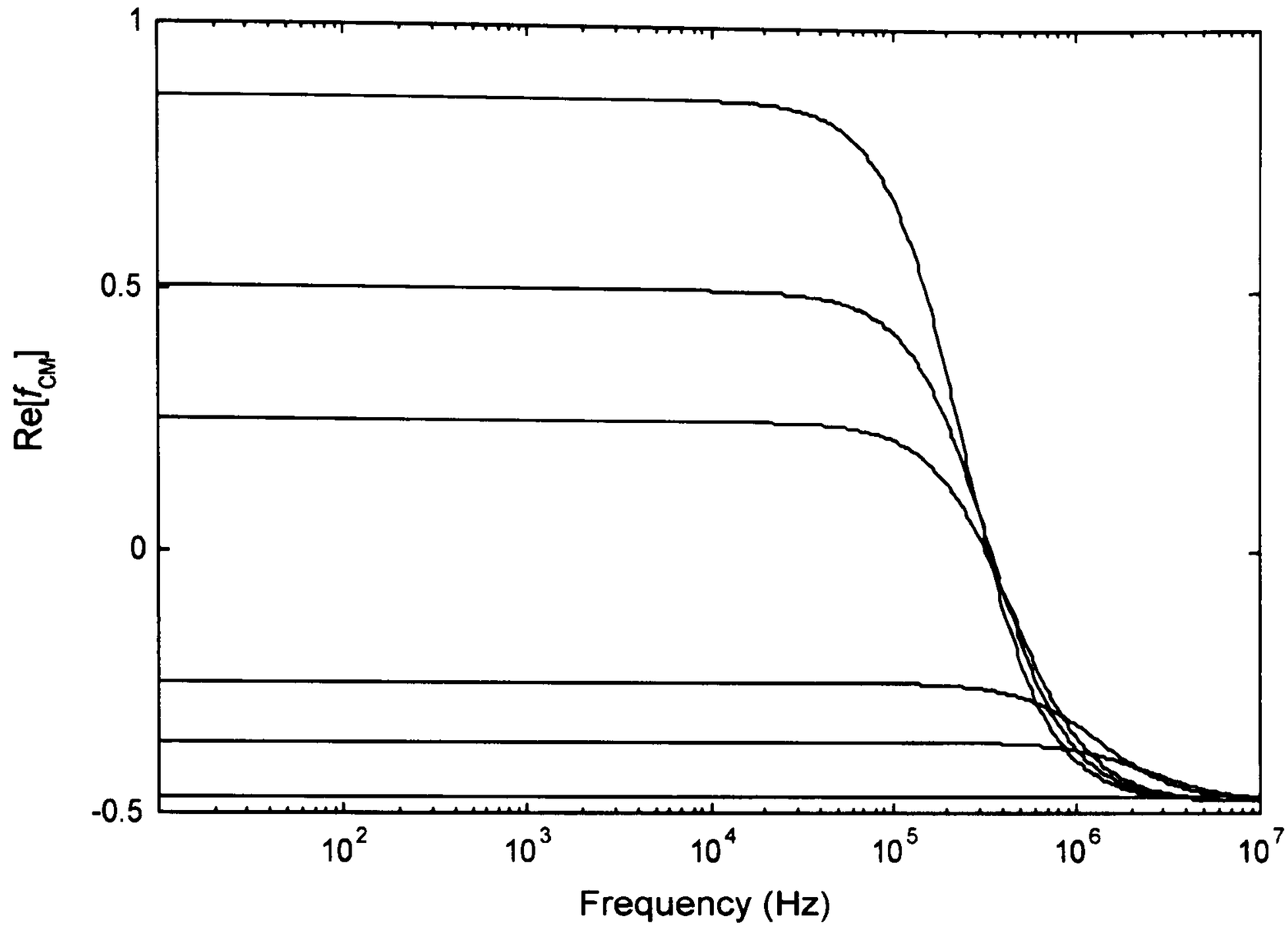

Figure 3-9. Effect of suspending medium conductivity on the real part of the Clausius-Mossotti factor for a 10μm latex bead, with $K_s = 2.44x10^{-9}$ S, and $\sigma_p = 1x10^{-9}$ Sm^{-1}. From top to bottom σ_m = 0.1, 0.5, 1, 5, 10, 50 mSm^{-1}.

3.11.2 Mammalian cells

Mammalian cells require pH and iso-osmotic conditions similar to the physiological state from which they have been removed. For the blood cells (both primary and cultured) and the trophoblast cells (obtained from the placental membranes) the pH should be in the region 6.8-7.4, and the osmolality of the suspension should be 290$mOsm^{-1}$. The conductivity should be sufficiently low such that the cells can undergo both positive and negative dielectrophoresis.

DEP cell manipulation is usually performed in the frequency range between 1kHz and 20MHz where cells will only achieve positive DEP if suspended in sufficiently low conductivity media. The vast majority of cell culture, suspending, and washing media are rich in ions, and are therefore highly conductive (e.g. PBS ~0.6 Sm^{-1}). Typically, the conductivity of dielectrophoretic separation media is in the range 20-70mSm^{-1}, tending to the higher end of this range so as to reduce ion leakage from the cells.

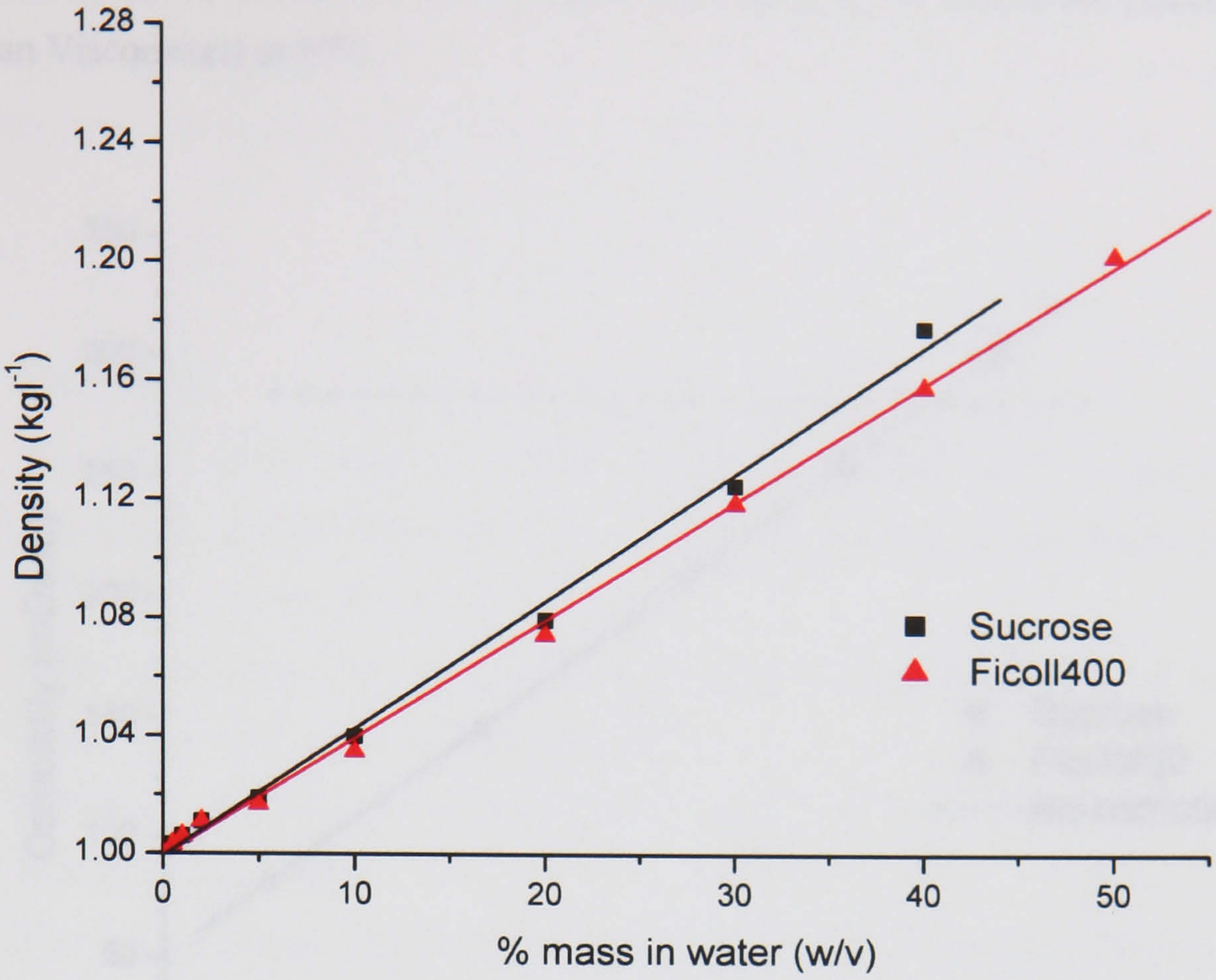

Figure 3-10. Variation in density with the addition of sucrose or Ficoll400.

To obtain the condition of neutral buoyancy (where the cell density is equal to that of the media) and hence eliminate the effects of sedimentation due to gravity, the 'standard' sucrose based dielectrophoretic separation medium (see for example [14]) was augmented. Ficoll400 (Sigma, F4375) a long chain poly-sucrose molecule was chosen; it is a neutral polymer and readily dissolves in aqueous media. The addition of Ficoll increases the density of a suspension in approximately the same way as sucrose (see figure 3-10). However, due to the size of the Ficoll molecule it is too large to permeate through the cell membrane, and as such its addition does not alter the osmotic balance of the medium. Figure 3-11 shows the effect that sucrose and Ficoll400 have on the osmolality of the medium when added to water.

The 'standard' dielectrophoretic separation medium used in this work consisted of:

- dH_2O (distilled water)
- 9% sucrose (w/v).
- 0.1% glucose (w/v)
- 0.8% BSA (w/v)
- 1mM EDTA.

The pH and conductivity were adjusted by the addition of small amounts of mono- or di-basic phosphate buffer to a density of 1.041kgm^{-3} and viscosity of 1.31mPa.s (measured using a Beckman Viscometer) at 25°C.

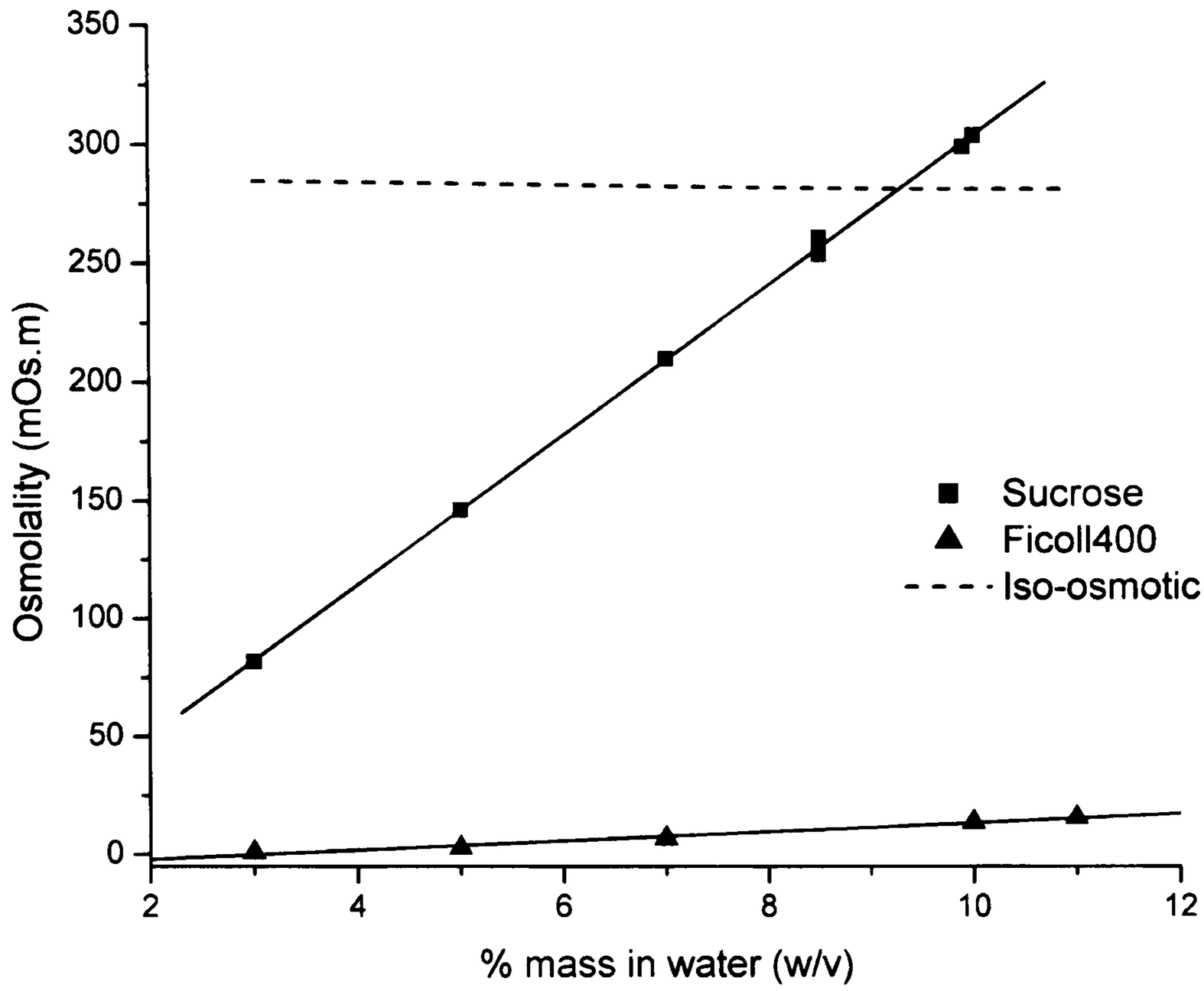

Figure 3-11. Variation in osmolality, with the addition of sucrose or Ficoll400 to water.

The Ficoll containing dielectrophoretic separation medium consisted of:

- dH_2O
- 9% sucrose (w/v)
- 3.5% Ficoll400 (w/v)
- 0.1% glucose (w/v)
- 0.8% BSA (w/v)
- 1mM EDTA.

with the pH and conductivity again adjusted by the addition of small amounts of mono- or di-basic phosphate buffer. This medium has a density of 1.065kgm^{-3} and viscosity of 1.50mPa.s at 25°C.

3.11.3 Bacteria

The bacterial cells were cultured as described in section 3.3. For DEP experiments these cells were washed and resuspended in a solution of 0.3% (w/v) D-Mannitol giving the correct osmolality, the conductivity was altered by the addition of PBS (see figure 3-8).

3.12 References

1. Alberts, B., *et al.*, *Molecular biology of the cell*. 3 ed. 1994, NY: Garland.
2. Bøyum, A., *Isolation of mononuclear cells and granulocytes from human blood.* Scand J Clin Lab Invest, 1968. **21**: p. 77.
3. *Cell separation methods and applications*. 1 ed, ed. D. Recktenwald and A. Radbruch. 1998, New York: Marcel Dekker Inc. 331.
4. Hudson, L. and F.C. Ha, *Practical Immunology*. 3 ed. 1989, Oxford: Blackwell Scientific Publishing.
5. Kliman, H.J., *et al.*, *Purification, characterization, and in vitro differentiation of cytotrophoblasts from human term placentae.* Endicronology, 1986. **118**(4): p. 1567-1582.
6. Shorter, S.C., *et al.*, Placenta, 1990(11): p. 505-513.
7. Barker, K., *At the bench: a laboratory navigator*. 1998: Cold Spring Harbor Laboratory Press.
8. Bio-Rad, I., *Bacterial transformation the pGLO system*, Bio-Rad.
9. Becton Dickinson, I., *BD FACScan User Manual*: Becton Dickinson, UK.
10. DAKO, I., *DAKO datasheets*.
11. McGee, 1982.
12. Milyenyi Biotech, I., *Instructions for Use, VarioMACS and SuperMACS*: Miltenyi Biotech.
13. Molecular Probes, I., *Acetoxymethyl (AM) and Acetate Esters*, , Molecular Probes.
14. Yang, J., *et al.*, *Differential analysis of human leukocytes by dielectrophoretic field-flow-fractionation.* Biophysical Journal, 2000. **78**(5): p. 2680-2689.
15. Campbell, S., *Dept. of Obstetrics and Gynaecology, GRI.* 2000, personal communication.
16. Cui, L., D. Holmes, and H. Morgan, *The dielectrophoretic levitation and separation of latex beads in microchips.* Electrophoresis, 2001. 22(18): p. 3893-3901.
17. Moore, K.L., *The developing human*. 5th edition, 1993: WB Saunders, Philadelphia.

A.3.1 Appendix 3.1 – Titration of JMB2 and Cyto-7

The optimal concentrations of the JMB2 and Cyto-7 antibodies for cell labelling were achieved by titration. These antibodies label the cytokeratin component of the cell cyto-skeleton (they are internal labels). Thin sections of placenta were cut using a Cryostat, these sections were then incubating with different concentrations of the JMB2 and Cyto-7 antibodies in order to find the required concentration for labelling. The antibody labelling was visualised using a DAB reaction, which forms a dark brown precipitate easily visible under a microscope.

The titration protocol was as follows:

- Sections were placed onto polylysine coated slides.
- Wash slides and store in freezer until needed at -70°C.

Fixation:

- Thaw section 10mins.
- Fix in acetone 10mins.
- Rinse in PBS 5mins.

Blocking peroxidase activity:

- 0.5% H_2O_2 / methanol 30mins.
- Wash in PBS 2 x 10mins.

Antibody labelling:

- A wax boundary circle was drawn around the area where the antibody was to be applied, this confined any liquid pipetted onto surface of slide.
- Block with 20% goat and 20% human serum 30mins at 25°C. (300µl onto each slide).
- Tap off blocking serum and add 1° Ab JMB2 (dilute in 2% goat serum) 1hour at 25°C in humidified box.
- Rinse in PBS 2 x 5mins.
- Add 2°Ab biotinylated anti mouse IgG (DAKO), 1:200 in 2% goat serum with 5% human serum added 30mins at 25°C in humidified box.
- Rinse in PBS 2 x 5mins.
- Add streptavidin, 1:400 in PBS 30mins.
- Rinse in PBS 2 x 5mins.

DAB reaction:

Make up DAB - 15ml 50mM Tris (pH 7.6) + 1 DAB tablet (Sigma, D5905) + 12µl H_2O_2.

- Add to slide through a filter leave for 10mins at 25°C.
- Wash in PBS 5mins then running tap H_2O.
- Stain in Haematoxylin for a few seconds then wash in H_2O.
- Dehydrate through alcohols to xylene (5mins each).
- Mount in DPX.
- View.

Images of the labelled placental cryo-sections are shown below in figures A-3-1 to A-3-3. These images show cross-sections through the placental villi. The villi are comprised of trophoblast cells, having a core of cytotrophoblast cells and a syncytiotrophoblast covering. A number of blood vessels can be seen in these images. Figure A-3-1 shows the control (no JMB2 or Cyto-7 labelling) sample with only the nuclear stain visible. Figure A-3-2 shows the pattern of cell labelled using the JMB2 antibody at a concentration of 1:200. JMB2 can be seen to label the trophoblast cells on the outer surface of the villi, but also labels a number of other cell types within the tissue. In particular the smooth muscle cells surrounding the blood vessels are strongly labelled by the JMB2. For comparison the pattern of labelling of the Cyto-7 antibody is shown in figure A-3-3. The Cyto-7 can be seen to label far fewer cells (if any) in this tissue, showing it to be far more specific than the JMB2 (this finding has been confirmed by others [15]).

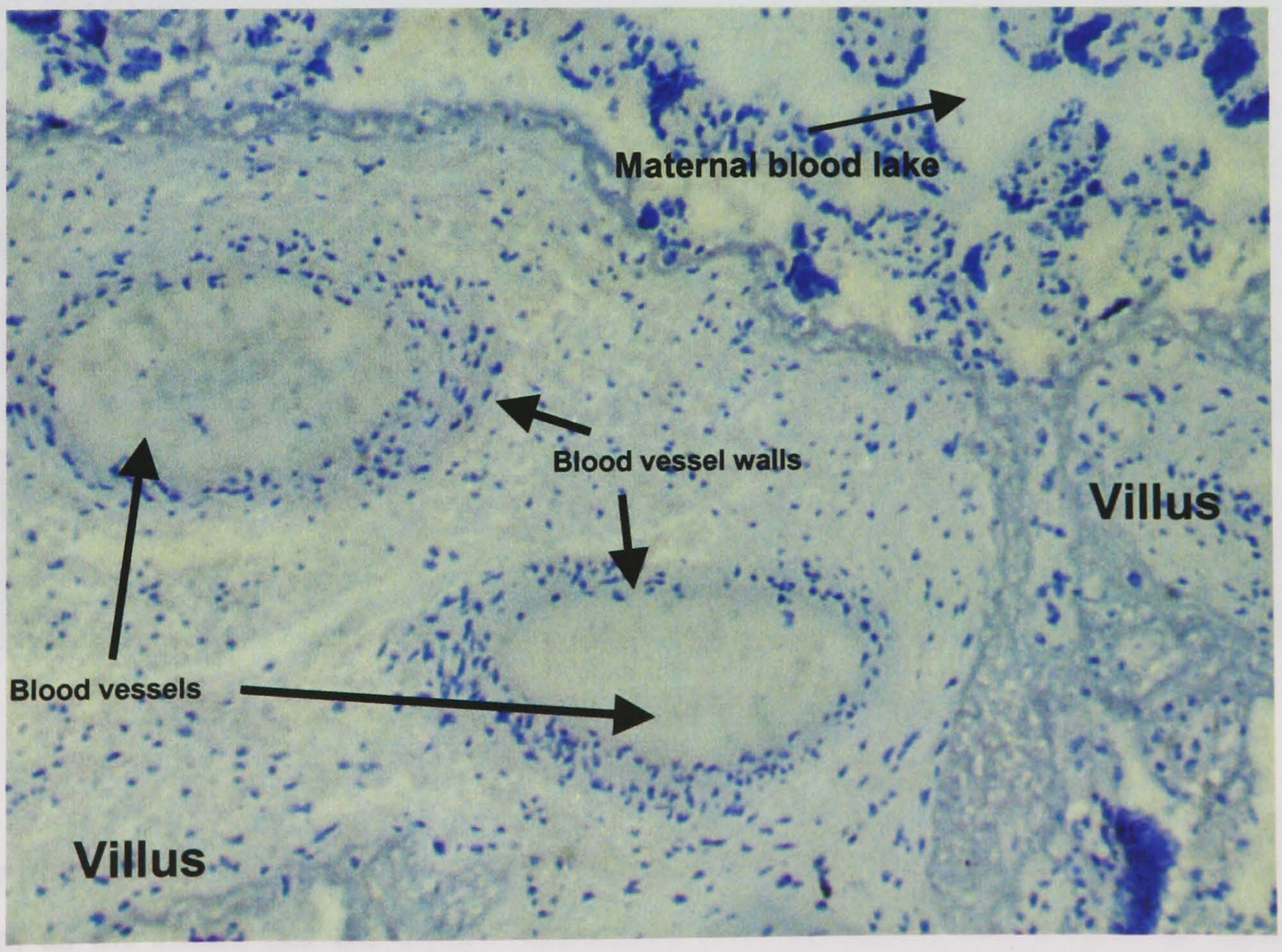

Figure A-3-1. Placental cryo-section incubated with no antibody – control (no brown).

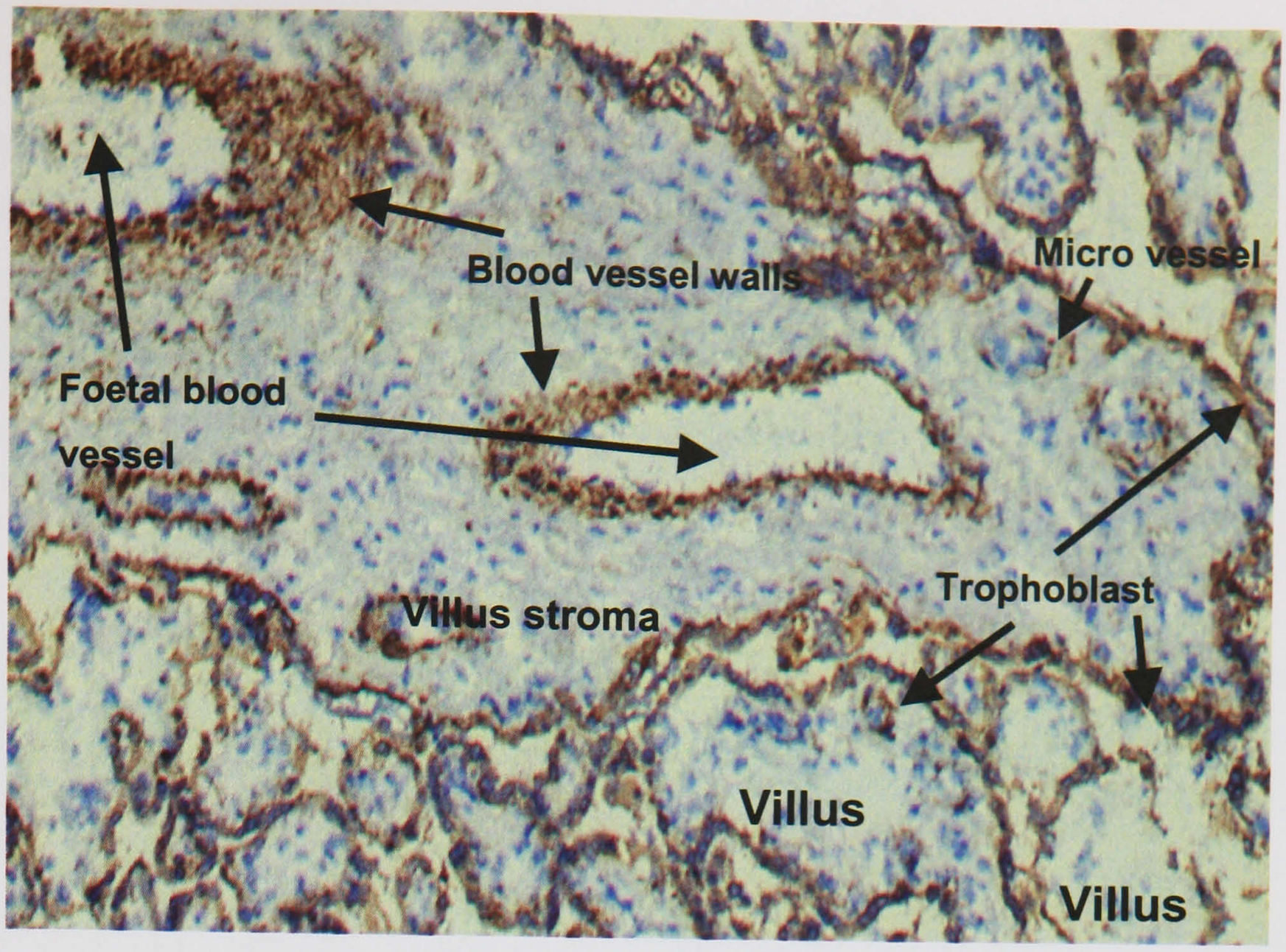

Figure A-3-2. Placental cryo-section incubated with JMB2 at a concentration of 1:200, showing staining of trophoblast and vascular smooth muscle).

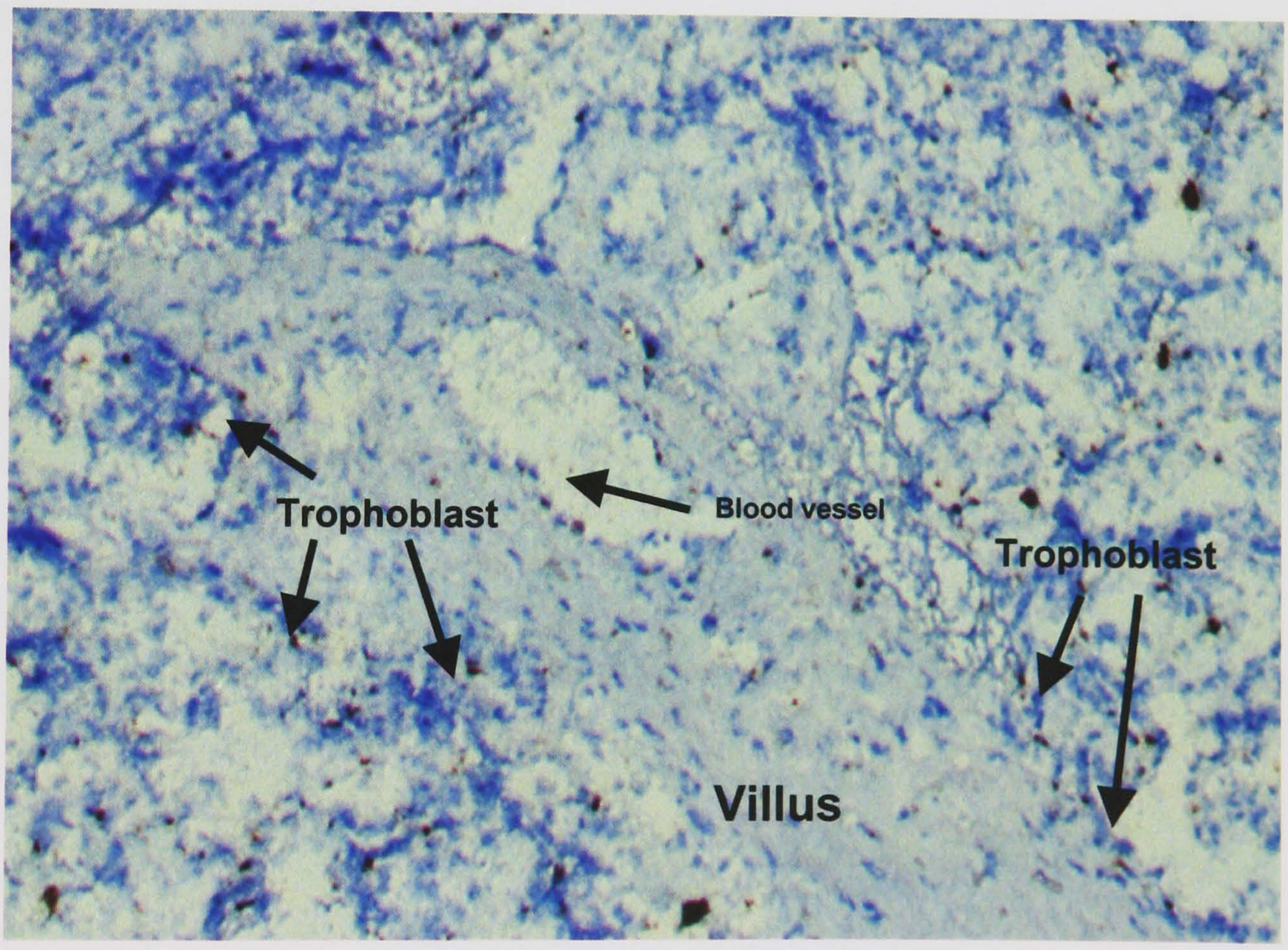

Figure A-3-3. Placental cryo-section incubated with Cyto-7 at a concentration of 1:25.

For the purposes of this thesis the non-specific labelling seen in figure A-3-2 should not be of concern, as the JMB2 nor the Cyto-7 antibodies label peripheral blood cells. In view of the above results the JMB2 antibody was chosen for use in this study.

Chapter Four: Fabrication and related technological considerations

4 Introduction

The experimental work in this thesis required the design and construction of a flow through dielectrophoretic particle separation device. This chapter describes the methods used in the construction of the device and the ancillary equipment built to control the device, as well as associated sample handling equipment.

4.1 Standard Electrode types

Dielectrophoresis uses non-uniform AC electric fields to generate forces on particles as described in chapter 2. In order to produce such fields, a variety of electrode configurations have been developed by various workers over the years. These range in complexity from simple wire and pin type electrode structures of early experimenters (see [1]), through planar electrode arrays [2] (e.g. interdigitated bar and castellated electrodes, parabolic, etc.) to examples of complex three-dimensional geometries such as those of Schnelle [3].

The majority of contemporary electrode designs rely upon microfabrication methods initially developed for the integrated circuits industry in the 1960's.

4.1.1 Microelectrode fabrication

Arrays of interdigitated microelectrodes were fabricated onto glass microscope slides using standard photolithography and either lift-off or wet etching techniques as described below. Electrode widths and inter-electrode gap size were in the range 10μm to 40μm. Figure 4-1 shows an example of a double electrode array fabricated using photolithography and wet etching.

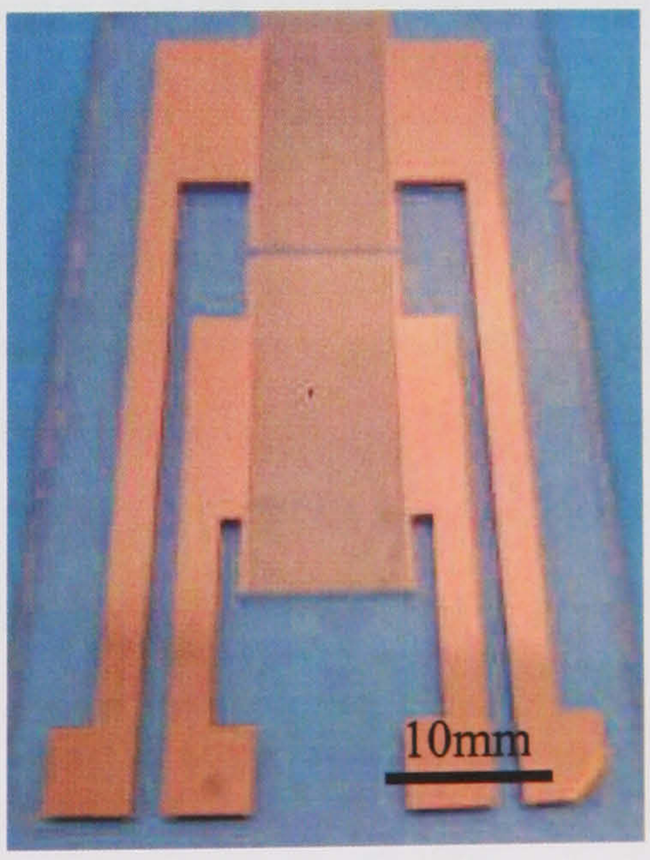

Figure 4-1. Photograph of the double array electrodes developed for this work.

4.1.2 Mask production

The electrode structures were designed using the CAD section of the microwave waveguide simulation package WAveMaker (WAM). These designs were saved in GDSII file format. The GDSII files were then transferred to a VAX workstation and converted to the CATS file type, readable by the CAD package used to process the pattern files for the beam-writer. A control file was then written for the beam-writer. The control file and pattern files were then sent to the beam-writer control workstation and chrome mask plates written.

4.1.3 Cleaning of glass substrate

Soda lime glass microscope slides of two sizes (76mm x 26mm x 0.8-1.0mm and 75mm x 38mm x 1.215mm) were used as substrates for the majority of devices fabricated in this project. A third glass substrate was used for some devices. 500μm polished glass sheets were purchased. The glass sheets were cut to size (75mm x 38mm) using a diamond tipped scribe.

Prior to device fabrication the glass was cleaned to remove any dust or organic material from its surface. This cleaning step was crucial for good adhesion of the multiple layers of metals and resists, which were deposited to make up the device.

4.1.3.1 Solvent cleaning

For solvent cleaning the slides were placed in beakers and ultrasonicated in the following:

- Optoclear W (Fluka, Switzerland) for 5mins
- Acetone for 5mins
- Methanol for 5mins
- Distilled water for 5mins
- Rinsed in distilled water and blown dry under a stream of filtered air.

4.1.3.2 Acid cleaning

Acid cleaning was used to remove any remaining organic material from the surface of the glass. H_2SO_4 was mixed 8:1 with H_2O_2 causing an increase in temperature to 80°C. The glass slides were placed in this aggressive liquid for 20 minutes then removed and rinsed with distilled water and blown dry under a stream of filtered air.

4.1.4 Electrode patterning

In order to form the electrode structures either a lift-off, or a wet etching technique was used. The first, lift-off requires that a thin layer of patterned photoresist be formed directly on to the

glass substrate on top of which a metal layer was then evaporated (see below). When the resist is removed it takes with it any metal not adhering directly to the glass. The second method, wet etching, required the metal layer be evaporated directly onto the cleaned glass surface. The patterned photoresist is then formed on top of the metal layer. The resist layer in this case acts as a mask protecting the metal directly beneath it from the etching solution. Figure 4-2 shows the various layers for lift-off and for wet etching.

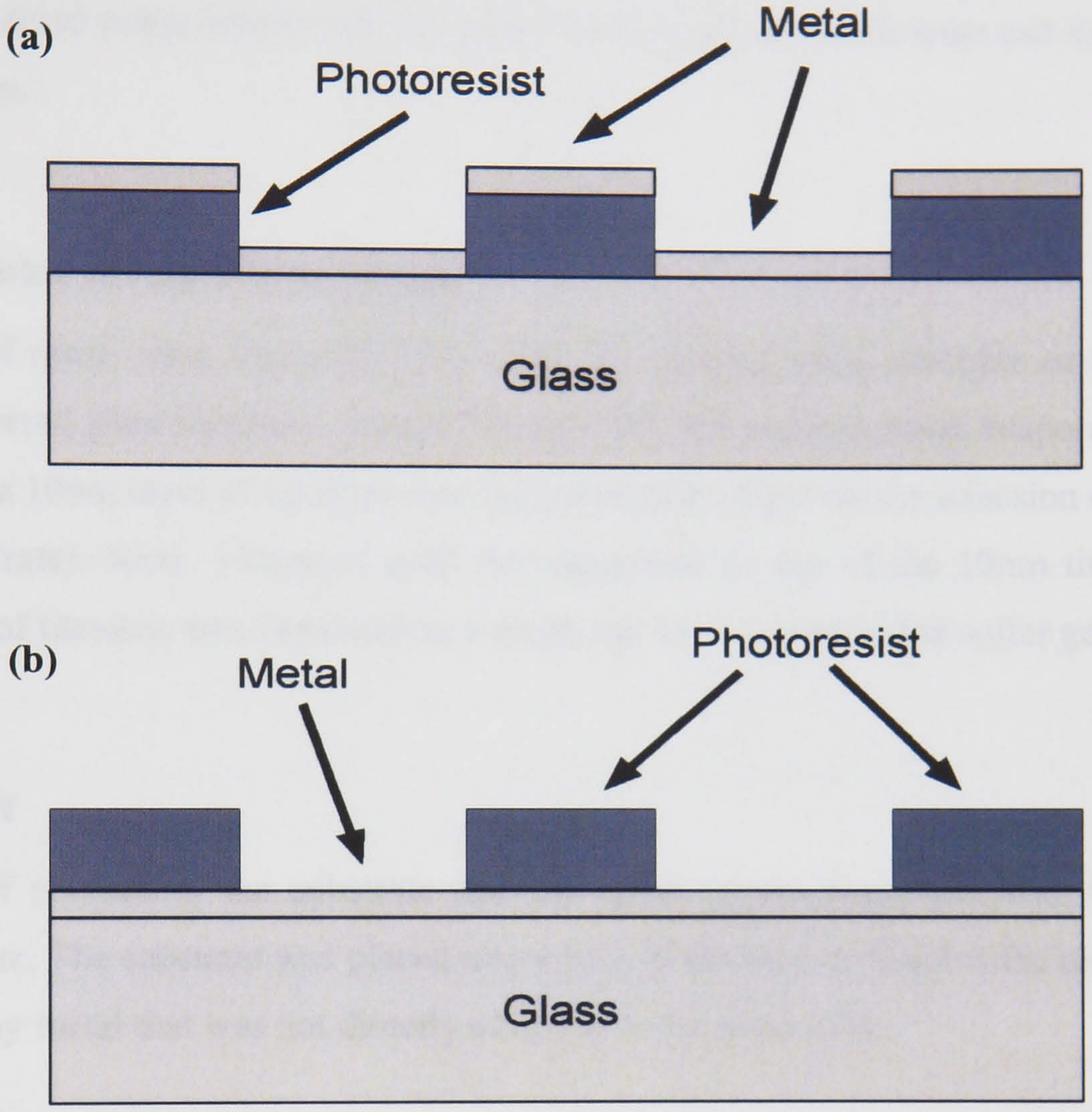

Figure 4-2. Fabrication levels for **(a)** lift off and **(b)** wet etching.

4.1.4.1 Photoresist patterning

Shipley S1818 positive tone positive photoresist (*Shipley*, UK) was processed as follows: a few drops of hexamethyldisilazane (HMDS) were placed on to the substrate, which was spun at 4000rpm for 10 seconds using a vacuum chuck spinner (*Headway Research,* UK). HMDS was used to enhance the adhesion of the S1818 photoresist to the underlying substrate material. This coated the substrate with a layer of methyl (CH_3) groups. The S1818 was then gently pipetted through a 0.45μm filter onto the substrate to cover the entire area in a bubble free layer. The sample was then spun at 4000rpm for 30 seconds, removed from the chuck and placed in an air forced oven at 90ºC for 15-20 minutes prior to exposure. This pre-exposure bake was used to dry off any remaining solvent in the resist.

Pattern transfer was achieved using a quartz-chromium photolithography mask and a UV mask aligner (HTG3, *Hybrid Technology Group,* USA). The substrate and mask were aligned and brought into hard contact, the resist was then exposed to light of wavelength 346nm, through the mask for 12 seconds at a power density of 120mW/cm^2.

To realise the resist profile the substrate was then immersed in a 1:1 mixture of developer (*Microposit,* UK) and RO water for 75 seconds under gentle agitation, before being rinsed in RO water and dried using filtered air. Only the areas of resist, which were not exposed to the UV light remain.

4.1.5 Deposition of thin film metal layers

Three layers of metal were deposited onto either the cleaned glass substrate or the patterned photoresist covered glass substrate, using a Plassys MEB450 electron beam evaporator (*Plassys*, France). First, a 10nm layer of titanium was deposited (this improves the adhesion of the gold to the glass substrate). Next, 100nm of gold was deposited on top of the 10nm titanium layer. Finally, 20nm of titanium was deposited as a tough top layer to protect the softer gold beneath.

4.1.6 Lift-off

For the lift-off procedure, the substrate had the metal layers deposited over the patterned photoresist layer. The substrate was placed into a bath of acetone to dissolve the resist layer and thus remove any metal that was not directly adhering to the glass slide.

It was found during initial fabrication tests that lift-off could be unreliable over large areas, especially for fabrication of the smaller 10μm wide electrode arrays. Occasionally, fragments of the "lifted-off" metal were deposit back onto the substrate resulting in the formation of short circuits on the final electrode array. Removal of these short circuits was possible but difficult.

Three methods were used to overcome the short circuit problem:

- Mechanical cutting of the short or the electrodes effected. However, this typically resulted in damaged to the electrode array over an area greater than that affected by the short.
- Application of a dc voltage of 20-30V across the electrode array resulted in a current flow that melted any small short circuits, and generally caused little damage to the surrounding electrodes. This method only worked for short circuits smaller than the

electrodes, for larger short circuits the electrodes themselves melted due to the current density being higher in the electrode than in the short.

- A wet etching technique was used; this method removes metal by dissolving it removing the possibility of re-deposition of metal fragments.

Furthermore, lift-off typically produced a ragged electrode edge (see figure 4-3(a)), where the waste metal has been torn away from the substrate. These ragged edges could potentially damage cells and other particles coming into direct contact with them; either by slicing into them mechanically or via electrical damage due to the high electric field strengths produced by the sharp protrusions.

4.1.7 Wet etching

The fabrication protocol for the wet etching procedure was similar to that for lift-off. However, for wet etching the metal was deposited prior to the photoresist. The S1818 photoresist pattern was then formed using photolithography as before but this time the photoresist pattern was used to protect the metal from the etchants. This results in a pattern of metalisation identical to that of the photoresist pattern. Following the wet etch procedure the substrate is rinsed in RO water and inspected using a microscope. Finally, the photoresist was removed by immersion in acetone, and rinsed in methanol then RO water and blown dry.

The standard etchants used are generally metal specific with different etch rates for each metal.

The two echants used were:

- Titanium etch - 1 part hydrofluoric acid (HF) to 26 parts RO water. All work with HF was carried out using PTFE dishes/beakers as HF etches glass, although at a slower etch rate compared to Ti.
- Gold etch – 16% (w/v) of potassium iodide (KI) and 4% (w/v) of iodine (I_2) dissolved in water.

Metal	**Etchant**	**Etch rate**
Ti	HF : RO water (1:26)	$2nm.s^{-1}$
Au	KI : I_2 : H_2O (32g:8g:200ml)	$1\text{-}2nm.s^{-1}$

Table 4-1. Etchants and etch rates for gold and titanium.

Table 4.1 shows the etch rates of these etchants for the pure metal. During fabrication it was found that the etch times had to be varied slightly, and etch times were defined visually during

the etch procedure. The reason for this change in etch rate is due to the formation of a thin alloy layer between the different metal layers as they are deposited in the evaporator. This interfacial alloying is only a few atoms thick, but can result in altered etch rates compared with the etch rate of the pure metal.

Figure 4-3 shows a comparison between lift-off and wet etch formed electrodes. The large horizontal scratches visible on figure 4-3(a) are due to handling the substrate prior to SEM and should be ignored. However, the ragged electrode edges are clearly visible. Figure 4-3(b) shows the smoother wet etched electrode edges. The wet etch image also shows the slight over etching and resultant pitting of the glass substrate due to this sample being left in the HF etch bath for too long.

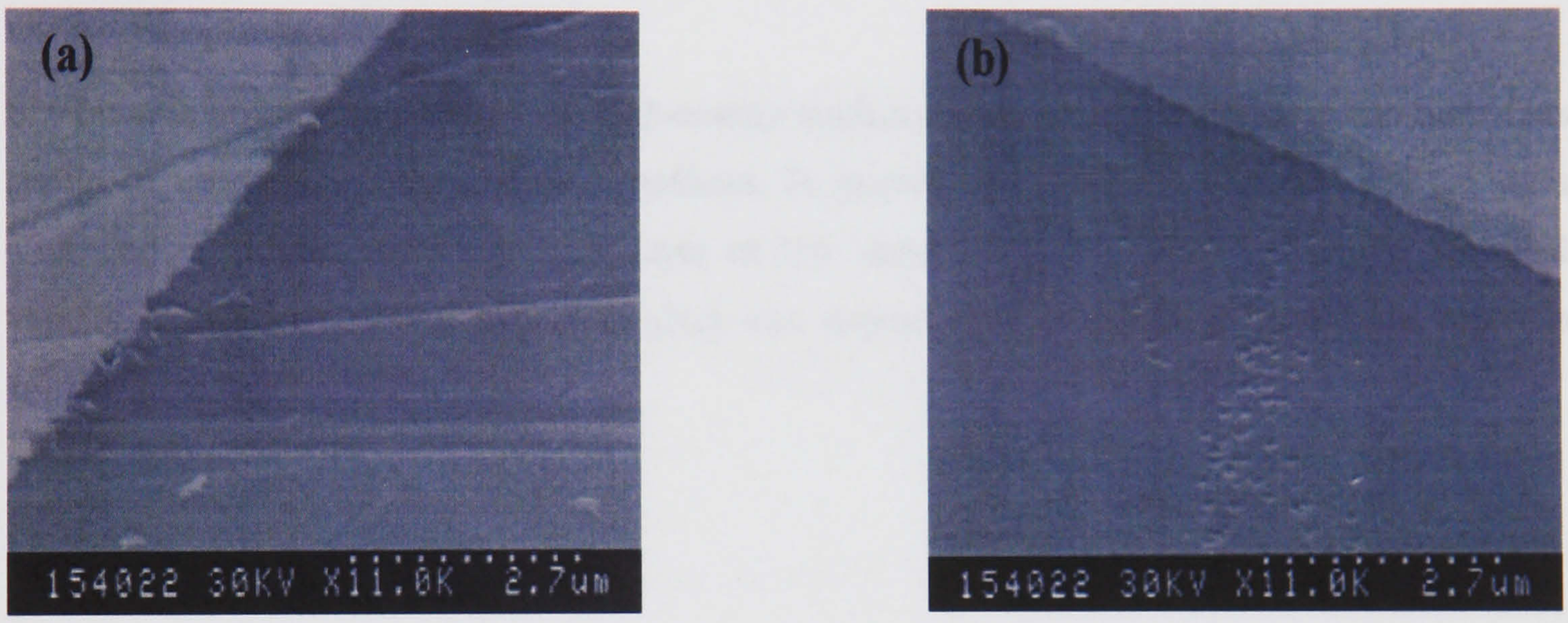

Figure 4-3. SEM images of showing **(a)** lift-off and **(b)** wet etch formed electrodes.

4.2 Flow channel

To contain the samples flowing over the electrode arrays a flow channel was formed with the upper and lower channel walls comprising of the electrode arrays. As the DEP force decreases exponentially with distance from the electrode array the height of the fluidic chamber must be sufficiently small such that the electric fields produced by the energised electrodes express their non-uniformity across the entire height of the channel (see chapter five for details). A channel height of 100μm was chosen for the devices.

The flow chamber were defined using either a thick photoresist and photolithoghaphy, or by forming the channel from a sheet of thermal adhesive, which was laminated between the upper and lower electrode substrates.

4.2.1 Thick photoresist layers - SU-8

SU8-1070 (*SOTEC Microsystems*, Switzerland) a negative tone photo-resist initially developed by IBM for thick and ultra thick resist applications, is now commonly used in MEMS research (Micro Electro Mechanical Structures) (see for example [4]). It is a chemically amplified resist system based on epoxy resin technology, and has been shown to possess adhesion characteristics superior to other conventional thick resists. It is sensitive in the near-UV, 365 nm, E-beam and X-ray regions. Low optical absorption in the UV region allows the formation of nearly vertical sidewall profiles in thick films. Aspect ratios of 20:1 have been achieved in films up to 400μm [5]. Crosslinked SU-8 is chemically resistant when cured above 100 °C and thermal stability is greater than 250 °C. This thermal stability allows high temperature processing techniques such as reactive ion etching (RIE) to be used in conjunction with this resist.

SU-8 has a low wetting ability for high-energy surfaces such as gold and silicon dioxide. This results in adhesion problems on these surfaces. To increase the adhesion of the SU-8 to the glass slide and electrodes, a 200nm thick layer of low stress PECVD (plasma enhanced chemical vapour deposition) silicon nitride (Si_3N_4) was deposited over the entire substrate prior to spinning the layer of SU-8.

SU8 was processed as follows:

- Si_3N_4 covered slides were cleaned in acetone then dehydrated in nitrogen filled oven for a minimum of 30mins at 200°C.
- SU-8 was pipetted onto the slide and allowed to spread. The SU-8 coated slides were then placed on a horizontally level flat surface and left for 1-2 hours to obtain a bubble free uniform layer.
- Samples were spun at 500rpm for 10 seconds, the speed was gradually increased to 2000rpm over 10 seconds, and held at 2000rpm for a further 15 seconds. The substrate was then left for 1-2 hours to remove any edge beading.
- Samples were soft-baked in an oven for 60 minutes at 90°C and allowed to cool slowly.
- Samples were exposed to light of 365nm through a chrome mask in three equal 100 second exposures, with 60 seconds between each exposure to allow cooling of the substrate, this was followed by a postexposure baked for 15 minutes at 95°C.
- After gradual cooling the samples were developed sequentially in Microposit EC solvent (*Shipley*, UK), then 1:1 Microposit EC solvent:isopropyl alcohol (IPA) mixture, rinsed in IPA and dried under a stream of filtered air.

Finally, the Si_3N_4 was removed to expose the electrode surfaces by dry etching with C_2F_6 using a Plasmateck BP-80 DRIE (deep reactive ion etching) machine (*Plasmateck, UK*).

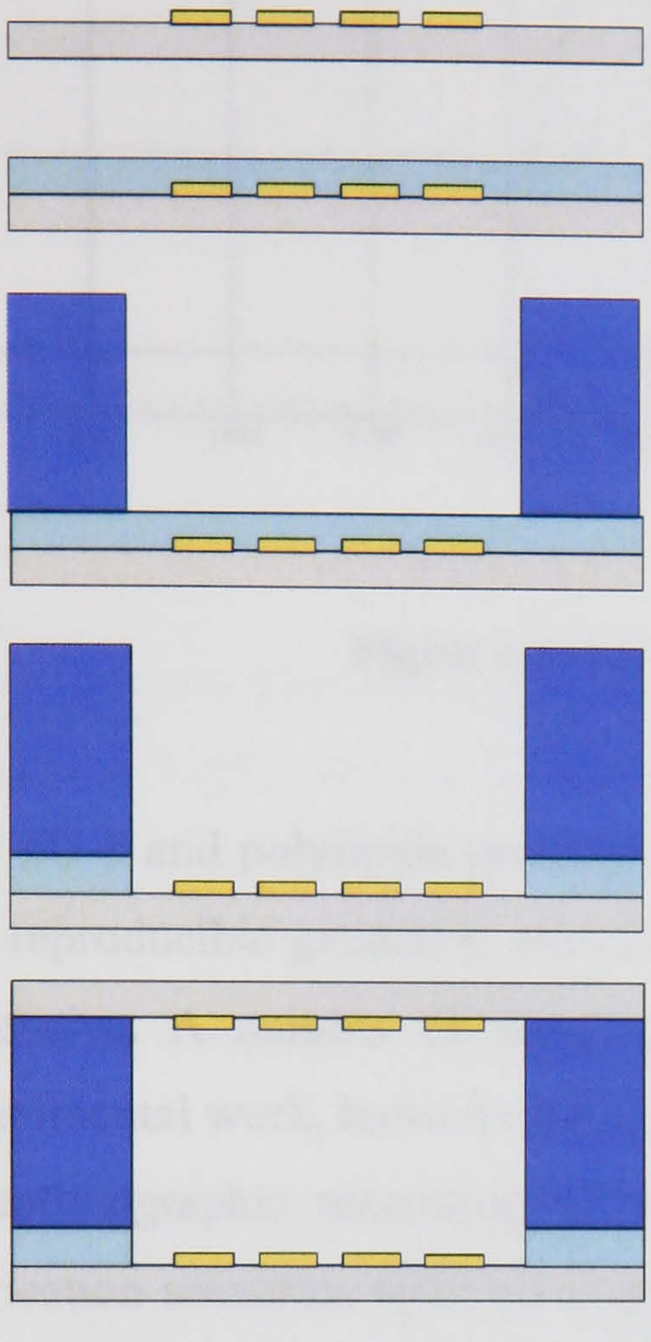

Figure 4-4. Fabrication protocol for SU8 channels

4.2.1.1 Alternative thick layer resists - Polyimide

SU-8 is only one of a number of thick film negative tone photoresists used in the MEMS industry. A number of test structures were built using an alternative resist - Durimide 7020, a polyimide based photoresist. Samples were processed in a similar fashion to the SU-8. However, problems with this resist's profile were encountered. Figure 4-5 compares the resist profiles for the polyimide and SU-8 resists. The Durimide channel structures had a tendency to shrink during the post-development bake (this is not required for SU-8). This resulted in the formation of a ridge around the channel shoulder. The ridge can be seen in trace (shown in figure 4-5b) obtained using a surface profiler.

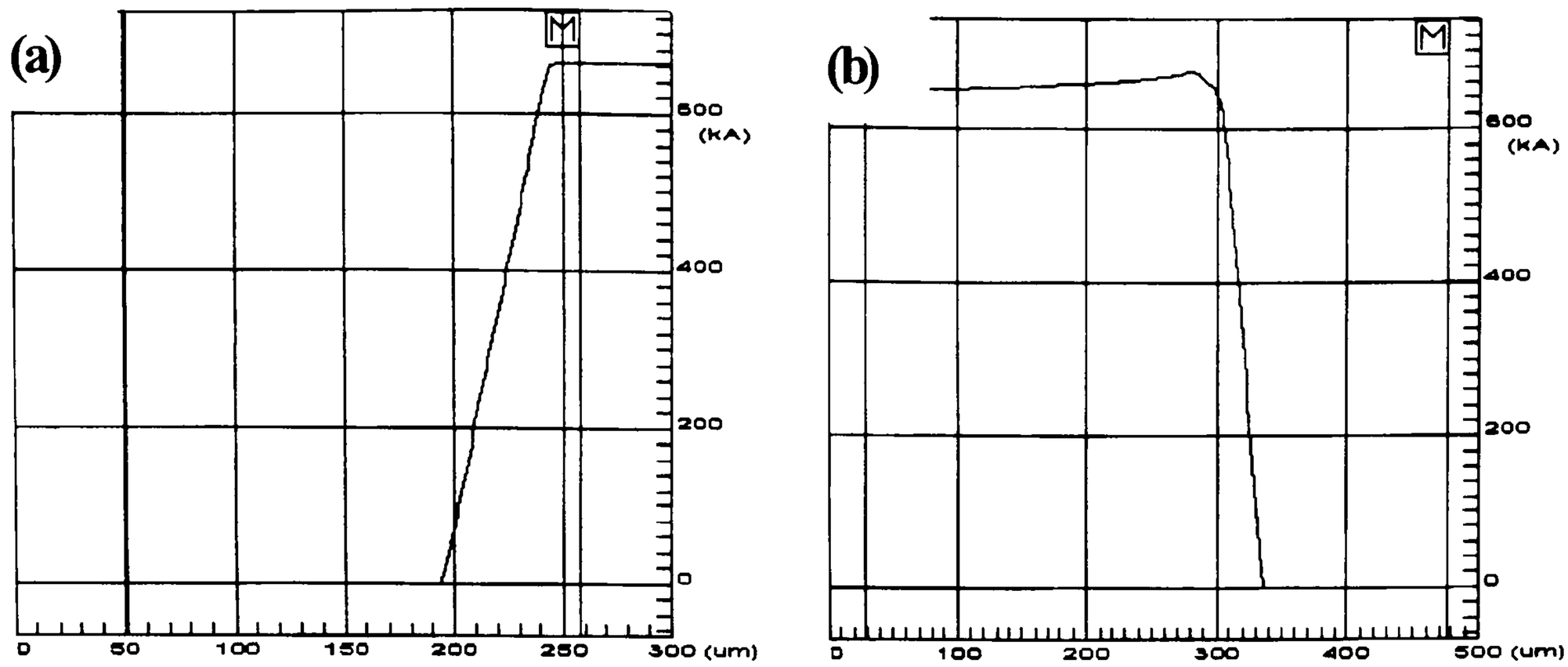

Figure 4-5. Resist profiles **(a)** SU-8 and **(b)** Durimide 7020.

The SU-8 and polyimide processes described above produce flow chambers of highly defined and reproducible geometry. However, the processing of these materials is time consuming and expensive. A number of these photoresist flow channels were produced and used in the experimental work, however the sizes of the flow channels (9mm x 50mm x 0.1mm) meant that photolithographic patterning of the channel was not necessary. As a result of this, other fabrication scenarios were investigated with the aim of simplifying device production. The use of a laminated adhesive hotmelt foil proved successful and is described below.

4.2.2 Hotmelt foil

The hotmelt foils (SIKA Werke, GmbH) were obtained as sheets, comprising an adhesive foil and a non-stick silicone-backing sheet. The flow channel was defined and cut out using a scalpel blade prior to bonding. The cut foil was placed between one half of the electrode array (i.e. the top or bottom substrate) and an unprocessed blank glass slide. The foil side was placed facing towards the electrode substrate and the non-stick silicone-backing sheet facing the blank glass slide. The samples were clamped using two medium sized bulldog clips and placed in the oven for 5 minutes at 110°C. The sample was removed from the oven and the bulldog clips removed allowing the blank glass slide and non-stick silicone paper to be removed. The second glass substrate with the mating electrode array was then placed in position with the top and bottom electrode arrays lined up precisely (see section 4.2.3) and clamped again using bulldog clips. The structure was then once again placed in the oven at 110°C for 5 minutes forming an hermetically sealed channel.

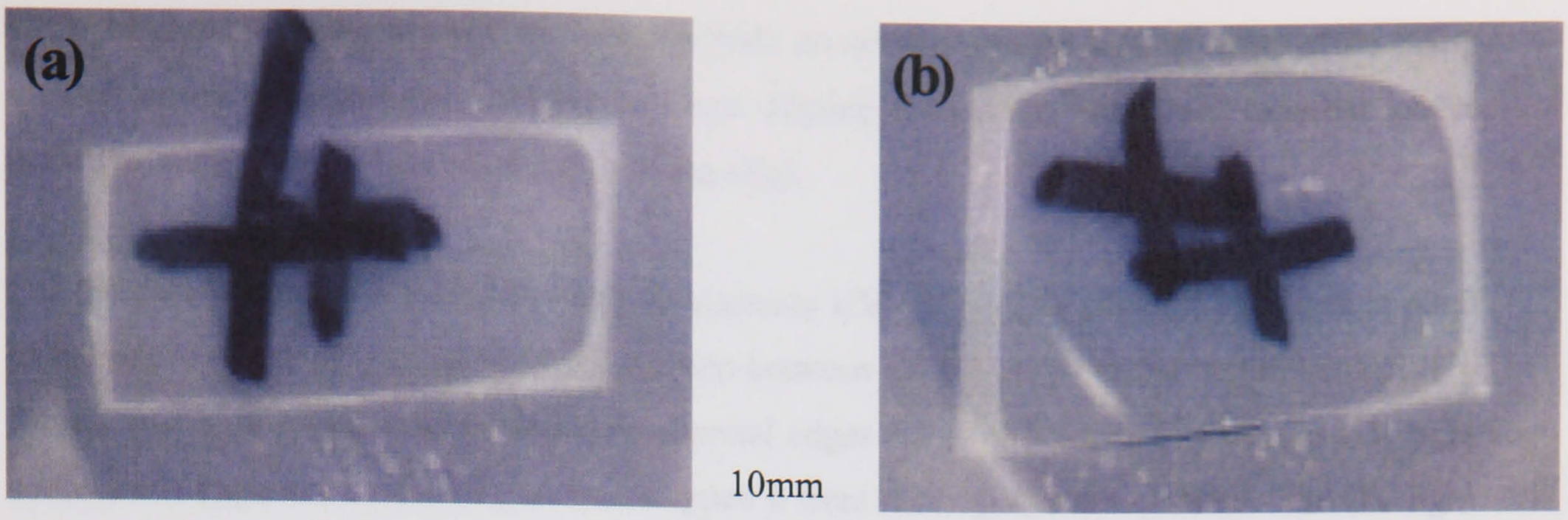

Figure 4-6. Hotmelt foil test samples showing distortion due to flowing **(a)** 110°C for 6 minutes, **(b)** 110°C for 7 minutes.

The minimum time needed for good bonding of the foil to the glass was approximately 5 minutes at 110°C. However, at this temperature, flowing of the foil will occur if the sample is left in the oven for longer than 5 minutes (see figure 4-6). Flow of the foil resulted in distortion of the channel relative to its original shape, and a reduction in channel height. An example of a channel produced using the hotmelt foil is shown in figure 4-7.

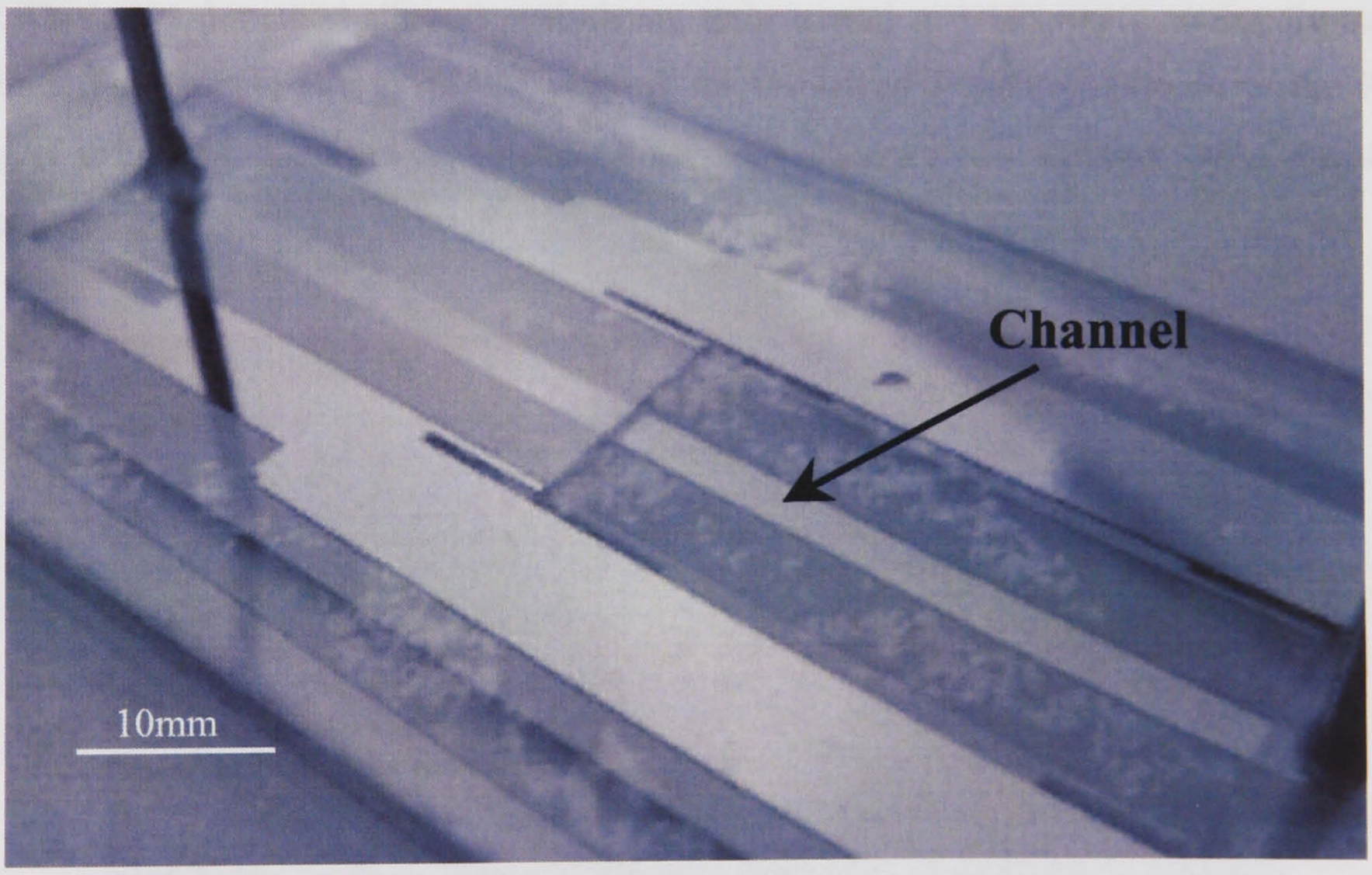

Figure 4-7. Photograph of a device made using the hot-melt foil.

4.2.3 Alignment and bounding of lid

To form a closed channel a second glass slide processed identically (but without the channel) was used to form the lid of the fluidic chamber. Inlet and outlet holes were drilled in the glass substrate prior to bonding of the lid, using 1mm diameter diamond tipped drill bits (*Diama*,

UK). Alignment of the top and bottom electrode arrays was carried out by hand while being viewed under a dissecting microscope. Once aligned the slides were held together under pressure using a spring-loaded clamp (bulldog clip).

For the case of the SU-8 channels medium viscosity UV curing glue (Loctite 350) was applied to the edges of the slides and allowed to creep between the slides under the action of capillary forces. Just as the glue reached the flow channel edges the device was exposed to a UV light source, this exposure cured the glue and stopped it from flowing into the channel. The UV light was focussed through a microscope objective allowing defined areas (1mm^2) of the device to be cured as necessary. The hotmelt foil channels were thermally bonded as described in the previous section.

4.3 Sample handling and injection

Prior to bonding inlet and outlet holes were drilled in the glass substrate using a diamond tipped drill. PEEK tubing was connected to the device either by directly glueing the tubing in place using epoxy resin, or by glueing Gripper fittings (*Omnifit*, UK) into place over the holes in the glass. This second method allowed push-fitting and removal of 1/16" PEEK tubing for sample handling. The Gripper fitting method allowed for the removal and replacement of the PEEK tubing if it became damaged or blocked. Figure 4-8 illustrates the gripper fitting method of connection.

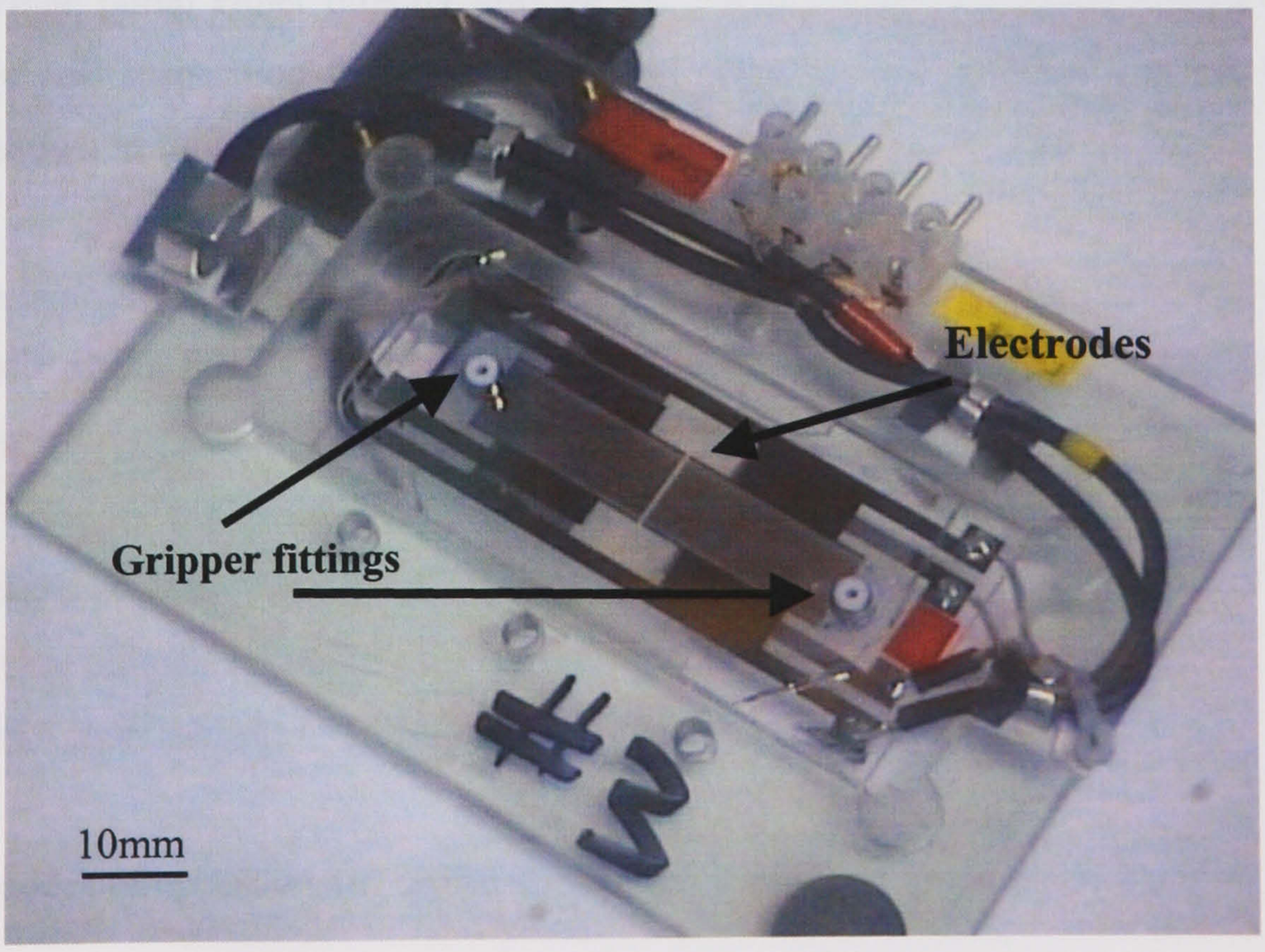

Figure 4-8. Device mounted on Perspex support (no heat sink), the gripper fittings are clearly visible.

4.3.1 Sample injection

The standard method for holding a sample prior to its introduction is to use a sample loop. Sample loops are coils of tubing of sufficient length to hold the required sample volume. This method works well for high flow rates where the velocity of the fluid passing through the loop is sufficient to carry with it all the particles (e.g. cells, beads, etc), even those which may have sedimented to the bottom of the tubing coils. This setup also works well for submicron-sized particles, where sedimentation is not a problem due to the influence of Brownian motion keeping the particles in suspension.

The sample volumes used in this work were large (0.5-2ml) compared to the device chamber size (~50μl) and the sample flow rates were relatively low (of the order of 2ml/h). In order to hold the sample volume in a loop of sufficiently low internal diameter so as to create flow velocities high enough to carry all the particles to the separation chamber, many meters of tubing would be required. This length of tubing inherently has a large internal surface area increasing the problem of cells adhering to the tubing.

The ideal method of getting the sample into the device would be to hold it in a vertical tube directly above the inlet port of the device. Any sedimentation would thus direct the cells into the device. A sample injection column was constructed with this in mind. A length of 1/8" PEEK tubing was cut to the desired length (i.e. volume). At either end, electronically controlled valves (Omnifit, UK) were fitted to allow vibration free switching of the fluid path. A third electronic valve was also required for this switching system to be realised. Cell free medium was pumped using a syringe pump either directly through the device or pumped to the sample column to displace the cell suspension from the column into the device. A diagram of the valves and column is shown in figure 4-9.

Each valve is controlled individually via switching circuitry housed in a separate control box. The positions of the three valves at any point in time can be controlled so as to allow one of three modes:

a) Sample column filling and displacement of air from column.
b) Device priming and flow of cell free medium through the device.
c) Injection of sample from column into device.

The three modes of operation are shown schematically in figure 4-9.

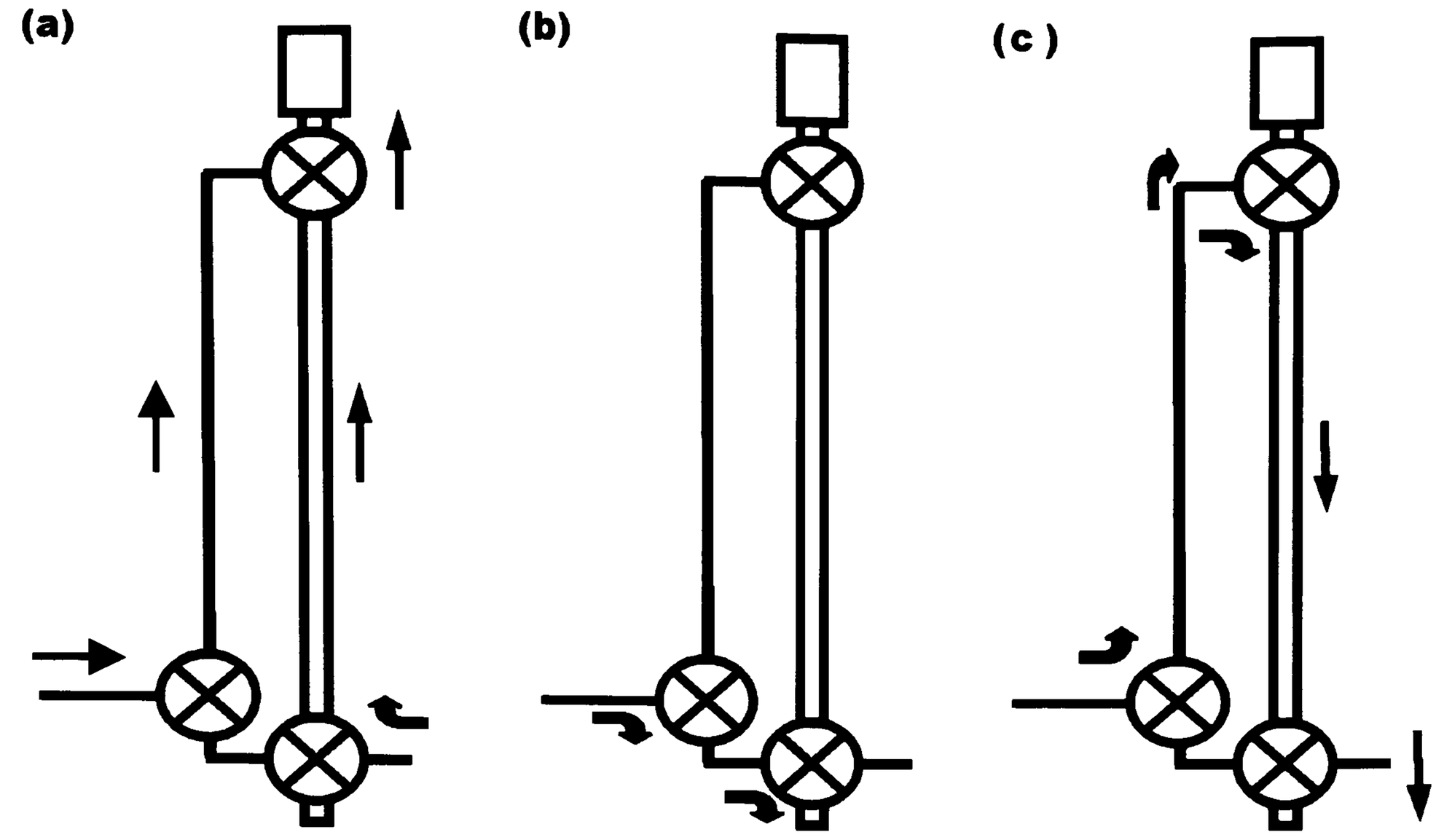

Figure 4-9. Column modes **(a)** sample filling (sample from the right, cell free medium from the left) **(b)** cell free medium into device **(c)** sample injection into device.

A diagram of the injection column and separation device is shown in figure 4-10 and a photograph of the sample injection column and separation device is shown in figure 4-11. A close up of the point where the column interfaces with the separation device is shown in figure 4-12.

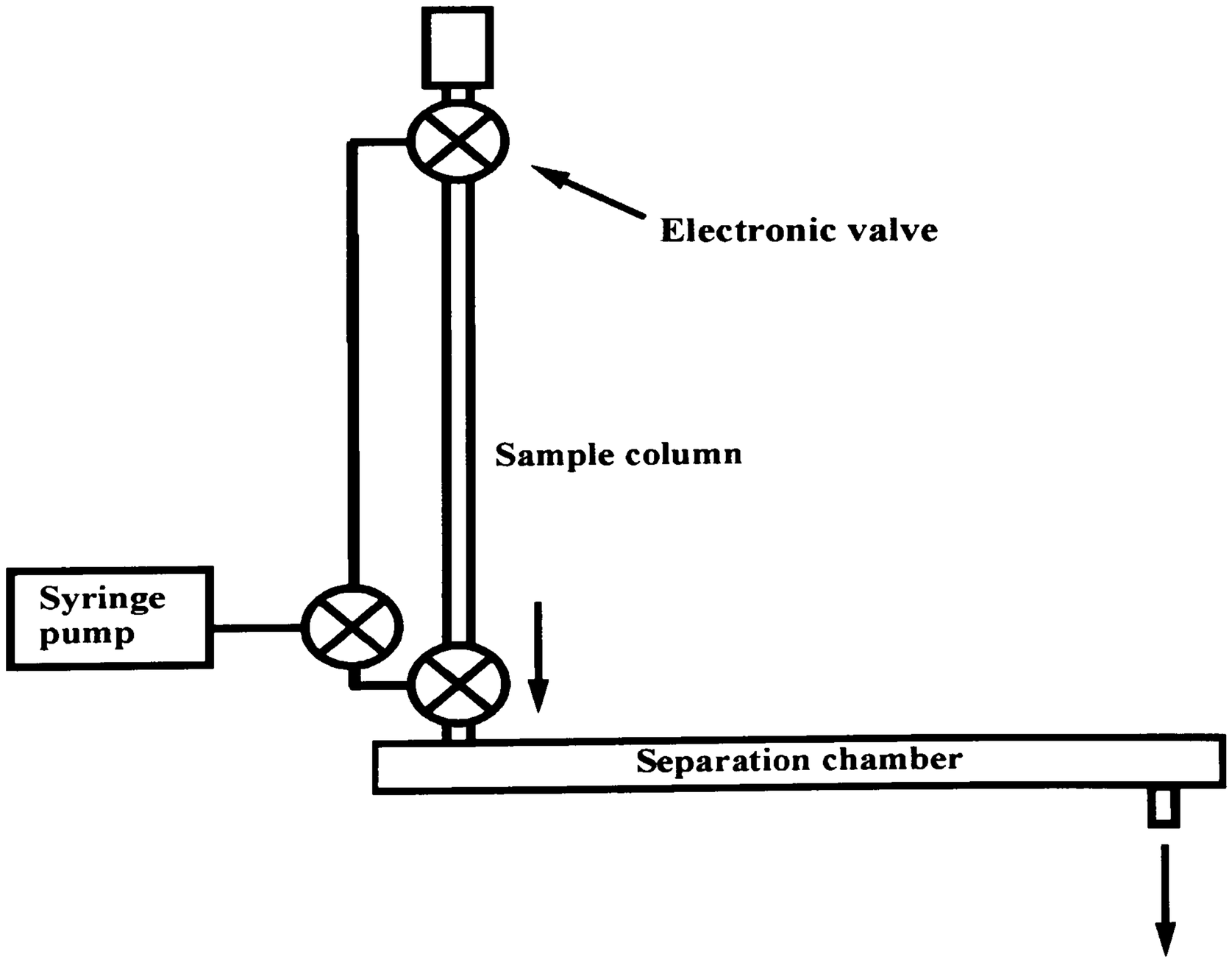

Figure 4-10. Schematic of the injection column attached to the DEP separation chip.

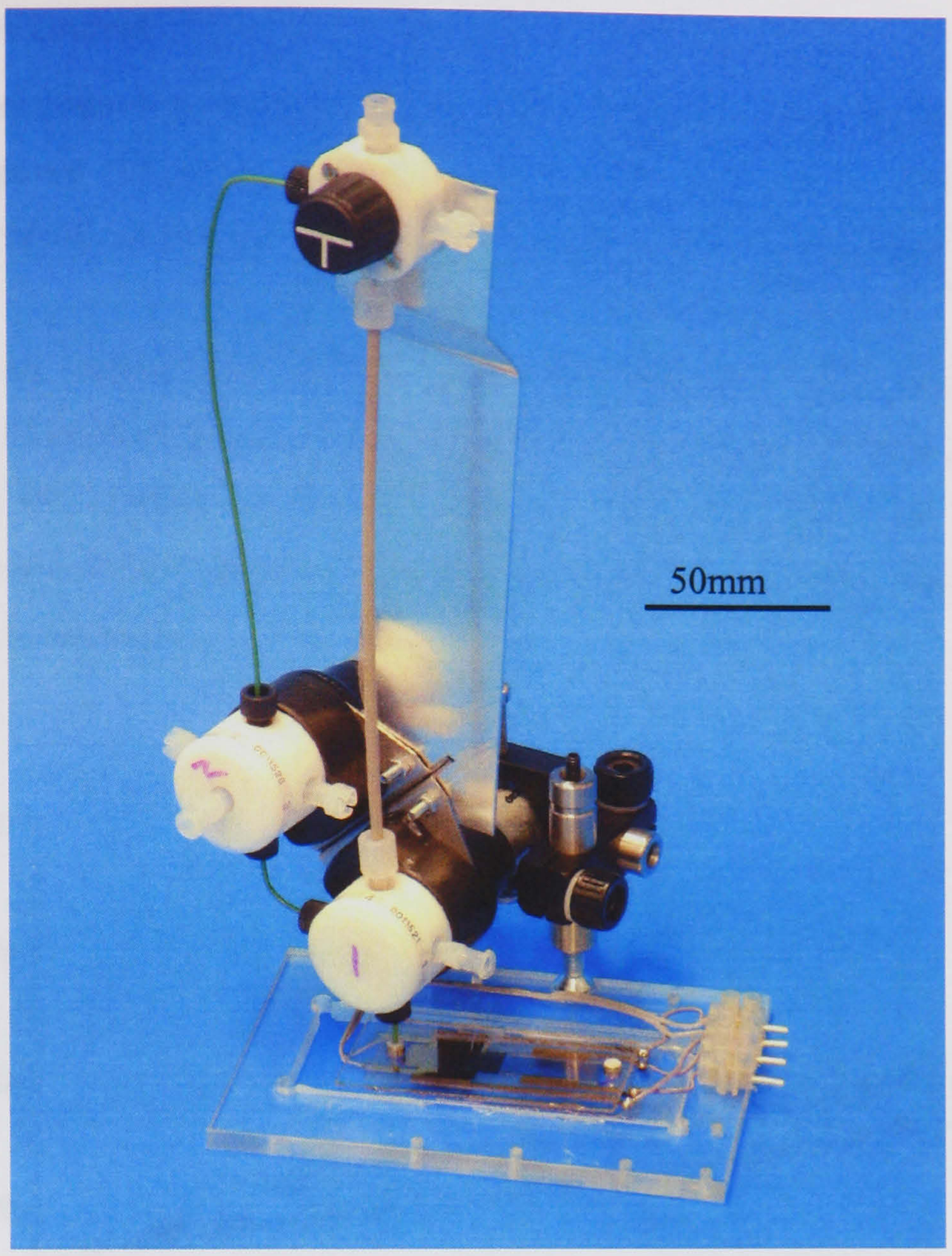

Figure 4-11. Photograph of the complete system showing the injection column and DEP separation chip.

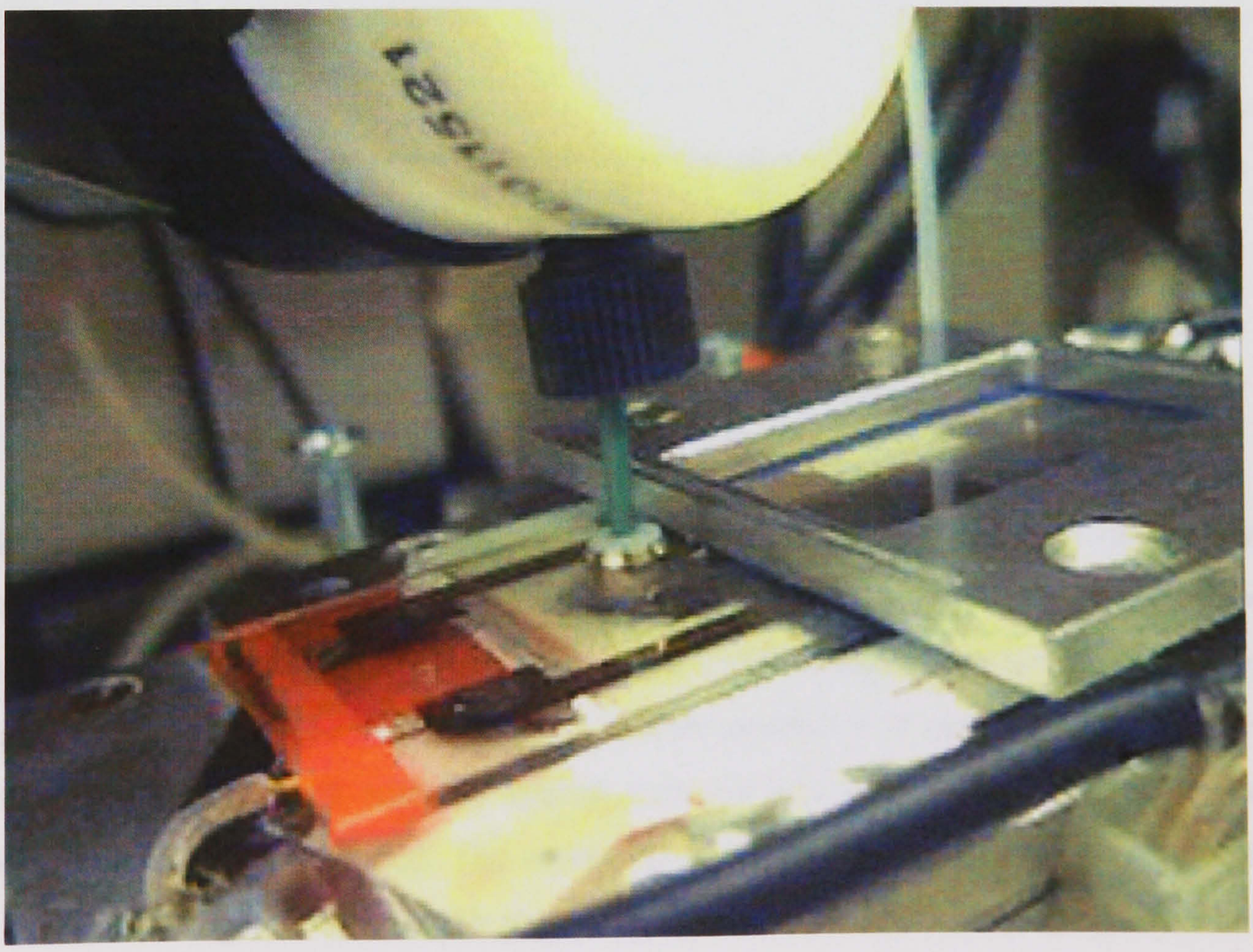

Figure 4-12. Detail of the injection column - separation device interface.

4.3 Temperature control

The large area electrode arrays (500mm^2) fabricated for this work can generate large amounts of heat due to the power dissipation in the device. This heat is potentially damaging to the cells and temperature variations will alter the dielectric properties of the suspending media.

Figure 4-13 shows measurements of the medium conductivity versus temperature for two concentrations of Ficoll400 in the standard DEP separation media described in section 3.11.2. The variation in the conductivity can be seen to be linear, with the small difference in the conductivity between the two samples being due to the addition of slightly different amounts of BSA and EDTA to the media.

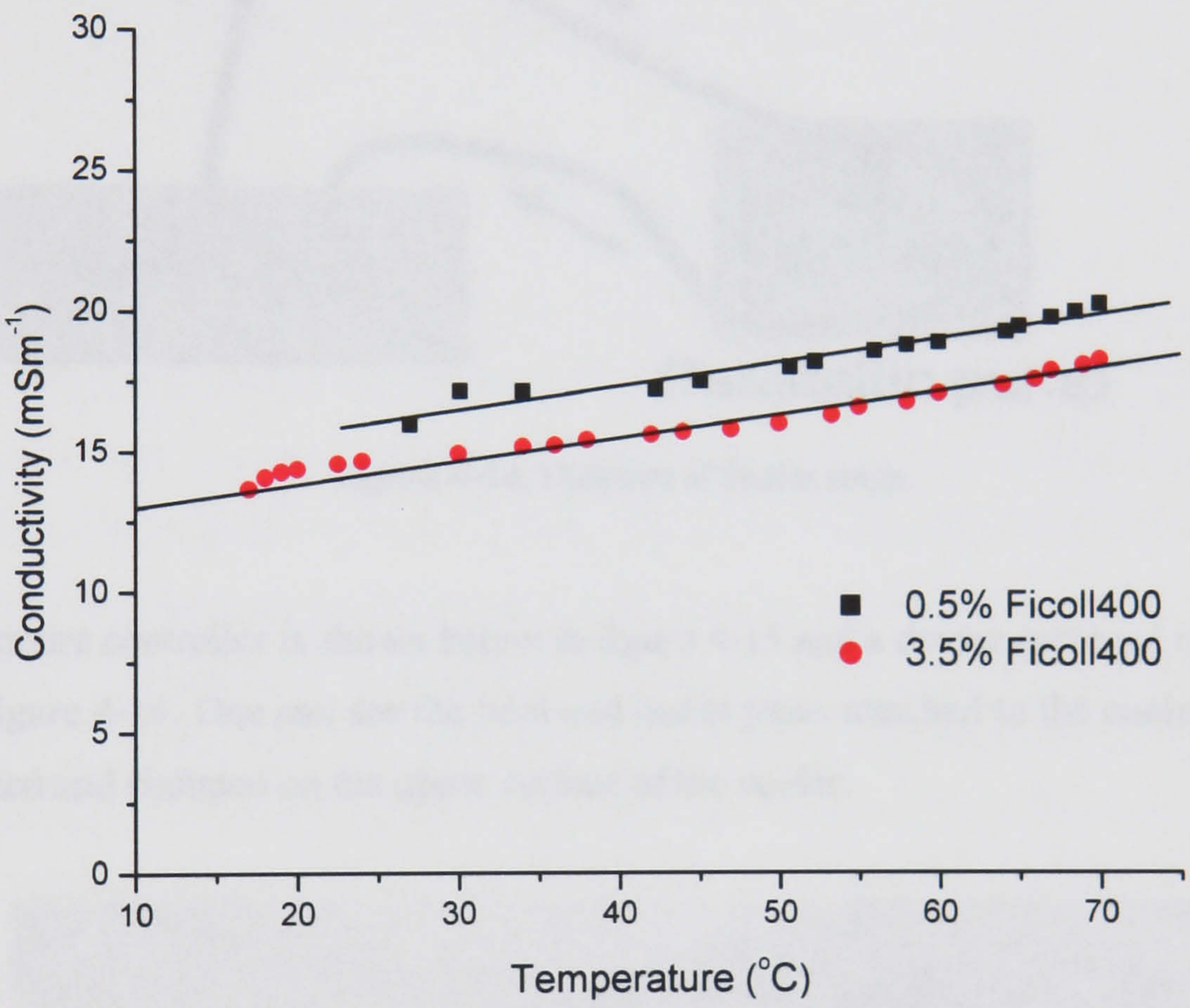

Figure 4-13. Effect of temperature change on medium conductivity.

In order to reduce the temperature in the chamber, the device was mounted (using heat sink compound) on a block of aluminium through which water of controlled temperature was pumped. The temperature of the water is controlled with a water bath and circulated using a peristaltic pump (see figure 4-14). The temperature controller is made up of two parts. The cooler, an aluminium block with an internal network of channels, through which water of controlled temperature is pumped. The second part is the clamp, made up of two aluminium plates this screws together to hold the glass separation device. The clamp has a twofold use; it

reduces the chance of leakage from the channel and allows the device to be fixed to the cooler block.

Figure 4-14 shows the temperature control system schematically. A peristaltic pump controls the flow of water from a water bath into the cooler. The temperature of the water in the water bath can be controlled, allowing thermal regulation of the cooler and DEP device.

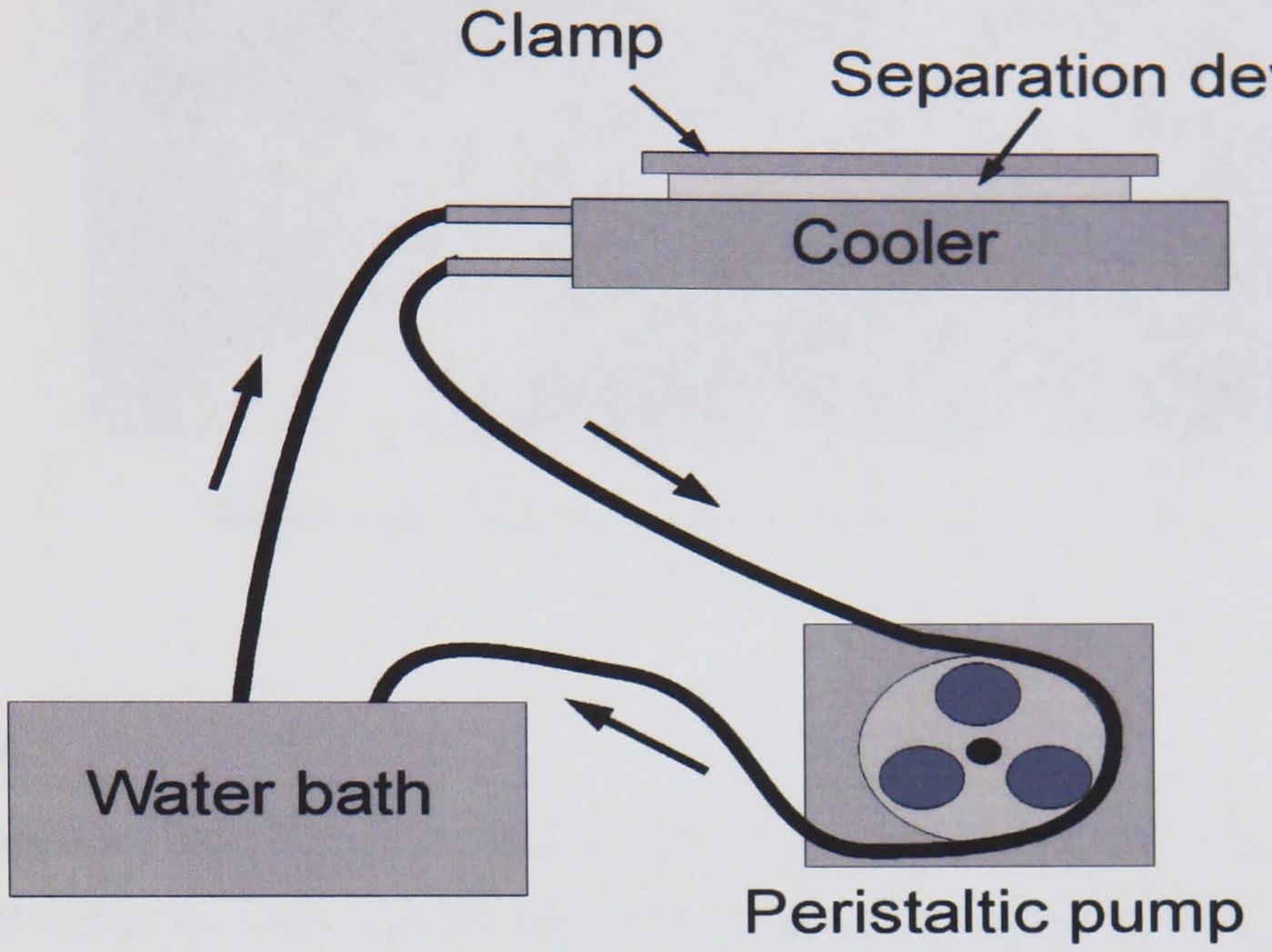

Figure 4-14. Diagram of cooler setup.

The temperature controller is shown below in figure 4-15 and a device mounted on the cooler is shown in figure 4-16. One can see the inlet and outlet pipes attached to the cooler and the DEP chip mounted and clamped on the upper surface of the cooler.

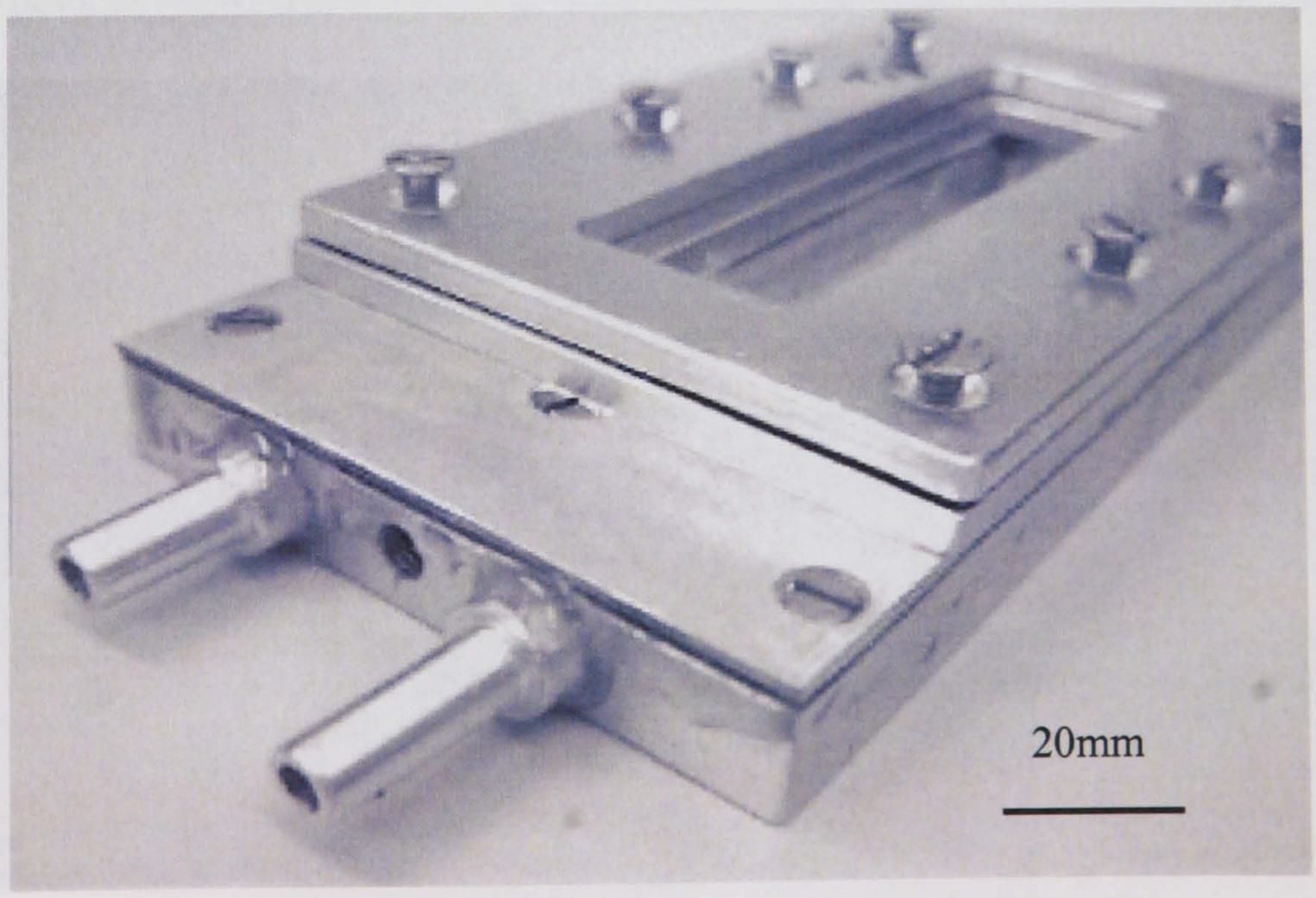

Figure 4-15. Temperature control block with device clamp attached.

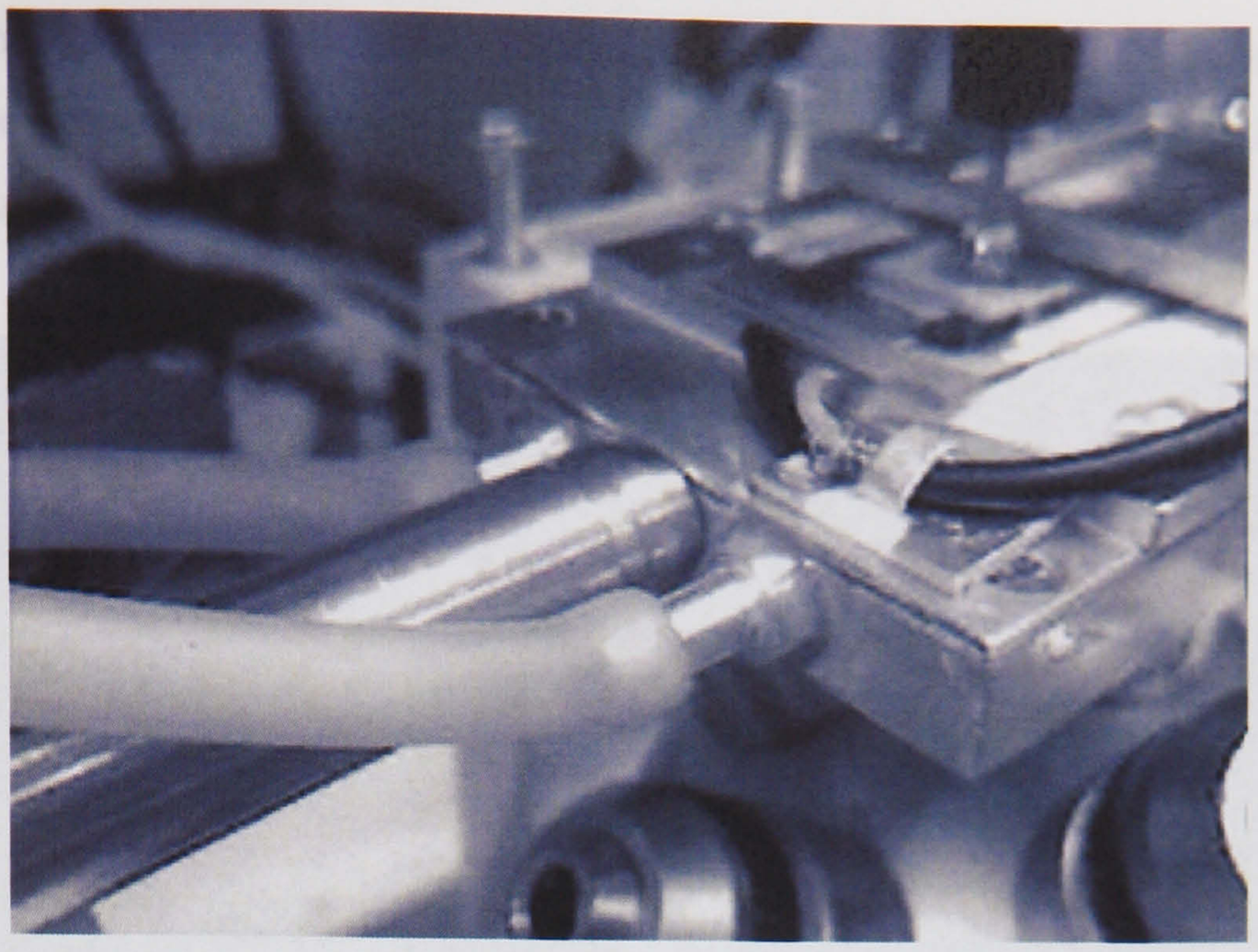

Figure 4-16. Close-up of inlet and outlet pipes for cooler.

4.4 Baffles

At high flow rates the cells held at the electrode edges by the DEP force become dislodged and tend to roll along the surface of the electrode array. In an attempt to avoid this problem and allow the use of high flow rates with reasonable applied voltages (i.e. voltages low enough such that the electric fields produced do not damage the cells trapped at the electrode edges and also to reduce heating effects) resist baffles were fabricated in the gaps between the electrodes. The aim being that as the particles are pulled down to the electrode edges they are shielded from the fluid flow in the spaces between the baffles. Thus reducing the viscous drag force tending to pull the cells from the electrode edges in the direction of the fluid flow. Experiments carried out using these devices showed that the resist baffles had no effect on cell capture (appendix A.5.1).

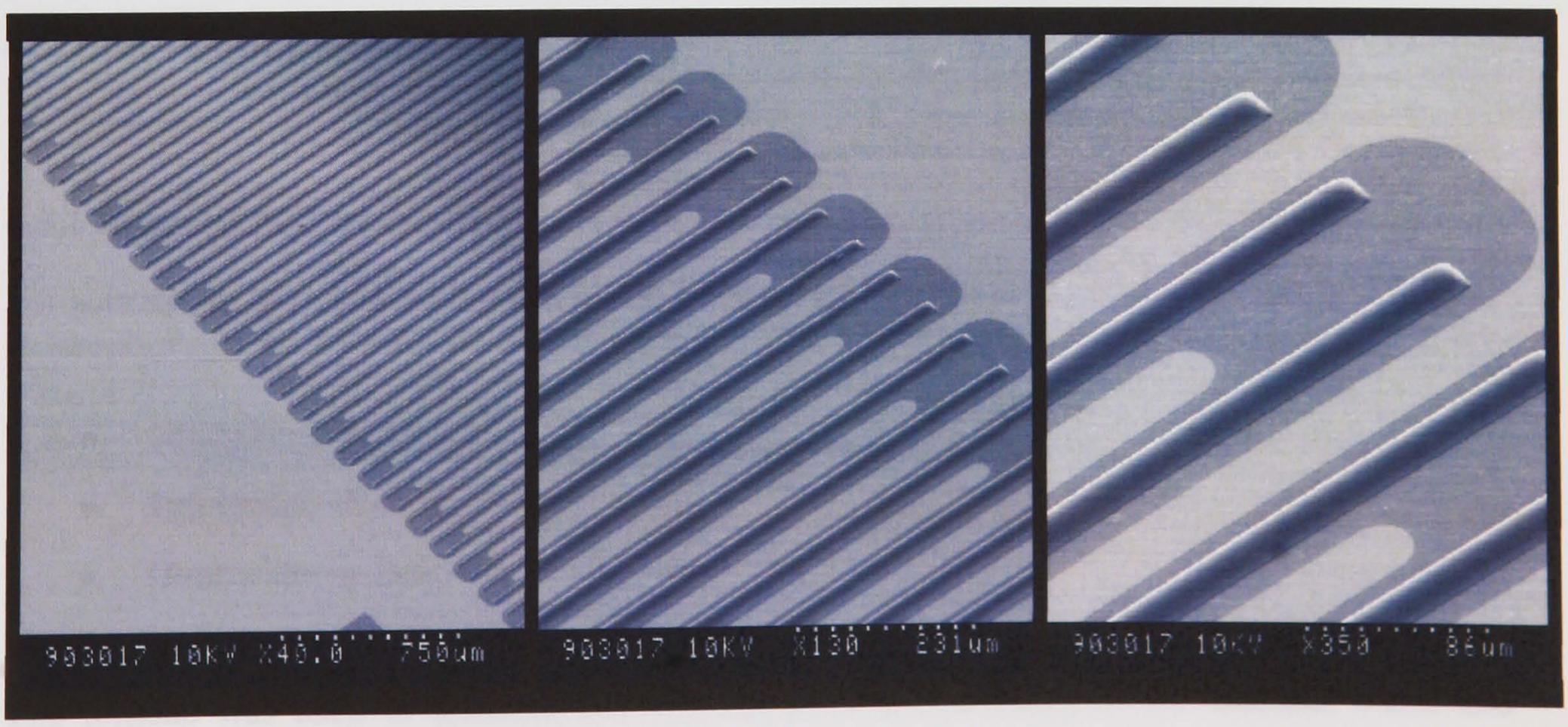

Figure 4-17. SEM of the DEP separation electrode array with resist "baffles" (black strips). The electrodes appear light grey and the glass surface of the device dark grey.

The positive tone photoresist AZ 4562 (*Clariant*, USA) similar to S1818 was used to produce the baffles. The processing was similar to that used for the S1818 resist in section 4.1.4.1. The resist baffles formed are shown in the series of SEM pictures in figures 4-17 and 4-18.

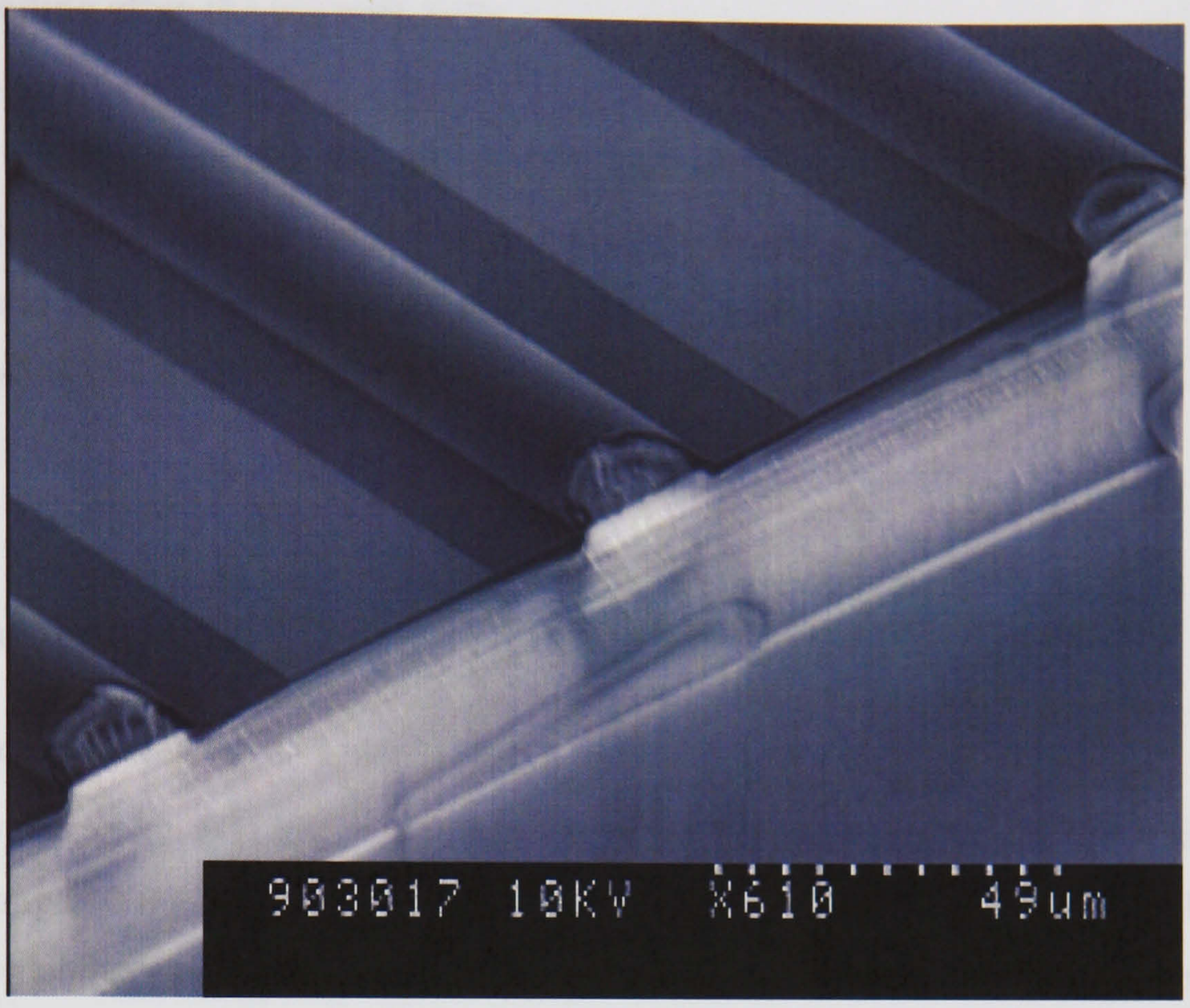

Figure 4-18. SEM of the DEP separation electrode array with resist "baffles" or "traps", the sample has been cleaved.

4.5 Cleaning

The devices were cleaned after use. The cleaning method depended on whether the experimental sample was biological or polymer based. The cleaning fluid was passed through the device as described below.

4.5.1 Removal of latex beads

For submicron latex beads cleaning of the device was as follows:

- 1ml toluene at 1ml/min.
- 1ml methanol at 1ml/min.
- 10ml water at 1ml/min.

The toluene was used to dissolve the latex beads, which adhered to the chamber walls and electrodes. However, the toluene also dissolves the polymer used to form the channel. It was

found that immediate washing with methanol and water following the toluene resulted in very little damage to the channel.

4.5.2 Cleaning after the use with cells

Following experiments involving cells, the channels were cleaned using a mixture of water and detergents. This solution was heated to 60°C and 20ml was pumped through the device at 1ml/min. The device was inspected and this cleaning step repeated if necessary. The cleaning solution found to be most effective consisted of 5% (w/v) Vircon and 1% (v/v) Tween20 in water, following this 20ml of water was passed through the device at 1ml/min.

4.6 Other equipment

4.6.1 Signal sources

Two Thurlby-Thandor TG120 function generators were used to supply sine wave signals in the frequency range 100Hz – 20MHz. These signals were amplified using an in-house built current amplifier, which boosted the signal power. Applied peak voltages of between 0V and 26V were achievable.

4.6.2 Microscopes and cameras

Various microscopes were used throughout the course of this work, they included; Zeiss Axiovert 200 inverted fluorescence microscope; Nikon Microphot upright fluorescence microscope; Nikon Microphot upright phase contrast microscope; Nikon inverted microscope; Leica dissecting microscope. Figure 4-19 shows the separation device mounted on the cooler, in position above a Nikon inverted microscope. The microscope stage has been removed to allow the device to be viewed (this was a result of the limited travel length of the objective when using the focus control, and the thickness of the cooler block and clamp). An x- y- z- micromanipulator (seen at the bottom right corner of figure 4-19) was used to move the separation device allowing the length and breadth of the electrode arrays to be scanned.

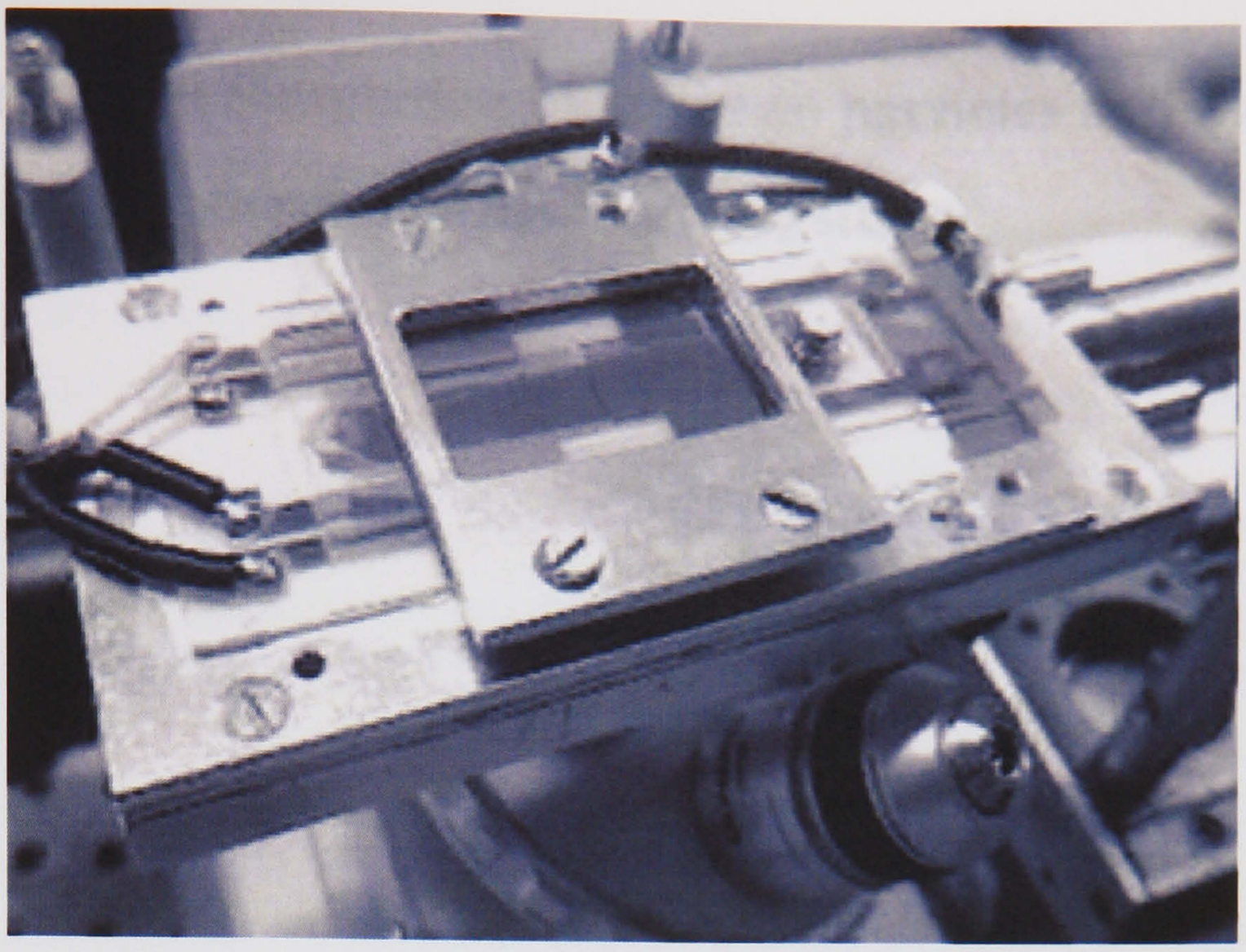

Figure 4-19. Device clamped and mounted on the cooler, above the modified Nikon inverted microscope.

The following cameras were used to capture either single images or video footage of experiments; Orca-ER (Hamamatsu Photonics, UK) controlled using SimplePCI ver5.0 (Compix Inc., PA, USA) camera control and imaging software. A filter wheel (Prior, USA) was also controlled by this software allowing the capture of multi-colour images. A JVC video camera was used to capture colour video footage over the duration of the experiments. This footage was recorded on S-VHS and frames were later "grabbed" onto computer using a Miro-DC30 (Pinnacle) image capture card.

4.7 References

1. Pohl, H.A., *Dielectrophoresis*. 1978, Cambridge: Cambridge University Press.
2. Pethig, R., *Dielectrophoresis: Using inhomogeneous AC electrical fields to separate and manipulate cells.* Critical Reviews in Biotechnology, 1996. **16**(4): p. 331-348.
3. Schnelle, T., *et al.*, *3-Dimensional Electric-Field Traps For Manipulation of Cells - Calculation and Experimental-Verification.* Biochimica Et Biophysica Acta, 1993. **1157**(2): p. 127-140.
4. *uTAS2000*. in *Micro Total Analysis Systems 2000, Proceedings*. 2000. Dordrecht: Kluwer Academic Publ.
5. Lorenz, H., *et al. EPON SU-8: a Low-Cost Negative Resist for MEMS*. in *Micromechanics Europe Workshop MME'96*. 1996. Barcelona.

Chapter Five: Simulation of forces on particles and their motion in DEP microsystems

5 Introduction

This chapter presents results of the numerical simulations used to calculate the forces experienced by particles as they pass through the particle separation system. The effect of the DEP force and the forces exerted on the particle by the fluid are used to predict the trajectories of particles as they pass through the system under different operating conditions.

The DEP separation system is based on the use of arrays of interdigitated bar micro-electrode arrays positioned on the upper and lower walls of a flow channel. The interdigitated bar electrode type was chosen as it generates a well-defined electric field for which a number of analytical solutions have been presented in the literature [1-4], one of which is used here [2].

Initially, the nature of the electric fields produced by arrays of interdigitated bar micro-electrodes is discussed. Knowledge of the electric field produced by such electrodes when energised with an alternating voltage of defined magnitude and frequency enables the calculation of the DEP force experienced by a particle. The forces arising from the interaction of the fluid with the particles are also discussed.

Owing to the complexity of the expressions involved, the development of an analytical solution for the problem would be difficult. Numerical techniques were therefore used to obtain a solution for the partial differential equations (PDE) involved. The Euler method [5] was used to iteratively calculate the forces on a particle at a particular position within the channel, and from this calculate the instantaneous velocity of the particle. The particle velocity was then used to calculate the new particle position and the process repeated until the particle reached a predetermined position within the channel.

A schematic diagram of the DEP-separator is shown in figure 5-1. The system consists of two separate arrays of interdigitated bar electrodes integrated into the one device. The two sections of the device are designed to perform different actions. The initial electrode array uses negative DEP to force particles away from the chamber walls and focus them into a narrow sheet midway between the top and bottom electrode arrays. The second electrode array, down stream from the first, is the separation electrode. This electrode array is energised such that all the particles experience positive DEP and are attracted and held at that array. For a given set of operating conditions the trajectory of a particle and its final position along the separation electrode array are defined by the particle's size, density, dielectric properties and the suspending medium conductivity, density, and viscosity.

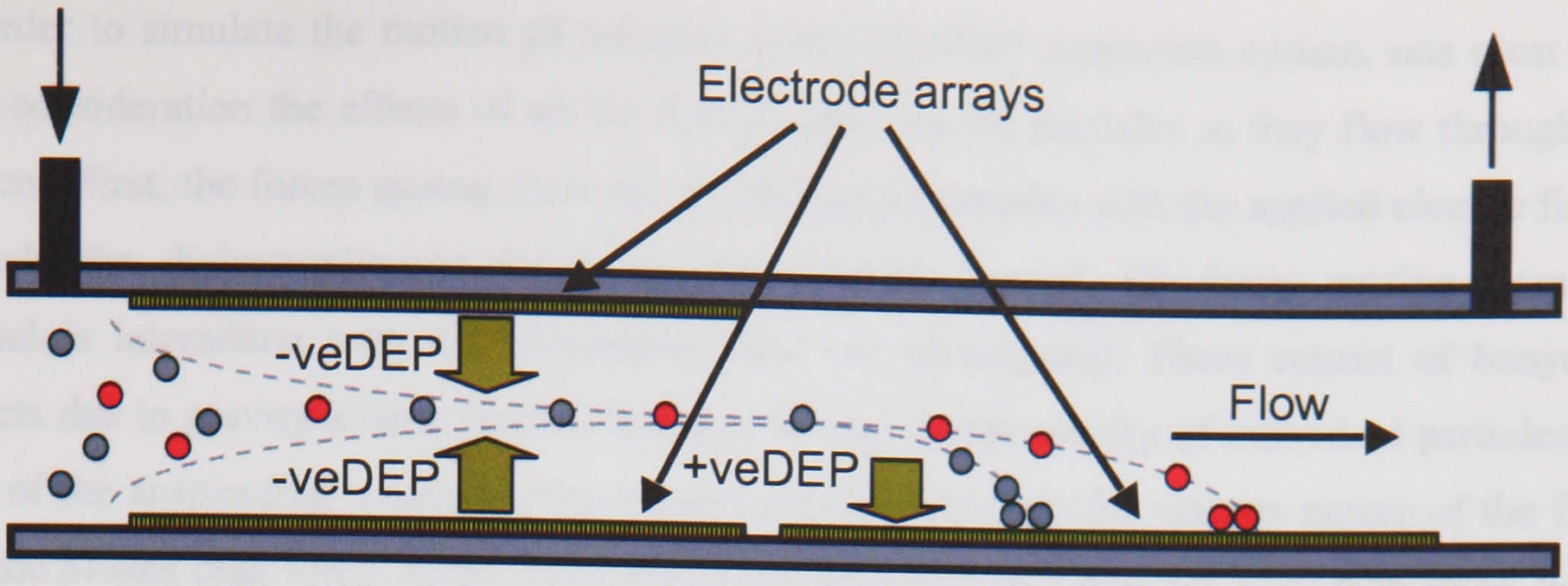

Figure 5-1. Schematic of DEP separation chip. The electrode array on the left uses –veDEP to focus all the particles into the mid-plane of the channel. The electrode array on the right uses +veDEP to attract particles to the bottom channel wall.

5.1 Methods

5.1.1 Modelling environment

Two software packages were used for the simulation work; FlexPDE (PDE Solutions, CA, USA) version 2.22, and MATLAB® (The Math Works Inc., USA) version 5.2. Simulations were run on an 850MHz Intel Pentium III personal computer running the Windows 2000 operating system.

FlexPDE is a finite element PDE solver [6]. The 2-D version of the software was used. The finite element method works by dividing the solution space into sub-regions comprised of small triangles, and solves over these simultaneously. The program solves the PDE by determining the values at discrete points at the corners of the triangles, and at the midpoints between these corners. To obtain values at other points an algorithm interpolates between the points and fits a polynomial function to each of the triangles. Details of the solution space, and boundary conditions are given in Appendix A.5.1.

The simulation programs used to numerically solve the motion of particle as they flow through the DEP separation system were written in MATLAB®. The plots of the electric field and its various components, obtained from the analytical solution of Morgan *et. al.* [2, 3] were calculated in MATLAB and the data transferred to Origin 6.1 (OriginLab, MA, USA) for plotting purposes. Particle trajectory simulations were either plotted using MATLAB's internal plotting functions or Origin. Further specific details of the numerical simulations are given in the text as and when these details become relevant.

In order to simulate the motion of particles within the DEP separation system, one must take into consideration the effects of all the forces acting on the particles as they flow through the system. First, the forces arising from the interaction of particles with the applied electric fields, namely the dielectrophoretic forces are investigated. Second, the forces arising from the particle's interaction with the suspending fluid are investigated. These consist of buoyancy effects due to gravity arising from differences in the average density of individual particles and that of the suspending medium. Also those forces arising from the viscous nature of the fluid, i.e. the Stokes drag force. Third, other forces are described including the Brownian force, which is considered in more detail at the end of this chapter.

5.2 Dielectrophoretic force

As described in chapter two, the time-averaged DEP force acting on a spherical particle is given by,

$$\boldsymbol{F} = \frac{1}{4} v Re[\alpha] \nabla \mid \boldsymbol{E} \mid^2 \tag{5-1}$$

where v is the volume of the particle, α the polarisability and $\boldsymbol{E}$ the electric field. For the particular case of a homogeneous spherical particle suspended in a liquid, the effective polarisability α is equal to $3\varepsilon_m f_{\mathrm{cm}}$, where ε_m is the permittivity of the liquid and f_{cm} is the complex Clausius-Mossotti factor [7, 8]. When this factor is positive particles experience positive DEP and move towards high field regions, when it is negative the opposite occurs.

The factor $\nabla \mid \boldsymbol{E} \mid^2$ in equation 5-1 is related to the gradient of the electric field and is dictated by the geometry of the electrodes. It has a direct influence on the DEP force on a particle, with large field gradients producing large DEP forces. For simple electrode geometries (such as the interdigitated bar electrode) analytical approximations for the field and gradient can be formulated [1-4]. Otherwise numerical techniques must be used to determine the DEP force [9].

5.2.1 Analytical solution for electric field and DEP force

An analytical solution for the electric field produced by an array of interdigitated bar microelectrodes is provided by Morgan *et. al.* [2, 3]. This solution uses Fourier series analysis to derive a simple one-dimensional expression for the force, at a distance of approximately one electrode spacing from the electrode array and beyond. A full analytical expression is also given

for the dielectrophoretic force in two dimensions. These analytical expressions were described briefly in chapter two and are presented here in greater detail.

The electrode arrays used in this work are fabricated on planar insulating substrates. Figure 5-2 shows the geometry, with electrode width d_1 and spacing d_2 as shown. The electrodes are oriented perpendicular to the direction of the fluid flow, and as such the particles will experience variations in the electric field, in both the horizontal and vertical direction, as they travel through the channel. Owing to the symmetry of this type of electrode geometry a number of assumptions and simplifications can be made [2]:

- The electrodes are much longer (z-axis) than their width d_1 so the problem can be reduced to that of two dimensions.
- The electrode array is assumed to be of infinite length so that symmetry arguments can be used to reduce the problem to a periodically repeated unit cell.
- Since the electrodes are much thinner (y-axis) than their width their thickness can ignored, allowing the potential on the electrodes to be specified as being at y=0.
- It is assumed that the potential between the electrodes is a linear function.
- The boundary condition for the electrodes is a fixed potential.

The reader is referred to the paper by Morgan *et. al.* [2, 3] for further details of the analysis.

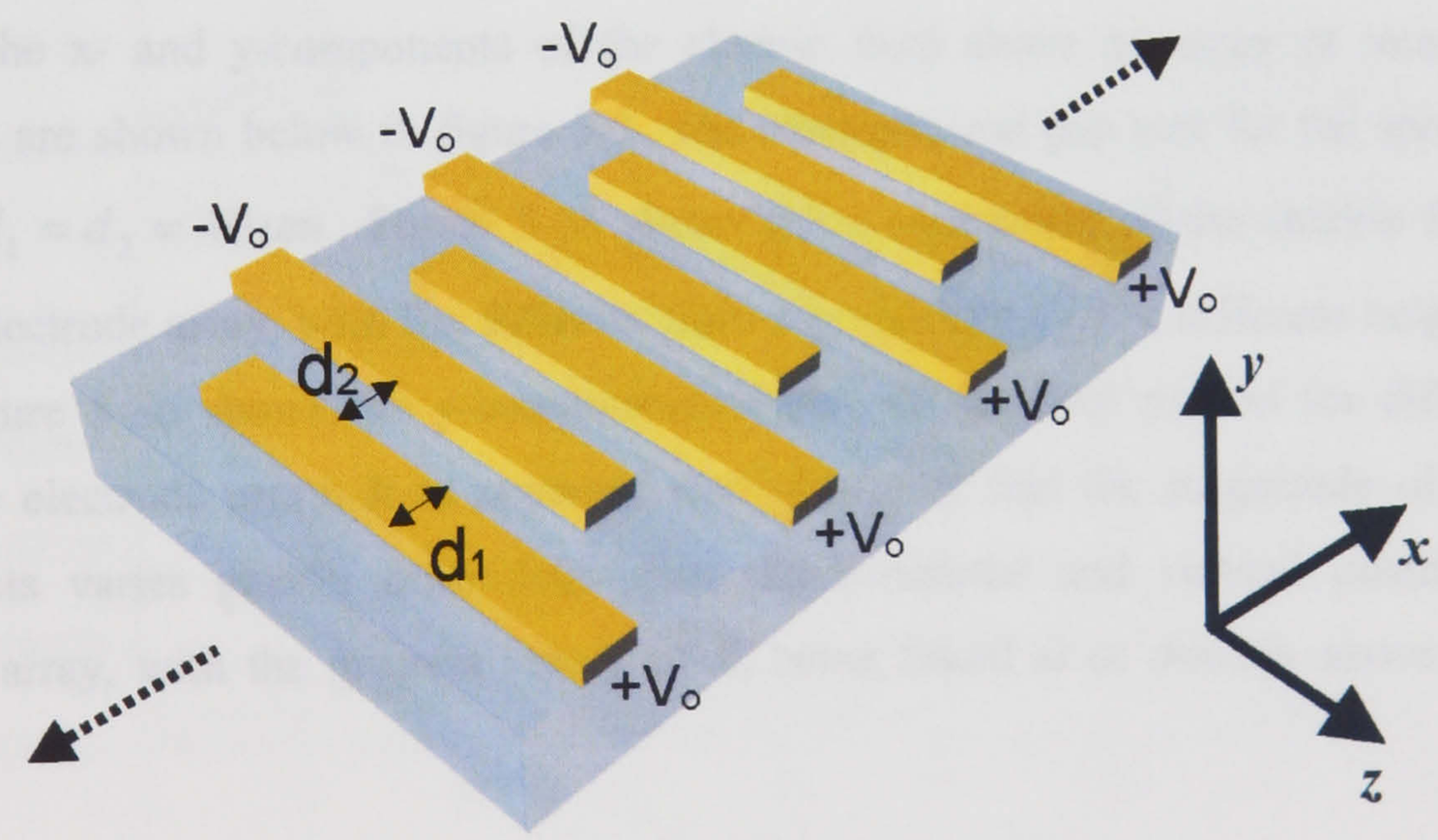

Figure 5-2. Enlarged view of an array of interdigitated micro-electrodes. d_1 and d_2 are the electrode and gap width respectively.

5.2.2 Full two-dimensional solution of DEP force

The analytical form for the two-dimensional electric field above an array of interdigitated bar electrodes is given by an infinite series sum. Assuming linear boundary conditions for the potential, and for the special case where $d_1 = d_2 = d$ the closed form expression for the horizontal and vertical components of the field at any point is given by,

$$E_x(x,y) = \frac{2V_o}{\pi d}\left[\tan^{-1}\left(\frac{\sin\hat{x}}{\sinh\hat{y}}\right) - \tan^{-1}\left(\frac{\cos\hat{x}}{\sinh\hat{y}}\right)\right] \tag{5-2}$$

and,

$$E_y(x,y) = \frac{V_o}{d\pi}\left[\ln\left(\frac{\cosh\hat{y}+\cos\hat{x}}{\cosh\hat{y}-\cos\hat{x}}\cdot\frac{\cosh\hat{y}+\sin\hat{x}}{\cosh\hat{y}-\sin\hat{x}}\right)\right] \tag{5-3}$$

where V_0 is the peak applied voltage, with V_0 and $-V_0$ applied to alternating electrodes giving a potential difference between consecutive electrodes of $2V_0$ and $\hat{y} = \pi y / 2d$ and $\hat{x} = \pi x' / 2d = \pi x / 2d + \pi / 4$, and $x' = x + d/2$.

Plots of the x- and y-components of the electric field above an array of interdigitated bar electrodes are shown below in figure 5-3. The electrode and gap size for the specific example are $d = d_1 = d_2 = 40\mu m$. Figure 5-3a shows the x-component of the electric field E_x above such an electrode array, with the different lines representing E_x at a different heights above the array. Figure 5-3b shows the y-component of the electric field plotted for different heights above the electrode array. It is apparent from the plots that the magnitude of electric field components varies greatly depending upon the horizontal and vertical position along the electrode array, with the greatest values of E_y being found at or directly above the electrode edges.

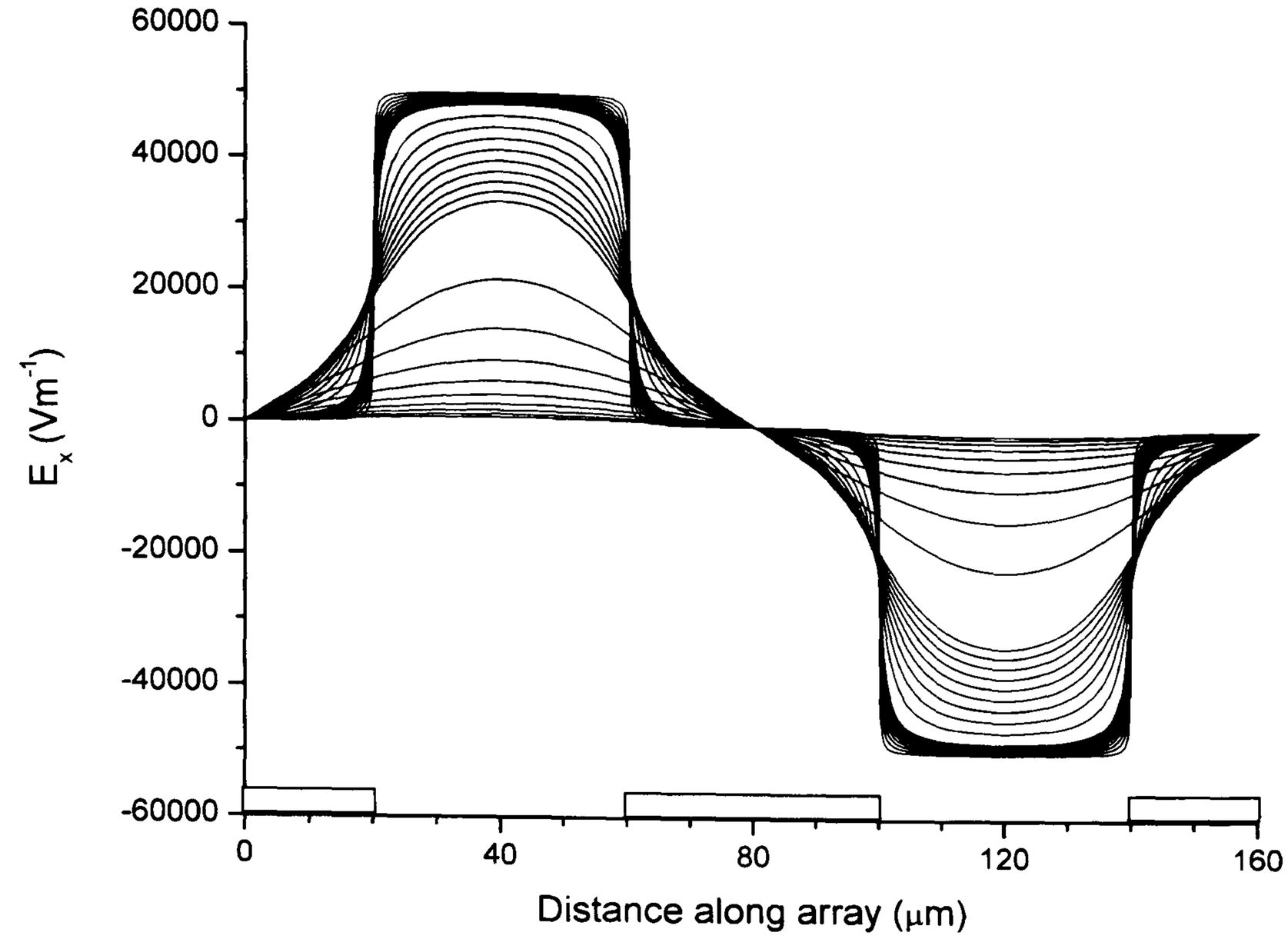

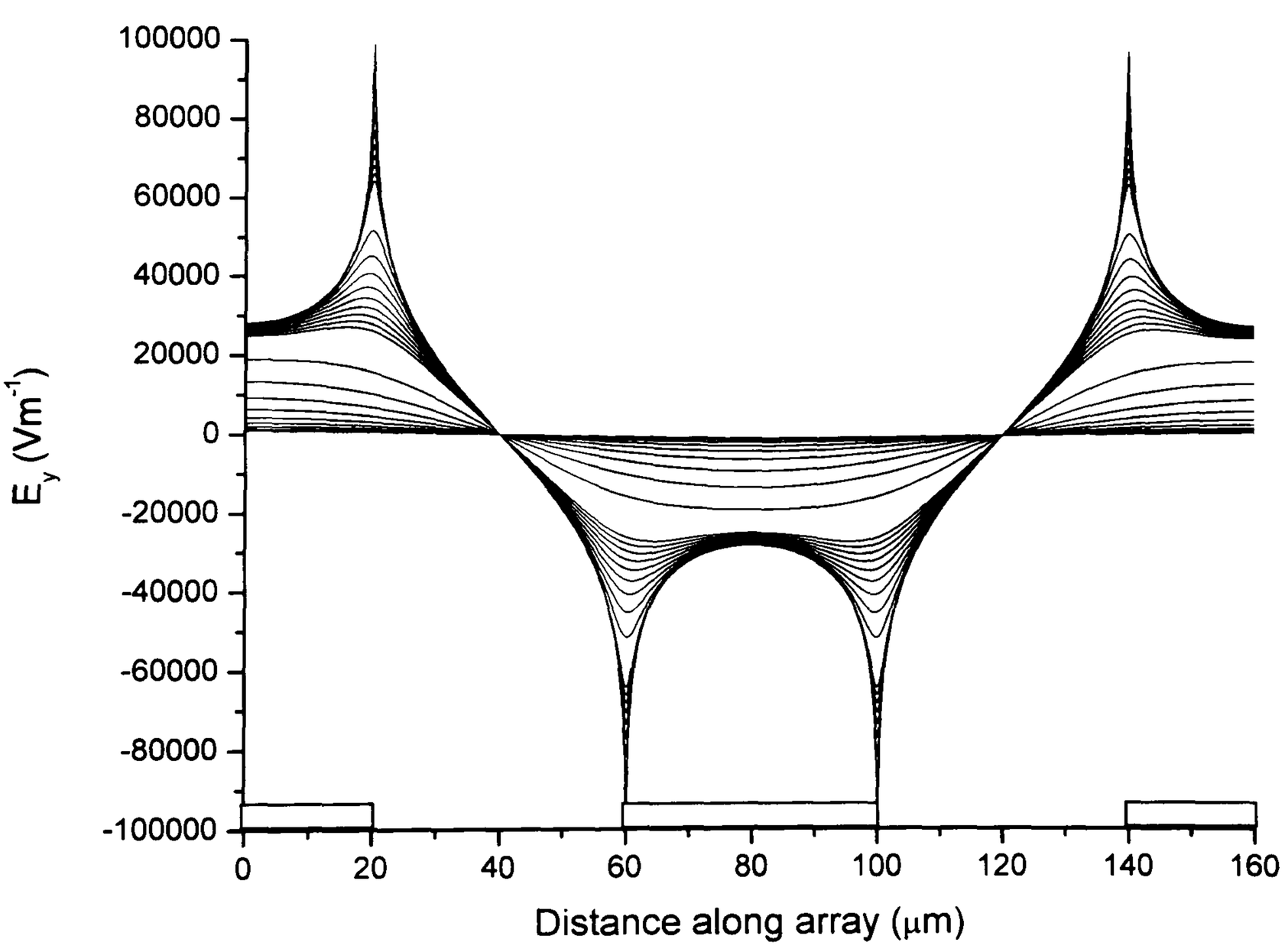

Figure 5-3. Variation of the (a) horizontal and (b) vertical components of the electric field along an interdigitated micro-electrode array. Individual lines represent the field at different heights[1] above the array, from 2μm to 100μm, with lines of higher value being closer to the electrode array. The characteristic electrode size and gap size $d = d_1 = d_2 = 40\mu m$.

[1] Heights = 2, 4, 6, 8, 10, 20, 30, 40, 50, 60, 70, 80, 90 and 100microns above the electrode array.

The DEP force is obtained from the derivatives of the electric field components, with explicit expressions for $E_{x,x}$, $E_{x,y}$, $E_{y,x}$ and $E_{y,y}$ given by:

$$E_{x,x}(x,y) = \frac{\partial E_x}{\partial x} = -\frac{\partial E_y}{\partial y} = -E_{y,y}(x,y)$$

$$= \frac{2V_o \sinh \hat{y}}{d^2}\left[\frac{\cos \hat{x}}{\cosh 2\hat{y} - \cos 2\hat{x}} + \frac{\sin \hat{x}}{\cosh 2\hat{y} + \cos 2\hat{x}}\right] \tag{5-4}$$

$$E_{x,y}(x,y) = \frac{\partial E_x}{\partial y} = \frac{\partial E_y}{\partial x} = E_{y,x}(x,y)$$

$$= \frac{2V_o \cosh \hat{y}}{d^2}\left[\frac{\cos \hat{x}}{\cosh 2\hat{y} + \cos 2\hat{x}} - \frac{\sin \hat{x}}{\cosh 2\hat{y} - \cos 2\hat{x}}\right] \tag{5-5}$$

Plots of the derivatives of the electric field components ($E_{x,x}$, $E_{x,y}$, $E_{y,x}$ and $E_{y,y}$) are shown below in figures 5-4a and 5-4b. The individual lines represent the field at heights of between 2μm and 100μm above the electrode surface.

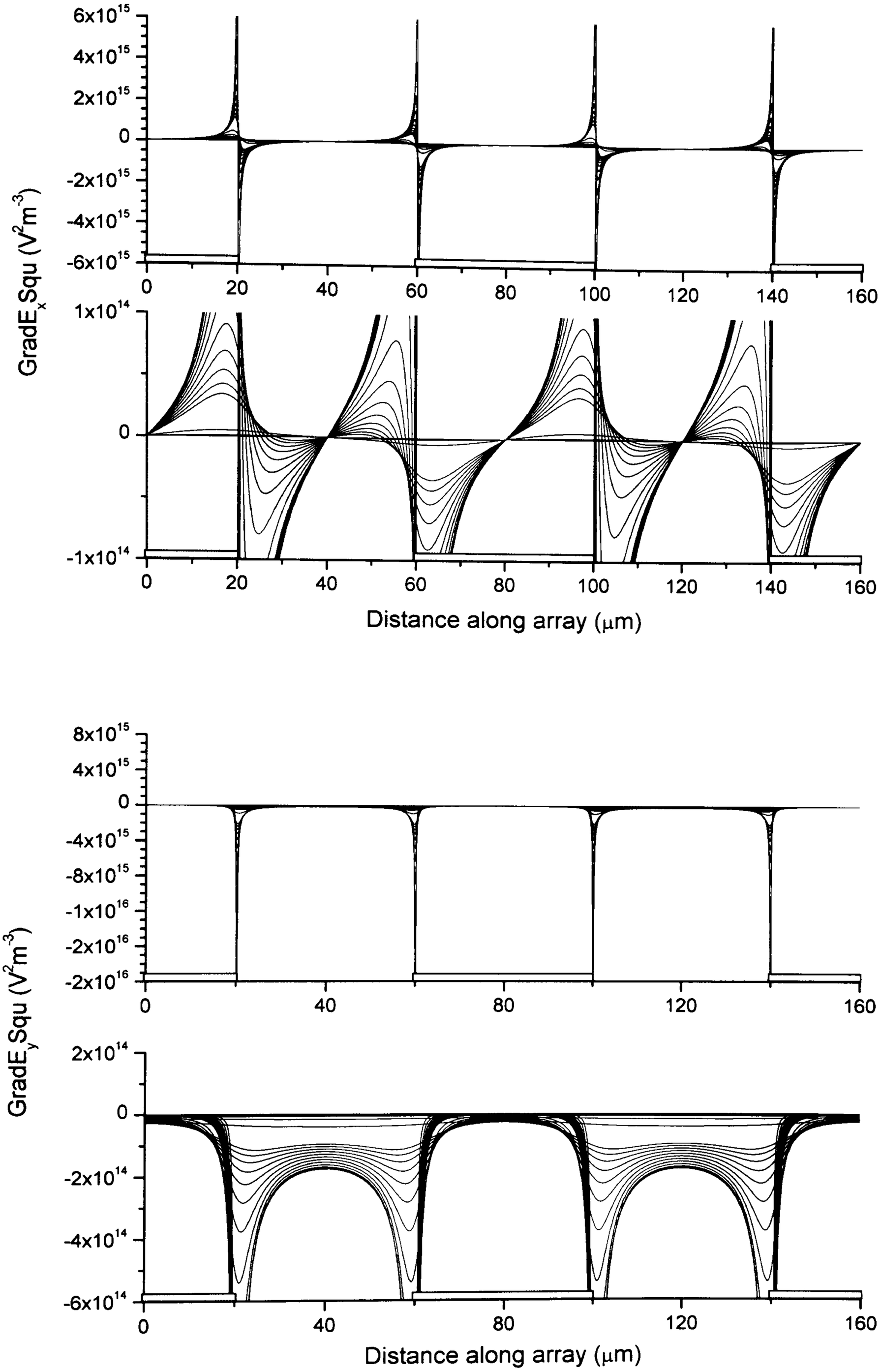

Figure 5-4. Variation of the (a) horizontal and (b) vertical components, of $\nabla \mid \mathbf{E} \mid^2$ along an interdigitated micro-electrode array. Individual lines represent the field at different heights above the array, from 2μm to 100μm. The characteristic electrode size and gap size $d = d_1 = d_2 = 40\mu m$.

The field gradient can be written,

$$\nabla(E_x^2 + E_y^2) = 2\mathbf{u}_x(E_x E_{x,x} + E_y E_{y,x}) + 2\mathbf{u}_y(E_x E_{y,x} + E_y E_{y,y}) \tag{5-6}$$

where $\mathbf{u}_x$ and $\mathbf{u}_y$ are unit vectors in the x and y directions.

The time averaged DEP force at any point above the electrode array is directly proportional to the field gradient of equation 5-6 and can be expressed as,

$$\langle \boldsymbol{F}_{DEP} \rangle = \frac{1}{4} v Re[\alpha] \nabla(E_x^2 + E_y^2) \tag{5-7}$$

Figure 5-5 shows how this factor varies, i.e. $\nabla(E_x^2 + E_y^2)$ varies with position along the array at different heights ranging from 2μm to 100μm above the electrode array. This is a direct measure of the DEP force.

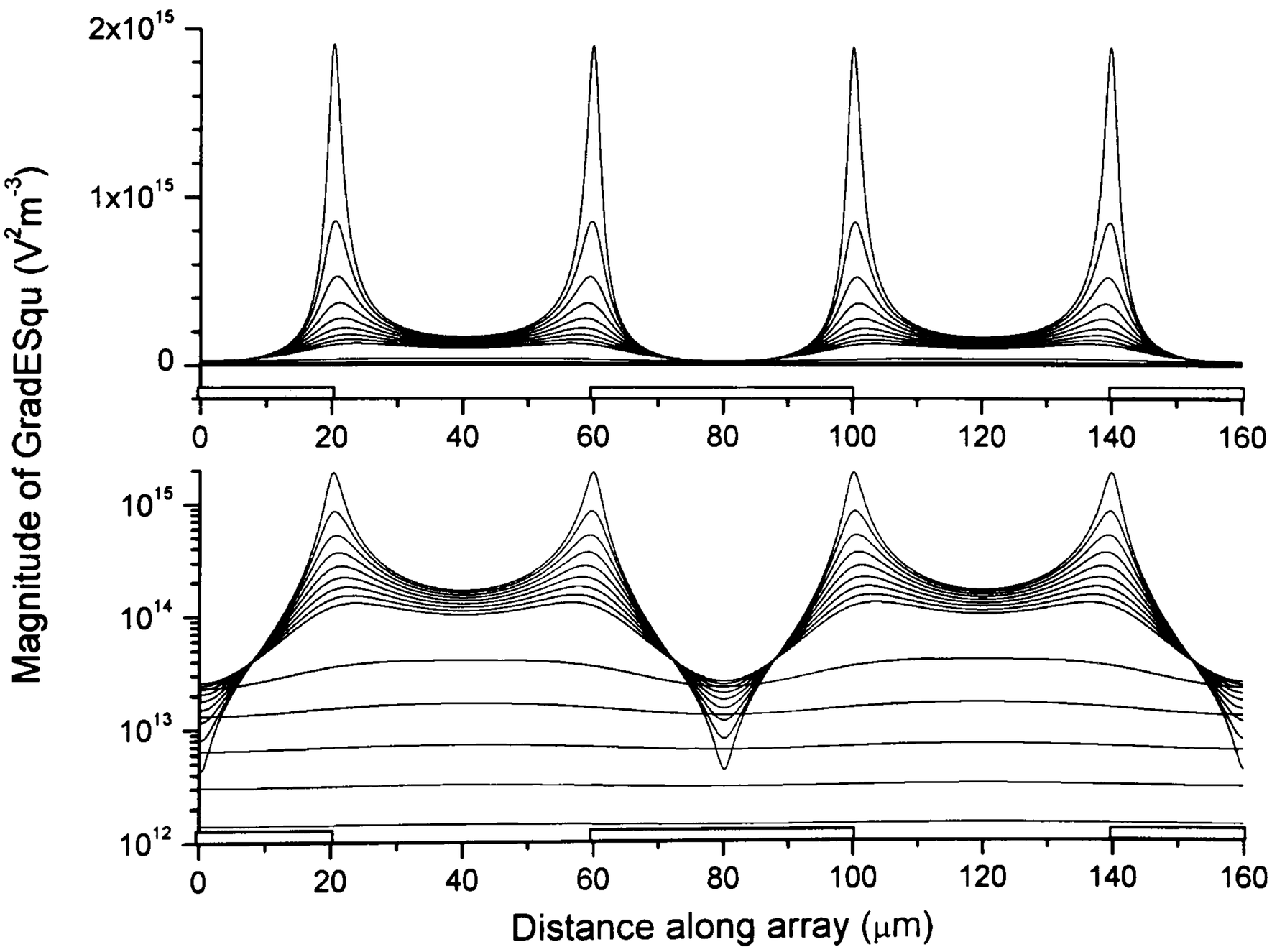

Figure 5-5. Variation of the magnitude of $\nabla |\mathbf{E}|^2$ along an interdigitated microelectrode array. This is directly proportional to the DEP force experienced by a particle. Individual lines represent the field at different heights above the array, from 2μm to 100μm. The characteristic electrode size and gap size $d = d_1 = d_2 = 40\mu m$.

5.2.3 Forces at heights greater than the characteristic electrode size *d*

The full expression for the force is an infinite series. However, at heights greater than d (where $d = (d_1+d_2)/2$) above the electrode array the higher order terms of the infinite series become negligible, and all but the first term can be neglected. This gives a simple analytical expression for the electric field gradient at heights greater than d. For the general case where $d_1 \neq d_2 \neq d$ the electric field gradient is given by,

$$\nabla|\boldsymbol{E}|^2 = -64\frac{V_o^{\,2}}{\pi d_2^{\,2} d}\cos^2\left(\frac{\pi d_1}{4d}\right)e^{-\frac{\pi y}{d}}\,\boldsymbol{u}_y \tag{5-8}$$

and the DEP force expression becomes,

$$\langle \boldsymbol{F}_{DEP} \rangle = -16\frac{V_o^{\,2}\nu}{\pi d_2^{\,2} d}\,Re[\alpha]\cos^2\left(\frac{\pi d_1}{4d}\right)e^{-\frac{\pi y}{d}}\,\boldsymbol{u}_y \tag{5-9}$$

For the special case where $d_1 = d_2 = d$ the electric field gradient is,

$$\nabla|\boldsymbol{E}|^2 = -32\frac{V_o^{\,2}}{\pi d^3}e^{-\frac{\pi y}{d}}\,\boldsymbol{u}_y \tag{5-10}$$

giving the DEP force as,

$$\langle \boldsymbol{F}_{DEP} \rangle = -8\frac{V_o^{\,2}\nu}{\pi d^3}\,Re[\alpha]e^{-\frac{\pi y}{d}}\,\boldsymbol{u}_y \tag{5-11}$$

Figure 5-6 (a) shows the variation of the magnitude of the electric field gradient for the one-dimensional expression versus height above an electrode array of electrode size $d_1 = d_2 = d = 40\mu m$ and peak applied voltages in the range 1 to 10V. Variation of $\nabla|\boldsymbol{E}|^2$ with height above electrode arrays of $d = d_1 = d_2$ =10μm, 20μm, and 40μm is shown in figure 5-6 (b).

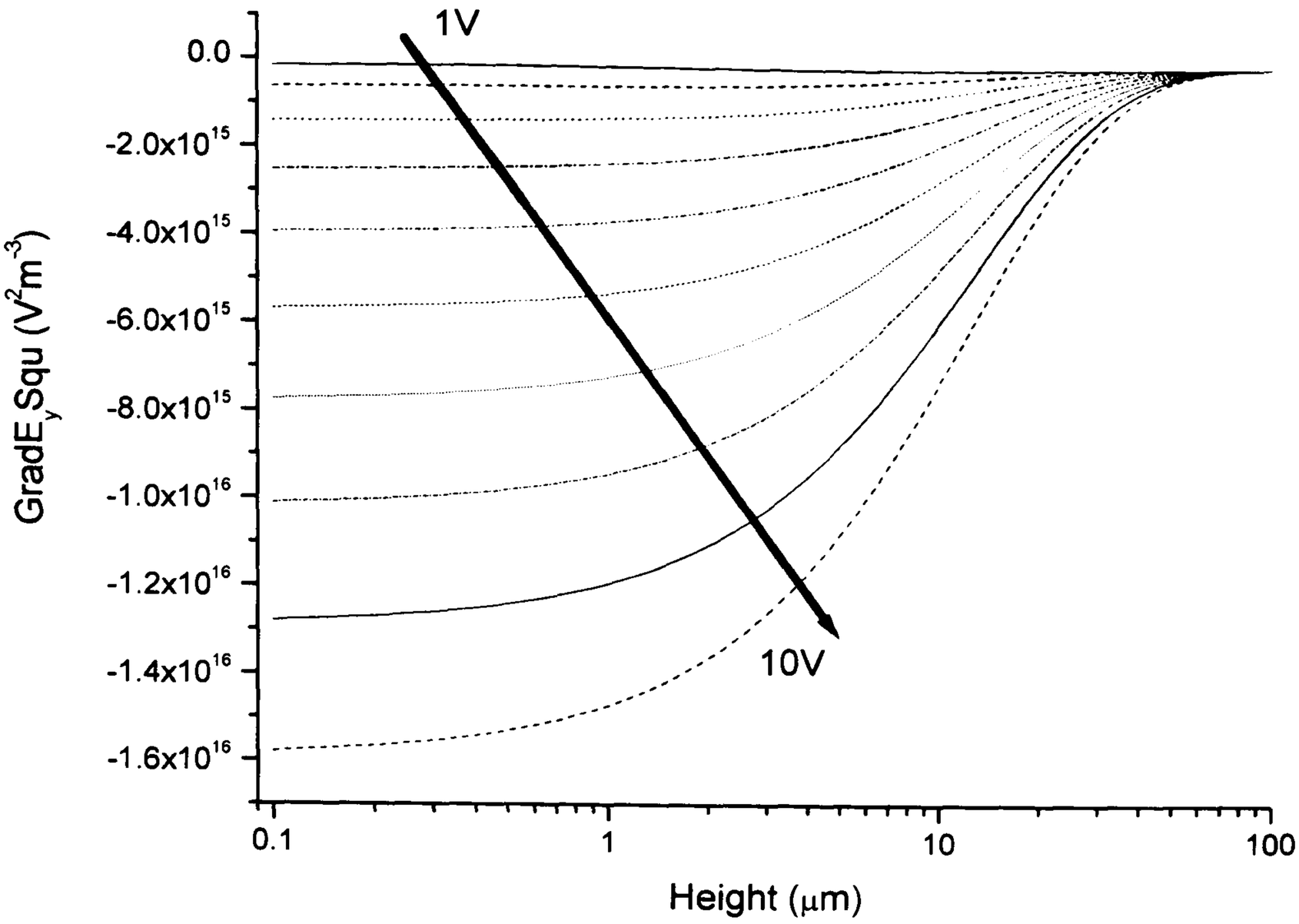

Figure 5-6 (a). Variation of the one-D magnitude of $\nabla |\mathbf{E}|^2$ versus the height above the electrode array for applied voltages from 1-10V, and $d = d_1 = d_2 = 40\mu m$.

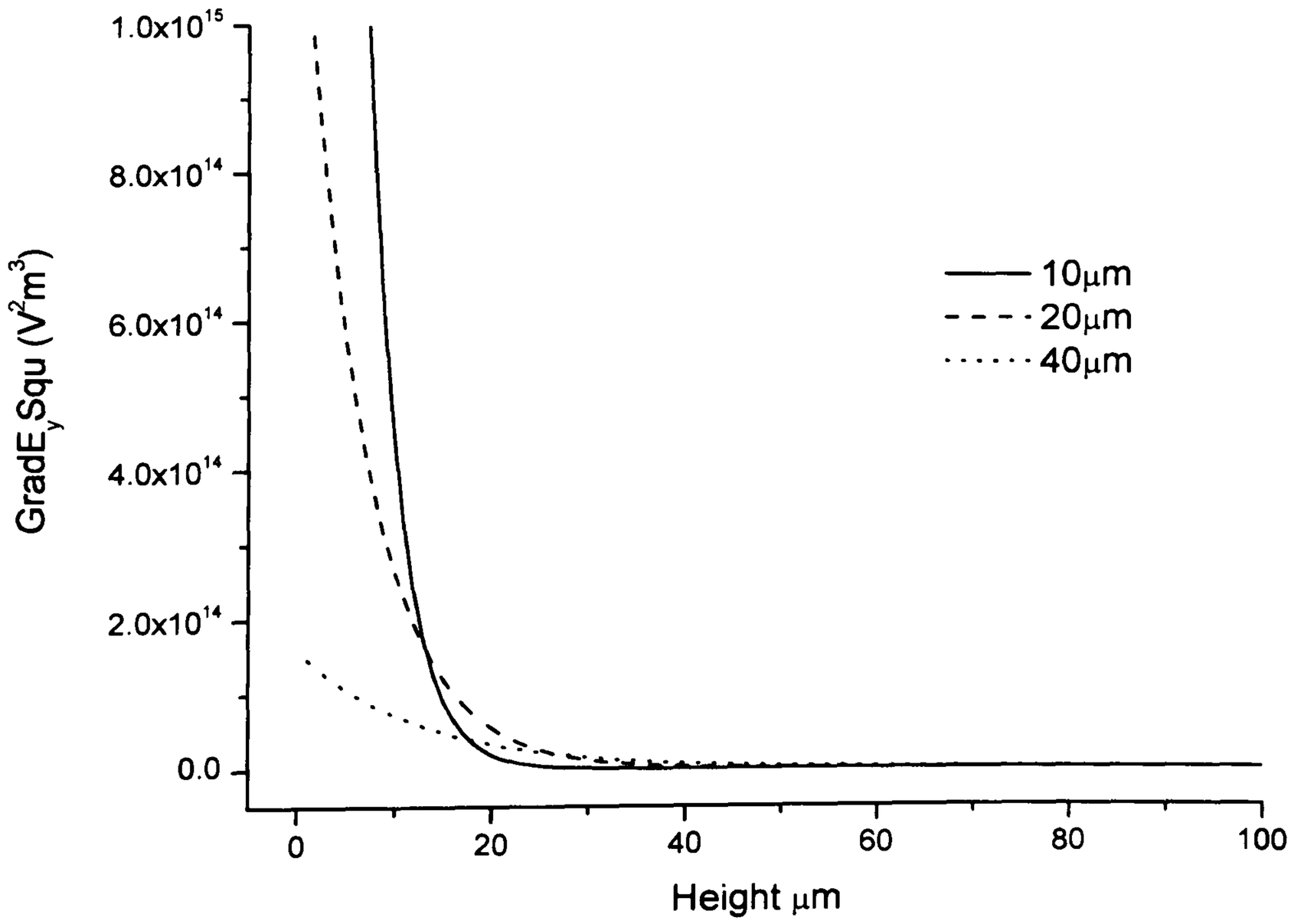

Figure 5-6 (b). Variation of $\nabla |\mathbf{E}|^2$ with height above electrodes of characteristic size $d = d_1 = d_2 = 10\mu m$, $20\mu m$, and $40\mu m$.

Figure 5-7 shows a comparison of the one-dimensional and two-dimensional electric field gradients as a function of height above an electrode array of electrode size $d_1 = d_2 = d = 40\mu m$ and applied peak voltage of 1V. The red line shows the one-dimensional field, while the black lines are plots of the magnitude of the electric field gradient variation with height along vertical slices passing through different positions along the electrode array.

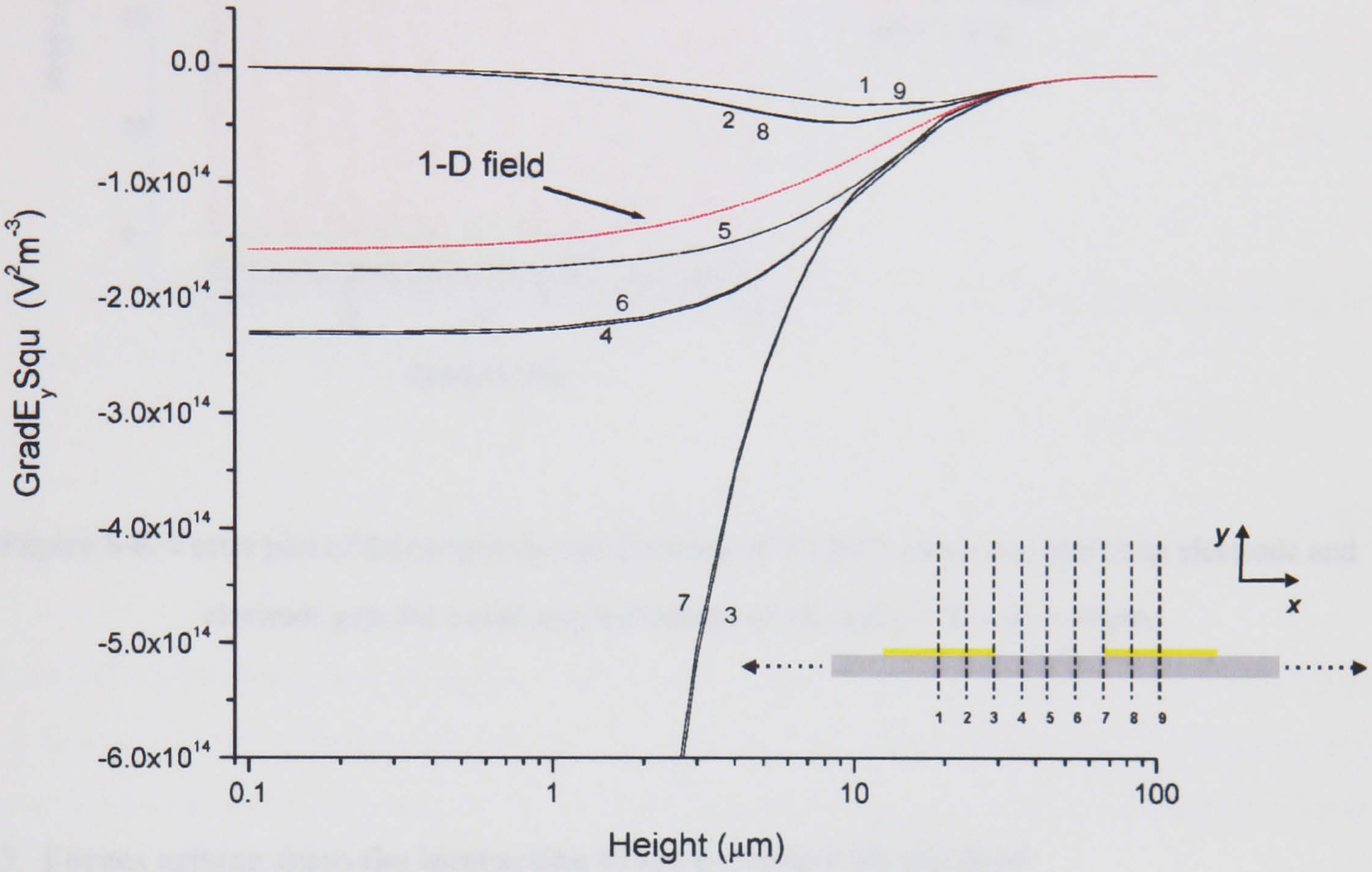

Figure 5-7. Comparison of the variation in the vertical component of $\nabla |\mathbf{E}|^2$, versus the height above the electrode array, plotted for the 1-D (red line) and 2-D (black lines) analytical solution. Peak applied voltage of 1V and $d = d_1 = d_2 = 40\mu m$. The different lines represent different cross sections through the electrode array.

When a particle is far from the electrode it initially experiences a force directed down towards the electrode array. As the particle approaches to a distance less than d, the force directs it towards the edge of one of the nearest electrodes. FlexPDE™ a 2D finite element method program for solving partial differential equations was used to solve Laplace's equation and calculate the vector field of $\nabla |E|^2$ (see Appendix A.5.1). Figure 5-8 shows the vector field above half an electrode and half a gap. This is the minimum-repeating unit space with the electric field generated by electrodes outside of this repeating unit being a mirror image of this domain. A plot of the two-dimensional field gradient in figure 5-5 shows that the variation in field above the electrode is most pronounced above or close to the electrode edges. For the case of –veDEP the vector field is the same but the direction of the vectors is reversed.

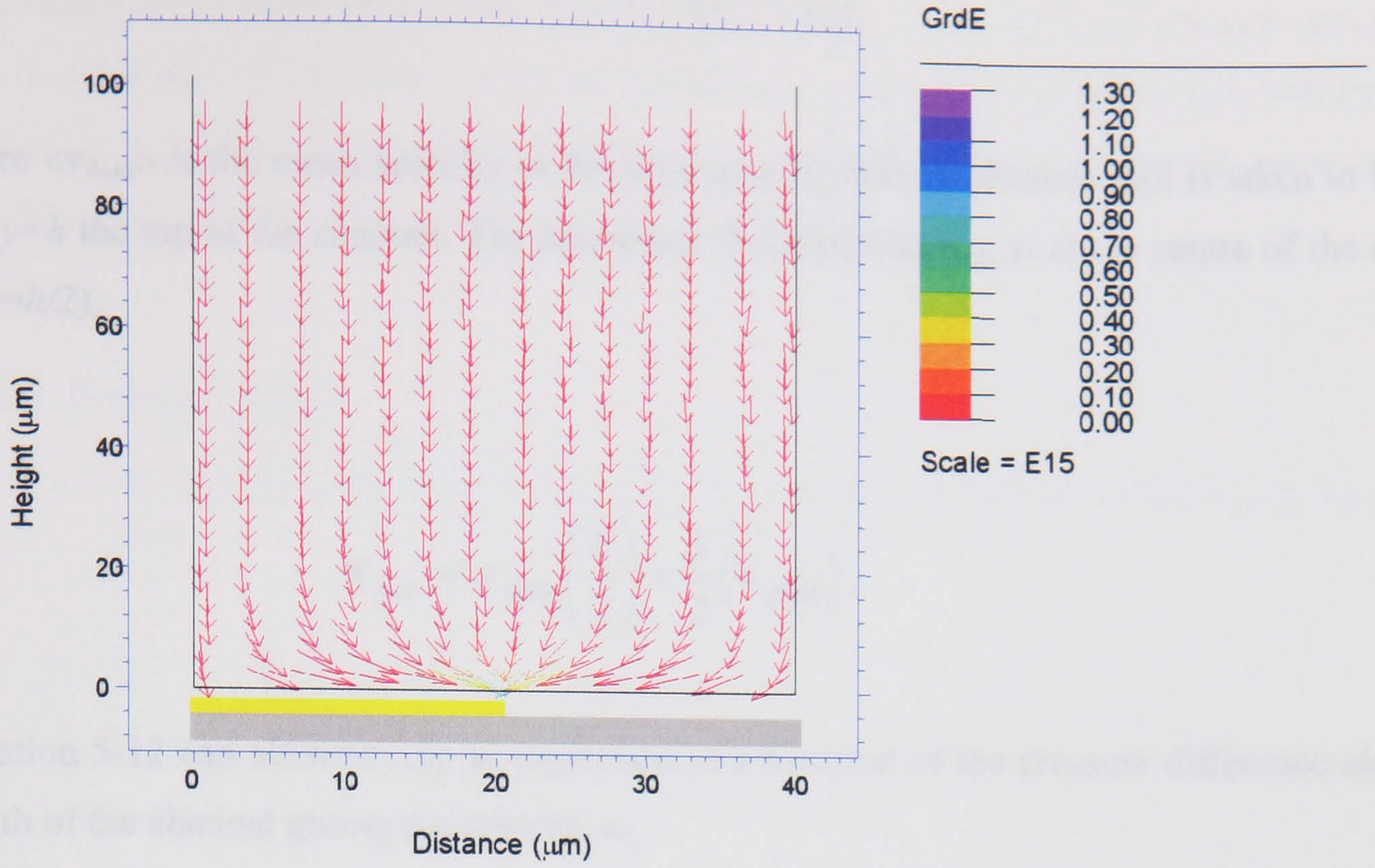

Figure 5-8. Vector plot of the magnitude and direction of $\nabla |\boldsymbol{E}|^2$, above one half of an electrode and electrode gap, for a peak applied voltage of 1V and $d = d_1 = d_2 = 40\mu m$.

5.3 Forces arising from the interaction of the particle with the fluid

This section describes the non-DEP forces exerted on a particle as it passes through the separation system. These forces arise due to the viscous nature of the fluid and the buoyancy force resulting from differences in the density of the particle and the suspending medium.

5.3.1 Fluid velocity profile

Due to the small size of the channel and the low fluid flow rates employed, the fluid exhibits low Reynolds number behaviour. This means that the fluid flowing through the system behaves in a laminar, i.e. non-turbulent manner. The pressure driven fluid flow in the channel takes on the characteristics of Poiseuille flow, resulting in the characteristic parabolic flow profile, with the maximum fluid velocity at the centre of the channel.

The analytical expression for the fluid velocity profile can be derived from the Navier-Stokes equations, and can be expressed in a simplified form to give the expression for the parabolic flow profile [10],

$$\mathbf{v}_{fluid}(y) = 6\langle \mathbf{v}_{fluid} \rangle \frac{y}{h}\left(1 - \frac{y}{h}\right) \tag{5-12}$$

where $<\mathbf{v}_{fluid}>$ is the mean velocity of the fluid and the bottom channel wall is taken to be $y=0$, and $y=h$ the top of the channel. The maximum fluid velocity $\mathbf{v}_{max}$ is at the centre of the channel (at $y=h/2$),

$$\mathbf{v}_{max} = \mathbf{v}_{fluid}\left(\frac{h}{2}\right) = \frac{3}{2}\langle \mathbf{v}_{fluid} \rangle . \tag{5-13}$$

Equation 5-12 can alternatively be expressed as a function of the pressure difference along the length of the channel giving the velocity as,

$$\mathbf{v}_{fluid}(y) = -\frac{1}{2\eta}\frac{\Delta P}{\Delta x}\left(hy - y^2\right) \tag{5-14}$$

where ΔP is the pressure difference, Δx the length of the chamber of height h and $y = 0$ defines the bottom of the chamber as before. For the sake of comparison with experiment it is convenient to calculate the volume flow rate Q (in cubic metres per second) through the device given by the integral of equation (5-14) over the channel dimensions,

$$Q = \frac{wh^3}{12\eta}\frac{\Delta P}{\Delta x} \tag{5-15}$$

where w is the width (in the z-axis) of the device and η is the viscosity of the medium.

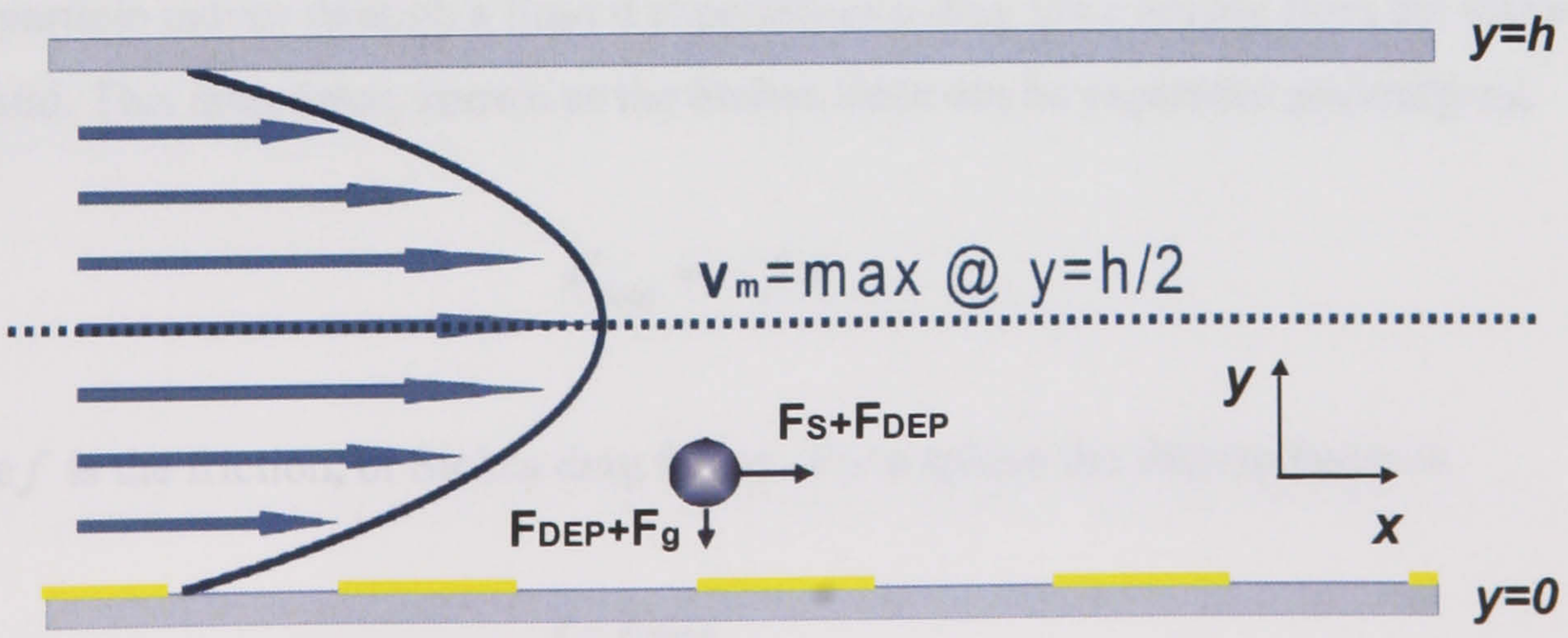

Figure 5-9. Deterministic forces experienced by a particle in the DEP separation system.

The forces arising from the pressure driven fluid flow can be considered to act only in the horizontal plane (x-direction). The formation of laminar flow within the channel ensures this, and for channels of the cross sectional dimensions used here (w=9mm and h=0.1mm) the laminar flow profile can be shown to be fully established within the first few microns of the inlet port [10]. This distance is known as the entrance length.

5.3.1.1 Entrance length

The entrance length L_h can be calculated based upon the hydraulic diameter D_h of the channel [10],

$$D_h = \frac{4A}{P} \tag{5-16}$$

where A and P are the cross-sectional area of the channel and the perimeter respectively. For the case of a channel where the cross section is a circle, D_h is simply the diameter of the circle. For a channel of rectangular cross section used in this work the value of D_h is approximately 200μm. This allows an estimate of the entrance length from the following relation [10],

$$\frac{L_h}{D_h} = 0.056 R_e \tag{5-17}$$

where R_e is the Reynold's number. If we take R_e = 1 (in reality $R_e << 1$) this gives an entrance length of approximately 11μm. The flow can therefore be assumed to be fully developed throughout the channel.

5.3.2 Viscous drag

As a particle moves through a fluid it experiences a drag force arising from the viscous nature of the fluid. This drag force, known as the Stokes force can be expressed generally as,

$$\boldsymbol{F}_{drag} = -f\,\mathbf{v} \tag{5-18}$$

where f is the friction, or Stokes drag factor. For a sphere the friction factor is,

$$f = 6\pi\eta a \tag{5-19}$$

5.3.3 Wall forces

Forces arising due to the interaction of the particles with the channel wall can also be considered, such as modified horizontal drag forces. These forces only occur when the particle is touching or in close proximity to the wall.

The horizontal drag on a cell in contact with the wall is given by the modified form of Stokes equation [11],

$$F_x \cong 6\pi\eta ac(\mathbf{v}_{fluid} - \mathbf{v}_p) \tag{5-20}$$

where c=1.7 , $\mathbf{v}_p$ is the cell velocity and $\mathbf{v}_{fluid}$ is the medium velocity at a above the wall.

The effects of these near wall forces on the motion of the particles in similar particle separation systems have been investigated by others and shown to be negligible [12, 13]. These forces were not included in the simulation.

5.3.4 Bouyancy forces

Particles also experience a force due to gravity, the magnitude and direction of which is related to the relative densities of the particle and fluid, and also the particle size. This force acts along the vector of the gravitational acceleration (i.e. along the y-axis). The force is given by,

$$F_g = \frac{4}{3}\pi a^3 \Delta\rho g \tag{5-21}$$

where g is the gravitational acceleration, $\Delta\rho$ the difference in density between the particle and fluid, and a the particle radius. This can either push the particle up or down depending on the relative densities of particle and suspending medium.

The buoyancy force is thus,

$$F_{Buoyancy} = \upsilon(\rho_p - \rho_m)g \tag{5-22}$$

where ρ_p and ρ_m are the density of the particle and suspending medium respectively.

5.4 Other forces

A number of other forces act upon a particle. These are described here briefly, as they were not included in the simulations. For a further discussion of these forces see chapters two and six.

5.4.1 Brownian forces

The effects of Brownian motion can be assumed to be negligible for particles greater than 1μm in radius, when compared to the DEP and fluid drag forces. The effect of thermal motion on particles is therefore neglected in the initial analysis, but returned to in section 5-8 and chapter six. It should be noted that the inclusion of Brownian motion components within the simulation increases the complexity of the computational problem resulting in it becoming very cumbersome, when run on a PC.

5.4.2 Particle-particle interaction

The model ignores the effect of particle–particle interaction. The assumption that the particles do not interact with each other is taken to be valid as the particle concentrations used in the experimental sections of this work are low (ca. 10^6 particles/ml [see ch.6]) and therefore the particles are well spaced. The typical distance beyond which particle-particle interactions no longer occur and can be ignored is typically about three particle diameters [7]. This is true for a particle suspended in a conductive medium, in which case the free charge in the electrolyte acts to screen the particle's charge. The field associated with the particle's charge therefore decays rapidly into the suspending medium. The only particle-particle interaction forces now available act over only very short distances, these are electrostatic interactions and van der Waals or Hamaker forces. See Morgan and Green for a discussion of particle-particle interactions and DVLO theory [14].

5.4.3 Electrode polarisation

Simply put the double layer capacitance can be thought of as a capacitor of reactance $1/j\omega C_{dl}$ in series with the suspending medium. As ω approaches zero the reactance goes towards infinity with all the potential being dropped across the double layer and none across the suspending medium. Electrode polarisation resulting from the build up of charge at the electrode solution interface is assumed to be negligible at the frequencies used (10kHz – 100MHz) and the effect that the electrical double layer has on the system is therefore neglected [14].

5.4.4 Electrohydrodynamic effects

Forces arising from the interaction of the electric field and the associated forces on the fluid are also neglected. The electrothermal forces and the electro-osmotic forces as described in chapter two are assumed to be negligible for the analysis [9, 15-17]. The effect of thermally induced changes in the viscosity of the medium is taken to be negligible.

5.5 Simulation

The forces acting on a particle can be divided into horizontal and vertical components, giving a pair of coupled differential equations (equations 5-24 and 5-25 below). The solution of these equations of motion gives the particle's trajectory. Considering the forces in the vertical or *y* direction first and ignoring the effects of hydrodynamic lift forces, particle-particle interactions, particle-surface interactions, and the random thermal effects due to Brownian motion, the equation of motion in the vertical direction can be expressed as,

$$m\frac{d\mathrm{v}_y}{dt} = F_{DEP_y} + F_{Buoyancy} + F_{Drag_y} \tag{5-23}$$

where F_{DEP_y} is the DEP force, $F_{Buoyancy}$ is the buoyancy force, F_{Drag_y} is the force due to viscous drag of the fluid on the particle, and v_y is the particle's velocity, all acting in the *y* direction, and *m* is the mass of the particle. Since the particles have very small masses (e.g. $4.5\text{x}10^{-15}$ kg for a latex particle of radius 1μm) and therefore little inertia, the viscous nature of the fluid dominates their behaviour. Under these conditions the particle can be assumed to reach its steady-state velocity instantaneously (e.g. a 1μm latex bead has a relaxation time of just 11ns, see section 2.4.2). Therefore, any variation in the velocity of the particle corresponds to a variation in the force on the particle. The left hand side of equation 5-23 contains the inertial component of the particle's motion and tends to zero giving a simplified equation for the *y*-component of the velocity,

$$\mathrm{v}_y = \frac{F_{DEP_y} + F_{Buoyancy}}{f}. \tag{5-24}$$

In the horizontal plane, and for a distance greater than *d* from the electrodes, the dominant force acting on the particle is the Stokes force due to the pressure driven movement of the fluid. In general and in the absence of any other forces, the particle velocity can be regarded as being the same as the fluid. As the particle approaches the electrode surface, the *x* component of the

electric field gradient becomes significant (see figure 5-8) and starts to influence the particle's motion. The velocity of the particle in this direction is given by the sum of the Stokes fluid drag force and the component of the DEP force in the x-direction as follows,

$$v_x = v_{fluid}(y) + \frac{F_{DEPx}}{f} \tag{5-25}$$

The motion of particles was calculated using an iterative Euler method written in MATLAB. The above equations of motion (equations 5-24 and 5-25) were solved using this iterative technique. The initial position of the particles was set, and from this the program calculated the forces on the particle, and hence the particle velocities in the x and y directions. Taking these velocities and multiplying them by a suitably small time step allows the incremental position of the particle to be calculated. The forces on the particle were recalculated giving the velocities in the x and y directions at this new position. The programme repeats, calculating the velocity and incremental position of the particle, until the particle reaches a predefined position in the channel, typically a predetermined height.

5.5.1 Time step

The time step was varied depending on the simulation. Typically, time steps of 1 microsecond were used in all the simulations, values less than this had no observable effect on the final results. Time steps longer than this were found to produce results of sufficient accuracy for simulations involving the motion of the particle at distances far from the electrode array. To reduce computation times a variable time step procedure was used, in which the time step was changed when a particle reached a specified distance from the electrode arrays. Time steps between 1 ms and 1μs were therefore used with the time step getting progressively smaller the closer the particle got to the electrode surface.

5.5.2 Comparison of simulation with theory and experiment

For the particular case of a homogeneous spherical particle, such as a latex sphere, suspended in a liquid, the effective polarisability α is equal to $3\varepsilon_m f_{CM}$. For the special case $d = d_1 = d_2$, the steady state particle levitation height can be found, by balancing the dielectrophoretic force (equation 5-11) with the gravitational force (equation 5-21) giving [2],

$$h = \frac{d}{\pi} ln\left[-\frac{24 V_o^2 \epsilon_m Re[f_{CM}]}{\pi d^3 \Delta \rho g} \right] \tag{5-26}$$

This assumes that the particle is experiencing -veDEP, and is repelled from the electrodes. Figure 5-10 shows a comparison of the levitation heights obtained from the theory (equation 5-26), the simulations of this chapter, and experimental results derived from the literature [18] for 6μm diameter latex particles suspended in water. Electrode arrays of characteristic size d = 10μm, d = 20μm and d = 40μm and applied peak voltages V_o between 2 and 4V. With a value of $Re[f_{cm}] = -0.5$, and the assumption that electrode polarisation effects are negligible. The density of latex and water were taken as 1055kgm^{-3} and 1000kgm^{-3} respectively.

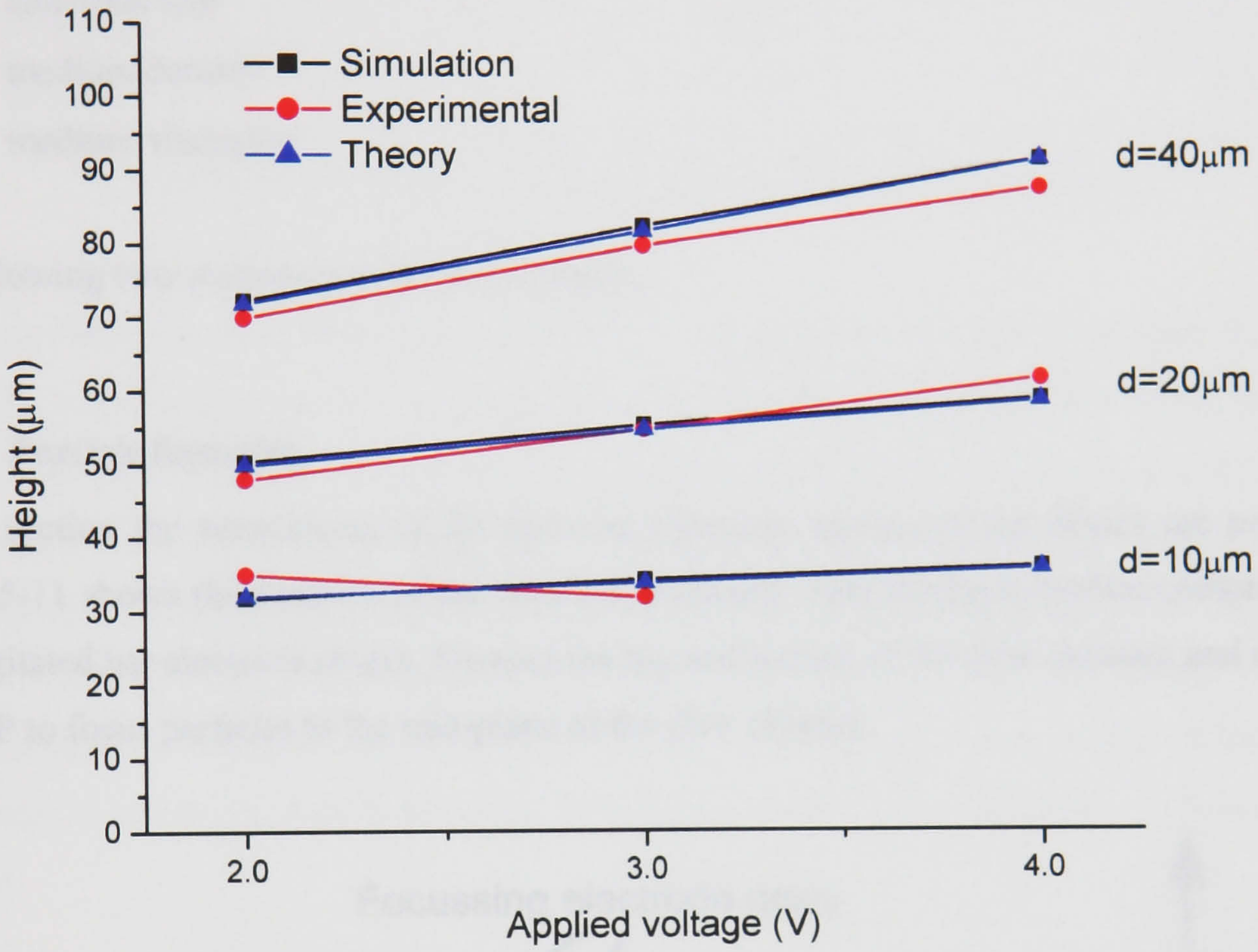

Figure 5-10. Comparison between theory, simulation and experimental [18] data for the steady state levitation height of 3μm diameter latex particles above three sizes of interdigitated electrode array.

The simulation and theoretical levitation heights are in good agreement with the experimental results. The limiting factor being the choice of small enough time step <1ms.

5.6 Particle trajectories

Trajectories were calculated for different experimental conditions. The effects of variation of the following parameters were investigated,

- applied voltage
- particle polarisability
- flow rate
- particle size
- electrode size
- medium density
- medium viscosity

The following two sections present these results.

5.6.1 Particle focussing

In this section the simulations of the focusing electrode section of the device are presented. Figure 5-11 shows the function of the focusing electrode. This electrode section comprises two interdigitated bar electrode arrays, forming the top and bottom of the flow channel, and uses –veDEP to focus particles to the mid-plane of the flow channel.

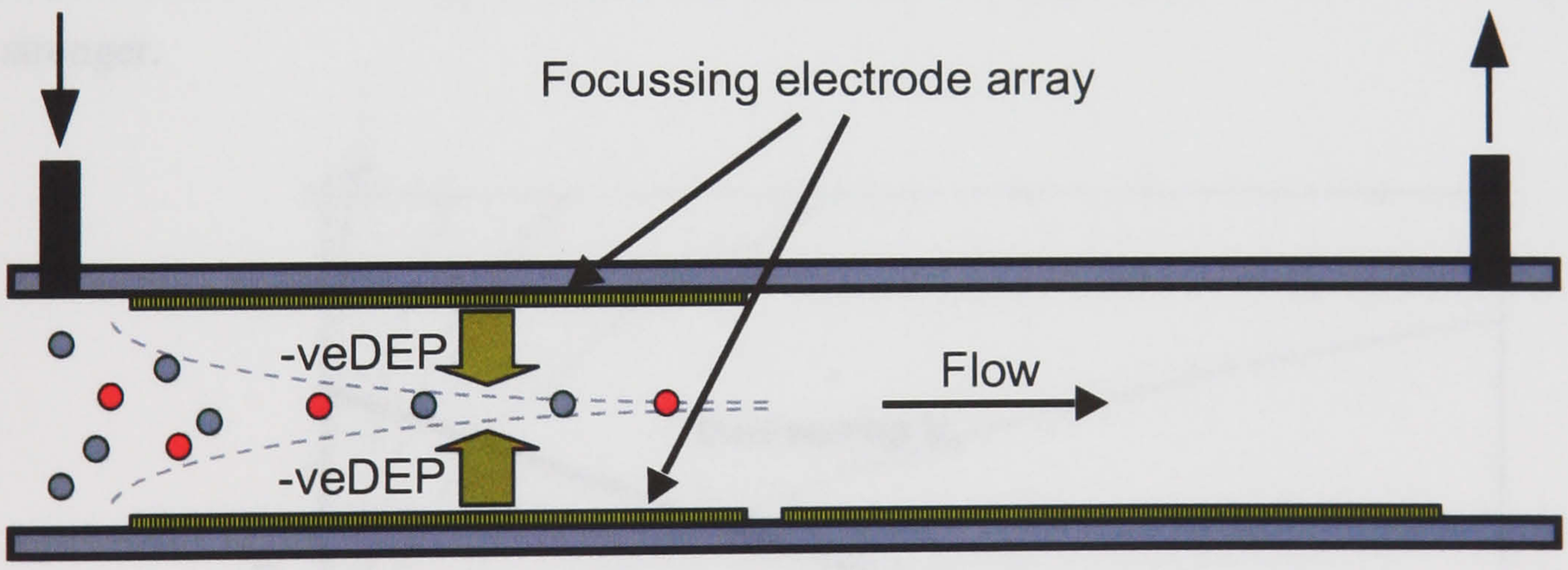

Figure 5-11. Schematic of the particle focussing system.

The channel is assumed for simulation purposes to have a height of 100μm and width of 9mm, giving a cross sectional area of 0.9mm^2. These dimensions are the same as that of the fabricated devices. Table 5-1 lists the values of the various parameters used in the simulation program. The values given in this table were used in all the simulations unless otherwise stated.

Parameter		Value
a	particle radius	5μm
V_o	applied peak voltage	2V
η	viscosity of medium	$1.5x10^{-3}$ kgms^{-1}
ρ_m	density of medium	1055 kgm^{-3}
ρ_p	density of particle	1055 kgm^{-3}
Q	volume flow rate	1mlhr^{-1}
$d=d_1=d_2$	size of electrode or gap	40μm
time step		$1x10^{-5}$ s
$Re[f_{CM}]$		-0.5

Table 5-1. Typical simulation parameters, for the focussing section.

A plot showing the simulated trajectories of a 5μm radius latex particle (chosen due to the similarity in size to the blood cells used in the experimental work) passing through the focussing region of the device is shown in figure 5-12. A 5μm radius particle was chosen, as this is similar to the size of blood cells. The initial height of the particle is 5μm above the bottom electrode array, the particles move from left to right and are being pushed towards the centre of the flow channel (i.e. towards the top of the plot). The simulation parameters are those shown in table 5-1, and the applied voltage is varied between 1V and 10V. The undulating profile of the particle trajectories is due to the particle passing over electrode edges where the electric field gradient is stronger.

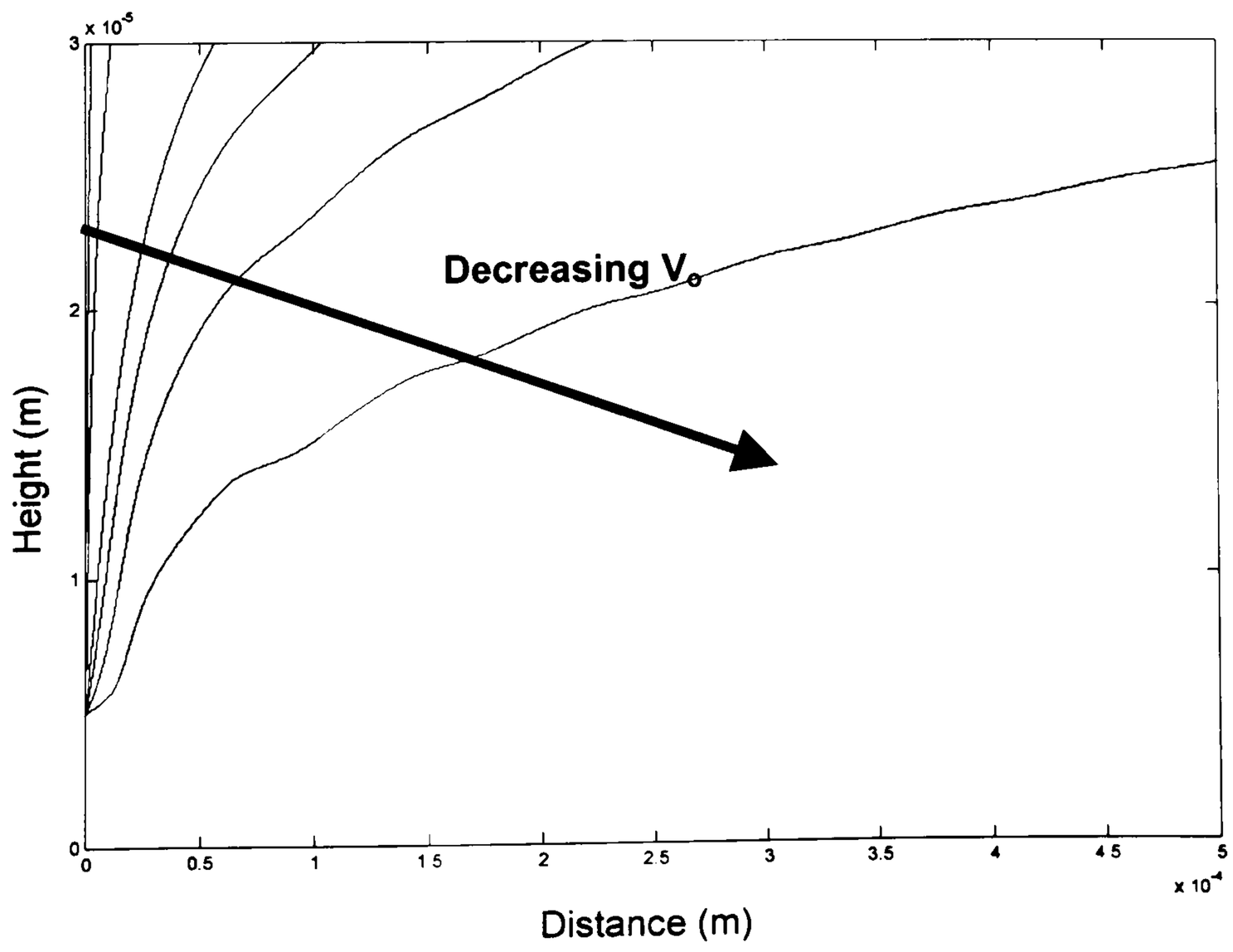

Figure 5-12. Particle trajectories in the focussing electrode array for different applied voltages.

We now define the 'focussing distance' of a particle flowing through the channel as the distance that that particle must travel before reaching a point *a* from the centre of the channel (i.e. a height (*h/2-a*) from the electrode array). For a 100μm high channel and a particle of radius 5μm this is the height of 50μm ± 5μm depending on whether the particle's initial position is above or below the centre of the channel.

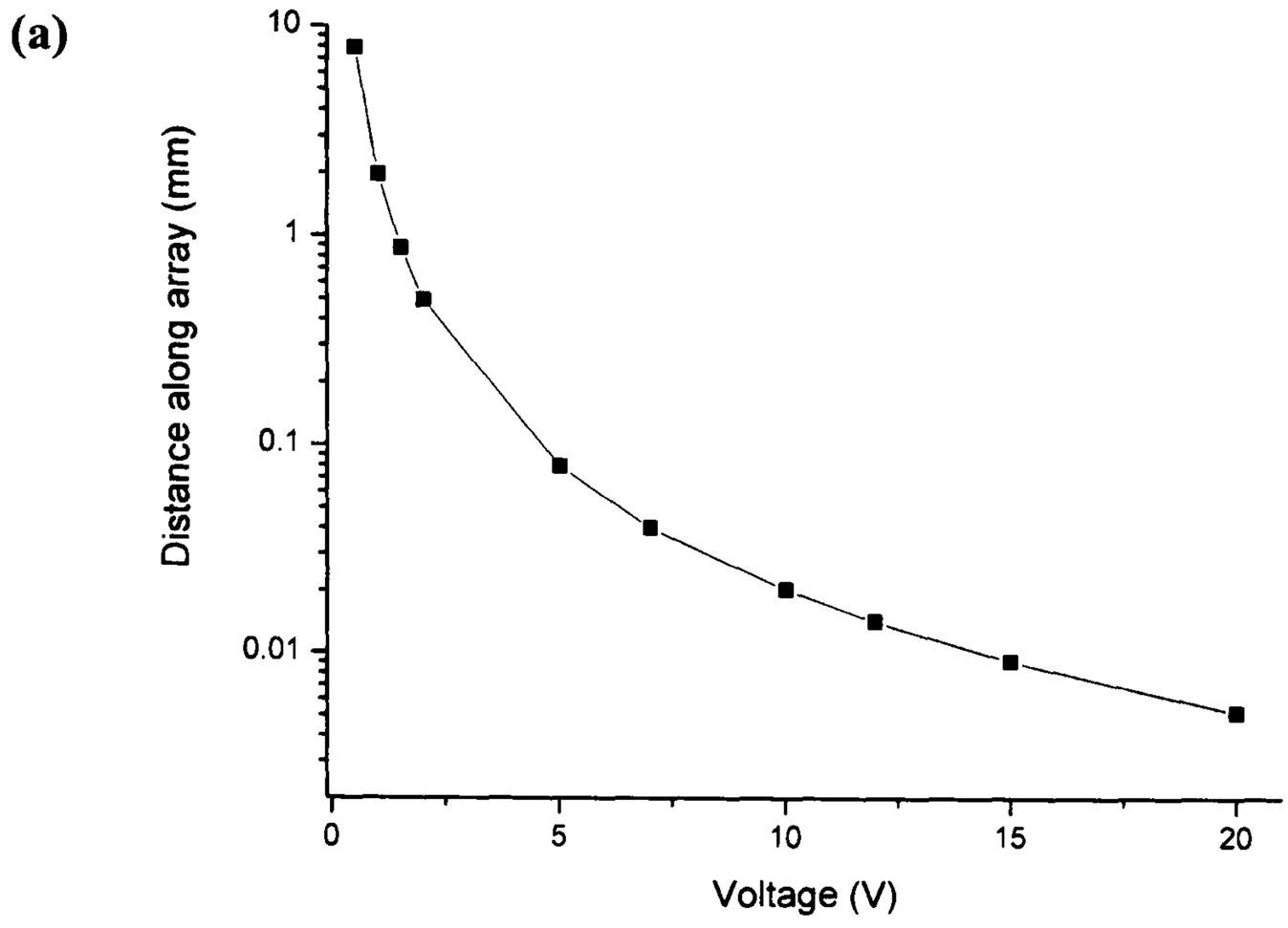

Figure 5-13. Variation of the distance along the electrode array a particle must travel before it is focussed versus **(a)** peak applied voltage and **(b)** characteristic electrode size.

Figure 5-13 shows how the focussing distance varies with applied voltage and the characteristic size of the focussing electrode array. An increase in applied voltage results in the particle becoming focussed more quickly requiring a shorter focussing distance. For the 40μm electrode

a focussing distance of only 100μm is required to bring a 5μm particle from near the chamber wall to within 5μm of the centre of a 100μm channel. It is apparent that very low voltages (<1V) can be used to manipulate particles given an electrode of sufficient length and neutral buoyancy conditions. However, if the particle is not of the same density as the suspending medium, there will be a threshold voltage below which the particle will not attain full focussing. If the applied voltage is not sufficient for the particle to attain a steady state levitation height (recalling section 5.5.2), at or above the mid-point of the channel then the particle will never become focussed. Variation in the electrode size d also has a marked effect on the focussing distance. Figure 5-6(b) shows $\nabla |\mathbf{E}|^2$ for different electrode sizes and the reason for this variation in focussing distance.

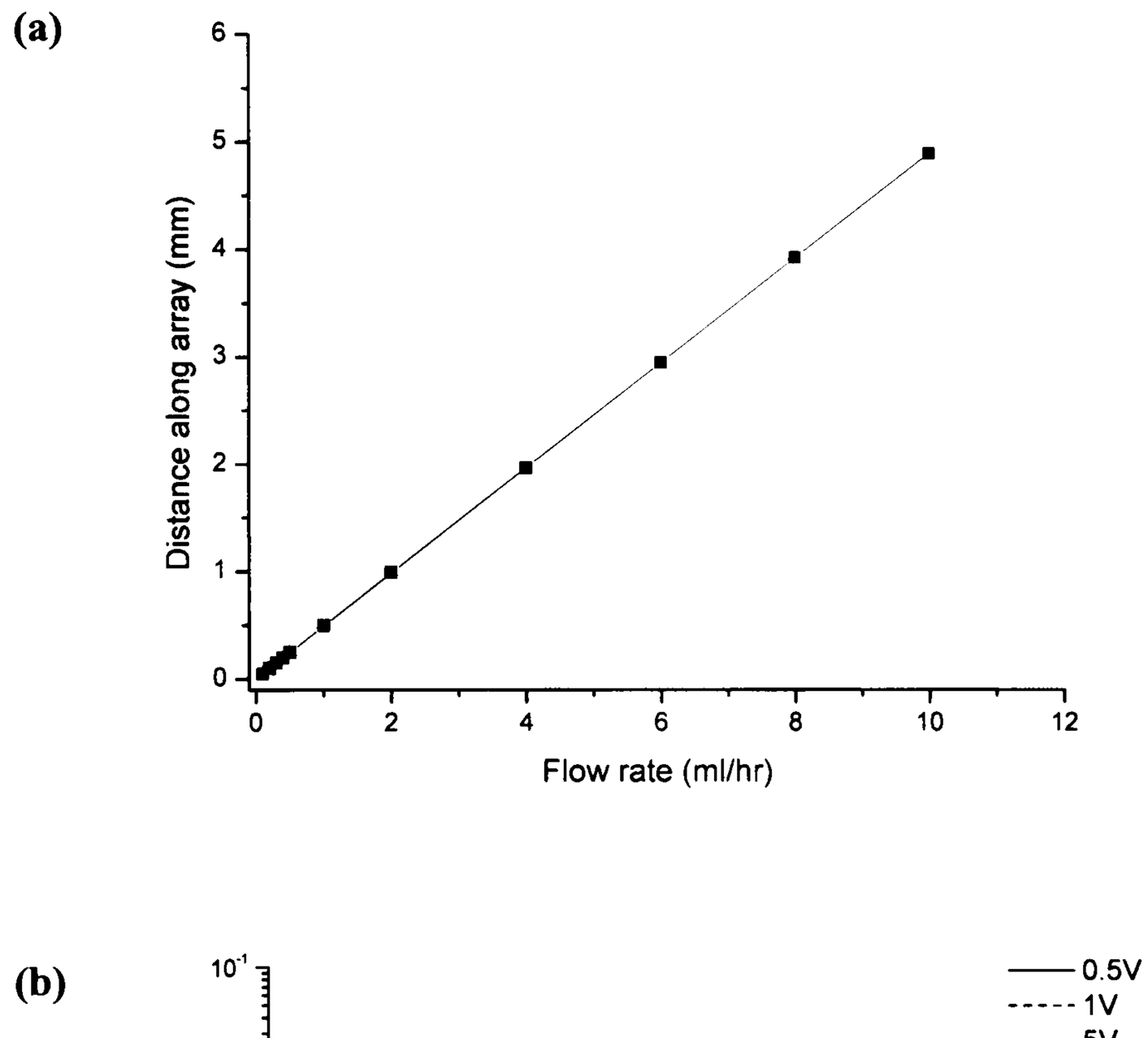

Figure 5-14. Variation of the distance along the electrode array a particle must travel before it is focussed versus **(a)** fluid flow rate and **(b)** initial particle height for various applied voltages.

Figure 5-14(a) shows a linear dependence of focussing distance with fluid flow rate as one would expect. The effect of the initial height of a particle on the focussing distance is shown in figure 5-14(b), this figure is symmetrical about its right hand side, with particles starting at heights greater than the channel centre (>50μm) requiring increasing focussing distances as the height away from the channel centre increases. Particles with initial height close to the electrode arrays will require the greatest time to become focussed and therefore represent the upper limit on focussing distance and time.

(a)

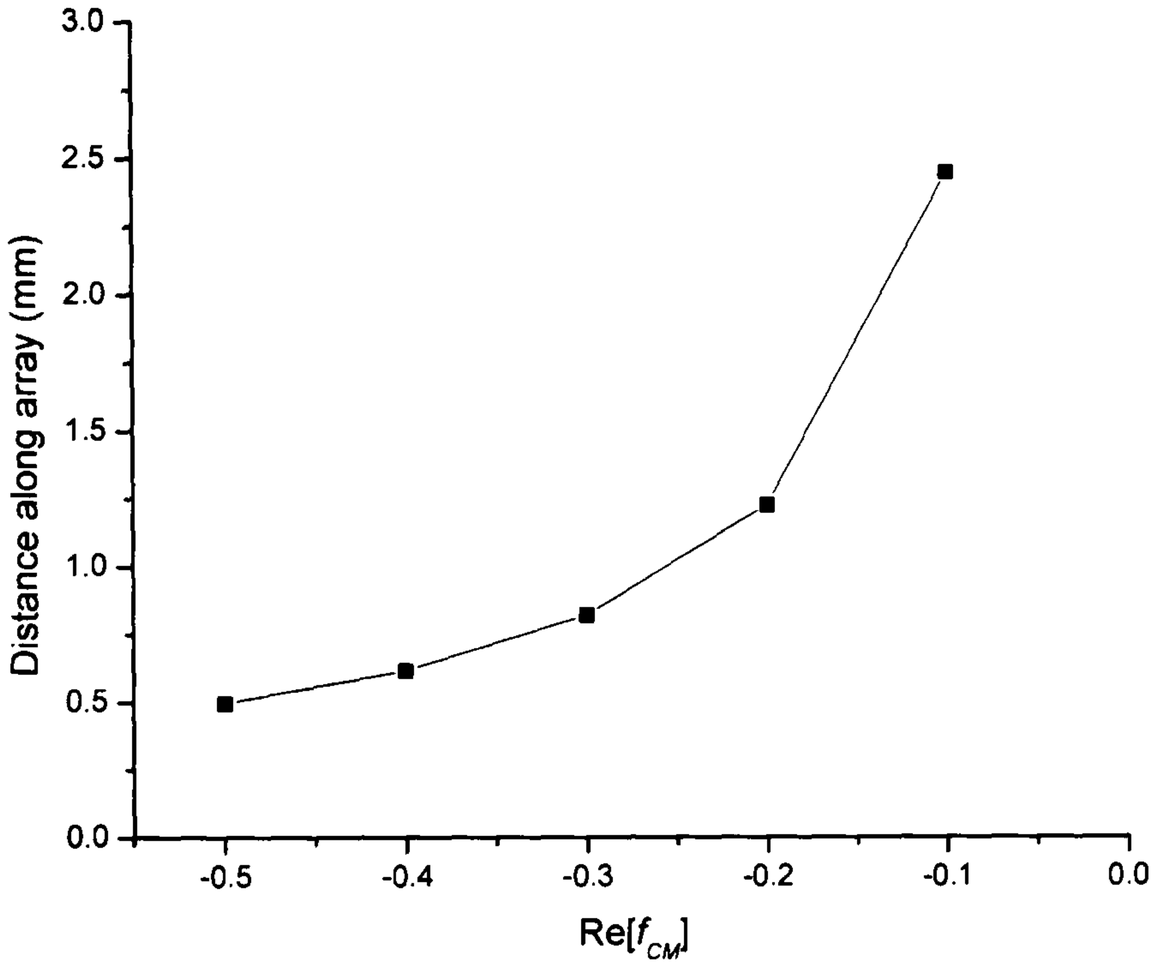

(b)

Figure 5-15. Variation in the particle trajectories for different values of particle polarisation.

Figure 5-15 shows how the focussing distance varies with a decreasing polarisability of the particle. As the polarisability of the particle decreases, the –veDEP force increases in magnitude resulting in a reduction in the required focussing distance, if all other parameters remain the same. Figure 5-15(b) illustrates this point with particle trajectory plots for 5μm particles with values of –0.5 to –0.1 for the real part of the *Clausius-Mossotti* factor.

Figure 5-16(a) shows how the focussing distance varies with the density of the suspending medium for the case of a latex particle of density 1055kgm^{-3}. This only applies to a particle originating near the bottom of the channel and moving upwards. For a particle starting near the top electrode array the focussing distance will increase with increasing medium density due to the reduction in the effective downward force due to gravity.

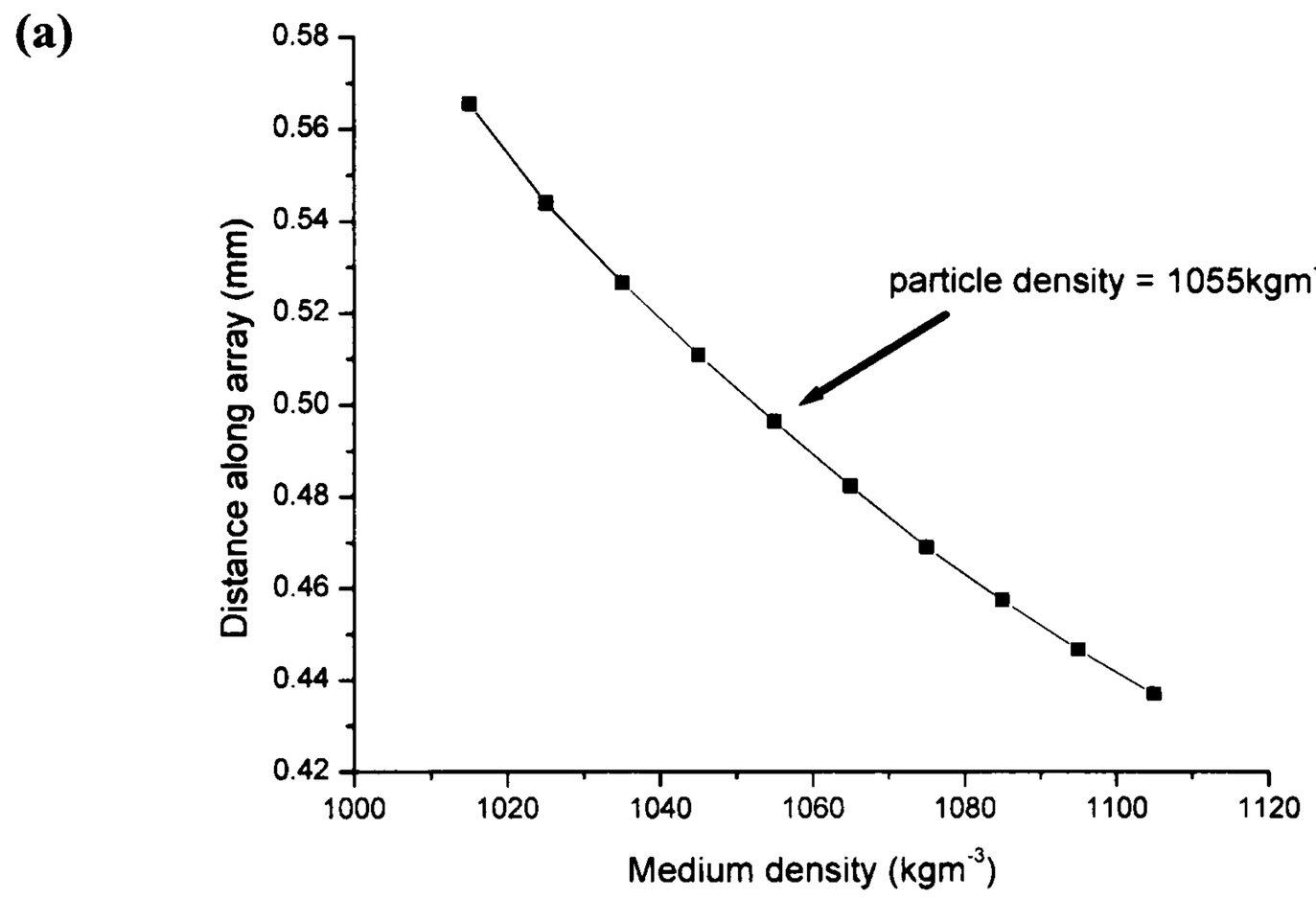

Figure 5-16. Effect of **(a)** suspending medium density and **(b)** particle size on the focussing distance a particle must travel before it is focussed to within 95% of the channel centre.

Figure 5-16(b) shows how the focussing distance varies with the size of the particle. For particle of radius less than 1μm the effects of Brownian motion become significant and must be factored into the simulation.

5.6.2 Particle separation

Once the particles have been focussed to the mid-plane of the device by the focussing electrode, they then travel further through the device and are attracted towards a second electrode array under the influence of +veDEP forces. This second array shall be referred to as the separation electrode array. A schematic of this is shown in figure 5-17.

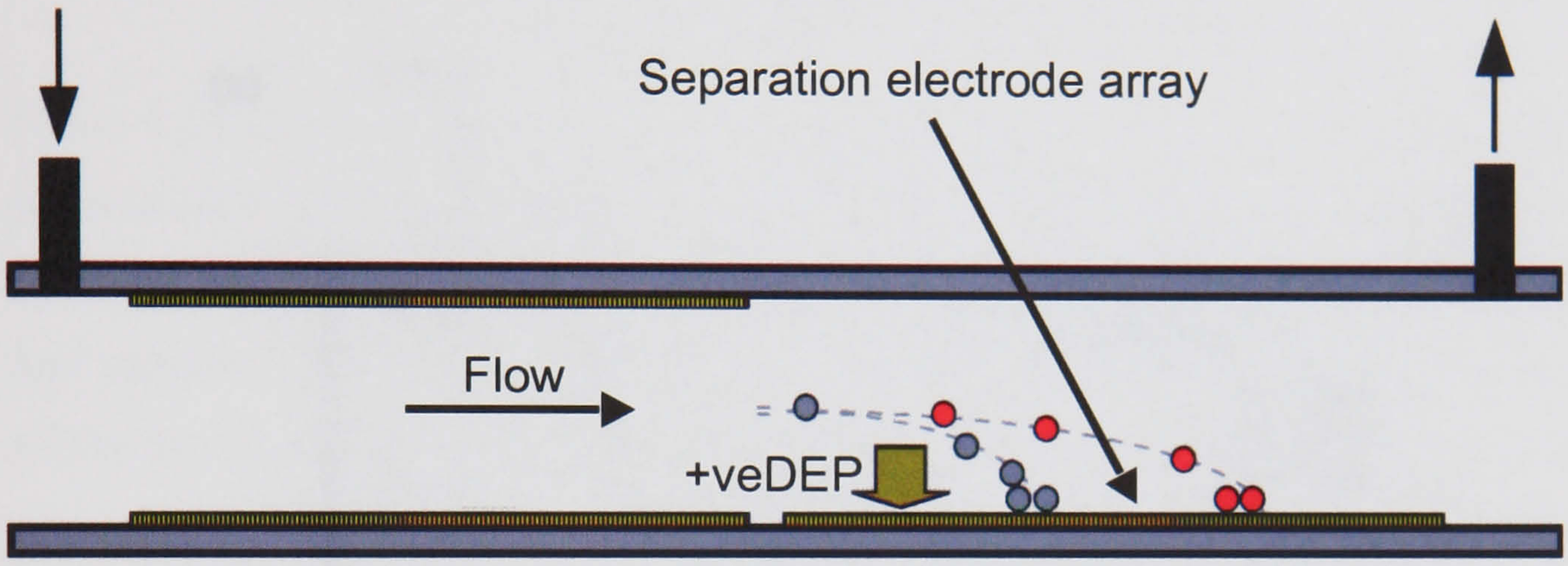

Figure 5-17. Schematic of the particle separation system.

Again the channel is assumed for simulation purposes to have a height of 100μm and width of 9mm, giving a cross sectional area of $0.9mm^2$. Table 5-2 lists the values of the various parameters used in the simulation program. The values given in this table were used in all the simulations unless otherwise stated.

Parameter		Value
a	particle radius	5μm
V_o	applied peak voltage	2V
η	viscosity of medium	$1.5x10^{-3}$ kgms^{-1}
ρ_m	density of medium	1055 kgm^{-3}
ρ_p	density of particle	1055 kgm^{-3}
Q	volume flow rate	1mlhr^{-1}
$d=d_1=d_2$	size of electrode or gap	40μm
time step		$1x10^{-5}$ s
$Re[f_{CM}]$		1

Table 5-2. Typical simulation parameters for the separation section of the system.

Figure 5-18 (a) shows the distance along the separation electrode array at which a 5μm particle is captured under the influence of +veDEP for initial starting heights of 40μm, 50μm and 60μm; and for various applied peak voltages. Figure 5-18 (b) shows the distance along the separation electrode array at which the same 5μm particle is captured and held under the influence of +veDEP for an initial starting height of 50μm and applied peak voltages of 1V, 5V and 10V for varying flow rates. The capture distance varies in a linear fashion (on the logarithmic scale) with flow rate for applied voltages of 1V and 5V. The particles are captured at discrete positions (electrode edges) along the electrode array resulting in the stepped line for 10V. The scale is logarithmic and this result in the step-like profile at low flow rates and high applied voltages, where the particle is captured on the first few electrode edges.

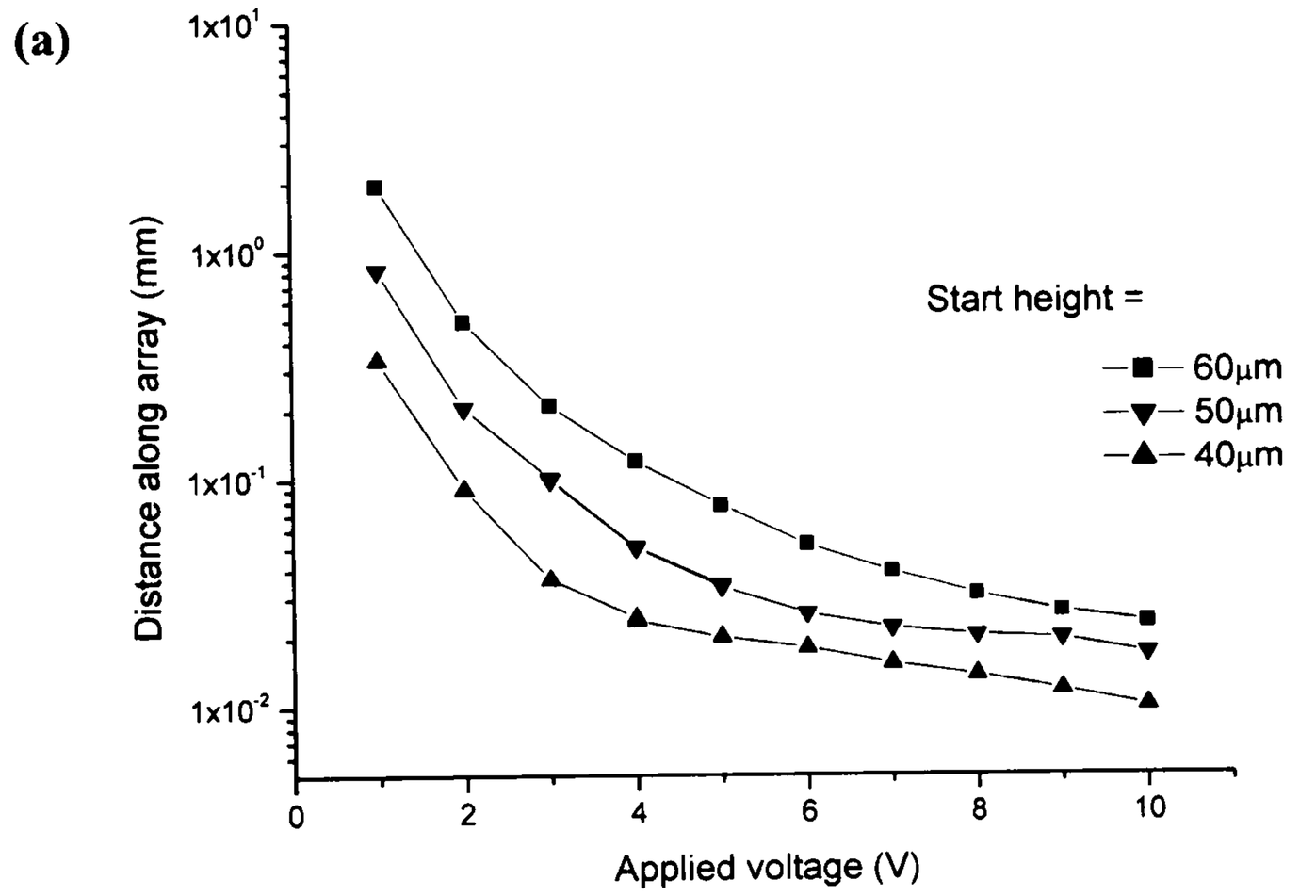

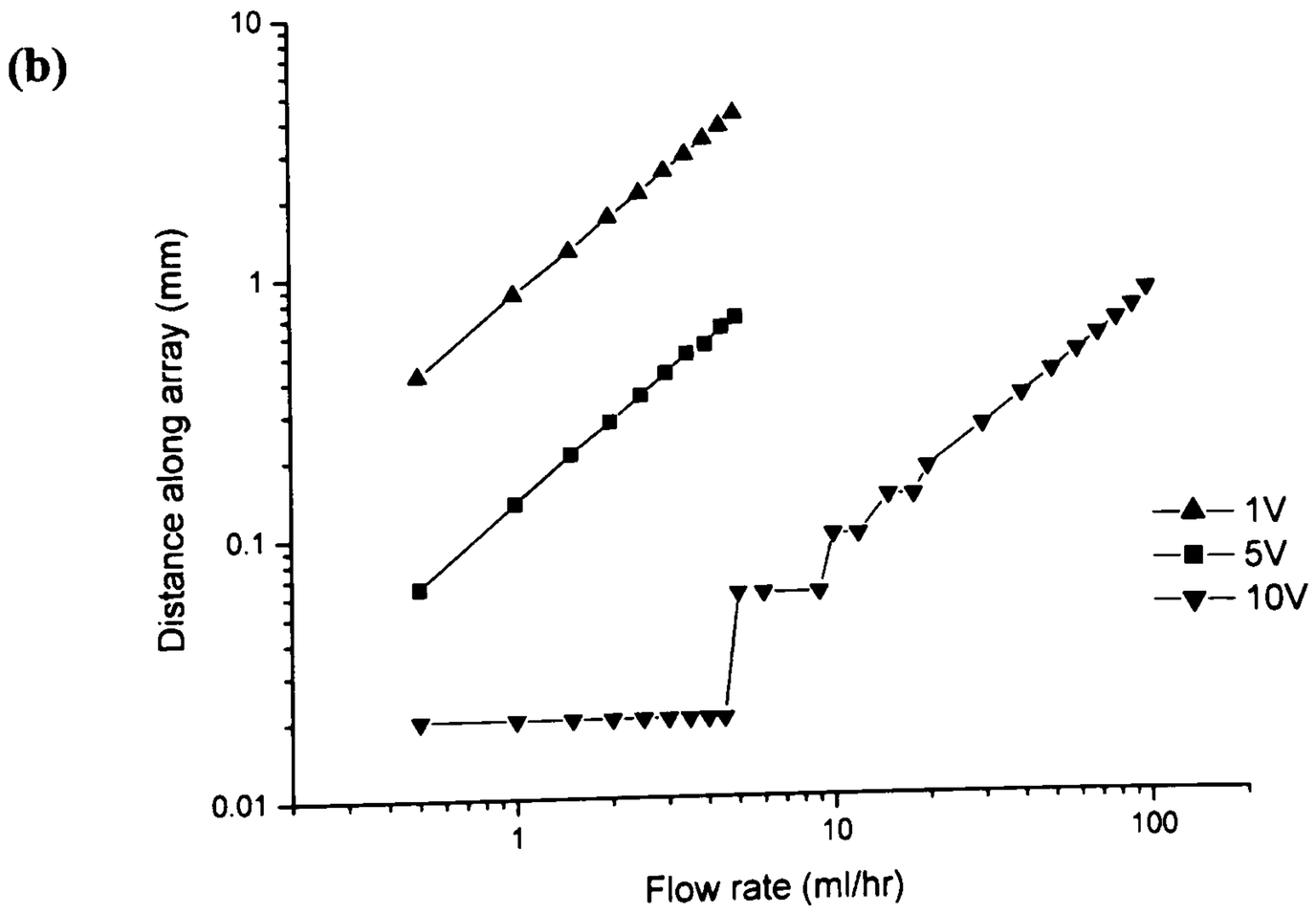

Figure 5-18. Variation of the distance along the separation electrode array versus **(a)** voltage for starting heights of 40μm, 50μm, and 60μm and **(b)** flow rate for peak applied voltages of 1V, 5V and 10V.

The distance along the separation electrode array at which a particle becomes trapped is divided into a set of discrete positions, corresponding to the position of the electrode edges. The simulation of the particle separation assumes that the particle is attracted to within one particle radius of the surface, at which point the simulation is terminated. The assumption that the particles reach the surface of the electrode array and are frozen in position allows for simplification of the simulation program. In reality upon reaching height r above the electrode surface particles tend to continue moving along the array under the influence of the fluid flow and the x component of the DEP force. Particle motion continues until the particle reaches an electrode edge where it becomes captured and remains there held under the influence of +veDEP. The condition for a particle being held at the electrode edge assumes that the fluid drag force is less than the DEP force holding the particle at the electrode.

Figure 5-19 shows the simulated particle trajectories for a 5μm radius particle with varying polarisabilities (values of Re[f_{CM}] between 0.1 and 1) for two different starting heights 40μm and 60μm. This plot of particle trajectories illustrates the need for effective particle focussing. Any variation in the initial height of the particle, due to poor focussing of the particle sample will be translated into a distribution of capture positions on the separation electrode array.

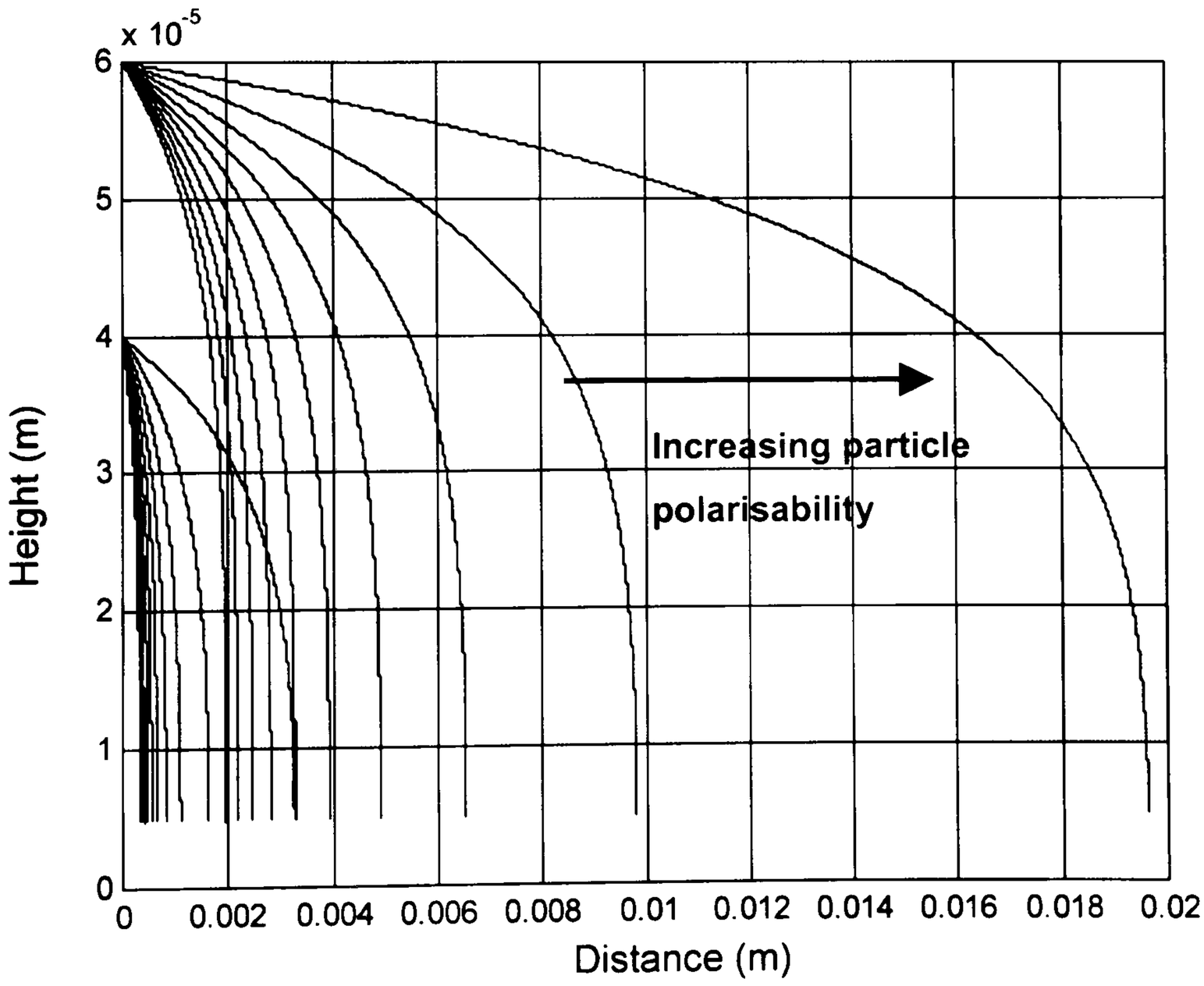

Figure 5-19. Variation of the distance along the separation electrode array versus polarisability. Re[f_{CM}] varying between 0.1 and 1 and for two strarting positions 40μm and 60μm.

Figure 5-20 (a) shows the capture distance along the separation electrode array, at which the 5μm particle is captured for initial starting heights of 40μm, 50μm and 60μm, versus particle size. The DEP force scales linearly with the volume of the particle, explaining the observed dependence of capture distance with size. Figure 5-20 (b) shows the effect of particle polarisability as illustrated in the trajectory plot of figure 5-19 above.

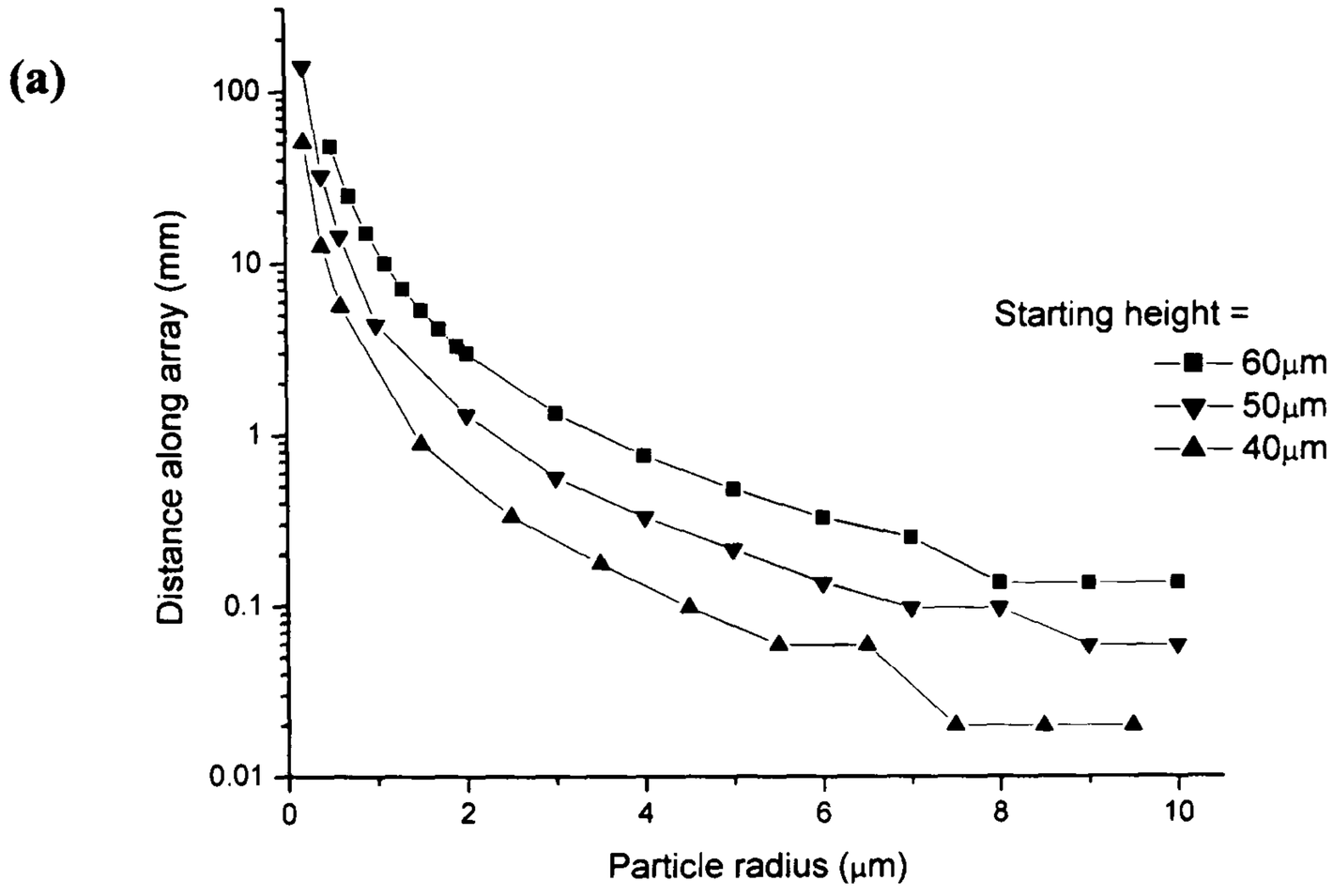

Figure 5-20. The distance along the separation electrode array before being captured versus **(a)** size and **(b)** polarisability. For starting heights of 40μm, 50μm and 60μm.

5.7 Conclusion

A simple analytical model has been developed which calculates the trajectories of particles as they flow through the DEP separation system. The effect of various experimentally controllable parameters has been investigated using the model. The simulations show the possibility of separating particles along the length of the separation electrode array, based on their dielectric properties and size. Effective focussing of the particle stream prior to entry in to the separation portion of the channel is necessary to obtain effective particle separation. The model is used in the next chapter where simulations (using the experimental parameters) are compared with experiment using a variety of particle types.

5.8 References

1. Clague, D.S. and E.K. Wheeler, *Dielectrophoretic manipulation of macromolecules: The electric field - art. no. 026605.* Physical Review E, 2001. **6402**(2): p. 6605-+.
2. Morgan, H., *et al.*, *The dielectrophoretic and travelling wave forces generated by interdigitated electrode arrays: analytical solution using Fourier series (vol 34, pg 1553, 2001).* Journal of Physics D-Applied Physics, 2001. **34**(17): p. 2708-2708.
3. Morgan, H., *et al.*, *The dielectrophoretic and travelling wave forces generated by interdigitated electrode arrays: analytical solution using Fourier series.* Journal of Physics D-Applied Physics, 2001. **34**(10): p. 1553-1561.
4. Wang, X.J., X.B. Wang, and P.R.C. Gascoyne, *General expressions for dielectrophoretic force and electrorotational torque derived using the Maxwell stress tensor method.* Journal of Electrostatics, 1997. **39**(4): p. 277-295.
5. Stephenson, G., *Mathematical methods for science students*. 1 ed. 1961, Glasgow: Longmans.
6. Backstrom, G., *Fields of physics by finite element analysis*. 2000, Malmo, Sweden: GB publishing. 266.
7. Jones, T.B., *Electromechanics of Particles*. 1995, Cambridge: Cambridge University Press.
8. Pethig, R., *Dielectrophoresis: Using inhomogeneous AC electrical fields to separate and manipulate cells.* Critical Reviews in Biotechnology, 1996. **16**(4): p. 331-348.
9. Green, N.G., A. Ramos, and H. Morgan, *Ac electrokinetics: a survey of sub-micrometre particle dynamics.* Journal of Physics D-Applied Physics, 2000. **33**(6): p. 632-641.
10. Sharp, K.V., *et al.*, *Liquid flows in microchannels*, in *The MEMS handbook*, M. Gad-el-Hak, Editor. 2002, CRC Press: Boca Raton. p. Chapter 6.
11. O'Neill, M.E., Chem Eng Sci, 1968. **23**: p. 1293-1298.

12. Wang, X.B., *et al.*, *Separation of polystyrene microbeads using dielectrophoretic/gravitational field-flow-fractionation.* Biophysical Journal, 1998. **74**(5): p. 2689-2701.
13. Yang, J., *et al.*, *Cell separation on microfabricated electrodes using dielectrophoretic/gravitational field flow fractionation.* Analytical Chemistry, 1999. **71**(5): p. 911-918.
14. Morgan, H. and N.G. Green, *AC Electrokinetics: Colloids and Nanoparticles*. 1 ed. Microtechnologies and Microsystems Series, ed. R. Pethig. 2003, Baldock, UK: Research Studies Press.
15. Ramos, A., *et al.*, *Fluid flow driven by a.c. electric fields in microelectrodes*, in *Electrostatics 1999*. 1999, Iop Publishing Ltd: Bristol. p. 137-140.
16. Ramos, A., *et al.*, *Ac electrokinetics: a review of forces in microelectrode structures.* Journal of Physics D-Applied Physics, 1998. **31**(18): p. 2338-2353.
17. Green, N.G., *et al.*, *Electrothermally induced fluid flow on microelectrodes.* Journal of Electrostatics, 2001. **53**(2): p. 71-87.
18. Markx, G.H., R. Pethig, and J. Rousselet, *The dielectrophoretic levitation of latex beads, with reference to field-flow fractionation.* Journal of Physics D-Applied Physics, 1997. **30**(17): p. 2470-2477.

A.5 Appendix 5 - Numerical Simulation using FlexPDE™

Two dimensional numerical simulation were carried out using a commercially available finite element based partial differential equation solver, FlexPDE™ (PDE Solutions Inc., USA).

A.5.1 FlexPDE™

First, a description of the problem to be solved is written in a scripted format understood by FlexPDE™. The problem description contains the partial differential equations system describing the problem, and the boundary conditions for the problem. FlexPDE™ solves the problem by converting the user-defined description of the problem into a finite element model, which is solved and outputted. The output can be presented either graphical or numerically. Specific details of how the software operates can be found in the FlexPDE™ online help or in [1].

A.5.2 The electrical problem - equations and assumption

Simulations of the electrical potential fields produced by the interdigitated bar electrode structures were carried out and from this the DEP force vector fields was obtained.

For the currents and frequencies used in this work and indeed those used in most AC electrokinetic systems, Maxwell's equations can be reduced to the quasi-electrostatic form [2, 3]. That is,

$$\mathbf{E} = -\nabla\phi \qquad \mathbf{E} \text{ is irrotational} \qquad \text{(A.5-1)}$$

$$\nabla \cdot \mathbf{J} + \frac{\partial \rho}{\partial t} = 0 \qquad \text{charge conservation equation} \qquad \text{(A.5-2)}$$

$$\nabla \cdot \mathbf{D} = \rho \qquad \text{Gauss' law} \qquad \text{(A.5-3)}$$

where ϕ is the electric potential, ρ is the free charge density, **J** is the free current density, and **D** is the electric flux density.

In order to obtain a solution for the DEP force we first solve numerically Laplace's equation for the electrical potential ϕ

$$\nabla \cdot (\varepsilon \nabla \phi) = 0 \qquad \text{(A.5-4)}$$

Where calculation of $\nabla\phi$ gives the magnitude of the electric field, and from this the normalised DEP force $\nabla\left|\nabla\phi\right|^2$ is obtained.

A.5.2.1 Boundary conditions and symmetry

For the sake of simplicity we make the assumption that the interdigitated electrodes are sufficiently long and the problem can be simplified and considered to be two-dimensional. This is possible as the length of the individual electrode fingers is large (10mm) when compared with the individual electrode finger's height (~100nm) and width (10-40μm). By taking into consideration the geometrical symmetry of such a system it is possible to further simplify the problem. If we assume that the electrode array is infinitely long the unit element, shown in figure A.5-1 is sufficient to describe the array assuming we impose suitable boundary conditions.

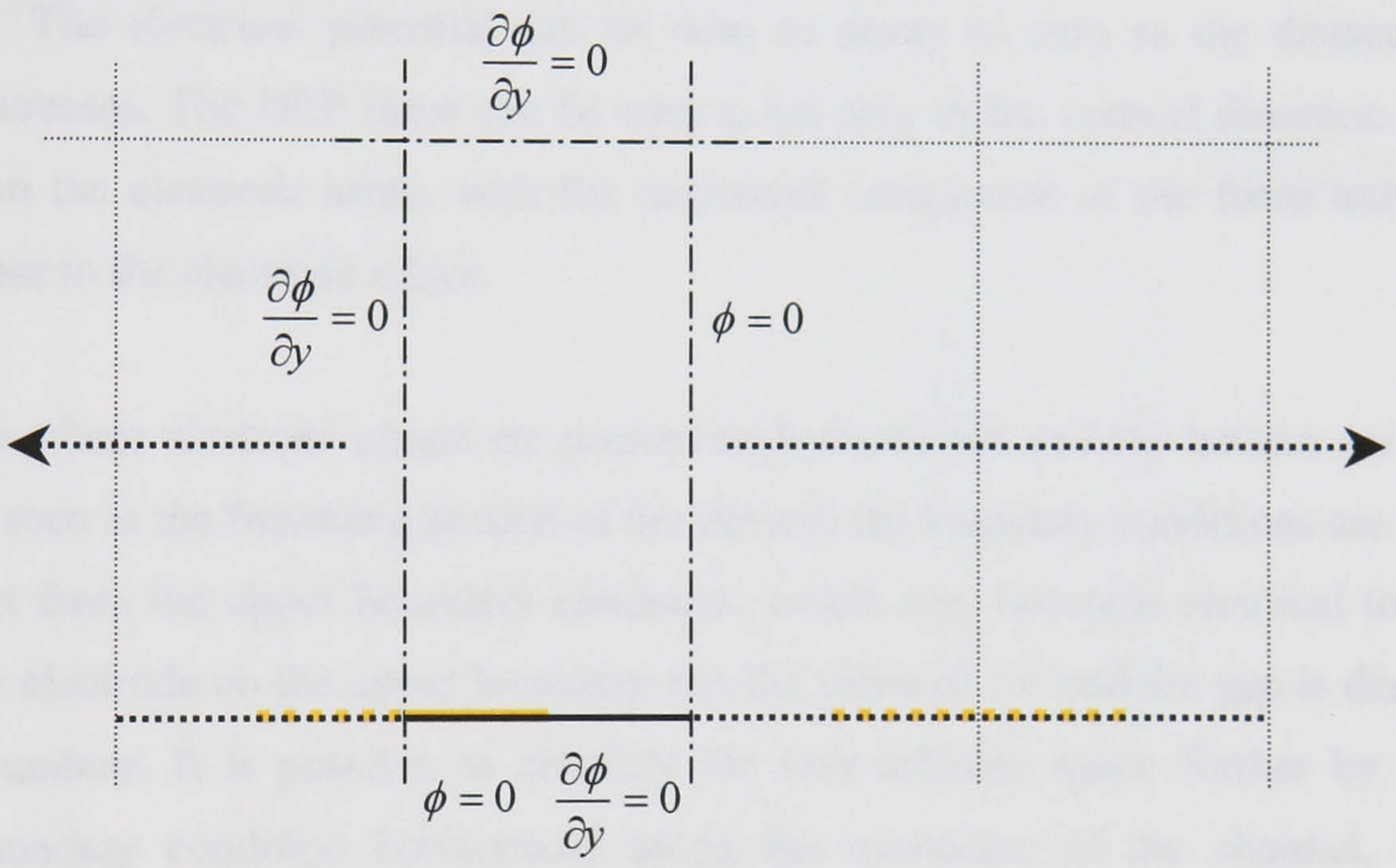

Figure A.5-1. Unit solution space; showing boundary conditions and symmetry.

Odd and even mirror boundaries are used to define the boundaries of the unit solution space. The Neuman ($\frac{\partial\phi}{\partial y}=0$) and the Dirichlet ($\phi=0$) boundary conditions are used for boundaries of even and odd symmetry respectively. The Neuman condition forms a boundary with the same charges or potentials on either side. The Dirichlet condition forms a boundary with opposite charges or potentials on either side. The electrodes are considered to be infinitely thin (a valid assumption as they are ~100nm thick whereas the electrode size is ≥10μm) and are therefore approximated as sections of the boundary and given the value of the applied potential (V_o). Such an approximation for the electrodes gives inaccuracies when very close to the electrode surface, but in any case the dipole approximation for the DEP force breaks down in this region [4, 5].

For the case where the electrode array is present only on the bottom surface of the channel the boundary conditions are as follows. At heights much greater than the characteristic electrode dimensions, the potential and hence the electric field both go to zero. Therefore, by taking the upper boundary sufficiently far from the electrodes allows us to specify either a Dirichlet or a Neuman condition. The left side of the solution space (i.e. the vertical line through the centre of the electrode) is defined with a Neuman boundary condition, giving even symmetry. The right side of the solution space (i.e. the vertical line through the centre of the gap) is defined with a Dirichlet or odd boundary condition. The electrode on the lower boundary has the value of 1V and the gap on the lower boundary is described by a Neuman boundary.

Figure A.5-2 shows the results of the numerical simulation of the electrical potential and normalised DEP force vector field above an array of interdigitated bar micro-electrodes of characteristic size $d = d_1 = d_2 = 40\mu m$ with an applied voltage of 1V. Electrodes are present only on the bottom wall of the channel, with half an electrode and half a gap shown in the simulation. The electrical potential can be seen to decay to zero as the distance from the electrode increases. The DEP force can be seen to act only in the vertical direction at distances of $>d/2$ from the electrode array, with the horizontal component of the force only becoming apparent close to the electrode edges.

For the case where electrode arrays are present on both the top and the bottom surfaces of the channel (as seen in the focussing section of the device) the boundary conditions are the same as before, apart from the upper boundary condition, which now becomes identical to that of the bottom. The electrode on the upper boundary has the value of 1V and the gap is described by a Neuman boundary. It is possible to simplify the unit solution space further by imposing a Neuman boundary condition horizontally along the mid-plane of the channel, but for the purpose of illustration the upper and lower electrodes are included in the simulations.

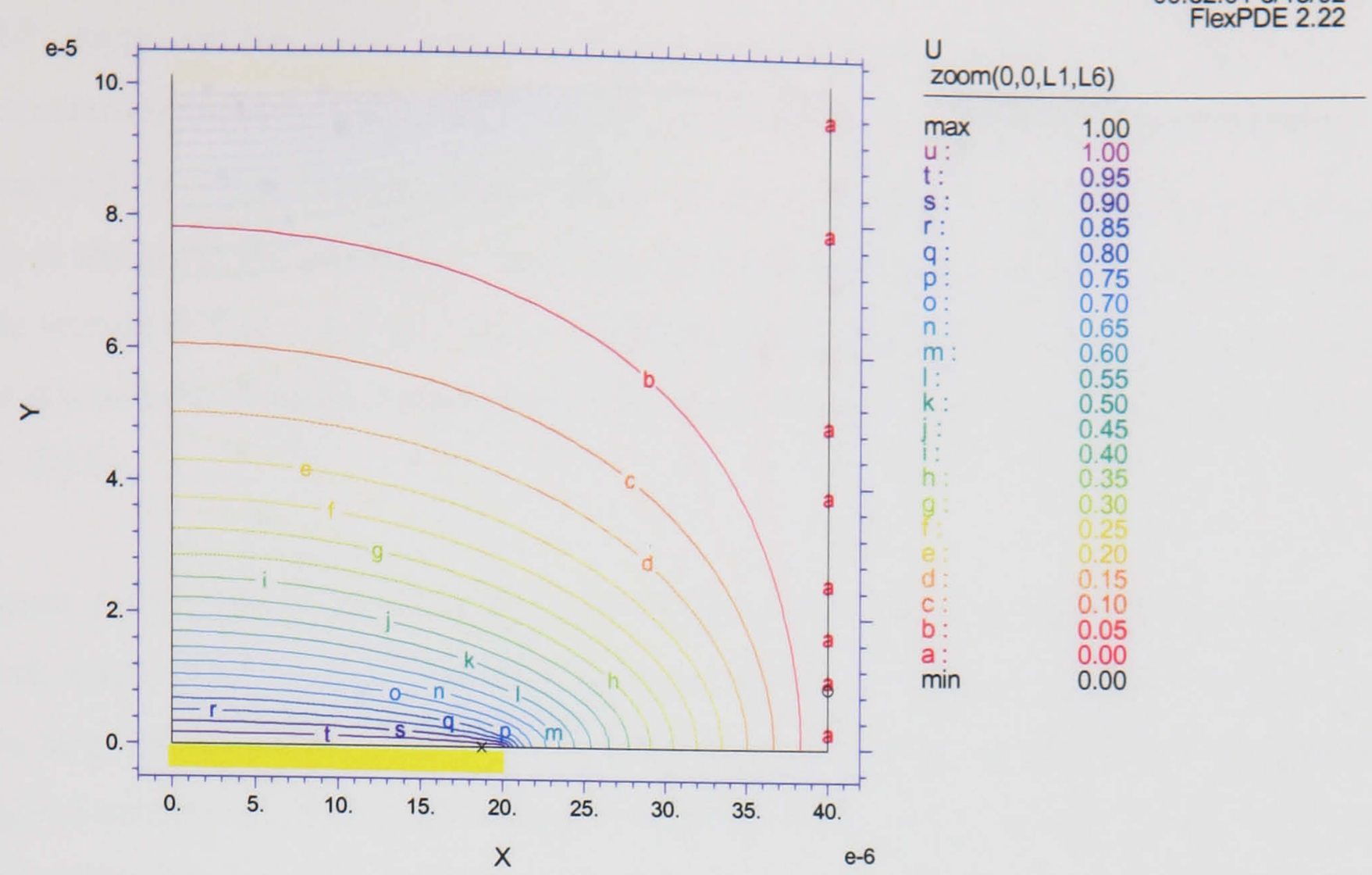

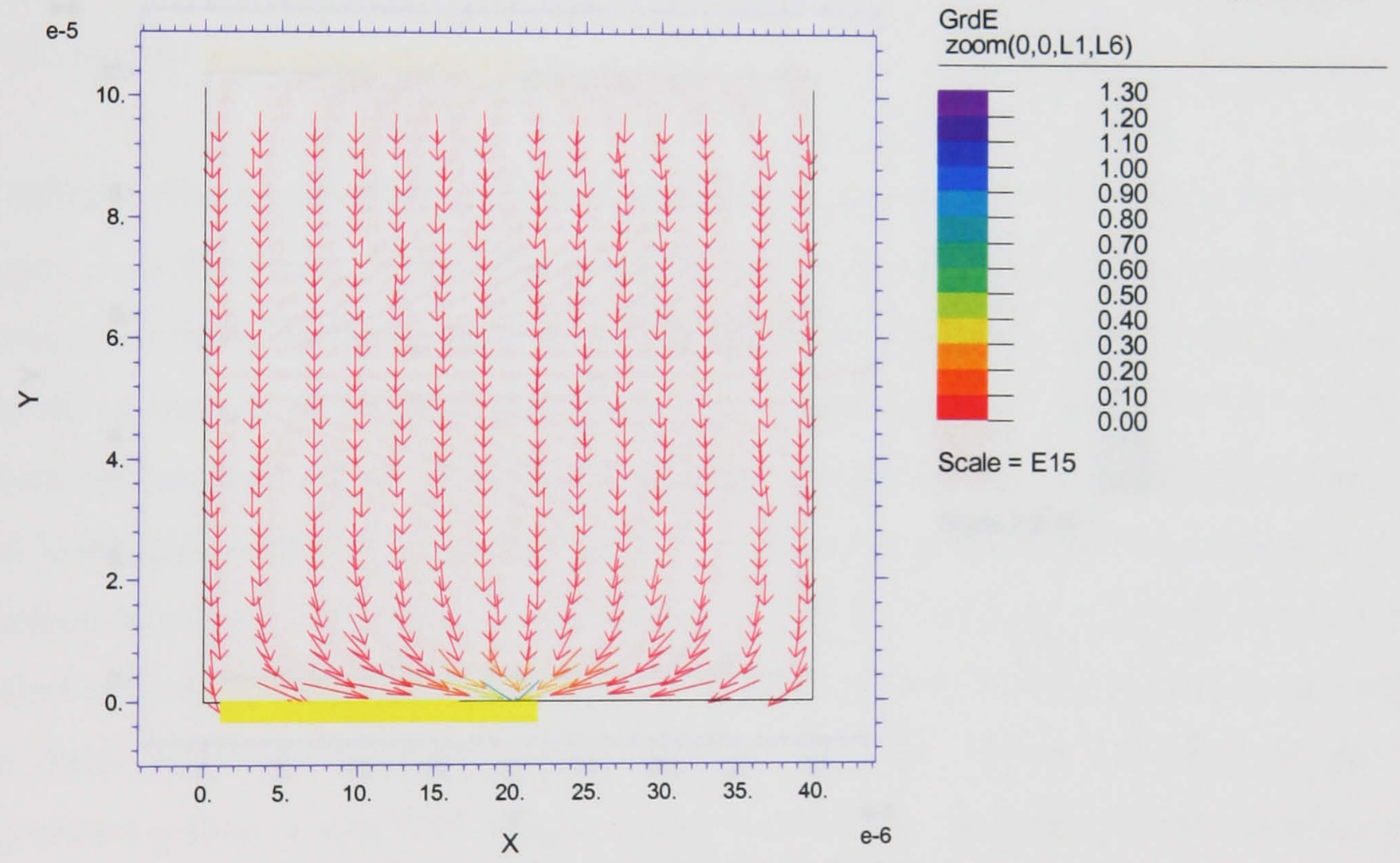

Figure A.5-2. Numerical simulation of **(a)** the electrical potential and **(b)** normalised DEP force vector field above an array of interdigitated bar micro-electrodes of characteristic size $d = d_1 = d_2 = 40\mu m$ with applied voltage of 1V. Electrode only on the bottom of the channel.

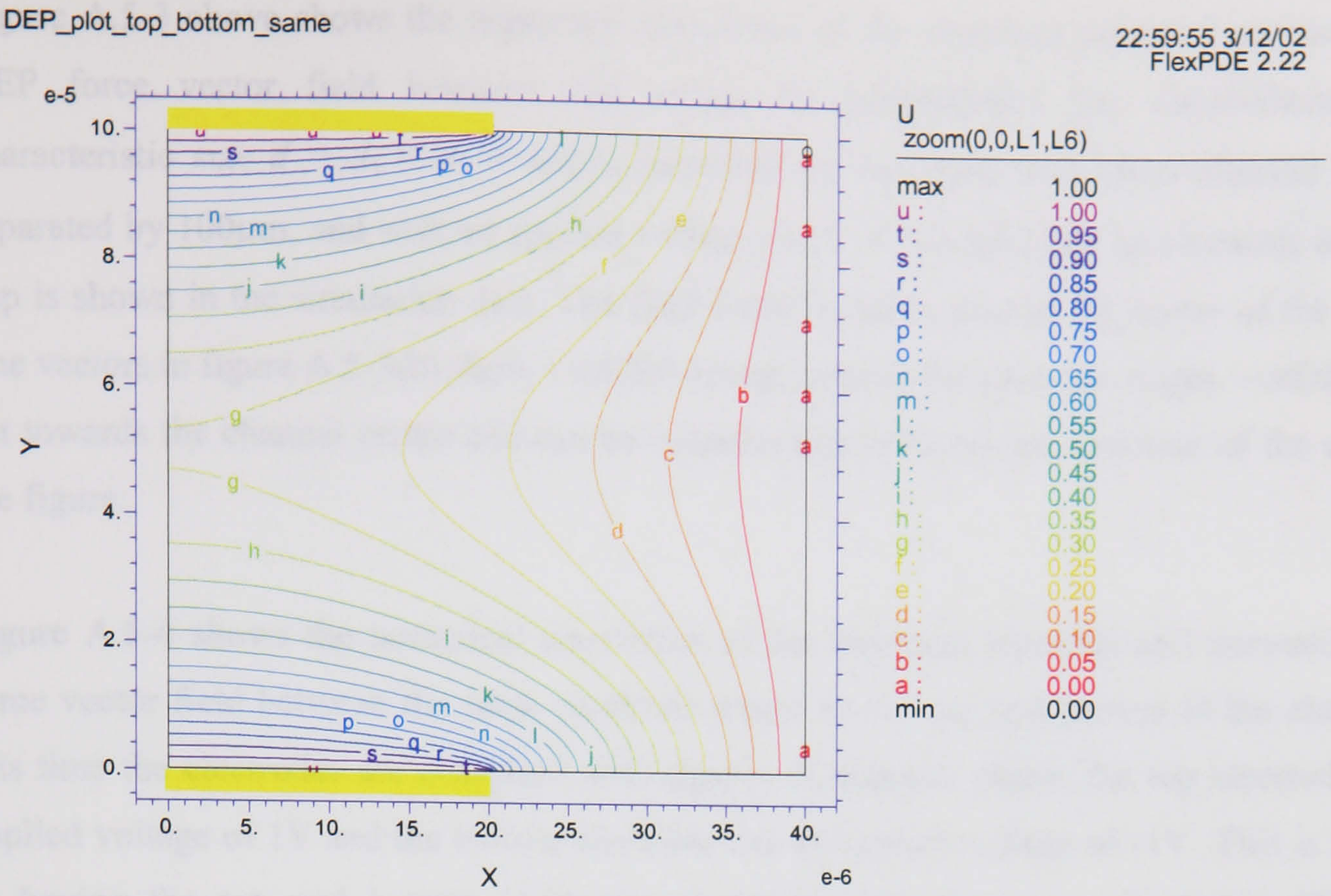

DEP_plot_top_bottom_same: Grid#0 p2 Nodes=16121 Cells=7920 RMS Err= 1.
Integral= 1.343050e-9

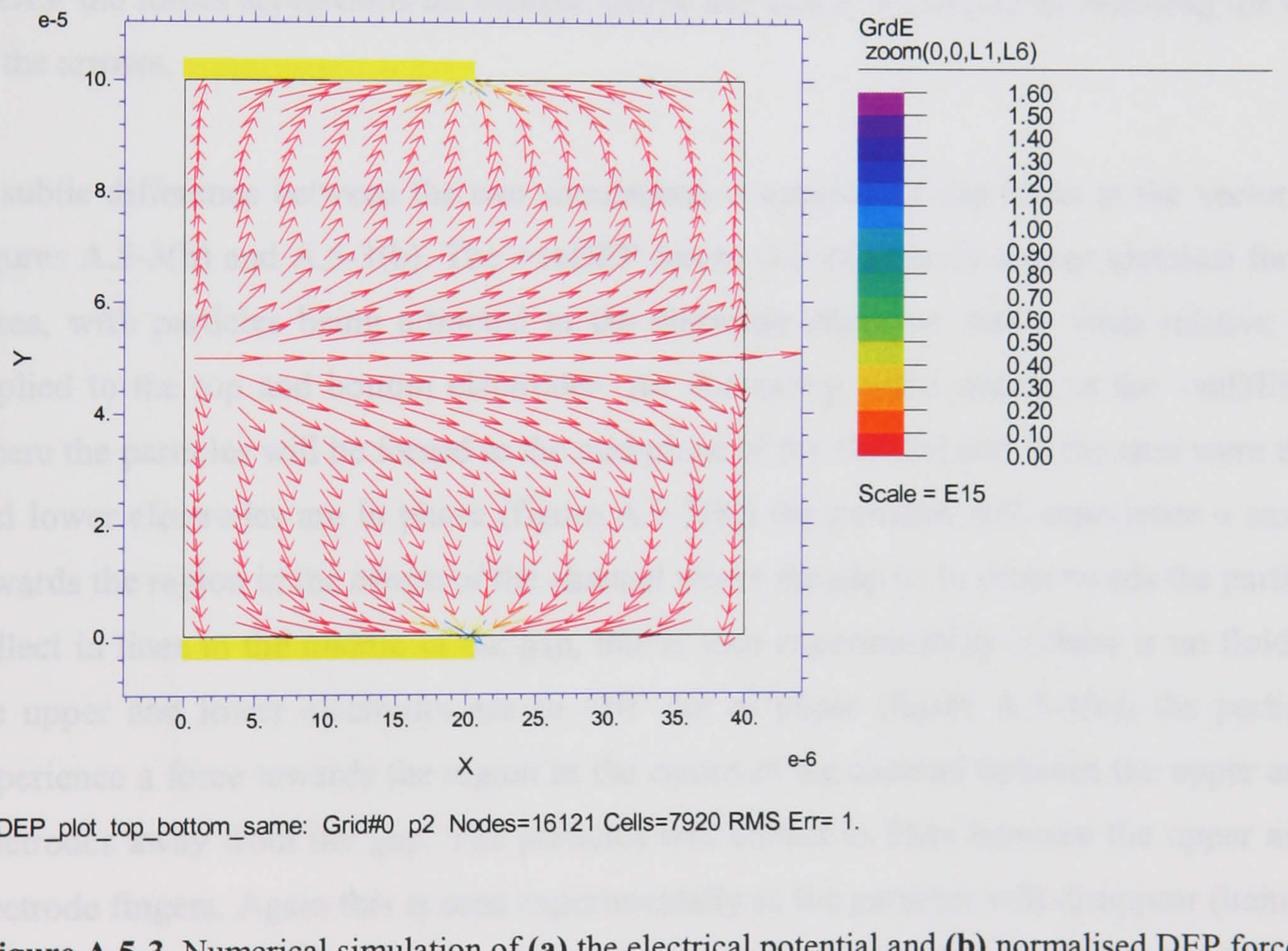

DEP_plot_top_bottom_same: Grid#0 p2 Nodes=16121 Cells=7920 RMS Err= 1.

Figure A.5-3. Numerical simulation of **(a)** the electrical potential and **(b)** normalised DEP force vector field above an array of interdigitated bar micro-electrodes of characteristic size $d = d_1 = d_2 = 40\mu m$ with applied voltage of 1V. Electrodes on the top and bottom of the channel, with electrodes directly above having the same applied potential.

Figure A.5-3 above shows the numerical simulation of the electrical potential and normalised DEP force vector field between two arrays of interdigitated bar micro-electrodes of characteristic size $d = d_1 = d_2 = 40\mu m$ patterned on the upper and lower channel surfaces, separated by 100μm, and with an applied voltage of 1V. Once gain half an electrode and half a gap is shown in the simulation data. The DEP force becomes zero at the centre of the channel. The vectors in figure A.5-3(b) show +veDEP acting towards the electrode edges. –veDEP forces act towards the channel centre and can be visualised by revesing the direction of the arrows in the figure.

Figure A.5-4 shows the numerical simulation of the electrical potential and normalised DEP force vector field between the same electrode arrays on the top and bottom of the channel but this time the electrodes are energised with signals of opposite phase; the top electrode has an applied voltage of 1V and the bottom electrode has an applied voltage of -1V. This is the same as having the top and bottom electrodes energised with the same signal but 180° phase difference between the two. The DEP force again becomes zero at the centre of the channel. The vectors in figure A.5-4(b) show +veDEP acting towards the electrode edges. For the case of –veDEP the forces act towards the channel centre and can be visualised by reversing the direction of the arrows.

A subtle difference between the two simulations is apparent if one looks at the vector plots in figures A.5-3(b) and A.5-3(b). The +veDEP forces will effectively appear identical for the two cases, with particles being attracted to the electrode edges no matter what relative phase is applied to the top and bottom electrodes. An interesting effect occurs in the –veDEP regime where the particles will be forced to the mid-plane of the channel and in the case were the upper and lower electrodes are in phase (figure A.5-3(b)) the particles will experience a small force towards the region in the centre of the channel where the gap is. In other words the particles will collect in lines in the middle of the gap, this is seen experimentally if there is no fluid flow. If the upper and lower electrodes are in 180° out of phase (figure A.5-4(b)) the particles will experience a force towards the region in the centre of the channel between the upper and lower electrodes away from the gap. The particles will collect in lines between the upper and lower electrode fingers. Again this is seen experimentally as the particles will disappear (being hidden by the opaque electrodes) when the electrodes are energised. Figure A.5-5 illustrates this schematically.

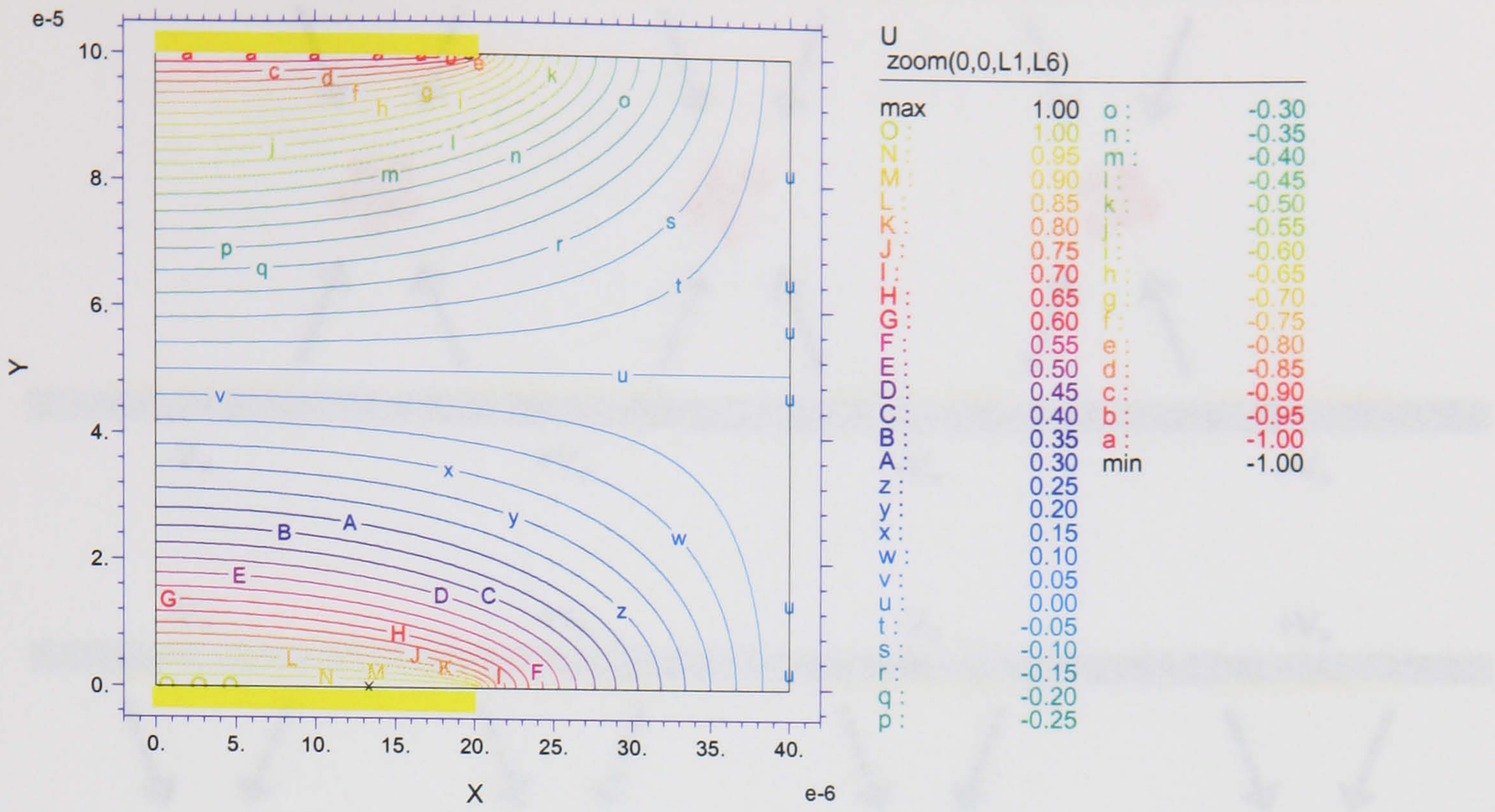

DEP_plot_top_bottom_different: Grid#0 p2 Nodes=36181 Cells=17880 RMS Err= 1.
Integral= 6.271854e-14

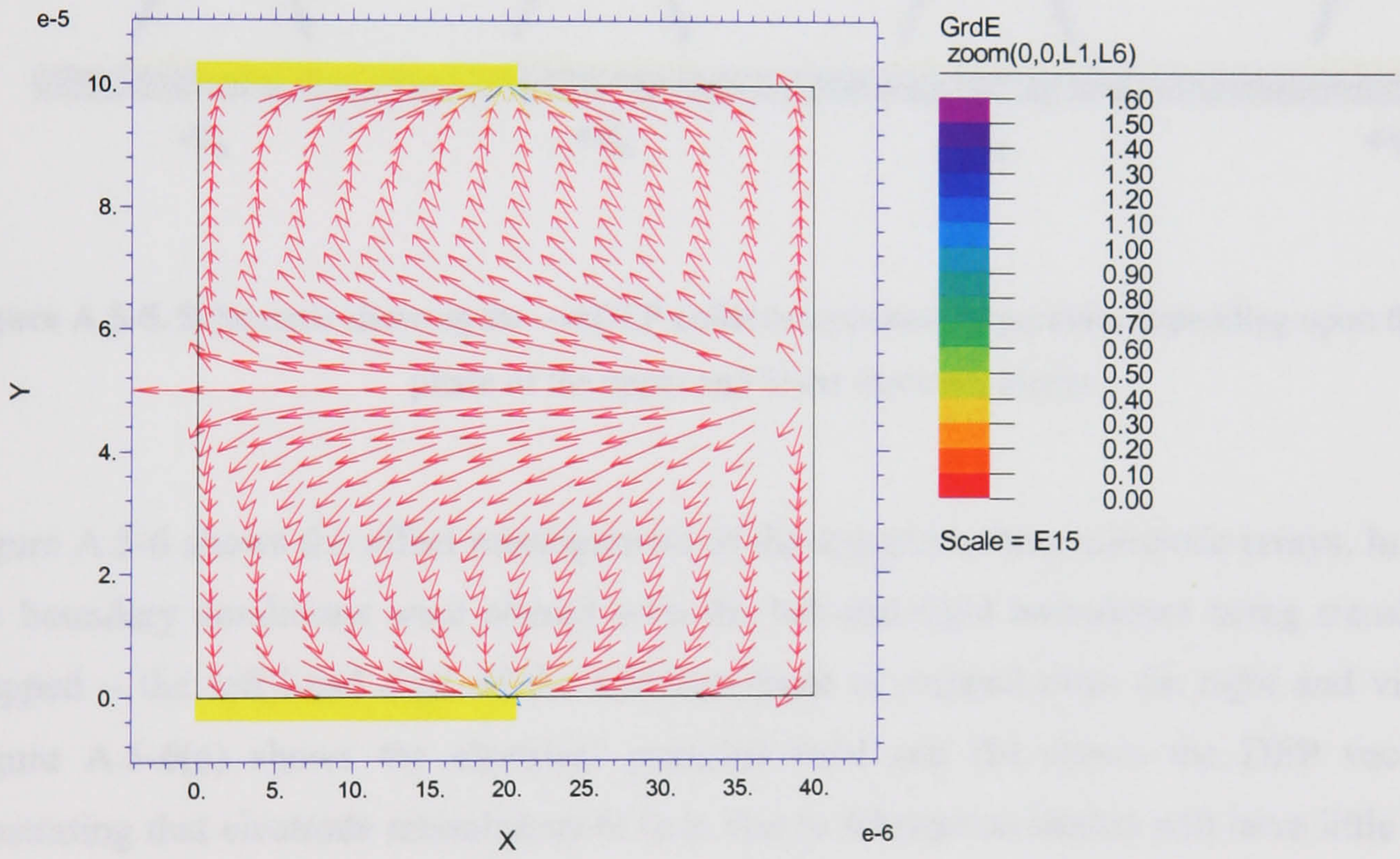

DEP_plot_top_bottom_different: Grid#0 p2 Nodes=36181 Cells=17880 RMS Err= 1.

Figure A.5-4. Numerical simulation of **(a)** the electrical potential and **(b)** normalised DEP force vector field above an array of interdigitated bar micro-electrodes of characteristic size $d = d_1 = d_2 = 40\mu m$ with applied voltage of 1V. Electrodes on the top and bottom of the channel, with electrodes directly above having opposite applied potentials.

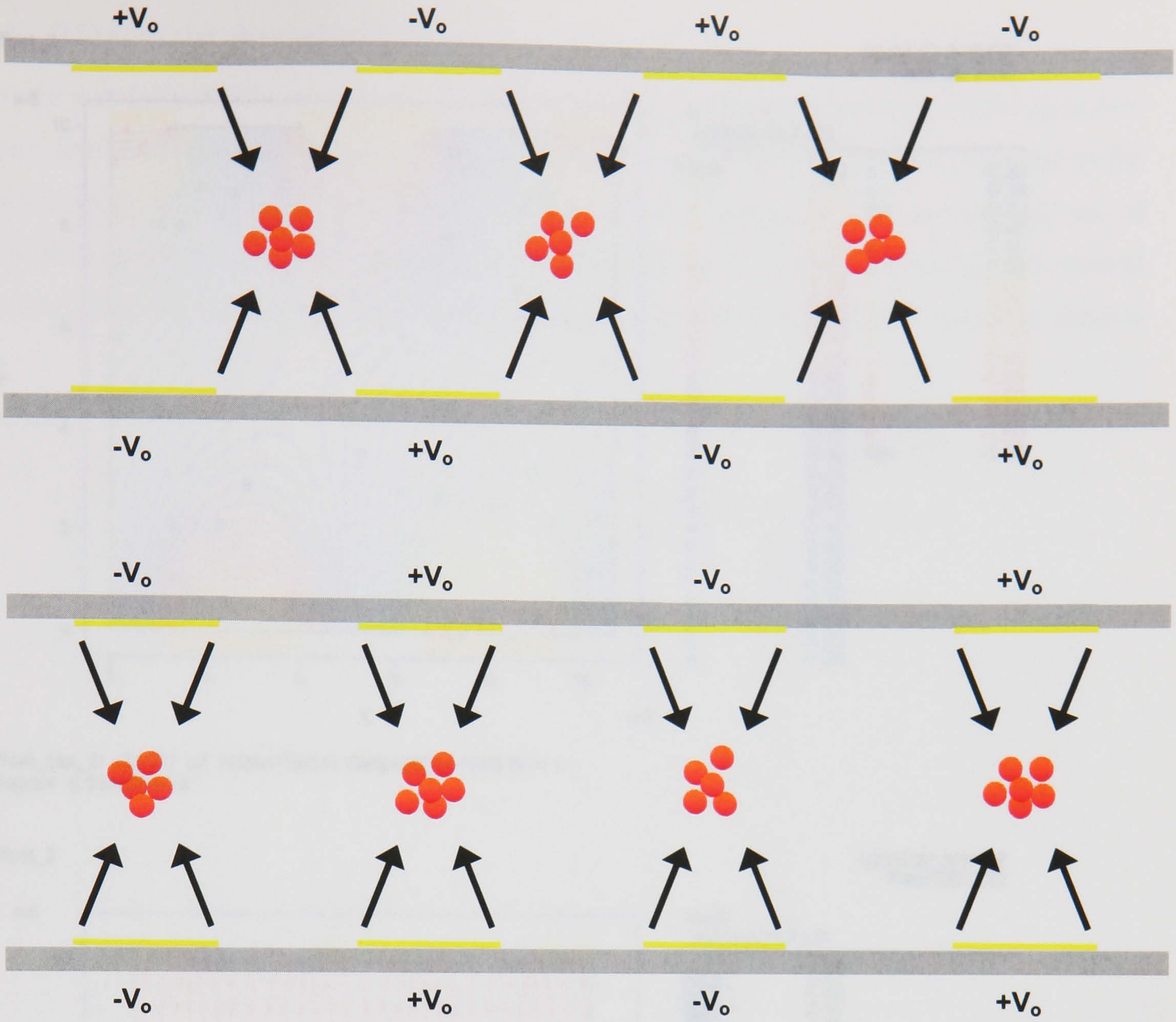

Figure A.5-5. Schematic showing the –veDEP collection position of particles depending upon the relative phase of the upper and lower electrode arrays.

Figure A.5-6 shows the effect misalignment of the top and bottom electrode arrays. In this case the boundary conditions were altered with the left and right boundaries being translationally mapped – the left hand edge of the solution space is mapped onto the right and vice versa. Figure A.5-6(a) shows the electrical potential field and (b) shows the DEP vector field, illustrating that electrode missalignment (e.g. due to fabrication limits) will have little effect on the overall DEP field and behaviour of the devices.

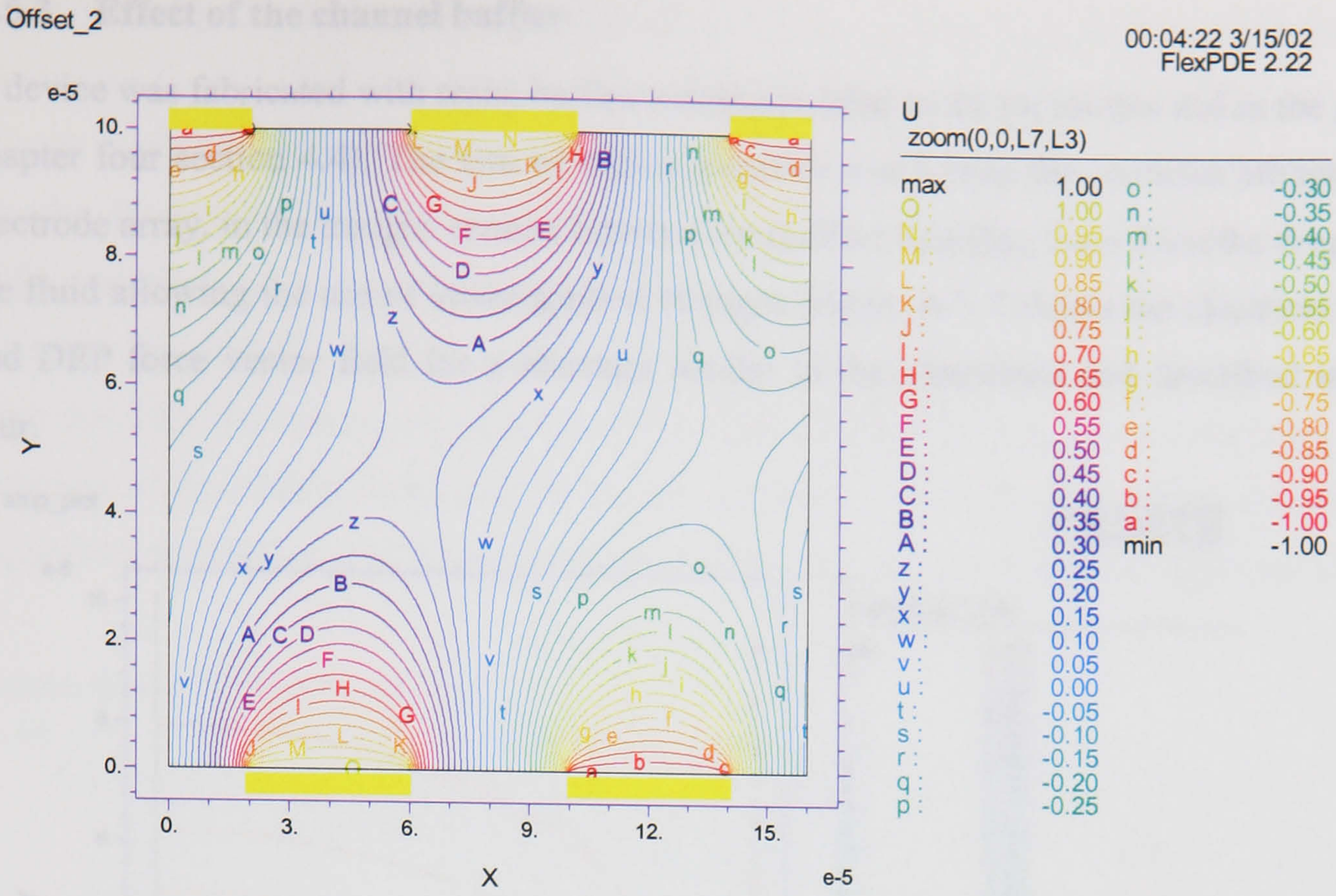

Offset_plot_2: Grid#0 p2 Nodes=56517 Cells=28014 RMS Err= 1.
Integral= 6.934899e-14

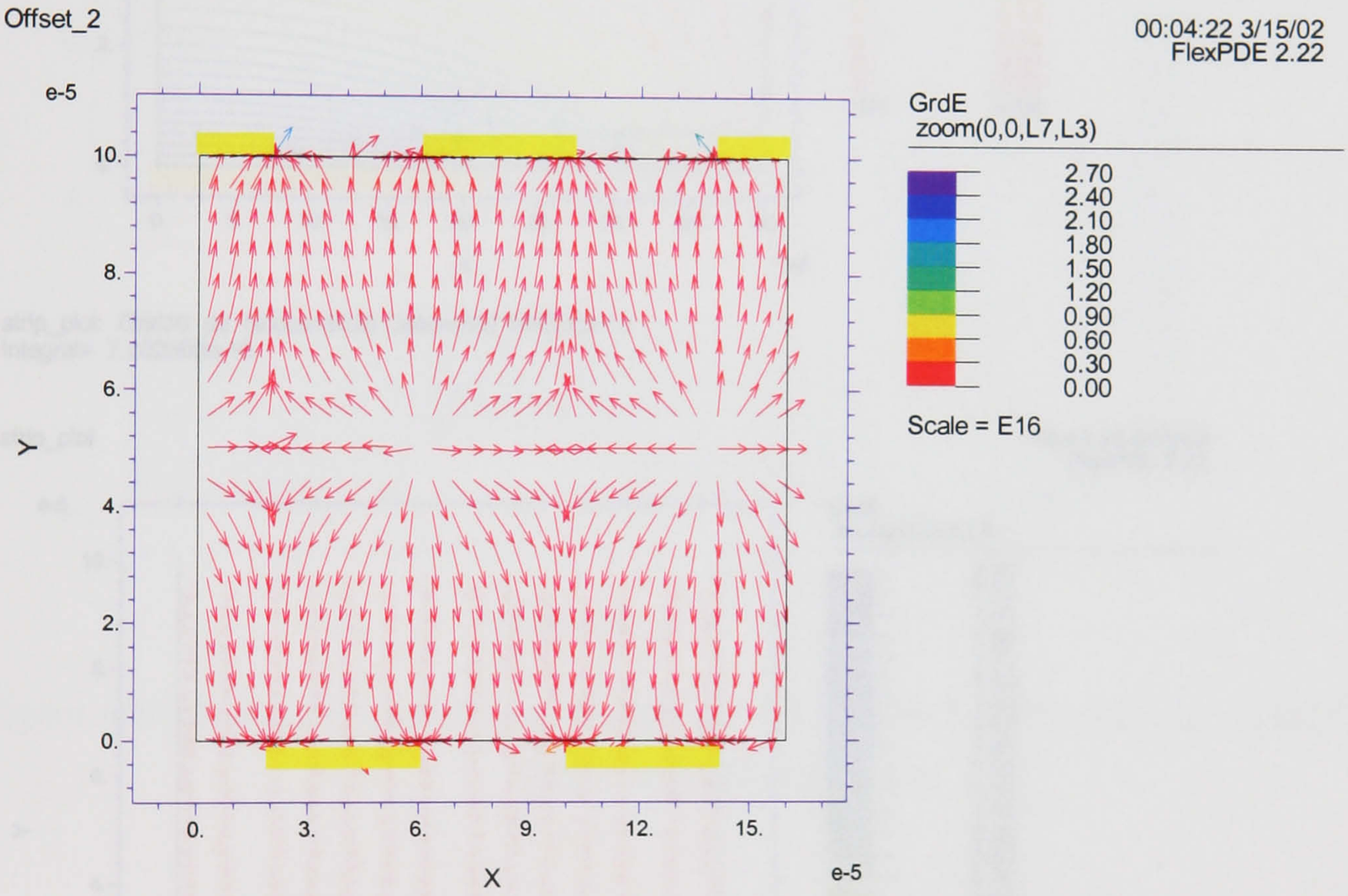

Offset_plot_2: Grid#0 p2 Nodes=56517 Cells=28014 RMS Err= 1.

Figure A.5-6. Numerical simulation of **(a)** the electrical potential and **(b)** normalised DEP force vector field above an array of interdigitated bar micro-electrodes of characteristic size $d = d_1 = d_2 = 40\mu m$ with applied voltage of 1V. With the top and bottom electrodes offset from one and other.

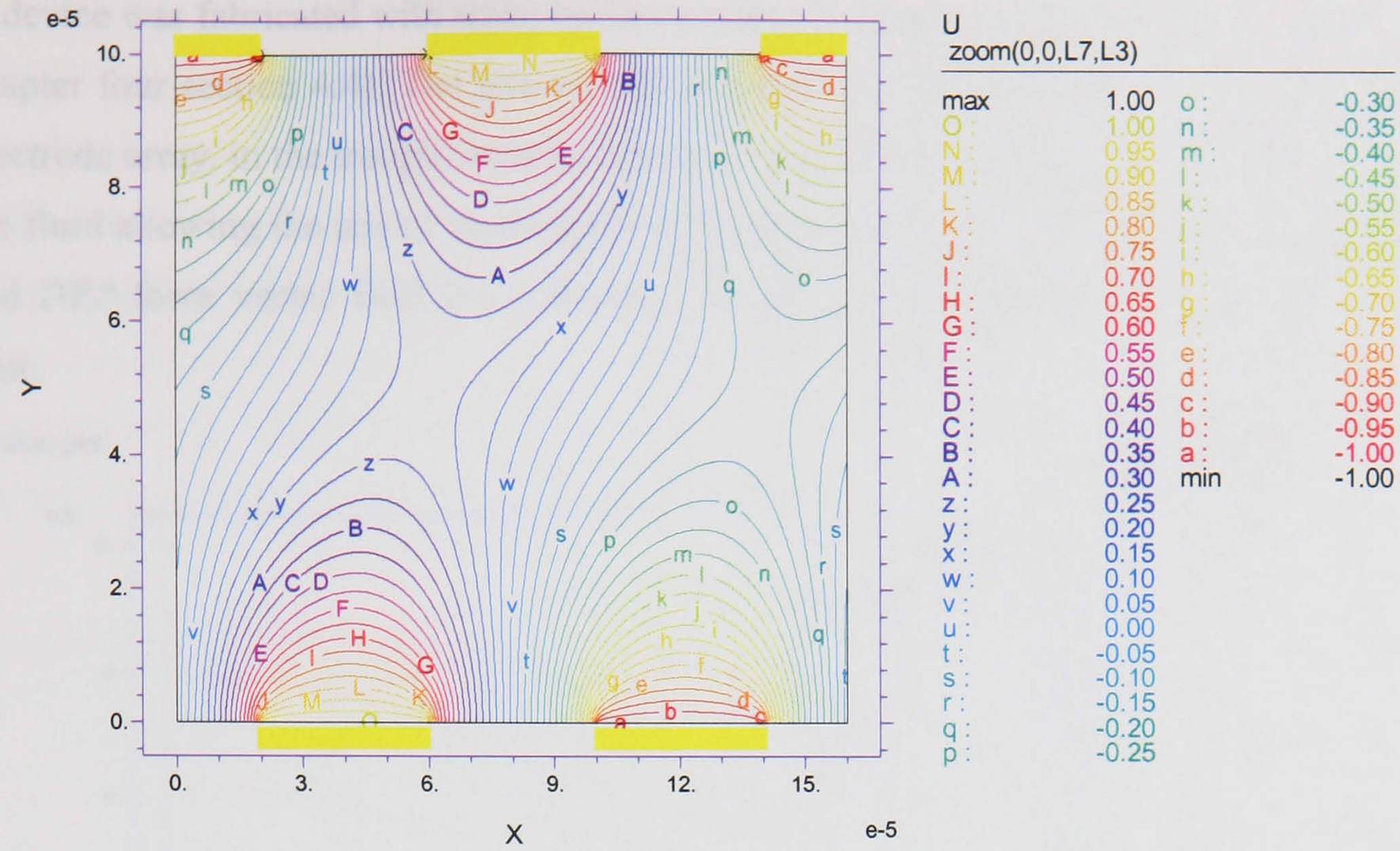

Offset_plot_2: Grid#0 p2 Nodes=56517 Cells=28014 RMS Err= 1.
Integral= 6.934899e-14

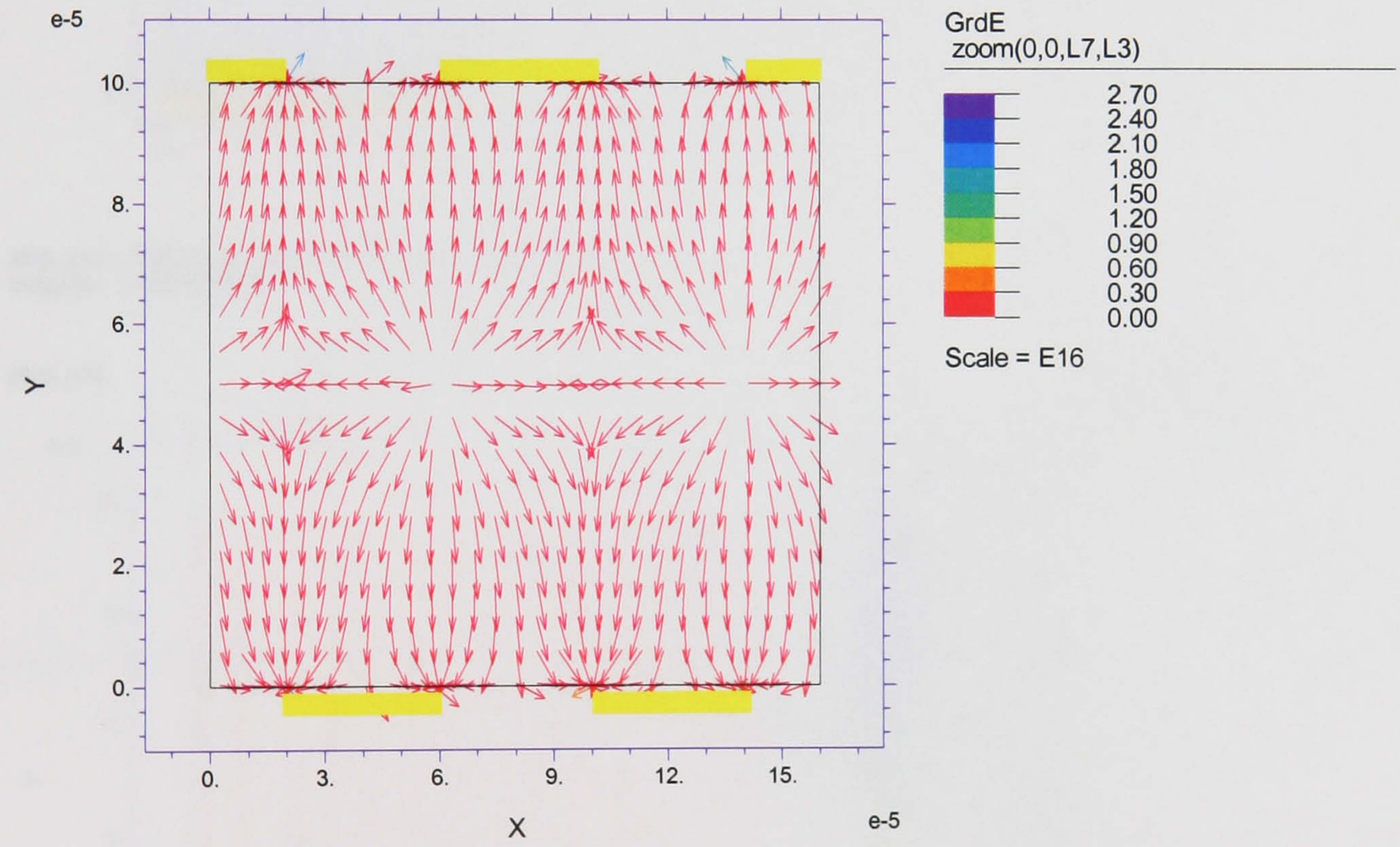

Offset_plot_2: Grid#0 p2 Nodes=56517 Cells=28014 RMS Err= 1.

Figure A.5-6. Numerical simulation of **(a)** the electrical potential and **(b)** normalised DEP force vector field above an array of interdigitated bar micro-electrodes of characteristic size $d = d_1 = d_2 = 40\mu m$ with applied voltage of 1V. With the top and bottom electrodes offset from one and other.

A.5.3 Effect of the channel baffles

A device was fabricated with resist baffles running parallel to the electrodes and in the gaps (see chapter four section 4.4). The aim of such a structure was to trap the particles attracted to the electrode array, in the troughs created between the baffles, shielding them from the drag force of the fluid allowing the use of lower applied voltages. Figure A.5-7 shows the electrical potential and DEP force vector field for a structure similar to that fabricated and described in chapter four.

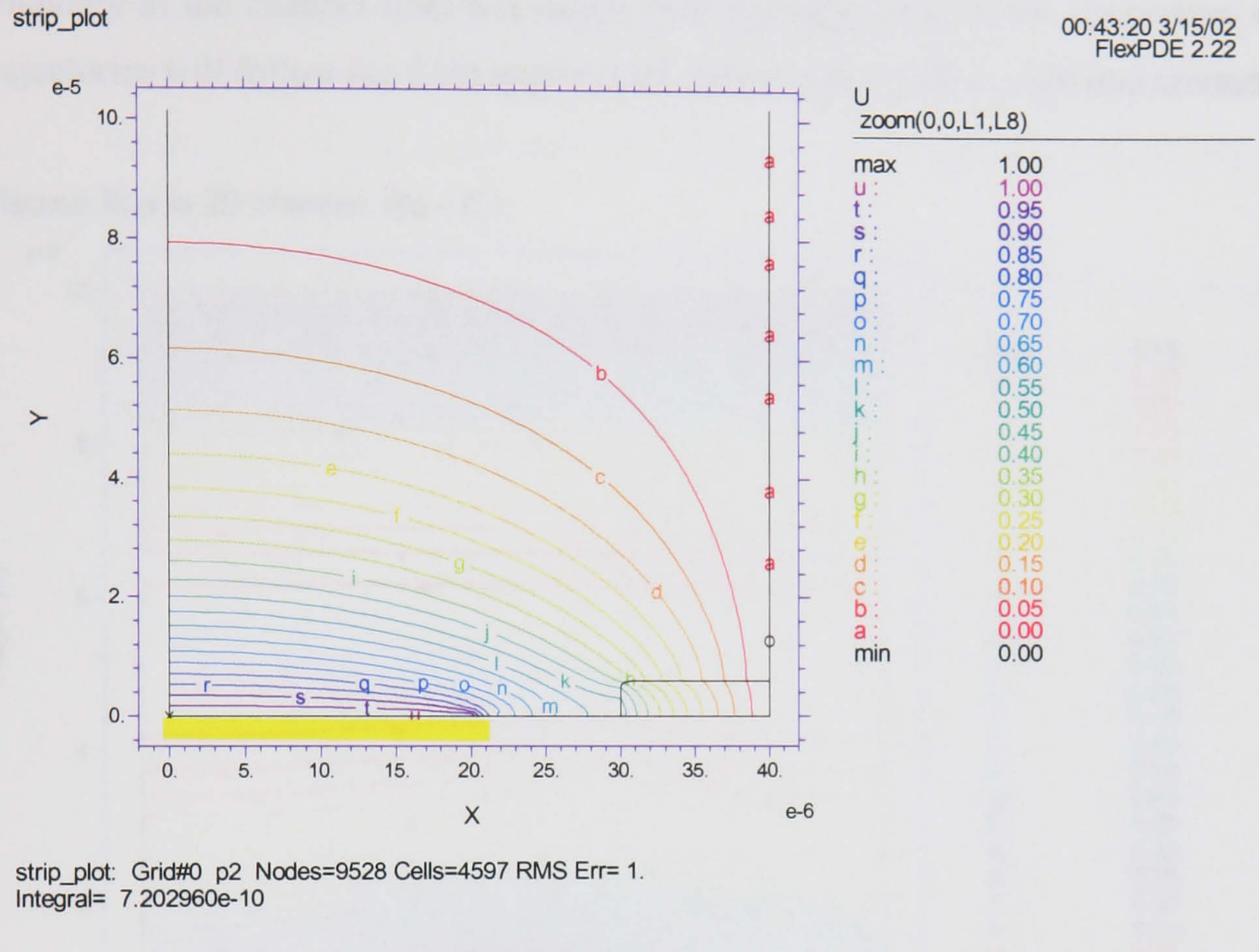

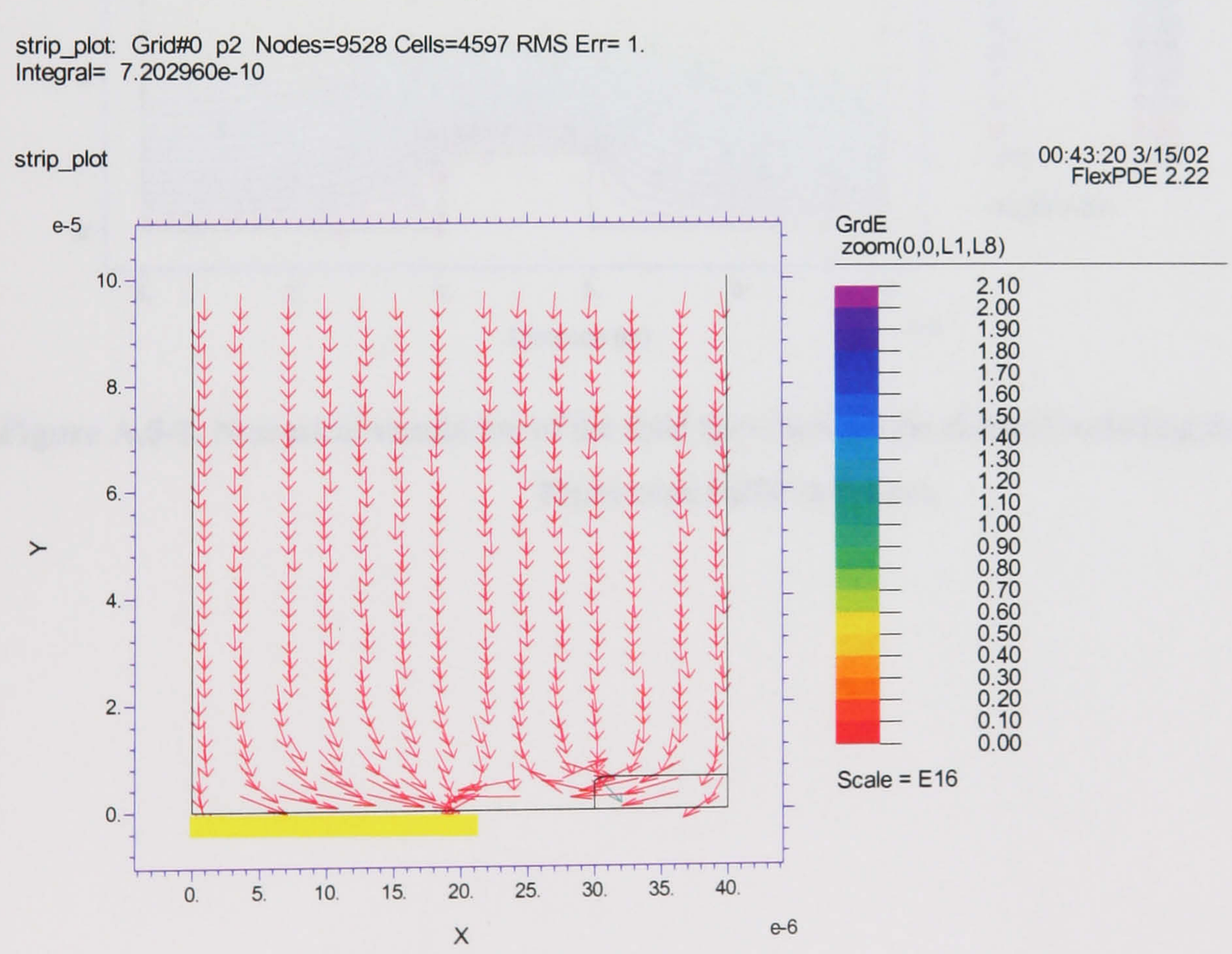

Figure A.5-7. Numerical simulation of **(a)** the electrical potential and **(b)** normalised DEP force vector field; including the baffle structure (10μm high and 20μm wide) for an array of characteristic size $d = d_1 = d_2 = 40\mu m$ with applied voltage of 1V.

Experimentally, the baffles had no measurable effect on the particle dynamics within the device. The reason for this can be attributed to the low Reynold's number flow in the channel; the fluid in such a structure is laminar and therefore flows around the baffle structure, in and out of the troughs. Figure A.5-8 shows numerical simulation of the fluid streamlines in such a system under conditions of pressure driven fluid flow from left to right. Again simulations were carried out using FlexPDE™, this time solving the Navier-Stokes equation. The boundary conditions were non-slip boundaries on the top and bottom channel surfaces, and a constant pressure boundary at the channel inlet and outlet (left and right sides of the simulation space). Particle trajectories will follow the fluid streamlines, flowing from left to right and around the baffles.

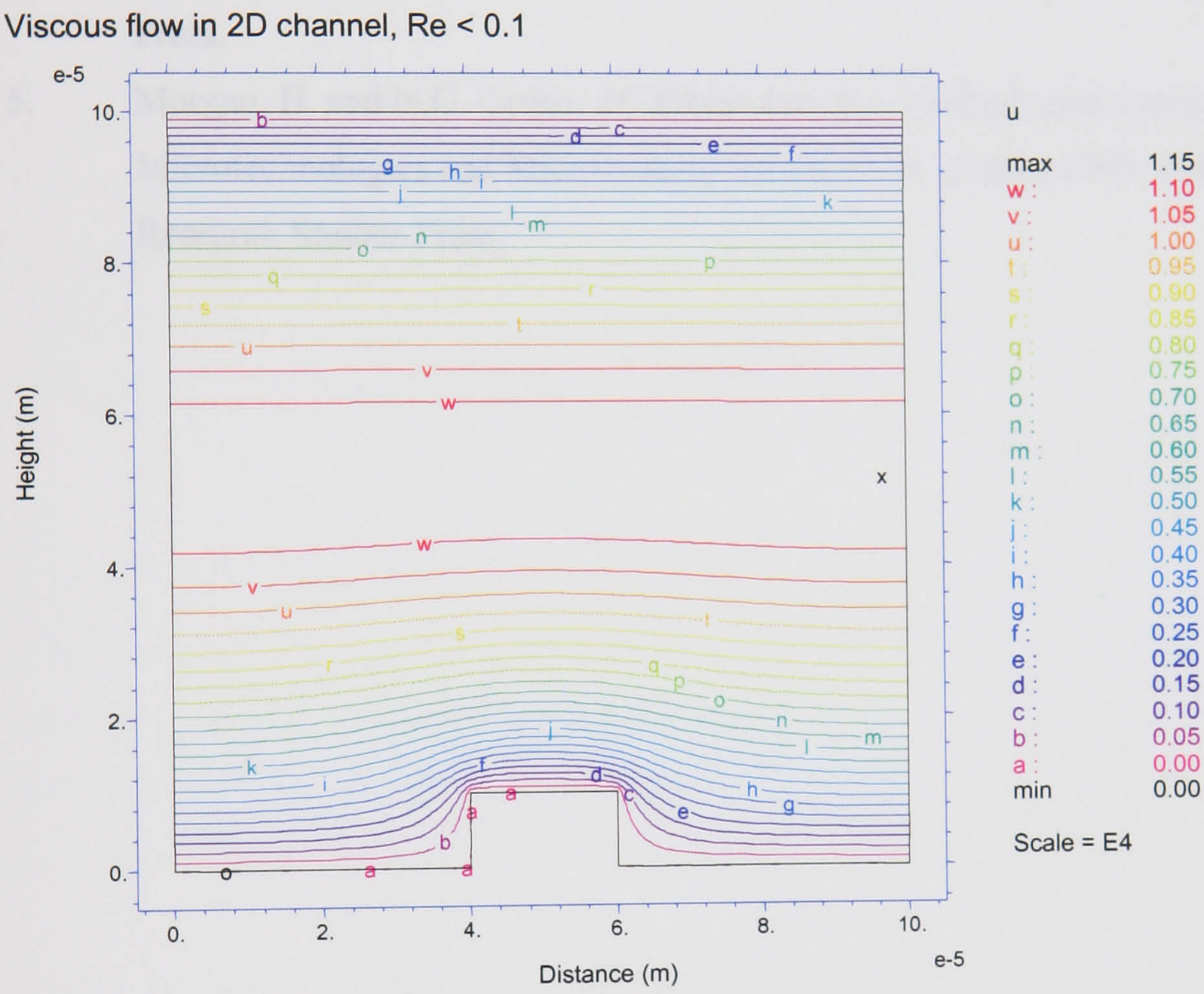

Figure A.5-1. Numerical simulation of the fluid flow through the channel including the 10μm high and 20μm wide baffle structures.

A.5.4 References

1. Backstrom, G., *Fields of physics by finite element method, an introduction*, Sweden: StudentLitteratur.
2. Morgan, H., *et al.*, *The dielectrophoretic and travelling wave forces generated by interdigitated electrode arrays: analytical solution using Fourier series.* Journal of Physics D-Applied Physics, 2001. 34(10): p. 1553-1561.
3. Morgan, H., *et al.*, *The dielectrophoretic and travelling wave forces generated by interdigitated electrode arrays: analytical solution using Fourier series (vol 34, pg 1553, 2001).* Journal of Physics D-Applied Physics, 2001. 34(17): p. 2708-2708.
4. Jones, T.B., *Electromechanics of Particles*. 1995, Cambridge: Cambridge University Press.
5. Morgan, H. and N.G. Green, *AC Electrokinetics: Colloids and Nanoparticles*. 1 ed. Microtechnologies and Microsystems Series, ed. R. Pethig. 2003, Baldock, UK: Research Studies Press.

Chapter Six: Dielectrophoretic chromatography

6 Introduction

This chapter presents the results of experiments undertaken to characterise the particle separation capabilities of the DEP separation system, based on the focussing/separation electrode geometry, described in the previous chapters. The focussing section of the device is discussed first, and the results of the experiments to characterise the functioning of this part of the device are presented. This is followed by the experimental characterisation of the separation section of the device. These results are discussed with reference to the simulation work of the previous chapter.

6.1 Materials and methods

A general description of the experimental protocols relevant to this chapter, are given here. Specific details of the device fabrication, and sample handling and labelling protocols used can be found in chapters three and four.

6.1.1 Experimental apparatus

Flow through DEP separation devices were fabricated, as described in chapter four. Two electrode sizes were used, with electrode and gap sizes $d = d_1 = d_2 = 20\mu m$ or $40\mu m$. The dimensions of the flow channels were measured for each device and this information was used in the simulations relating to specific experiments.

The experimental set-up is shown schematically in figures 6-1 and a photograph is shown in figure 6-2. The channels were viewed using an inverted microscope in either phase contrast or epi-fluorescence mode. Images were recorded using a CCD camera onto S-VHS, or captured directly to a PC.

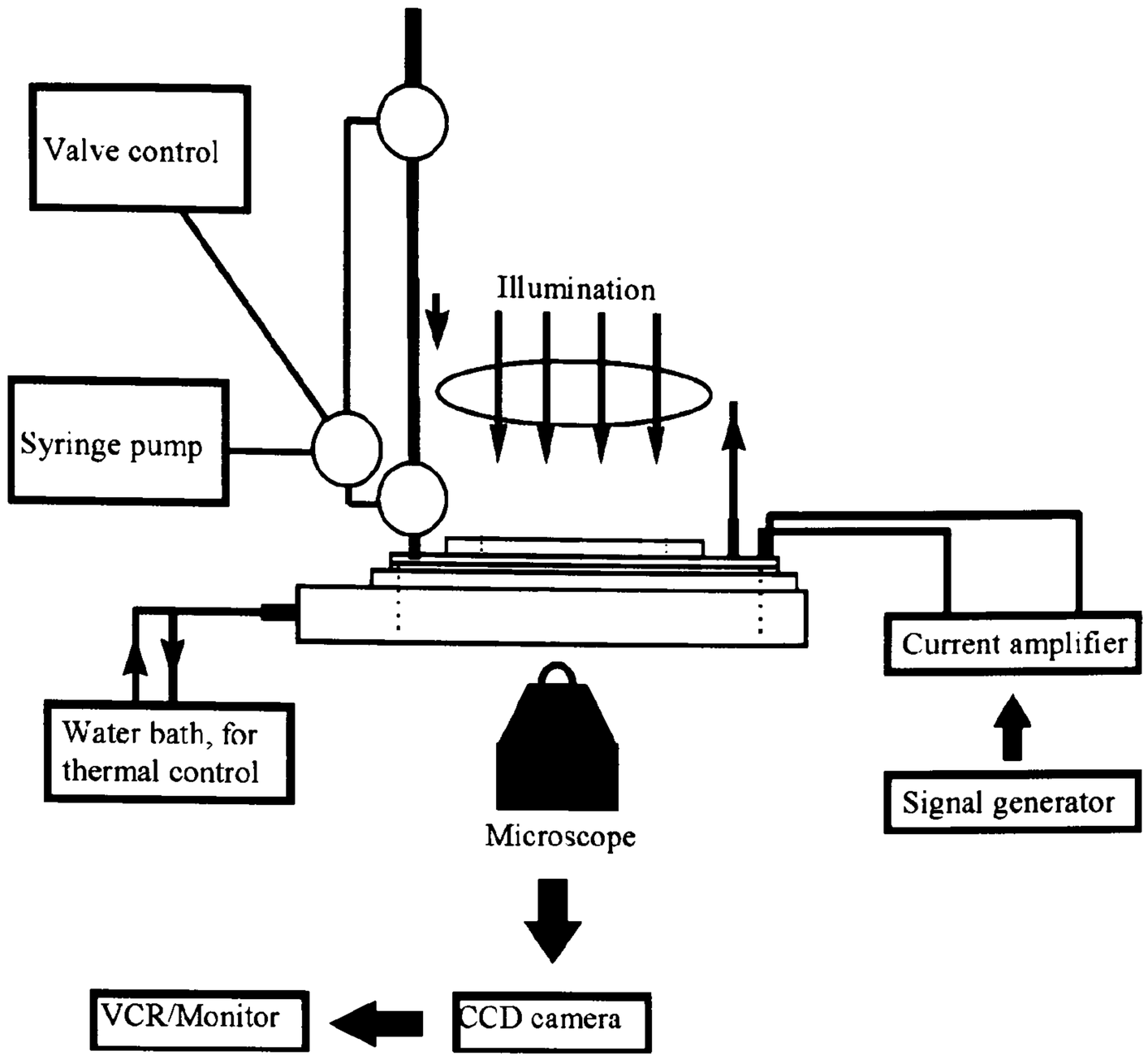

Figure 6-1. Schematic of experimental setup, showing the DEP separation device mounted on the cooler, the sample injection column, and the other apparatus.

The photograph in figure 6-2 shows the experimental setup used for the experiments involving non-fluorescently labelled particles. The fluorescence microscopy setup (shown on figure 7-2) is identical to that shown in figure 6-2, apart form the use of a Zeiss Axiovert200 inverted epi-fluorescence microscope.

The DEP separation devices were mounted on the temperature controller (see section 4.3). Water at room temperature was pumped through the controller in order to dissipate any heat produced by the device during the course of the experiments, maintaining the device at a constant temperature (~25°C). The whole device was held in position using an *x*- *y*- micromanipulator, allowing the entire flow channel to be viewed. The focus control of the microscope allowed observation at different heights within the flow channel. The entire apparatus (microscope, *x*- *y*- micromanipulator, etc.) was mounted on a vibration free platform, comprising a heavy steel plate resting on rubber mountings. The fluorescence set up was mounted on a pneumatically isolated optical bench (a gift from IBM, Greenock). Movement of the device for viewing purposes was therefore relatively vibration free. This was an important consideration as initial experiments showed that, even small vibrations (e.g. due to people walking in the lab) were sufficient to cause cells to be released from the electrode edge and flow further along the separation electrode array before becoming captured once more.

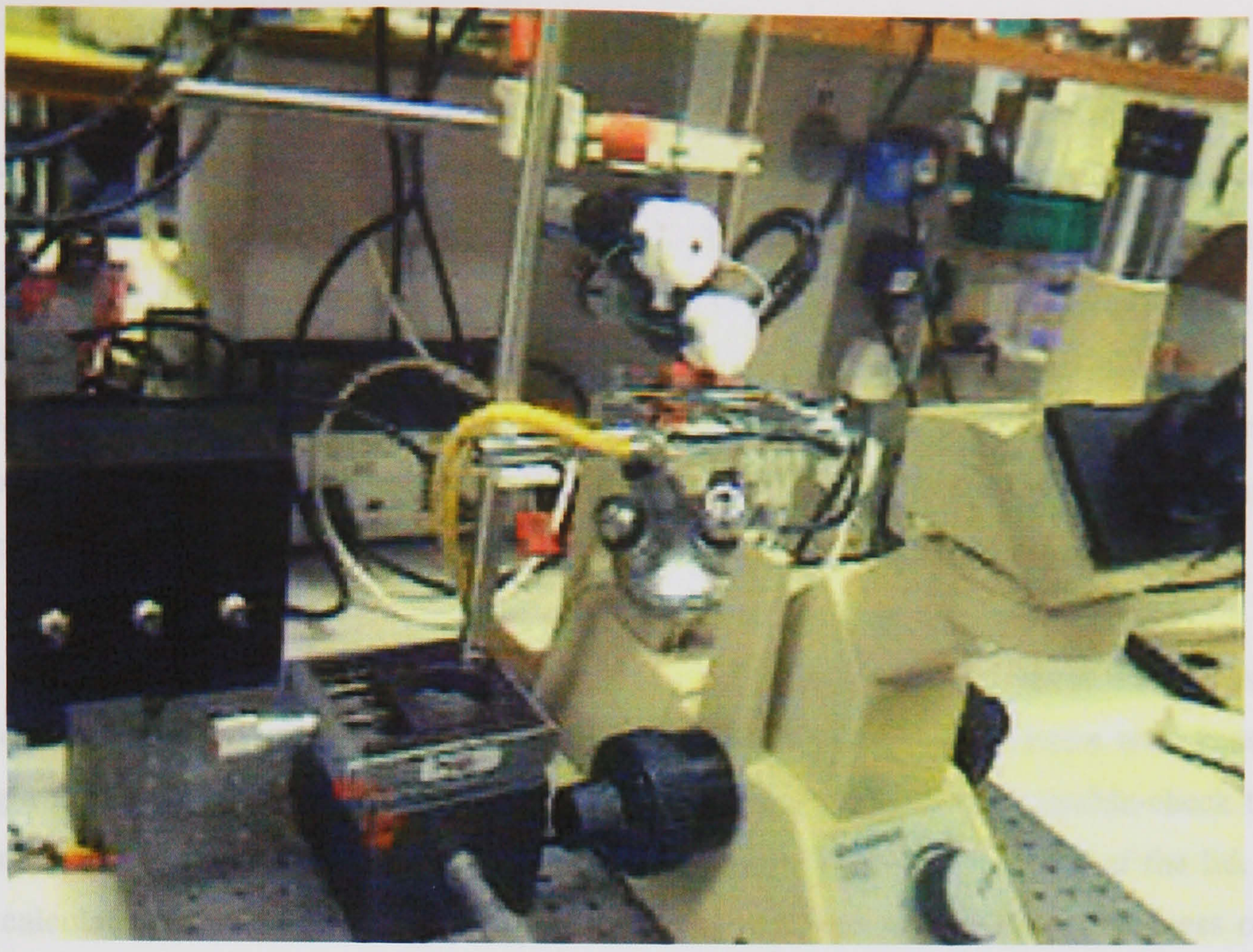

Figure 6-2. Photograph of the experimental setup used for non-fluorescence experiments.

6.1.2 Sample preparation

Particles (i.e. cells or latex beads) were suspended at known concentrations in the relevant DEP separation media (see section 3.11 for details) of known conductivity. The particle samples were prepared and loaded into the injection column of the device. The sample was then forced from the injection column and flowed through the separation device under the influence of pressure driven fluid flow applied using a programmable syringe pump. The rate of fluid flow through the device was controlled by manually programming the syringe pump.

6.2 Particle focussing

The DEP separation system can be divided into two distinct functional parts. The focussing section where all particles undergo -veDEP and are forced into a thin sheet midway between the top and bottom electrode arrays, and the separation section where particles are attracted under the influence of +veDEP to that electrode array. This section describes the experiments carried out to investigate the operation of the focussing electrode section of the device. Experiments were carried out using two sizes of latex beads (diameters 10μm and 557nm). Due to the difficulty of accurately measuring particle positions (with the fluid flow on) the measurements were made under zero flow conditions. Observations of the particle positions with the fluid flowing gave qualitatively similar results.

6.2.1 Steady state particle levitation heights

In order to establish the functioning of the focussing device, steady state levitation heights of particles were measured in the absence of fluid flow. Figure 6-3 shows a graph of the steady-state levitation height plotted against the peak applied voltage (logarithmic scale) for 10μm diameter latex spheres. Measurements were made with the top and bottom electrode arrays energised with the same applied voltage on each array. The particle levitation heights were measured using the calibrated focus control on a Nikon Microphot microscope used in brightfield mode, using a x10 magnification lens. The measurement resolution for such a system is determined by the graduations on the focus control and is approximately ±1μm.

Prior to conducting levitation height measurements, the graduated focus knob of the microscope was calibrated against the thickness (height) of the channel (channel thickness was measured using a DEKTAK™ surface profiler prior to bonding the channel lid). To double-check this a micrometer was used to measure the height of the channel following bonding of the lid. This was calculated from the measured thickness of the device less the measured thickness of the glass substrates used for the upper and lower channel walls. Both measurements gave the channel height of 100μm, resulting in a focus control calibration factor of 1.37 for the x10 dry lens with a numerical aperture of 0.3. The axial distance measured (i.e. the height in the channel) using the focus knob is then multiplied by this calibration factor to give an accurate measurement of axial distance.

Three measurements were made to calculate the height of individual particles: the position of the bottom electrode array, the position of the top electrode array, and the position of the particle when it's mid-plane appeared in focus (i.e. measurements were made focussing at the centre of the particle). The position of the focus knob was noted at each of these three positions and the particle position was calculated. The data was collected with a suspending medium conductivity of $1mSm^{-1}$, at a frequency of 10MHz, where all the beads experience -veDEP, and the factor $Re[f_{CM}]$ was calculated to be -0.476 (this value for the real part of the Clausius-Mossotti factor was derived from values measured by Cui *et. al.*[1]). The density of latex is $1055kgm^{-3}$, and the beads were suspended in dilute KCl solution (density of $1000kgm^{-3}$). Particle concentrations were approximately $1.0x10^6$ beads per ml. At this concentration and for this size of bead the likelihood of the particles interacting is small, the volume of a single 10μm bead is $\sim 5.2x10^{-19}m^3$ and the channel volume is $\sim 5x10^{-9}m^3$, it would therefore require 10^{10} 10μm beads to pack the channel.

An analytical solution for the steady state levitation height above a single electrode array was given (section 5.5.2, equation 5-26) for a homogeneous spherical particle (e.g. a latex sphere) suspended in a liquid. For the special case $d = d_1 = d_2$, an expression for the steady state focusing position of a particle can be found, by balancing the dielectrophoretic force due to the top and bottom electrode arrays (equation 5-11) with the gravitational force (equation 5-22). For the case where there is an electrode array on the top and bottom of the channel the equation is,

$$e^{\frac{-\pi y}{d}} - e^{\frac{-\pi(h-y)}{d}} = -\frac{24V_o^2\varepsilon_m \mathrm{Re}[f_{CM}]}{\pi d^3 \Delta\rho g} \qquad (6\text{-}1)$$

where h is the channel height, g is the gravitational acceleration, $\Delta\rho$ the difference in density between the particle and fluid, V_o is the applied peak voltage, $Re[f_{CM}]$ the real part of the Claussius-Mosotti factor, ε_m the permittivity of the medium, and y is the particle height. The terms on the left of equation 6-1 express the exponentially decaying nature of the DEP force at distances greater than d from the top and bottom electrode arrays. Simplification of this equation to give the theoretical value of levitation height versus applied voltage is not easily achievable due to the two exponential expressions on the left of equation 6-1. Figure 6-3 shows experimentally derived values for the levitation heights, and the simulated levitation heights (see chapter five for details of the simulations) in the focussing array versus the peak applied voltage.

The beads were levitated to a stable position where the buoyancy force is balanced by -veDEP levitation forces [1-4]. A settling time of 5 minutes was allowed following the change in the applied voltage; this allowed time for the beads to reach their equilibrium position. It can be seen that the experimental and simulated particle positions are comparable, and that when the top and bottom electrodes are energised, particles are focussed (rather than levitated) to a constant height half that of the chamber height. The focussing position does not vary with applied voltage, above a threshold of 3V peak for the 40μm electrode and 4V peak for the 20μm electrode arrays, for channels of height 100μm.

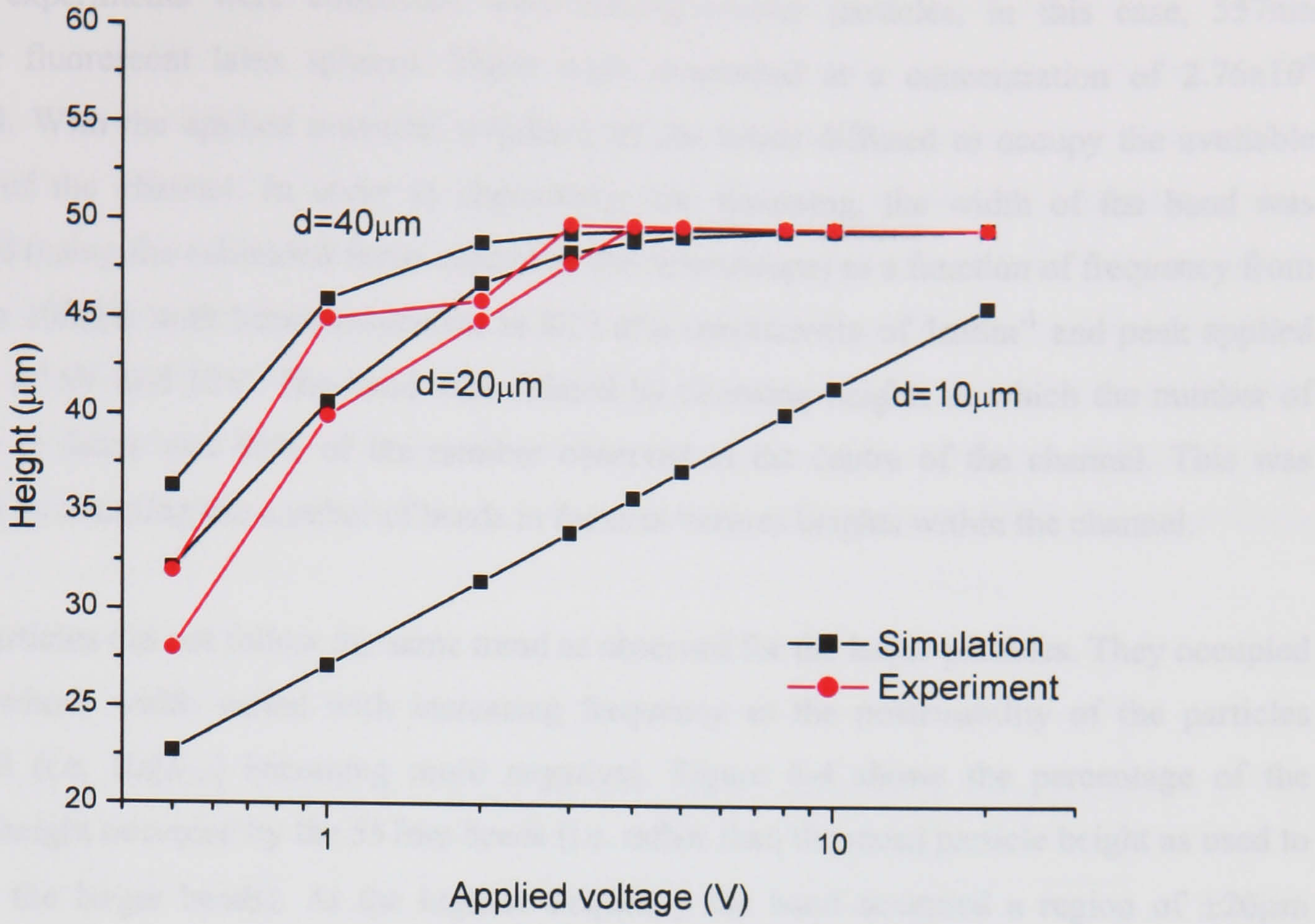

Figure 6-3. Comparison between simulated and measured steady state focussing heights for 10μm diameter latex particles, between focussing electrodes comprising either the 10μm, 20μm or 40μm electrode arrays. Experimental data is shown for the 20μm and 40μm electrode arrays.

Levitation height measurements were not made using 10μm electrodes due to difficulties in fabricating arrays of such small feature size over large areas (5cm x 1cm). Measurements were also made with beads flowing through the device. It was observed that particles were levitated to the mid-plane of the chamber within a short distance (few millimetres) of the start of the electrodes, which corresponded roughly with the trajectory calculations of chapter five, although accurate values were difficult to obtain.

All the particles were focussed and confined to a narrow sheet, one particle diameter wide, with uniform particle distribution across the width of the chamber. Upon exiting the focussing section of the device, the particles continued to travel along the middle of the chamber where the fluid flow velocity was greatest. No particles were observed adhering to any of the chamber walls within this section of the separation device, even after many repeat experiments on the same device. Similar results were found for experiments carried out using blood cells. The fact that no beads or cells could be seen adhering to the section of the channel where the applied DEP was negative suggests that the technique may be a useful method for antifouling, although the use of –veDEP for antifouling has previously been proposed by others (e.g. [5]).

6.2.2 Focussing of submicron particles

Similar experiments were conducted with sub-micrometer particles, in this case, 557nm diameter fluorescent latex spheres. These were suspended at a concentration of 2.76×10^6 beads/ml. With the applied potential switched off the beads diffused to occupy the available volume of the channel. In order to characterise the focussing, the width of the band was measured (using the calibrated focus control on the microscope) as a function of frequency from 1MHz to 10MHz with beads suspended in KCl at a conductivity of $1 mSm^{-1}$ and peak applied voltages of 5V and 10V. The band was defined by choosing heights at which the number of particles in focus was 90% of the number observed at the centre of the channel. This was achieved by counting the number of beads in focus at various heights within the channel.

These particles did not follow the same trend as observed for the larger particles. They occupied a band whose width varied with increasing frequency as the polarisability of the particles increased (i.e. $\mathrm{Re}[f_{CM}]$ becoming more negative). Figure 6-4 shows the percentage of the channel height occupied by the 557nm beads (i.e. rather than the mean particle height as used to describe the larger beads). At the highest frequency the band occupied a region of ±20μm around the mid-point of the channel. When the voltage is removed the particles rapidly diffused to occupy the entire volume of the channel in a few seconds.

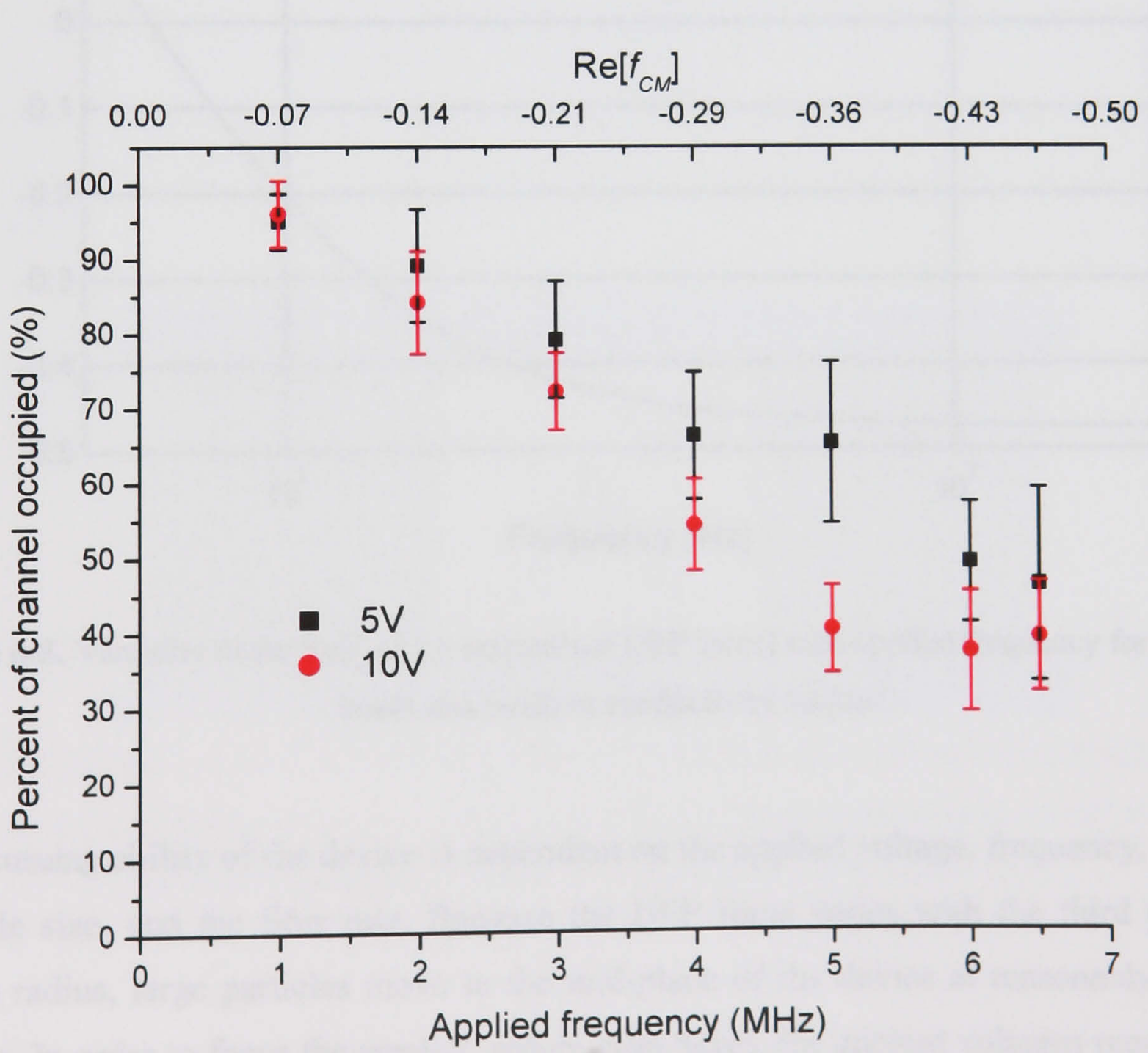

Figure 6-4. Thickness of the band of 557nm latex beads when focussed between two electrode arrays of 40μm separated by 100μm as a function of applied voltage 5V and 10V frequency.

The characteristics of the 557nm latex beads have been investigated previously [6] and their polarisability versus frequency data is shown in figure 6-5. These beads experience –veDEP between 1 to 10MHz for the suspending medium conductivities used (σ_m = 1mSm^{-1}). The thickness of the band of 557nm beads corresponds to the variation in the applied dielectrophoretic force around this frequency. As the frequency increases the magnitude of the -veDEP force increases and thus confines the beads to a narrower band as shown in figure 6-4. In this frequency range the 557nm beads always experience negative DEP, but the value of Re[f_{CM}] changes from -0.2 at 1MHz to –0.48 at 10MHz. Measurements correspond to three standard deviations of the particle distribution. The band thickness is due to a balance of fluxes, and is broader at lower frequencies because J_{DEP} (i.e. the particle flux due to DEP) is less at lower frequencies as shown in figure 6-5. This is further discussed in section 6.6.1.

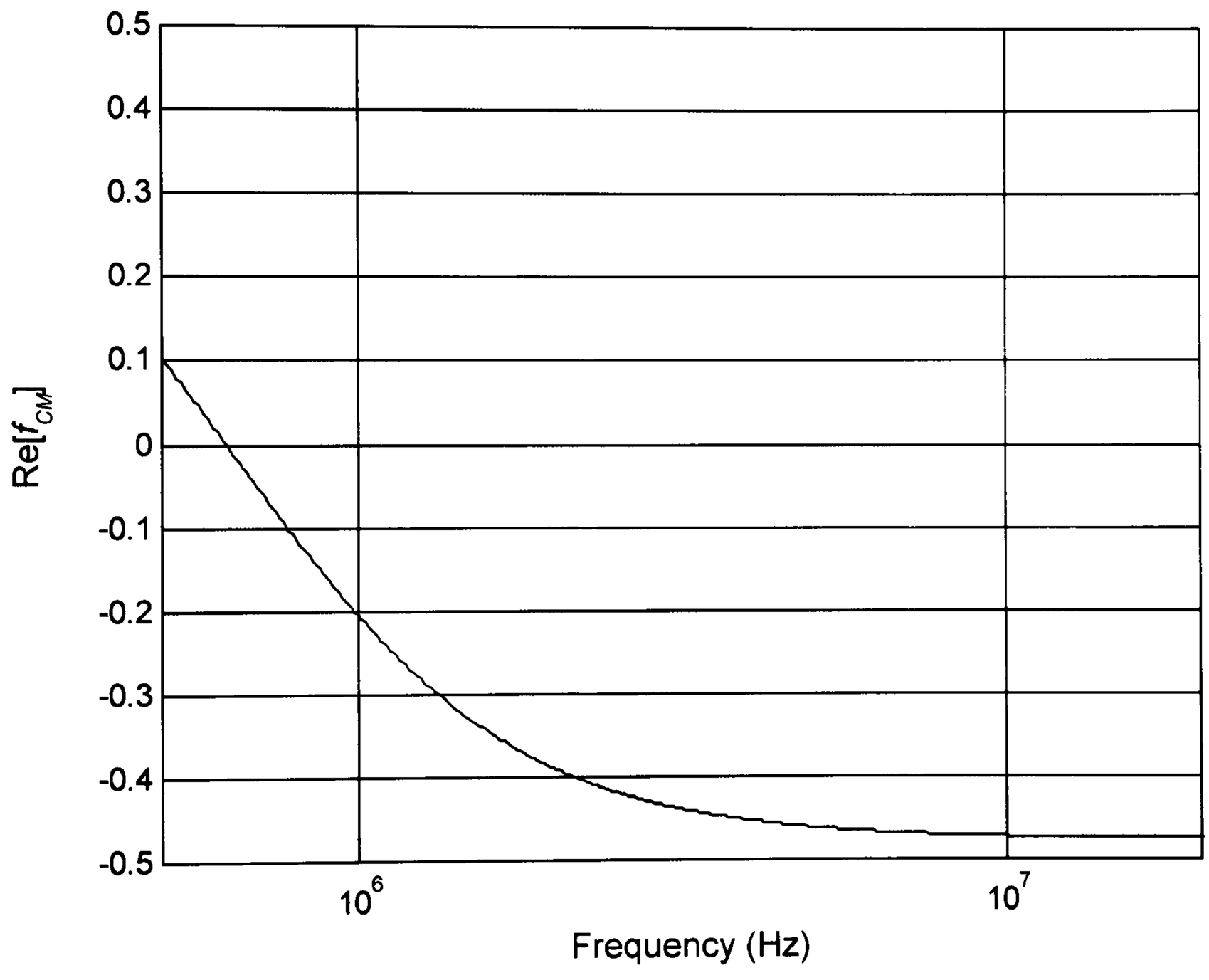

Figure 6-5. Variation in the Re[f_{CM}] (or normalised DEP force) with applied frequency for 557nm latex beads and medium conductivity 1mSm^{-1}.

The focussing ability of the device is dependent on the applied voltage, frequency, particle size, electrode size, and the flow rate. Because the DEP force varies with the third power of the particle radius, large particles move to the mid-plane of the device at reasonably low applied voltages. In order to focus the smaller, sub-micron beads, the applied voltages required must be large (>10V) for the 40μm electrode and 100μm channel height. These large voltages cause a large amount of heat to be dissipated into the system. Focussing (in this case taken as the middle

10% of the channel height) of the sub-micron beads was not fully achievable using this electrode design.

In order to produce a device capable of confining particles to a small sample volume in a microfluidic channel the devices used here could be scaled down. This would result in a larger DEP force at the channel centre without the need for increasing the applied voltages with the consequent temperature rise that this voltage increase would bring. 2D focussing could also be achieved by using an extruded quadropole electrode geometry along the length of a microfluidic channel as illustrated schematically in figure 6-6(a).

(a)

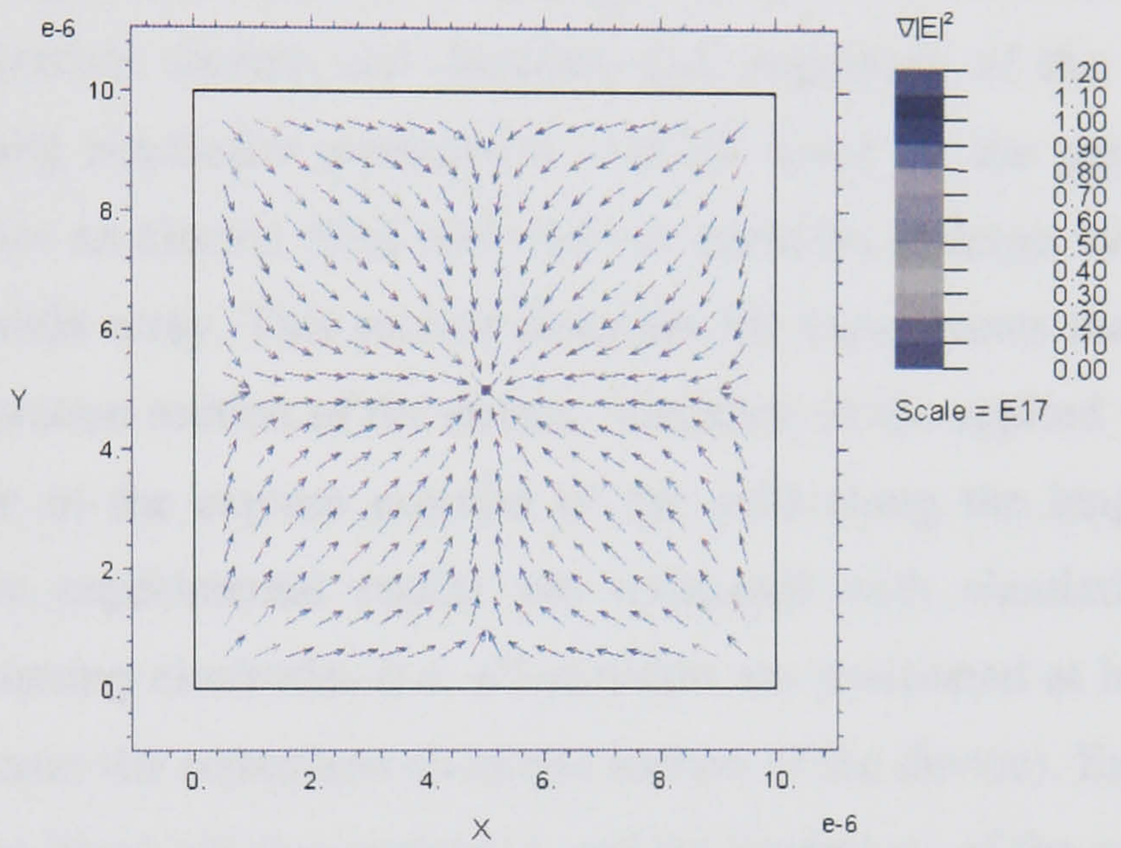

(b)

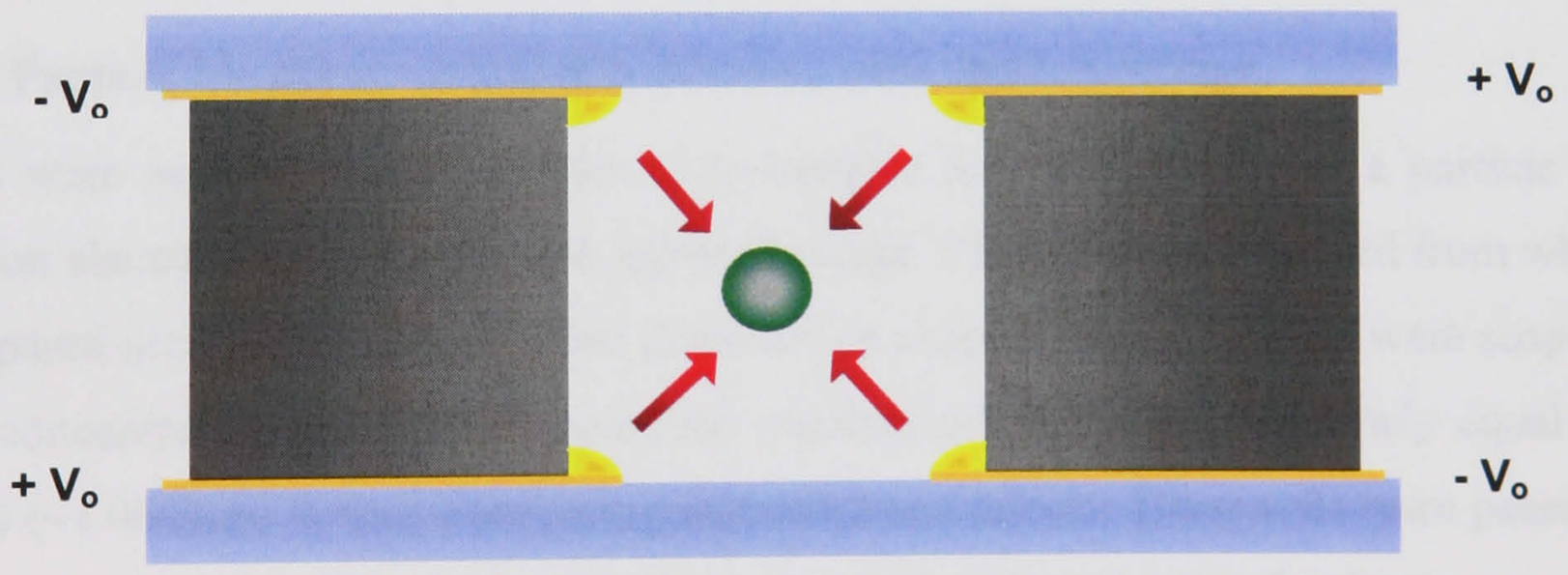

Figure 6-6. (a) Schematic of 2D focussing electrodes positioned in the corners of a microfluidic channel. **(b)** Numerical simulation of the 2D focussing electrode arrangement showing) a vector plot of the DEP force, directing particles radially into the centre of the flow channel.

To illustrate the focussing effect for the system shown in figure 6-6(a) the values of $\nabla|E|^2$ were determined across a 2-D slice through the such a system. FlexPDE™ (PDE Solutions Inc.) was used to solve Laplace's equation using voltages of +1V and –1V on each electrode. A vector

plot of $\nabla|E|^2$ is shown in figure 6-6(b). Note that the direction of the DEP force vectors push particles away from the electrode edges at the corners and into the centre of the flow channel. Particles experiencing a –veDEP force from the electrodes will therefore become focused into a stream of single particles as they flow along such a channel.

6.3 Particle separation

After passing through the focussing section of the device, all the particles should ideally be positioned at a height halfway between the upper and lower channel walls. From the preceding work it was shown that this is true for particles of the size of a typical mammalian cell, with a suitable applied voltage and frequency. As a particle flows from the focussing section of the device into the separation section, the direction and magnitude of the forces on it change. Whereas the focussing electrodes produced a –veDEP force on the particles, the separation electrode array applies an electric field such that the particles undergo +veDEP and are pulled down onto the electrode array. This section describes the experiments that were carried out to characterise the separation section of the device. Variation of the applied voltage and flow rate resulted in a change in the capture position of the cells along the length of the separation electrode array. The experimental results are compared with simulations, assuming ideal operation of the focussing electrodes (i.e. all particles are positioned at height h/2 in the flow channel when they enter the separation electrode section of the device). Experiments using sub-micron beads (557nm latex) are also presented, and the limitations of the system are discussed.

6.3.1 Particle banding: variation in position with applied voltage

PBMCs were used as model particles to investigate how the position of a particle along the separation electrode array varies with applied voltage. PBMCs were collected from whole blood and prepared according to the methods described in chapter three. The cells were suspended at a known concentration in the DEP separation medium of density approximately equal to that of the cells (~1.060kgm^{-3}), thus eliminating sedimentation effects. These cells were passed through the separation device under similar conditions but with different applied voltages.

Figure 6-7 shows the experimental results for banding of PBMCs using 40μm electrodes for different applied voltages. The other experimental parameters did not change between runs, the flow rate was 0.4mlhr^{-1}, medium conductivity 21mSm^{-1}, and applied frequency 5MHz. The mean position of the band of cells is shown, with the error bars indicating the distance within which >95% of the cells were captured on the electrode array.

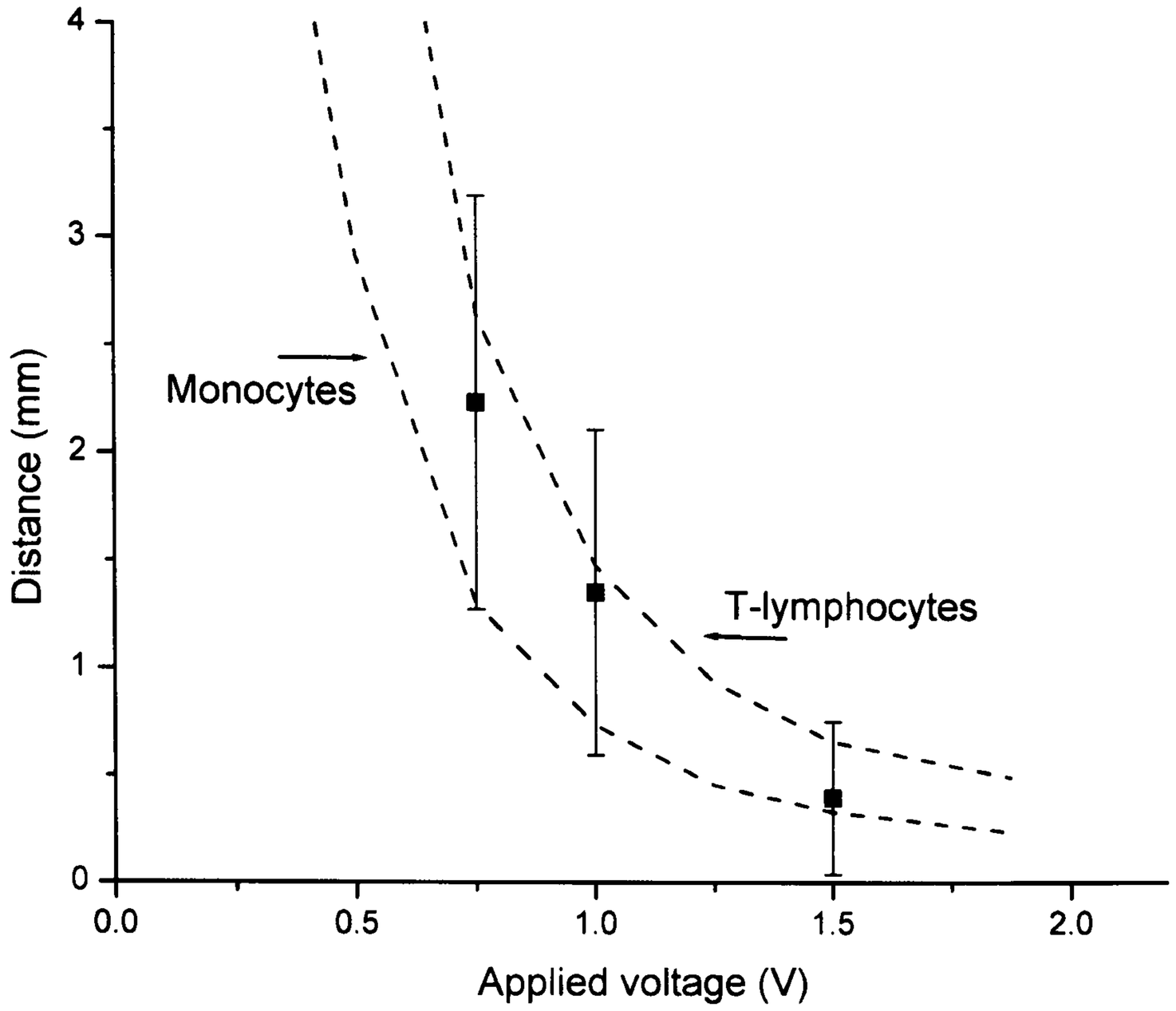

Figure 6-7. Variation in capture position along the separation electrode versus applied voltage. Dashed lines show position expected from simulations for monocytes and T-lymphocytes.

The dashed lines in figure 6-7 show the simulated banding position of monocytes (r=4.63um, $Re[f_{CM}]$=0.869) and T-lymphocyte (r=3.29um, $Re[f_{CM}]$=0.845) using the size and specific membrane capacitance values given by Yang *et. al.* [7]. The simulations were carried out using the same parameter values as that of the experiments only varying the applied voltage. Of the cells present in PBMCs, monocytes and T-lymphocytes have, respectively, the highest and lowest values of specific membrane capacitance (i.e. the monocytes and T-lymphocytes experience the highest and lowest DEP forces, attracting them towards the electrode array, of all the PBMC sub-populations). These cells therefore represent the upper and lower limits of the mean capture position for the PMBC subpopulations.

6.3.2 Particle banding: variation in position with flow rate

THP-1 cells were grown in culture and collected according to the methods described in chapter three. These cells were resuspended in DEP separation media. In order to characterise the dielectric properties of the THP-1 cells, crossover measurements were made on these cells (see section 2.9.3 for details). The data from the crossover measurements is presented in figure 6-8.

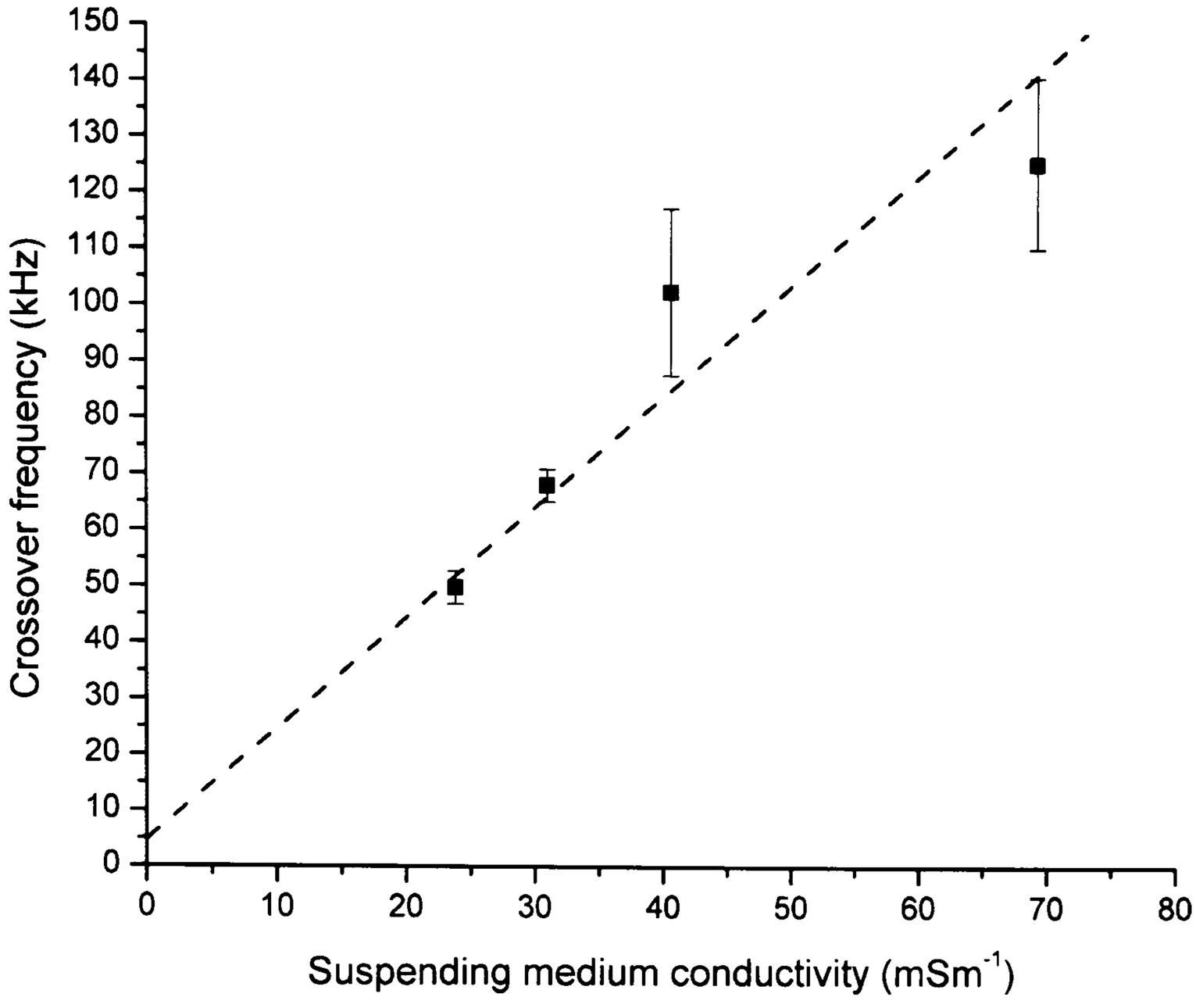

Figure 6-8. Crossover frequency versus suspending medium conductivity for THP-1 cells.

From the crossover measurement data the specific membrane capacitance of the THP-1 cell type was calculated to be $C_{mem} = 17.7 \pm 2.7$ mFm^{-2}, the cell radius was r = 6.4 ± 1.0 μm (as measured manually using the image analysis software (see section 4.6.2).

Figure 6-9 shows the experimental results obtained for the mean banding position along the separation electrode array at which the THP-1 cells were captured. In these experiments two electrode sizes ($d = d_1 = d_2$ = 20μm or 40μm) were used. The focussing section of the device was $d = d_1 = d_2$ = 40μm in both cases. The conditions for the 20μm electrode array experiments were applied peak voltage Vo = 1.5V, field frequency 100kHz, and σ_m = 28mSm^{-1}. For the experimental runs using the 40μm array, the applied peak voltage was Vo = 1.25V, field frequency of 1MHz, and σ_m = 26.9mSm^{-1}. The dashed lines show the results of simulations based on the parameters used in the experiments, and using the dielectric properties of the THP-1 cells as measured (ignoring the effect of membrane conductance).

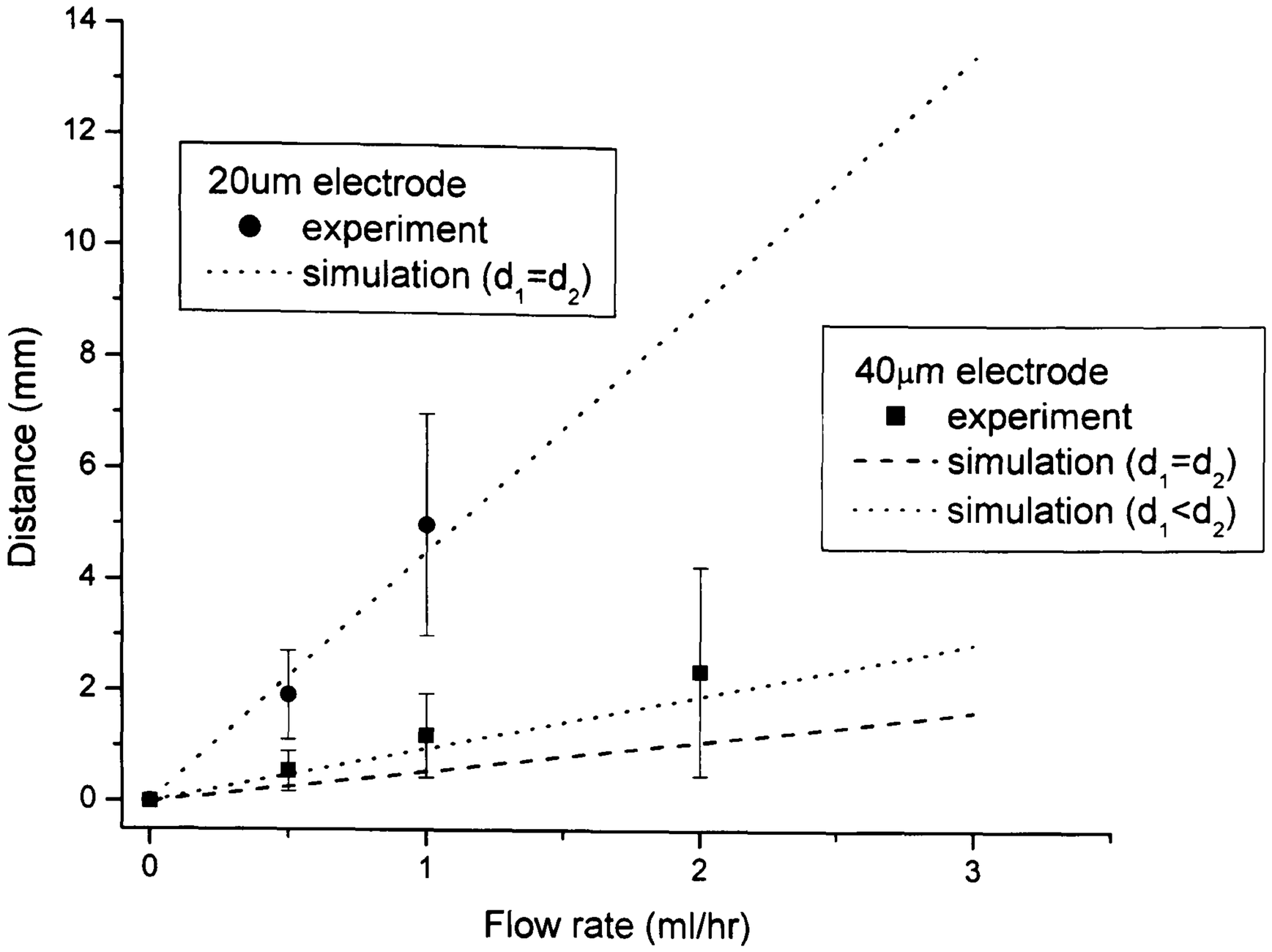

Figure 6-9. Banding position of THP-1 cells on 20μm and 40μm electrode arrays for different flow rates. Dashed lines represent the simulation taking d_1=d_2 and the dotted line shows the simulation with d_1=36μm and d_2=44μm. Error bars span the upper and lower limits where cells were captured on the electrode arrays.

Part of the discrepancy between the calculated banding position and experiment for the 40μm electrodes is due to the electrode and gap size not being equal. The electrode and gap sizes were measured and found to be d_1 = 36μm and d_2 = 44μm respectively. In order to account for the variation in the electrode/gap size, as measured for the larger sized array, a 1D expression for the DEP force was implemented in the simulation (dotted line in figure 6-9), this allowed the electrode/gap size difference to be included in the calculation. The effect of this was to reduce the discrepancy between the calculated and experimental results. EHD effects may also have a slight disruptive effect on the banding positions of the cells.

Figures 6-10(a) and (b) shows a micrograph of the banding of the THP-1 cells for two of the separation runs using the 40μm separation electrode arrays. Figure 6-10(a) shows the captured cells after 0.5ml of sample had passed through the device at a flow rate of 0.5mlhr^{-1}; figure 6-10(b) shows the results for the same experiment but using a higher flow rate of 1.0mlhr^{-1}. There is obviously some distribution in the captured position of these cells.

The spread of cells captured on the separation electrode can be attributed to a number of factors:

- the build up of cells on the electrode array distorts the field geometry resulting in an altered DEP force, which acts on the upstream cells upon entry into the separation electrode
- the heterogeneous nature of the cell population (i.e. distribution in f_{CM} and size, resulting in a distribution in the DEP force acting on the individual cells)
- imperfect focusing (before entering into the separation electrode) of the particle stream as it flows through the focussing section of the device (see figures 5-18 to 5-20)
- EHD fluid flow

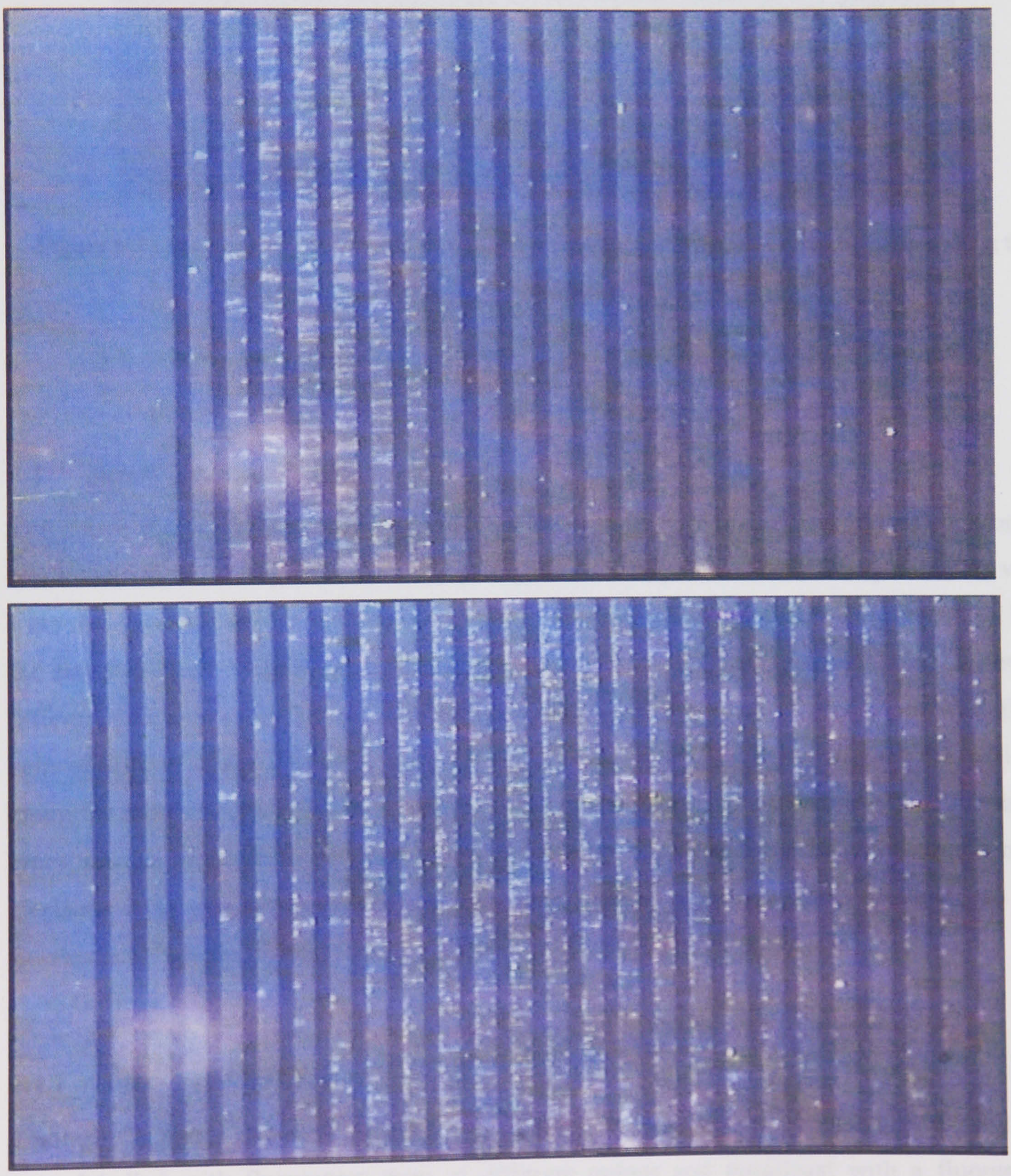

Figure 6-10. Banding of THP-1 cells showing the capture of particles at defined positions along the length of the 40μm electrode array, at flow rates of **(a)** 0.5mlhr^{-1} and **(b)** 1.0mlhr^{-1}.

Figure 6-11 shows how the position at which the THP-1 cells come down on the separation electrode array varies with the size of the cell. The flow of sample was from left to right as in the above figures. Assuming that the specific membrane capacitance of the THP-1 cells remains constant, then the DEP force experienced by individual cells will vary with the size of the cell. In this example all the cells were attracted to the separation electrode under the influence of the +veDEP force, the larger THP-1 cells can be seen to have collected further upstream than the smaller cells.

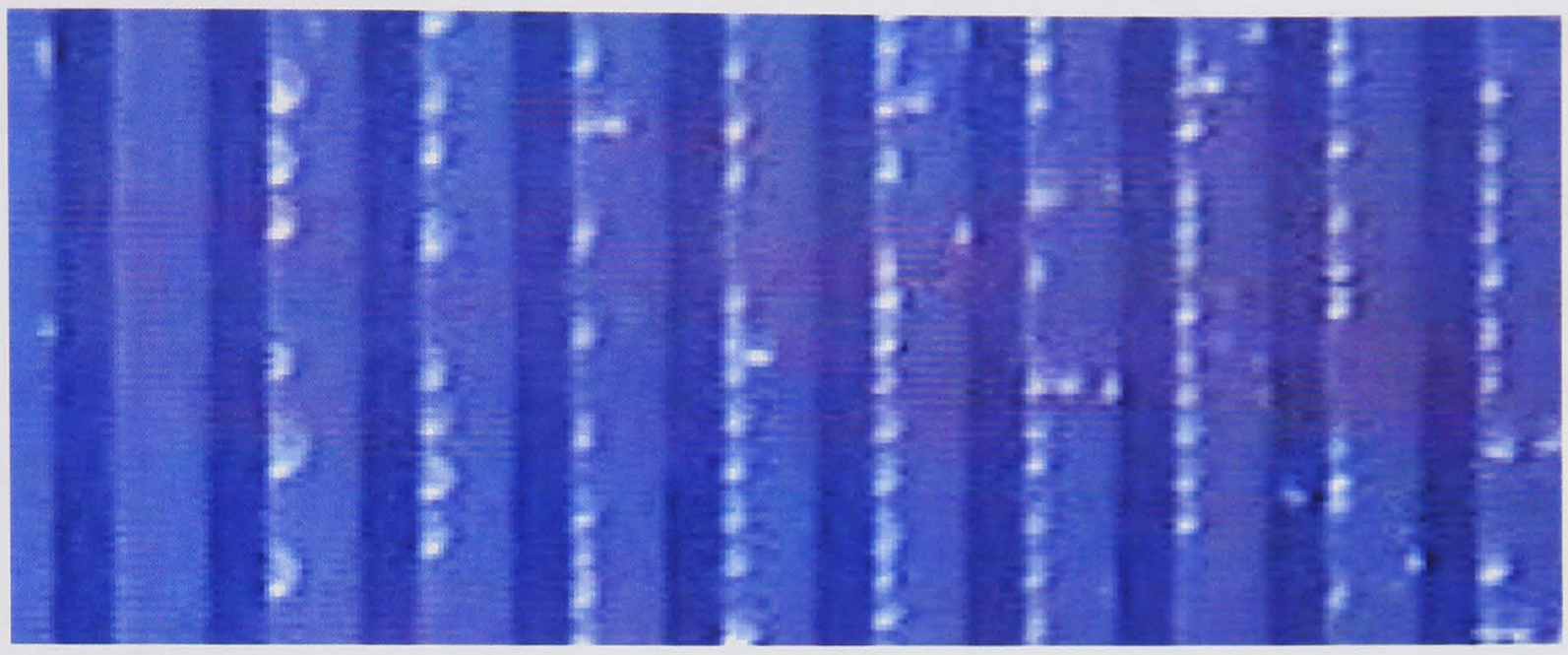

Figure 6-11. Banding of THP-1 cells showing the separation of particles according to size along the length of a 40μm electrode array.

6.4 Binary mixture of cells

The above discussion describes the ability of the system to pull particles out of solution and retain them at the electrode surface, under the influence of positive DEP. The parameters varied were the flow rate and the applied voltage, with all other parameters remaining the same. From the simulations of chapter five it is predicted that cells of different type should come down at different positions along the length of the separation electrode array (as seen above with THP-1 cells of different size). The experiments of section 6.3, using PBMCs shows that cells will band along the electrode array. However, it was not possible to distinguish between the different cell types on the electrode array, and ascertain whether their position along the length of the electrode array corresponded to a particular cell type. In order to achieve this the cells were fluorescently labelled with different colours according to the cell type.

6.4.1 THP-1 and PBMCs

To allow the identification of different cell types within the separation device, specific cell types were labelled with fluorescent dyes of different colour and visualised with a fluorescence microscope using epi-fluorescence illumination. THP-1 cells, and PBMCs (isolated from whole human blood) were labelled with CellTracker™ fluorescent dyes (Molecular Probes). The THP-

1 cells were incubated with the blue CellTracker™ dye (CMHC, 372nm/470nm) and PBMCs were incubated with the green CellTracker™ dye (CMFDA, 492nm/516nm). The labelling procedure for this dye is described in chapter three.

6.4.1.1 Methods

The THP-1 cells were grown in culture and harvested prior to experiments as described in section 3.2.1. Blood samples were obtained 1-2 hours prior to the experiments and the PBMC cell fraction isolated as described in section 3.1.1. The two cell populations were labelled separately with different coloured CellTracker™ dyes, according to the protocol given in section 3.7. The two populations were then mixed together at known cell concentrations (~10^6 cells per ml) and resuspended in DEP separation media of conductivity σ_m = 26.3mSm^{-1}. The variation in the value of Re[f_{CM}] with frequency for the THP-1 cells, monocytes, and T-lymphocytes is shown in figure 6-12.

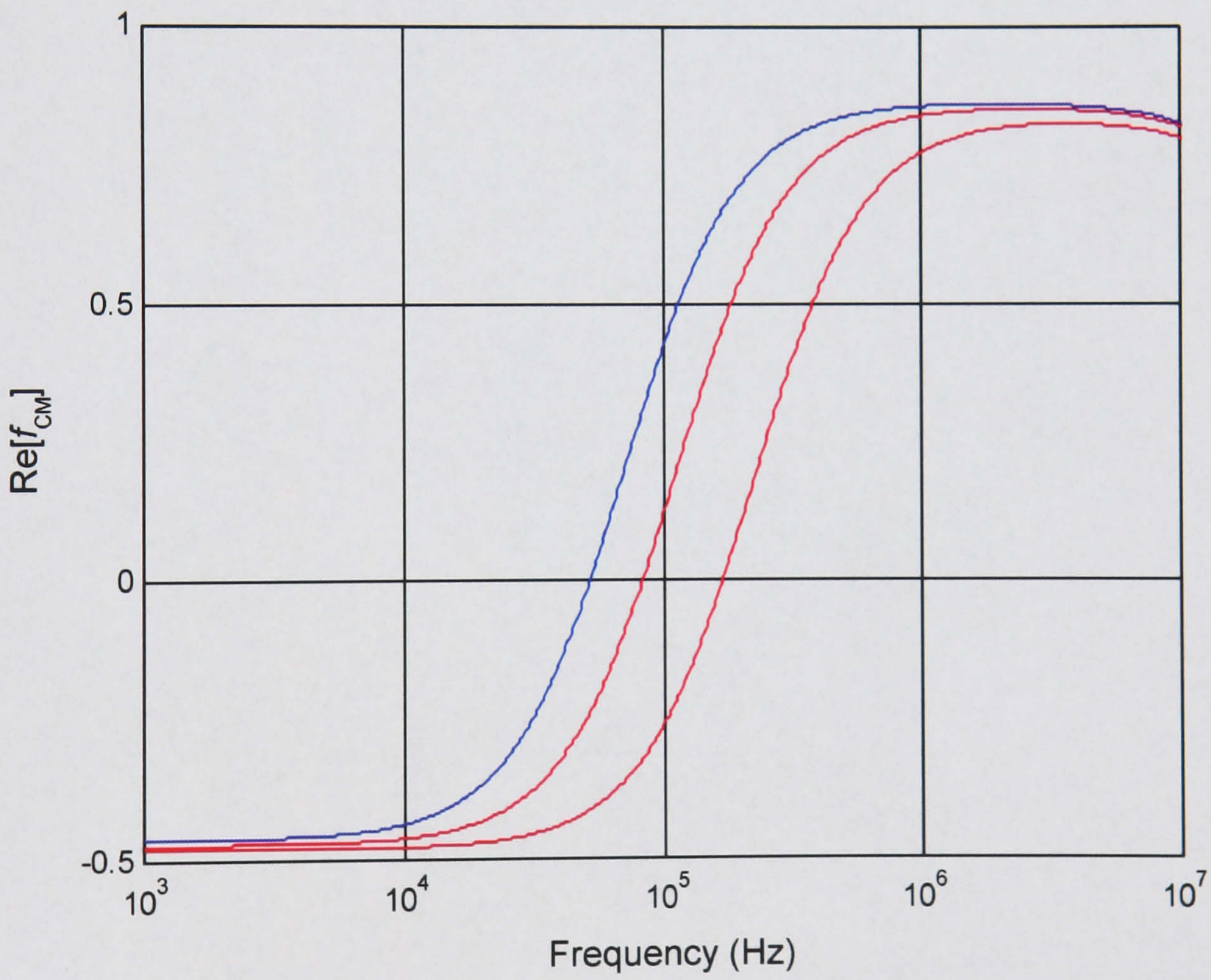

Figure 6-12. Variation in the Re[f_{CM}] with applied frequency for THP-1 cells (blue) and monocytes (red, left) and T-lymphocytes (red, right). Medium conductivity = 26.3mSm^{-1}.

6.4.1.2 Results

It should be noted that the following fluorescence images were captured using a monochrome camera (Orca ES, Hamamatsu), with images of the different fluorescent dyes captured using

different filters. The monochrome images were then combined to form the complete image, with each of the monochrome images represented by pseudo colour, i.e. red, green or blue. The image shown in figure 6-13 is therefore a pseudo colour image, with the THP-1 cells appearing in green (although they were labelled with a blue dye) and the PBMCs appearing red (despite being labelled with a green fluorescent dye).

Figure 6-13 shows a fluorescence image of a portion (640μm by 800μm) of the separation electrode array after a mixture of labelled THP-1 cells (green) and PBMCs (red) were passed through the device. The majority of the THP-1 cells were attracted and captured by the first few electrodes, while the majority of the PBMCs were captured in a wider band further along the electrode array. This distribution of the two cell types, although not completely separated in this experiment, demonstrates the principle of DEP cell separation using this electrode configuration.

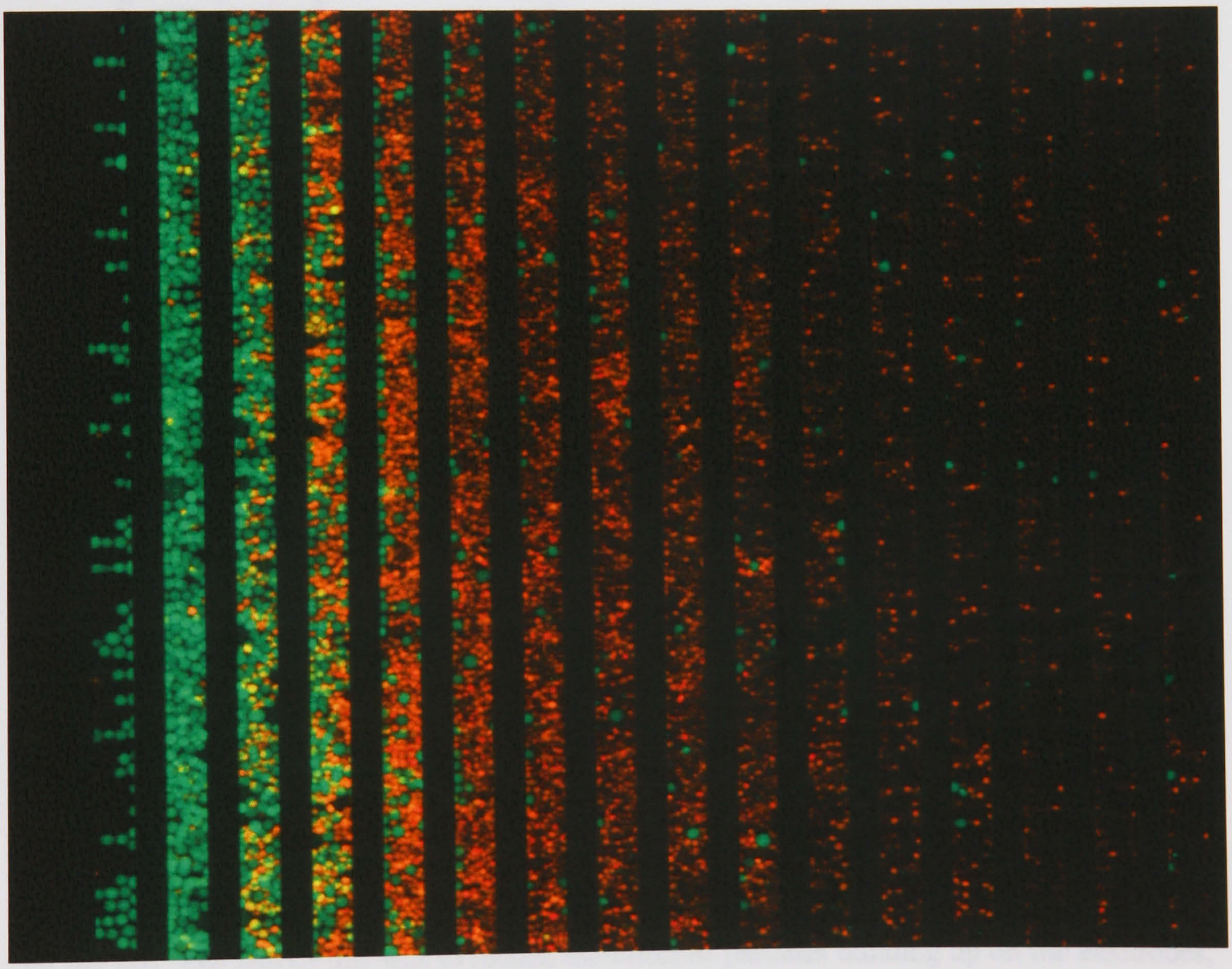

Figure 6-13. Fluorescence image of THP-1 cells (green) and PBMCs (red) banding on a 40μm separation electrode array. Flow rate of 0.5mlhr^{-1}, applied peak voltage of 1.5V at 150kHz.

The data from the experiment shown in figure 6-13 is presented in figure 6-14 in graph form. The number of cells and the cell type in the gaps between the electrode fingers were counted. The distribution of the two cell types can be represented with reasonable accuracy using

Gaussian distributions fitted using the statistical routines in Origin 6.1. The Gaussian fit to the THP-1 data has an R^2 value of 0.95957 and is centred around the second electrode gap with a width of 2 gaps, the Gaussian curve for the PBMC data has an R^2 value of 0.85486 and is centred on electrode gap number 7 with a width of 6.5 electrode gaps.

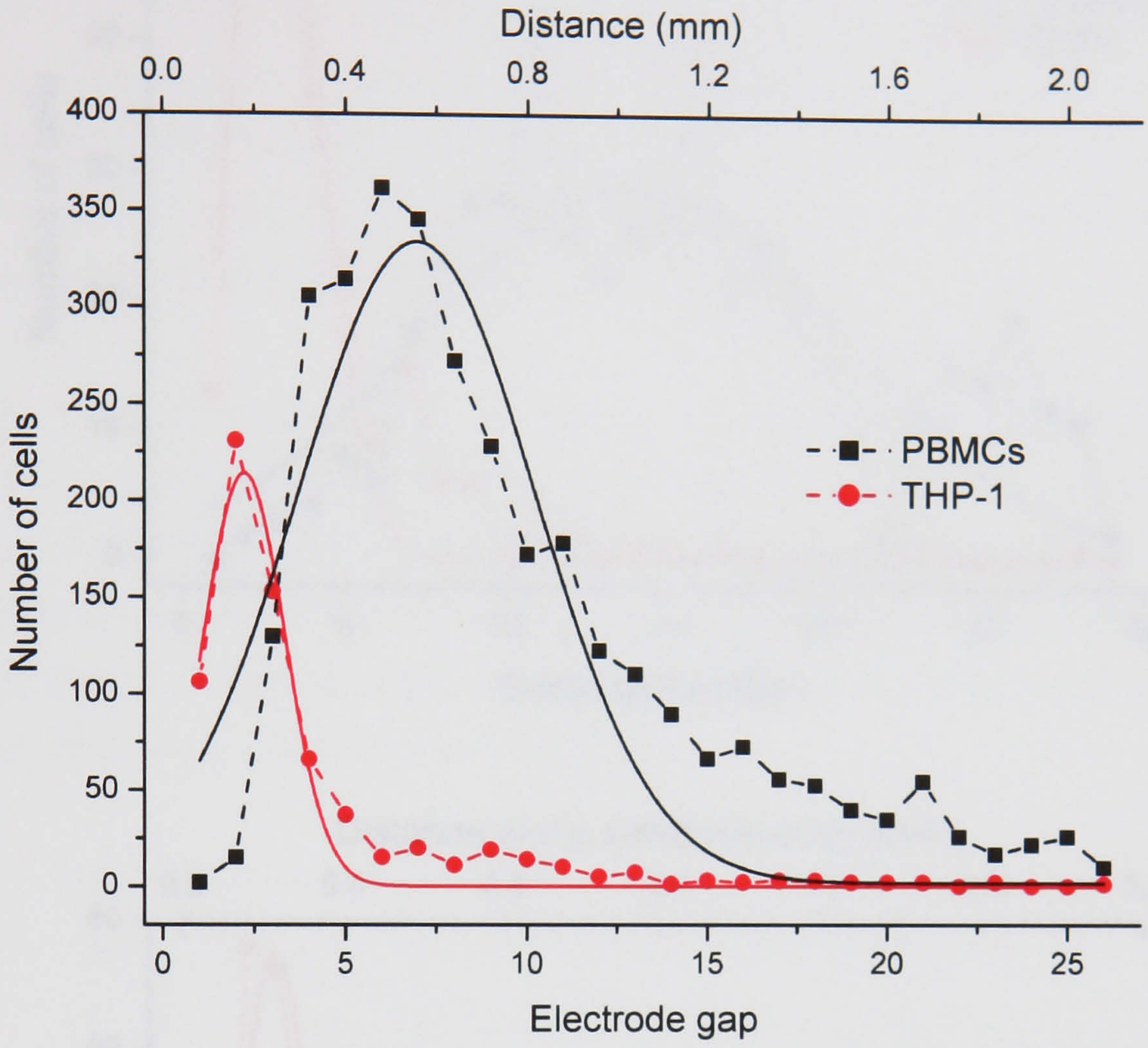

Figure 6-14. Distribution of THP-1 cells and PBMCs on the 40μm separation electrode array.

It should be noted that particle build up on the electrodes distorts the electric field produced by the electrode arrays, leading to disruption of the particle trajectories and alteration in the positions at which the cells band on the separation electrode array.

6.4.2 THP-1 and PBMC fractions

The above experiment was repeated with lower numbers of THP-1 cells and PBMCs (~$5x10^4$ cell per ml). The aim of this was to reduce the effect of particles building up on the electrodes, and hence reduce the disruption of the electric field and fluid flow caused by this. Figure 6-15 shows the results. The THP-1 cells showed a similar distribution to the previous experiment, collecting on the first few electrodes. However, the PBMC distribution can be seen to be wider than that of the previous experiment, and shows an indication of having more than one peak.

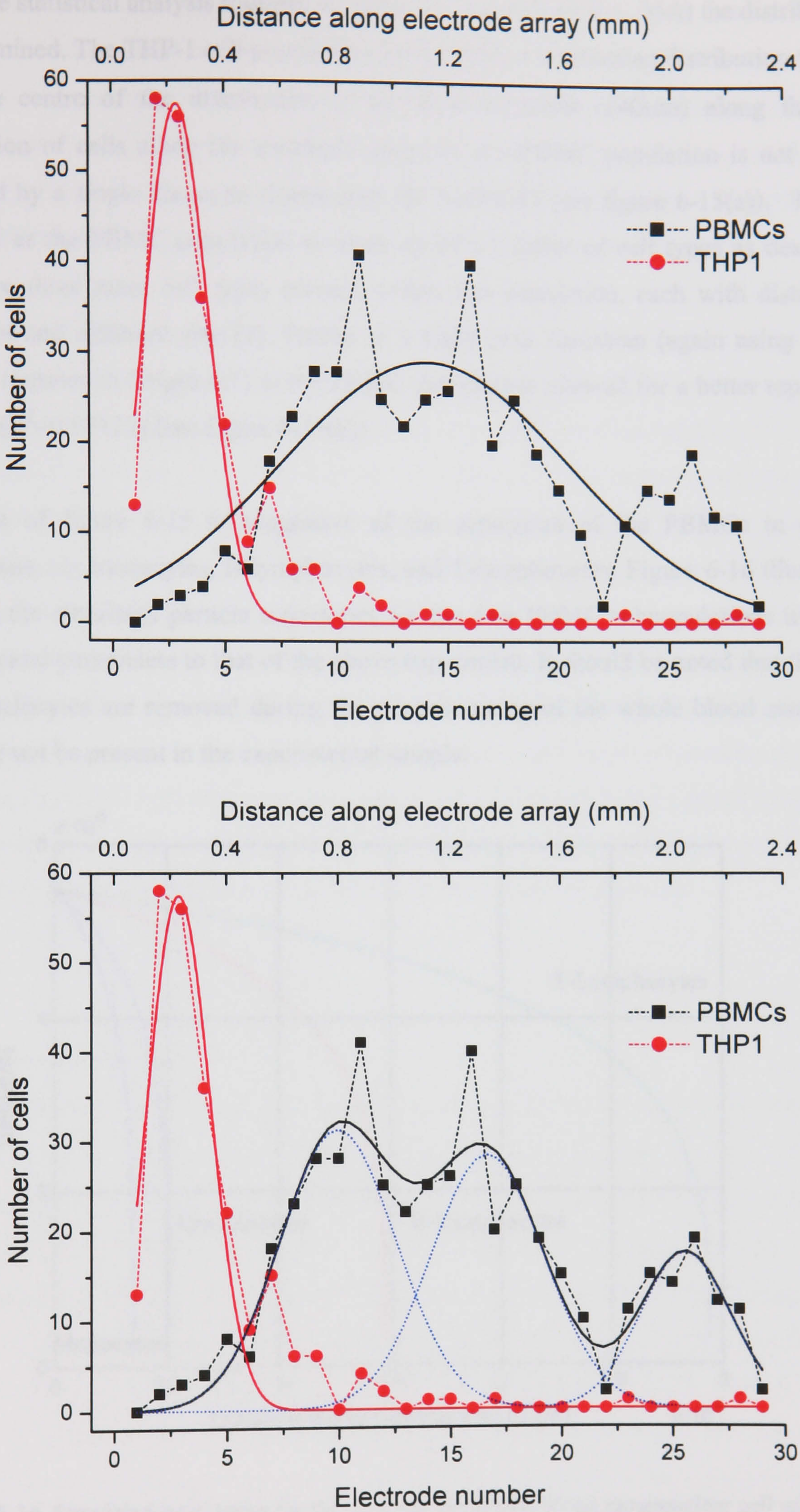

Figure 6-15. Distribution of THP-1 cells and PBMCs on the 40μm separation electrode array, **(a)** single Gaussian fit to the data and **(b)** fitting of a triple Gaussian to the PBMC data.

Using the statistical analysis routines in Origin 6.1 (OriginLab Co., MA) the distribution of cells was examined. The THP-1 cell population can be fitted to a Gaussian distribution (R^2= 0.92598) with the centre of the distribution at the third electrode (240μm) along the array. The distribution of cells along the electrode array for the PBMC population is not as accurately modelled by a single Gaussian distribution (R^2=0.65418) (see figure 6-15(a)). This would be expected as the PBMC population is made up of a number of cell types as described above. There are three main cell types present within this population, each with distinct dielectric properties and different size [7]. Fitting of a triple peak Gaussian (again using the statistical analysis routines in Origin 6.1) to the PBMC distribution allowed for a better representation of the data (R^2=0.87127) (see figure 6-15(b)).

The data of figure 6-15 is suggestive of the separation of the PBMCs in the their sub populations, i.e. monocytes, B-lymphocytes, and T-lymphocytes. Figure 6-16 illustrates this by showing the simulated particle trajectories for the four PBMC subpopulations using the same experimental parameters to that of the above experiment. It should be noted that the majority of the granulocytes are removed during the pre-processing of the whole blood sample, and will therefore not be present in the experimental sample.

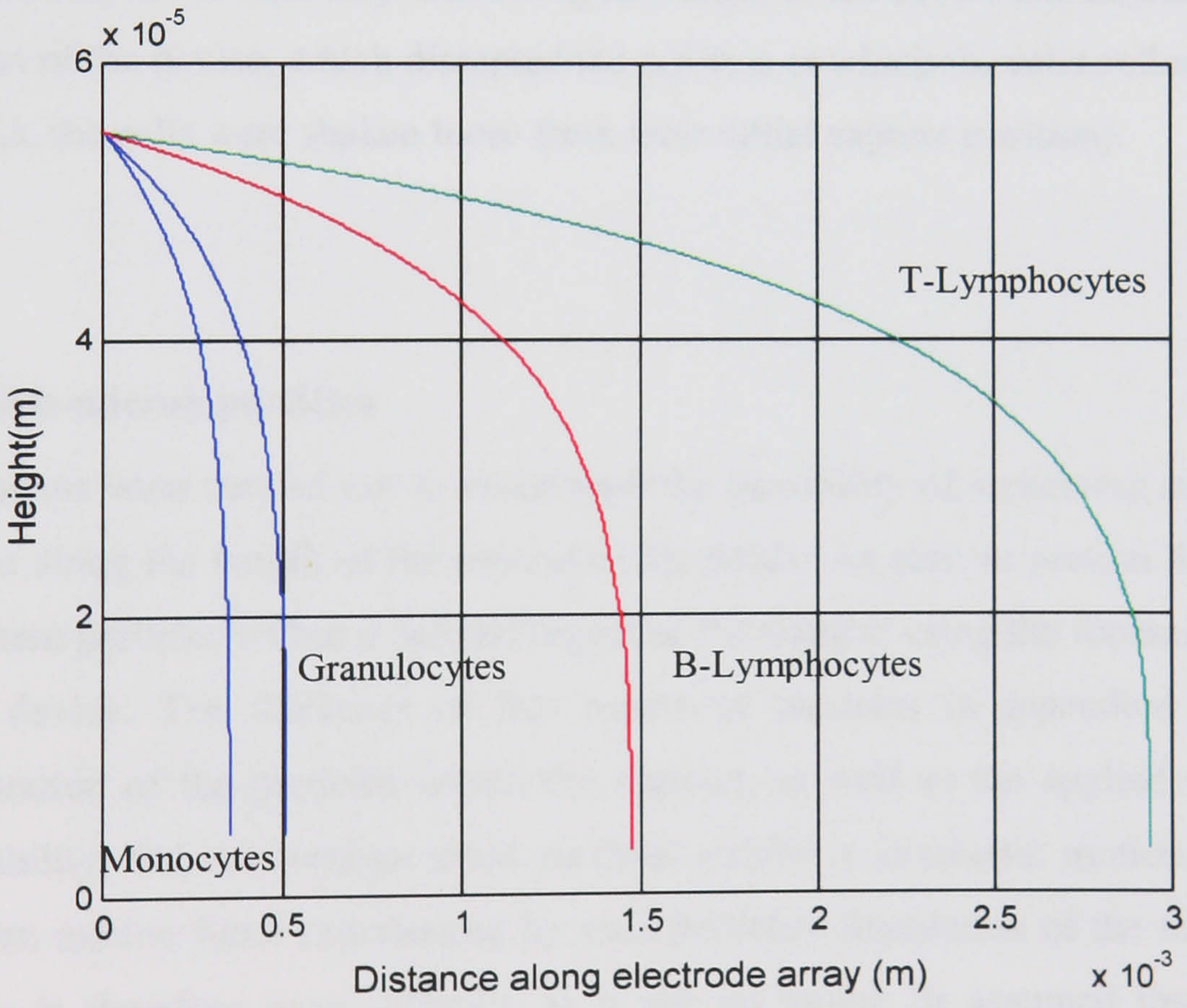

Figure 6-16. Simulated trajectories for the different peripheral blood mononuclear cell sub-populations, using data corresponding above experiment (section 6.4.2). Applied peak voltage was 3V at 250kHz with medium conductivity of 33mSm^{-1}, and the chamber was 110μm in height. PBMC properties from [7].

In this experiment, using the lower numbers of cells, the cells were again captured on the separation electrode giving a similar distribution to that of the previous experiments. However,

this time the cells were generally captured and held at the electrode edges. The cells were distributed evenly along the length of the individual electrode fingers, and showed no sign of clumping; suggesting that the disruption to the cell trajectories caused by the build up of cells on the electrodes had little effect on the capture position when the cell concentration is low. The cells were therefore captured on the electrode array at a position more closely related to the cell's dielectric properties and size than in the experiment of section 6.4.1.2.

A further set of experiments was carried out with the aim of demonstrating conclusively, that the PBMC cells were indeed being separated along the length of the separation electrode array. The PBMC sample was obtained as described above and labelled (section 3.5.1) with CD69-Cy5 (T-lymphocyte specific - 630/660nm) and CD14-FITC (monocytes specific - 488/515nm) fluorescent antibodies. Unfortunately, the fluorescence set up, used for these experiments, was not sensitive enough to image the fluorescently labelled cells while using the low magnification lens (x4) needed to image a suitably large section of the electrode array (the CD69 and CD14 fluorescent molecules only label the cell surface, unlike the CellTracker^{TM} dyes which fill the interior of the cells and are therefore far brighter). Use of a x20 objective lens allowed the cells to be imaged however it was not possible to measure their absolute position on the electrode array. An attempt to manually scan along the length of the device and capture images resulted in vibration of the device, which disrupted the position at which the cells collected on the electrode array (i.e. the cells were shaken loose from their initial capture position).

6.5 Sub-micron particles

Experiments were carried out to investigate the possibility of separating sub-micrometre sized particles along the length of the separation electrode. As seen in section 6.2.2 it is possible to focus these particles within a defined region of the channel using the focussing electrode section of the device. The thickness of this region of particles is dependent upon the size and concentration of the particles within the channel, as well as the applied voltage and particle polarisability. Sub-micrometre sized particles exhibit a stochastic motion due to the random Brownian motion force experienced by such particles. Simulation of the motion of these small particles is therefore more difficult, as it can no longer be assumed that the particles have reached their terminal velocity instantaneously in the time frame of the computational step.

6.5.1 Experimental results

Fluorescently labelled (FITC) latex particles of diameter 557nm were suspended in dilute KCl ($\sigma_m = 1 mSm^{-1}$) and passed through the separation system. These particles can experience both

–veDEP and +veDEP, as shown in the normalised force-frequency plot of figure 6-5. This plot shows the theoretical behaviour of such particles when suspended in water with conductivity $1mSm^{-1}$.

The focussing electrodes were energised with an applied peak voltage of 5V at a frequency of 10MHz, and the separation electrodes were energised with an applied peak voltage of 3.75V at 100kHz. The particles were observed using a fluorescence microscope and FITC filter set, with images being captured to video.

The particles were partially focussed by the focussing electrode array, away from the channel walls and towards the mid-plane of the channel, in a manner similar to that described in section 6.2.2. Estimation of the exact thickness of the focussed particles was difficult, but the majority of the 557nm particles appeared to be within 20 - 25μm above or below the mid-plane of the channel by the time they reached the end of the focussing electrode array. The separation array showed particles undergoing +veDEP and being captured at either the electrode edges, or in bands on top of the individual electrodes of the separation electrode array. The capture mode varied depending on the frequency of the signal applied to the separation electrode. Lower applied frequencies resulted in EHD fluid motion (see chapter two) driving the particles from the electrode edges to a stable position on top of the electrodes.

Figure 6-17. 557nm latex beads as they pass through the focussing electrode array. The image is focussing on the mid-plane of the channel; particles above or below this are seen to be out of focus.

Particles were observed to collect along the entire length of the separation electrode array; banding of these particles was not observed in either mode of operation. This lack of particle banding is probably due to the poorly focussed stream of particles, passing from the focussing section of the device into the section containing the separation electrode array. Simulations in

chapter five demonstrated the effect that poor or imperfect focussing had on the final position of 10μm particles travelling through the device. Small variations in the focussing height translated into relatively large shifts in the final position of particles on the separation electrode array. For the case of the 557nm beads, the majority of the particles were observed to be within 20 – 25μm of the centre of the channel, the focussing is therefore rather poor. Simulations (ignoring Brownian motion effects) show that the majority of the particles (i.e. those initially focussed to within ±20μm of the channel centre) would be attracted to the separation electrode array and become captured at distances along the entire length of the separation electrode array (see figure 6-18).

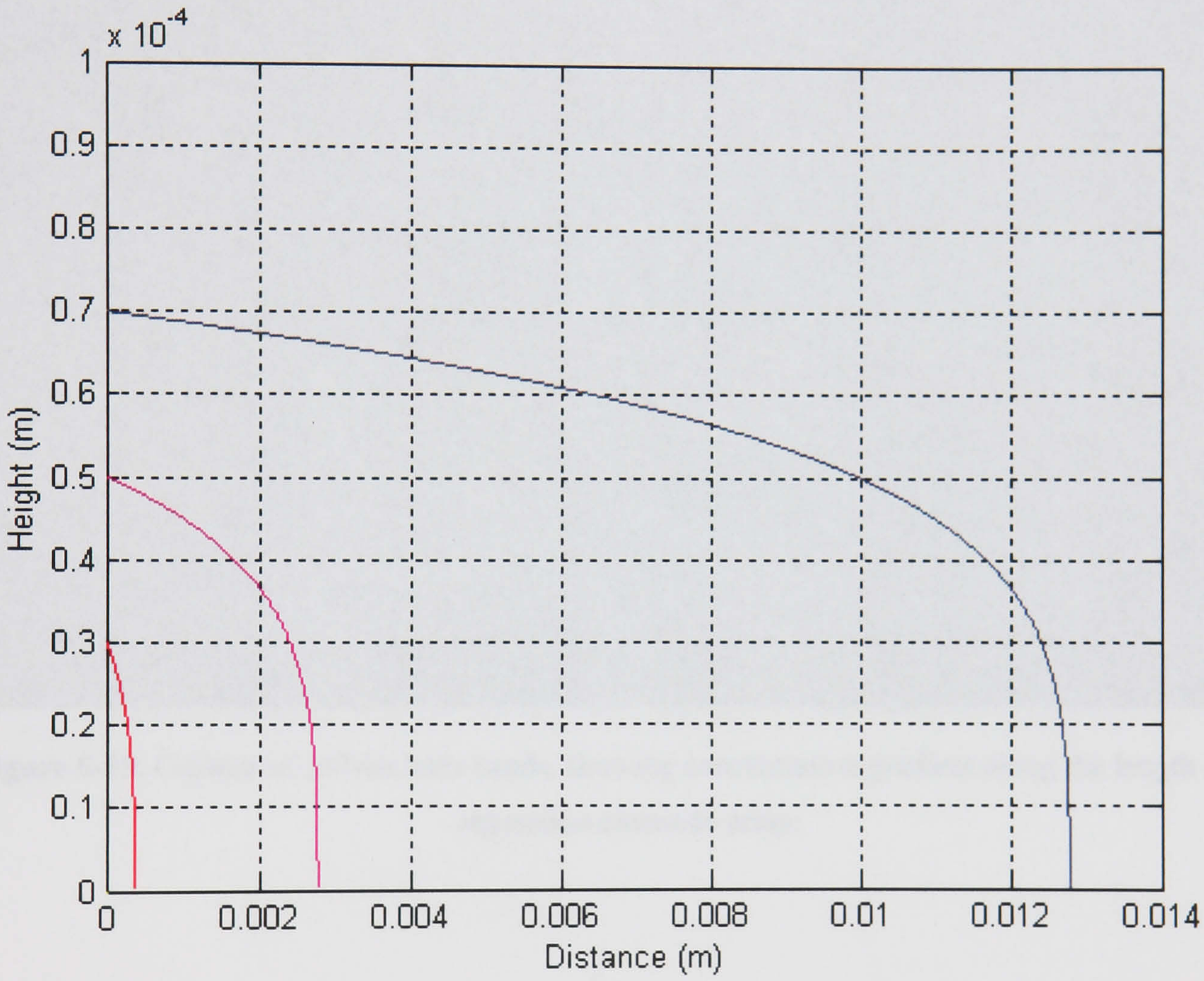

Figure 6-18. Simulation of the trajectories of 557nm latex beads with applied peak voltage of 3.75V and various starting heights. Brownian motion was neglected in the simulation.

The effect that Brownian motion has on these particles must also be considered. The DEP force constantly attracts particles towards the electrode array as they flow through the device, individual particles were observed to have their motion disrupted by jumping about due to this random force. The particle trajectories due to the deterministic forces acting on the particles (i.e. the DEP force, fluid motion and the gravitational force) are therefore modified by the superposition of a random walk. Thus altering the position on the separation array at which individual particles become captured.

The combination of the poorly focussed particle stream, and the Brownian motion resulted in particles being evenly distributed along the electrode array. Some experiments did however show a slight gradient in the particle concentration along the length of the separation electrode array, with an initially high particle concentration at the start of the array reducing as the distance along the array increased (see figure 6-19). In these experiments, a higher applied voltages or low flow rate was used. The particles were depleted from the suspension as they flowed through the device. The ability of the system to remove (filter or deplete) small numbers sub-micron particles from suspensions is investigated in chapter seven.

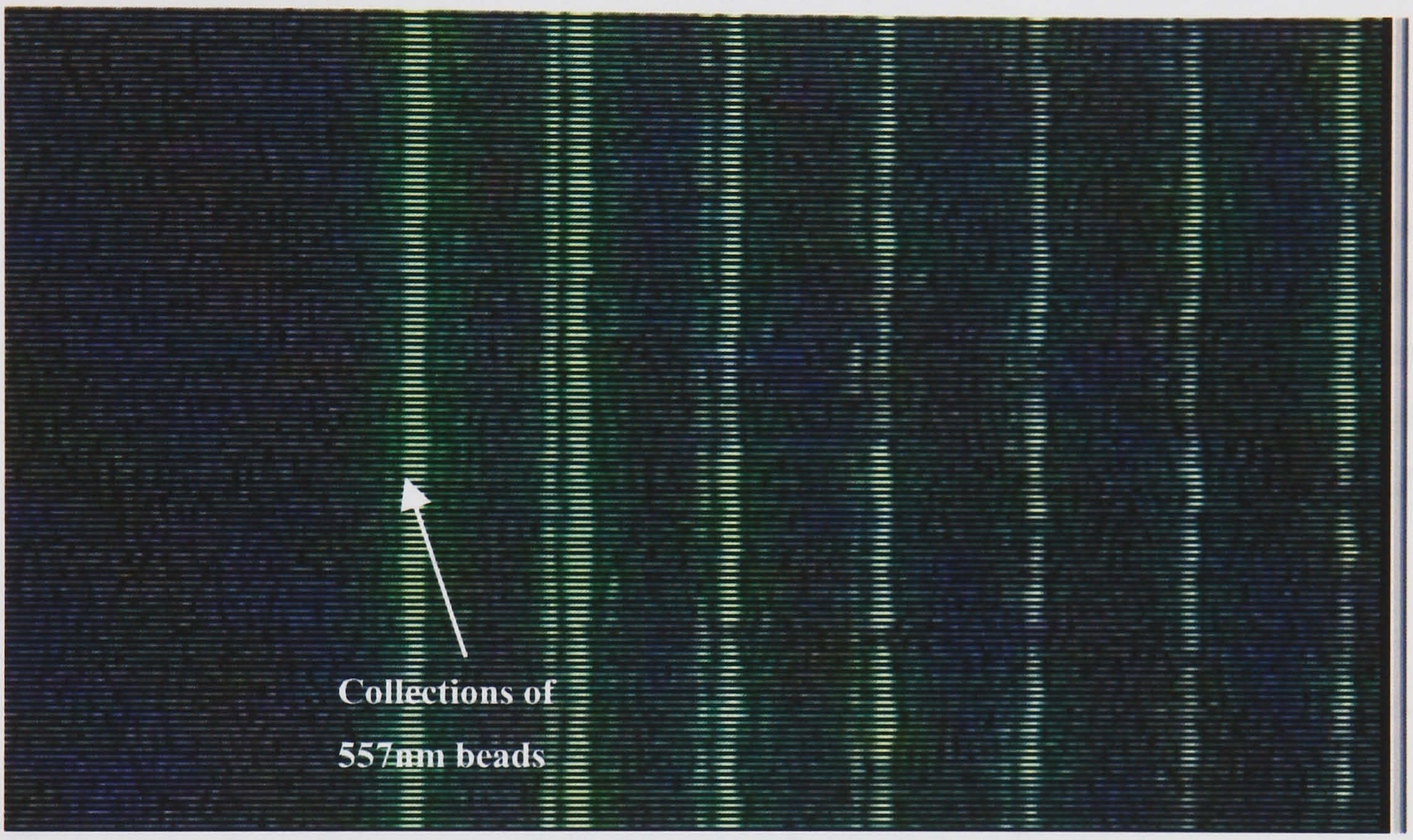

Figure 6-19. Capture of 557nm latex beads, showing concentration gradient along the length of the separation electrode array.

6.6 Discussion

The experimental results presented demonstrate that the DEP separation system operates as predicted for large particles. The simulations based on the work presented in chapter five are in reasonably good agreement with the experimental results for large particles (i.e. those greater than 2μm in diameter and not significantly affected by the disruptive force of Brownian motion). The focussing section uses –veDEP forces to confine particles to the central region of the flow channel. For the separation section of the device to function it was important that the focussing section works effectively. As shown in figures 5-18 to 5-20 the banding position of a particle varies considerably with the accuracy of the particle focussing.

Owing to fabrication considerations, both the focussing and separation electrode arrays were the same length (25mm). Future devices could be fabricated with electrode sizes tailored to the

particular application and particle type being used. Smaller sizes of separation electrodes would allow higher resolution separations and the use of lower applied voltages. Furthermore, variation in the spacing of the interdigitated electrodes could be used as a means of varying the DEP force along the length of the separation electrode. With such a structure the force experienced by the particles could be tailored to give a more uniform acceleration towards the electrode surface (i.e. reduce the steepness of the particle trajectories as the particles approach the electrode surface). The uniformly spaced interdigitated bar electrodes were used in this work solely to allow a straightforward comparison between the experimental results, and the simulation work based on the analytical solution for the DEP force available for such electrodes.

6.6.1 Sub-micrometre particle concentrations

Simulation of the particle concentration profiles for sub-micron particles within the focussing section of the device was carried out using FlexPDE™ (see chapter five for details). At steady-state the concentration profile in one dimension, across the channel height between the upper and lower focussing electrode arrays is given by the balance of the DEP and diffusion fluxes. The total flux of particles is made up of the diffusion, sedimentation and DEP fluxes, $\boldsymbol{J}_D$, $\boldsymbol{J}_g$, and $\boldsymbol{J}_{DEP}$ respectively. In the steady state these fluxes balance such that,

$$\boldsymbol{J}_D = \boldsymbol{J}_g + \boldsymbol{J}_{DEP}. \tag{6-2}$$

If we assume that sedimentation effects are negligible we get the following (see section 2.8),

$$-D\nabla c + \frac{c\boldsymbol{F}_{DEP}}{6\pi\eta a} = 0 \tag{6-3}$$

where D is the diffusion constant of the particles, c is the particle concentration, ∇c is the particle concentration gradient, $\boldsymbol{F}_{DEP}$ the DEP force, and $6\pi\eta a$ is the friction factor.

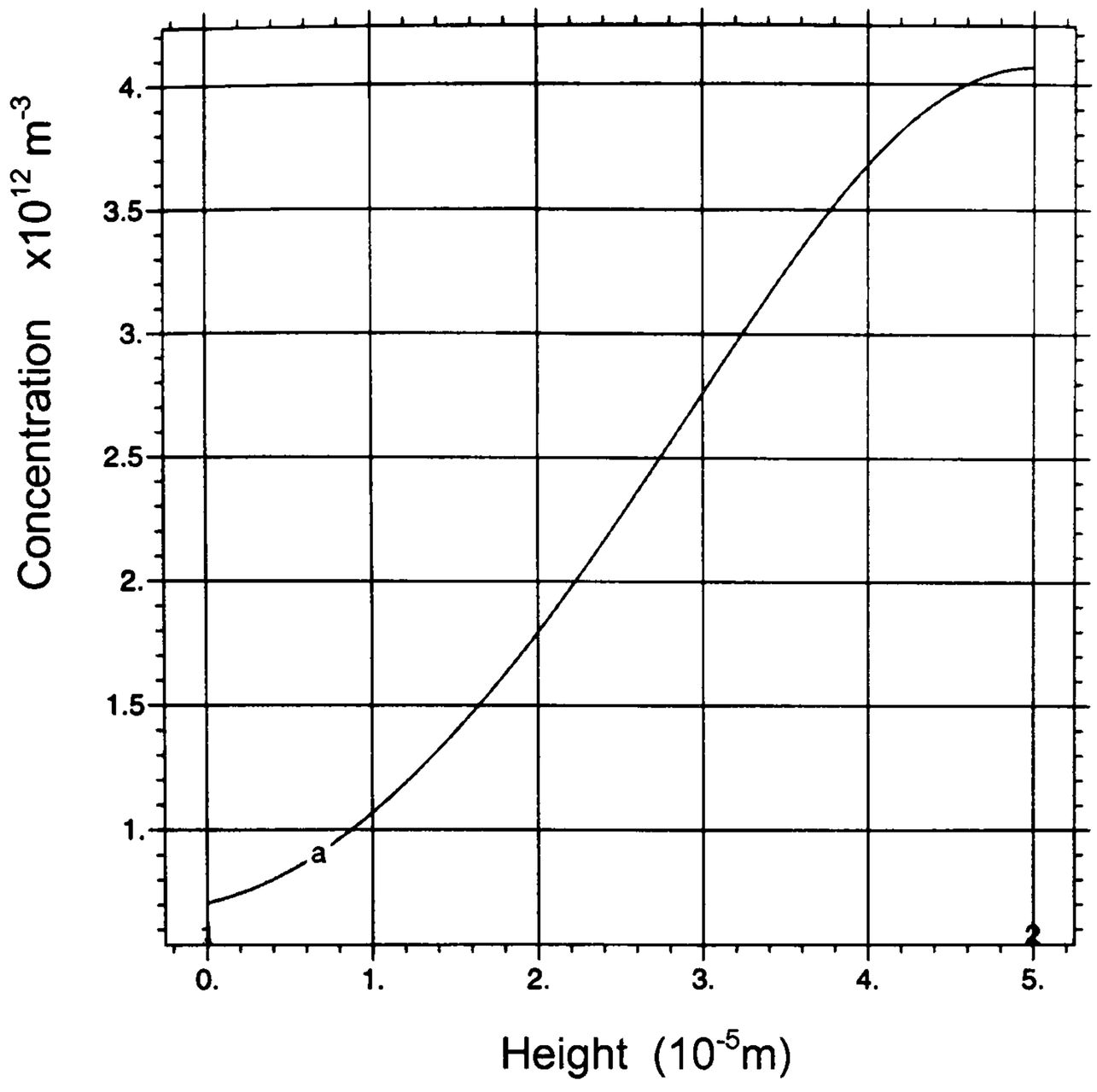

Figure 6-20. Numerical simulation of the particle concentration profile of sub-micron beads in the focussing section of the DEP separation system.

Figure 6-20 shows the particle concentration profile calculated from equation 6-3. The profile is given for half the channel and is symmetrical about the right hand side of the plot. The particle distribution can be seen to have Gaussian-like profile with the maximum concentration of particles in the centre of the channel and very few particles near the electrodes. The simulation gives a qualitative representation of the particle distribution within the device. Unfortunately, the simulation only converged under a very limited set of particle concentrations, and comparison with the experimental results could therefore not be made.

6.7 References

1. Cui, L., D. Holmes, and H. Morgan, *The dielectrophoretic levitation and separation of latex beads in microchips.* Electrophoresis, 2001. **22**(18): p. 3893-3901.
2. Markx, G.H., R. Pethig, and J. Rousselet, *The dielectrophoretic levitation of latex beads, with reference to field-flow fractionation.* Journal of Physics D-Applied Physics, 1997. **30**(17): p. 2470-2477.
3. Huang, Y., *et al.*, *Introducing dielectrophoresis as a new force field for field- flow fractionation.* Biophysical Journal, 1997. **73**(2): p. 1118-1129.

4. Morgan, H., *et al.*, *The dielectrophoretic and travelling wave forces generated by interdigitated electrode arrays: analytical solution using Fourier series (vol 34, pg 1553, 2001).* Journal of Physics D-Applied Physics, 2001. **34**(17): p. 2708-2708.
5. Schnelle, T., *et al.*, *Adhesion-inhibited surfaces. Coated and uncoated interdigitated electrode arrays in the micrometer and submicrometer range.* Langmuir, 1996. **12**(3): p. 801-809.
6. Green, N.G. and H. Morgan, *Dielectrophoresis of submicrometer latex spheres. 1. Experimental results.* Journal of Physical Chemistry B, 1999. **103**(1): p. 41-50.
7. Yang, J., *et al.*, *Dielectric properties of human leukocyte subpopulations determined by electrorotation as a cell separation criterion.* Biophysical Journal, 1999. **76**(6): p. 3307-3314.

Chapter Seven: Particle isolation and enrichment

7 Introduction

This chapter presents the results of experimental work carried out to characterise the particle separation system's ability to isolate an individual particle type from a mixture of particles. The work follows on from that of the preceding chapters, with many of the experimental procedures having already been discussed in those chapters. An introduction to the general field of particle sorting and separation was given in chapter one and the reader is referred back to this chapter for a discussion of the "state-of-the-art" in DEP particle separation systems.

In this chapter the application of the system to the problem of isolating cells from latex beads, and trophoblast from peripheral blood mononuclear cells (PBMCs) is investigated. The trophoblast/PBMC model system was chosen as it has relevance to the problem of isolating foetal cells from maternal blood samples for prenatal diagnostics (for discussion see section 1.2). The use of the system for the removal of low numbers of cells and virus-sized particles (460nm latex beads) is investigated.

In the last decade there has been a major drive to isolate and enrich foetal cells from the maternal circulation, in order to perform non-invasive prenatal diagnostic tests. To date all the enrichment strategies are antibody based, typically with the antibodies attached to a fluorescent or a magnetic label. The lack of specificity of the antibodies used, and the fact that they often only target a sub-population of the target cells has meant that contamination is a major problem. This makes such diagnostic tests less reliable than the traditional invasive prenatal diagnostic methods. The potential to enrich foetal cells using a non-antibody based strategy, which exploits differences in the dielectric properties of PBMCs and trophoblast cells is of great interest.

7.1 DEP particle separation

The trophoblast cells of the placenta form the interface between foetal and maternal circulation and are present from very early on in pregnancy. They are shed directly into the maternal circulation. Since trophoblast cells are morphologically and functionally distinct from peripheral blood cells, one would expect that the dielectric properties of these two cell types should be distinctly different. In recent work it has been shown that trophoblast cells do indeed behave differently when placed in a non-uniform AC electric field when compared with maternal blood cells [1]. That is to say trophoblasts do have different dielectric properties from that of the average PBMC.

DEP is a sensitive method of discriminating between different populations of cells and uses AC electric fields to separate cells according to their membrane capacitance and conductance (see chapter two). This method has been used to achieve selective separation of sub-populations of cells, such as breast cancer cells, leukaemia cells and CD34 + cells [2-6]. The DEP force varies (both in magnitude and direction) with the applied electric field frequency and magnitude, the medium conductivity and permittivity, cell volume and the intrinsic dielectric properties of the each individual cell. These last properties are governed by the morphology of the cell, in particular the membrane structure, protein and carbohydrate content and charge. Groups of similar cells will therefore experience similar DEP forces. If two populations of cells have sufficiently different dielectric properties then the resulting difference in DEP force can be exploited to separate the cells into sub-populations.

Variation of the frequency of the applied electric field causes the magnitude and direction of the DEP force to vary. It is therefore possible to select an applied field frequency such that different cell types will experience diametrically opposite DEP forces. DEP separation systems have been demonstrated that are capable of isolating single cell types from heterogeneous mixtures of cells (see chapter one and the review paper by Pethig [4] for details). For bulk separation of particles from mixtures all current DEP based separation systems work essentially in only one dimension, i.e. at the surface of the electrode array.

The systems operate along the following basis; all the cell types are initially attracted by +veDEP and held at the electrode edges. One of the physical parameters controlling the relative DEP force on the cells is altered (e.g. field frequency [7], medium conductivity [8], etc.), such that all the cells experience –veDEP or extremely weak +veDEP and are released from the electrodes and carried away in a fluid stream. The systems are all limited in their usefulness, having limited separation purity due to problems of non-specific adhesion to the separation chamber walls, or of steric hindrance (i.e. cells being retained at the electrode surface not by the +veDEP force but being held their amongst other trapped cells). Most of these systems work in a "stop-go" mode and are therefore very slow or are limited to processing only very small sample volumes <100μl.

To overcome these problems a new electrode configuration has been developed, which allows separation to occur in 2-dimensions. Details of the design and construction of the device are discussed in the previous chapters. Details of the various particle sorters including DEP based systems were presented in chapter one and are therefore only discussed briefly in the present chapter.

7.2 The DEP particle separation system

The principle of the DEP separator developed for this work is outlined in figure 7-1. It differs from previous DEP separation systems in that it has an initial particle-focussing element incorporated up stream of the separation electrodes. This allows a controlled feed of the particle sample into the region of the separation electrode array.

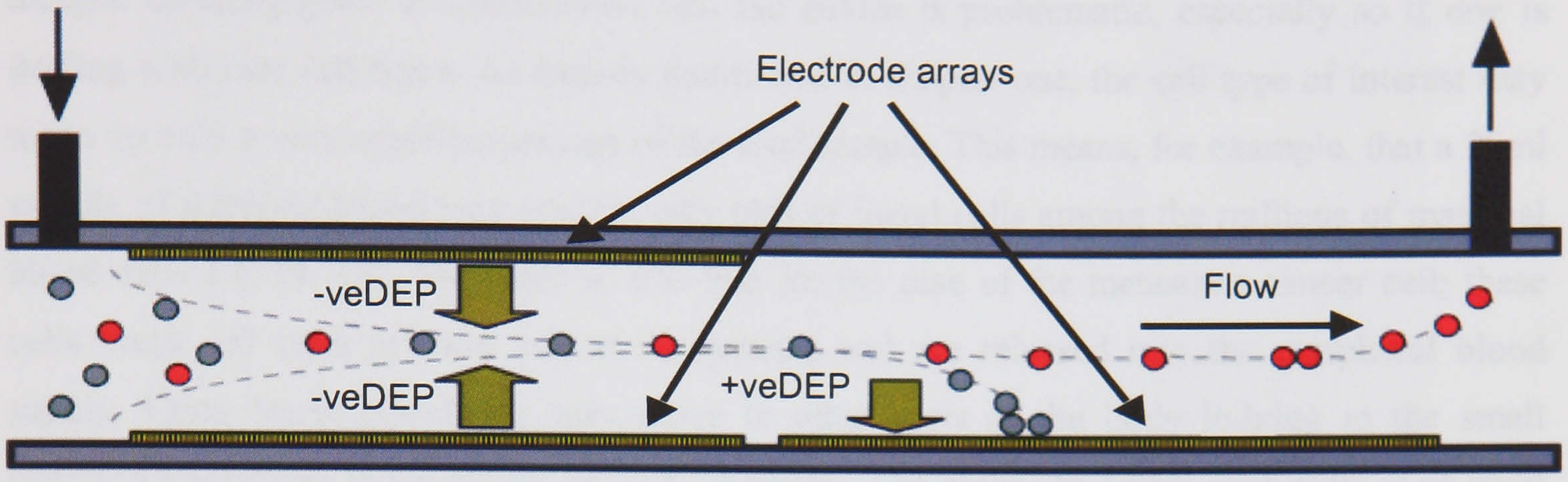

Figure 7-1. Principle of DEP cell separation for the isolation of single cell or particle types from mixture.

The basic operation is as follows; when particles enter the device they are carried in a fluid stream and are distributed randomly throughout the volume. Using -veDEP forces, the electrode arrays concentrate this wide distribution of particles entering the device into a well-defined sheet 5-10μm thick (i.e. one particle diameter), positioned midway between the upper and lower electrode arrays. The functioning of the focussing electrode was described in the previous chapter. It has been noted in the previous chapters that the formation of a sheet of particles only occurs for particles large enough such that the DEP force acting on the particles is sufficient to overcome the disruptive influence of Brownian motion. Following focussing particles enter the second separation electrode array, which is energised such that the DEP forces acting on the particles pull the desired sub-population of particles out of solution onto the electrode surface under the influence of +veDEP. The remaining particles experience a -veDEP force and remain in the high fluid velocity streamlines, which exist in the centre of the chamber (under laminar flow) these particles are thus rapidly eluted from the device. Those particles held at the electrode can be eluted for further processing by removal of the electric field (or application of a frequency to initiate negative DEP) whilst continuing to flow fluid through the device.

7.3 Materials and methods

All the experiments in this chapter use electrodes of characteristic electrode widths and inter-electrode gap sizes of $d_1 = d_2 = 40\mu m$ and channel cross-section 100μm x 900μm.

7.3.1 Sample handling

Sample handling prior to introduction into the device is problematic, especially so if one is dealing with rare cell types. As already mentioned in chapter one, the cell type of interest may make up only a very small percentage of the total sample. This means, for example, that a 20ml sample of maternal blood may contain only tens of foetal cells among the millions of maternal blood cells e.g. [9, 10]. The same is also true for the case of the metastatic cancer cell; these cells break off from primary cancerous tumours and are released into the peripheral blood supply. Once freely circulating they move to other parts of the body lodging in the small capillaries resulting in secondary tumour formation. The ability to detect such cells is of great importance, as potentially only one cell is needed to form a new tumour. For detection to be relevant and clinically useful the ability to detect very low numbers of cells is of paramount importance. To this end, careful sample handling prior to introduction into the device is necessary to avoid losing the cells of interest.

Large particles, such as cells will sediment to the bottom of any tubing or sample injection loops during the 30 minutes or so required to process a typical experimental sample. Under the low flow rate conditions used in this work (typically <2ml/hr) the particles remain in the tubing and are not carried into the device by the fluid. To achieve sufficiently high flow rates such that all the particles are carried along with the fluid requires the use of sample injection loops consisting of long coils of narrow bore tubing. This results in a large surface to volume ratio with the associated problems of particles adhering to the tubing walls. To overcome this problem a vertical sample injection column was designed and built (see section 4.3). This ensures that all cells enter the separation device and are not lost in the tubing. The experimental setup is shown in figure 7-2, using the device shown in figure 4-11, it consists of a section of 0.125" internal diameter PEEK tubing that is filled with the sample and held vertically above the inlet port of the chamber. Also shown in figure 7-2 is the valve arrangement, which allows cell-free suspending medium to be flowed through the device with minimum of dead volume. The electronic control valves also reduce the mechanical shocks to the system, which occur when using manually switched valves.

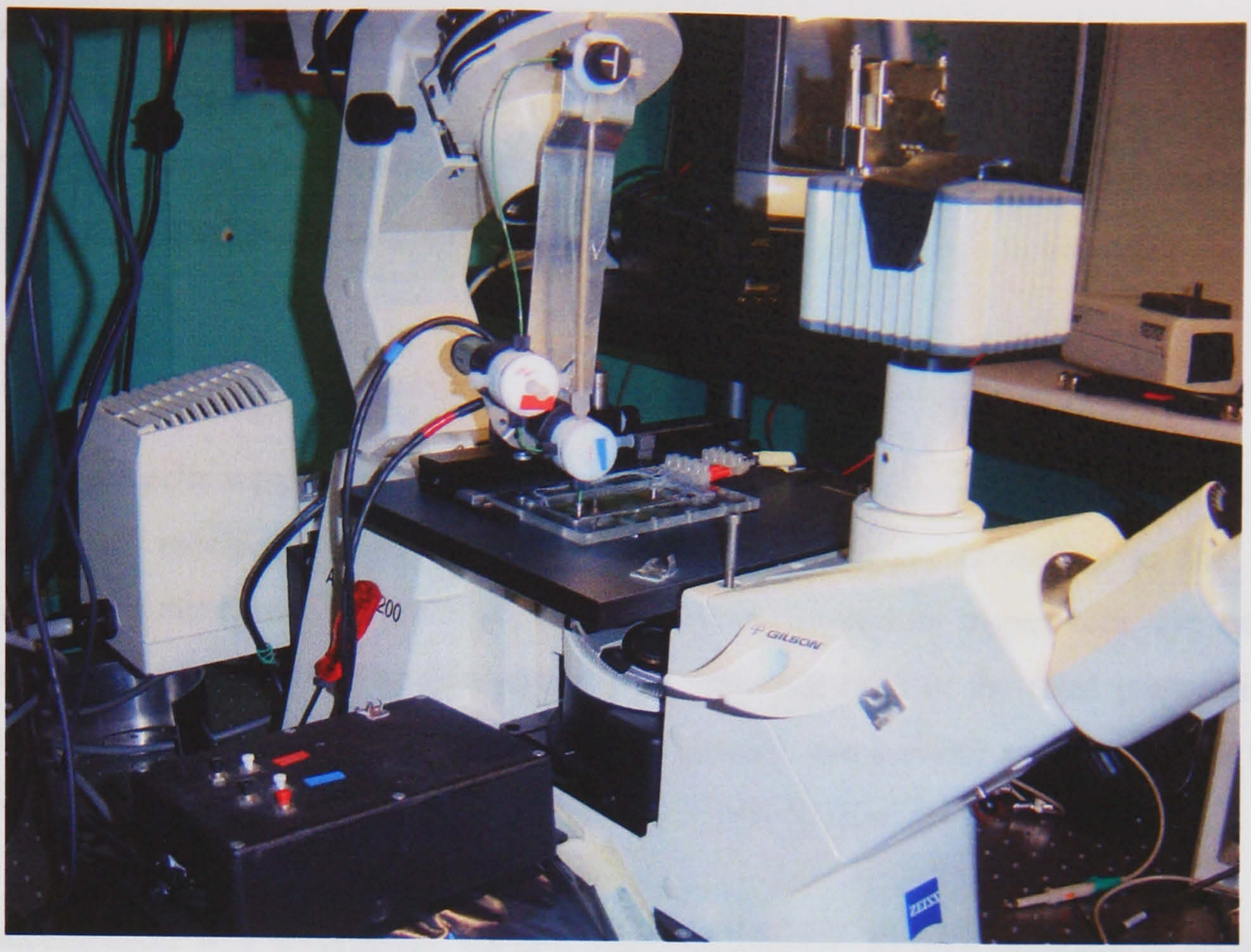

Figure 7-2. Separation device showing complete system including the fluidic and electrical connections.

7.3.2 Cell and bead samples

Cell and bead samples were prepared as described below, with all samples having their conductivities measured prior to the experiment.

7.3.2.1 Beads

Latex beads of two sizes (6μm and 460nm diameter) were obtained from Polysciences Inc. They were washed twice in suspending media and then seeded at known concentrations into the samples. A Coulter counter was used to measure the number of 6μm beads in the samples. The 460nm beads are supplied as a percentage weight of latex per unit volume, allowing the calculation of the particle numbers. The beads could then be serially diluted to the required concentrations.

7.3.2.2 PBMCs and THP-1 cells

Peripheral blood samples were collected into EDTA coated tubes (Vacutainer, Becton Dickson) from healthy volunteers and processed according to the protocol in section 3.1.1. THP-1 cells were grown in culture and harvested when required according to the protocol in section 3.2.1. These cells were washed twice in Ficoll-free dielectric separation medium (dH_2O with 9% w/v sucrose, 0.1% w/v glucose), following the washing step the cell pellet was resuspended in dielectric separation medium containing Ficoll (dH_2O with 9% w/v sucrose, 0.1% w/v glucose,

3.5% w/v Ficoll) of the correct osmolality ~290mOsm^{-1}. This two step washing procedure was necessary as the density of the Ficoll containing medium renders the cells neutrally buoyant, making centrifugation problematic. Cell counts were performed using a Coulter counter, with serial dilutions carried out as required.

7.3.2.3 Trophoblast cells

The trophoblast cells were prepared from the amniochorionic membranes of the placenta using a combination of mechanical and enzymatic digestion techniques, according to the method described in chapter three [11, 12]. Cell viability was examined by trypan blue dye exclusion test and found to be >90%. The percentage of trophoblast cells in the final preparation was evaluated by flow cytometry using the trophoblast specific cytoskeletal antibody JMB2 to label the trophoblast, and the leukocyte specific antibody CD45 to label the blood cells.

Cell concentration was determined using a haemocytometer. Known numbers of trophoblast cells were mixed with PBMCs and resuspended in dielectric separation medium (H_2O containing 9% w/v sucrose, 3.5% w/v Ficoll, 0.1% w/v glucose, 0.8% w/v BSA and 1mM EDTA), pH 6.8-7.2 and osmolality ~290mOsm^{-1}.

7.3.2.4 Bacteria

E.coli bacteria (K-12 strain) were grown in culture. To aid visualisation these cells were genetically transformed to express Green Fluorescent Protein (GFP). The culture procedure and transformation details are given in section 3.3. The cells were harvested and washed twice in suspending medium of known conductivity prior to the experiments.

7.3.2.5 Flow cytometry analysis

Flow cytometric analysis was performed on FACScan® (Becton Dickinson UK) using standard instrument setting (see chapter three for further details).

7.4 Separation of binary mixtures

To test the ability of the system to separate mixtures of particle types two model systems were investigated. The first, involved the separation of human PBMCs from mixtures of PBMCs and 6μm latex spheres. The second, and more interesting model system involves the separation of placentally derived trophoblast cells from a mixture of these trophoblast cells and human PBMCs.

7.4.1 PBMCs from 6μm latex beads

To demonstrate the separation of cells from beads, mixtures of cells and 6μm diameter carboxylated latex beads were introduced into the device at typical concentrations of ~10^6 particles per millilitre. The applied electric field frequency and suspending medium conductivities were chosen such that the cells were attracted to and retained at the separation electrodes while the beads experienced –veDEP and were repelled from the electrodes. Flow rates between 0.5ml and 2ml per hour were used and applied voltages of between $3V_{pp}$ and $6V_{pp}$. The DEP force frequency spectra for a T-lymphocyte [13] and a 6μm bead (K_s=1.5nS, [14]) were calculated for a medium conductivity of 20mS.m^{-1} and are shown in figure 7-3.

20:1 mixtures of PBMCs and 6μm latex beads suspended in low conductivity sugar solution were passed through the device and showed almost complete removal of PBMCs from the sample (see figure 7-4). Observation of the beads and cells as they flowed through the device showed that the particles were focussed to the mid-plane of the chamber in a short distance. Particles were observed to form a sheet with an equal number density across the width of the chamber. Upon exiting the focussing section of the device the beads continued to travel along the middle of the chamber where the fluid flow was greatest. The cells were attracted to the separation electrodes, where they tended to collect in a band. The position of the band varied depending on the flow rate and applied voltage, as described in chapters five and six. No particles were observed adhering to any of the chamber walls even after many repeat experiments on the same device.

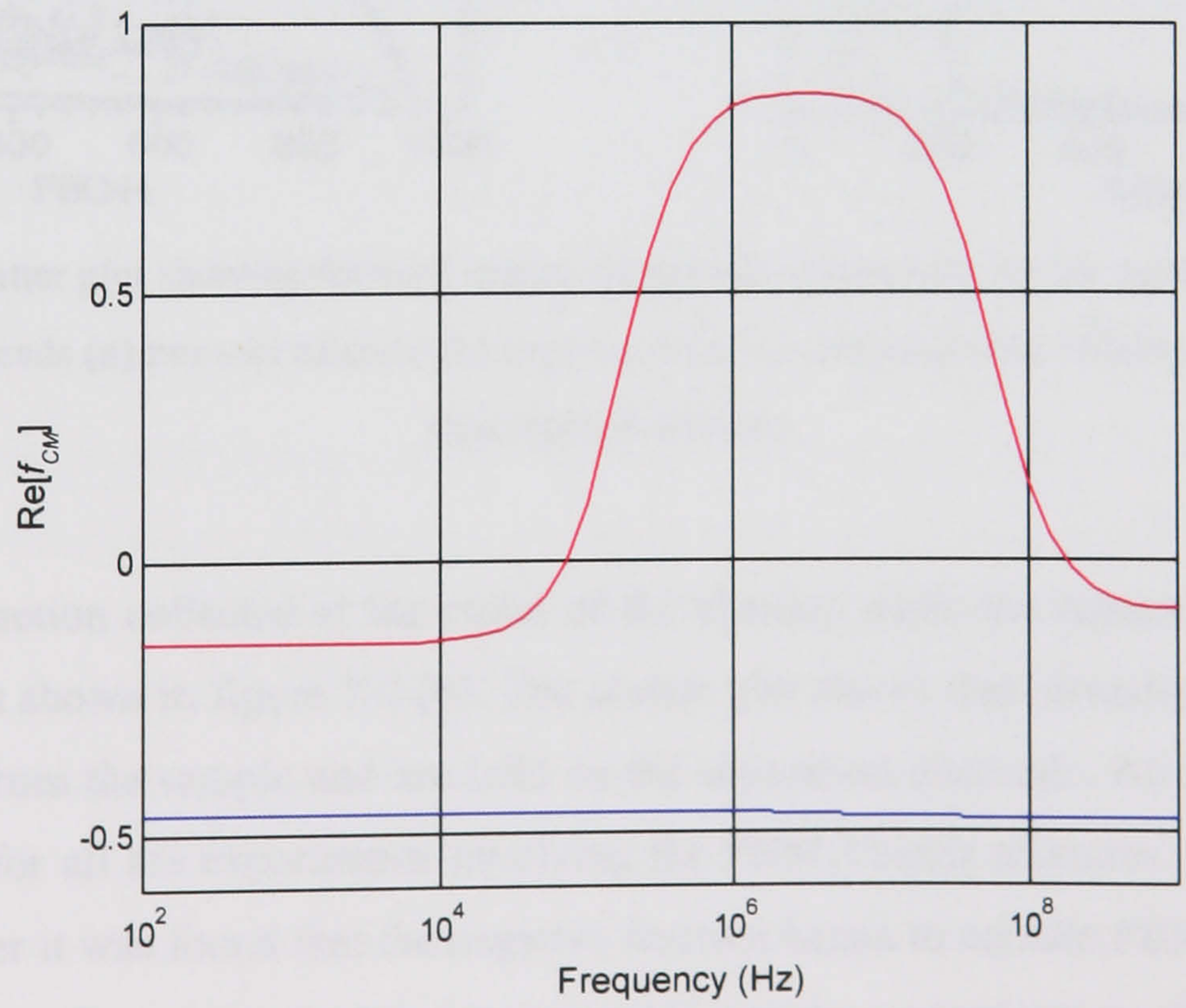

Figure 7-3. Real part of the *Clausius-Mossotti* factor versus frequency for 6μm latex beads with surface conductance K_s=1.5nS [14] (blue line) and PBMCs [13] (red line) at a suspending medium conductivity of 20mS.m^{-1}.

The results of a typical experiment are shown below in figure 7-4. The medium conductivity of the cell/bead mixture was measured to be 21mS.m^{-1}, and a flow rate of 0.4ml.hr^{-1} was used. The focussing electrode arrays were energised with 6Vpp at 10kHz. A 5MHz signal at 4Vpp was applied to the separation electrode array. Figure 7-4 (a) shows the scatter plots obtained by flowcytometry analysis of a portion of the sample prior to passing through the DEP sorting device and figure 7-4(b) shows the same analysis for the sample collected while the electric field was still applied to the separation electrodes.

When observed through the microscope it was clear that the cells collected on the separation electrode array. It was also observed that during the course of the separation experiment not a single latex bead collected on the separation electrodes. The positive fraction held at the separation electrode array under the influence of +veDEP forces contained no latex beads (held under steric hinderance, or otherwise) when examined under the microscope.

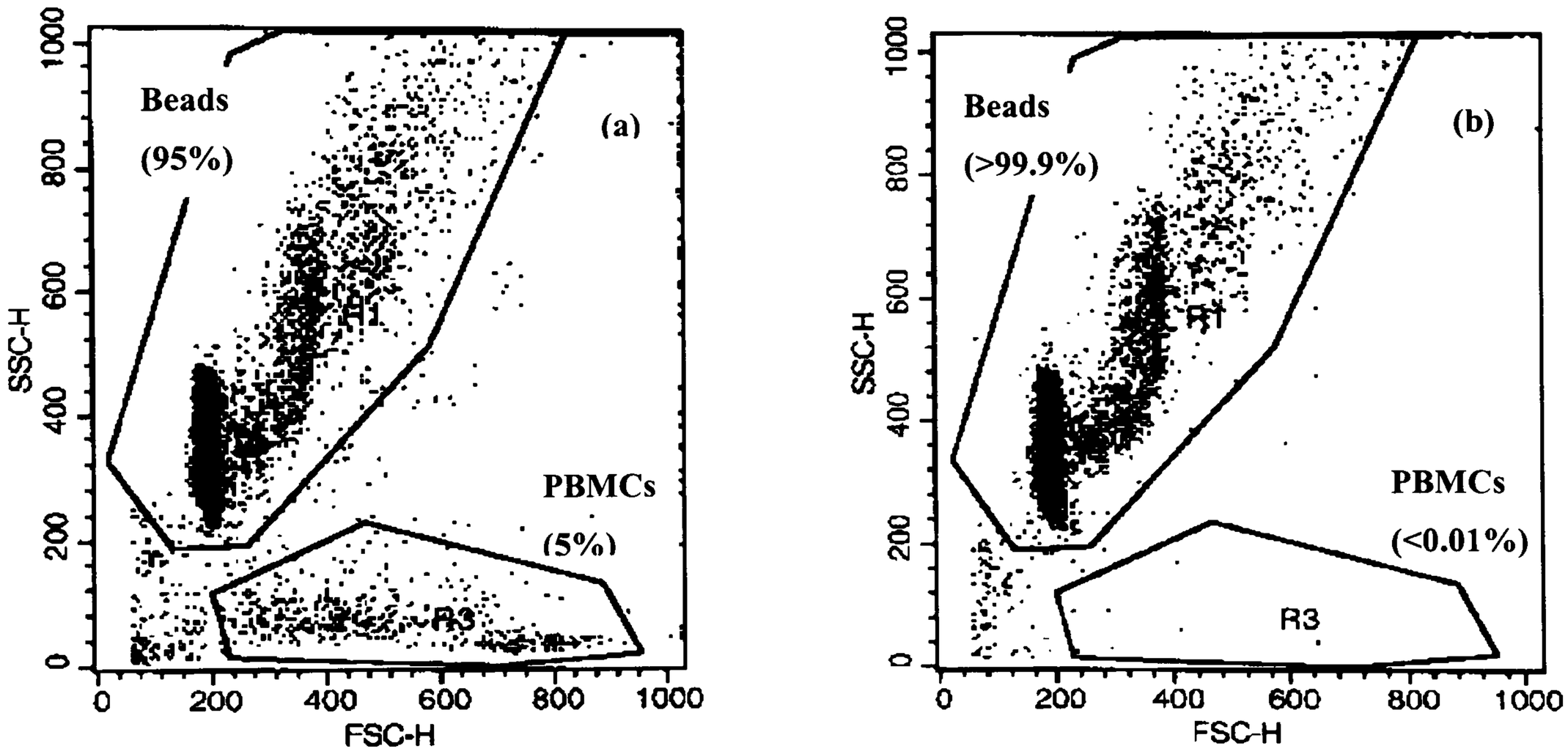

Figure 7-4. Scatter plot showing forward scatter versus side scatter data for the separation of PBMCs from 6μm latex beads **(a)** pre-sort mixture **(b)** negative fraction collected with 5MHz signal applied to the separation electrodes.

The negative fraction collected at the outlet of the channel while the separation electrode was still energised is shown in figure 7-4 (b). The scatter plot shows that virtually all the cells have been removed from the sample and are held on the separation electrode. An applied voltage of $4V_{pp}$ was used for all the experiments involving the PBMC/beads mixtures. With flowrates of 4mlhr^{-1} or greater it was found that the negative fraction began to contain PBMCs as well as the beads, with higher flow rates resulting in increased sample contamination. The reason for this was that the DEP force was not sufficiently strong to hold the cells at the electrode edges against the drag force due to the fluid flow. Higher applied voltages improve the separations at higher flow rates but the higher electric field strengths will tend to damage the cells.

7.4.2 Bacteria from PBMCs

Similar experiments were carried out separating bacteria from mixtures of blood cells. Due to the size of the *E.coli* (ca. 1μm x 2μm) they could not be detected using the FACS machine. A further limitation of the experimentation with these *E.coli* cells is that they do will not undergo –veDEP at suitably low frequencies. At the medium conductivities used, the crossover frequency for the GFP expressing bacteria was experimentally found to be ~160MHz. A high frequency signal generator and tuned amplifier were used to energise the focussing electrode arrays. This allowed only very weak focussing of the sample due to the signal loss arising from the impedance mismatch between the 50Ω signal source and the electrode array. Further engineering of the device is required to enable such devices to work in this high frequency region.

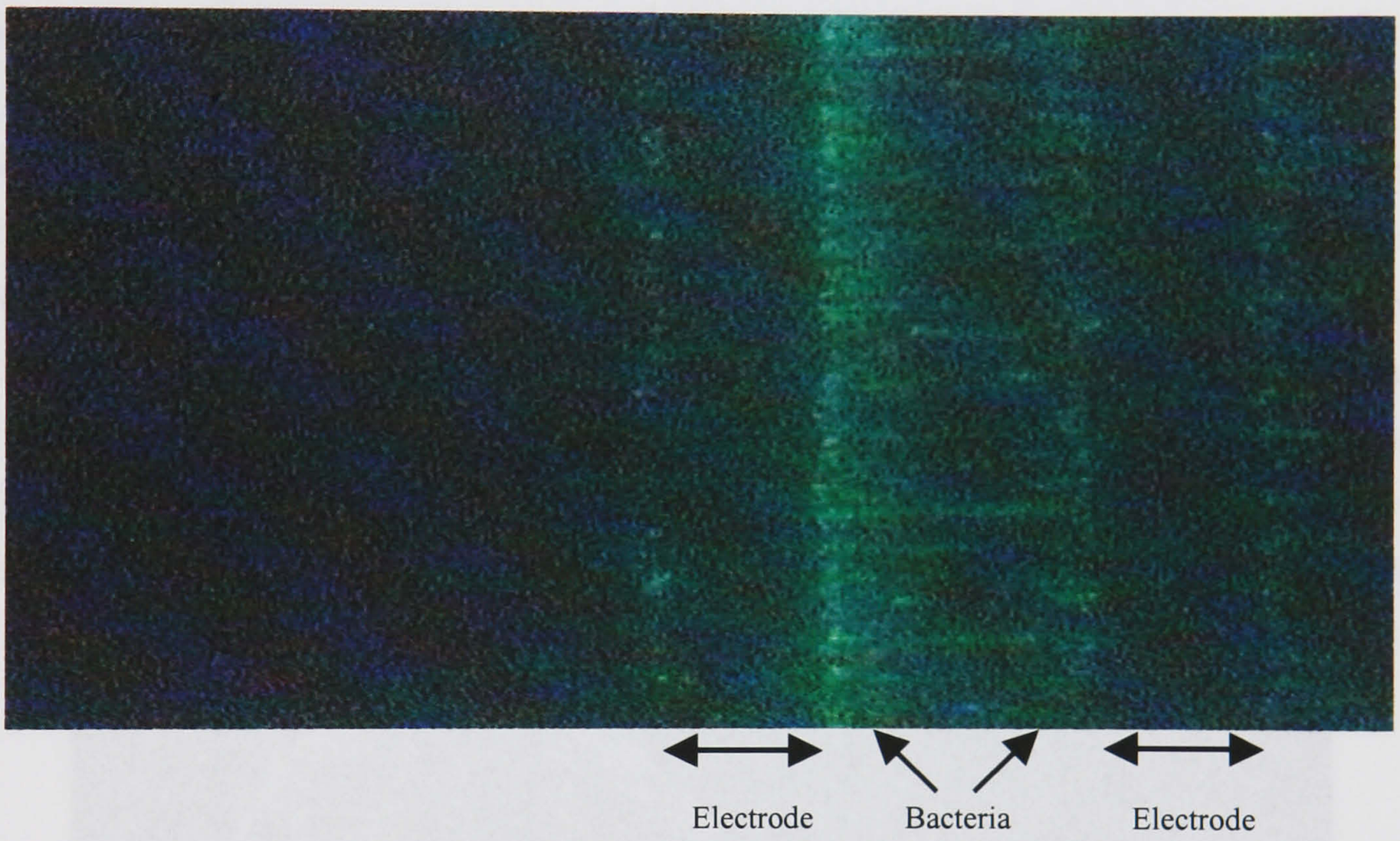

Figure 7-5. GFP expressing *E.coli* captured onto the separation electrode array under the influence of +veDEP from a mixture of PBMCs and *E.coli*.

Figure 7-5 shows an experimental image of *E.coli K12* captured on the separation electrode array under the influence of +veDEP. The medium conductivity of the cell/bacteria mixture was measured to be 38mS.m^{-1}, and a flow rate of 0.5ml.hr^{-1} was used. The focussing electrode arrays were energised with 24Vpp at 180MHz (the voltage actually seen on the electrodes was probably considerably less than this, due to impedance mismatches). A 10kHz signal at 6Vpp was applied to the separation electrode array, in this region the PBMCs experience –veDEP and the *E.coli* are attracted to the electrodes under +veDEP. Most of the bacteria were seen to collect on the initial few electrodes of the separation electrode.

7.4.3 Trophoblast from PBMCs

The dielectric properties of the human trophoblast cells have been characterised [1]. In this work the authors investigated the dielectric properties of the trophoblast cells and PBMCs using electrorotation and crossover measurements. The PBMC data was found to be in close agreement with that of Yang *et. al.* [13]. Trophoblast cells obtained from two sources

1. enzymatic digestion of placental membranes (method described in section 3.1.2)
2. isolated from retroplacental blood samples

have been shown to have distinctly different dielectric properties from those of the human PBMCs [1, 13] and also that of RBCs [15]. The aim of the current section is to assess whether these differences, measured by Chan *et. al.* [1], can be exploited to separate artificial mixes of trophoblast cells and PBMCs using DEP sorting techniques.

Figure 7-6 shows an SEM image of a pair of cells (thought to be trophblast) prepared from the amnionic membranes of a human placenta by enzymatic digestion of the amnionic membranes (this figure also appears in the paper by Chan *et. al* [1]). The morphology of these cells appears distinctly different from that of the PBMCs as seen in the work of Yang *et. al.* [13] (reproduced in chapter one, figure 1-9). It is likely that morphological differences between the cytoplasmic membranes of the cells shown in figure 7-6 and those seen in figure 1-9 accounts for the difference in membrane capacitance measured for the trophoblast cell type [1] and the PBMCs [1,13].

Figure 7-6. SEM of (probable) trophoblast cells isolated from placental membranes [1].

From the dielectric spectra shown in figure 7-7 one can see that, if the frequency of the applied field is chosen correctly (i.e. choosing a frequency within the shaded region), it should be possible to selectively attract trophoblast to the electrode surface under the influence of +veDEP and retained them there, while the PBMCs experience -veDEP and are repelled from the electrode surface. Any cells not held by the +veDEP force will pass through the chamber.

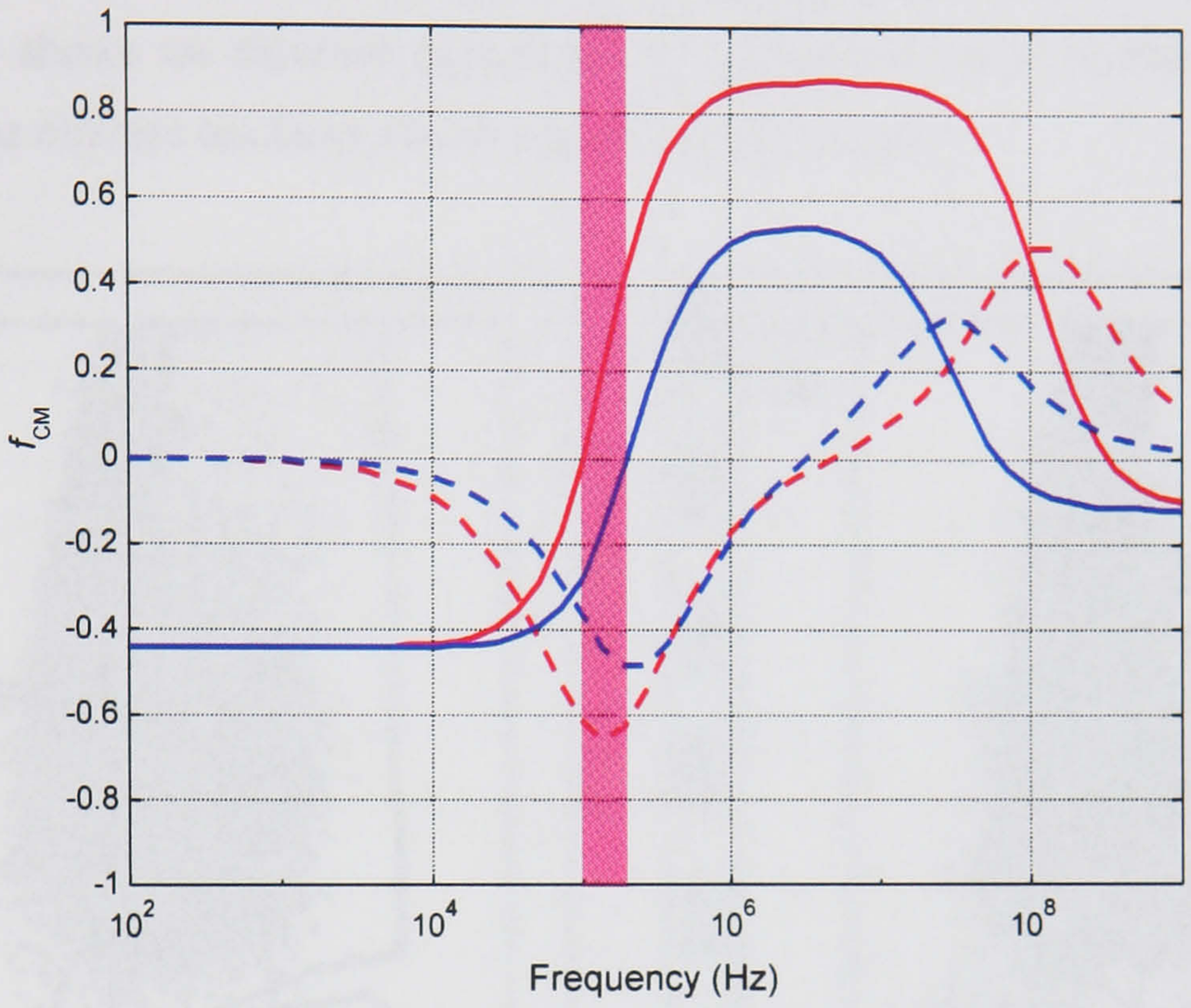

Figure 7-7. Plot of real part (solid lines) and imaginary parts (hatched lines) of the Clausius-Mossotti factor (i.e. normalised force) versus electric field frequency for a typical trophoblast [1] (red) and T-lymphocyte [13] (blue). Suspending medium conductivity of 50mS.m^{-1}. Shaded area shows window of useable separation frequencies.

To test this, mixtures of trophoblast and PBMCs were passed through the separation system with the electrodes energised, using AC voltages of 1 to 5V_{pp} in the frequency band ranging from 0.1MHz to 0.5MHz depending on the suspending medium conductivity used. The negative fraction was first collected i.e. those cells not held at the electrode by the electric field. Cell-free conductivity medium was then allowed to flow through the chamber and the field was switched off releasing the cells held under +veDEP (positive fraction).

The pre-sort mixture, and the post-separation positive and negative fractions were fluorescently labelled with antibodies (as described in section 3.5) specific to trophoblast[1] (JMB2) and PBMCs (CD45). The fractions of the artificial mixture were analysed using FACS allowing the degree of enrichment of trophoblast in the positive sorted fraction and the degree of

[1] JMB2 may label other cell types but has been shown not to label PBMCs [16].

contamination with PBMCs to be calculated from an initial 1:1 mix. Figure 7-8 (i)-(iii) show the FACS data from a separation experiment. Figure 7-8 (i) shows approximately equal concentrations of trophoblast and PBMCs in the pre-sort sample. The FACS instrument settings were chosen such that events in region R2 show fluorescently labelled cells. The populations Following separation the negative fraction (i.e. that collected at the outlet of the device with the field on, figure 7-8 (ii)) is comprised of approximately equal numbers of trophoblast and PBMCs. The positive fraction (i.e. that collected following release of the field) shown in figure 7-8 (iii) clearly shows an enriched population of trophoblast cells. Furthermore the PBMC component of the mixture has been almost completely eliminated.

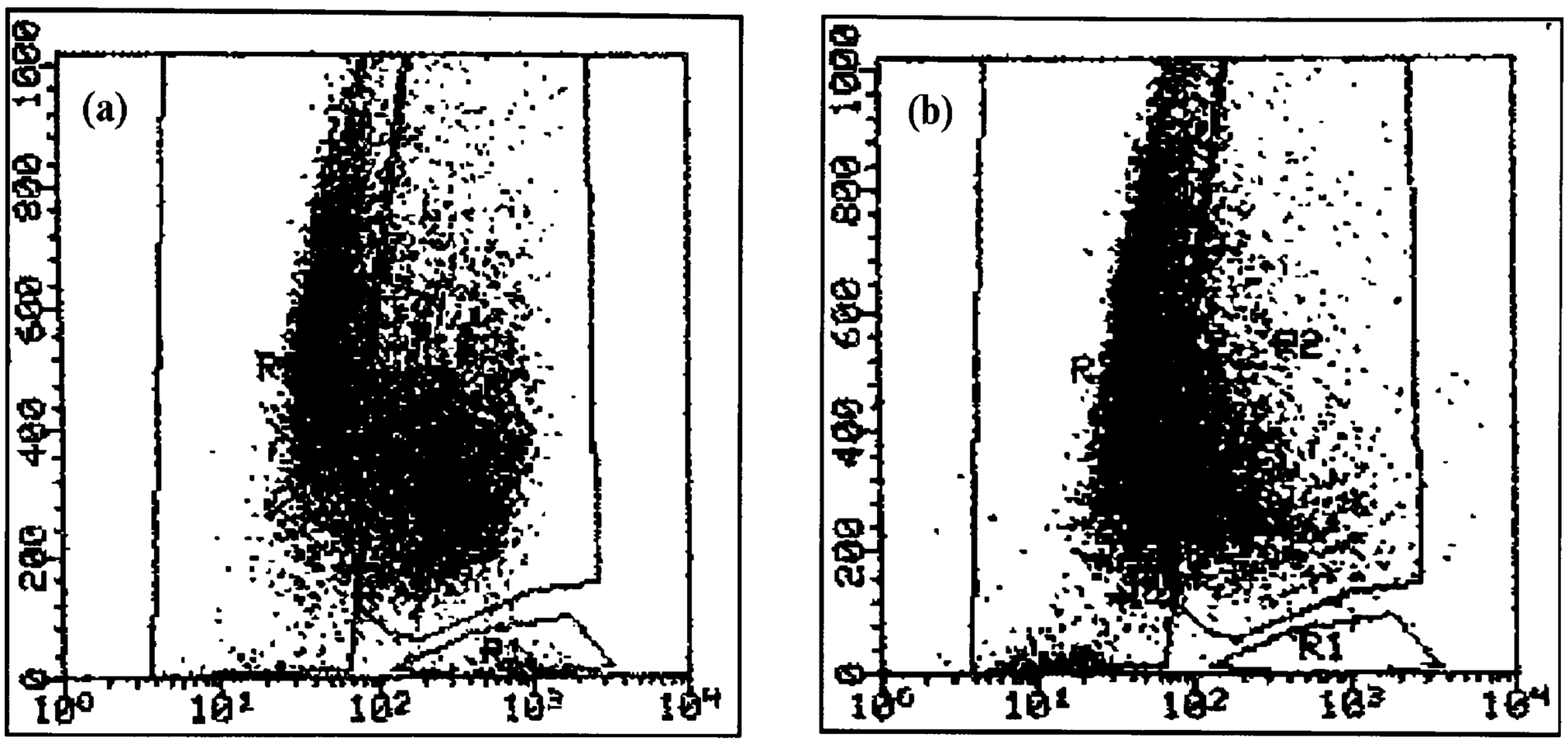

Figure 7-8(i). FACS scatter plot of SSC versus FL1 for the pre-sort mixture of trophoblast and PBMCs showing **(a)** CD45 labelled cells (PBMCs) and **(b)** JMB2 labelled cells (trophoblast).

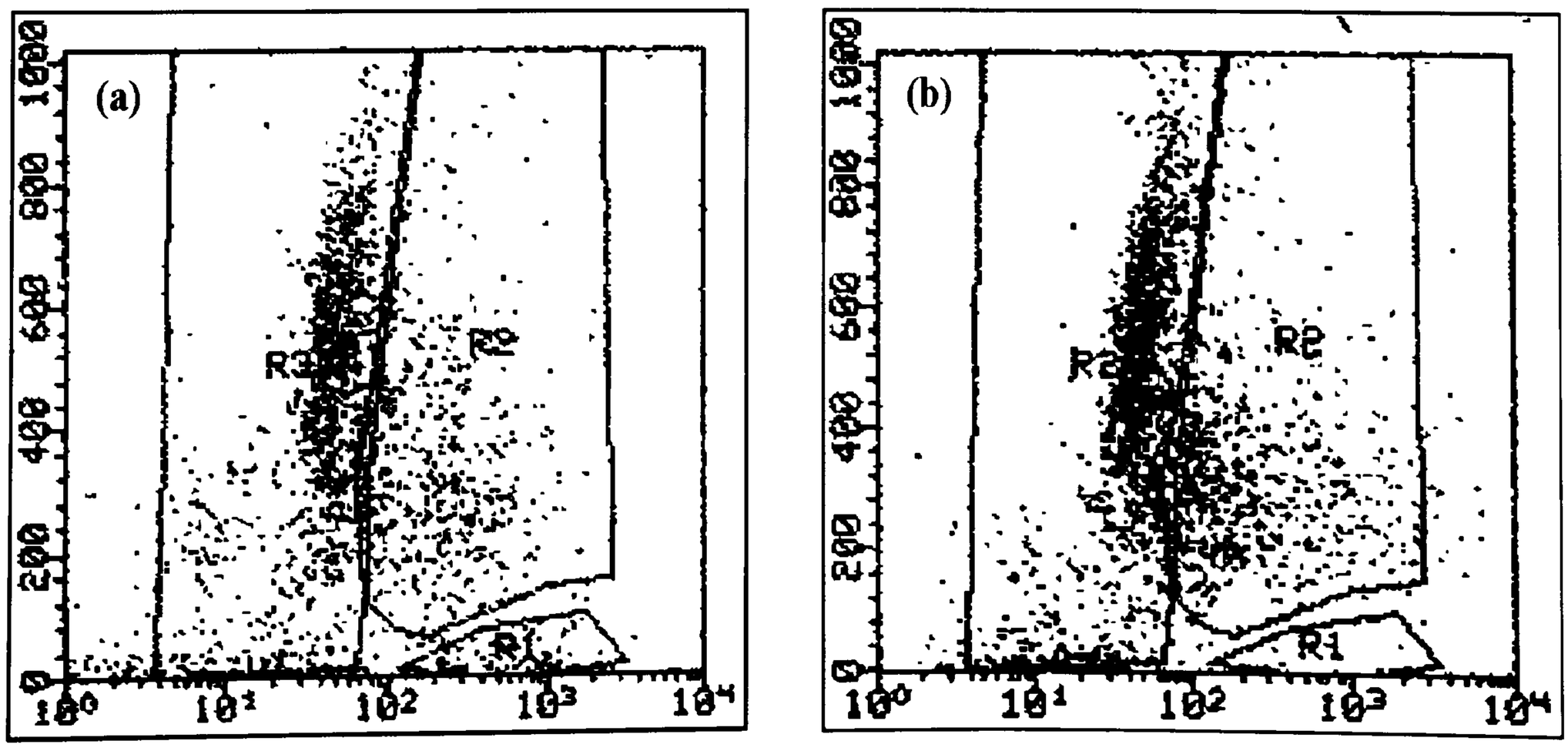

Figure 7-8(ii). FACS scatter plot of SSC versus FL1 for the negative fraction showing roughly equal numbers of **(a)** PBMCs and **(b)** trophoblast.

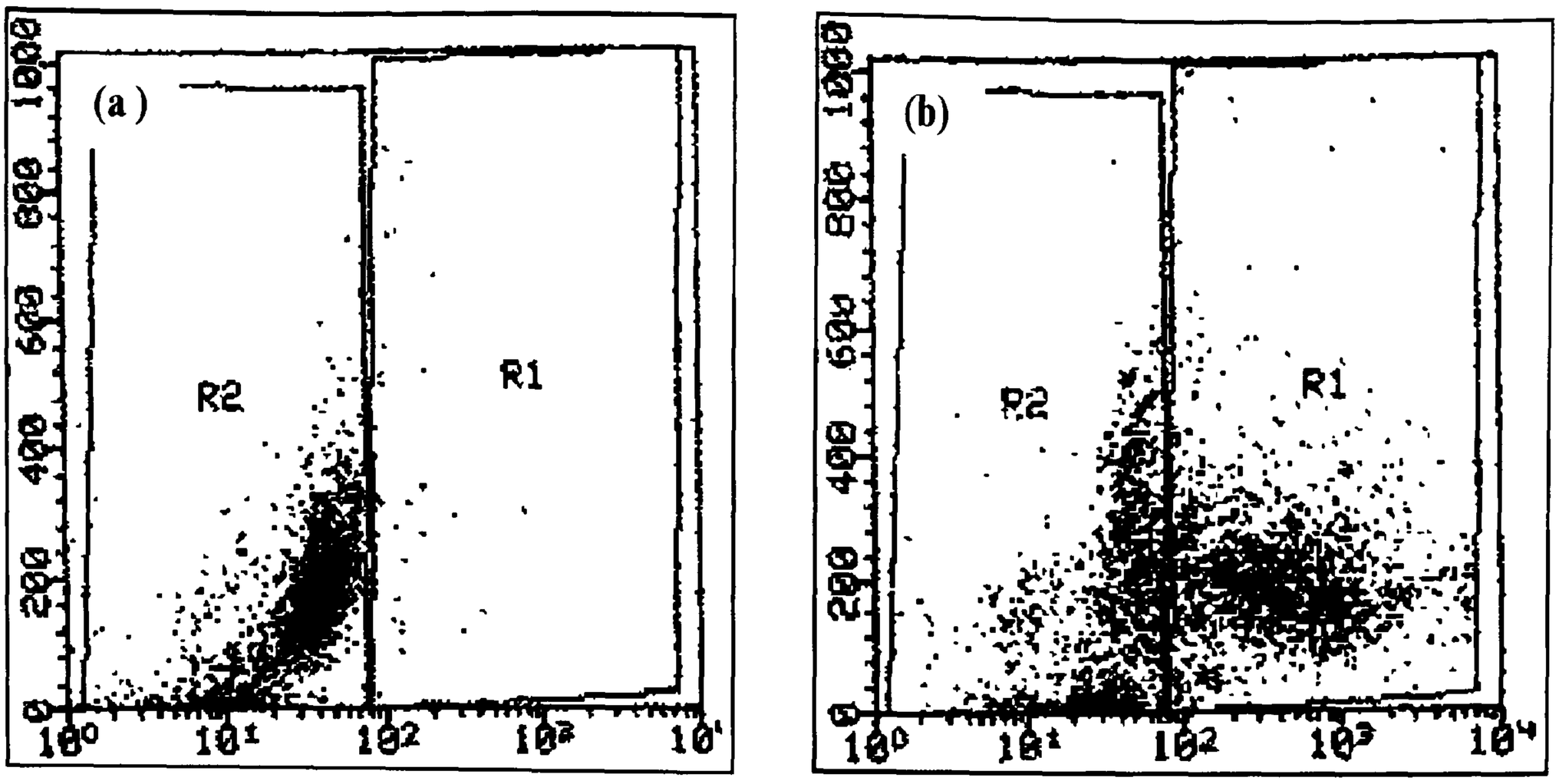

Figure 7-8(iii). FACS scatter plot of SSC versus FL1 for the positive fraction showing **(a)** the majority of PBMCs have been removed and **(b)** the enriched trophoblast fraction.

From the FACS analysis data above a thirty-fold enrichment of trophoblast was demonstrated using the separation system, with a concurrent 99% depletion of lymphocyte cells under the following experimental conditions:

- 1:1 mixture of trophoblast to PBMCs
- 10^6 cells per ml
- sample conductivity = 46.4mS.m^{-1}
- flow rate = 0.4ml.hr^{-1}
- volume of sample processed = 0.5ml
- focussing electrode = 6Vpp at 10kHz
- separation electrode = 3Vpp at 120kHz

Figure 7-9 shows the image looking down the microscope and shows cells collecting on the electrode edges under the influence of +veDEP. This image was captured under similar experimental condition to those described above. The cells are likely to be trophoblast cells. This assumption is based on two factors; firstly, their morphology many of the cells in figure 7-9 are different in morphology from that of PBMCs, which appear spherical when in suspension and secondly, the flowcytometery data which shows enrichment for cells positively labelling with the anti-JMB2 and therefore likely to be trophoblast.

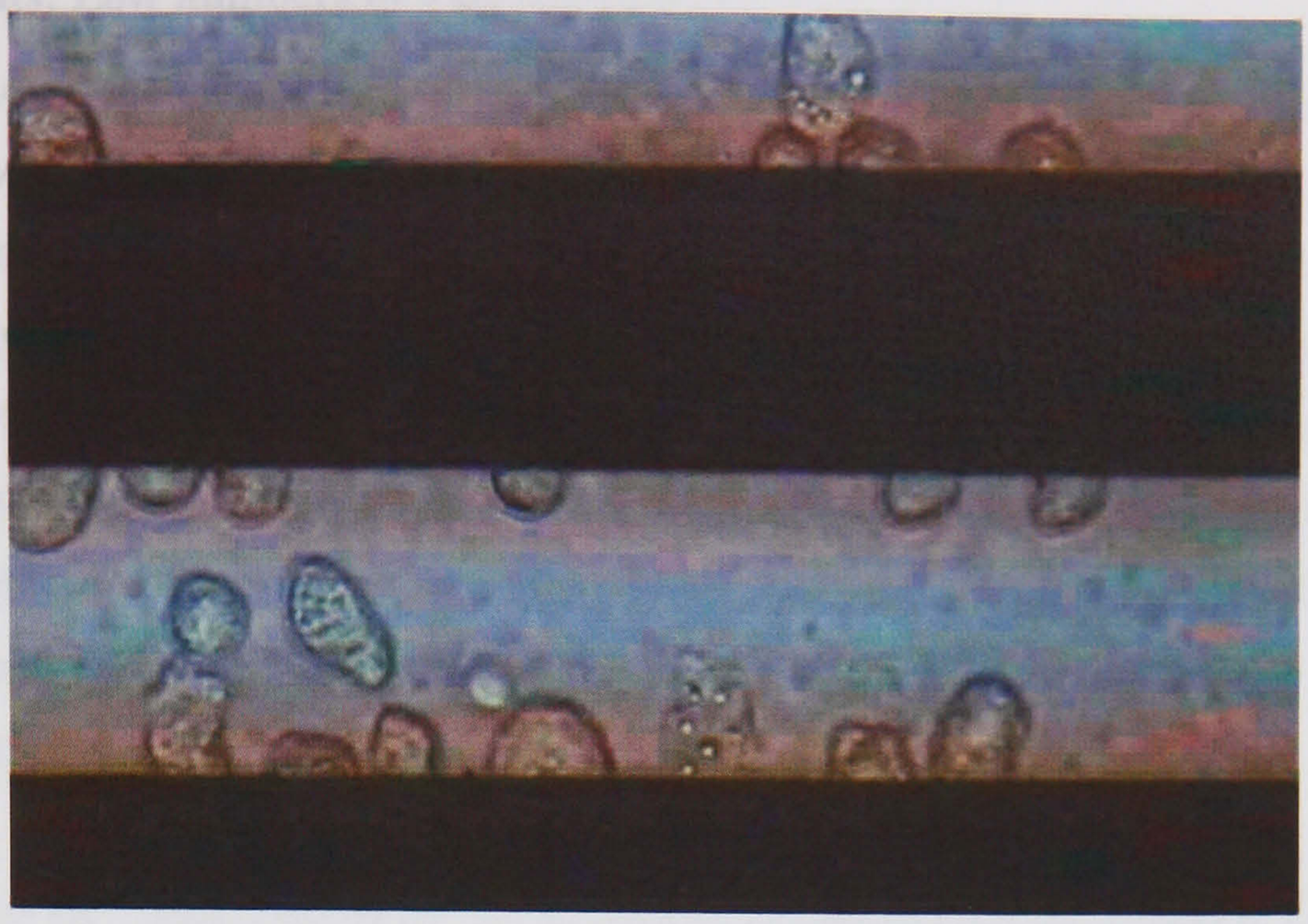

Figure 7-9. Micrograph showing +veDEP of a mixture of cells held at the separation electrode during experiment relating to that of figure 7-8.

7.5 Rare particle isolation

One of the major requirements for many analytical devices is the capability of the system to retrieve small numbers of particles from relatively large volumes. Applications include removal of a rare cell type from a mixture, isolation of small numbers of viral particles from a fluid, separation of bacteria from blood supplies, water, food, etc. This section discusses the ability of the DEP-based separation system to remove, concentrate and retain small numbers of particles from a continuous fluid stream, and also the usefulness of the system for isolating low numbers of cells or particles from large volumes of fluid. The device operates as described above by pulling particles out of a fluid stream onto the separation electrode using +veDEP.

7.5.1 Materials and methods

Samples containing small numbers of particles were passed through the separation system. The particles used were either THP-1 cells or 460nm diameter latex beads. The initial number of particles in each of the samples was measured first by either Coulter counter (in the case of the cells) or calculated from the percent latex value given on the datasheet supplied with the 460nm beads. Samples underwent serial dilution to reduce the particle number per unit volume. These samples were then passed through the device and both the positive and negative fractions were collected and the number of particles within each of the fractions was counted. As a cross check the number of particles held on the energised separation electrode array were also counted by scanning the microscope along the length of the device.

7.5.2 Results: Low numbers of THP-1 cells

Table 7-1 shows the data collected for passing low numbers of THP-1 cells through the separation system at different particle concentrations and under different experimental conditions. The medium conductivity of the sample, flow rate and cell concentration are shown. The focussing and separation electrode arrays were energised with 6Vpp at 10kHz and 6Vpp at 1MHz respectively for all experiments. One millilitre of sample was passed through the device for each of the four runs, this was followed by 0.2ml of cell-free suspending medium (i.e. 4x the chamber volume) to ensure all the particles had time to enter the device. Runs 1-3 were carried out using a separation electrode array of gap and electrode size 40μm. While run 4 was carried out using a 20μm electrode array.

Run	Cells per ml	Flow rate ($ml.hr^{-1}$)	σ_m ($mS.m^{-2}$)	Cells on device	Cells in collection tube
1	700	0.5	8.5	753	0
2	127	0.5	10.6	153	0
3	13	0.5	9.8	0	0
4	850	1	8.0	460	28

Table 7-1. Low numbers of THP-1 cells passed through device.

The number of cells held on the electrode array was counted using the microscope and scanning along the length of the electrode array. The medium flowing through the device with the separation electrodes energised was collected in a 1.5ml sample tube. This was centrifuged to form a pellet and the medium drawn off. The pellet was resuspended in 50μl of PBS and pipetted onto a microscope slide for examination.

Runs 1 and 2 showed greater than 100% collection of the cells, this is due to errors introduced by the dilution process (i.e. cells adhering to sample tube, etc.) and illustrates problems associated with counting such low numbers of particles. Run 3 resulted in no cells being captured by the separation electrodes, again probably due to problem with the accuracy of the serial dilution when dealing with such low numbers of particles.

Run 4 used a 20μm electrode array and a higher flow rate of $1ml.hr^{-1}$. In this sample only 460 cells were counted on the electrode (54%). For this experiment 28 cells were counted in the collection tube. The reasons for this are probably due again to errors in the serial dilutions and also problems with the loss of cells in the outlet tubing and cells adhering to the tube.

7.5.3 Results: Low numbers of sub-micron beads

At higher concentrations these particles did not follow the same trend as observed for the larger particles. The sub-micron particles occupied a band ±20μm around the mid-point of the channel. The reason for this is that a diffusion flux is generated which is opposes the DEP flux. When the voltage is removed the particles rapidly diffuse to occupy the entire volume of the channel in a few seconds. For the situation where the particle concentrations are sufficiently low, such that there is no diffusion flux acting counter to the DEP force, focussing is possible. Observation of the 460nm latex beads passing through the focussing section of the device showed that they can be focussed into the centre of the channel. Banding however was not observed for these beads and this is due to the disruption of the particle's motion by the Brownian force. This randomising force can act both towards or away from the separation electrode array resulting in some particles being captured earlier then expected and others being captured further down stream in the channel than simulation (without inclusion of the Brownian motion) would suggest. The overall result was the capture of the 460nm beads along the entire length of the separation electrode array.

Experiments were conducted passing low numbers of the 460nm beads through the separation system. The beads were suspended in dH_2O and passed through the device at flowrates of $0.5mlhr^{-1}$. Serial dilutions of the particle samples were performed to give particle concentrations of ~100 beads/ml. Sample volumes of 10ml were then passed through the device, with applied voltages of 20Vpp at 5MHz on the focussing electrode arrays and 5Vpp at 10kHz on the separation electrode arrays. The samples were left to run undisturbed overnight and the particle numbers on the separation electrodes counted after the entire 10ml sample had flowed through. In these experiments only the number of beads on the separation electrode array were counted. Table 7-2 shows the number of beads collected on the separation electrode array.

Run	Beads on device
1	643
2	821
3	675

Table 7-1. Low numbers of 460nm latex beads passed through device.

Due to the large volumes used in this series of experiments it became problematic to centrifuge and isolate the beads present in the collection tube (i.e. those beads passing through the device having not been captured by the separation electrode array).

7.5.4 Discussion

A major problem with DEP-based separation systems is non-specific adhesion of unwanted cells on the separation or collection electrodes. One application of a device is the isolation of small numbers of rare cells from a large population of unwanted particles with minimum contamination. This is minimised by the use of the initial particle focussing electrodes. Since all the particles entering the device are initially pushed away from the channel walls by a –veDEP force, only the cells that undergo +veDEP and are attracted to the separation electrode come into contact with the channel walls. The result of this is to reduce any chances for steric trapping and adhesion of contaminant cells at or to the channel walls.

The ability of the system to separate binary mixtures of cell sized latex beads and peripheral blood mononuclear cells (PBMCs), as well as mixtures of PBMCs and placentally derived trophoblast cells has been demonstrated. Removal of almost all the PBMCs from the beads mix was achieved with a pure sample of PBMCs held at the separation electrode. Problems with particles being retained in the fluidic tubing of the device restricted the analysis although visual inspection of the electrodes showed extremely good separation purity. The same is likely to be true for the trophoblast/PBMC experiments, and one could argue the that the enrichment of trophoblast cells of up to thirty times, with almost complete depletion of contaminating PBMCs represents a lower limit on the system's resolution.

Problems were encountered removing the cells from the separation electrode array. Although the majority of the cells were released with the cessation of the +veDEP signal, or the application of a –veDEP to the separation electrode array, a small percentage (approx. 5-10%) of the cells remained stubbornly attached to the electrodes. The addition of the Ficoll400 (MW = 400,000) to the suspending media had the beneficial effect of reducing the number of trapped cells. The mechanism by which this occurs is not known, one hypothesis is that this large polysucrose molecule forms a molecular layer between the cells and the channel walls, on top of which the cells sit when held at the electrodes, thus acting as a cushion keeping the cells from intimately contacting the glass or electrode surfaces (the non-stick effect of the Ficoll containing medium requires further investigation).

It has been shown that low numbers of particles can be isolated from large volumes of liquid allowing the continuous separation and concentration of a variety of particle types. THP-1 cells were captured and concentrated with almost 100% efficiency from dilute samples. Although the experiments involved the isolation of particles of a single type from large volumes the ability of the system to isolate rare particles from mixtures of particles follows from this. All the particles are initially focussed to the centre of the channel and therefore, if the particles are sufficiently well distributed so that they do not interact and the relative DEP forces on the particles are

suitably different, rare particle isolation should be possible. Similar experiments were carried out using low numbers the sub-micron (460nm) latex beads showing that they too can be focussed in the device, however the disruptive effect of Brownian motion stops these particles from banding on the separation electrode array. The ability of the system to concentrate low numbers of these particles from large sample volumes was demonstrated.

Unfortunately, time did not allow for the full characterisation of the separation system and therefore the data needed to describe the resolution of the device is not available. The work of the next chapter attempts to address this point, but by the very nature of the clinical samples used, the exact number of rare cells in these samples is not known.

7.6 Conclusions

The system described can be used for the continuous isolation and/or concentration of rare particles from large samples as well as separate single cell types from binary mixtures of particles. Further work is required to optimise the system in order to increase the enrichment factor with the aim of allowing the isolation of subpopulations of cells which are otherwise impossible to separate using the traditional antibody based techniques. The example of the trophoblast in the maternal blood arises once again and is investigated in chapter eight. The numbers and proportions of the trophoblast types within the maternal circulation may vary with gestation; this physiological trait could possibly be investigated using a dielectrophoretic isolation system of the type described here.

7.7 References

1. Chan, K.L., *et al.*, *Measurements of the dielectric properties of peripheral blood mononuclear cells and trophoblast cells using AC electrokinetic techniques.* Biochimica Et Biophysica Acta-Molecular Basis of Disease, 2000. **1500**(3): p. 313-322.
2. Gascoyne, P.R.C., *et al.*, *Dielectrophoretic separation of cancer cells from blood*, in *IAS '95 - Conference Record of the 1995 IEEE - Industry Applications Conference/Thirtieth Ias Annual Meeting, Vols 1-3*. 1995. p. 1366-1373.
3. Gascoyne, P.R.C., *et al.*, *Dielectrophoretic separation of cancer cells from blood.* Ieee Transactions On Industry Applications, 1997. **33**(3): p. 670-678.
4. Pethig, R., *Dielectrophoresis: Using inhomogeneous AC electrical fields to separate and manipulate cells.* Critical Reviews in Biotechnology, 1996. **16**(4): p. 331-348.

5. Becker, F.F., *et al.*, *The Removal of Human Leukemia-Cells From Blood Using Interdigitated Microelectrodes.* Journal of Physics D-Applied Physics, 1994. **27**(12): p. 2659-2662.

6. Becker, F.F., *et al.*, *Separation of Human Breast-Cancer Cells From Blood By Differential Dielectric Affinity.* Proceedings of the National Academy of Sciences of the United States of America, 1995. **92**(3): p. 860-864.

7. Markx, G.H., *et al.*, *Dielectrophoretic Characterization and Separation of Microorganisms.* Microbiology-Uk, 1994. **140**: p. 585-591.

8. Markx, G.H., P.A. Dyda, and R. Pethig, *Dielectrophoretic separation of bacteria using a conductivity gradient.* Journal of Biotechnology, 1996. **51**(2): p. 175-180.

9. Adinolfi, M., *Noninvasive or Minimally Invasive Prenatal Diagnostic-Tests On Maternal Blood-Samples or Transcervical Cells.* Prenatal Diagnosis, 1995. **15**(10): p. 889-896.

10. Bianchi, D.W., *Fetal cells in the maternal circulation: Feasibility for prenatal diagnosis.* British Journal of Haematology, 1999. **105**(3): p. 574-583.

11. Kliman, H.J., *et al.*, *Purification, characterization, and in vitro differentiation of cytotrophoblasts from human term placentae.* Endicronology, 1986. **118**(4): p. 1567-1582.

12. Shorter, S.C., *et al.*, Placenta, 1990(11): p. 505-513.

13. Yang, J., *et al.*, *Dielectric properties of human leukocyte subpopulations determined by electrorotation as a cell separation criterion.* Biophysical Journal, 1999. **76**(6): p. 3307-3314.

14. Cui, L., D. Holmes, and H. Morgan, *The dielectrophoretic levitation and separation of latex beads in microchips.* Electrophoresis, 2001. **22**(18): p. 3893-3901.

15. Gascoyne, P., *et al.*, *Dielectrophoretic detection of changes in erythrocyte membranes following malarial infection.* Biochimica Et Biophysica Acta-Biomembranes, 1997. **1323**(2): p. 240-252.

16. Sargent, I.L., personal communication, 1999.

Chapter Eight: Isolation of foetal cells from maternal blood - real systems and associated technical considerations

8 Introduction

The work presented in this chapter follows on from that of chapter seven, and was designed to test the ability of the DEP separation system to isolate rare cells from biologically relevant samples. The aim of these experiments was to isolate trophoblast (foetal cells) from maternal blood samples. A number of maternal blood samples were donated for these experiments. These samples, following some pre-processing, were passed through the DEP separation devices as described in the previous chapters. The results of the experiments are presented and discussed in this chapter.

As discussed earlier (chapter one) there are a number of foetal cell types present in the maternal blood. All of these cells could potentially be used for prenatal diagnostic purposes if a method could be found to reliably isolate them from maternal blood samples. Work was undertaken to characterise the dielectric properties of the foetal nucleated RBC (fnRBC). The fnRBC is unique among the other foetal blood cell types found within the maternal blood. Whereas most of the foetal blood cell types have an abundance of maternal counterparts in the maternal blood supply, the nucleated RBC (nRBC) is rare in the maternal circulation (in general nRBCs are rare in adult blood). The dielectric properties of nucleated RBCs (nRBC) were calculated using data obtained from crossover measurements made on nRBCs isolated from umbilical cord blood (i.e. of foetal origin).

A major problem with all biological material is that it has a tendency to adhere to surfaces. Many cell types require solid substrates on which to grow and multiply, they therefore tend to adhere to a surface when they come into contact with it. The final part of this chapter looks at the results of work done to chemically alter the channel and electrode surfaces. The aim was to reduce the non-specific adhesion of blood cells (i.e. the non target cell type) within the device, while at the same time enhance the affinity of the channel surfaces for the target cell type (i.e. the trophoblast). The adhesion properties of a variety of molecules were investigated using Interference Reflection Microscopy (IRM).

8.1 Isolation of foetal cells from maternal blood samples

The isolation of foetal cells from the maternal circulation for prenatal diagnostic purposes was first proposed by Walknowska *et. al.* in the late 1960's [1]. Many groups have investigated the possibility of recovering these cells from the maternal circulation as an alternative, non-invasive method of obtaining foetal cells for cytogenetic analysis. The background to this work is given in chapter one. Presently, there are no antibodies specific to foetal cells that would allow these cells to be reliably isolated from samples of maternal blood. As such, a major part of the work

presented in this thesis was directed toward developing a novel DEP based separation method capable of isolating rare cells from heterogeneous mixtures. As discussed in the previous chapters, the DEP separation technique relies upon the inherent difference in the dielectric properties of the trophoblast cell type, and those of the peripheral blood mononuclear cells. The technique therefore dispenses with the need for complex and expensive, and often unavailable labelling protocols and techniques.

Trophoblast cells isolated from a variety of sources; e.g. whole placenta, placental membranes, and retroplacental blood, have been shown to have markedly different dielectric properties when compared to those of the PBMCs sub-populations present in the maternal blood [2]. These distinct characteristics are attributable to highly folded cellular membrane of the trophoblast cells (figure 7-6 shows such folded membrane morphology in what is thought to be a pair of trophoblast cells). This suggests that the trophoblast cell type may be amenable to isolation from samples of maternal blood using techniques such as DEP. Artificial mixtures of trophoblast cells (isolated from placental membranes), and PBMCs were made up in known ratios. These mixtures were passed through the DEP separation system in order to test the feasibility of DEP separation. The results of these experiments presented in chapter seven demonstrate that, in principle, the enrichment of trophoblast (JMB2 positive cells) from blood cells is possible using DEP. However, the percentage of trophoblast cells present in these samples was relatively large ($\geq$10%) when compared with the numbers typically reported for maternal blood (1-10 per ml of whole blood).

As well as the non-representative cell ratios used in the experiments presented in the previous chapter, there is also some doubt as to whether the trophoblast cells used in the model system are truly representative of the trophoblast cells that make their way into the maternal circulation and are found in the maternal blood. That is to say, the dielectric properties of the trophoblast cells, as measured by Chan *et. al.* [2] may be different from those of the cells present in the maternal circulation. Furthermore, the enzymatic digestion protocol used to isolate the trophoblast cells from the placental membranes was rather aggressive, and potentially damaging to the cells. This may have altered the dielectric properties of the trophoblast cells, and could affect their responses to the applied electric fields. There is therefore some doubt as to the relevance of the dielectric properties of the cells presented in the paper by Chan *et. al.*, to the cells present in the maternal blood, despite having measured the properties of trophoblast derived from a number of sources.

A number of maternal blood samples were therefore obtained from healthy volunteers, and these were run through the DEP separation system in order to test the system's ability to isolate trophoblast from maternal blood samples.

8.2 Maternal blood samples

Women who had undergone prenatal diagnostic testing, and therefore knew the sex of their baby, were asked to donate blood samples if they were carrying a male foetus. A number of maternal blood samples were collected. These were pre-processed as described below and passed through the DEP separation system.

The blood samples were pre-processed to remove the majority of the RBCs (as described in chapter three), and a MACS protocol was used to remove as many leukocytes ($CD45^+$ cells) and monocytes ($CD14^+$ cells) as possible. The remaining cells were suspended in separation medium at known conductivity and the samples were passed through the DEP separation system under defined operating conditions. The various post-sort fractions were analysed using PCR to detect Y chromosomal DNA (i.e. evidence of male and therefore foetal cells), or the cells were allowed to sediment onto glass slides and ICC was carried out. ICC involved labelling the cells with the trophoblast specific antibody JMB2 [34], the details of which are described in chapter three. This enabled identification of trophoblast cells when the samples were viewed using a microscope.

8.2.1 Methods

Approximately 20ml of blood was collected from each pregnant female volunteer into sterile Vacutainer™ tubes containing EDTA anticoagulant. The red blood cells were removed by density gradient centrifugation, using a Histopaque 1077 gradient, as described in chapter three. The MACS cell separation system was then used to remove the majority of $CD45^+$ and $CD14^+$ cells (i.e. leukocytes and monocytes respectively) from the sample. The monocytes cells were specifically targeted for removal using the CD14 conjugated MACS beads as these cells have been shown to have similar dielectric properties to that of the trophoblast cells [2, 3]. To reduce the total number of maternal cells in the sample, CD45 conjugated MACS beads were used to remove as many leukocytes as possible from the sample. This pre-processing was carried out to reduce the sample volume from 20ml (maternal blood sample) to approximately 1ml, thus allowing the entire sample to be processed in a reasonable time (<1 hour) using the experimental DEP separation devices.

The cells remaining in the samples after density gradient centrifugation and MACS pre-processing steps were resuspended in DEP separation media, and the conductivities of the samples adjusted to approximately $30mSm^{-1}$, with a pH of between 6.8 and 7.4.

Experiments were carried out as described in chapters six and seven, with specific experimental conditions for each experiment given in table 8-1. The protocol was as follows: the positive

fractions (i.e. those cells retained by the separation electrode) were collected. Each of the collected samples were split into two; one portion was used for the PCR analysis, the cells in the rest of the sample were sedimented onto glass microscope slides and subjected to immunocytochemical (ICC) labelling. The PCR work was carried out in collaboration with staff at the Duncan Guthrie Institute, Yorkhill Hospital Glasgow. Primers specific for human Y-chromosome DNA were used, with the reactions performed as described in the protocol given in chapter three. The post reaction samples were then run on a gel electrophoresis system, and the DNA bands visualised autoradiographically. Adult male and female PBMC samples were used as controls with each of the PCR reactions.

The frequency and applied voltages for the experiments were chosen according to values for the properties of the cells reported in the literature [2, 4, 5]. A computer program written in MATLAB was used to calculate the optimal frequency for separation of the trophoblast and PBMCs. Figure 8-1 shows a typical plot obtained for a suspending medium conductivity of $30mSm^{-1}$. The plot illustrates the frequency range over which the separation of trophoblast from PBMCs should be possible.

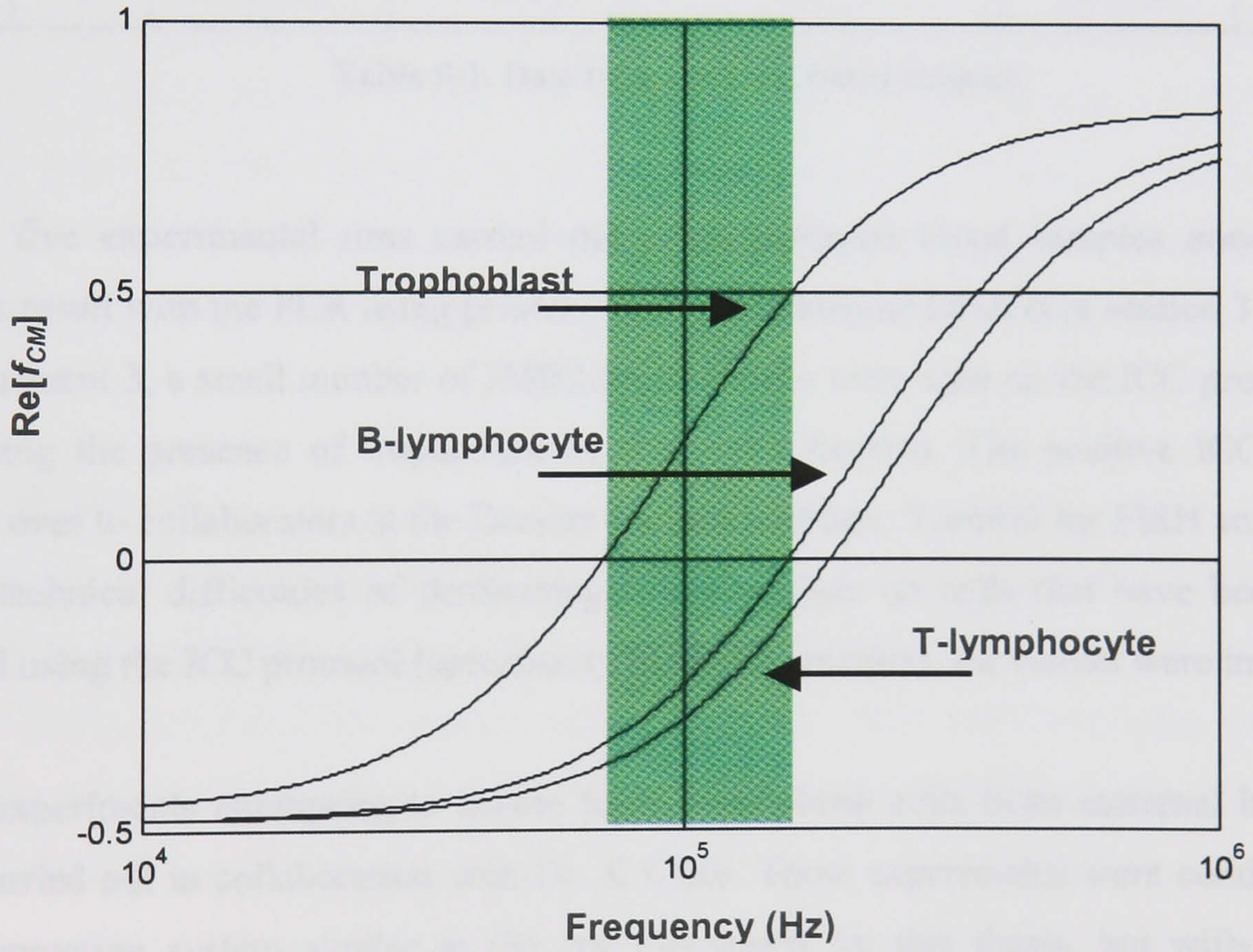

Figure 8-1. Force frequency plot showing the real part of the *Clausius –Mossotti* factor for trophoblast and T- and B-lymphocytes versus frequency for a suspending medium conductivity of $30mSm^{-1}$. The shaded region shows the band of separation frequencies.

From figure 8-1 it can be seen that for a suspending medium conductivity of $30mSm^{-1}$, applied frequencies of between 80kHz and 180kHz would result in trophoblast cells experiencing a +veDEP force, and lymphocytes experiencing a –veDEP force. Separation experiments were

therefore carried out using frequencies within this region. The conductivities of the cell suspensions, applied field frequencies, applied peak voltages, and fluid flow rates for the individual experimental runs are shown in table 8-1.

8.2.2 Results

Five experimental runs were carried out using blood donated by five women, all of whom were in the third trimester of their pregnancies and expecting baby boys. Table 8-1 shows the experimental conditions and the results obtained using PCR and ICC (see section chapter 3 for details).

Expt.	PCR	ICC (+ve)	Frequency	V_o (peak voltage)	Flow rate	σ_m
1	-ve	0 cells	100kHz	5V	0.6ml/hr	$30.2mSm^{-1}$
2	-ve	0 cells	120kHz	6V	0.6ml/hr	$37.8mSm^{-1}$
3	-ve	3 cells	120kHz	6V	0.5ml/hr	$33.0mSm^{-1}$
4	-ve	0 cells	120kHz	6V	0.5ml/hr	$30.8mSm^{-1}$
5	-ve	0 cells	120kHz	6V	1ml/hr	$30.9mSm^{-1}$

Table 8-1. Data from maternal blood samples.

Of the five experimental runs carried out using maternal blood samples none produced a positive result with the PCR using primers for Y-chromosome DNA (see section 3.8). However, in experiment 3, a small number of JMB2 positive cells were seen on the ICC processed slides, suggesting the presence of trophoblast in the sorted fraction. The positive ICC sample was handed over to collaborators at the Duncan Guthrie Institute, Yorkhill for FISH analysis. Owing to the technical difficulties of performing FISH analysis on cells that have been previously labelled using the ICC protocol (specifically the DAB reaction), the results were inconclusive.

Initial experiments attempting to isolate foetal trophoblast cells from maternal blood samples were carried out in collaboration with Dr. K Chan. These experiments were conducted using a DEP separation system similar to the one developed for this thesis, but without the initial focussing electrode array. Of the 10 experimental runs conducted on maternal blood samples using this system, a number of positive results were obtained using PCR to detect Y-chromosomal DNA. The PCR products for these experiments, as well as that for the controls, are shown on the gel reproduced in figure 8-2. It should be noted that these maternal blood samples were obtained post-partum (i.e. following delivery), rather than 3rd trimester as above.

Figure 8-2. PCR results from maternal blood samples passed through an earlier DEP separation system.

In three samples, DNA from the X- and Y-chromosomes is present, indicating the presence of male (i.e. foetal) cells in the sample. In the first positive result, the Y signal was relatively strong, requiring 30 rounds of PCR to obtain sufficient amount of the amplified product for visualisation on the gel. The other two positive results (to the right of the first) were only visible after a further 10 rounds of PCR amplification (i.e. 40 rounds in total) after which a faint band showing Y product became visible. This requirement for further rounds of PCR, to produce bands in these two male samples, is probably due to smaller amounts of foetal DNA being present (i.e. a lower number of foetal cells) in these samples. Ideally an additional control for the extra PCR rounds would be required to ensure the reliability of this result.

8.2.3 Discussion

Although all the experiments carried out on maternal blood samples using the DEP separation device with the focussing section were negative for Y-DNA PCR, the fact that one sample showed JMB2 positive cells suggests that some foetal cells may have been isolated by the separation system. There are a number of possibilities as to why the system failed to isolate more foetal cells:

1. very few or no foetal cells in the sample
2. cells were lost in pre-processing steps
3. cells were lost in tubing, stuck in device, etc.
4. the DEP system may not be sensitive enough

Owing to the small number of experiments where maternal blood was used (five), and the known variability of foetal cell numbers in the maternal circulation, no firm conclusion can be reached as to whether the DEP separation system is sufficiently sensitive to extract these rare

cells. The positive PCR results, based on work carried out using an earlier design of electrode suggests that DEP isolation of these cells may well be possible. The number of trophoblast present in the maternal circulation is known to vary throughout the course of the pregnancy and varies with the gestational age of the foetus [6-8]. However, as these experiments used blood samples from mothers who had already given birth, the levels of foetal cells present in these samples was probably significantly higher than that commonly reported in typical, healthy pregnancies pre-partum [9, 10].

It should be noted that the specificity of the JMB2 antibody, although excellent with respect to PBMCs may result in the labelling of other epithelial cells (e.g. skin cells) present in the sample. For conclusive evidence of the foetal origin of the cells isolated by the DEP system, analysis by FISH would be required.

More experimental runs are required to ascertain whether the DEP separation of trophoblast from maternal blood is possible using the current separation system. The uncertainty about the true DEP characteristics of the foetal cells in the maternal circulation, and possibility of loss of already rare cells during the sample pre-processing steps (e.g. loss of cells in the density gradient) need to be investigated. Ideally a large number of maternal blood samples require to be run through the DEP separation system, under a variety of experimental conditions. The post sort fractions of these experiments could then be analysed.

In order to improve the chances of isolating foetal cells from maternal blood samples, other foetal cell types should be targeted as well as that of the trophoblast. As there is no data in the literature regarding the dielectric properties of the other foetal cell types known to be present in the maternal blood during pregnancy, it was of interest to study these cell types. The next section discusses measurements that were carried out to measure the dielectric properties of foetal nucleated RBCs derived from cord blood.

8.3 Measurement of the dielectric properties of foetal erythroblasts

As described above, trophoblast are likely to have distinct dielectric properties compared with PBMCs. Foetal blood cells, on the other hand, would be expected to have similar dielectric properties to that of their maternal counterparts making DEP separation impossible. The case of the fnRBC is somewhat different. nRBCs are present in both the maternal and foetal blood supply. However, nRBCs are rare in the maternal blood, and enrichment for nRBCs to produce a purified sample of fnRBCs from a maternal blood sample could still be extremely useful. The number and purity of fnRBCs derived from maternal blood increases with increasing gestational

age, ranging from 50 to 500 fnRBCs per 20ml blood sample, and from 0.1 to 1% (fnRBCs as a percentage of the total maternal nRBCs population), from the 6th week of gestation to term [11].

The number of fnRBCs also varies depending upon the health of the mother and that of the foetus. For example, mothers carrying a foetus with an aneuploide (e.g. extra X or Y chromosomes, or other genetic abnormality) have an increased likelihood of foetal cell transport into the maternal blood, and therefore an increase in the number of foetal cells present in the maternal blood. Pregnancies with pre-eclampsia show an increase (up to a factor of 10) in the number of fnRBCs [12].

Durrant *et. al.* [13] demonstrated the usefulness of targeting multiple foetal cell types. The trophoblast cells were sorted using paramagnetic beads labelled with a novel monoclonal antibody (Mab34). This was followed by triple density gradient enrichment to remove maternal lymphocytes and red blood cells. Nucleated red blood cells (nRBC) were sorted by incubation with ferromagnetic particles coated with CD71 (an antitransferrin receptor monoclonal antibody), and separation was carried out using a mini-MACS column. Sorted cells were sexed using nested PCR for the Y chromosome and the results compared with the karyotypic analysis of the CVS. They found that the sensitivity in determining a male pregnancy by isolating fnRBC alone was 38% and isolating trophoblasts alone was 39%. Sorting for both cell types correctly predicted a male pregnancy in 10/18 or 56%. Of the 10 males correctly identified, 3 were diagnosed using nRBCs alone, 3 using trophoblast alone and 4 with both cell types.

This section describes the results of crossover measurements made on nRBCs isolated from umbilical cord blood samples. Other foetal cell types have been shown to be present in the maternal circulation, and these may also have suitable dielectric properties, which would allow their separation from maternal blood using dielectrophoretic techniques. As discussed in chapter one, there are potentially a number of different foetal cell types in the maternal blood, only one of which has had its dielectric properties characterised. The dielectric properties of human trophoblast cells were characterised by Chan *et. al.*[2], and this information was used to calculate suitable applied field frequencies for the DEP separation experiments of this chapter, and those of chapter seven. In order to investigate the dielectric properties of other foetal cell types, work was carried out in collaboration with Dr Diana W. Bianchi at the New England Medical Center, Tufts University, Boston. The aim of this collaboration was to characterise the dielectric properties of the foetal nucleated red blood cell (fnRBC). Dr Bianchi's laboratory is at the forefront of research into the basic physiology of the fnRBC, and has a particular interest in developing methods for isolating fnRBC from the maternal blood [14-21].

8.3.1 Materials and methods

The enrichment procedure described here concentrated the cell sample for nucleated RBCs, and not specifically for fnRBCs. However, as the blood samples were obtained directly from the foetal cord, the majority of the cells should be foetal in origin, and therefore most of the nRBCs present in the sample can be assumed to be fnRBCs.

Cord blood was collected into sodium citrate tubes, and processed as described in chapter three. Briefly, the blood was pre-processed by spinning over a Ficoll 1119 density gradient and the mononuclear cell layer was collected (see section 3.1 for further details). The denser Ficoll 1119 gradient was used instead of the standard 1077 gradient to ensure that none of the nfRBCs present in the sample were lost within the gradient [22]. nRBCs unlike RBCs are mononuclear cells (i.e. they have a nucleus) and as such are less dense than erythrocytes, to which they are the precursor. Following the density gradient centrifugation step, the nRBCs are found in the buffy coat layer along with the other mononuclear cells.

A two-step MACS protocol was used to deplete PBMCs from the sample and enrich for nRBCs. To achieve this, the collected mononuclear cell layer was washed by re-suspending the cord blood sample 1:1 in Hanks buffered saline solution (HBSS) and centrifuging at 500g for 15mins. The pellet was resuspended in 1ml HBSS with 0.5% BSA and 5mM EDTA. 30µl of CD14, CD15 and CD45 conjugated MACS beads were added to the sample, and incubated for 30min at 4°C. The sample was then passed through the MACS separation system. Cells not retained by the magnetic field were collected, and incubated with 30µl of CD71 conjugated MACS beads. These were then passed through the MACS system once again (using a fresh column). This time the cells retained by the magnetic field were collected.

The use of the combination of CD14, CD15 and CD45 conjugated MACS beads (Myltenyi Biotech, Germany) allowed the removal of the majority of the white blood cells from the sample. CD71 (Myltenyi Biotech, Germany) was then used to positively select for nRBCs, as this label targets the transferrin receptor present on the surface of nRBCs but not RBCs. This nRBC enriched cell sample ($CD14^-$, $CD15^-$, $CD45^-$, and $CD71^+$) was split into two aliquots. The cells in the first aliquot were used for FACS analysis, the rest of the sample was resuspended in separation medium and used for DEP crossover measurements. For FACS analysis and sorting, the cells were fixed in 4% formaldehyde in HBSS and fluorescently labelled with fluorescent probes specific for leukocytes (anti-CD45-FITC), DNA (Hoechst 33342), and the foetal protein γ-haemoglobin (made in house by a collaborator), according to the protocols described in chapter three. Two cord blood samples were obtained and processed as described above. Figure 8-3 shows the FACS data obtained for the nRBC enriched sample, each dot represents the fluorescence from a single cell. Region R1 was chosen as being the fnRBC population as it

selects for cells that label positive for foetal haemoglobin and also negative for leukocyte antigens. From the data it is apparent that there are very few cells labelling as leukocytes in the population. The majority of the events detected and showing up in the lower left hand sector of figure 8-3 are likely to be non-nucleated (i.e. mature) erythrocytes or dead cells, both of which are distinctly different in appearance from fnRBC when viewed down the microscope.

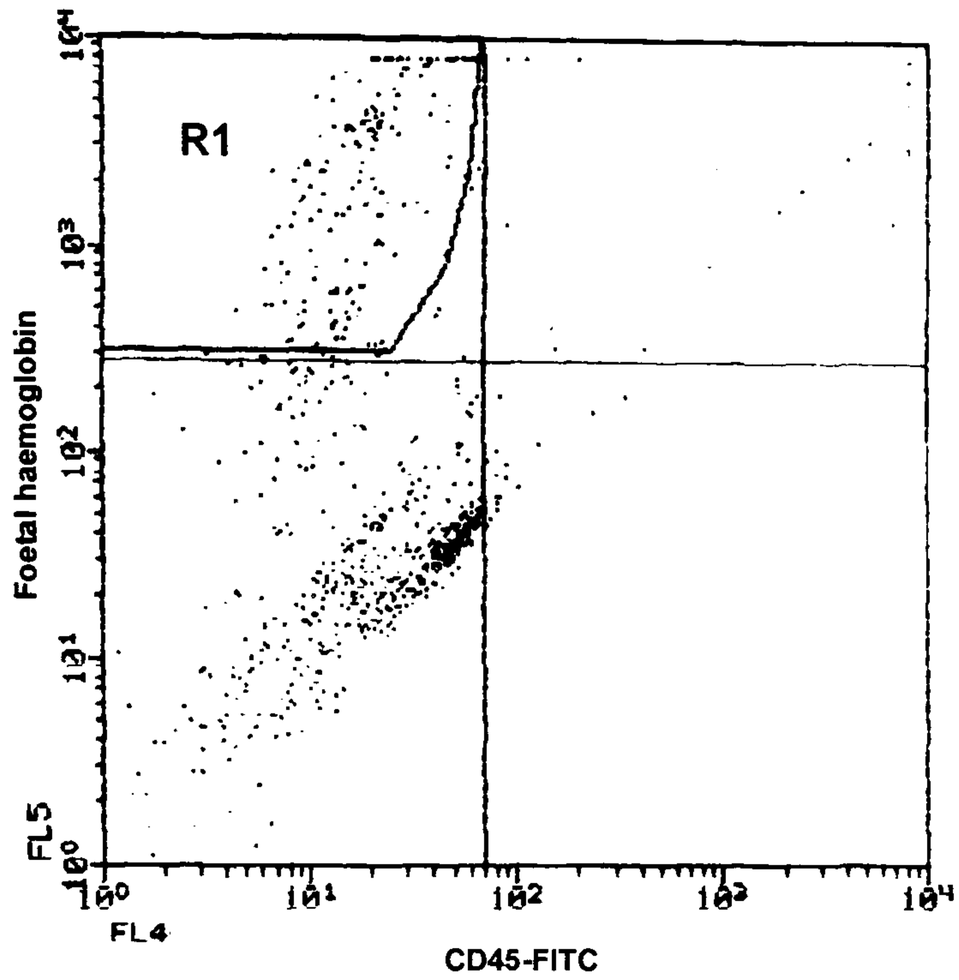

Figure 8-3. FACS data showing the purity of fnRBCs derived from cord blood following enrichment using density gradient centrifugation and the $CD14^-$, $CD15^-$, $CD45^-$, and $CD71^+$ MACS protocol. Region R1 contains cells labelled as fnRBCs.

The samples were analysed using a FACS sorter to ascertain concentration of fnRBCs in the sample. The FACS data of figure 8-3 shows that, following the enrichment protocol described above, approximately 30% of the cells in the sample were fnRBCs. Two different cord blood samples gave similar purities for fnRBCs following pre-processing and labelling steps. To conclusively demonstrate that the cells gating in region R1 of the FACS plot were foetal in origin, cells from this region were sorted onto glass slides using the FACS machine. The cells were identified for sorting by gating on the fluorescence signal associated with the fluorescence label of the gamma-chain of foetal haemoglobin (anti-HbF), and the fluorescence of the nuclear staining (Hoechst 33342). Additionally, the cells had to be CD45 negative (i.e. non leucocytes).

A fluorescence image of a labelled fnRBC isolated with the gating conditions described above is shown in figure 8-4. This cell was sorted onto a glass slide and subsequently FISH labelled (see chapter three), to demonstrate the cell's foetal nature. The X- and Y-chromosomes were labelled and can be seen as the pale blue and pink spots within the cell nucleus. The diffuse blue staining is DNA labelled with the Hoechst dye, and the orange halo around the cell is the γ-hemoglobin. All the cells sorted onto the glass slides, under the above conditions, exhibited similar labelling.

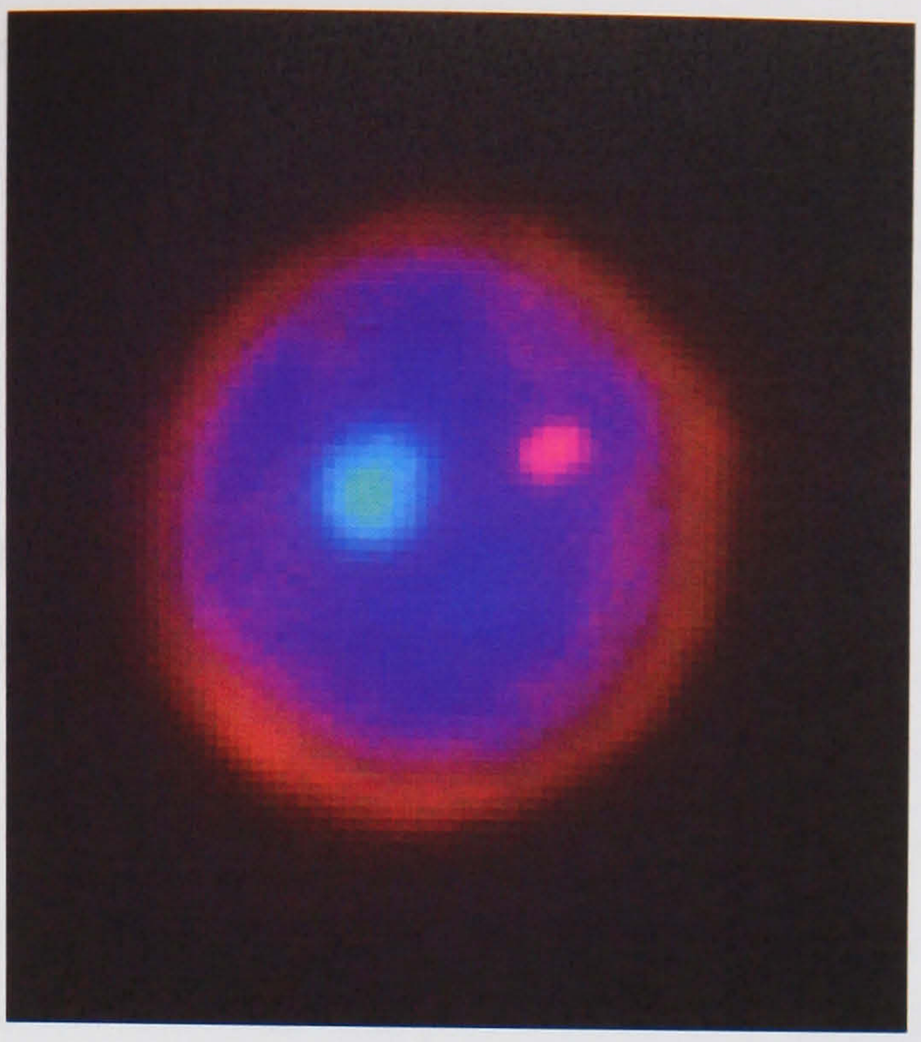

Figure 8-4. Fluorescence image of a fnRBC showing the X- and Y-chromosomes (pale blue and pink respectively), the nucleus (blue) and the γ-haemoglobin (orange on the inside of the cellular membrane).

The cells not used for FACS analysis, were suspended in a suspending medium of known conductivity. The osmolality of the separation medium could not be measured (and therefore finely adjusted), due to the lack of an osmometer in the Boston lab. There is therefore some doubt as to the exact value of the suspending medium osmolality, but should be in the region of ~290mOsm^{-1}. The suspending medium consisted of dH_2O with 9% (w/v) sucrose, 0.1% (w/v) glucose, 0.8% (w/v) BSA and 1mM EDTA. The pH (6.8-7.2) and conductivity were adjusted by the addition of phosphate buffer.

30μl of the cell suspensions at each of the conductivities (in the range 20 – 120mSm^{-1}) were applied to an array of interdigitated castellated micro-electrodes (similar to those shown schematically in figure 1-10) patterned onto a glass microscope slide. These electrode arrays had a typical feature size of 50μm. A coverslip was placed over the suspension allowing the cells to be viewed using a microscope. A signal generator was used to apply a voltage of approximately $5V_{pp}$ to the electrodes in the 100kHz – 1MHz frequency range. Adjustment of the frequency caused the cells to undergo either +veDEP or -veDEP (i.e. movement to or from the electrode edges), at the crossover frequency point the cells experienced neither +ve or –veDEP and remained stationary with respect to the electrode edge. Increasing the frequency caused the cell to be attracted to the electrode edge and a decrease in frequency caused the cell to be repelled from the electrode edges. The motion of the cells was observed as the applied field frequency was varied and the crossover frequency for individual cells noted. Visual identification of the cells used for the cross-over measurements was carried out to select for fnRBCs, with identification being based on the rejection of RBC (bi-concave disc morphology) and cell debris.

Control samples were also run to ascertain whether the presence of MACS beads on the surface of the cells change the cell's dielectric properties. Female RBCs were obtained, from a volunteer, and crossover measurements made on these cells with and without glycophorin-A (GPA, an erythrocyte specific antigen) conjugated MACS beads attached to their surface.

8.3.2 Results and discussion: DEP crossover measurements on fnRBCs

Measurements of the crossover frequencies were performed on multiple cells (typically 15-20 cells) for various measured suspending medium conductivities. Two samples of cord blood were collected. The first, sample 1 was used for crossover measurements with suspending medium conductivities in the 70 – 120mSm^{-1} range. The second sample (sample 2) was used for crossover measurements in the lower conductivity region 20 – 40mSm^{-1}. The measurement data is plotted in figures 8-5 and 8-6. The size of the cells was measured as $a = 3\mu m$.

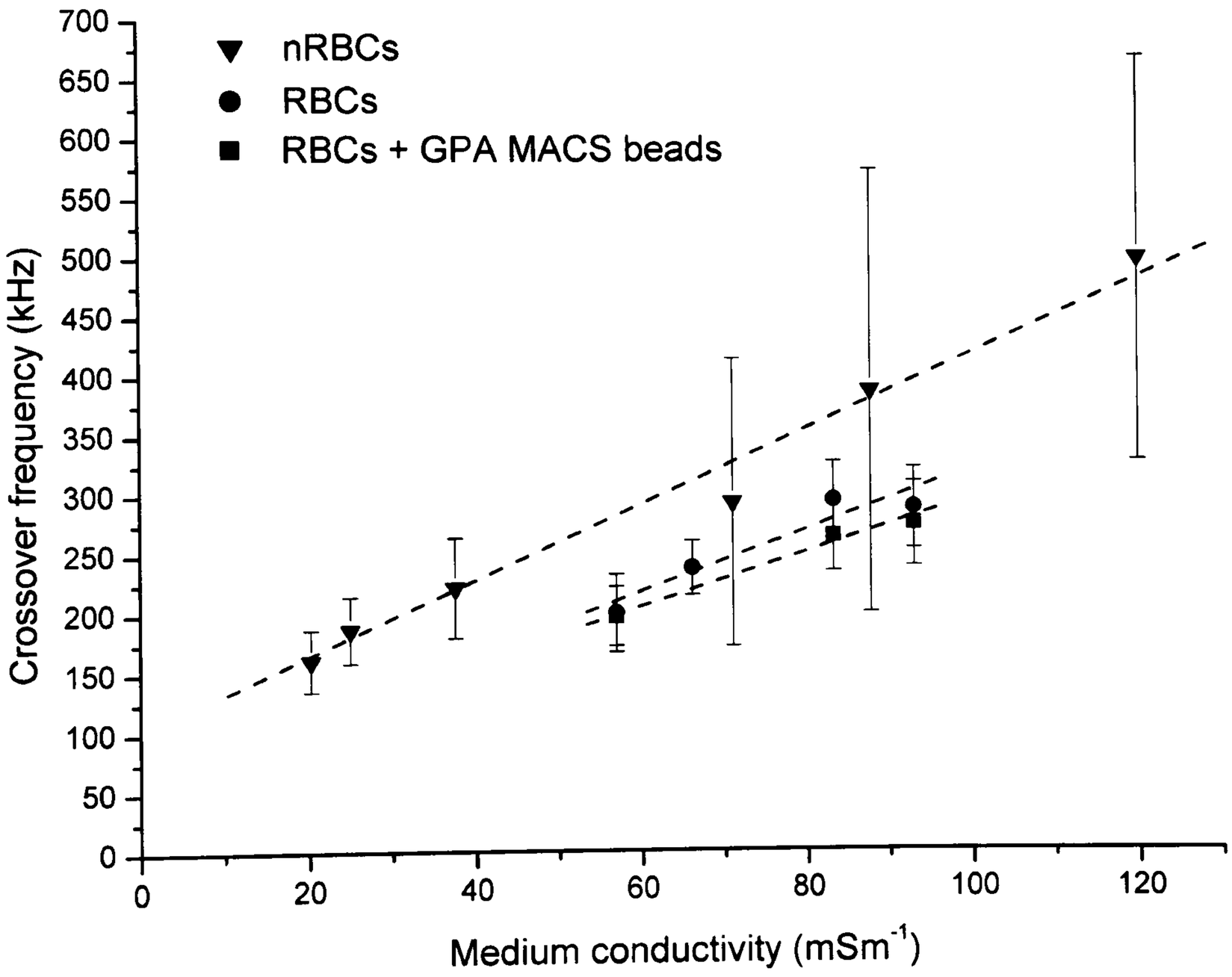

Figure 8-5. Variation of crossover frequency with suspending medium conductivity for nRBCs, and RBCs (with and without attached MACS beads).

8.3.2.1 RBC controls

Equation 2-60 in chapter two gives the value for the DEP crossover angular frequency. This can be written in terms of DEP crossover frequency f_x as in equation 8-1 below.

$$f_x = \frac{1}{2\pi}\left(\frac{(\sigma_m - \sigma_p)(\sigma_p + 2\sigma_m)}{(\varepsilon_0\varepsilon_p - \varepsilon_0\varepsilon_m)(\varepsilon_0\varepsilon_p + 2\varepsilon_0\varepsilon_m)}\right)^{\frac{1}{2}} \quad (8\text{-}1)$$

where ε is the permittivity and σ is the conductivity, and the subscripts p and m represent the particle and the medium respectively.

Equation 8-1 can be simplified to the form [23],

$$f_x = \frac{\sqrt{2}}{8\pi R C_{Smem}}\left((4\sigma_m - aG_{smem})^2 - 9a^2 G_{Smem}\right)^{\frac{1}{2}} \quad (8\text{-}2)$$

where $C_{Smem} = \varepsilon_{mem} / d$ is the effective specific membrane capacitance and $G_{Smem} = \sigma_{Smem} / d$ is the specific membrane conductance, where d is the membrane thickness, and ε_{mem} and σ_{smem} are the membrane permittivity and conductivity. ε_{mem} is derived from the slope of the graph in figure 8-5 and σ_{smem} is derived from the horizontal axis intercept using the following relations [23, 24],

$$C_{smem} = \frac{\sigma_m}{\pi\sqrt{2} f_0 a} \quad (8\text{-}3)$$

and,

$$G_{smem} = \frac{4\sigma_m \times intercept}{f_0 a^2}. \quad (8\text{-}4)$$

The crossover measurements for the control RBCs resulted in a calculated membrane capacitance of 21mFm^{-2}. This value is quite different to that expected from previous studies ~9mFm^{-2} [24]. The reason for this is unclear, but is probably due to sub-optimal suspending medium conditions. RBCs are highly susceptible to suspending medium osmolality, more so than most nucleated cell types. Unfortunately, due to the lack of an osmolality metre in Dr Bianchi's lab, there was no way of measuring the osmolality of the suspending mediums used for these experiments. Any variation in the medium osmolality away from the ideal, iso-osmotic condition would result in the RBCs swelling or shrinking. This stress on the cells could account for the anomalous results. The use of RBCs as a control was therefore not a good choice. The ability of nRBCs to cope with changes in the osmolality conditions is not known. However, one would assume that nRBCs would be less affected by osmolality variations than the RBCs, due to the presence of a nucleus and the small cytoplasmic volume of this cell type.

8.3.2.2 RBCs with GPA-conjugated MACS beads

The control sample containing the RBCs with conjugated MACS beads had a similar membrane capacitance to that of the naked RBCs. This suggested a common problem with the suspending medium osmolality. The MACS beads are typically 20nm in diameter. There was no observable difference in the dielectric properties of the RBCs, with or without the GPA (Glycophorin A) conjugated MACS beads attached to the cell's surface. Typically, an erythrocyte has between $2x10^5$ and $1x10^6$ GPA receptors on its cell membrane. Therefore it is to be expected that nRBCs have a similar number of CD71, transferrin receptors on their surfaces, and consequently a similar number of MACS beads would be expected to be present on the surface of the nRBCs.

The lack of effect on the dielectric properties, with MACS beads attached to the surface of the RBCs, is in agreement with observations made on cells derived from the monocytic cell line THP-1 (see chapter six). The crossover frequency of THP-1 cells was observed, with and without CD14 MACS beads attached to their surface. No difference in the crossover frequency, and therefore no change in the cell's dielectric properties were observed with the MACS beads attached. Measurements of the electrophoretic mobility of these cells, with and without the MACS beads attached, showed no change when measured using a zeta potential analyser (DELSA440, Beckman Coulter, (data not shown)). Similar observations have been reported in the literature, Yang *et. al.* [5] describe DEP separation of the main leukocyte subpopulations using DEP-FFF (see chapter one). In these experiments they observed no difference in the elution time of the cells from their DEP-FFF device for cells with or without MACS beads attached to their surfaces. Their separation system relies upon –veDEP forces to levitate the cells within the flow channel. Differences in the mean levitation heights of the different leukocyte subpopulation within the flow channel, results in the cell populations having different mean velocities in the channel, and therefore different elution profiles. One would expect any changes in the dielectric properties, as a result of the attachment of the MACS particles to the cell's surface to be seen as a change in the elution profiles. As these changes were not observed, it was concluded that the attachment of the MACS beads has no observable effect on the dielectric properties of a cell under the experimental conditions used.

8.3.2.3 fnRBC

Only approximately 30% of the cells in the processed cord blood samples (used for crossover measurements) were fnRBCs (see FACS data of figure 8-3). Many of these cells were likely to have been contaminating cells not removed by the pre-processing steps. Visual identification and selection of nRBCs was therefore necessary for the crossover measurements.

The data of figure 8-3 shows that there is a difference in the measured membrane capacitance of the fnRBCs, compared with that of the typical mature RBCs (i.e. ~9mFm^{-2}). This would be expected as nRBCs have quite different morphology to RBCs. Whereas RBCs have a bi-concave disc morphology, nRBCs and fnRBCs are spherical and have an average radius of approximately 4μm making them similar in size and shape to leukocytes.

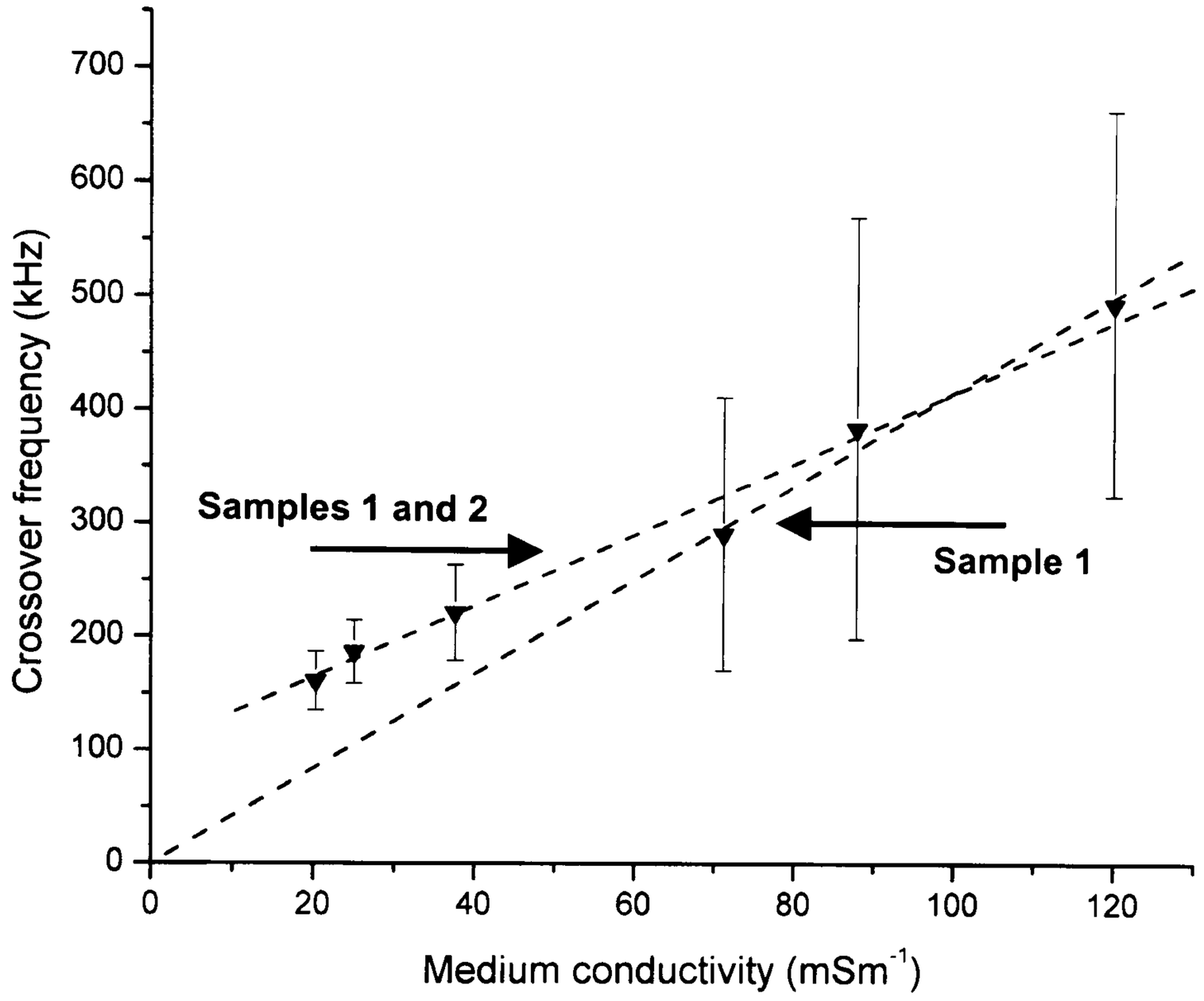

Figure 8-6. Variation of crossover frequency with suspending medium conductivity for nRBCs. The slope of higher gradient was calculated using the crossover data obtained from the three highest suspending medium conductivities.

Figure 8-6 shows the variation in crossover frequency with suspending medium conductivity for nRBCs. The lines of best fit are shown using the crossover data obtained combining both samples, and using only sample 1 (i.e. the three highest medium conductivities). The results of the crossover measurements for both cord blood samples (samples 1 and 2) gives a value of 17.7mFm^{-2} for the specific membrane capacitance. Previous studies have demonstrated the detrimental effect of ion leakage from cells undergoing electrorotation and DEP crossover measurements while suspended in media of low ionic strength (e.g. [25]). The duration over which the cells remained in the experimental media while the crossover measurements were being made, could be expected to have resulted in substantial changes to the cell's physical and dielectric properties. Using the data obtained from only sample one gives a value of 13.4mFm^{-2} for the membrane capacitance. This figure suggests that the dielectric properties of the fnRBC

are not significantly different from that of the other blood cell types, considering only the preliminary results obtained using sample one.

If one considers both samples 1 and 2, and takes the value at which the line of best fit intersects the horizontal axis, the specific membrane conductance is calculated to be 127,000 Sm^{-2}. The data from sample 1 is too scattered to give a meaningful value of specific membrane conductance. Typical values for the specific membrane conductance of blood cells are given in the literature and are of the order 3300 Sm^{-2} for leukocytes [2, 3].

Unfortunately, the cell samples measured were contaminated with other cell types, and although visual identification of the sample was used to try and select for fnRBCs, inevitable errors will have been made. It might be expected that a number of distinct populations, representing different cell types with different dielectric properties, would appear from the data if the number of cells measured had been greater. However, as the sample size was relatively small, with approximately 15-20 cells being measured at each of the different conductivities, this effect remains hidden. The relatively high value of 17.7mFm^{-2} for the membrane capacitance, suggests that the fnRBC type may also be amenable to isolation using the DEP separation methods described in this thesis. The more reasonable value of 13.4mFm^{-2} would suggests that the fnRBC has dielectric properties similar to that of the human leucocytes, thus making the prospects for separation of fnRBCs from maternal blood using the DEP methods rather poor.

8.3.3 Conclusion

Further work is required in order to overcome some of the problems associated with the measurements made on the fnRBC samples. However, the data is suggestive of a slight difference in the dielectric properties of these cells compared with that of the average PBMC. Whether DEP separation techniques would be sufficiently sensitive to isolate these cells from maternal blood samples is therefore still unclear. Due to the work having been carried out while visiting another lab it was not possible to take this work further.

8.4 Surface functionalisation of the separation chamber

Application of a +veDEP force within the separation device results in the collection of cells at the edges of the energised electrodes. Cells also collect over the electrodes and in the spaces between the electrodes. The cells are therefore held in close proximity to the channel wall under the influence of the +veDEP force for the duration of the experiment (30min – 60min), allowing time for interaction with the channel surfaces. Cessation of the applied electric field, or application of a –veDEP force field ejects the majority of these cells from the electrode surfaces,

but it was found that 5-10% of the cells consistently remain attached to the surface (see section 7.5.4). This adhesion of cells occurs non-specifically and disrupts experiments. In order to facilitate the release of these cells from the chamber surfaces, and allow the retrieval of all the cells from the separation device, a number of approaches involving the alteration of the flow channel surfaces were investigated.

The investigations had a two-fold aim; firstly to alter the device surfaces in order to reduce the non-specific adhesion of blood cells, and secondly to attempt to increase the system retention specifically for trophoblast cells. As a model system, glass coverslips were functionalised by the addition of various molecules. These included BSA, human anti-CD45, whole laminin (derived from human placenta), and a laminin peptide fragment.

Loke *et al.* [26-28] has shown that human extravillous trophoblast cells could be isolated from a mixture of PBMCs using laminin-coated magnetic beads. Other extracellular proteins (e.g. fibronectin) have been shown to interact with trophoblast but not as specifically as laminin. The effect of chemically functionalising the inner surfaces of the separation chamber with these molecules was investigated for this thesis.

A non-stick polymer poly(MPC-co-33-BMA) was also tested for its anti-adhesive properties. The polymer is synthesized from 2-methacryloyloxyethyl phosphorylcholine (MPC) and butyl methacrylic acid (BMA), and forms a polymeric surface coating when applied to the glass substrate. The polymer coating is composed of phospholipid polar groups and has a structure similar to a phosphotidylcholine biomembrane. The glass surface of the separation device, when coated with the polymer, presents a biomimetic surface to approaching proteins, platelets and cells. This family of polymers have been shown to have excellent *in vivo* non-thrombogenicity. No studies to date have investigated the polymers usefulness as an anti-adhesive coating with respect to cell types other than that of blood cells, with the majority of the studies concentrating on the polymer's efficacy for reducing adhesion of platelets.

8.4.1 Materials and methods

Glass coverslips were functionalised as described below. Suspensions of trophoblast and suspensions of PBMCs were made up at defined cell concentrations in either PBS or the Ficoll free dielectrophoretic separation medium (see section 3.11.2). The samples were pipetted onto the functionalised glass coverslips and the cells left to sediment onto the slides for 30 minutes. This time was chosen to simulate the time cells would spend in the separation chamber during a typical separation experiment. The coverslips were washed gently and the percentage of cells, as a measure of the original cell concentration, adhering to the glass was determined by counting.

The strength of adhesion of individual cells was observed using interference reflection microscopy (IRM) (see below). The distance between the cell and the substrate has been shown to correlate with the strength of adhesion of the cell to the substrate [33].

8.4.1.1 Preparation of PBMCs and trophoblast

Peripheral blood samples were obtained from both healthy male and pregnant female volunteers, according to the protocol given in chapter three. Peripheral blood mononuclear cells (PBMCs) were obtained by diluting whole blood 1:2 with PBS (1mM EDTA). Samples were processed on a Histopaque 1077 gradient with the buffy coat collected, washed, and the cell pellet resuspended in PBS or separation medium (dH_2O with 9% w/v sucrose, 0.1% w/v glucose, 0.8% w/v BSA and 1mM EDTA).

Trophoblast cells were obtained from placental membranes using the enzymatic digestion technique described in chapter three. Placentas were obtained from healthy non-smokers undergoing caesarean section. The cells were resuspended at known concentration in PBS or separation medium. Cell counts were performed using a haemocytometer. The dielectric separation media had pH 6.8-7.2 and osmolality ~290mOsm^{-1}.

The surface of the glass coverslips were functionalised as described below, and the cells were allowed to sediment out of solution onto these surfaces. After a predefined time (30 minutes), the slides were washed gently in PBS and the cells were fixed with 2% formaldehyde in PBS. The number of cells adhering to the glass substrates was counted using an inverted microscope, in phase contrast. These same substrates were then used for the IRM and SEM work. The SEM samples required an additional dehydration protocol (see chapter three).

8.4.1.2 Surface functionalisation

Glass coverslips (22mm x 22mm x 0.1mm) were cleaned in Caro's acid (7:1, H_2SO_4:H_2O_2) for twenty minutes, to remove any organic matter and expose the surface hydroxyl groups. 3-Aminopropyltrimethoxysilane (APTS) (Sigma, A1435) was dissolved in 95% ethanol, 5% dH_2O to give a 1% solution. The glass coverslips were immersed in the APTS solution for 2 minutes. This provided surface amino groups for attachment of secondary molecules.

Romagnano *et. al.* [29] reported experiments carried out to study the interaction of trophoblast with laminin *in vitro*. They found that trophoblast attachment and spreading on laminin matrices was competitively inhibited in the presence (in solution) of the laminin peptides YIGSR (Tyr-Ile-Gly-Ser-Arg), RGD (Arg-Gly-Asp), and IKVAV (Ile-Lys-Val- Ala-Val). This suggests that the adhesion molecules responsible for adhesion of the trophoblast to the laminin matrix were

binding these peptides and becoming blocked. The laminin peptide chosen for use in the current study contained the IKVAV sequence. It should be noted that the above study was carried out using mouse trophoblast cells, whether the peptide sequence used in this study is present in the human placenta cytotrophoblast basement membrane needs clarification.

Laminin peptide fragment: Cys-Ser-Arg-Ala-Arg-Lys-Gln-Ala-Ala-Ser-Ile-Lys-Val-Ala-Val-Ser-Ala-Asp-Arg (Sigma, C6171) was attached to the glass surface via a heterobifunctional crosslinker, sulfo-GMBS (Pierce, No.22324, Illonois USA). A 0.2mM solution of sulfo-GMBS in 50mM phospate buffer (pH8) was allowed to react with the amine derivitised surface of the glass for 1 hour at room temperature. The glass was then rinsed with PBS and dH_2O. 1μM synthetic laminin peptide in phosphate buffer (pH7) was subsequently applied to the surface for 2 hours. The cover slips were finally rinsed with PBS.

Whole human laminin molecule (Sigma, L6274), bovine serum albumin (BSA) (Sigma, A3294), and monoclonal anti-human CD45 antibody (Sigma, C7556) were attached via a simpler two-step process. After silanisation the glass was immersed in a solution of 2% gluteraldehyde (Sigma, G7526) in PBS with 40mM sodium cyanoborohydride ($NaCNBH_3$) (Sigma, S8628) for 1 hour at R.T. The glass was rinsed with dH_2O. 0.1μg/ml solutions of each of the proteins (in PBS with 40mM $NaCNBH_3$) were applied to the glass surface and allowed to react for 1 hour at R.T. The slides were washed twice in PBS and then immersed in 0.1M glycine (Sigma, G7403) in PBS for 1 hour, before rinsing with PBS. All the reagents and solution were freshly made.

The poly(MPC-co-33-BMA) was supplied by Dr Peter Rolfe, University of Keele. The polymer came as a dry powder, and was dissolved 1:50 (w/v) in ethanol. The polymer solution was applied to the surface of the glass cover slips by pippetting a small amount of the solution onto the surface of the glass, leaving for a few seconds and then rinsing with dH_2O. This procedure forms a layer of adsorbed polymer on the surface of the glass.

8.4.1.3 Interference reflection microscopy

Interference reflection microscopy (IRM) is an optical technique for measuring the thickness of thin films. Curtis was the first to apply it to the study of cell adhesion in 1964 [33]. For the case of a cell adhering to glass there is a thin film of intercellular medium between the cell's plasma membrane and the glass. Differences in the refractive indices of the glass, medium and plasma membrane result in reflective interfaces between the different materials. When an intense beam of monochromatic light is projected with normal incidence onto the interfaces, interference occurs due to phase differences in the light reflected from the different interfaces. The intensity

of the reflected light is related to the separation of the interfaces. Distances down to about 50Å can be accurately measured. IRM allows quantitative analysis of distance between the adhering cell and the glass surface. Cells adhering more strongly to glass substrates typically have higher numbers of focal adhesion points, which appear as darker regions in the IRM image. Focal adhesion points are regions of close contact between the glass and the cell [33].

Interference reflection microscopy (IRM) of adhering cells was carried out using equipment in the laboratory of Prof. ASG Curtis, Centre for Cell Engineering, IBLS, Glasgow University. The coverslips with the adhering cells were fixed in formaldehyde and gently rinsed with dH_2O to remove any salt crystals from the sample (residue from evaporated PBS) and mounted cell side down on oil filled cavity slides. The cells were viewed using the IRM microscope with attached video camera and image capture and analysis software.

8.4.2 Results and Discussion

The number of cells adhering to the glass coverslips were counted and expressed as a percentage of the total number of cells in the sample. Cell numbers were counted for each glass coverslip, the data is shown below in tables 8-2 and 8-3. The cell samples were suspended in either PBS or the sucrose based (Ficoll free) dielectric separation medium. The dashes in tables 8-2 and 8-3 represent missing data points, resulting from loss or damage of the coverslips during the course of the experimental work.

Suspending medium	Laminin	Laminin peptide	BSA	MPC	Glass	Anti-CD45
PBS	12	12	12	37	62	-
PBS	8	16	16	39	31	-
PBS	42	34	-	17	59	93
PBS	36	54	28	17	50	84
Medium	17	34	84	-	-	84
Medium	29	27	67	10	20	62

Table 8-2. Percentage PBMCs from the suspension adhering to the substrate after 30 minutes.

Suspending medium	Laminin	Laminin peptide	BSA	Poly MPC-co-BMA	Glass
PBS	8	10	8	4.5	3
PBS	7.5	9.75	8.25	3	3
PBS	21	84	-	-	63
PBS	21	84	25	9	9
Medium	14	8	11	1	1.5
Medium	44	44	-	-	22
Medium	12	8.25	11.25	1.5	1.5
Medium	44	44	34	5	8

Table 8-3. Percentage trophoblast from the suspension adhering to the substrate after 30 minutes.

The human anti-CD45 antibody was chosen as a control molecule. This antibody recognizes the CD45 leukocyte common antigen family present on all cells of leukocyte lineage; it should therefore bind all PBMCs with good affinity. This was indeed observed, with the PBMCs having a high affinity for the anti-CD45 coated surface, indicating that the surface functionalisation was working.

Due to the small size of the data set and variability of the data no clear differences in the pattern of adhesion is immediately apparent. Statistical analysis of the data was therefore undertaken to determine if there was any significant difference between the various substrates, or differences between the use of PBS or the sugar solution suspending media. A two-factor ANOVA (analysis of variables) with repeated measures test was used to analyse the data. This was followed by a post hoc Tukey-test. For the PBMCs a weakly significant ($p=0.039$) difference was found between the cells adhering to the MPC and BSA substrates, with more cells adhering to the BSA coated substrate. No difference was found for the different suspending media. As mentioned above the anti-CD45 coated surface showed a marked increase in the number of PBMCs adhering to it and a statistically significant increase in the percentage of cells adhering to this substrate ($p=0.0011$).

For the trophoblast data the two-factor ANOVA with repeated measures test was again used and in this case showed a minor statistical differences between the substrates. Further analysis of the data using a post hoc Tukey-test showed a weak statistically significant ($p=0.0656$) difference between the number of cells adhering to the glass substrate and the MPC layer.

Analysis of the difference in the adhesion properties between the two cell types and all the substrates showed very little difference between the various surface functionalisations. The trophoblast showed a reduced adhesion to the MPC layer when compared with the PBMCs. The idea that the whole laminin or the laminin peptide could be used to increase the affinity of the channel walls to retain the trophoblast cells on the interior of the separation chamber (in preference to PBMCs) has not been demonstrated by this data.

The results of this study do not show an advantage for using the whole laminin or the laminin peptide instead of the untreated glass. It has been shown by others that the adhesion of trophoblast cell lines is strongly influenced by the laminin type [30]. Further investigation of different laminin subtypes might be expected to reveal differences, and give more positive results.

The non-stick polymer appears to reduce the adhesion of trophoblast compared with the untreated glass surface. The BSA functionalised surfaces had little effect on the surface adhesion for both cell types, when compared with the untreated glass surface. This was surprising as BSA is widely used to block surfaces and reduce non-specific protein interactions at surfaces. Protein adsorption onto a surface is widely recognised as a pre-cursor to cellular adhesion.

The interaction of cells with laminins and fibronectin is mediated largely by integrin type receptor family subunits [31]. For example the pattern of staining for the alpha5, alpha6, beta1 and beta4 subunits indicates that the integrins expressed by trophoblast are predominantly the alpha5beta1 and the alpha6beta4 heterodimers [30]. It has been shown that early trophoblast cells adhere to peptide in the E8 domain of laminin using a mechanism that is independent of the one used for adhesion to fibronectin [32], suggesting that laminin should be a better choice for this work. Choosing a peptide fragment containing the above-mentioned heterodimers may result in increased adhesion of the trophoblast cells to the substrate.

Figure 8-7 shows an SEM image of an isolated trophoblast adhering to an untreated glass surface. The cell can clearly be seen to be starting to spread across the glass surface with projections emanating from all sides of the cell. The image is typical for a trophoblast after only 30 minutes incubation on such a substrate.

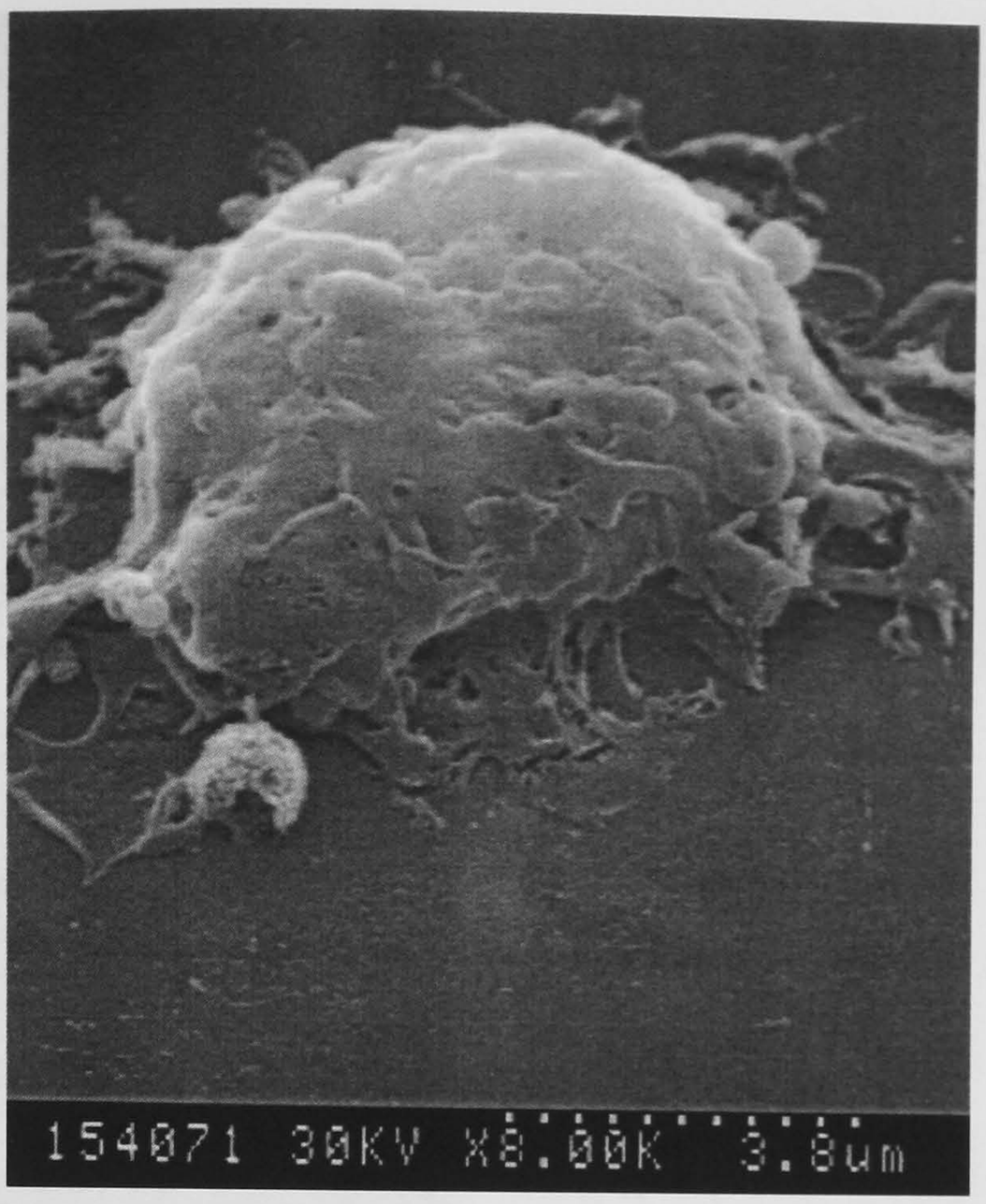

Figure 8-7. SEM of an isolated trophoblast on glass.

8.4.2.1 Interference reflection microscopy

The IRM data are presented in figure 8-8. Briefly, IRM images are produced due to reflections arising at the interfaces between the glass, medium and the cell's plasma membrane. Interference occurs due to phase differences in the reflected light arising from the different interfaces. The intensity of the reflected light is directly related to the distances a cell is from the glass substrate, down to a lower limit of 5nm. IRM therefore allows quantitative analysis of the adhesion of a cell to a transparent surface. Points of strong adherence (i.e. small cell to substrate distances) correlate with dark areas on the IRM images.

The IRM data in figures 8-8 (a) – (c) show the trophoblast cells interacting with the surfaces. The trophoblast on the laminin coated surfaces (figures 8-8 (b) and (c)) give IRM images with a much darker profile. These cells are exhibiting a much stronger interaction with the laminin surfaces, than that of the glass coated with non-stick polymer. Regions of focal contact (dark spots) can be clearly seen in these images. The IRM images of the trophoblast cells on the non-stick polymer coated slide (figure 8-8(a)) show weak adhesion of these cells to the glass surface. The same effect was seen for the PBMCs plated onto this surface.

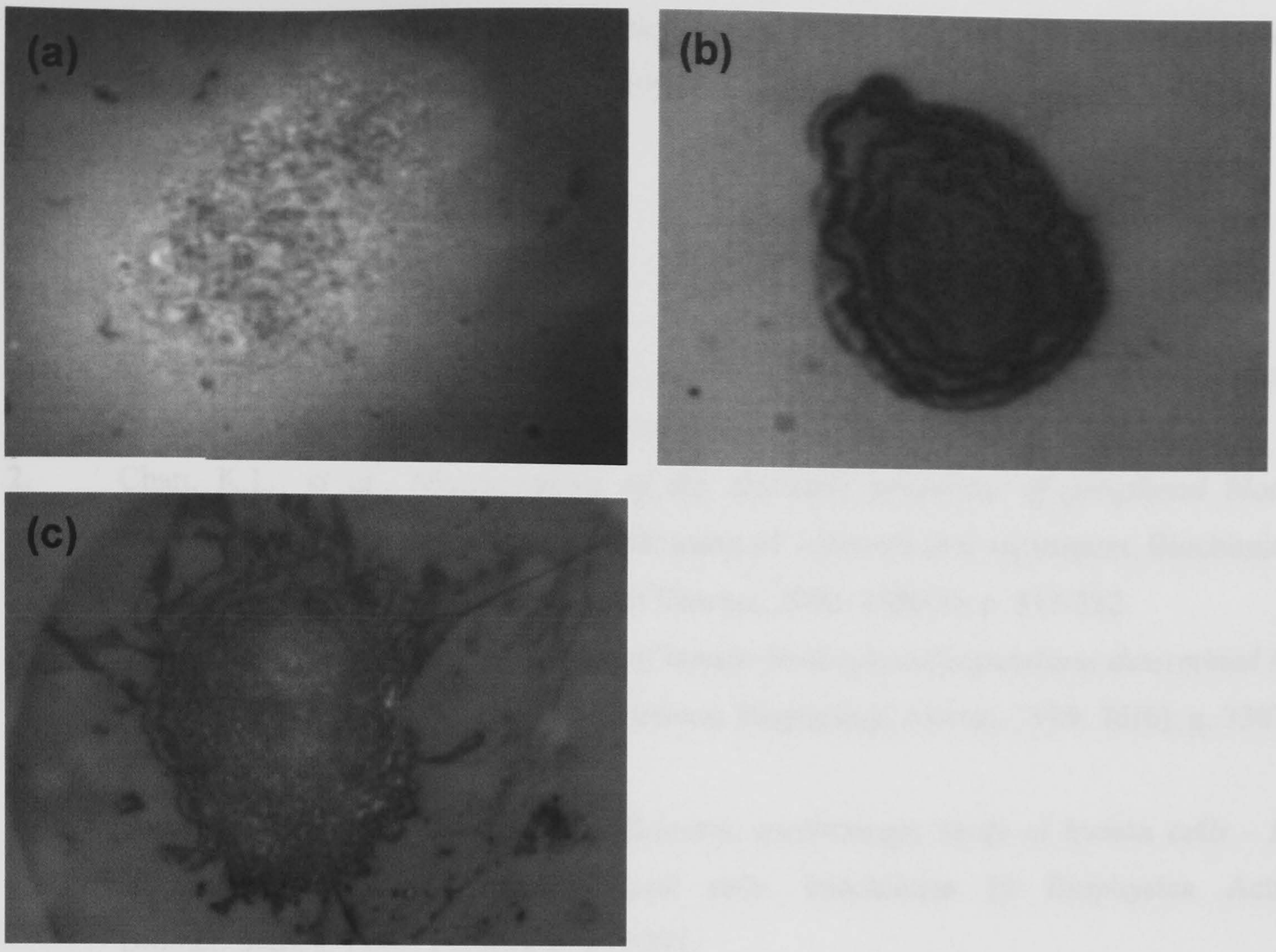

Figure 8-8. IRM images of trophoblast cells adhering to glass surfaces with (a) no surface functionalisation, (b) whole laminin surface, and (c) laminin peptide surface.

It has been reported that isolated trophoblast cells assume a flattened, sessile phenotype when cultured on laminin but tend to exhibit a more spreading, motile morphology when plated onto fibronectin coated surfaces [30]. The whole laminin coated surface exhibited strong cell adhesion (large numbers of cells adhering, and lots of black in the IRM image) but with few outgrowths (lamellaepodea etc.), in accordance with the previous study [30]. However, cells adhering to the glass functionalised with the laminin peptide showed greater spreading, more like that expected from cells plated on fibronectin coated substrates. One possible reason for this is that the functional epitope on the laminin and fibronectin molecules is the RDG sequence. This is the integrin binding epitope and is the main functional, binding part of these molecules. Differences in the structures of the molecules containing this RDG sequence results in differences in their binding efficacies. The laminin peptide used does not contain a RDG sequence and may therefore cause effects more like that expected of the fibronectin molecule than that of the whole laminin molecule.

Based on the above results the internal glass and electrode surfaces of the separation device could be modified, by the addition of proteins and other forms of chemical functionalisation. Judicious choice of peptide fragment could allow enhanced performance of these surfaces. This

would allow the cells flowing in the separation system to not only interact with the electric fields (DEP forces) but also to have a strong differential affinity for the channel walls.

8.5 References

1. Walknowska, J., F.A. Conte, and M.M. Grumbach, *Practical and theoretical implications of fetal/maternal lymphocyte transfer.* Lancet, 1969. **i**: p. 1119-1122.
2. Chan, K.L., *et al.*, *Measurements of the dielectric properties of peripheral blood mononuclear cells and trophoblast cells using AC electrokinetic techniques.* Biochimica Et Biophysica Acta-Molecular Basis of Disease, 2000. **1500**(3): p. 313-322.
3. Yang, J., *et al.*, *Dielectric properties of human leukocyte subpopulations determined by electrorotation as a cell separation criterion.* Biophysical Journal, 1999. **76**(6): p. 3307-3314.
4. Polevaya, Y., *et al.*, *Time domain dielectric spectroscopy study of human cells - II. Normal and malignant white blood cells.* Biochimica Et Biophysica Acta-Biomembranes, 1999. **1419**(2): p. 257-271.
5. Yang, J., *et al.*, *Differential analysis of human leukocytes by dielectrophoretic field-flow-fractionation.* Biophysical Journal, 2000. **78**(5): p. 2680-2689.
6. Covone, A.E., *et al.*, *Trophoblast cells in peripheral blood from pregnant women.* Lancet, 1984(Oct 13): p. 841-843.
7. Bruch, J.F., *et al.*, *Trophoblast-Like Cells Sorted From Peripheral Maternal Blood Using Flow-Cytometry - a Multiparametric Study Involving Transmission Electron-Microscopy and Fetal Dna Amplification.* Prenatal Diagnosis, 1991. **11**(10): p. 787-798.
8. Johansen, M., *et al.*, *An Investigation of Methods For Enriching Trophoblast From Maternal Blood.* Prenatal Diagnosis, 1995. **15**(10): p. 921-931.
9. Bianchi, D.W., *et al.*, *Fetal cells in maternal blood: NIFTY clinical trial interim analysis.* Prenatal Diagnosis, 1999. **19**(10): p. 994-995.
10. Bianchi, D.W., *Fetal cells in maternal blood: from pregnancy to autoimmune disease.* Clinical Chemistry, 2001. **47**(2): p. 7.
11. Bianchi, D.W., *et al.*, *Possible Effect of Gestational-Age On the Detection of Fetal Nucleated Erythrocytes in Maternal Blood.* Prenatal Diagnosis, 1991. **11**(8): p. 523-528.
12. Ganshirt, D., *et al.*, *Enrichment of fetal nucleated red blood cells from the maternal circulation for prenatal diagnosis: Experiences with triple density gradient and MACS based on more than 600 cases.* Fetal Diagnosis and Therapy, 1998. **13**(5): p. 276-286.
13. Durrant, L.G., *et al.*, *Isolation of fetal trophoblasts and nucleated erythrocytes from the peripheral blood of pregnant women for prenatal diagnosis of fetal aneuploides.* Early Human Development, 1996. **47**: p. S79-S83.

14. Bianchi, D.W., *et al.*, *Development of a model system to compare cell separation methods for the isolation of fetal cells from maternal blood.* Prenatal Diagnosis, 1996. **16**(4): p. 289-298.

15. Herzenberg, L.A., *et al.*, *Fetal cells in the blood of pregnant women: detection and enrichment by fluorescence-activated cell sorting.* Proceedings of the National Academy of Sciences U.S.A., 1979. **76**(1): p. 1453-1455.

16. Iverson, G.M., *et al.*, *Detection and isolation of fetal cells from maternal blood using the fluorescence-activated cell sorter (FACS).* Prenatal Diagnostics, 1981. 1(61-73).

17. Zheng, Y.L., *et al.*, *Demonstration of Spontaneously Dividing Male Fetal Cells in Maternal Blood By Negative Magnetic Cell Sorting and Fish.* Prenatal Diagnosis, 1995. **15**(6): p. 573-578.

18. Zheng, Y.L., *et al.*, *Search for the optimal fetal cell antibody: Results of immunophenotyping studies using flow cytometry.* Human Genetics, 1997. **100**(1): p. 35-42.

19. Zhen, D.K., *et al.*, *Poly-FISH: A technique of repeated hybridizations that improves cytogenetic analysis of fetal cells in maternal blood.* Prenatal Diagnosis, 1998. **18**(11): p. 1181-1185.

20. Bianchi, D.W., *et al.*, *Erythroid-Specific Antibodies Enhance Detection of Fetal Nucleated Erythrocytes in Maternal Blood.* Prenatal Diagnosis, 1993. **13**(4): p. 293-300.

21. Bianchi, D.W., *Current knowledge about fetal blood cells in the maternal circulation.* Journal of Perinatal Medicine, 1998. **26**(3): p. 175-185.

22. Samura, O., *et al.*, *Comparison of fetal cell recovery from maternal blood using high density gradient for initial separation step: 1.090 vs. 1.119.* American Journal of Human Genetics, 1999. **65**(4): p. 2089.

23. Huang, Y., *et al.*, *Membrane changes associated with the temperature-sensitive P85(gag-mos)-dependent transformation of rat kidney cells as determined by dielectrophoresis and electrorotation.* Biochimica Et Biophysica Acta-Biomembranes, 1996. **1282**(1): p. 76-84.

24. Gascoyne, P., *et al.*, *Dielectrophoretic detection of changes in erythrocyte membranes following malarial infection.* Biochimica Et Biophysica Acta-Biomembranes, 1997. **1323**(2): p. 240-252.

25. Arnold, W.M., A.H. Jager, and U. Zimmermann, *The Influence of Yeast-Strain and of Growth-Medium Composition On the Electrorotation of Yeast-Cells and of Isolated Walls*, in *Dechema Biotechnology Conferences, Vol 3, Pts a and B*. 1989. V C H Verlagsgesellschaft: Weinheim. p. 653-656.

26. Loke, Y.W., T. Burrows, and A. King, *Adhesion Molecules and Trophoblast Invasion.* Contraception Fertilite Sexualite, 1995. **23**(9): p. 573-575.

27. Loke, Y.W., L. Gardner, and A. Grabowska, *Isolation of Human Extravillous Trophoblast Cells By Attachment to Laminin-Coated Magnetic Beads.* Placenta, 1989. **10**(4): p. 407-415.

28. Burrows, T.D., *et al.*, *Human Trophoblast Adhesion to Matrix Proteins - Inhibition and Signal-Transduction.* Human Reproduction, 1995. **10**(9): p. 2489-2500.

29. Romagnano, L. and B. Babiarz, *Mechanisms of Murine Trophoblast Interaction With Laminin.* Biology of Reproduction, 1993. **49**(2): p. 374-380.

30. Burrows, T.D., A. King, and Y.W. Loke, *Expression of Integrins By Human Trophoblast and Differential Adhesion to Laminin or Fibronectin.* Human Reproduction, 1993. **8**(3): p. 475-484.

31. Engvall, E., *Laminin Variants - Why, Where and When.* Kidney International, 1993. **43**(1): p. 2-6.

32. Armant, D.R., *Cell-Interactions With Laminin and Its Proteolytic Fragments During Outgrowth of Mouse Primary Trophoblast Cells.* Biology of Reproduction, 1991. **45**(5): p. 664-672.

33. Curtis, A.S.G., *The mechanism of adhesion of cells to glass. A study by interference reflection microscopy*. Journal of Cell Biolology, 1964. **20**: 199-215.

Chapter Nine: Conclusions and future work

9 Achievements of this thesis

The realisation of a novel dielectrophoretic particle separation system, for the isolation of rare particles from large sample volumes and complex particle mixtures, involves a number of different technical issues. As a result of this, the work presented in this thesis is truly interdisciplinary in nature, and falls within the field of bioelectronics. A number of the techniques developed are potentially applicable to the technologies described as Lab-on-a-chip and micro-Total Analysis Systems. The review of cell separation methods given at the start of the thesis focussed on the recent developments in the field of microfabricated cell sorters. At present the development of such systems is proceeding with great speed.

Dielectrophoresis for cell separation was first postulated 50 years ago [1] and is currently enjoying renewed vigour as a separation technique in micro-systems – each year an increasing number of new papers are published on some application of dielectrophoresis. Indeed dielectrophoresis is becoming a widely recognised tool for particle separation, growing alongside more traditional separation techniques such as electrophoresis, FACS, MACS, centrifugation and others.

A new configuration of DEP particle separation device has been developed and constructed. Associated equipment to aid with sample injection and handling was also developed. The ability of the system to manipulate a variety of cell types (i.e. human blood, *E.coli* bacteria) and particles (sub-micron latex beads) types has been demonstrated. Furthermore, these experimental results were compared with a numerical model that was developed to simulate the trajectories of particles within the system. Variation in the applied signal (voltage and frequency) and characteristic electrode size were examined and the experimental results were found to vary in accordance with the predictions of the numerical model. Prediction of the mean banding position of THP-1 cells using the measured value of specific membrane capacitance ($17.7 \pm 2.7 mFm^{-2}$) is in good agreement with the actual experimental data. Similar experiments using peripheral blood mononuclear cells gave equally good agreement with the simulations (cell parameters taken from the literature [2]).

Dielectrophoretic particle chromatography is introduced as a novel means of particle separation. The proof of concept is demonstrated by the separation of two cell types labelled with different wavelength fluorescent probes. THP-1 cells were spatially separated from PBMCs along the length of an interdigitated electrode array of with individual electrode size 40μm.

The ability of the system to isolate rare particles from model systems such as artificial mixtures of cell types and latex beads (sizes ranging from 460nm to 10μm in diameter) was investigated.

Concentration of low numbers of cells as well as sub-micron latex beads from large sample volumes was demonstrated. Samples with particle concentrations in the region of 100 particles per mL were used. Scaling up of the separation system to allow the use on even greater sample volumes is potentially possible simply by running a number of similar devices in parallel.

The experimental work described in chapter eight, proved unsuccessful in its attempt to completely purify foetal cells from maternal blood samples. However, in the scope of this project, this was not entirely unexpected due to the shear magnitude of the problem. The dielectric properties of the particular cells targeted (i.e. trophoblast) were predicted from measurements made on cells isolated from the placental membranes by Chan *et. al.* [3]. These cells are probably not representative of the cells that make their way into the maternal circulation (i.e. they may have different dielectric properties), and therefore may not experience +veDEP at the frequencies used. The presence and number of foetal cells also varies throughout the course of pregnancy, and therefore the number of foetal cells in the samples prior to sorting was not known. Further work is required to test the ultimate resolution of the DEP separation system, and to assess its potential for rare cell isolation.

9.1 Suggestions for future work

A number of improvements to the system are possible, some of which have been discussed in the preceding chapters, but were not investigated due to time constraints.

9.1.1 Further characterisation of the lower limits of cell detection

As alluded to above, further characterisation of the system is required to allow quantification of the lower limit of particle numbers that can be isolated from a sample. Similarly, the absolute resolution of the system for separating mixtures of cell types is still unclear, this requires further experimental work. It is therefore necessary that a number of samples be run through the device under various operating conditions, and the pre- and post-sort samples analysed (by FACS, FISH, PCR, or other suitable methods). Work carried out by Bianchi *et. al.* [4] describe the use of a model system, where low numbers (down to the level of single cells) of 'model' male foetal cells were mixed into female peripheral blood mononuclear cells. The three main cell separation methods for the isolation of foetal cells from maternal blood were then compared (FACS, MACS, and immunomagnetic beads). Foetal cell yields and purities were assayed by a quantitative polymerase chain reaction (qPCR) using chromosomes Y- and 7-specific sequences. The use of a similar experimental protocol, to quantify the DEP separation system's ability to isolate rare cells, would allow the resolution of the system to be demonstrated.

9.1.2 Cyto-genetic analysis on-chip

Currently, the aim of much research and development in the microfluidic bio-chip area is the development of particle (e.g. cells, proteins) separation and manipulation techniques, equally as important is the performance of various analytical measurements. Integration of these separation and analysis steps into a single device is one of the central philosophies driving this area of research forward. The benefits arising from such 'complete' systems are huge and include: reduced size and cost of clinical diagnostic and scientific research systems, reduction in the size of sample required, increased speed of analysis, reduced reagent costs, portable systems.

On-chip analysis of the cells isolated by the separation device would reduce the need for sample handling and the loss of cells that this generally entails. This is obviously of greater importance when dealing with very low numbers of cells, as is the case for the foetal cells in maternal blood problem. Retention of the cells using +veDEP is limited by the requirements of a suspending medium of low conductivity. Unfortunately, most cell labelling and analysis protocols require the use of high conductivity media for the washing and labelling steps. Such high conductivity media result in -veDEP forces acting upon the cells at the frequencies used.

Functionalisation of the separation electrode array (see chapter 8) could potentially allow cells to be retained within the device, even when the DEP force was removed. The cells could then be labelled allowing cyto-genetic analysis (e.g. FISH) of the cells within the device, with the various buffers and labelling probes being introduced into the device via the channel inlet and outlet. The small volume of the channel (50μL) would lead to a reduction in the volumes of probes and buffers required. Laminin has been suggested as an adhesive substrate for trophoblast (see chapter 8), however there exists a plethora of possible surface functionalisation molecules which could be used to promote cell adhesion, depending on the cell type under investigation.

9.1.3 Development of the system

DEP has been shown to be useful for the separation and isolation of various cell types. The work presented in this thesis goes some way towards the development of a practical DEP cell separator.

9.1.3.1 Towards a bench-top DEP cell separation system

Many current cell separation techniques are moving further towards fully automated sample handling and analysis, with the operator introducing the sample (following minimal pre-treatment) into the system, and with the sorted cells being outputted after a short period of time.

Initial attempts using the LabVIEW™ programming language, to control the various components of the DEP separator were made with the aim of making the system semi-automated. With further automation the system could be developed to run as a fully automated cell separation system, with all pumps, valves and applied signals under microprocessor or PC control.

9.1.3.2 Expand useable applied frequency range

Changes in the electrode design to enable the use of higher applied signal frequencies would allow the efficient manipulation of bacteria and other particles, which may require the use of frequencies in excess of 100MHz to achieve -veDEP. To achieve suitable field strengths at such high frequencies requires that the impedance of the microelectrode arrays are matched to that of the signal source driving the electrodes (typically 50Ω). The design and construction of electrode arrays for use at frequencies of 200MHz or higher is possible with the use of strip-line techniques.

9.1.3.3 Increased sample handling capabilities

At present the system is capable of sorting particle samples at a rate of typically 1-2mLh^{-1}. Paralleling-up of the system would allow a linear increase in sample throughput, with relative ease, and is only a matter of fabrication. Issues of plumbing and heat production could potentially limit the practical size of such separation systems. However, practical systems capable of isolating cells from sample volumes of a few litres, in 15 minutes or so, should be relatively simple to realise.

9.1.4 Ideas for micro-flowcytometers

Using the interdigitated electrode array geometry, particles could be focussed into a narrow sheet but not a beam. However, it would be relatively simple to construct an orthogonal electrode array, which would confine the particles into a narrow beam. One example of such an electrode has been published by Fuhr's group [5]. The ability to produce such a well-defined narrow beam of particles would allow all the particles to be passed through a small detection zone in a manner similar to FACS systems. Furthermore, the positioning of the particles at the very centre of a channel would allow rapid sorting of the particles based on a method by which the particles are pushed away from the central axis by some force (e.g. optical pressure of -veDEP) and carried into one of a number of outlet channels.

Figure 9-1 shows preliminary work on a particle focussing system using an arrangement of four electrodes (two on the top and two on the bottom of the channel). The fluid is moving from left to right and the particles focused by the –veDEP forces into the centre of the flow channel (it should be noted that the channel has a constant cross-section along its entire length and only the electric fields are responsible for the particle focussing).

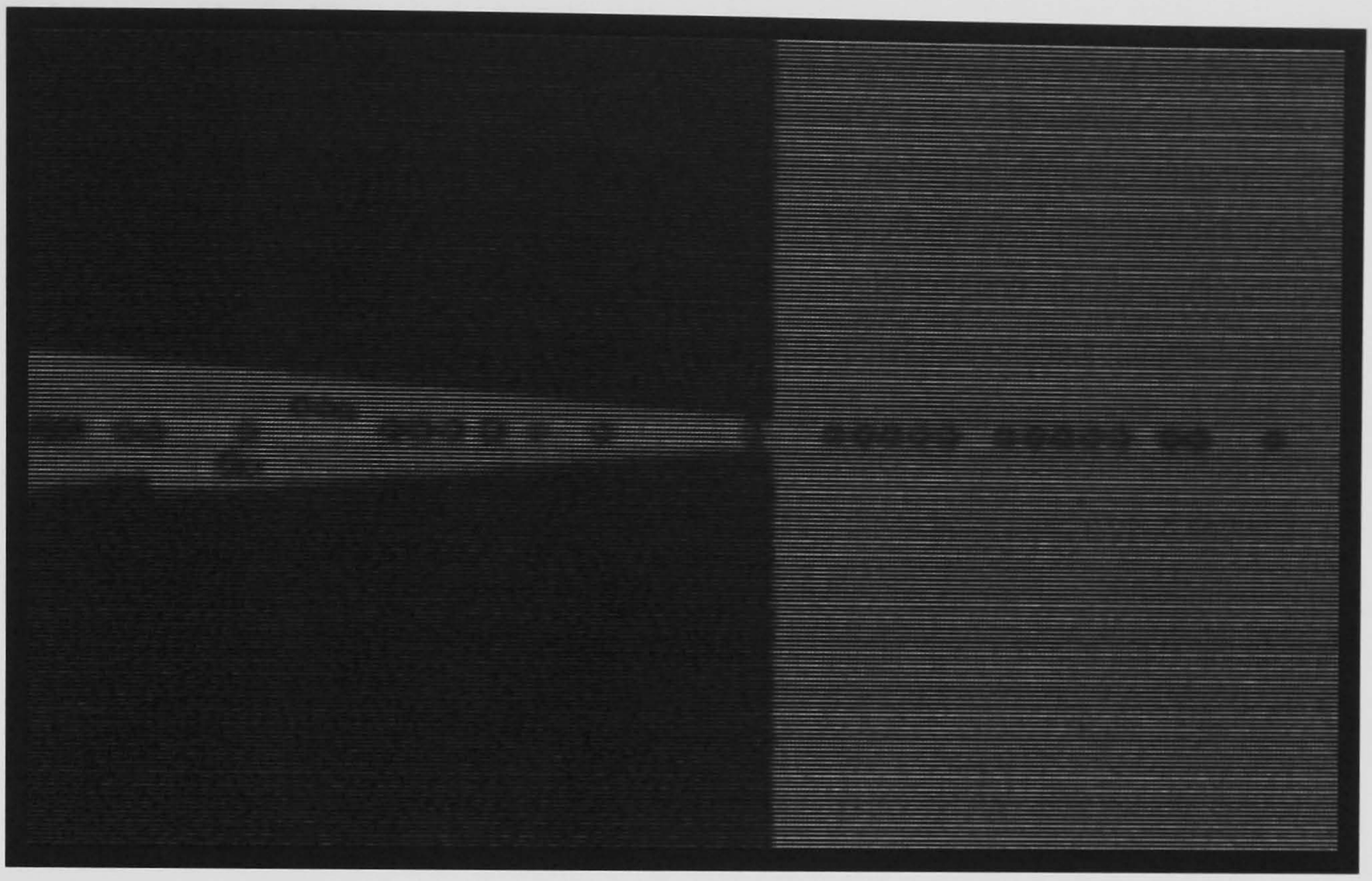

Figure 9-1. Method of creating a beam of particles (ongoing work of the author).

The benefit of such a system would be the rapid sorting of cells in a microsystem based on optical and/or impedance measurements carried out on individual particles. The technique could potentially be useful for sorting smaller particles such as single viruses and even single molecules, if scaled down sufficiently [6]. 'Bolting-on' of such a device to the end of the DEP separator proposed in this thesis would allow detection of, and counting of the cells as they flow to the channel outlet.

9.2 References

1. Pohl, H.A., *The motion and percipitation of suspensoids in divergent electric fields.* Journal of Applied Physics, 1951. **22**: p. 869-871.
2. Yang, J., *et al.*, *Dielectric properties of human leukocyte subpopulations determined by electrorotation as a cell separation criterion.* Biophysical Journal, 1999. **76**(6): p. 3307-3314.
3. Chan, K.L., *et al.*, *Measurements of the dielectric properties of peripheral blood mononuclear cells and trophoblast cells using AC electrokinetic techniques.* Biochimica Et Biophysica Acta-Molecular Basis of Disease, 2000. **1500**(3): p. 313-322.

4. Bianchi, D.W., *et al.*, *Development of a model system to compare cell separation methods for the isolation of fetal cells from maternal blood.* Prenatal Diagnosis, 1996. **16**(4): p. 289-298.
5. Schnelle, T., *et al.*, *Paired microelectrode system: dielectrophoretic particle sorting and force calibration.* Journal of Electrostatics, 1999. **47**(3): p. 121-132.
6. Morgan, H., D. Holmes, and N.G. Green. *AC electrokinetic focussing in microchannels: micro- and nanoparticles.* in *Electrostatics 2003*. 2003. Heriot-Watt University, Edinburgh: IOP Publishing Ltd.

Publications arising from this work.

Journal papers

1. Cui, L., D. Holmes, and H. Morgan, *The dielectrophoretic levitation and separation of latex beads in microchips*. Electrophoresis, 2001. **22**(18): p. 3893-3901.
2. Holmes, D., and H. Morgan, *New methods in dielectrophoretic cell separation.* (in preperation, 2003).
3. Holmes, D., N.G. Green and H. Morgan, *Nano-particle focussing using dielectrophoresis.* IEE Proceedings – Nanobiotechnology (in preperation, 2003).
4. Holmes, D., N.G. Green and H. Morgan *Dielectrophoretic flow-through separation systems: Comparison of experimental and numerical simulations.* IEEE – EMBS (submitted, 2003).

Conference proceedings

1. Theodorides, D., *et al.*, *Assessment of dielectrophoresis for sorting trophoblast from blood*, in *Fetus As a Patient*. 2000, Monduzzi Editore: 40128 Bologna. p. 403-408.
2. Holmes, D., M. Thomas, and H. Morgan, *Dielectrophoretic separation/isolation of rare particles/cell types form a heterogeneous suspension within a microfluidic system*, in *Micro Total Analysis Systems 2000, Proceedings*. 2000, Kluwer Academic Publ: Dordrecht. p. 115-118.
3. Theodorides, D., *et al. A novel AC electrokinetic method for the isolation of fetal cells from maternal blood.* in *6th World Hellenic Biomedical Congress*. 2000. Hilton Hotel, Athens, Greece: Ministry of Foreign Affairs Ministry of Health, University of Athens.
4. Theodorides, D., *et al. Assessment of dielectrophoresis for sorting trophoblast from blood.* in *XVI International Congress The Fetus as a Patient*. 2000. Fiuggi (Rome), Italy: Parthenon Publishing.
5. Holmes, D. and H. Morgan. *Particle focussing and separation using dielectrophoresis in a microfluidic channel.* in *Micro Total Analysis Systems 2001, Proceedings*. 2001. Monterey, USA: Kluwer Academic Publ.
6. Holmes, D. and H. Morgan. *Dielectrophoretic chromatography of cells.* in *Micro Total Analysis Systems 2002, Proceedings*. 2002. Nara, Japan: Kluwer Academic Publ.

7. Holmes, D. and H. Morgan. *Dielectrophoretic chromatography of cells*. in *NanoTech2002: The 6th Annual European Conference On Micro & Nanoscale Technologies for the Biosciences*. 2002. Montreux, Switzerland.
8. Holmes, D. and H. Morgan. *Cell Sorting And Separation Using Dielectrophoresis*. in *Electrostatics 2003*. 2003. Heriot-Watt University, Edinburgh: IOP Publishing Ltd.
9. Morgan, H., D. Holmes, and N.G. Green. *AC electrokinetic focussing in microchannels: micro- and nanoparticles*. in *Electrostatics 2003*. 2003. Heriot-Watt University, Edinburgh: IOP Publishing Ltd.